Environmental and landscape responses to abrupt climatic change during the Last Termination (*ca.* 21-11 cal ka BP) in the Vale of Pickering, NE England

Paul Christopher Lincoln

Thesis submitted for the degree of Doctor of Philosophy, Royal Holloway, University of London

January 2017

Institution of study:
Centre for Quaternary Research
Department of Geography
Royal Holloway
University of London

Declaration of Authorship

I, Paul Christopher Lincoln, hereby declare that this thesis and the work presented in it is entirely my own. Where I have consulted the work of others, this is always clearly stated.

The following publications includes original results reported in this PhD thesis:

Lincoln, P.C. Eddey, L.J., Matthews, I.P., Palmer, A.P. and Bateman, M.D. (eds.). .2017. *The Quaternary of the Vale of Pickering: Field Guide*. Quaternary Research Association, London.

Signed: Date:

Abstract

The Last Termination *ca.* 21-11 cal ka BP, including the Last Glacial-Interglacial Transition (LGIT) *ca.* 16-11 cal ka BP, represents the most recent period of abrupt climate change in which high amplitude cooling and warming events occurred on a sub-millennial scale. These events, best recorded in the Greenland ice-core records, had significant impacts on landscape change in NW Europe. Whilst there are a number of European continental sequences in which responses to these climatic shifts have been investigated, there have been limited studies in NE England. The Vale of Pickering (VoP), offers the opportunity to investigate landscape and biological response during the LGIT due to range of terrestrial archives preserved in the area which can be correlated to the LGIT. In addition, there is also archaeological evidence for repeated phases of early human occupation during this climatically unstable period in the valley. However, the lack of quantitative climatic reconstructions, detailed geomorphic mapping, and poor chronological control precludes a full understanding of the magnitude of climatic shifts, and the phasing of terrestrial responses through the Last Termination in the eastern Vale of Pickering (eVoP).

On this basis, a systematic geomorphological and sedimentological reinvestigation of the eVoP was undertaken. First, detailed geomorphic mapping of the Vale, followed by depositional modelling using new and previously published sedimentary records from the Wykeham Quarry area was undertaken in order to identify new sequences in which palaeoenvironmental information can be derived. Second, sedimentological, biological (pollen, macrofossils and coleopteran) and geochemical (^{18}O and ^{13}C stable isotopes) techniques were applied to these sequences in order to reconstruct past climatic and environmental changes. Third, robust chronologies were developed for these sequences using radiocarbon, SAR-OSL, tephrostratigraphy and Bayesian age modelling.

The results from this investigation indicate that cooling and warming events the eVoP during the LGIT are broadly in phase with the Greenland ice core record, but differ in amplitude to those recorded elsewhere in the British Isles and Western Europe. Additionally, there is evidence for dynamic hydrological, vegetational and geomorphic responses in the eVoP to the abrupt warming and cooling events. These are broadly in phase with those elsewhere in northern Europe, however the nature of these responses differs, indicating spatial variability in landscape change during this period. This has important implications for the interpretation of the archaeological record and environmental context of early human occupation during the LGIT.

Acknowledgements

Firstly, I'd like to thank my supervisors **Ian Matthews**, **Adrian Palmer** and **Simon Blockley** who have been an immeasurable help in the completion of this thesis. The support and guidance you have provided throughout this project is greatly appreciated.

Andy Josephs, and the **Oxford Archaeology team** are thanked for their help, particularly in the early stages of this project in coordinating research efforts and keeping me abreast of planned quarrying schedules which have significantly strengthened the output of this work. In regards to fieldwork, I would first like to thank members of Hanson Aggregates including **Ben Ayres**, **Stuart Laws**, **Dan Senkans** and **Tim Harvey** who have made working at Wykeham Quarry an enjoyable and rewarding experience. Thanks are also extended to **Robert Pigg** and **Robert Sword** who provided access to the WYKNE15 and WYKSE14 sites for field excavations. **John Lowe** and **Ian Candy, Claire Tye, Ash Abrook,** and in particular **Rhys Timms** are thanked for their help through all aspects of the fieldwork in this project, particularly Ash and Rhys' continued determination to extract cores from a cold, submerged field in a Yorkshire January, with a 'broken down' equipment van a mile up the road. A special mention is also extended to Simon in this regard, whose 'cheeky' fieldtrips to Scarborough have been one of the highlights of this project for me (especially the enthusiastic late evening expeditions for a decent pint and a curry). Cheers guys! **Scott Elias** and **Simon Armitage** are thanked for their help with the coleopteran and SAR-OSL data presented in this thesis whilst Ian Candy is also acknowledged for all of his help and assistance associated with stable isotopic work. I would also like to extend a huge thanks to **Richard Staff** for his undying optimism and enthusiasm throughout my week at ORAU running radiocarbon samples. It was a fantastic experience and I am greatly appreciative of the time devoted that you devoted to me. **Jim Rose** is thanked for the enthusiasm he has shown for this project, and the provision of some critical papers for interpretation. Thank you also to all of the RHUL PhD students including**, Jacob Bendle, Julian Martin, Rachael Squire, Dan Webb, Pappa Spyridoula,** and **Gareth Tye**, as well as the Geography department as a whole who have made RHUL a fun and interesting place to work. A huge thank you is especially reserved for the RHUL technical staff**: Iñaki Valcarcel, Marta Perez, Claire Mayers** and **Katy Flowers** with whom many a laugh has been had over the past 6 or so years since I turned up at RHUL. A big thank you to my family- **Diana**, **John** and **Dave Lincoln** who have always been incredibly supportive through all of my academic endeavours, which is greatly appreciated. Last but not least, a special thank you to my soulmate **Jenni Sherriff** who has been fantastic throughout this project and has kept me smiling through the hard months. I could not have completed this without you.

This thesis is dedicated to Jack Wilcox (1989-2012).

List of Contents

List of Figures

Chapter 1 – Introduction

Chapter 2 – Climatic variability in the North Atlantic and surrounds during the Last Termination (*ca*. 21-11 ka BP)

Chapter 3 – NE England through the Last Termination

Chapter 4 – Research Methodology

Chapter 5 – Developing a landscape model for the eastern Vale of Pickering through the Last Termination

Chapter 6 – Palaeoenvironmental reconstructions from Wykeham Quarry

Chapter 7 – Developing an LGIT palaeoclimatic event stratigraphy for the eastern Vale of Pickering

Chapter 8 – Regional comparisons to the eastern Vale of Pickering palaeoclimatic event stratigraphy

Chapter 9 – Reconstructing landscape response to hydroclimatic changes in the eastern Vale of Pickering during the Last Termination

List of Tables

Chapter 6 - Palaeoenvironmental reconstructions from Wykeham Quarry

Chapter 7 – Developing an LGIT palaeoclimatic event stratigraphy for the eastern Vale of Pickering

List of Abbreviations

ABUN	Macrofossil abundance scale
AMOC	Atlantic Meridional Overturning Circulation
b2k	Years before 2000 AD on the GICC05 timescale
C-IT	Chironomid-inferred temperatures
cal BP	Calibrated radiocarbon years before present (1950 AD)
$\delta^{18}O_{bulk}$	$\delta^{18}O$ values from bulk lacustrine carbonate
DEM	Digital elevation model
DTM	Digital terrain model
EH	Early Holocene
eVoP	eastern Vale of Pickering
E-WI	Early Windermere Interstadial
GICC05	Greenland Ice-core Chronology (Rasmussen *et al.,* 2006)
GI-	Greenland Interstadial
GS-	Greenland Stadial
IRD	Ice-rafted debris
ka	Thousand years
LfA	Wykeham Quarry Lithofacies Assemblage
LGIT	Last Glacial-Interglacial Transition (*ca.* 14.7-11 cal ka BP)
LGM	Last Glacial Maximum
LLS	Loch Lomond Stadial
MCR	Mutual Climatic Range
MIS	Marine Isotope Stage
M-L-WI	Mid-Late Windermere Interstadial
m OD	Metres above ordinance datum (UK sea-level)
NADW	North Atlantic Deep Water
NGRIP	North Greenland Ice Core Project
NSIL	North Sea Ice Lobe
PBO	Preboreal Oscillation
SAR-OSL	Single aliquot regenerative optically stimulated luminescence
sp.	Taxa not identified to species
VOYL	Vale of York Ice Lobe
WI	Windermere Interstadial
WN-I	Wykeham Northern Extension isotope zone
WN-L	Wykeham Northern Extension lithozone
WN-M	Wykeham Northern Extension macrofossil zone
WS-L	Wykeham Southern Extension lithozone
WS-M	Wykeham Southern Extension macrofossil zone
WS-P	Wykeham Southern Extension pollen zone
WYKNE15	The Wykeham Northern Extension 2015 record
WYKSE14	The Wykeham Southern Extension 2014 record
YD	Younger Dryas

1. Introduction

1.1. Scientific rationale

It is now widely accepted that anthropogenic practices are substantially affecting the global climatic system, with forecasts by the Intergovernmental Panel on Climate Change (IPCC) highlighting the potential of abrupt changes in climatic regime in the future (Solomon *et al.,* 2007; Stocker *et al.,* 2013). Abrupt (millennial-decadal scale) climatic events in the North Atlantic region have been demonstrated to have occurred repeatedly in the past (Rasmussen *et al.,* 2014), and considered to have been caused by changes in ocean circulation patterns in the North Atlantic, driven by large influxes in freshwater, disrupting the transfer of latent heat to continental margins (Broecker and Denton, 1989; Broecker *et al.,* 1990). These shifts are therefore most pronounced in the North Atlantic and surrounds. This is significant as currently, the melting of ice sheets in this region is enhancing the influx of freshwater into the North Atlantic and perturbing rates of ocean circulation (Dickson *et al.,* 2002; Vellinga and Wood, 2002; 2008; Rhein *et al.,* 2013; Rahmstorf *et al.,* 2015). The study of past climatic intervals in which these freshening events are previously occurred allows for an assessment to be made regarding the environmental and landscape response to these events, thereby improving our understanding of the impact of future climatic change to terrestrial systems.

The proximity of the British Isles to the North Atlantic means it is particularly sensitive to abrupt climatic changes, making it an ideal location to study the effects of past climatic changes on landscapes. Additionally, the stratigraphy of the British Isles is well understood, meaning potential sequences able to reconstruct palaeoclimatic regimes can be readily identified. Principal to this understanding is the identification of past glacial limits of the British-Irish Ice Sheet (BIIS) which repeatedly advanced and retreated across Britain through the Quaternary (Bowen *et al.,* 1984; 2002; Clark *et al.,* 2004; Evans *et al.,* 2005), eroding pre-existing landforms and conditioning the landscape via proglacial and paraglacial readjustment processes upon retreat (Ballantyne, 2002; Palmer *et al.,* 2008; 2015; Livingstone *et al.,* 2011). Palaeoenvironmental records from lake basin infills formed in these environments have provided a readily available source of evidence for past climatic change, significantly enhancing our understanding of the climatic structure in the British Isles through previous periods of climatic instability (Brooks and Birks, 2000a; Marshall *et al.,* 2002; Candy *et al.,* 2016; Tye *et al.,* 2016).

The last deglaciation of the BIIS occurred during the most recent period of pronounced climatic instability in Earth's history, termed as the Last Termination between *ca.* 21-11 cal ka BP, where a series of abrupt climatic events have been recorded. The Last Termination is one of the most extensively studied intervals in relation to past climatic variability, as it is the most recent period of Earth's history where the global climate system underwent large-scale reorganization of ocean

and atmospheric circulation (Rasmussen *et al.,* 2014; Heiri *et al.,* 2014; Rahmstorf *et al.,* 2015). Additionally, the wealth of preserved geomorphological, lithostratigraphical, and biostratigraphical evidence in the British Isles provides a means to reconstruct climatic and environmental changes at a high temporal resolution, constrained to more precisely dated age models than earlier Quaternary stages (Walker, 2001; Rasmussen *et al.,* 2014). This is critical for climate models attempting to assess the manifestation of future abrupt climatic events on landscapes due to the rapidity and spatial complexity in which these episodes can occur (Steffensen *et al.,* 2008; Brauer *et al.,* 2008; Heiri *et al.,* 2014; Rach *et al.,* 2014). The Last Termination in the British Isles therefore provides a valuable analogue for future instabilities in the global climate system and landscape change (Vellinga and Wood, 2002; Hegerl *et al.,* 2007; Heiri *et al.,* 2014; Rahmstorf *et al.,* 2015).

1.1.1. The Last Termination

The climatic structure of the Last Termination is best expressed in the Greenland ice core stratigraphy, which indicates that the interval was characterised by a substantial warming trend superimposed with a series of abrupt and short-lived (millennial to sub-centennial scale) climatic oscillations. These repeatedly shifted between near interglacial to almost full glacial conditions (Rasmussen *et al.,* 2006; Lowe *et al.,* 2008), in sub-decadal timescales (Steffensen *et al.,* 2008), with shifts most prevalent between 14.7-11 cal ka BP (the last glacial-interglacial transition -LGIT; Björk *et al.,* 1998). The mechanism for these climatic shifts is widely accepted to originate from fluctuations in the strength and position of North Atlantic Ocean circulation, driven by freshwater forcing from deglaciation of Northern Hemisphere ice sheets (Broecker *et al.,* 1989; Alley, 2007). This interval provides significant potential for palaeoclimatic reconstruction in the British Isles due to the wealth of geomorphological, lithostratigraphical, and biostratigraphical evidence preserved, meaning it can be studied in much higher temporal resolution and dated more precisely than phases of climatic instability during earlier Quaternary intervals (Walker, 2001; Rasmussen *et al.,* 2014).

1.1.2. Key British sites

Palaeoclimatic records derived from biological, sedimentological and geochemical evidence in British lacustrine sequences demonstrate a similar climatic pattern through the Last Termination to that documented in the Greenland ice cores (Atkinson *et al.,* 1987; Lowe *et al.,* 1995; Walker *et al.,* 2003). Furthermore, high resolution records from sites such as Hawes Water and Whitrig Bog have been able to identify multiple abrupt climatic events through the LGIT which appear to correspond to those identified Greenland (Brooks *et al.,* 2012) and elsewhere in continental sequences in western Europe (von Grafenstein *et al.,* 1999; van Raden *et al.,* 2013), demonstrating that terrestrial systems were affected by this climatic instability across large parts of the North Atlantic region (Yu and Eicher, 1998).

However, the phasing, timing, amplitude, and spatial homogeneity of palaeoclimatic change, and palaeoenvironmental responses has remained difficult to quantify, owing primarily to: a) the difficulty found in constructing robust chronologies from these palaeoenvironmental records, b) the lack of high resolution records in various regions, meaning changes occurring in areas such as the eastern British Isles remain poorly constrained. Additionally, the focus of palaeoenvironmental reconstructions in Britain has been principally associated with changes in temperature and/or vegetation cover, meaning other aspects of climate and environmental systems, such as regional hydrology remain poorly-/un-quantified (Huijzer and Isarin, 1997; Huijzer and Vandenberghe, 1998; Hoek and Bohncke, 2002).

Areas such as the Vale of Pickering (VoP), located in north east (NE) England, provide significant potential in which to develop understanding of palaeoclimatic, and palaeoenvironmental regimes through the Last Termination based upon the following criteria: a) it is situated on the east coast of the British Isles, an area where chronologically constrained high resolution palaeoclimatic records are lacking, b) the eastern VoP (eVoP) was inundated by the BIIS during the Dimlington Stadial (Kendall, 1902; Evans *et al.,* 2016), meaning palaeolake basins formed via glacial and paraglacial readjustment processes, preserving sediments viable for palaeoenvironmental reconstruction through the LGIT, are likely to exist in the valley (Palmer *et al.,* 2015).

1.2. Site introduction and previous work

This thesis focuses on improving the understanding of the palaeoclimatic structure and landscape evolution of the eVoP during the Last Termination through the integration of geomorphic, sedimentological, chronological, biological and geochemical techniques. This section outlines previous work undertaken in the VoP, and from sedimentary sequences at Wykeham Quarry in the eVoP, which forms a major component of this study.

1.2.1. The Vale of Pickering (VoP)

The Vale of Pickering (VoP), located in north-eastern England is a broad, elongate, east–west trending valley, bounded to the north by the North York Moors, and to the south by the Yorkshire Wolds (Figure 1.1). At the start of the Last Termination, the valley was inundated by two lobes of the BIIS from the North Sea, which inundated the eVoP, and from the Vale of York, which dammed drainage, forming a proglacial lake in the valley (Kendall, 1902; Evans *et al.,* 2016). By the onset of the LGIT (*ca.* 14.7 cal ka BP), ice had receded, and the proglacial lake drained to form a more constrained water body in the eVoP, termed Palaeolake Flixton (PF). PF is interpreted to have formed via the paraglacial reorganisation of the landscape (dead-ice melt-out from outwash sediments) after ice recession from the eVoP (Palmer *et al.,* 2015). Palaeoenvironmental signals, consisting principally of pollen analysis have been reconstructed from the infill of PF, demonstrating evidence of climatic complexity (vegetation assemblage

turnover) through the LGIT (Day, 1996; Mellars and Dark, 1998; Cummins, 2003). The margins of PF have been found to preserve abundant evidence of Upper Palaeolithic, and Early Mesolithic activity (Clark, 1954; Moore, 1954; Schadla-Hall, 1987; Mellars and Dark, 1998; Conneller *et al.,* 2016), making the eVoP the most important, and well documented Early Mesolithic site in Britain (Gonzalez and Huddart, 2002; Mellars and Dark, 1998). Whilst the timing of early human occupation of the eVoP is chronologically constrained, the palaeoenvironmental records from the basin have been difficult to date, principally due to the potential of hard water error, and the lack of plant macrofossil remains in the LGIT sediments (Cloutman, 1988a; b; Day, 1996; Dark, 1998), meaning the timing and duration of environmental changes through the Last Termination are not well resolved.

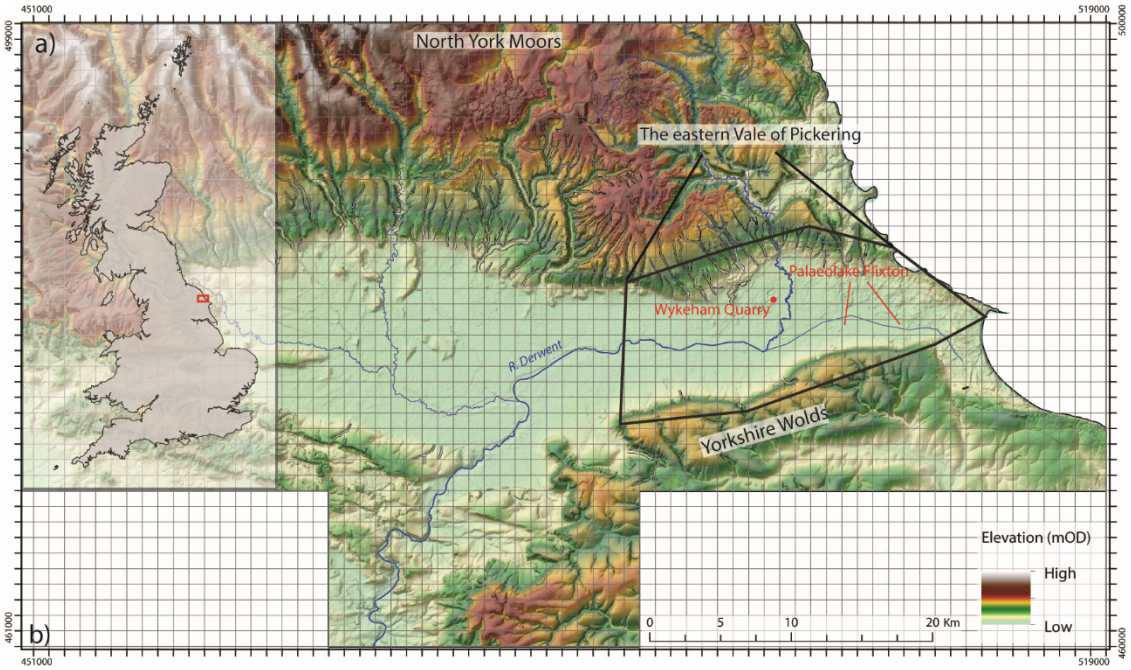

Figure 1.1. *a) The location of the Vale of Pickering (VoP; red triangle) in the British Isles, b) Digital Elevation Model of the VoP, showing the location of sites mentioned in text. The extent of the eVoP, which forms the main focus of this thesis is shown alongside the locations of Palaeolake Flixton and Wykeham Quarry which are discussed in sections 1.21 and 1.2.2 respectively.*

1.2.2. Wykeham Quarry

Wykeham Quarry (SE 98231 82344) is located in the central area of the eVoP, *ca.* 2 km to the west of PF (Figure 1.1). The quarry is run by Hanson Quarry Products Europe Limited, and has been in operation since 1981, extracting aggregates (sands and gravels), via stripping and dragline extraction. Since 2004, the quarry has expanded in two stages. An initial extension was excavated between 2004 and 2013 (termed as the present quarry area in Figure 1.2). Owing to the proximity of the site to the archaeological sites preserved around PF, a- series of trial trenches and a watching brief was placed on the extraction phases, aimed at identifying sites of potential for archaeological preservation, and recording the characteristics of deposits preserved in the quarry area.

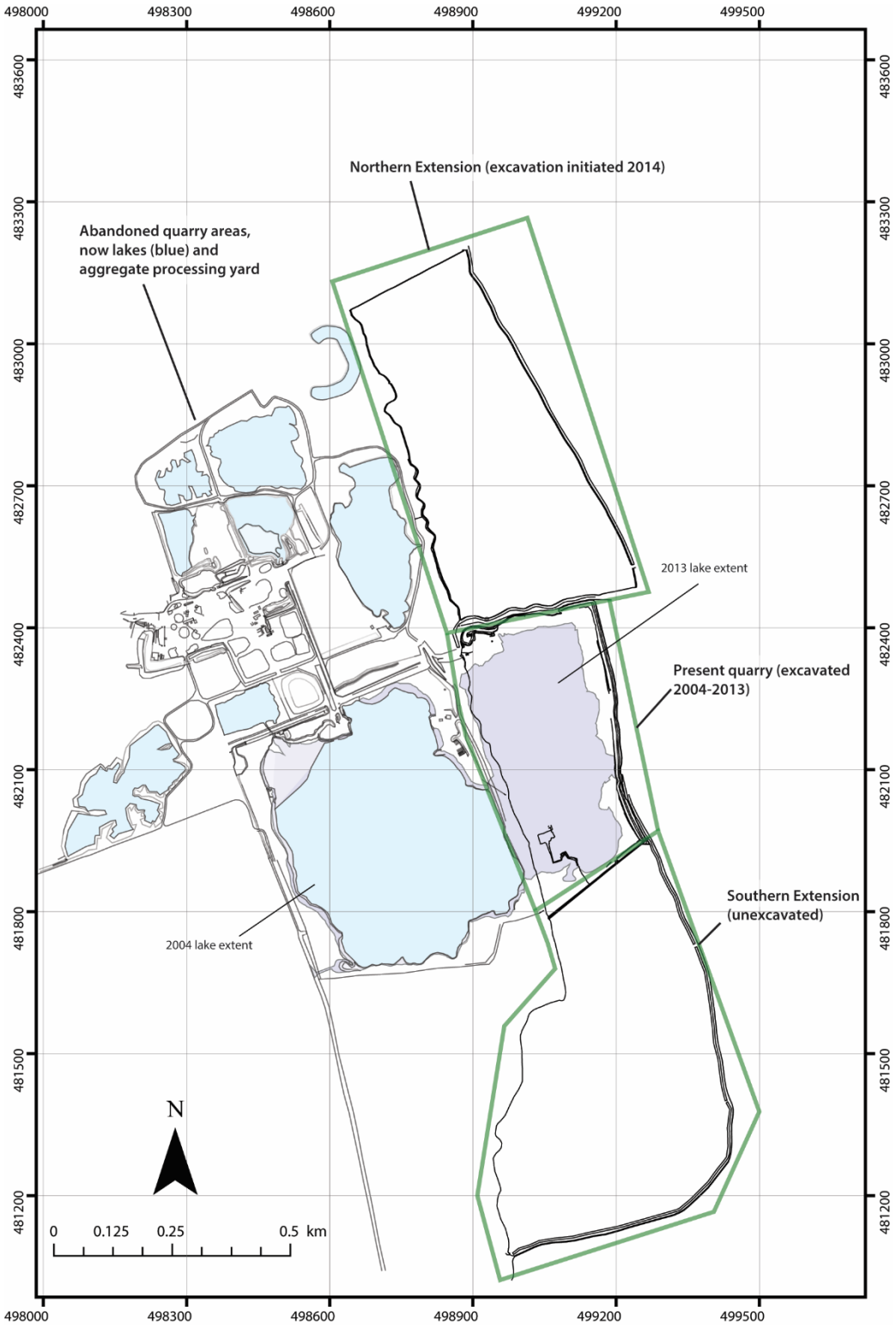

Figure 1.2 *Map of Wykeham Quarry in the eVoP (location shown in Figure 1.1), showing the locations of the present quarry area, Northern and Southern Extension areas discussed in text. The extent of lakes formed after aggregate extraction are shown to demonstrate the extent of quarrying undertaken between 2004 and 2013. As of 2013 nearly all of the present quarry area had been excavated, meaning in situ deposits had been entirely removed.*

Although to date, no Early Mesolithic or Upper Palaeolithic remains have been identified from the quarry excavation, these records contain complex sequences of fine-grained and fossiliferous deposits, viable for multiproxy palaeoenvironmental reconstruction and radiocarbon dating, through intervals of the Last Termination across the present quarry area (Fraser *et al.,* 2009; Cloutman *et al.,* 2010).

In 2012, permission was granted for a second extension phase, to the north, and the south of the present quarry site (areas termed as the Northern and Southern Extension areas respectively in Figure 1.2). Prior to the excavation of these areas, a detailed auger survey was performed by Batchelor (2009), aimed at assessing the thickness and extent of fine grained deposits across the site and identify sites of potential for archaeological remains. This survey identified additional complexity in the sedimentary sequences including the presence of alluvial, and in some cases carbonate rich deposits with potential for palaeoenvironmental reconstruction. The mode of formation, and development of these deposits in association with climatic changes during the Last Termination however remained poorly constrained. In line with this evidence, Hanson Aggregates provided funding to Royal Holloway for the undertaking of this PhD to investigate the deposits at Wykeham Quarry, and develop understanding of the evolution of the eVoP through the Last Termination. The following section outlines the principal research aims and objectives of the project.

1.3. Research aims and objectives

The overarching goal of this research is to improve understanding of climatic, hydrological, and geomorphic shifts during the LGIT in the eastern Vale of Pickering (eVoP). This can be split into three principle research aims:

1. Develop a model of landscape evolution through the Last Termination from the eVoP using GIS mapping techniques coupled with sedimentological analysis of deposits.
2. Identify sites viable for high resolution palaeoclimatic, palaeohydrological, and palaeoenvironmental reconstructions in the eVoP through the LGIT.
3. Produce well dated, high resolution palaeoenvironmental records using a combination of sedimentological, geochemical and palaeoecological techniques, which can be compared to other palaeoenvironmental records from the North Atlantic and surrounds.

To achieve the aims stated above, a number objectives needed to be achieved:

1. The VoP was mapped using desk based techniques to remap and synthesise existing landforms identified in the valley associated with geomorphic activity through the Last Termination. (Aim 1)

2. Further landforms were identified using desk based mapping techniques which: a) developed understanding on the phasing and mode of deglaciation in the VoP, and geomorphic activity through the Last Termination b) have the potential to contain sedimentary sequences viable for high resolution palaeoenvironmental reconstructions through the LGIT (Aims 1-2).
3. The sedimentary sequences from Wykeham Quarry was synthesised and supplemented by additional, targeted boreholes taken in the field where required. The stratigraphic data was analysed and modelled to develop understanding on the spatial distribution of analogous sedimentary sequences, and used to identify sites of optimum potential for palaeoenvironmental reconstruction, and radiocarbon dating (Aims 1 and 2).
4. Sites of optimum potential for palaeoenvironmental reconstruction were identified from the sediment models constructed in objective 3. In order to fulfil the criteria, sedimentary sequences must: a) have been deposited through the LGIT, and b) contain evidence of sedimentological complexity, which may represent variability in climatic, landscape, and/or hydrological regimes (Lewis and Maddy, 1999; Schnurrenberger *et al.,* 2003). (Aims 2 and 3).
5. The sedimentology of selected sequences was established using standard macro- and micro-scale techniques in order to understand the nature of sediment deposition, and associated prevailing, environmental conditions. (Aims 2 and 3).
6. Biological (pollen, plant macrofossils and coleoptera) and geochemical techniques (bulk sediment stable isotopes from freshwater carbonates) were used to identify periods of palaeo-climatic, -hydrological, and -environmental variability, in the selected sedimentary sequences, which enabled the correlation of records to other sites in NE England. (Aim 3).
7. Chronological techniques (radiocarbon dates from terrestrial plant macrofossils, single-aliquot-regenerative optically stimulated luminescence (SAR-OSL), and cryptotephra) were utilised on selected sequences to assign absolute ages to sedimentary sequences, enabling robust correlations to palaeoenvironmental records across the N Atlantic region to be constructed (Björk *et al.,* 1998; Lowe *et al.,* 2008). (Aim 3).

1.4. Thesis structure

This thesis is split into 10 Chapters. Chapter 2 provides a review of the structure and mechanisms responsible for climate change in the North Atlantic and surrounds during the Last Termination. Chapter 3 describes the existing geomorphic, palaeoclimatic, palaeoenvironmental, and archaeological records through the Last Termination in both NE England, and specifically the VoP. Chapter 4 provides a description of the scientific rationale and analytical techniques used in this study to address the aims and objectives. Chapter 5 presents the results of the desk based geomorphic mapping of the VoP, and the sedimentology and stratigraphy of deposits at Wykeham Quarry, used to develop understanding the model of landscape evolution through the Last Termination and identify potential sites for palaeoenvironmental reconstruction. Chapter 6 presents the results of sedimentological, palaeoenvironmental, and chronological records

constructed from selected sediment sequences from Wykeham Quarry. Chapter 7 synthesises palaeotemperature and palaeohydrological records from the eVoP through the LGIT which are used to create a regional palaeoclimatic event stratigraphy. Chapter 8 discusses the eVoP event stratigraphy in relation to other palaeoclimatic records from the British Isles and NW Europe. Chapter 9 discusses the landscape evolution of the eVoP in relation to hydroclimatic changes reconstructed in the eVoP. The main conclusions of this study are presented in Chapter 10.

2. Climatic variability in the North Atlantic and surrounds during the Last Termination (*ca* 21-11 cal ka BP)

2.1. Introduction

The period marking the end of the last glacial (Devensian in the British Isles, Weichselian in Europe, Termination 1 in the North Atlantic) and the present Interglacial (MIS-1; the Holocene), between *ca.* 21 to 11 cal ka BP (the Last Termination hereafter), was one of substantial interhemispheric climatic variability in and around the North Atlantic (Björk *et al.,* 1998; Lowe *et al.,* 2008). This period includes the interval between *ca.* 14.7 and 11 cal ka BP, which is commonly referred to as the last glacial-interglacial transition (LGIT; Björk *et al.,* 1998; Lowe *et al.,* 2008), considered to represent the most recent Dansgaard-Oeschger (D-O) event (Dansgaard *et al.,* 1993). The LGIT is characterised by a series of abrupt and short-lived (millennial to sub-centennial scale) climatic oscillations, shifting between near interglacial, and almost full glacial conditions (Rasmussen *et al.,* 2006; Lowe *et al.,* 2008). This is one of the most extensively studied intervals of the entire Quaternary period for two reasons: First, the wealth of preserved geomorphological, lithostratigraphical, and biostratigraphical evidence means it can be studied in much higher temporal resolution and potentially dated more precisely than earlier Quaternary phases (Walker, 2001; Rasmussen *et al.,* 2014). Second, it is the most recent period of Earth's history where the global climate system underwent large-scale reorganization of ocean and atmospheric circulation, therefore potentially providing a valuable analogue for contemporary, and future instabilities in the global climate system (Vellinga and Wood, 2002; Hegerl *et al.,* 2007; Heiri *et al.,* 2014; Rahmstorf *et al.,* 2015).

In order to understand how landscapes in the British Isles evolved during this period, it is first necessary to review the regional climatic parameters under which these landscapes were formed. It has long been assumed that climatic and environmental trends in the North Atlantic region are broadly in phase (within chronological errors) during this interval (Lowe *et al.,* 1995; 2008), highlighting the common causal mechanism for the observed changes across the region. However, well resolved records from Northern Europe have recently shown that the local manifestation of these hemispheric climatic oscillations can be offset by up to two centuries across the mid-high latitudes of the Northern Hemisphere (Brauer *et al.,* 2008; Lane *et al.,* 2013; Rach *et al.,* 2014; Muschitiello *et al.,* 2015). This suggests that the mechanisms producing these climatic oscillations are complex, and their manifestation across the North Atlantic and surrounds was spatially and temporally heterogeneous (e.g. Muschitiello *et al.,* 2015; Candy *et al.,* 2016).

This chapter seeks first to review the climatic structure of the Last Termination and the LGIT

in the North Atlantic and surrounds between *ca.* 21-11 cal ka BP (section 2.2), and second, assess the principal drivers for these changes (section 2.3). The chapter concludes by assessing the potential that palaeoclimatic records from Northeast (NE) England have for recording climatic and environmental oscillations through the Last Termination.

2.2. Stratigraphy, and climatic structure of the Last Termination

The following section summarises the previous methods used to subdivide palaeoclimatic/palaeoenvironmental signals through the Last Termination and LGIT in the British Isles, and Northwest Europe, which are summarised in Figure 2.1.

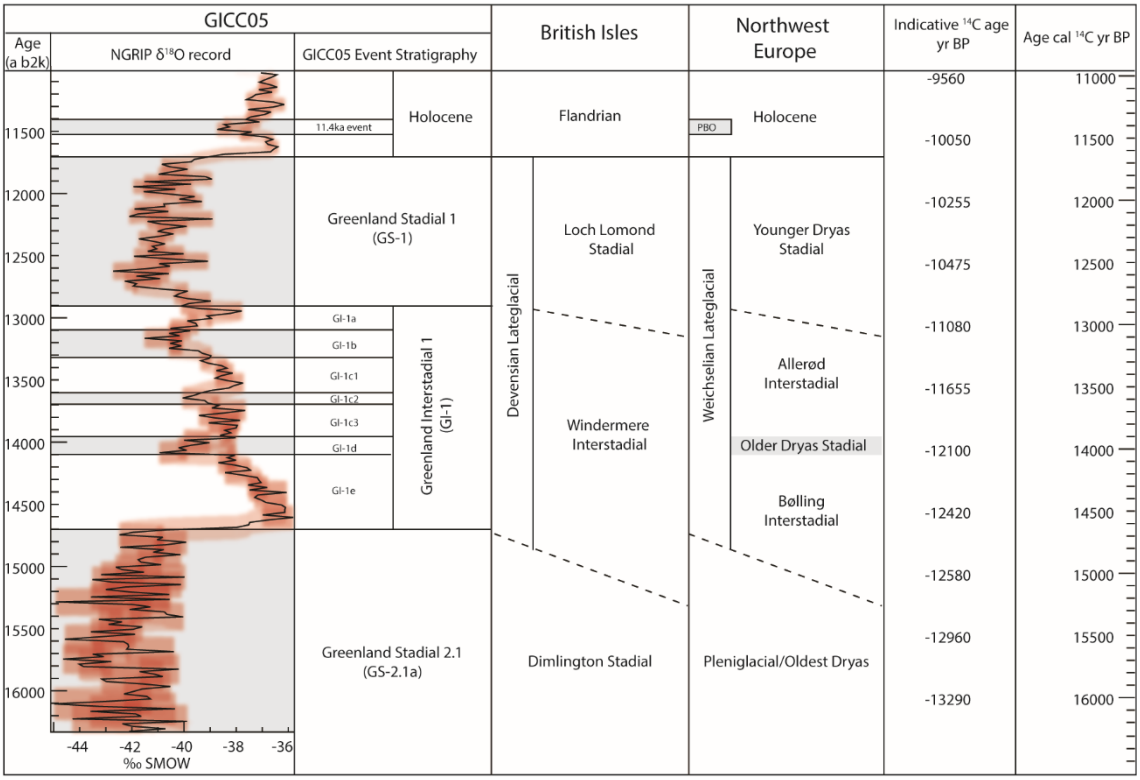

***Figure 2.1**. δ18O record from NGRIP plotted against the GICC05 timescale (Figure 2.2), the North Atlantic Event Stratigraphy (left), and the stratigraphic subdivision of the LGIT in the British Isles and Northwest Europe. The calibrated calendar timescale is shown on the right alongside 'indicative'/average 14C ages (after Lowe and Walker, 2014).*

2.2.1. Traditional stratigraphies of terrestrial records

The Last Termination, and in particular the LGIT are classically correlated to the palynological biozones obtained from lacustrine and wetland sediments in southern Scandinavia (Iversen, 1954; Mangerud *et al.,* 1974). This scheme is termed the Norden model and subdivides the LGIT into two warm phases (interstadial episodes) named the Bølling (13-12 ^{14}C ka BP), and the Allerød (11.8-11 ^{14}C ka BP), separated by two cold phases named as the Older Dryas (12-11.8 ^{14}C ka BP), and the Younger Dryas (YD; 11-10 ^{14}C ka BP). Preceding the LGIT was a cold stage termed as the Oldest Dryas/Pleniglacial (>13 ^{14}C ka BP) whilst proceeding the Younger Dryas was the initial stage of the Holocene termed as the Preboreal (10-9^{14}C ka BP).

In the British Isles, chronologically bounded bio- and lithozones have also traditionally been used to subdivide the Last Termination (Late Devensian) into four climatostratigraphic periods (Coope, 1977; Pennington, 1977; Rose, 1985). These are: a) The Dimlington Stadial between 26-13 ^{14}C ka BP, b) the Windermere Interstadial (WI) between 13-11 ^{14}C ka BP, c) the Loch Lomond Stadial (LLS) between 11-10 ^{14}C ka BP, and the Flandrian/Holocene <10 ^{14}C ka BP.

As the boundaries of the Norden Model biozones are assigned radiocarbon derived ages by Mangerud *et al.* (1974), they have since been widely used as chronozones (time parallel events) with which to assign observed climatic episodes in other sequences distal to Scandinavia, which are assumed to be approximate in time, (e.g. Markgraf, 1991), but for which the Norden scheme was never intended (Björk *et al.,* 1998). This introduces problems when attempting to assess the mode of climatic changes during this interval for two reasons: First, the Norden Model is constructed from biozone boundaries (reflecting the response of vegetation to thresholds in the antecedent climatic and/or environmental conditions), which are known to be time transgressive (e.g. Pennington, 1986; Walker, 1995; Wohlfarth, 1996; Birks and Birks, 2014) and therefore do not represent a time parallel horizon with which to compare and correlate climatic records (Björk *et al.,* 1998; Lowe *et al.,* 2008). Second, the chronostratigraphy of the Norden Model is constructed from bulk limnic radiocarbon dates which are known to contain recurrent site-, sample-, or laboratory specific errors including contamination of older and younger material, and reservoir offsets (Wohlfarth, 1996; Walker, 2001; Blockley *et al.,* 2007; Lowe *et al.,* 2008). Furthermore, the wide uncertainties on these ages make it difficult to assign precise age ranges to centennial scale climatic oscillations through the LGIT (Lowe *et al.,* 2007; *see below*). This means the Norden model cannot be used to reliably assess the regional chronology of the abrupt climatic changes through the LGIT.

2.2.2. GICC05 - the regional stratotype for climatic variability during the Last Termination

For the reasons outlined above, the International Working Group known as INTIMATE (INTegration of Ice, MArine, and TErrestrial records) proposed that the Norden Model should be replaced as the North Atlantic stratotype by a North Atlantic Event Stratigraphy, using the high resolution isotopic signals from the Greenland Ice cores as a regional template (Björk *et al.,* 1998; Lowe *et al.,* 2001; Lowe *et al.,* 2008; Blockley *et al.,* 2012). This record is preferential for a number of reasons. First, it is constructed from a series of stable isotopic signals which have been shown to be sensitive- and respond rapidly- to climatic variations (Johnsen *et al.,* 1992; Dansgaard *et al.,* 1993; Steffensen *et al.,* 2008; Rasmussen *et al.,* 2014). The most widely utilised of these signals is the water isotope $\delta^{18}O_{bulk}$ record, which is a proxy for past air temperature at the sampling site, (Johnsen *et al.,* 1992; Dansgaard *et al.,* 1993; Steffensen *et al.,* 2008) and δD which is a proxy for the moisture source of precipitation (Masson-Delmotte *et al.,* 2005; Jouzel *et al.,* 2007; Steffensen *et al.,* 2008). These proxy records are underpinned by a robust, and highly

resolved timescale based upon multiparameter layer counting of multiple ice cores termed the GICC05 timescale (Rasmussen *et al.,* 2006; Rasmussen *et al.,* 2014), which provides high age precision (maximum counting error of *ca* 3 %) through the Last Termination (Figures 2.1-2.2). The GICC05 timescale enables climatic events during the Last Termination to be resolved at a temporal resolution that cannot be achieved in most terrestrial archives. The North Atlantic Event Stratigraphy therefore provides the most robust framework with which to assess climatic variability in the North Atlantic during the Last Termination. Furthermore, it provides a basis with which to compare other palaeoclimatic, and palaeoenvironmental records, allowing assessments on the spatial manifestation of climatic variability in the North Atlantic region, as well as potential leads and lags in the climate system during the Last Termination (Björk *et al.,* 1998; Lowe *et al.,* 2008).

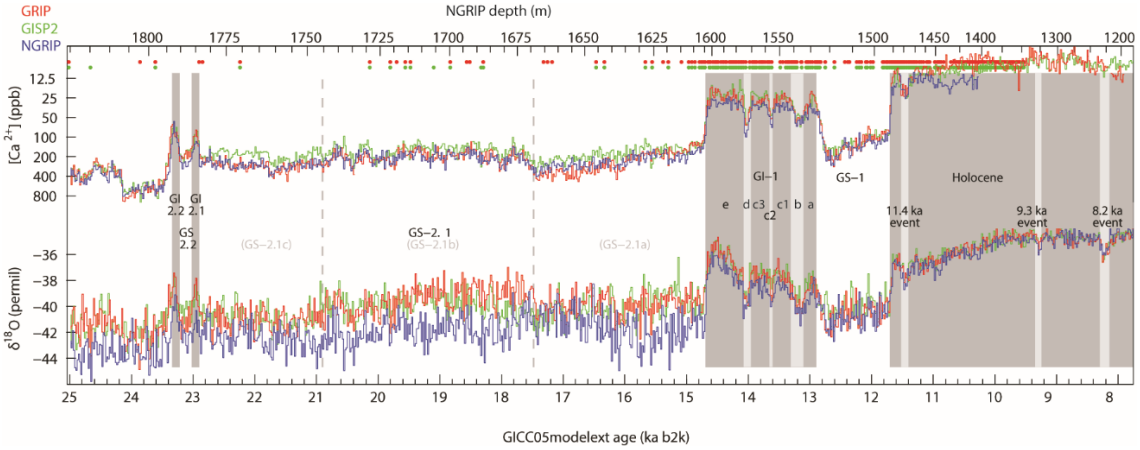

***Figure 2.2**. 20-year average values of $\delta^{18}O$ and Ca^{2+}: see text for data sources from GRIP (red), GISP2 (green), and NGRIP (blue) ice cores on the GICC05 timescale between 8 and 25 ka b2k (from Rasmussen et al., 2014). This record forms the North Atlantic Event Stratigraphy for the Last Termination. Greenland stadial and interstadial numbers discussed in text are labelled.*

In order to test the phasing of climatic response, INTIMATE propose that palaeoenvironmental records should be constructed using independent, and quantifiable proxy data, and defined using local stratigraphic terminology. To enable comparisons to other records, each stratigraphy should contain an independent high-precision age model (Lowe *et al.,* 2008). This provides a means to test how the palaeoclimatic, and palaeoenvironmental signals correlate with other records. These criteria are therefore adopted here (Chapter 4).

2.2.3. Climatic structure of the Last Termination in the North Atlantic and surrounds

The GICC05 $\delta^{18}O$ record divides the Last Termination into two stadials termed Greenland Stadial-2.1 (GS-2.1 *ca.* 23-14.7 ka b2k) and GS-1 (12.9-11.7 ka b2k), and one interstadial termed Greenland Interstadial-1 (GI-1, *ca.* 14.7-12.9 ka b2k), prior to the onset of the present interglacial (The Holocene) at *ca.* 11.7 ka b2k (Rasmussen *et al.,* 2014). GI-1 is further subdivided into 7 alternate cold and warm episodes (GI-1e, GI-1c1, GI-1c3, GI-1a, and GI-1d, GI-1c2, and GI-1b respectively, whilst a short-lived cooler episode in the Early Holocene (EH) between 11.5 and

11.4 ka b2k is termed as the 11.4 ka event (Rasmussen *et al.,* 2007; Rasmussen *et al.,* 2014, Table 2.1; Figures 2.1-2.2). GS-2.1 has also previously been subdivided into three sub-stages (GS-2a to 2c) by Björk *et al.* (1998), with GS-2b representing an episode of warmer conditions. Recent comparisons of multiple ice cores by Rasmussen *et al.* (2014) suggest that this subdivision is not replicable across multiple cores, and further work is required to determine whether these changes reflect a regional climatic signal or regional climatic contrasts between drill-sites.

Table 2.1. *Onset of events in the revised GICC05 timescale, which is used as the event stratigraphy for the North Atlantic and surrounds (from Rasmussen et al., 2014).*

Event	NGRIP depth (m)	Age (a b2k) and definition uncertainty	Maximum counting error (yr)
End of 11.4 ka BP event	1476.16	11,400	96
Start of 11.4 ka BP event	1482.32	11,520	97
Start of Holocene	1492.45	11,703 ±4	99
Start of GS-1	1526.52	12,896 ± 4	138
Start of GI-1a	1534.5	13,099	143
Start of GI-1b	1542.1	13,311	149
Start of GI-1c1	1554.75	13,600	156
Start of GI-1c2	1557.08	13,660	158
Start of GI-1c3	1570.5	13,954	165
Start of GI-1d	1574.8	14,075	169
Start of GI-1e	1604.64	14,692 ± 4	186
Start of GS-2.1a	1669.09	17,480	330
Start of GS-2.1b	1745.31	20,900	482
Start of GS-2.1c	1783.62	22.900	573

In this scheme, GS-2.1 broadly corresponds to the Dimlington Stadial in Britain and the Pleniglacial/Oldest Dryas in the Norden model. The succeeding Interstadial (GI-1) encompasses the Windermere Interstadial (WI) in Britain, and the Bølling-Allerød (B-A) in the Norden Model. The WI is not subdivided further, but the Norden Model can be compared to the North Atlantic event stratigraphy as follows: GI-1e is representative of the Bølling, GI-1d is representative of the Older Dryas, and GI-1c-GI-1a representative of the Allerød in the Norden Model. GS-1 broadly corresponds to the Younger Dryas (YD), and the Loch Lomond Stadial (LLS) in the Norden and British sequences respectively (Lowe *et al.,* 2001; Lowe and Walker, 2014; Figure 2.1). It is again noted that these periods are not assumed to be synonymous, nor time-parallel due to the criteria outlined above (Björk *et al.,* 1998; Walker *et al.,* 1999; Lowe *et al.,* 2008),

Hereafter, the principal focus of this section is on the LGIT (*ca.* 14.7-11 cal ka BP) for which evidence for abrupt and rapid climatic oscillations are best expressed, and most readily observed in terrestrial archives beyond Greenland.

2.2.3.1. Windermere Interstadial/Bølling-Allerød/GI-1

The GICC05 $\delta^{18}O$ record shows that the transition from stadial to interstadial conditions at the onset of the LGIT (GS-2.1 to GI-1e) occurred in under 3 years (Steffensen *et al.,* 2008), and corresponded to a warming of 9 ± 3 °C on the summit of the ice sheet (Severinghaus *et al.,* 1999), The thermal conditions in the subsequent *ca.* 100 yr of GI-1e were the mildest of the entire of GI-1 (Rasmussen *et al.,* 2014), before temperatures started to decline < *ca*. 14.5 cal ka BP. A steady cooling trend followed through GI-1e to GS-1 (*ca*. 14.5-12.9 cal ka BP), and was interrupted by three short-lived cold excursions, defined as GI-1d, GI-1c2, and GI-1b. GI-1d and GI-1b are the most pronounced of these excursions, both in terms of duration and amplitude (121 and 203 years respectively), with GI-1c2 lasting only *ca*. 60 years (Rasmussen *et al.,* 2014).

Palaeoclimatic records derived from coleopteran mutual climatic ranges (MCR) of the WI in Britain show a similar structure to GI-1, with the warmest temperatures potentially occurring early in the WI, before steadily declining into the LLS (Atkinson *et al.,* 1987; Walker *et al.,* 1993; Lowe *et al.,* 1995; Walker *et al.,* 2003), although this trend is less pronounced in other palaeotemperature indicators (e.g. Brooks and Birks 2001; van Asch *et al.,* 2012). Recent high-resolution records have also been able to identify abrupt climatic events within the WI that are similar to those in the GICC05 record, being readily correlated to GI-1d, GI-1c2, and GI-1b (Brooks and Birks, 2000; Marshall *et al.,* 2002; van Asch *et al.,* 2012; Brooks *et al.,* 2012; Brooks *et al.,* 2016; Candy *et al.,* 2016; Figure 2.3). The most readily identifiable of these events is from climatic deteriorations between the Borrobol and Penifiler tephras (14.14–13.95 and 14.09–13.65 cal ka BP respectively) in Scotland, which correspond closely in timing to GI-1d in the GICC05 record, and the Older Dryas in the Norden model (Brooks *et al.,* 2012; Brooks *et al.,* 2016; Candy *et al.,* 2016), Chironomid inferred temperatures (C-ITs) show this event was manifested as a deterioration in summer temperatures of *ca.* 6 °C, which is larger in amplitude than other pre-LLS climatic events identified in the British Isles. Correlatives to GI-1b in the British Isles are consistently of a lower amplitude than correlatives of GI-1d (Marshall *et al.,* 2002; Brooks and Birks, 2000; Brooks *et al.,* 2012; 2016; Candy *et al.,* 2016; Figure 2.3), which suggests this event was of a lower magnitude. This contrasts with the Greenland $\delta^{18}O$ record (Rasmussen *et al.,* 2014), and other terrestrial records around the North Atlantic (e.g. Yu and Wright, 2001), which suggest that the climatic deterioration associated with the GI-1b oscillation was more severe (e.g. Heiri *et al.,* 2007). These spatial differences highlight the importance of local factors such as site latitude, longitude, and altitude on the manifestation of palaeoclimatic signals. At present, too few high-resolution and chronologically constrained records exist to adequately investigate the importance of these local factors on the amplitude of high-resolution climate change.

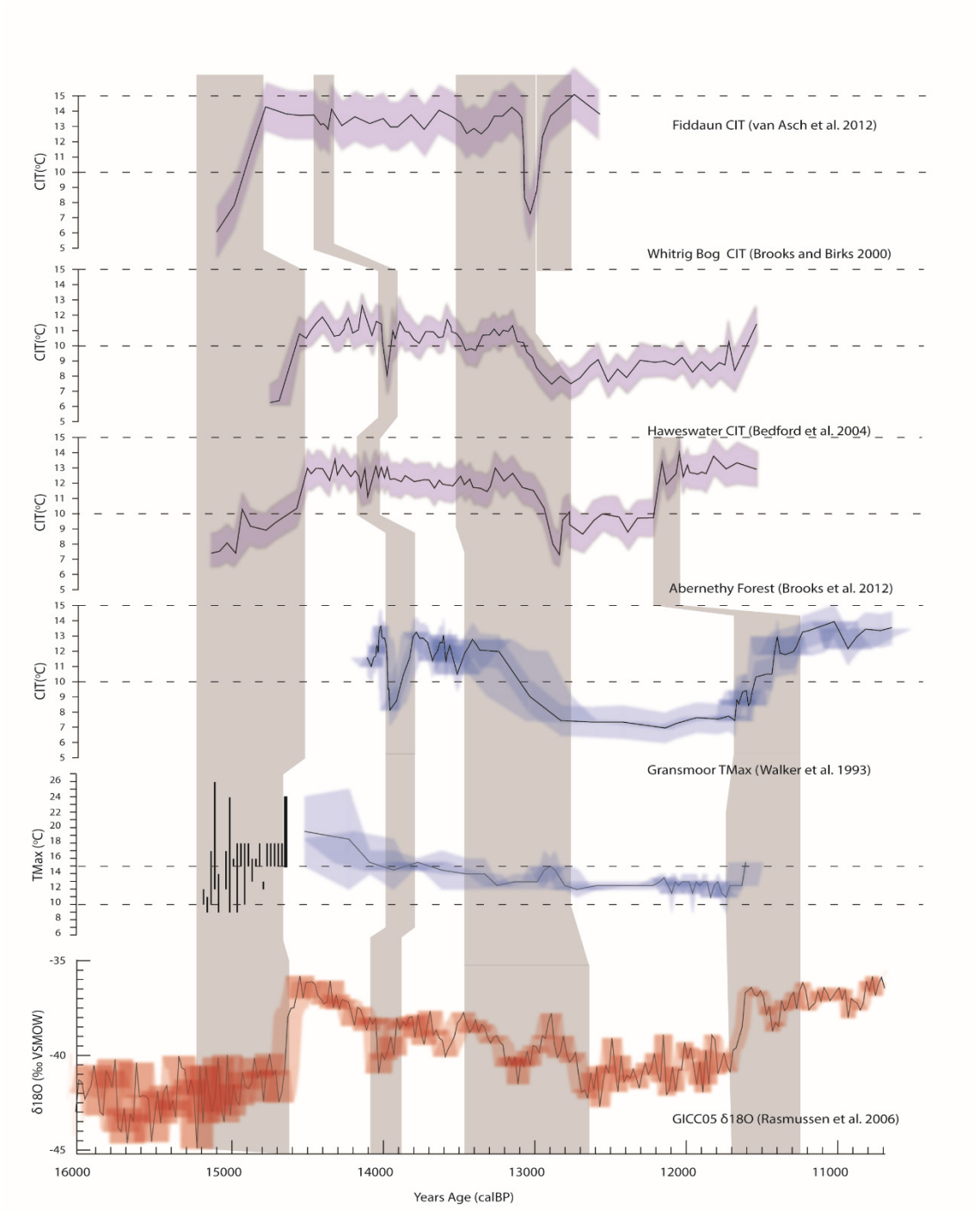

Figure 2.3. *Comparison of British July temperature records to the North Atlantic Event Stratigraphy. The records show a consistent structure and evidence for abrupt climatic oscillations similar to those identified in the Greenland ice cores. Of these records, only Gransmoor and Abernethy Forest have an independently derived chronology meaning the timing of these abrupt climatic oscillations remain temporally unconstrained. With the exception of the Gransmoor record which temperatures are calculated via the mutual climatic rang (MCR) of coleoptera (Walker et al., 1993), all temperatures are derived from chironomid inferred temperatures (C- ITs).*

2.2.3.2. Loch Lomond Stadial/Younger Dryas/GS-1

GS-1 is characterised by a marked and abrupt shift in δD values (1-3 yr) at *ca.* 12.9 ka b2k, reflecting an abrupt change in polar circulation, followed by a cooling transition (reflected in $\delta^{18}O$ values), that lasted for over 200 yr (Steffensen *et al.,* 2008). Cold conditions persisted for *ca.* 1000 yr before a similarly abrupt shift in δD, was followed by a warming transition of *ca.* 60

yr (in $\delta^{18}O$; Steffensen *et al.,* 2008), which marks the Pleistocene-Holocene boundary, and the onset of the present interglacial at *ca.* 11.7 ka (Walker *et al.,* 2009; Rasmussen *et al.,* 2014).

The transition from the Allerød/WI into the Younger Dryas/LLS is well documented across European records and it relates to widespread declines in summer and winter temperatures (Atkinson *et al.,* 1987; Walker *et al.,* 1993; Renssen *et al.,* 2015). However, the timing of climatic deterioration into the LLS in Britain is poorly constrained, principally due to the lack of well dated quantitative temperature estimates (e.g. Walker *et al.,* 2003; Brooks *et al.,* 2012; Muschitiello and Wohlfarth, 2015). Cooling trends are reported prior to the onset of GS-1 at Abernethy Forest, but cannot be reliably considered owing to the lack of radiocarbon dates through this transition. Biotic responses to regional cooling have also recently been reported to occur as early as 13.1 cal ka BP in Northern Ireland, *ca.* 200 yr before the onset of GS-1 in Greenland (Muschitiello and Wohlfarth, 2015).

Recently published work from high resolution lacustrine sequences in Germany, Norway, and Sweden demonstrate that the onset of the YD in Northern Europe was spatially heterogeneous across the North Atlantic region, with climatic conditions associated with cooling, occurring through various proxy archives between *ca.* 13.1 and 12.7 ka BP (Brauer *et al.,* 2008; Neugebauer *et al.,* 2012; Lohne *et al.,* 2013; Rach *et al.,* 2014; Muschitiello and Wohlfarth, 2015; Muschitiello *et al.,* 2015). The transgressive response is best expressed in the high resolution varved record at Meerfelder Maar in west Germany (Brauer *et al.,* 2008; Rach *et al.,* 2014). This record shows that although climatic cooling at the onset of GS-1/the YD can be shown to occur quasi-synchronously with Greenland (Brauer *et al.,* 2000), the hydrological response to this cooling was delayed by *ca.* 170 years (Rach *et al.,* 2014; Figure 2.4.). These changes can in turn be used to explain the delayed vegetation response at the onset of the YD in many records (Muschitiello and Wohlfarth, 2015), and further illustrates the need for independently derived chronologies of high integrity for palaeoenvironmental sequences (Lowe *et al.,* 2008; see above). Furthermore, it is highly likely that similar spatial lags are also present at different stages of the LGIT but have yet to be identified owing to a lack of focus on these intervals. The climatic variables responsible for this asynchrony are discussed further in section 2.3.

Recent work on highly resolved continental records have also shown that the YD itself contains climatic structure (Brauer *et al.,* 2000; Bakke *et al.,* 2009; Lane *et al.,* 2013), which consists of the coldest conditions occurring early in the stadial, followed by less cold, more humid and unstable conditions during the latter stages (Walker, 1995; Bakke *et al.,* 2009; Lane *et al.,* 2013). The initial phase was characterised by high zonal wind systems, increased storm intensity and aridification, with the development of permafrost, and the re-expansion of ice masses in upland regions. Increased climatic instability is inferred from enhanced, but unstable glacial meltwater production (Ti counts) at Kråkenes in Norway (Bakke *et al.,* 2009), and expansion signals from the Loch

Lomond Readvance ice cap in Scotland (MacLeod *et al.,* 2011) which point towards warmer, wetter but more unstable conditions during this phase (Bakke *et al.,* 2009).

The timing of this change, hereafter termed as the 'mid-YD transition' (Lane *et al.,* 2013) occurs in close association with the deposition of the Vedde Ash at 12.02 ± 0.04 cal ka BP (Bronk Ramsey *et al.,* 2015). By comparing palaeoenvironmental signals with respect to the position of the Vedde Ash at Meerfelder Maar, and Kråkenes, Lane *et al.,* (2013) demonstrate that the mid-YD transition was time-transgressive by *ca.* 120 yr between these sites. This therefore represents a significant palaeoclimatic shift which is not consistently recognised in many records across NW Europe, and likely relates to the inadequate sampling resolution of many palaeoclimatic records. Furthermore, this shift is not characterised in the $\delta^{18}O$ record in Greenland (Rasmussen *et al.,* 2014), demonstrating the regional heterogeneity of the climate system, and the need for more highly resolved palaeoclimatic records from different continental areas to better quantify how these leads and lags are manifested.

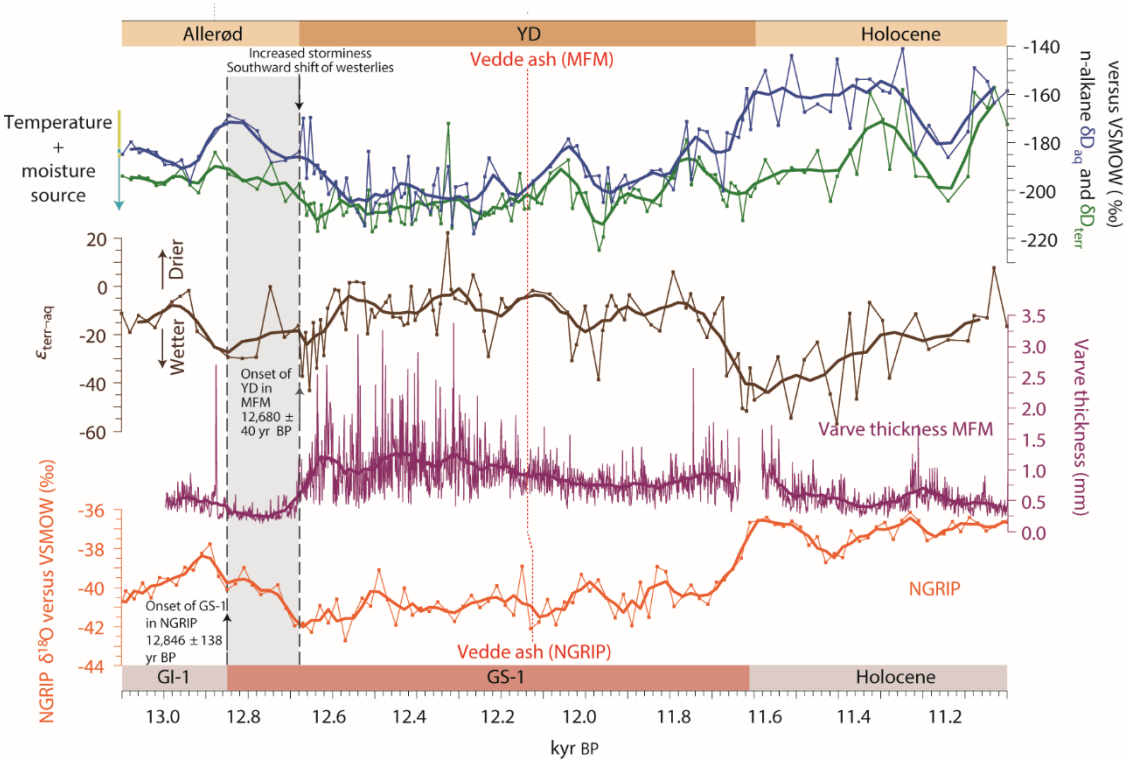

Figure 2.4. *From Rach et al. (2014) demonstrating the ca. 170 yr lag in the onset of the YD at Meerfelder Maar in relation to GS-1 (marked in grey). The onset of the YD is characterised by an increase in varve thickness (purple), and an increase in ε terr-aq (dDterr in green and dDaq in blue), representing drier conditions. This illustrates the spatial heterogeneity of climatic change at the onset of the LLS in the North Atlantic region.*

2.2.3.3. The Holocene

The transition into the Holocene in the GICC05 record occurs at 11.65 ± 0.1 cal ka BP (Walker *et al.,* 2009; Rasmussen *et al.,* 2014), and is characterised by a 2–3 ‰ decrease in δD followed by a rise in $\delta^{18}O$ over the proceeding 60 yr, representing a rapid change in atmospheric

circulation (Masson-Delmotte *et al.,* 2005), and a subsequent increase in temperature (of *ca.* 10 ± 4 °C Severinghaus *et al.,* 1998) respectively (Steffensen *et al.,* 2008; Walker *et al.,* 2009). This shift in the GICC05 record has been adopted as the Global Stratotype Section and Point (GSSP), for the base of the Holocene epoch (Walker *et al.,* 2009).

In other terrestrial sequences around the North Atlantic, the Pleistocene-Holocene boundary is apparent in a wide range of proxy records, all of which point toward a marked reorganisation of the global climate system suggesting that the final climatic transition from a Glacial to Interglacial mode was uniformly rapid (Brauer *et al.,* 2000; Litt *et al.,* 2001; Ralska-Jasiowiczowa *et al.,* 2003; Steffensen *et al.,* 2008; Lohne *et al.,* 2013), occurring at 11.53-11.59 cal ka BP (Litt *et al.,* 2001) over *ca.* 50-100 years. High resolution evidence has shown that the amelioration may have also been interrupted by a decadal scale climatic reversal during the amelioration (Vincent and Cwynar, 2016). The short duration of this event however means that it is infrequently recorded in terrestrial sequences.

The 11.4 ka event represents a *ca.* 120 year cooling interval *ca.* 200 year after the Pleistocene-Holocene boundary which is characterised by a *ca.* 2 ‰ decrease in $\delta^{18}O$ values in the GICC05 record (Rasmussen *et al.,* 2007; Rasmussen *et al.,* 2014). This event is correlated to a climatic deterioration termed as the Preboreal Oscillation in terrestrial records in Northern Europe, where it is characterised by a re-expansion of open ground vegetation, and a decline in lake catchment biomass (Björk *et al.,* 1997). Low amplitude oscillations in C-ITs have also been identified in British sequences (Lang *et al.,* 2010; Brooks *et al.,* 2012), but are difficult to precisely correlate to the 11.4 ka event due to the *ca.* 600 year long radiocarbon plateau at the beginning of the Holocene, which produces large uncertainties on calibrated radiocarbon dates (Björk *et al.,* 1997; Lowe *et al.,* 2001; Walker *et al.,* 2009).

2.2.3.4. Summary

Palaeoclimatic evidence from terrestrial sequences around the North Atlantic indicate that the climatic structure of the Last Termination is broadly congruent with the palaeoclimatic data from Greenland. Furthermore, they can be considered to occur quasi-synchronously, within dating errors to the North Atlantic Event Stratigraphy (Lowe *et al.,* 1995; Brauer *et al.,* 2000). High-resolution records however have demonstrated that the abrupt climatic events during the LGIT were spatially and temporally heterogeneous, varying in magnitude, duration, and timing across NW Europe (Heiri *et al.,* 2007; Brauer *et al.,* 2008; Bakke *et al.,* 2009; Neugebauer *et al.,* 2012; Lane *et al.,* 2013; Rach *et al.,* 2014; Muschitiello and Wohlfarth 2015; Engels *et al.,* 2016). Further palaeoclimatic records are therefore required in order to better assess the regional picture of palaeoclimatic evolution in the North Atlantic and surrounds during the Last Termination. Firstly

however, it is important to review the mechanisms that have been used to explain the observed changes in palaeoclimatic signals through the Last Termination.

2.3. Drivers of climate change in the North Atlantic and surrounds during the Last Termination

This section provides a brief review of the principal drivers used to explain the climatic changes observed in the North Atlantic and surrounds (section 2.2). It is acknowledged that this is a complex, and wide-ranging topic, encompassing the interplay between a series of mechanisms, and global teleconnections within and between both hemispheres (Broecker, 1998; Blunier *et al.,* 1998). A comprehensive review is therefore beyond the scope of this thesis. Instead, this section focusses on the most widely accepted hypotheses for: a) the initiation of the Last Termination *ca.* 21 ka BP, b) the mechanisms controlling abrupt climatic oscillations during the LGIT in the North Atlantic. The factors leading to the climatic changes observed in the Last Termination are largely accepted to result from three mechanisms. These are: a) Orbital forcing, b) Oceanic forcing, and c) Atmospheric forcing. Whilst a more recent hypothesis, attributing extra-terrestrial forcing (a bolide impact in N.America) to the onset of the YD has been posited (Firestone *et al.,* 2007; Bunch *et al.,* 2012), this remains highly controversial (Surovell *et al.,* 2009; Pinter *et al.,* 2011; Holliday *et al.,* 2014), and is therefore not discussed further here.

2.3.1. Orbital forcing

It is well established that glacial-interglacial cycles are driven primarily by secular variations in insolation (solar radiation received at the top of the atmosphere) which are controlled by changes in the Earth's orbital parameters, associated with the shape (eccentricity) of the Earth's orbit with the Sun, and the configuration of the Earth's axis (obliquity and precession) on a range of timescales (Milankovitch, 1941; Berger and Loutre, 1991; Berger and Loutre, 2010).The distribution of summer insolation at 65 °N (dominated by changes in precession) in particular is thought to be critical in the growth and decay of ice sheets (Milankovitch, 1941; Imbrie and Imbrie, 1980). This hypothesis is supported by the frequencies in the spectra of $\delta^{18}O$ records from marine sediments (which are a proxy for global ice volume (Shackleton and Opdyke, 1973)), that show consistent correspondence to changes in orbital forcing, and are therefore determined to govern the pacing of glacial-interglacial cycles, including the Last Termination (Hays *et al.,* 1976; Lisiecki and Raymo, 2005; Cheng *et al.,* 2009; Denton *et al.,* 2010; Figure 2.5).

The relatively abrupt nature of the Last Termination indicates that orbital forcing alone cannot account for the transition in its entirety, and that positive feedbacks must exist in the climate system, which amplified climatic changes once a critical threshold was reached (Berger and Loutre, 2010; Denton *et al.,* 2010; Figure 2.5). It is hypothesised that the rise in Northern

Hemisphere summer insolation at *ca.* 24-21 ka initiated the Last Termination, but other factors in the climate system were responsible for manifesting the unstable climatic signal observed across the North Atlantic. The large Northern Hemisphere ice sheets, which had reached their maximum extent at *ca.* 21 ka, straddled the North Atlantic during the LGM (Mix *et al.,* 2001). The melting of these ice masses as Northern Hemisphere insolation increased is thought to have led to large changes in snow-ice albedo (Stott *et al.,* 2007; Severinghaus, 2009), ventilation of oceanic CO_2 (Skinner *et al.,* 2010), and changes in oceanic circulation (see below), all of which acted as positive (and negative) feedbacks in the climate system (Denton *et al.,* 2010).

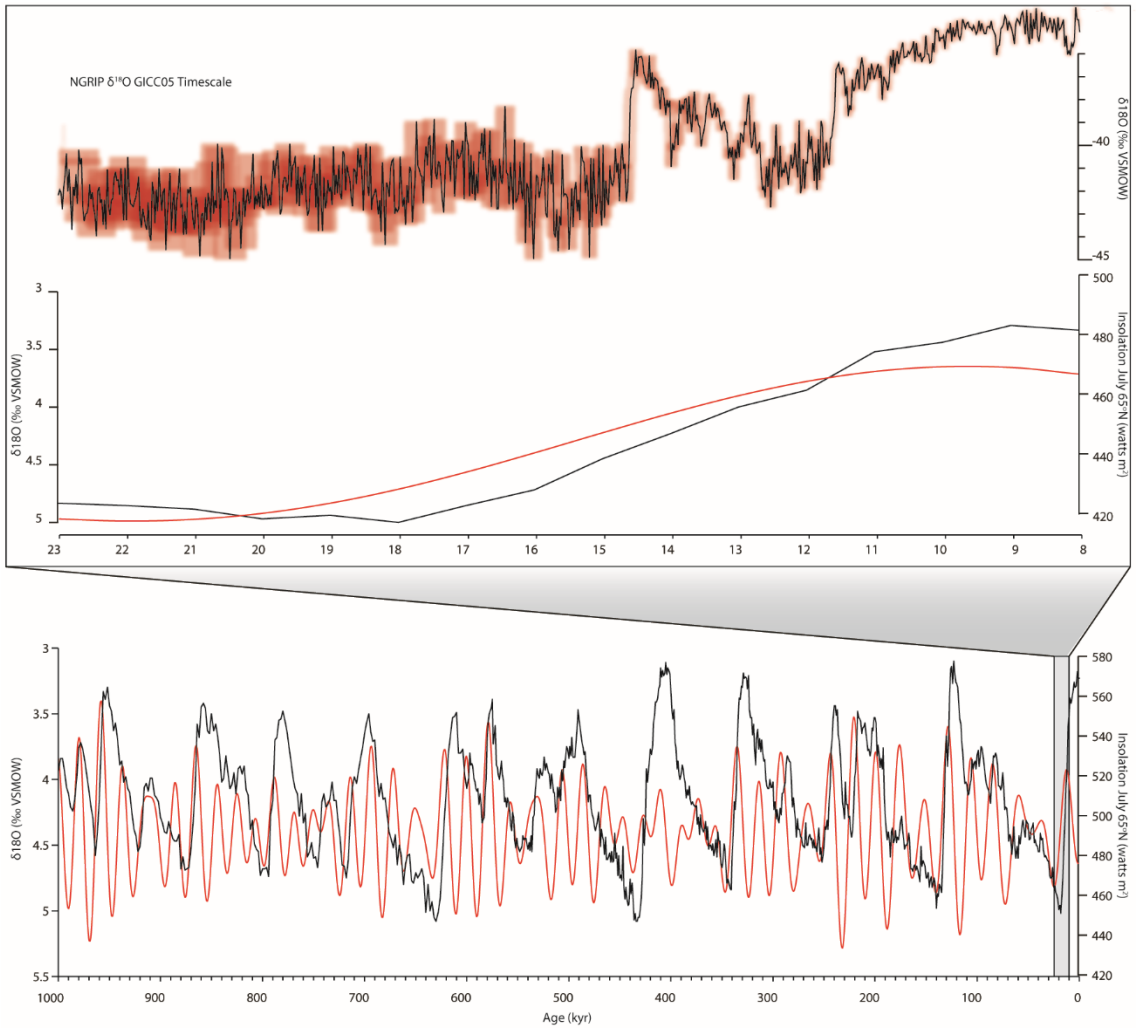

Figure 2.5. *Comparison of the stacked benthic oxygen isotope record (black; Lisiecki and Raymo, 2005), representing glacial-interglacial variations in global ice volume (Shackleton and Opdyke, 1973), compared with summer insolation at 65°N (red; Berger and Loutre, 1991) over the past 1 million years. A consistent link in glacial-interglacial terminations and rising insolation can be seen. The Last Termination, discussed in text is outlined in grey. When compared to the high resolution $\delta^{18}O$ record from the Greenland ice cores over the Last Termination (top), it is evident that the abrupt climatic oscillations cannot be explained by orbital forcing in isolation.*

2.3.2. Oceanic and atmospheric forcing

Increases in solar insolation alone cannot account for the climatic episodes observed in climatic records across the North Atlantic. This is especially true for the transitions into abrupt, centennial to millennial scale warm/cold oscillations through the LGIT which occurred on up to annual-decadal timescales (Steffensen *et al.,* 2008), and therefore must relate to higher resolution

climatic mechanisms. The feedback which provides the most convincing criteria for controlling Dansgaard-Oeschger (D-O) cycles is the variability in oceanic heat transport into the high northern latitudes via the thermohaline circulation (Broecker *et al.,* 1989; Clark *et al.,* 2002; Cheng *et al.,* 2009).

In the North Atlantic, surface flow is presently dominated by the North Atlantic current, which is driven by south-westerly prevailing winds, bringing warm salty water from the lower latitudes to the east Atlantic seaboard. As this water travels northward it progressively cools, increases in density and sinks in the Norwegian Sea to form North Atlantic Deep Water (NADW) which flows southward to the Southern Ocean (Figure 2.6). This process is termed as the Atlantic Meridional Overturning Circulation (AMOC) and acts as a heating system for the North Atlantic region, transferring latent heat to NW Europe, keeping it considerably warmer than equivalent latitudes on the western seaboard (Broecker and Denton, 1989; Rahmstorf, 1996; Clark *et al.,* 2002). The strength of AMOC and the position of NADW formation have been envisaged by Broecker and Denton (1989) and Broecker *et al.* (1990) to provide a mechanism to explain the abrupt climatic oscillations observed during the LGIT in the North Atlantic and surrounds (Clark *et al.,* 2001). In order to cessate the northerly AMOC heat-flow, a viable method of preventing NADW formation in the Nordic Seas is required. This is most readily attributed to the injection of freshwater into the North Atlantic from terrestrial realms, leading to a reduction in surface water salinity and density in the high latitude North Atlantic (Broecker *et al.,* 1989), inhibiting NADW formation (Clark *et al.,* 2001; Clark *et al.,* 2002). The rise in solar insolation at the onset of the Last Termination would have led to enhanced ablation and instability of the Northern Hemisphere ice sheets during the Last Termination, leading to the incursion of high volumes of meltwater into the North Atlantic. Catastrophic influx of meltwater, either via ice sheet collapse and iceberg rafting (Bond *et al.,* 1992), or proglacial lake drainage from the Laurentide (Teller *et al.,* 2002), and/or the Fennoscandian Ice Sheets (Muschitiello *et al.,* 2015b), is therefore a viable model to produce repeated weakening or shutdown of AMOC, and abrupt cooling events in the North Atlantic region (Broecker and Denton, 1989; Broecker *et al.,* 1990).

Both of these scenarios are supported by abundant lines of evidence. The episodic presence of ice-rafted debris (IRD) rich layers in North Atlantic marine cores are derived from the influx of iceberg armadas from neighbouring ice sheets. These episodes, termed as Heinrich events, point towards the periodic collapse of the Laurentide Ice Sheet during the last cold stage (Bond *et al.,* 1992; Hemming, 2004), flushing high volumes of freshwater into the North Atlantic and temporarily diminishing NADW formation. During the Last Termination, Heinrich Event 1 occurred between *ca.* 18-15 cal ka BP (termed H1), which is broadly coincident with GS-2.1a in the Greenland ice cores, the Oldest Dryas in the Norden model, and the Dimlington Stadial in the British Isles, immediately prior to the LGIT in the GICC05 stratigraphy (Clark *et al.,* 2001;

Denton *et al.,* 2006; Rasmussen *et al.,* 2014). H1 is interpreted to have brought temporarily colder conditions back to NW Europe, and has been correlated to temporary re-advances of Northern Hemisphere ice sheets (e.g. McCabe *et al.,* 2007; Sejrup *et al.,* 2015; Toucanne *et al.,* 2015).

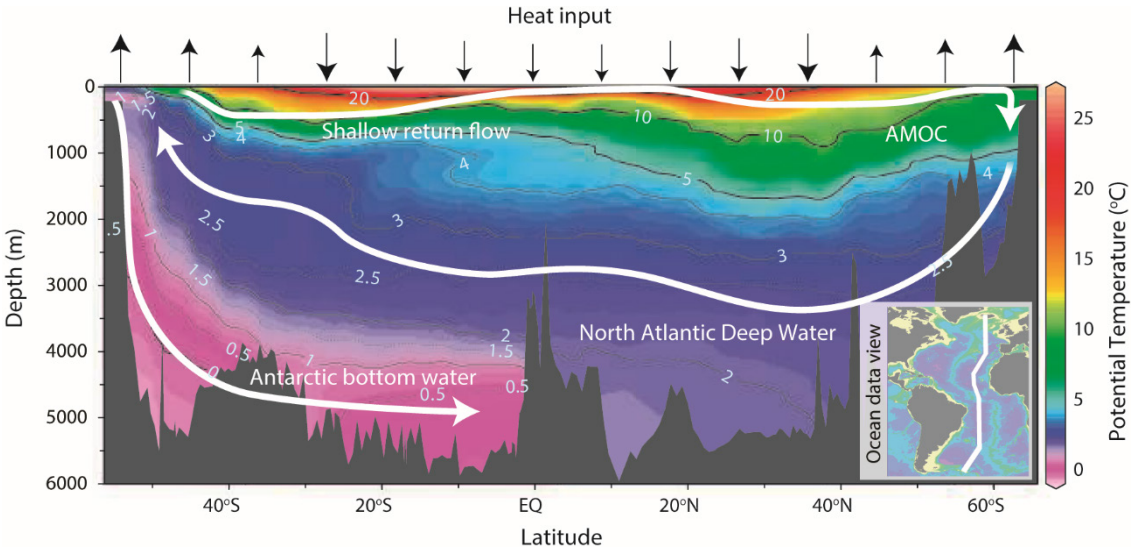

Figure 2.6*. Schematic cross-section of the North Atlantic showing the thermal stratification, surface heat exchange areas and primary current flows (white arrows) discussed in text (adapted from Hegerl and Bindoff, 2005). These processes provide the principle mechanisms which drive AMOC, and provide latent heat transfer to northwest Europe.*

In later parts of the LGIT, proglacial lake drainage is thought to have driven the abrupt climatic oscillations. Most significantly it has been implicated for driving the onset of GS-1/YD/LLS at *ca.* 12.9 ka. The drainage of Glacial Lake Agassiz in North America, which was formed from the ablation of the Laurentide Ice Sheet is the most likely candidate for meltwater influx into the North Atlantic (e.g. Broecker *et al.,* 1989; Teller *et al.,* 2002; Murton *et al.,* 2010; Rayburn *et al.,* 2011), although meltwater sourced from the Fennoscandian Ice Sheet has also been posited (Bodén *et al.,* 1997; Muschitiello *et al.,* 2015b). Catastrophic drainage of meltwater into the North Atlantic is thought to have diminished AMOC strength and/or led to a southerly displacement of NADW formation which caused sea-ice to expand southward (Denton *et al.,* 2005; Brauer *et al.,* 2008; Figure 2.7). This in turn affected atmospheric circulation, with an increased winter sea-ice cover in the North Atlantic (Isarin *et al.,* 1998; Denton *et al.,* 2005) leading to a southerly diversion of the polar front (Ruddiman and McIntyre 1981; Bakke *et al.,* 2009), and the precipitation bearing westerly storm tracks (Kageyama *et al.,* 1999; Brauer *et al.,* 2008). Atmospheric conditions therefore provided a substantial positive feedback on deteriorating climates in Northern Europe, with evidence of the development of extremely cold and dry conditions, and more zonal, high intensity westerly winds (Brauer *et al.,* 2008), bringing more seasonal climatic regimes to Central Europe (Atkinson *et al.,* 1987; Walker *et al.,* 1993; Walker *et al.,* 2003; Denton *et al.,* 2005).

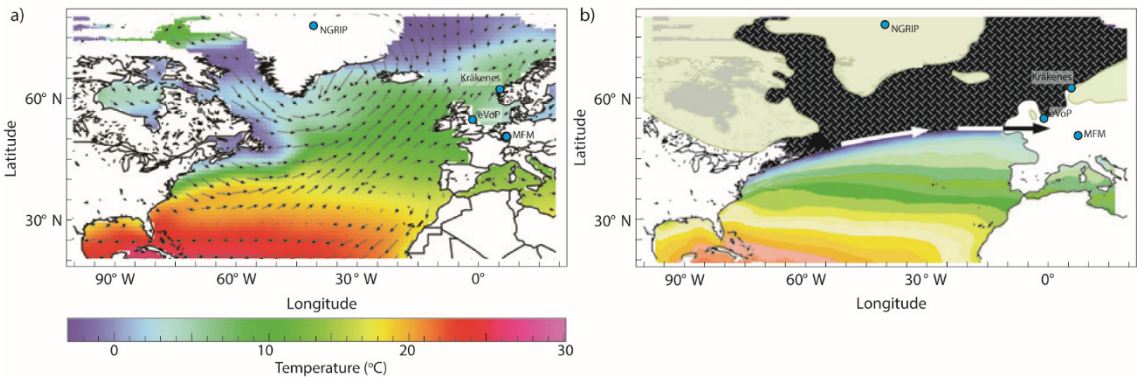

Figure 2.7. *Model of winter sea surface temperatures (colours) and surface wind fields (arrows), in the mid-North Atlantic during a) the present day, and b) the YD. The locations of the eVoP, Meerfelder Maar, Kråkenes and NGRIP are provided for reference (adapted from Brauer et al., 2008).*

The role of AMOC in climatic variability during the LGIT is also supported by the high resolution analysis of terrestrial European lake deposits through the YD (Brauer *et al.,* 2008; Bakke *et al.,* 2009; Rach *et al.,* 2014). The mid-YD transition is explained by a strengthening AMOC/northerly displacement, bringing warmer Atlantic waters into the North Atlantic and temporarily breaking up the extensive sea-ice cover. This in turn affected atmospheric circulation, releasing the westerly winds from their depressed southerly mode (Bakke *et al.,* 2009), and pushing the polar front northward (Lane *et al.,* 2013). Temporarily warmer climates re-invigorated the melting of marine and terrestrial ice, temporarily reducing AMOC strength again (Bakke *et al.,* 2009). The time transgressive expression of this climatic signal can therefore be attributed to the time taken for sea-ice to melt, and subsequent northerly movement of the polar front Meerfelder Maar and Kråkenes. This transition is calculated to occur at a rate of *ca* 10 km/yr (Lane *et al.,* 2013). These data therefore all corroborate the role that AMOC has in mediating climatic conditions in the North Atlantic and surrounds, both via direct oceanic forcing, and well as indirect effects on atmospheric circulation patterns.

In summary, freshwater forced reductions in AMOC strength provide the most credible explanation for the abrupt and repeated climatic cooling episodes observed across the North Atlantic and surrounds during the Last Termination (Alley, 2007). Two processes can explain the abrupt climatic oscillations observed through the LGIT in the North Atlantic and surrounds. These are:

a) Sharp transitions to cold conditions in Europe driven by the reduction in AMOC strength/the southerly movement of NADW formation, and the development of sea-ice in the N. Atlantic.
b) Changes in precipitation regimes driven by latitudinal displacement of atmospheric circulation patterns, particularly the position of westerly precipitation bearing wind systems.

This explanation has principally focussed on H1 and the initiation of the LGIT (Denton *et al.,* 2006), and the start of the YD/GS-1 (Broecker *et al.,* 1989), but the mechanisms discussed above

are also applicable to the lower amplitude climatic oscillations identified during the LGIT (Clark *et al.,* 2001; Kleiven *et al.,* 2008), as well as variability within individual climatic oscillations (Bakke *et al.,* 2009).

2.4. Relevance to the Vale of Pickering

The principal aim of this review is to provide a framework with which to compare any palaeoclimatic, and palaeoenvironmental signals obtained in the eVoP. The climatic structure of the Last Termination across the North Atlantic region is broadly concordant, owing primarily to the mediation of temperature regimes by the variable strength in AMOC (section 2.3). The eVoP is proximal to the North Atlantic, meaning that palaeoclimatic conditions in the valley should also have been principally controlled by AMOC variability during the Last Termination. This is supported by other palaeoclimatic records in the British Isles, and Southern Scandinavia which record analogous climatic events to the North Atlantic Event Stratigraphy (e.g. Heiri *et al.,* 2014). Whilst the eVoP lies in a more distal locality to the North Atlantic than most of the British records, the fact that similar climatic perturbations are also recorded across Scandinavia, and NW Europe support the continual influence of AMOC across more distal localities during the Last Termination.

The eVoP also lies at a latitude inferred by Bakke *et al.* (2009) and Lane *et al.* (2013) to have been susceptible to variations in atmospheric circulation during the LLS/YD. Shifts in atmospheric circulation would have led to the development of spatially heterogeneous climatic gradients meaning that further high-resolution, quantitative palaeoclimatic records in this region are required both to better constrain the nature of climatic heterogeneity during the LLS, and also identify further intervals where these heterogeneous signals exist. In summary therefore, the eVoP is a location of high potential with which to identify and test previous models of palaeoclimatic regimes in the North Atlantic and surrounds during the Last Termination. Based on the mechanisms outlined above, one would expect broadly comparable trends in palaeotemperature trends to other North Atlantic records through the LGIT, but variable hydrological responses and amplitudes of abrupt climatic oscillations driven by spatially heterogeneous changes in atmospheric circulation patterns.

3. NE England through the Last Termination

3.1. Introduction

The unstable climatic regimes during the Last Termination significantly impacted land surfaces across NW Europe, with changes in climatic regime affecting terrestrial environments at different rates and scales (Walker *et al*., 1994; Huijzer and Vandenberghe, 1998; Hoek and Bohncke, 2002; Antoine *et al.,* 2003). Understanding the regional timing, phasing and amplitude of these responses to climatic change is now essential to further our understanding on how unstable climatic regimes affect terrestrial environments, and in turn how these changes may impact anthropogenic activity on palaeolandscapes.

In NE England, the Last Termination was characterised initially by the deglaciation of the British Irish Ice Sheet (BIIS) during the Dimlington Stadial (Rose, 1985; Clark *et al.,* 2012), which led to lowland landscapes undergoing significant paraglacial readjustment after the ice retreated. This led to the formation of irregular topography in recently deglaciated areas which was preconditioned to form isolated lake bodies (e.g. Bridgland *et al.,* 2011). The sedimentary infill of these lake bodies has provided a valuable archive with which to reconstruct palaeoenvironmental, and landscape regimes post ice recession. This is best demonstrated by palaeoclimatic records from sites such as Hawes Water in the Lake District, and Gransmoor on Holderness (Marshall *et al.,* 2002; Walker *et al.,* 1993) which show a similar climatic structure to that recorded in the North Atlantic Event Stratigraphy through the LGIT. These changes dramatically affected the timing and phasing of landscape development in NE England (e.g. Pennington, 1986; Rose, 1995; Innes *et al.,* 2009; Birks and Birks, 2014).

This Chapter reviews palaeoenvironmental and landscape reconstructions from NE England through the Last Termination. First, a review of the existing evidence for Late Quaternary environmental change in the region is presented, concentrating on the evidence for glacial advance and retreat in the region, climatic reconstructions, and palaeoenvironmental trends through the LGIT. Second, the chapter reviews present models of the landscape evolution in the Vale of Pickering (VoP). The chapter concludes by synthesising the potential that the eastern VoP (eVoP) has to improve understanding on the palaeoclimatic, palaeoenvironmental, and palaeogeomorphoc evolution through the Last Termination in NE England.

3.2. The physiography of NE England and the North Sea

Northern England is topographically separated by the north to south trending Pennine Hills (including the North Pennines, The Yorkshire Dales, the South Pennines, and the Peak District; Figure 3.1). To the west of the Pennines, the Lake District National Park, contains the most

elevated topography in the country (≤ 978 m OD), before the Irish Sea forms a western barrier. To the east of the Pennines, the more subdued North York Moors (≤ 454 m OD) and Yorkshire Wolds (≤ 240 m OD) form the most prominent topography of the region. Interspersed with these topographically elevated regions, are a series of low lying and broad valleys, the most prominent of which being the north to south trending Vale of York and Vale of Mowbray lying directly to the east of the Pennines. To the east of the Vale of York, the lowlands of Holderness, the VoP and the Tees Valley are topographically separated by the Yorkshire Wolds and the Nork York Moors respectively. Precipitation patterns in the lowlands of NE England are characterised by a well-developed rain shadow, as the moisture from dominant westerly air masses is rained-out via orographic precipitation over the highlands of Lake District and the Pennines (Figure 3.2). To the east of the region, lies the North Sea. The southern sector of the North Sea basin (< 56°N) is shallow (< 40 m deep), whilst to the north of Yorkshire (> 56 °N), the basin deepens to between 100-150 m, before reaching in excess of 200 m deep at the margins of the continental shelf. The North Sea provides a cooling influence for the coastal regions particularly in the summer months, which, when coupled with the regions latitude and longitude, and topography (which makes the region exposed to cool northerly winds, and a rain-shadow), makes this England's coolest and driest region (Wheeler *et al.,* 2013).

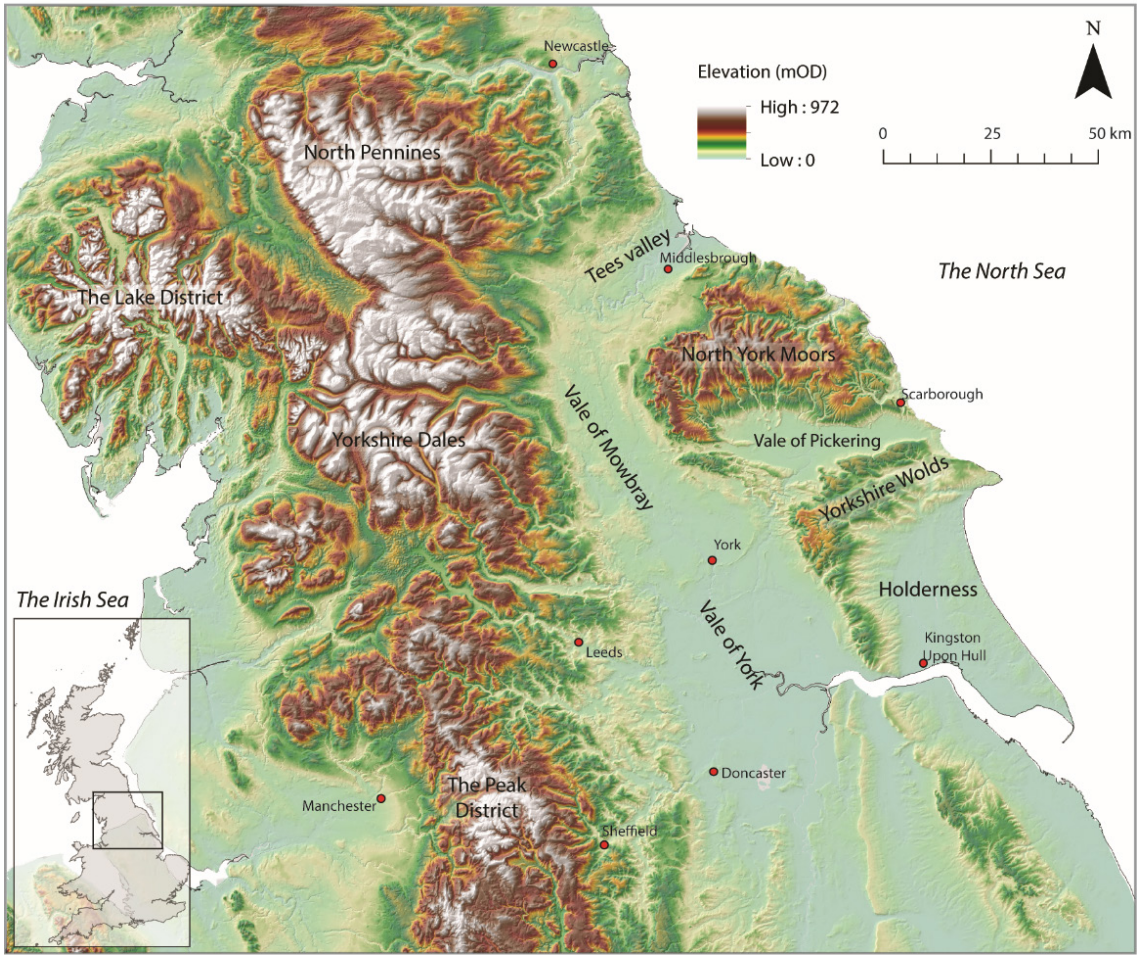

Figure 3.1. *Digital terrain model (DTM) of Northern England marking the location of sites discussed in text.*

The upland areas of northern England have been repeatedly glaciated during the Middle and Late Pleistocene (Bowen *et al.,* 1986; Evans *et al.,* 2005; Catt, 2007; Gibbard and Clark, 2011), and have provided local sources of ice that merge with ice moving southward from Scotland and into the lowland plains of the Irish Sea Basin to the west and the North Sea Basin to the east (Bowen, 1973; Ehlers and Gibbard, 2004; Clark *et al.,* 2004). This review concentrates on evidence for glaciation in the lowlands situated to the east of the Pennines (i.e. the Vales of York, Mowbray and Pickering and Holderness), which have been affected by Quaternary glaciation through at least two glacial stages in MIS 12 and 2 (Bowen *et al.,* 1986; 2002) and possibly during MIS 10 and 8 (Shotton, 1986; White *et al.,* 2016) although the evidence for the extent and timing of these glaciations is more equivocal (e.g. Pawley *et al.,* 2008). This is partly due to the erosive effect of the most recent glacial episode during MIS 2 and as such the review will concentrate on the evidence for glacial advance and retreat during this period.

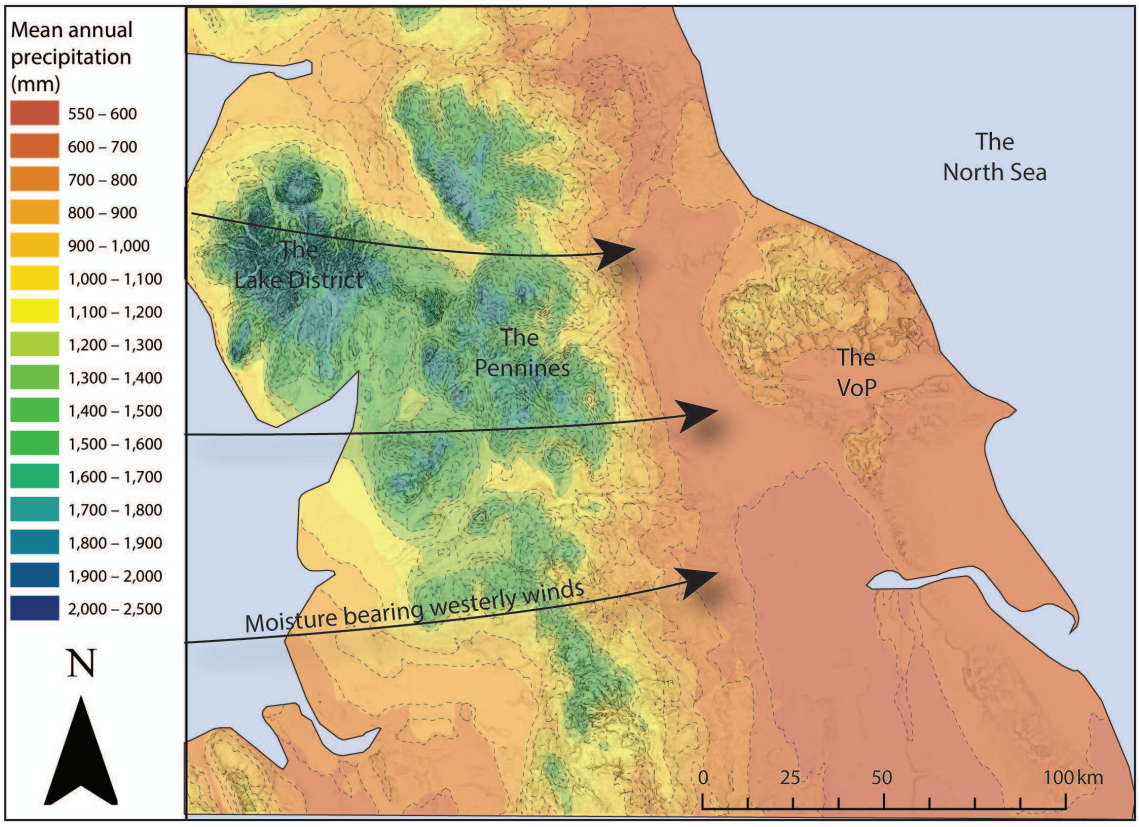

Figure 3.2. *Worldclim model showing the variability of mean annual precipitation values (mm) across northern England (Hijmans et al., 2005). The model shows the longitudinal gradient that exists from the west to the east of the country, with the lowlands of NE England (including the VoP) receiving significantly lower amounts of precipitation then the NW. This is attributed to a rain-shadowing effect on the lee-side of the hills and mountains in the Lake District and the Pennines which promotes the rainout of moisture from westerly winds via orographic precipitation. This shows that: a) the climatic regime in NE England is driven principally by the distribution of heat and moisture from the North Atlantic Ocean, b) the presence of these gradients are linked to heat and moisture delivery from AMOC, c) too few quantitative palaeoclimatic records exist from the region to reconstruct temporal changes in these climatic gradients, particularly when changes in AMOC strength have occurred (i.e. the LGIT).*

3.3. Landscapes and palaeoenvironments of NE England through the Last Termination

3.3.1. The Last Glacial Maximum (LGM)

Critical to the understanding of the evolution of the eVoP through the Last Termination is the role of two ice lobes: a) the North Sea Ice Lobe (NSIL) and the Vale of York Ice Lobe (VOYL), which advanced to the east, and the west of the North York Moors respectively during the Dimlington Stadial, leaving much of the VoP ice free (Bowen *et al.,* 2002; Clark *et al.,* 2004; Evans *et al.,* 2005; Catt, 2007; Chiverrell and Thomas, 2010; Figure 3.3). However, the complex interaction between these two ice lobes significantly affected the geomorphology of the VoP. Furthermore, much of the geomorphic evidence from surrounding areas implies that the Quaternary landscape evolution in NE England was driven largely by associated glacial processes (Catt, 2007; Rose, 2010). The following sections summarise the evidence for a series of glacial advances in the North Sea, and the Vale of York during the Dimlington Stadial.

The North Sea Ice Lobe (NSIL)

The stratigraphic record of the NSIL of the British-Irish Ice Sheet (BIIS) is well established from the east Yorkshire coast (Catt and Penny, 1966; Catt, 2007), where three diamicts are separated and in places interbedded with stratified silts and sands at Flamborough Head (Farrington and Mitchell, 1951; Valentin, 1957; Catt and Penny, 1966), Holderness (Catt, 1991b; 2007; Evans *et al.,* 1995; Boston *et al.,* 2010; Evans and Thomson, 2010), the Humber Estuary, and North Lincolnshire (Suggate and West, 1959; Straw, 1961; Straw and Clayton, 1979; Gaunt, 1981; Bateman, 2008; 2015). From these deposits, sedimentological- (e.g. Madgett and Catt, 1978; Davies *et al.,* 2009; Boston *et al.,* 2010; Bateman *et al.,* 2011; Busfield *et al.,* 2015), and geomorphic evidence (e.g. Evans and Thomson, 2010), have been used to propose limits of an Early Devensian glacial advance, followed by two later re-advance phases in Eastern Yorkshire. (Evans *et al.,* 2001; Catt, 2007; Bateman *et al.,* 2011).

The oldest glacigenic deposit recognised from the east Yorkshire coast is the Basement Till which underlies the Ipswichian raised beach at Sewerby, indicating that it was deposited prior to the Last Interglacial (MIS 5; Bisat, 1939; Catt and Penny, 1966; Catt, 2007; Murphy and Lundberg, 2009). On the Holderness coast, the Basement Till is overlain by the Skipsea, and Withernsea Tills, both of which are Late Devensian in age (Madgett and Catt, 1978; Rose, 1985; Bateman *et al.,* 2011; 2015; Figure 3.4).

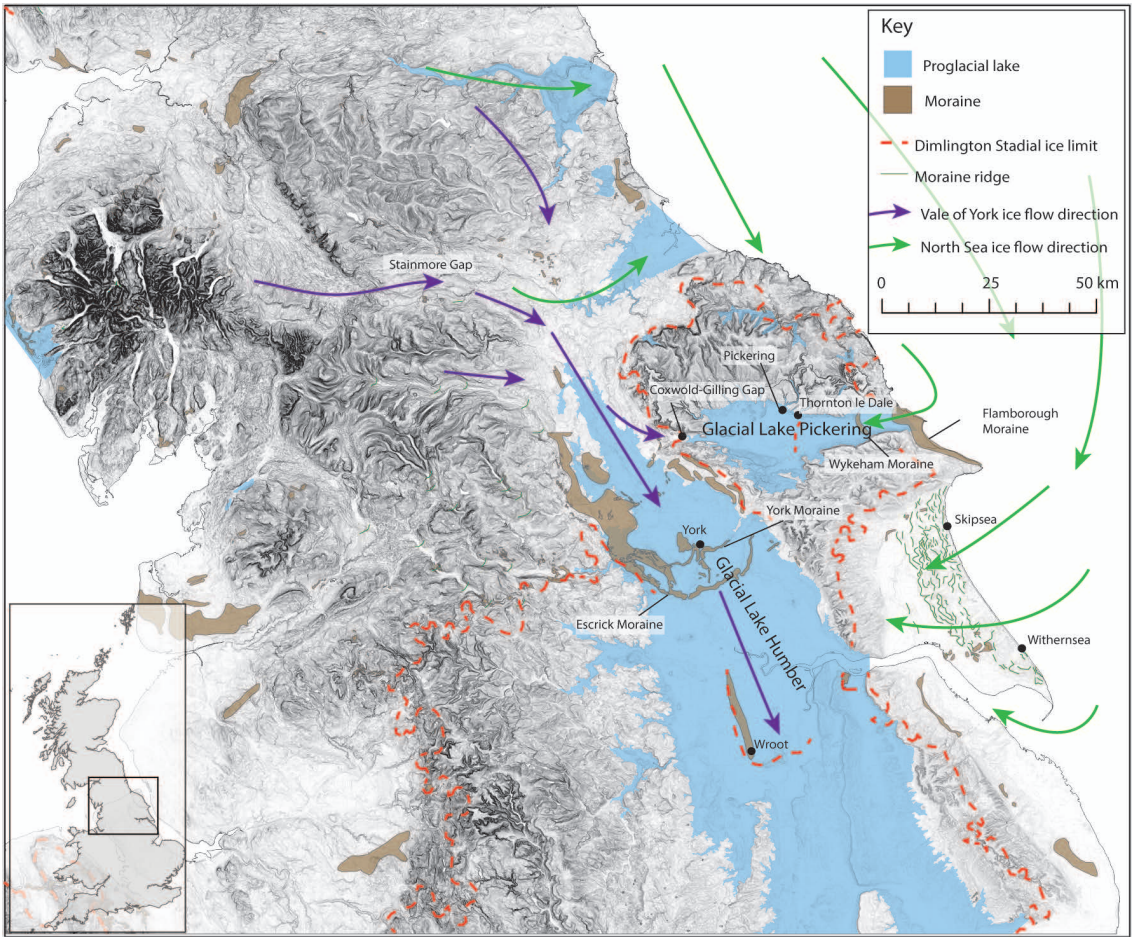

Figure 3.3. *Map showing the major flow directions of the NSIL (green) and VOYL (purple) during the Dimlington Stadial. Moraines, moraine ridges and proglacial lakes (from Clark et al., 2004), and sites discussed in text are listed for reference.*

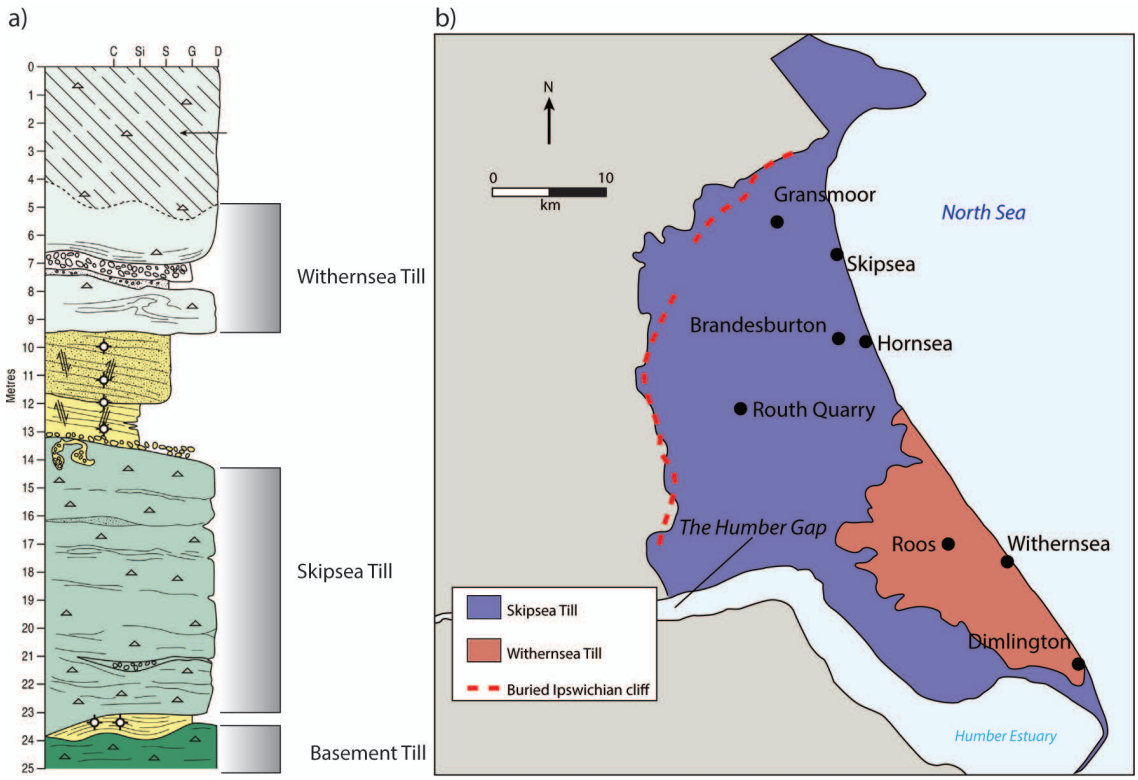

Figure 3.4. *a) Composite vertical profile log for the LGM typesite at Dimlington showing the stratigraphy of glacigenic deposits of the NSIL (modified from Bateman et al., 2015), b) Map of the distribution of till deposits on Holderness (after Bateman et al., 2011). The location of the Humber Gap mentioned in text is also labelled.*

The ice that deposited the Skipsea Till likely originated from the Midland Valley in Scotland and NE England, flowing southward down the North Sea basin (Carr *et al.,* 2006; Catt, 2007; Busfield *et al.,* 2015), and onto the North Yorkshire coast (Madgett and Catt, 1973; Catt, 2007; Evans *et al.,* 2005), blocking the eVoP (Kendall, 1902; Evans *et al.,* 2016). The Withernsea Till, which overlies the Skipsea Till was also sourced from ice flowing from the Lake District, via the Stainmore Gap and into the North Sea during a later re-advance (Catt, 2007; Evans and Thomson, 2010; Figure 3.1). The maximum NSIL extent is inferred from the presence of the Skipsea Till on the dipslope of the Yorkshire Wolds, with the Withernsea Till outcropping a smaller area on the southern margins of Holderness (Rose, 1985; Evans *et al.,* 2005; Catt, 2007; Figure 3.4).

The Vale of York Ice Lobe (VOYL)

Ice sourced from southern Scotland and the Lake District advanced southeast, via the Stainmore Gap (Lewis, 1894; Boulton *et al.,* 1985; Catt, 2007), joining with local ice from Upper Teesdale (Mitchell, 2007), and the Pennines (Kendall and Wroot, 1924; Raistrick, 1926). This ice flowed into the Vale of York from the north, damning regional drainage, and forming three distinct moraines (Evans *et al.,* 2005; Catt, 2007; Bateman *et al.,* 2015), and with the NSIL blocking the Humber Estuary, creating a large ice dammed lake (Clark *et al.,* 2004; Bateman *et al.,* 2008), termed Glacial Lake Humber (Gaunt, 1976; 1981; Fairburn, 2009; Fairburn and Bateman, 2016).

A retreat and stabilisation of the ice lobe is indicated by a complex suite of ridges, consisting of till and poorly sorted gravels (Catt, 2007), deposited across wide swathes of the valley, near York, which are termed the York and Escrick Moraines (Melmore, 1935). On the eastern margins of the Vale of York, the moraines extend onto the foothills of the Howardian Hills, blocking the Coxwold-Gilling gap at the western extent of the VoP (Kendall, 1902; Kendall and Wroot, 1924; Catt, 2007). At this stage, Glacial Lake Humber existed at 30-33 m OD (Gaunt, 1981; Clark *et al.,* 2004; Fairburn and Bateman, 2016).

Eight proglacial lake terraces have been identified at 42, 40, 33, 30, 25, 20, 15 and 10 m OD (Fairburn, 2009; 2011; Fairburn and Bateman, 2016) which enable an eight-stage model of proglacial lake development to be constructed. This mode demonstrates that the level of Glacial Lake Humber progressively declined through the Dimlington Stadial, being driven by changes in the position and presence of ice/moraine dams in the Humber Gap (location shown in Figures 3.3-3.4) and the elevation of drainage cols through the Dimlington Stadial (Bateman *et al.,* 2015; Fairburn and Bateman, 2016).

3.3.2. Chronology

The timing of Late Devensian ice movement in northeast England was poorly constrained, confined primarily to bulk radiocarbon dates from kettlehole basins, providing fragmented and indirect minimum ages for advance and recession (e.g. Beckett, 1981; Keen *et al.,* 1984; Rose, 1985; Figure 3.5). More recently the BRITICE CHRONO project has attempted to better delimit the rate and timing of BIIS decay during the Dimlington Stadial (Clark *et al.,* 2012; Bateman *et al.,* 2015; Evans *et al.,* 2016). This section briefly summarises the chronological evidence used to constrain Late Devensian ice sheet advance and retreat of the NSIL and VOYL, which directly affected the VoP. A summary of these data are presented in Figure 3.6.

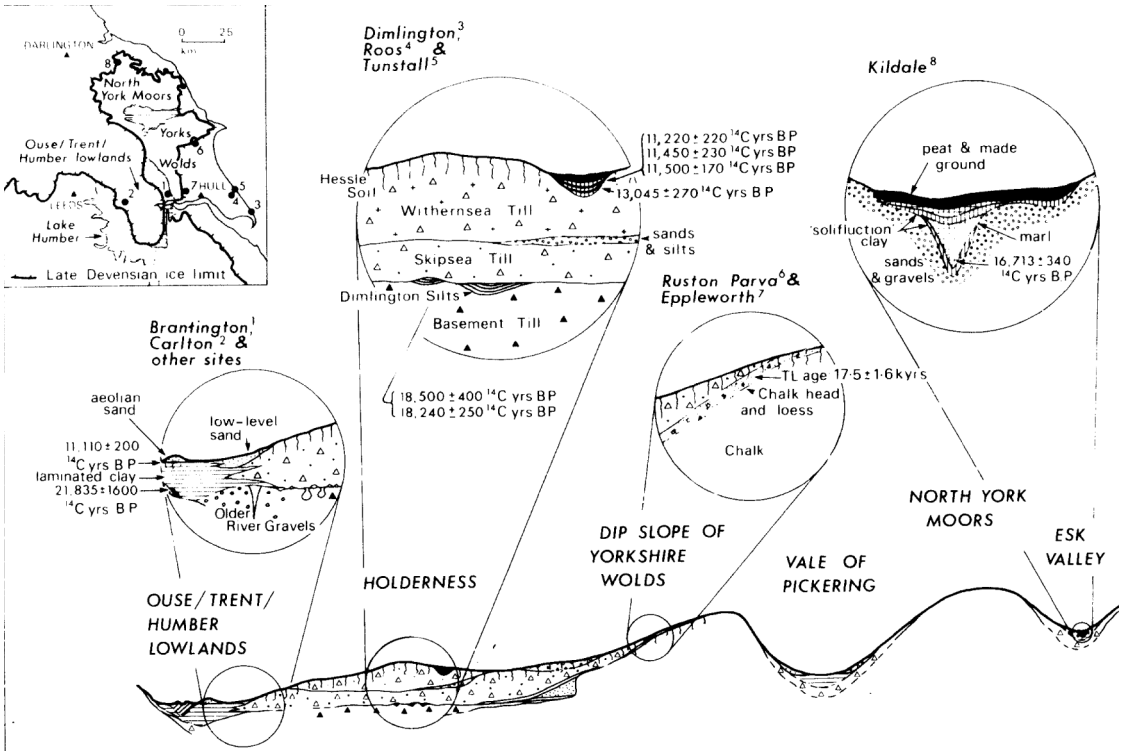

Figure 3.5. *Schematic representation of the stratigraphic, and chronological evidence for Dimlington Stadial advances of the NSIL onto the NE Yorkshire coast (from Rose, 1985). This demonstrates the fragmentary and imprecise age estimates for phases of ice advance and retreat in the North Sea.*

3.3.2.1. The NSIL

Radiocarbon ages from plant remains lying in-between the Basement and Skipsea Tills of 18.5 ± 0.4 ^{14}C years BP (22.41 ± 0.97 cal ka BP) at Dimlington (Penny *et al.,*1969), corroborated by OSL ages on the same deposits, of 20.5 ± 1.2 ka and 21.2 ± 1.5 ka BP (Bateman *et al.,* 2015), provide a maximum age for the onset of Late Devensian ice advance of the NSIL onto the Holderness coast (Rose, 1985). OSL ages from interbedded sandur deposits inbetween the Skipsea and Withernsea tills at Dimlington, further constrain the deposition of the Skipsea Till to between 21.7-16.2 ka BP (Bateman *et al.,* 2011). The southern extension of these ice lobes is argued to

coincide with a slight warming episode observed in the GICC05 timescale termed GS-2.1b (Bateman *et al.,* 2015).

The NSIL receded from Holderness at *ca.* 17.3 ± 0.95 ka BP, leading to the development of subaerial deposits, lying between the Skipsea and Withernsea tills at Dimlington (Bateman *et al.,* 2011). The extent of the ice retreat into the North Sea Basin is not constrained, but is inferred to have maintained a local presence to the North Yorkshire coast between. Local presence is also inferred in the Humber estuary, which the ice lobe continued to dam drainage paths from the Vale of York which sustained the 33 m OD level of Glacial Lake Humber (Fairburn and Bateman, 2016; Figure 3.6, 18-17 ka).

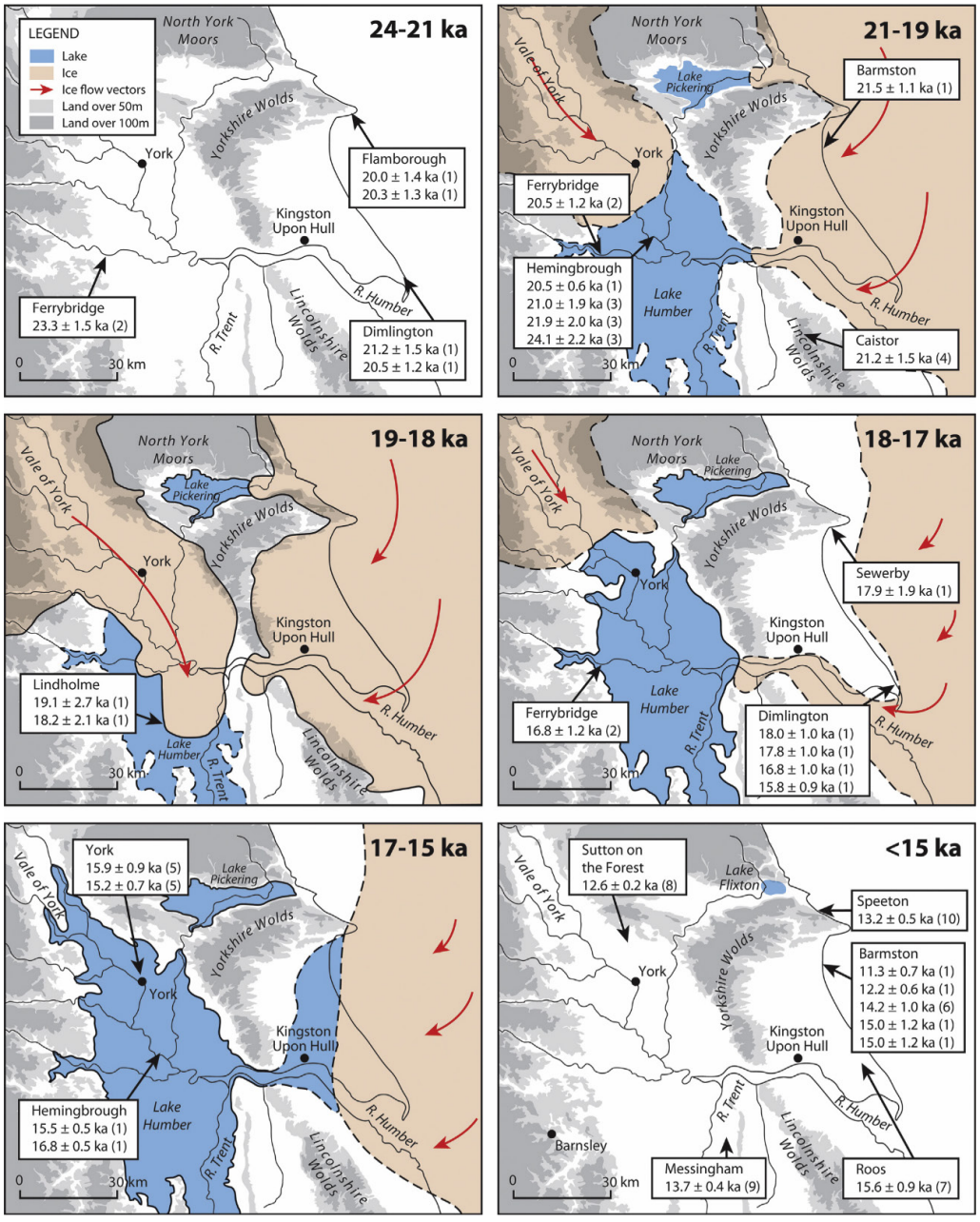

Figure 3.6. *Schematic reconstruction of the relative ice movements of the NSIL and VOYL constrained by OSL and ^{14}C dates (Bateman et al., 2015). Ice margins are illustrative and based, where available, on dated stratigraphic and geomorphic evidence indicating either ice free or ice inundated conditions. This indicates the significantly larger amount of chronological information available to reconstruct the interlobate dynamics of the BIIS since the publication of Rose (1985; Figure 3.5), and the mapping of landforms in the VoP.*

The NSIL re-advance that deposited the Withernsea Till is bracketed between OSL ages of 17.3 ± 0.95 ka BP and 14.9 ± 0.44 ka BP (Bateman *et al.,* 2015). A constraining minimum age for its deposition is provided by a radiocarbon date on basal organics from a kettle hole at Roos, of 13.05 ± 0.27 ^{14}C ka BP (15.59 ± 0.88 cal ka BP; Beckett 1981; Figure 3.5). This re-advance coincides with other re-advances from the BIIS, including the Irish Sea ice lobe (McCabe *et al.,* 2007; Thrasher *et al.,* 2009) and the Witch Ground Basin in the northern sector of the North Sea (Lekens *et al.,* 2005; Sejrup *et al.,* 2015). Overall however, this readvance is overprinted upon a general trend of BIIS retreat at other localities (Clark *et al.,* 2012), indicating that the NSIL was acting independently of the BIIS during the latter stages of deglaciation, most likely as a result of surge activity, driven by internal ice sheet dynamics (Boulton and Hagdorn, 2006; Boston *et al.,* 2010; Livingstone *et al.,* 2012).

3.3.2.2. The VOYL

Ice advance into the Vale of York is proposed to have occurred between 25-21 ka BP by Livingstone *et al.* (2012), where it formed a low level proto-Glacial Lake Humber prior to 21.9 ± 1.6 ka BP (Murton *et al.,* 2009; Bateman *et al.,* 2015). The maximum southern extension of ice to the limit at Wroot, in the Vale of York has been dated to 18.7 ± 0.63 ka BP based upon two OSL ages (19.1 ± 2.7 ka BP and 18.2 ± 2.1 ka BP) at Lindholme (Bateman *et al.,* 2015; location shown in Figure 3.3). Between 18-17 ka BP, the VOYL retreated, and stabilised in the vicinity of the York and Escrick Moraines, before retreating northward (Bateman *et al.,* 2015). By 16.4 ± 0.75 ka BP Glacial Lake Humber had attained an altitude of 33 m OD, which then proceeded to lower in stages (25-15 m OD) between 15.9 ± 0.9 and 15.2 ± 0.7 ka BP (Fairburn and Bateman, 2016). The final drainage of Glacial Lake Humber occurred between 14.65 and 13.01 cal ka BP, significantly after the ice recession from the Vale of York (Metcalfe *et al.,* 2000).

3.3.2.3. Summary

The chronological models of glacial deposits in NE England has developed understanding on the dynamics of ice lobe growth and decay during the Dimlington Stadial (e.g. Clark *et al.,* 2012; Bateman *et al.,* 2015). These data demonstrate that the maximum ice advance of the NSIL and VOYL occurred at *ca.* 19-18 ka BP, and initial retreat occurred at *ca.* 18-17 ka BP. This suggests that the two ice lobes were acting equivalently between 19-17 ka BP at a millennial timescale (although the large uncertainties on OSL ages do not allow a firm conclusion to be drawn on the exact synchroneity of advance and retreat). Between *ca.* 17-15 ka BP however, evidence suggests that the two ice lobes were acting independently of each other, with the VOYL retreating and collapsing, but the NSIL re-advancing (Bateman *et al.,* 2015). The diachronous response suggests that lowland ice masses sourced from dispersal centres in northern England (e.g. the Lake District and Pennines) largely collapsed (e.g. the VOYL), whilst those sourced from

more northerly dispersal centres (e.g. the NSIL) were able to re-advance between *ca.* 18-16 ka BP (Livingstone *et al.,* 2015). This indicates the dynamic mode of deglaciation of the BIIS between *ca* 18-15 ka BP, which significantly impacted the timing and phasing of landscape development in NE England. Further work is required to develop understanding on how landscapes responded to the dynamic, and diachronous recession of these ice lobes, and to increase precision on the timing of ice recession, particularly for the VOYL (e.g. Bridgland *et al.,* 2011), where limited ages exist for the retreat of ice north of the York Moraine (Bateman *et al.,* 2015).

3.4. The LGIT in NE England

The palaeoclimatic and palaeoenvironmental responses to LGIT climatic change in NE England have been determined via beetle-derived estimates of temperature (Walker *et al.,* 1993), palynological signals recorded in lacustrine sediments (Bartley, 1962; Bartley *et al.,* 1976; Walker *et al.,* 1993a; Gearey, 2008), and sedimentological analysis of fluvial deposits (Rose, 1995; Gao *et al.,* 2007; Bridgland *et al.,* 2010). These deposits are most commonly sourced from kettle-hole lakes and abandoned meltwater channels, formed in lowland areas previously inundated by ice during the Late Devensian (Figure 3.7), and when dated they provide useful minimum age estimates of the timing of deglaciation and an understanding of the palaeoenvironmental conditions through the LGIT. The following sections outline the climatic variability through the LGIT in NE England, then discusses vegetation and geomorphic trends before briefly outlining challenges for future research in the region.

3.4.1. Palaeoclimatic reconstructions

Quantitative, and well dated climatic proxy records from the lowlands of NE England are confined to the coleopteran mutual climatic range (MCR) record from Gransmoor on Holderness (Walker *et al.,* 1993; Lowe *et al.,* 1995; Elias and Matthews, 2013; Figure 3.7). This record has become a type sequence for LGIT climatic variability, principally because: a) few other records exist; b) the TMax ranges show a climatic structure through the Windermere Interstadial (WI) that is consistent with the GICC05 record of GI-1, with an early thermal optimum and subsequent decline until the onset of the Loch Lomond Stadial (~ GS-1; Lowe *et al.,* 1995; 2008; Björk *et al.,* 1998); c) it is one of the few quantitative palaeoclimatic records in the British Isles that records the climatic amelioration at the onset of the WI.

At the base of the Gransmoor record, TMax temperatures rise by 12-14 °C to a peak of between 18 to 23 °C during initial warming in the WI (Walker *et al.,* 1993). TMin temperatures are more poorly constrained and range between -4 and 9 °C. These temperatures demonstrate mild summer temperatures similar to contemporary ranges, but larger annual ranges, representative of a more continental climate than the present day (average 16 °C summers and 4 °C winters in eastern Yorkshire). This relative peak in TMax temperatures was relatively short-lived and

concluded prior to 14 cal ka BP (Walker *et al.,* 1993; Blockley *et al.,* 2004). From 14 cal ka BP to the onset of the Loch Lomond Stadial, the Gransmoor coleopteran record suggests relatively lower but broadly stable summer temperatures between 12-16 °C, while winter temperatures are reconstructed between 0- -12 °C, consistent with a more continental climatic regime in NE England. Elsewhere in the British Isles (NW England and Scotland) however, the climatic structure through this interval is less stable, and characterised by between one and three abrupt oscillations in chironomid-inferred temperature (C-ITs; Brooks and Birks, 2001a; Brooks *et al.,* 2012; 2016) and $\delta^{18}O_{bulk}$ records (Marshall *et al.,* 2002; Whittington *et al.,* 2015; Candy *et al.,* 2016). These events are consistently correlated to GI-1d, GI-1c2, and GI-1b in the GICC05 record (Rasmussen *et al.,* 2014), but with the exception of the C-IT record at Abernethy Forest (where an oscillation of 5.8 °C is chronologically correlated to GI-1d; Matthews *et al.,* 2011) the timing of these climatic oscillations in the British Isles remain undated, precluding precise comparisons on regional leads and lags in the climatic system.

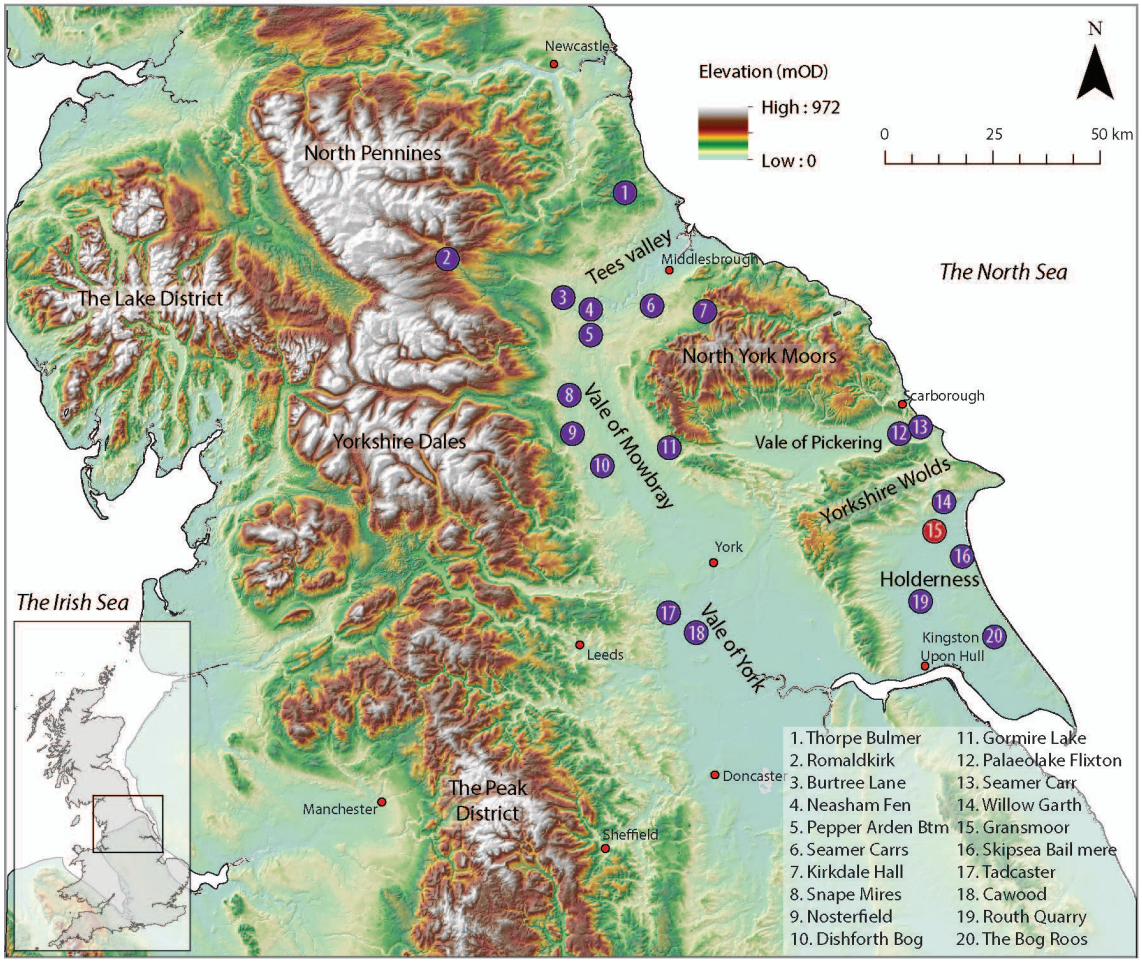

Figure 3.7. *Key LGIT records in NE England (after Innes et al., 2009). Sites in purple consist of pollen records whilst sites in red (only Gransmoor) consist of multiproxy, palaeoencironmental reconstructions allied with a robust chronology.*

The LLS saw the spread of many obligate, cold adapted taxa to NE England, with summer temperatures decreasing by 4-5 °C (Renssen *et al.,* 2015), to *ca* 9-11°C (Walker *et al.,* 1993; Coope *et al.,* 1998). Winter temperatures also fell to as low as -15 to -20 °C at Gransmoor

(Walker *et al.,* 1993). This represents a decline of *ca.* 12°C in relation to peak WI values (Walker *et al.,* 1993; Walker *et al.,* 1995), indicating a more continental climatic regime (Isarin *et al.,* 1998; Denton *et al.,* 2005), with minimum mean annual temperatures in northern England falling to *ca.* -5 °C (Atkinson *et al.,* 1987).

LLS aged aeolian deposits in the Vale of York, Lincolnshire (Gaunt *et al.,* 1971; Bateman *et al.,* 1998; Bateman, 2001), and the VoP (Schadla-Hall, 1987) also demonstrate periods of enhanced aridity during this interval in NE England (Isarin *et al.,* 1998; Bridgland *et al.,* 2011). Elsewhere in the British Isles, palaeoglacial reconstructions have suggested the development of strong west-east precipitation gradients during the LLS (Bendle and Glasser, 2012; Boston *et al.,* 2015). At present however, little supporting evidence of palaeoprecipitation/palaeohydrological change through the LGIT exists in the British Isles, particularly through the preceding WI.

Gransmoor does not record the climatic amelioration at the onset of the Holocene but the nearest quantitative records from palaeolake basins in the Lake District (Marshall *et al.,* 2002; Bedford *et al.,* 2004; Lang *et al.,* 2010) and Scotland (Brooks and Birks, 2000a; Brooks *et al.,* 2012; 2016), show a similarly abrupt amelioration as that recorded in Greenland and across Northern Europe. A shift in the seasonality of rainfall, from an initially continental (i.e. high summer precipitation low winter precipitation) to a progressively more maritime climatic regime (more equal summer and winter precipitation regimes) is also inferred from isotopic records through the first *ca.* 3000yr of the EH in NE England (Candy *et al.,* 2015).

Whilst the Gransmoor record provides a valuable palaeoclimatic reconstruction for NE England, it is limited in the following ways. The earliest radiocarbon date obtained from the sequence comes from 226 cm, the re-calibrated age of which is 14.55-14.15 cal ka BP (re-calibrated using IntCal13). The position of this date is significant as it post-dates the abrupt climatic amelioration and climatic optimum in the MCR record. The age model for the Gransmoor MCR therefore is not reliably constrained below 226 cm, particularly as the sediment composition below this interval switches from organic-rich gyttjas to sands and silts (Walker *et al.,* 1993), which likely represents a significant change in sedimentation rate (Bronk Ramsey, 2008).

The Gransmoor sequence as reported in Walker *et al.* (1993) is also split into two sections, consisting of an open face (0-235cm from top of sequence), where most of the palaeoenvironmental data are sourced from (S25-235), and a second section, horizontally offset from the S25-235 samples, consisting of the aforementioned sands and silts, with evidence of faulting and partial slumping, where a further 26 MCR ranges are derived (B1 to 26; Figure 3.8). The climatic amelioration at the onset of the WI is contained within this second section, in which there is no chronological information (see above). Within this section, the amelioration ranges reported in Walker *et al.* (1993) consist only of the TMax and TMin of samples from the lower

and upper limit of this period as represented stratigraphically, (S230-B1 and B24-26), with the samples from intervening stratigraphic horizons discounted due to a lack of overlap with the 'upper' and 'lower' limit temperature ranges. Consequently, the local timing of climatic amelioration, and the duration of the apparent climatic optimum during the early WI cannot be reliably assessed using the Gransmoor MCR record.

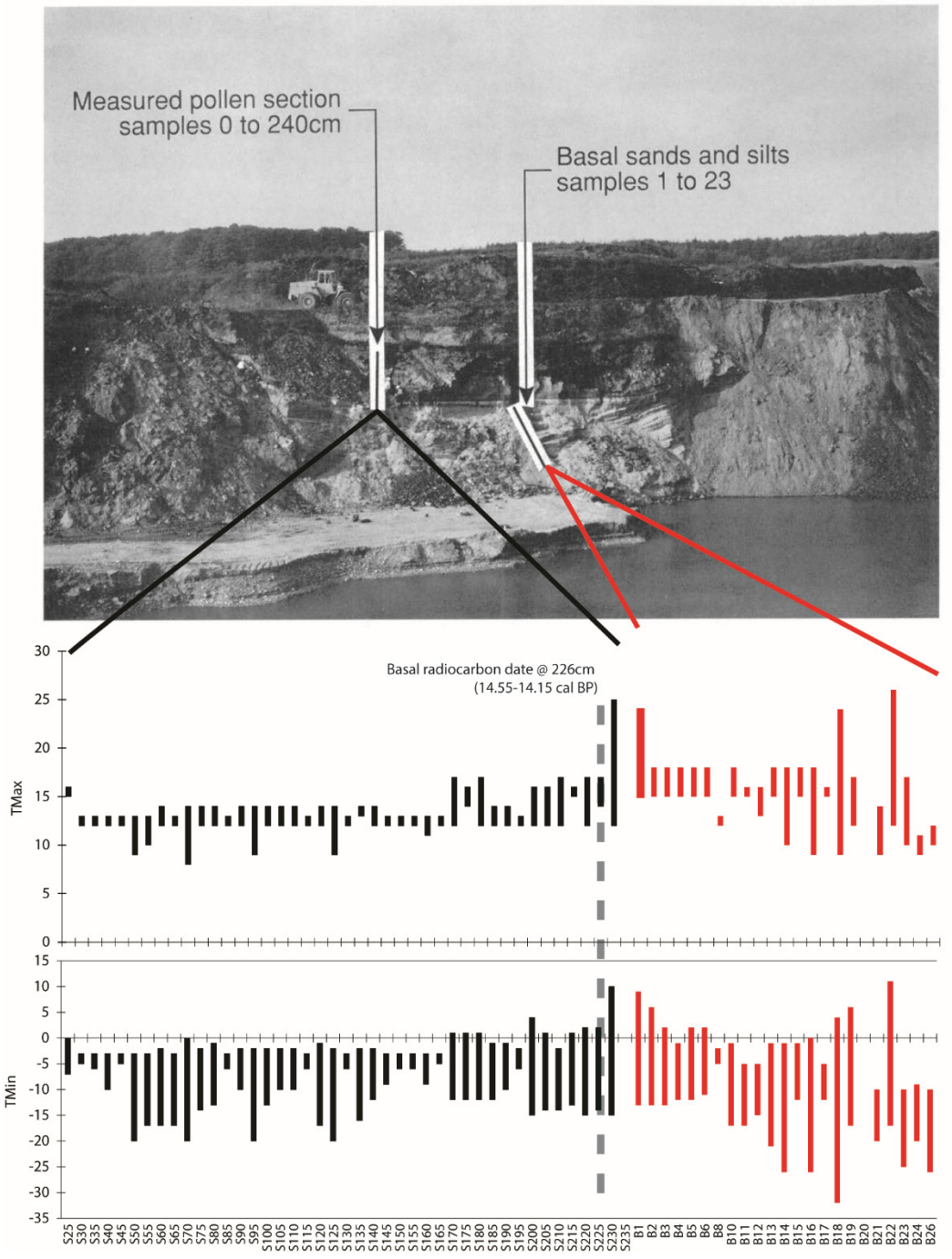

Figure 3.8. *Coleopteran MCRs from the two sections at Gransmoor (Walker et al., 1993). The image illustrated the two localities which samples were taken from, and the location of the basal radiocarbon date from the sequence which post-dates the climatic amelioration associated with the WI at ca. 15 cal ka BP.*

Additionally, the abrupt centennial scale climatic oscillations in the LGIT which are identified in the Greenland ice-core records, and are also identified elsewhere in the British Isles are not well resolved in the Gransmoor MCR sequence. It is unclear whether this relates to: a) the sensitivity of coleopteran MCRs to distinguish these events, b) an inadequate sampling resolution to adequately resolve the amplitude of the oscillations, c) a spatially heterogeneous climatic signal between NE England and the rest of the British Isles. The presence of similar high-resolution climatic oscillations elsewhere in the British Isles (Marshall *et al.,* 2002; Brooks *et al.,* 2012; 2016; Candy *et al.,* 2016) and Europe (e.g. von Grafenstein *et al.,* 1999; Heiri *et al.,* 2007; van Asch *et al.,* 2012) suggests that it is most likely that the Gransmoor record is of too low resolution to determine these events. At present therefore, no quantitative palaeotemperature records constrained by a robust chronology exist to the east of the Pennines, limiting precise reconstructions and regional correlation. Furthermore, other climatic variables such as palaeohydrological variability has not been quantitatively assessed in the British Isles, particularly through the WI.

Improved palaeoclimatic records from NE England are required to test the spatial manifestation of climatic signals through the LGIT, which are hypothesised to have varied across latitudinal, longitudinal, and altitudinal gradients (Coope *et al.,* 1998; Brooks and Langdon, 2014; Candy *et al.,* 2016). These types of records are important as changes in the climatic regime are a primary controlling factor on local geomorphic, ecological, and archaeological trends (Rose, 1995; Blockley *et al.,* 2006; Jacobi and Higham, 2011; Birks and Birks, 2014). Therefore, high-resolution, quantitative, and multiproxy palaeoclimatic records from this region would enable robust comparisons to other regional palaeoclimatic records to test the spatial heterogeneity of the climatic system (Lane *et al.,* 2013; Muschitiello *et al.,* 2015) and develop multiproxy palaeoenvironmental reconstructions through the LGIT.

3.4.2. Vegetation

Palaeoenvironmental reconstructions from NE England through the LGIT are derived almost entirely from pollen records from lowland basins in Holderness (Beckett, 1974; 1981; Hunt *et al.,* 1984; Walker *et al.,* 1993; Tweddle, 2000; Geary and Lillie, 2001); the Vales of York and Mowbray (Bartley, 1962; Jones, 1977; Innes *et al.,* 2009); the Tees Valley (Bellamy *et al.,* 1966); the foothills of the North York Moors (Keen *et al.,* 1984); the VoP (Walker and Godwin, 1954; Cloutman, 1988a; b; Day, 1996; Mellars and Dark, 1998); and Southern County Durham (Bartley *et al.,* 1976; Figure 3.7). Remarkably these sites show largely concordant trends throughout the LGIT, with subtle differences thought to represent the variability of pollen source catchments and edaphic factors (Cloutman, 1988b; Walker *et al.,* 1993; Dark, 1998; Tweddle, 2001). The following section discusses the pollen derived vegetation trends using the summary pollen diagrams from four key records: Palaeolake Flixton (Day, 1996), Gransmoor (Walker *et al.,* 1993;

Figure 3.9), Thorpe Bulmer (Bartley *et al.,* 1976), and Tadcaster (Bartley, 1962). These are selected as they contain a full record of the LGIT and in the case of Gransmoor also have associated chronological information. Other sites shown in Figure 3.7 are used to support the key trends from these records.

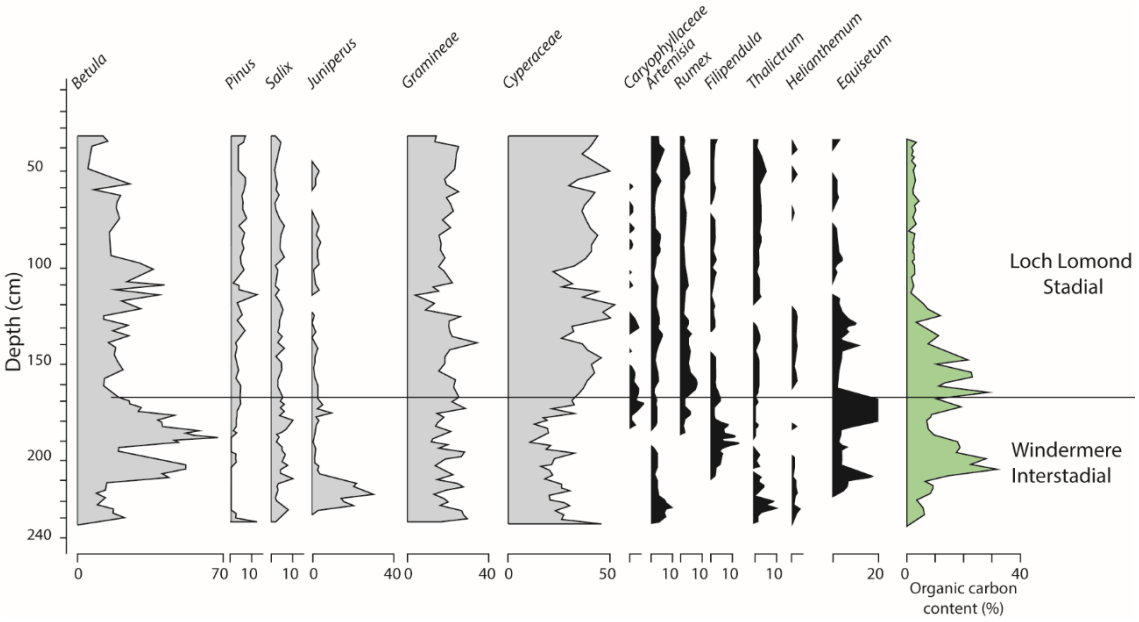

Figure 3.9. *Pollen diagram from Gransmoor, illustrating shifts in vegetation assemblages that are consistently recorded in LGIT records across NE England (modified from Walker et al., 1993).*

The vegetation succession during the early WI is characterised by the increase of *Betula* (to *ca.* 25 % (Bartley, 1962; Beckett, 1981; Day, 1996; Walker *et al.,* 1993; Figure 3.9), with at least some of this rise attributed to *Betula nana*, and a proportional fall of Poaceae, suggesting the regional colonisation of shrubs and isolated trees. At all four of sites, *Artemisia* and *Rumex* are present throughout this period, and a similar trend can be seen in other lowland sites in NE England, such as Routh Quarry (Geary and Lillie, 2001) and Snape Mires (Innes *et al.,* 2009). The influx of thermophilous taxa, such as *Juniperus.* are frequently assumed to directly relate to the rapid warming at the onset of the WI (Tweddle, 2001; Innes, 2002). However, the records selected here suggest a delay in the expansion of *Juniperus* in NE England, with the Gransmoor sequence, demonstrating that polleniferous sediments including *Juniperus* occurred after the climatic optimum, and possibly as late as 13.9 cal ka BP (Walker *et al.,* 1993). If this inference is correct, it suggests that by the time higher vegetation development had been initiated, summer temperatures were as much as 4-5 °C lower than the thermal optimum at the onset of the WI (Walker *et al.,* 1993). The *Juniperus* expansion consistently occurs directly after a reduction in *Betula* and increases in open and/or disturbed ground indicators e.g. *Artemisia*, *Rumex, Helianthemum* and pre-Quaternary spores. Lithostratigraphic changes are also reported in the Palaeolake Flixton record during this interval, with high amounts of siliclastic material in the record during this time (Day, 1996). These changes all suggest a link to a wider climatic event, closely associated with the expansion of *Juniperus* in NE England.

After this interval, there is a subsequent well-documented expansion of *Betula* to its WI maximum (≤ 80 % of total land pollen), eventually replacing *Juniperus* in the landscape (Beckett, 1981; Walker *et al.,* 1993; Geary and Lillie, 2001; Innes *et al.,* 2009). To the north, in the Tees valley, arctic and alpine herbaceous taxa persist throughout the WI, suggest the development of an open-park tundra rather than birch forests (Blackburn, 1952), a pattern also recorded at Kildale Hall (Jones, 1977). Consequently, Thorpe Bulmer is the northernmost site in NE England to preserve a distinct *Betula* peak, and this is suggested to represent the northern limit of birch woodland expansion during the mid-late WI in Britain (Tweddle, 2001; Innes, 2002). The potential that *Betula* pollen has for long distance transport however, means that the local presence of tree birch can only be confidently verified via macrofossil records (Mortensen *et al.,* 2014; Birks and Birks, 2014) few of which exist from LGIT records in NE England. To the south and west of this area, tree birch macrofossils are not recorded at Llanilid in S. Wales until 13.6 cal ka BP (Walker *et al.,* 2003), or at Hawes Water until after *ca.* 14 cal ka BP (Jones *et al.,* 2002), a pattern which is also observed in NW Europe during the Allerød period (Mortensen *et al.,* 2011; 2014). These trends support that: a) landscape stability in NE England increased during WI and at *ca.* 14 cal ka BP became suitable for *Betula* growth; b) The diachronous response of *Betula* migration may relate to latitudinal gradients in climate; and c) topographic and edaphic controls are locally important and may have limited the spread of closed forests to the lowlands of NE England. The distribution range of *Betula* pollen grains mean that in isolation, pollen records cannot confidently reconstruct the local changes in vegetation cover. Plant macrofossil analysis coupled with the palynological records are therefore required to more accurately reconstruct the local scale shifts in vegetation cover across NE England (Birks, 2000).

A distinct second decline in *Betula* pollen is evident at Thorpe Bulmer (710 cm), Gransmoor (195 cm), and Lake Flixton (540 cm). This decline is associated with increases in open ground taxa e.g. Poaceae and *Filipendula* and has been suggested to relate to a second climatic event within the WI (Walker *et al.,* 1993). This second event may not directly relate to summer temperature changes as although it can be recognised at Gransmoor there is no concurrent oscillations within the beetle-derived temperature estimates. This may relate to the sampling resolution of the beetle-MCR data however, meaning that the temperature reconstructions from Gransmoor lacks sufficient resolution to capture this event (see above).

The transition to the LLS is characterised by increased abundances of open ground taxa in pollen records, with an increased dominance of Poaceae and Cyperaceae and high abundances of open/disturbed herb taxa such as *Rumex* and *Artemisia* (Beckett, 1981; Tweddle, 2001). *Betula* and *Salix* remain present in low abundances, in the lowlands, with isolated stands of *Betula pubescens* suggested to have persisted in sheltered areas before recolonising during the EH (Mayle *et al.,* 1999; Tweddle, 2000). This transition however is poorly dated, with most records presuming changes in litho- and/or bio-stratigraphic records, represents the transition into the

LLS (e.g. Bartley, 1962; Cloutman, 1988 a; b; Day, 1996; Tweddle, 2001; Innes *et al.,* 2008). Direct chronological control on these vegetation changes is sparse, being constrained only from Gransmoor and the Roos Bog on Holderness (e.g. Beckett, 1981; Walker *et al.,* 1993). Further chronological control is required through this interval to more accurately assess the palaeoecological response intervals to the climatic deterioration through the LLS.

The vegetation succession through the EH is well documented in NE England. Rapid climatic amelioration resulted in the development of species-rich, shrubby grasslands, with an initial expansion of *Empetrum, Juniperus,* and *Salix,* which replaced open grasslands developed during the LLS (Tweddle, 2001; Innes *et al.,* 2009). An expansion of *Juniperus* and *Betula* (Bartley, 1966; Turner and Kershaw, 1973; Bartley *et al.,* 1976), led to declines in thermophilic fen herbs such as *Typha* and *Fllipendula.* Macrofossil analysis in the VoP reveal that most of the *Betula* pollen was from downy birch (*Betula pubescens*), with small amounts of dwarf birch (*Betula nana*) persisting during the initial rise in the pollen records from the lowlands (Dark, 1998). Macroremains of European aspen (*Populus tremula*) are also prevalent during this initial woodland expansion, but are poorly represented in pollen diagrams due to the susceptibility of *Populus* pollen to deterioration in sedimentary records (Cloutman, 1988b; Mellars and Dark, 1998). As with the WI, the development of tree birch communities in NE England was not coincident with Pleistocene-Holocene boundary, lagging the climatic amelioration by several centuries (Pennington, 1986). The rise of *Corylus avellana* from EH pollen records in NW Europe (e.g. Smith, 1984; Edwards, 1990; Day, 1996), is well recognised, where it replaces the *Betula* dominated vegetation records. This rise is reported to occur in Palaeolake Flixton between 10.89 ± 0.33 cal ka BP (Cummins, 2003), and 9.99 ± 0.25 cal ka BP (Mellars and Dark, 1998).

3.4.3. Geomorphology

Low eustatic sea levels left the southern North Sea Basin subaerially exposed throughout the LGIT, connecting eastern England to continental Europe via a low-lying landmass termed Doggerland (Coles, 1998; Figure 3.10). This landmass was not entirely inundated until the mid-Holocene (Jelgersma, 1979; Bickett and Tizzard, 2014; Ward *et al.,* 2016), via a combination of rising eustatic sea-level (Lambeck *et al.,* 2014), slowing glacio-isostatic adjustment (Smith, 2004; Bondevik, *et al.,* 2005), and the Storegga Slide tsunami at *ca.* 8.2 ka BP (Weninger, *et al.,* 2008).

The palaeogeography of NE England, is believed to have played a significant role in the development of fluvial systems through the LGIT (Rose, 1995; Bridgland *et al.,* 2010). During the early stages of the WI, a uniform phase of incision is identified in most lowland British rivers (Bull, 1991; Rose, 1995; Tebbens *et al.,* 1999; Bridgland *et al.,* 2010). This is largely attributed to the low sea-levels coupled with diminishing sediment loads in river catchments (Rose, 1995), and high rates of glaco-isostatic adjustment in recently deglaciated catchments. These phases of

incision led to the formation of distinct fluvial terraces in the larger river valleys (Bridgland *et al.,* 2010). During the mid to latter stages of the WI, lowland river catchments in England consistently transition from incising to aggrading modes, with fine-grained clastic and organic-rich sediments consistently recorded. A similar change is also well documented across many northern European river systems (Kozarski, 1983; Lipps and Caspers, 1990; Vandenberghe *et al.,* 1994; Antoine *et al.,* 2003; Kasse *et al.,* 2005; Turner *et al.,* 2013), but the precise timing of these transitions is too poorly constrained to make inter-catchment comparisons. Towards the end of the WI, a phase of incision is recorded in some lowland rivers in eastern England such as the River Gipping (Rose and Boardman, 1983).

During the LLS, lowland rivers systems in NE England are consistently characterised by a shift to braided, aggradational planforms (Rose *et al.,* 1980; Rose, 1995; Gao *et al.,* 2007), with inorganic sands and gravels deposited across floodplains and occasional organic facies in palaeochannel infills (e.g. Dinnin, 1997). In the EH, river activity diminished in lowland catchments (Gao *et al.,* 2007; Rose, 2010), with fine grained alluvium being deposited across lowland floodplains (Rose, 1995).

Whilst the development of fluvial systems are relatively well understood in NE England, many of these reconstructions lack supporting palaeoenvironmental and chronological information with which to assess changes in catchment dynamics (e.g. vegetation cover, particle sizes, and palaeoclimatic reconstructions), meaning the leads and lags of river catchments changes to climatic and environmental forcing is inadequately constrained (Rose, 1995). Further records encompassing palaeofluvial development, catchment dynamics, and palaeoclimatic evolution are required therefore to quantify the inter-relationship of these systems.

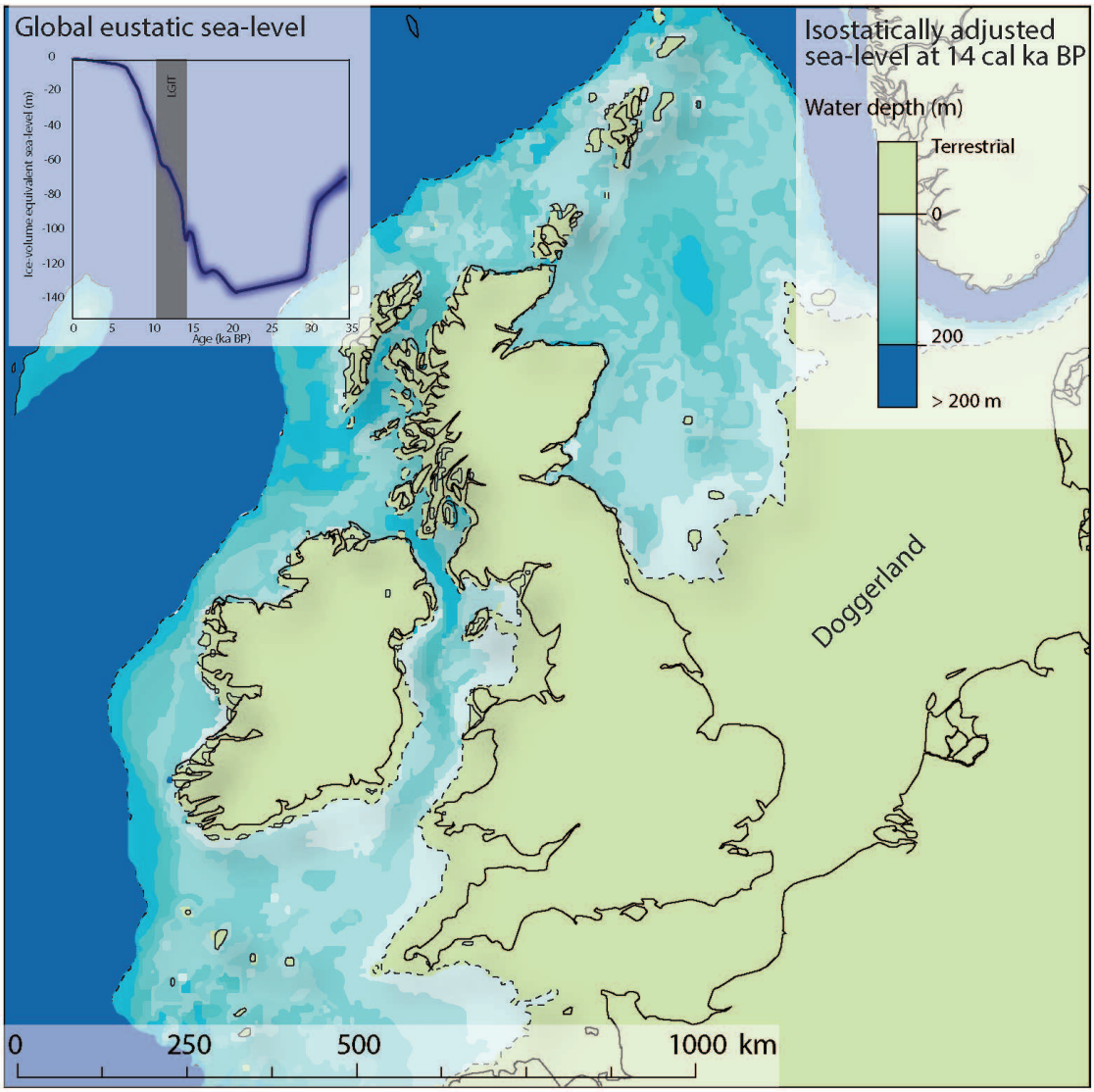

Figure 3.10. *Reconstruction of the palaeoshorelines of the British Isles at 14 cal ka BP through the LGIT. The inset figure shows the reconstruction of global eustatic sea-level from Lambeck et al. (2014) whilst the mapped shorelines are derived from the glacio-isostatically adjusted models of Ward et al. (2016). These conditions left the southern North Sea basin subaerially exposed through the entire LGIT, meaning the palaeogeography of NE England differed significantly from the present day. The subaerially exposed landmass has been termed as Doggerland.*

3.5. The Vale of Pickering

The Vale of Pickering has significant potential with which to improve understanding of climatic and landscape development through the Last Termination. The following sections summarise the physiography and geology of the VoP before reviewing evidence previously identified from the valley for geomorphic and palaeoenvironmental evolution during this interval.

3.5.1. The physiography and geology of the VoP

The VoP, is a broad, elongate, east–west trending valley, bounded to the north by the North York Moors, and to the south by the Yorkshire Wolds (Figure 3.11). The valley extends *ca.* 45-50 km from the coast at Filey in the east, to Helmsley in the west. It has a maximum width of *ca.* 12 km between Malton and Pickering, narrowing eastwards to *ca.* 4 km at Seamer. Along its

central axis, the elevation of the Vale floor declines in the eastern VoP between Filey and Low Marishes (40 to 20 m OD) before steadily rising in the west to Helmsley (20 to 60 m OD). The western end is enclosed by two areas of elevated topography known as the Hambleton Hills, and the Howardian Hills, which are separated by the Coxwold-Gilling Gap, that forms a watershed at and an outflow path into the Vale of York.

The geology of the VoP is composed of three stratigraphic units. The Tabular Hills/Corallian dipslope and the North York Moors, which lie directly to the north of the VoP (Figure 3.12), are formed of a complex sequence of Jurassic calcareous sandstones and limestones, which are termed the Corallian group (Figure 3.12). These hills are incised by a series of short valley forms that are oriented mainly N-S, directly down the dipslope. Of these valleys, only four breach the watershed. Two of these valleys (The Forge Valley and The Mere Valley) have been discussed in association with landform development through the Last Termination in the eVoP. The southern escarpment of the Corallian Dipslope is lithologically controlled by an E-W trending syncline fault in the eVoP, which extends along the valley side. To the south of this feature, Kimmeridge clay mudstones extend across the floor of the valley (Figure 3.12). In the eVoP the Kimmeridge clay is replaced by Speeton clay across a series of faults that trend from E-W and form part of the Hunmanby Fault complex. The presence of these fault lines promotes spring formation in the eVoP (Menuge, 2001; Bearcock *et al.,* 2015). These deposits are overlain by superficial sands, gravels and alluvium in the eVoP, which progressively fine to the west where they consist of sands, silts, and alluvium.

The Yorkshire Wolds are formed of Cretaceous chalk, and comprise a natural escarpment, and southern limit to the VoP. By contrast with the Corallain dipslope to the north of the VoP, the Wolds escarpment is uniform, with very few valley form trending into the VoP. In the central VoP, the chalk escarpment turns southward, and is replaced by Jurassic Limestone of the Howardian Hills. At the transition between these lithologies, there is an embayment leading south to Kirkham Gorge. This embayment presently provides the principal exit for water out of the VoP via the River Derwent.

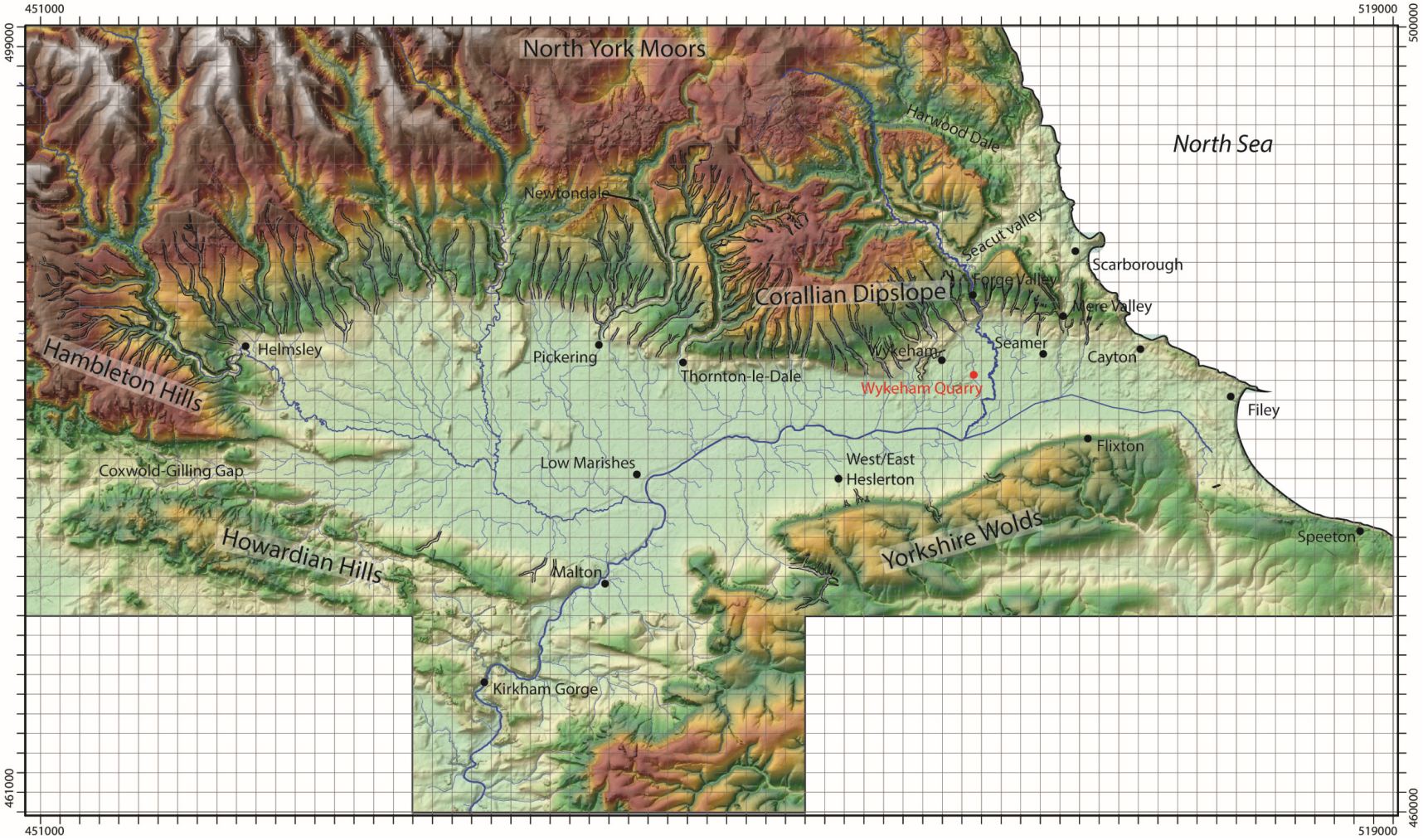

Figure 3.11. *Map of the Vale of Pickering showing the location of key sites mentioned in text. The main contemporary drainage route of the River Derwent is shown flowing into the valley through the Forge Valley in the eVoP, before coming confluent with the River Hertford south of Wykeham Quarry, and the River Rye at Low Marishes. The river drains out of the VoP through the Kirkham Priory gorge in the western VoP.*

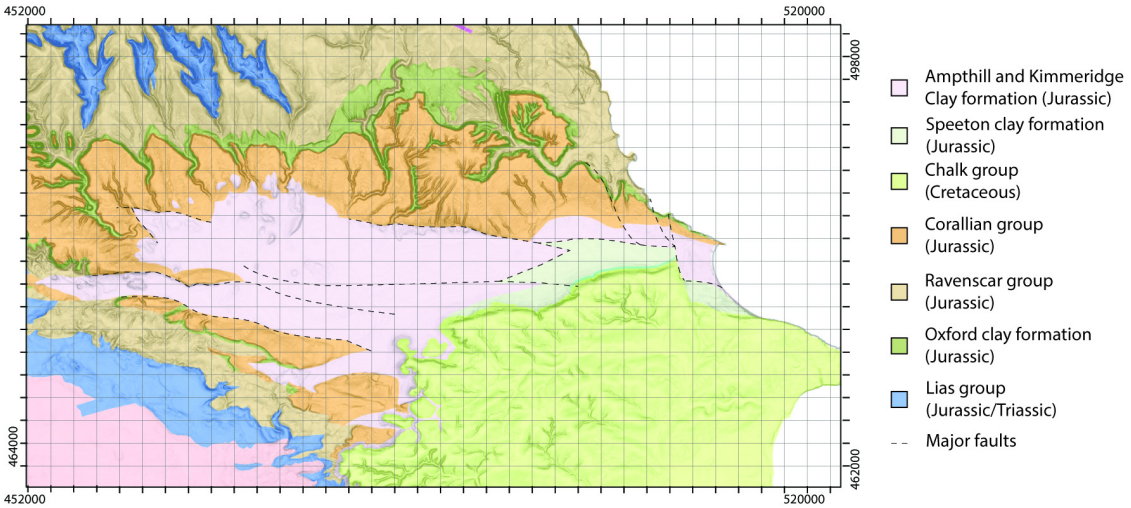

Figure 3.12. *Bedrock geology of the VoP.*

3.5.2. Landscape evolution through the Dimlington Stadial

Landforms associated with glacial activity of the VOYL and the NSIL in the VoP have been mapped extensively (Table 3.1), and have been used to reconstruct phases of ice advance and retreat (Table 3.2). Much of the interpretation of the landscape evolution of the VoP therefore hinges upon the interpretation of the interrelationships between these landforms, in relation to ice advance into the VoP from the NSIL and VOYL (Kendall, 1902; Evans *et al.,* 2016). These interpretations have led to a generally accepted model of a two stage, Late Devensian, ice advance in the eVoP (Penny and Rawson, 1969), Coinciding with these ice advances is evidence for the formation of a proglacial lake, dammed by the two ice lobes and graded to a series of elevations (Kendall, 1902; Evans *et al.,* 2016), for up to 6,000 years (Livingstone *et al.,* 2012; Bateman *et al.,* 2015). Interpretations of these landforms are supported by recent chronological evidence from East Heslerton by Evans *et al.* (2016), and palaeoenvironmental evidence from PF (Day, 1996; Dark, 1998; Candy *et al.,* 2015), which enable the Late Devensian geomorphic evolution of the VoP to be categorised into 5 stages. This model is based principally on the interpretation of the landforms made by Kendall (1902) and Evans *et al.* (2016). These stages (Stage 1-5) are briefly reviewed in the following section, incorporating the interpretations of the landforms in previous research (Tables 3.1 and 3.2 and Figures 3.13-3.14).

***Table 3.1**: Summary table listing previous reports of the geomorphology in the VoP. The landforms described in text derive entirely from these reports.*

Study	Type of mapping	Relevant area covered	Methods	Landforms identified
Kendall (1902)	Descriptions and schematic maps	VoP and Upper Derwent Valleys	Field based mapping	Overflow/meltwater channels, glacial deposits demarked by topography
Kendall and Wroot (1924)	Descriptions of features	eVoP north to Hackness	Field based	Overflow and meltwater channels
Farrington and Mitchell (1951)	Description and schematic mapping	eVoP	Field based mapping	Glacial topography, interpreted as moraines
Penny and Rawson (1969)	Schematic mapping and description	eVoP	Field based mapping	Glacial topography,
Straw (1979)	Schematic mapping and description	eVoP	Unknown	Glacial topography, lacustrine terraces.
Foster (1985)	Sedimentology, schematic mapping, description	VoP and the Yorkshire Wolds	Field based mapping, sediment logging and analysis	Glacial topography, meltwater channels, outwash trains.
Franks (1987)	Sedimentology, field based mapping, description	eVoP and upper Derwent Valleys	Field based mapping , sediment logging and analysis	Glacial topography, meltwater channels, terraces, palaeolakes.
Cloutman (1988a,b)	Auger surveying for subsurface bathymetry, sedimentology,	Western margins of Palaeolake Flixton	Field based augering and sediment description to delineate palaeolake extent and bathymetry	Palaeolake margins.
Palmer *et al.* (2015)	Auger surveying for subsurface bathymetry	Western margins of Palaeolake Flixton	Field based augering and sediment description to delineate palaeolake extent and bathymetry	Bathymetry of glacial deposits, palaeolake margins.
Evans *et al.* (2016)	Remote sensing using NEXTMAP DTM	VoP with specific reference to the western extent	Remote sensing identifying glacially derived sediments and glacial lake outflows	Glacial topography, additional lake overflows
Powell *et al.* (2016)	Sedimentology and remote sensing using NEXTMAP DTM	the western VoP	Sedimentology identifies tills in the western VoP	Pre-Late Devensian glacial deposits

3.5.2.1. Stage 1: Prior to the Last Glacial Maximum (>*ca* 21 cal ka BP)

Landforms relating to activity prior to Late Devensian ice advance are poorly preserved. Reconstructions of the pre-Devensian topography of the VoP from borehole evidence, suggest that the centre of the valley was a topographic depression, as low as -15 m OD, dipping to the east (Edwards, 1978). At this time, the River Derwent flowed eastward either through the Sea Cut Valley (Kendall, 1902; Franks, 1987), or Harwood Dale, and into the Scarborough Bay area (Straw, 1979). Owing to the extensive alteration of the landscape caused by the Late Devensian ice advances (Stages 2 to 3), little else is known about the geomorphology of the eVoP at this time. A series of Kimmeridge clay hills in the western VoP capped by diamicton have been attributed to a plateau icefield in the North York Moors during a glacial event preceding the Dimlington Stadial, possibly during MIS 8 (Powell *et al.,* 2016). These deposits may relate to a similar glacial episode as the Basement Till on the east Yorkshire Coast, but no chronological evidence is available to support these claims. The preservation of these deposits also support the view that the western VoP remained outside the maximum extent of the LGM ice limit (Bowen *et al.,* 2002; Clark *et al.,* 2004).

***Table 3.2**: Summary of the landforms identified by previous workers in the VoP. Each landform is named in relation to local terminology, and correspond to the landforms mapped in Figure 3.13. The previous workers who have interpreted the landform are listed alongside a brief description of the landforms characteristics. The interpretations listed correspond to the generally accepted mode of formation for each landform, which are used for the summary presented in text.*

Landform	Identification	Classification	Interpretation	Alternative interpretation	Active during
Kimmeridge clay hills	Kendall (1902); Edwards (1978)	Isolated hills in the centre of the western VoP, comprised of Kimmeridge clay and till	Pre-Late Devensian tills representing expansion of a plateau icefield in the Tabular Hills (Powell *et al.,* 2016)	Pre-Late Devensian landforms, controlled by fault based uplift	Stage 1
Thornton-le-Dale till	Edwards (1978); Foster (1985); Evans *et al.* (2016)	Undulating topography consisting of a diamicton of various lithologies	Ice terminus of the North Sea Ice Lobe	Formed by glacial activity prior to the Late Devensian	≥Stage 2?
Ampleforth Moraine	Kendall (1902); Straw (1979); Evans *et al.* (2005)	Elevated ridge composed of glacial till, crossing the Coxwold-Gilling Gap	Ice terminus of the Vale of York Ice Lobe		Stage 2
Hutton Buscel terrace	Kendall (1902); Edwards (1978); Franks (1987)	Flat topped, horizontal-gently graded landform (60-70 m OD), perched upon the valley side in the eVoP	Kame terrace formed during the 'Wykeham Stage' when ice stood at the Wykeham		Stage 2
Hunmanby Gap	Evans *et al.* (2016)	Deeply incised valley, through the watershed of the Yorkshire Wolds scarp.	Submarginal spillway, draining the 70 m OD Glacial Lake Pickering during Stage 2		Stage 2
Subglacial, Marginal/Submarginal meltwater channels	Kendall (1902); Edwards (1978); Straw (1979); Foster (1985); Franks (1987)	Channel forms running outside contemporary drainage, obliquely to the valley side, or as misfit features in contemporary systems	Meltwater channels formed underneath or at the margin of a glacier		Stage 2-3?
Hutton Buscel sands and gravels	Franks (1987); Evans *et al.* (2016)	Irregular collection of mounds and ridges, with frequent flat based depressions	Kettle-kame topography (Franks 1987)	Outwash from the Forge Valley forming a deltaic deposit (Fraser *et al.,* 2009)	Stages 2-3
Thorn Park sands and gravels	Franks (1987)	Narrow ridge of sand and gravel, oriented parallel to the a-axis of the Seacut Valley	Glaciolacustrine and glacifluvial sediments, eroded by subglacial meltwater		Stage 2-3

Kirkham Gorge	Kendall (1902);	Deeply incised, sinuous valley, incised through the Howardian Hills watershed	Spillway for the 45 m OD Glacial Lake Pickering, during the Late Devensian	Subglacial meltwater channel formed prior to the Late Devensian (Edwards 1978; Franks 1987)	Stage 2-3
Mere Valley	Kendall (1902)	Deep and wide valley, incised from the eVoP, to the Scarborough Bay.	Pre-existing valley utilised as a meltwater spillway.		Stage 2-3
Forge Valley	Kendall (1902); Franks (1987)	Deeply incised valley through the Corallian DIpslope watershed.	Spillway for Glacial Lake Hackness into the eVoP.	Pre-existing valley utilised as a meltwater conduit through the Corallian Dipslope (Foster 1985)	Stages 2-4?
Glacial Lake Pickering	Kendall (1902); Clark *et al.,* (2004); Evans *et al.* (2016)	Clays spread across the lowlands of the VoP	Ice/moraine dammed, proglacial lake occupying a 70-60, 45 and 30 m OD lake levels		Stages 2-4
Sherburn Sands	Fox-Stragways (1881); Foster (1985); Franks (1987); Evans *et al.* (2016)	Undulating, variably benched deposits 60-25 m OD, across the northern scarp slope of the Yorkshire Wolds	Scarp fed fan deltas, fed by nival runoff from the Yorkshire Wolds (Evans *et al.,* 2016)		Stages 3-4
Seamer sands and gravels	Kendall (1902); Penny and Rawson (1969); Straw (1979); Evans *et al.* (2016)	Low angled-graded deposit of sand and gravel, with hummocky topography at the eastern margin	Ice proximal outwash fan from the Mere Valley, when ice stood in the Seamer vicinity		Stage 3
Flamborough Moraine/Cayton-Speeton Moraine	Kendall (1902); Farrington and Mitchell (1951); Penny and Rawson (1969); Edwards (1978); Foster (1985); Evans *et al.* (2016)	Two tiered diamicton, correlated to the Skipsea till on Holderness	Ice contact landform corresponding to ice positioned in this locality >17.3 ka BP (Evans *et al.,* 2016)	Till cored drumlins formed by ice flow remnants at the 'Cayton-Speeton' Stage retreat (Penny and Rawson 1969)	Stage 3
Palaeolake Flixton	Clark and Godwin (1954); Cloutman (1988a;b); Palmer *et al.* (2015)	Lacustrine sediments in the eVoP	Palaeolake formed within kettle-kame topography in the eVoP, post ice recession from the VoP.		Stage 5

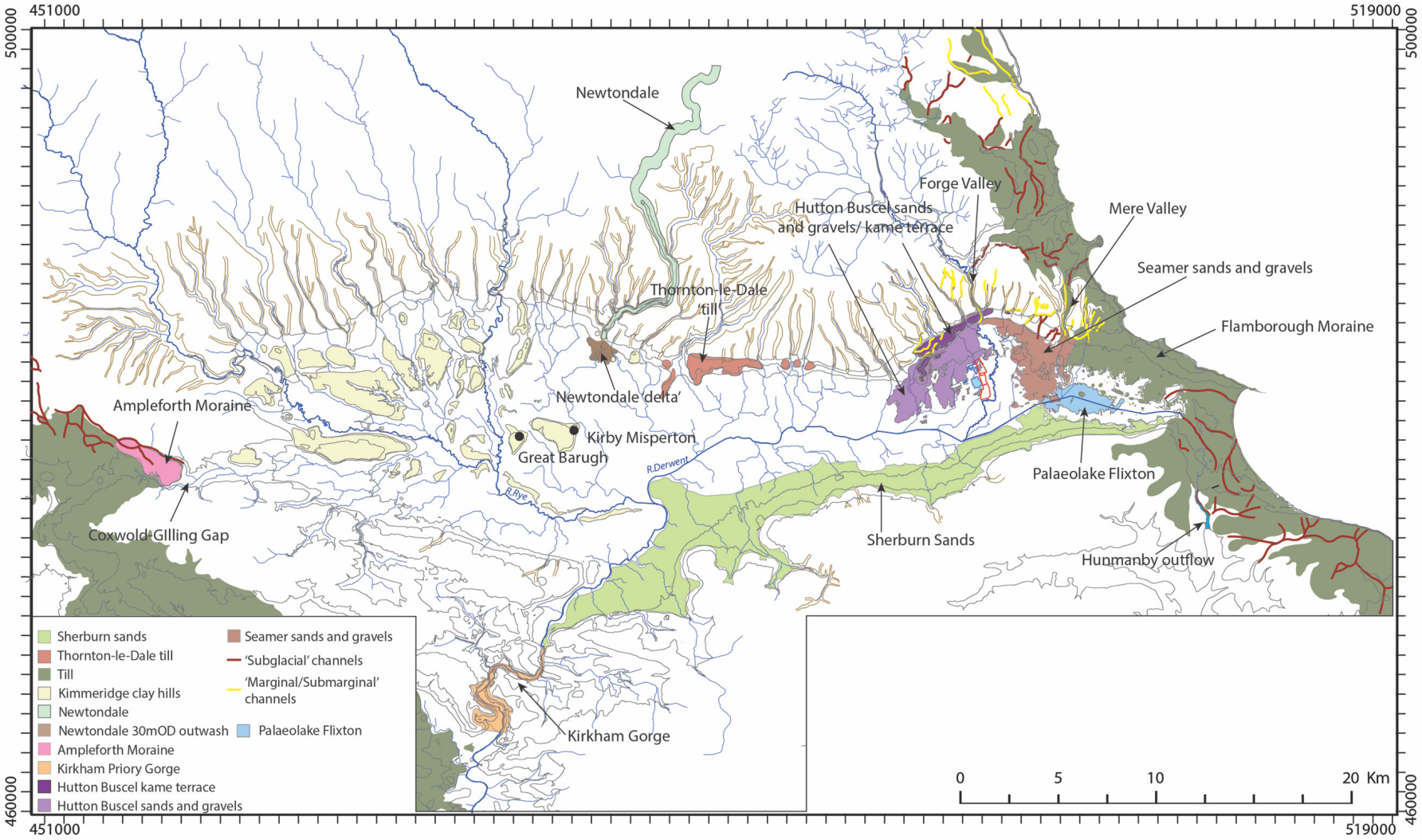

***Figure 3.13**. Summary of landforms identified in the VoP and surrounds associated with geomorphic activity through the Last Termination. Details of these landforms are summarised in Table 3.2.*

3.5.2.2. Stage 2: Ice advance and retreat in Wykeham/Thornton-le-Dale *ca.* 21-18 ka BP

Between *ca.* 21-18ka BP ice advanced to its maximum positions in the VoP, damning outflows and leading to the highest elevation lake levels in Glacial Lake Pickering (Figure 3.14). To the west of the VoP, irregular hummocky topography blocks the Coxwold-Gilling Gap, culminating in a series of raised, linear landforms, and subglacial meltwater channels between Wass and Ampleforth (Kendall and Wroot, 1924), termed the Ampleforth Moraine, (Evans *et al.,* 2005; Figure 3.13). These units can be traced into the Escrick Moraine in the Vale of York and mark an ice advance into the Coxwold-Gilling gap as the VOYL flowed southward down the Vale of York. At this time, ice is also interpreted to have blocked outflows in the Howardian Hills (i.e. at Kirkham), although its terminal position is poorly constrained (Evans *et al.,* 2005).

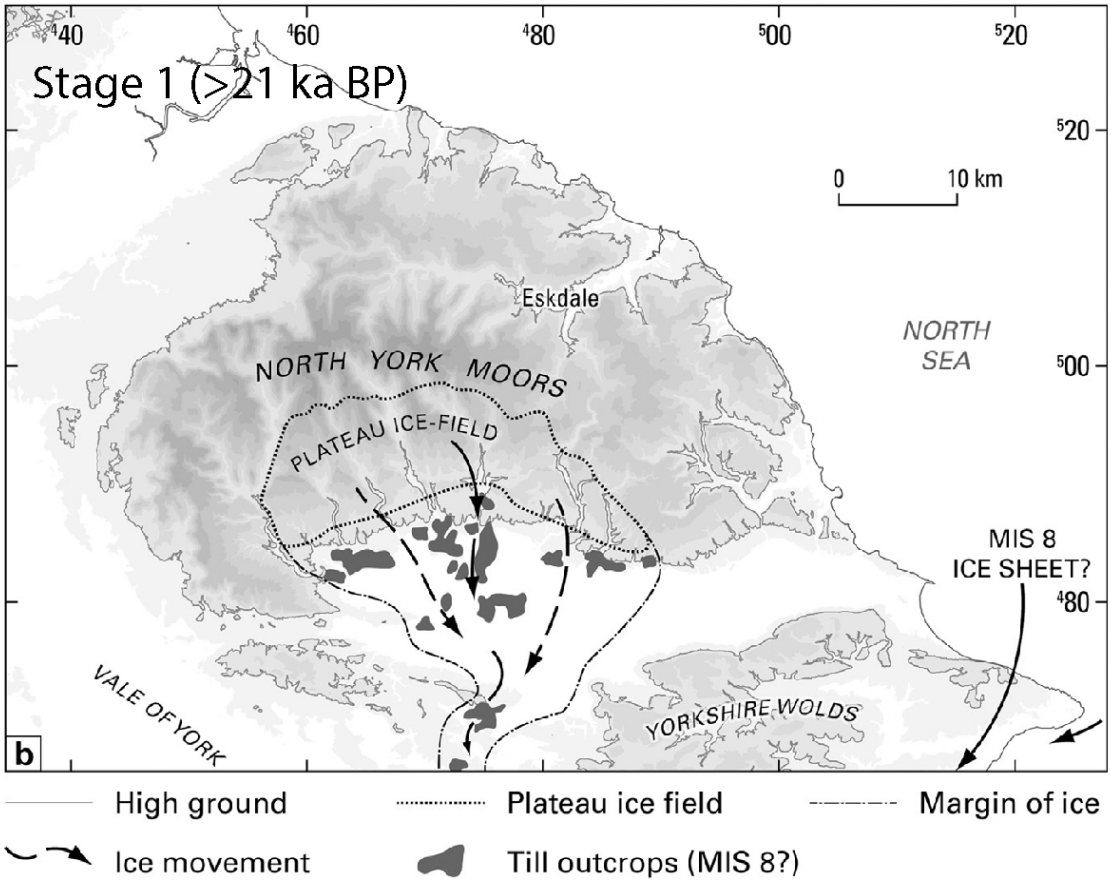

Figure 3.14. *(see next page)*

In the eVoP, the limit of the NSIL is contested. It is accepted to have advanced to at least as far as Wykeham (Kendall, 1902; Straw, 1979; Evans *et al.,* 2016), covering Wykeham Quarry (Figure 3.14). This advance is delimited by the *ca.* 3.5 km long, Hutton Buscel kame terrace. Lateral

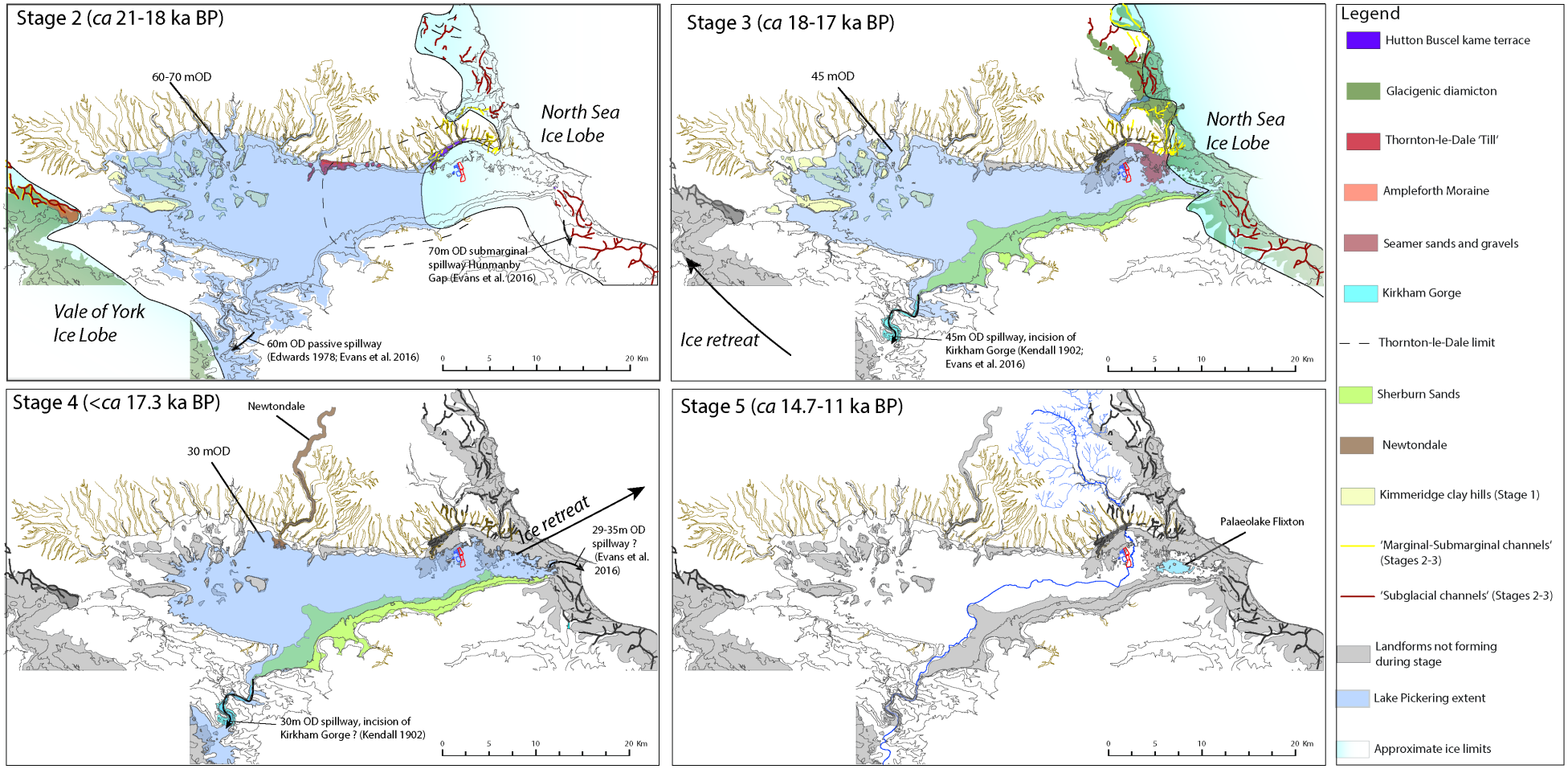

Figure 3.14. *Summary of the landscape evolution of the VoP incorporating the 5-stage model constructed from the landform evidence presented in Table 3.2 and Figure 3.12. Stage 1 follows the model of Powell et al. (2016), invoking the advance of a plateau icefield into the VoP, forming the 'Kimmeridge hills' prior to the Late Devensian ice advance. Stages 2-5 incorporate the landform evidence mapped by the author with lake levels mapped to the contours outlined by previous authors, with the chronological criteria outlined in Bateman et al. (2015) and Evans et al. (2016; Table 3.1). Landforms actively forming, are coloured in each stage, whilst landforms already present, but determined to have ceased active formation are greyed out. From this model it is evident that landforms assigned to Stage 5 (the LGIT) are confined only to PF in the eVoP.*

meltwater channels extend across the terrace surface, suggesting the feature was subaerially exposed, and fed by meltwater emanating from the east (Edwards, 1978; Foster, 1985; Franks, 1987), as well as the Forge/Seacut Valleys (Kendall, 1902; Penny and Rawson, 1969; Franks, 1987). This interpretation is supported by E-W trending, obliquely angled channels graded to similar elevations as the terrace (Kendall, 1902; Edwards, 1978; Franks, 1987), and N-S trending, marginal meltwater channels and Corallian dipslope valleys (Franks, 1987), and the Forge Valley (Kendall, 1902) respectively.

The landform is interpreted by Kendall (1902) and subsequent researchers (Penny and Rawson, 1969; Franks, 1987) as an ice limit, and used to define the 'Wykeham Stage' advance of Penny and Rawson (1969). The elevation of the Hutton Buscel terrace grades to between 68 to 60 m OD, and has been used to infer the altitude of an early stage Glacial Lake Pickering, with estimates ranging between 60-70 m OD (Kendall, 1902; Straw, 1979; Evans *et al.,* 2016). As the Coxwold-Gilling Gap, and the Kirkham area are reconstructed to be inundated by a VOYL ice dam at this time, a highstand *ca.* 70 m OD lake is reconstructed to drain submarginally through an easterly col at Hunmanby by Evans *et al.* (2016). A *ca.* 60 m OD col exists to the east of the present-day Kirkham Gorge (Edwards, 1978), that may have had the potential to drain the lake to the lower base level reconstructed from the Hutton Buscel terrace, provided the VOYL had retreated sufficiently to open this col.

A more westerly limit for the NSIL, in the centre of the VoP is reconstructed from a unit of hummocky topography exposed at Thornton-le-Dale (Edwards, 1978; Foster, 1985), and termed as the Thornton-le-Dale limit by Evans *et al.* (2016). An extreme westerly limit, terminating at Pickering was envisioned by Foster (1985), and proposed using glacial meltwater channels mapped on the Wolds escarpment, coupled with the distribution of the Sherburn sands along the foot of the Wolds slope, which were interpreted as an outwash train. During the remapping of landforms in this project, none of the meltwater channels reported by Foster (1985) were identified, and when coupled with the reinterpretation of the depositional context of the Sherburn sands by Evans *et al.* (2016), leave little supporting evidence for this ice limit remaining. As such, this limit is not considered further. The Thornton-le-Dale limit also remains equivocal without further detailed geomorphic and sedimentological evidence, which is beyond the scope of this thesis.

3.5.2.3. Stage 3: Ice stabilisation to the east of Seamer *ca.* 18-17 ka BP

Subsequent to Stage 2 there is evidence of limited NSIL retreat, reconstructed using geomorphological, and sedimentological evidence for glacial landforms, lake shorelines and fluvial sediments. This retreat is interpreted to be linked to a lowering of Glacial Lake Pickering to *ca.* 45 m OD based upon the graded elevation of an outwash fan delta splaying out across the eVoP

at Seamer (termed as the Seamer sands and gravels by Franks, 1987). These deposits are interpreted to have been formed when ice receded to the east of the Mere Valley (Kendall, 1902). Directly to the east of the Seamer sands and gravels lies further hummocky topography, that can be traced southward to a series of prominent ridges buttressed against the Wolds scarp. These landforms are termed the Flamborough Moraine by Farrington and Mitchell (1951), and represent an ice margin during the 'Cayton-Speeton Stage' (Penny and Rawson, 1969; Straw, 1979). Below the scarp of the Yorkshire Wolds, between Muston and the intake of the Kirkham Gorge, an elongate strip of sediments grading to between *ca.* 60 and 25 m OD are termed the Sherburn Sands by Foster (1985) and Evans *et al.* (2016). Evans *et al.* (2016) interpret these deposits as subaerial, nival fed alluvial fans, which coalesced along the scarp base of the Wolds, when Lake Pickering stood at ≤ 45 m OD.

As outlined above, the lake levels of Glacial Lake Pickering are reconstructed to fall in this stage. For this to occur, the ice dam formed by the VOYL must have receded from the margins of the VoP, to the north of the Escrick Moraine (Bateman *et al.,* 2015), allowing water to outflow via downcutting in the Kirkham Gorge (Edwards, 1978; Evans *et al.,* 2016), to an altitude governed by the elevation of Glacial Lake Humber in the Vale of York, which at this stage was lowering from between 42 to 33 m OD (Fairburn and Bateman, 2016; Figure 3.14). No evidence presently exists either from the VoP or Kirkham Gorge however to substantiate these claims, meaning the link between the two water bodies is poorly resolved.

3.5.2.4. Stage 4: Ice recession from the eastern Vale of Pickering *ca.* <17-14.7 ka BP

Stage 4 represents the evacuation of ice from the eVoP which coincided with a decline in the lake level of Glacial Lake Pickering from 45 to 30 m OD (Kendall, 1902; Figure 3.14). This altitude is derived from the elevation of a gravel delta at the mouth of the Newtondale spillway at Pickering, interpreted as an alluvial fan, graded to the altitude of Glacial Lake Pickering (Kendall, 1902). The lake level decline is presumed to be controlled either by further downcutting in the Kirkham Gorge (Kendall, 1902), or back drainage through a 29-35 m OD spillway in the Flamborough Moraine (Evans *et al.,* 2016), but remains poorly constrained. The timing of ice retreat from the eVoP is tentatively constrained to 17.3 ± 1 ka BP based upon the interpretation presented above (Evans *et al.,* 2016), which broadly coincides with a recession of the NSIL in Northern England (Bateman *et al.,* 2015). The phasing and timing of downcutting in the Kirkham Gorge through this interval is also poorly resolved meaning that the mechanism responsible for incision to its present altitude are insufficiently explained in these models. Further work is therefore required to establish the link between Glacial Lake Pickering and Glacial Lake Humber through Stages 3 and 4.

3.5.2.5. Stage 5: The LGIT, *ca.* 14.7-11 cal ka BP

With the exception of PF, no landforms are attributed to this phase in previous studies meaning the transition between Stages 4-5 is not reconciled. PF was formed as an isolated body of water, within kettle and kame topography in the eVoP (Palmer *et al.,* 2015). At its maximum extent (*ca.* 25 m OD), PF was restricted to the depression existing between the Seamer sands and gravels, and the Flamborough Till, with an outflow to the west of the basin, presumed to flow between the Seamer sands and gravels and the Sherburn sands.

The lack of landforms assigned to Stage 5 arises from: a) a focus primarily upon the glacial evolution of the valley b) any landforms formed post ice-recession are likely to be more subtly expressed in comparison to the glacially derived features formed in Stages 2 to 4, and therefore not identified during previous field based mapping. On present understanding, little connection exists between the glacial landscape in the VoP during the Dimlington Stadial, and the LGIT environments, partly due to poor chronostratigraphic control through this interval, but also due to the lack of identified archives from the valley.

3.5.2.6. Conflicting interpretations

It is acknowledged that this 5-stage model remains equivocal, largely due to ambiguities in the mechanisms controlling the size and drainage of Glacial Lake Pickering (Edwards, 1978; Foster, 1985; Franks, 1987). These conflicting arguments assert Kirkham Gorge was a pre-existing feature, possibly being formed as a subglacial drainage conduit during a glacial episode prior to the Late Devensian (i.e. The Anglian/MIS 12 and/or MIS 10/8; Edwards, 1978; Franks, 1987). This is principally based on: a) the fact that the gorge is incised from an elevation of > 76.2 m OD, meaning erosion cannot be entirely explained by the drainage of a 70 m OD lake, and b) the presence of drainage routes at lower elevations through the Howardian Hills ($\leq$ 60 m OD). This is used to suggest that the lake was never as extensive as that originally envisaged by Kendall (1902).

Additionally, the lack of lacustrine deposits overlying the Kimmeridge clay hills (which lie at altitudes of 30-70 m OD and are interpreted to have formed prior to the Late Devensian) is used by Edwards (1978) to argue that the Late Devensian proglacial lake never reached elevations of 60-70 m OD as envisaged by Kendall (1902) and Evans *et al.* (2016). To resolve these ambiguities, further investigations are required to: a) more accurately map the palaeolake levels of the glacially dammed lake, b) develop more robust sedimentological models of the interaction between the ice masses that dammed the lake. Further analysis of the glaciolacustrine sediments in the centre of the VoP may help in establishing whether the Glacial Lake existed over a longer period of the Late Devensian than current models have established and the extent of this water body. In addition, understanding the sedimentology of the deposits that reflect the

NSIL retreat and fall in lake levels, when the eVoP reverted from a subaqueous to subaerial environment (Stage 4-5 in the model) will be of equal importance to resolving some of these ambiguities.

3.5.3. The LGIT

Lithostratigraphic and palaeoenvironmental records from Palaeolake Flixton

Palaeoenvironmental records from the VoP are monopolised by sedimentary sequences obtained from PF in the eVoP (Moore, 1950; Walker and Godwin, 1954; Cloutman, 1988a; b; Cloutman and Smith, 1988; Day, 1993; Day and Mellars, 1994; Innes, 1994; Day, 1996; Mellars and Dark, 1998; Dark, 2000; Cummins, 2003; Taylor, 2011; Palmer *et al.,* 2015; Candy *et al.,* 2015). Auger surveys across the western extent of PF by Palmer *et al.* (2015), show an undulating bathymetry, consisting of an irregular surface of gravels, interpreted as kettle and kame topography, formed after the recession of the NSIL in Stage 3 (Franks, 1987; Palmer *et al.,* 2015). The basin infill is characterised by four lithofacies (LFA 1-4), consisting of two inorganic units (LFA 1 and 3), indicative of low organic productivity and cold climates, interbedded with silty marls (LFA 2a and 2b) characteristic of stable catchment conditions under temperate climatic regimes (Palmer *et al.,* 2015). This sequence has been interpreted as a 'tripartite sequence', infilling through the LGIT, with LFA 1 correlated to the Dimlington Stadial, LFA 2a to the WI, LFA 3 to the LLS, and LFA 2b to the EH. The lake deposits are capped by humified peat (LFA4 of Palmer *et al.,* 2015), signalling the shallowing, and infilling of the lake, through hydroseral succession, developing fen or carr woodland across the eVoP during the EH (Cloutman, 1988a; b; Cloutman and Smith, 1988; Taylor, 2010). This sedimentary sequence is most readily preserved in the deepest bathymetric depressions of the basin, with shallower sequences containing an incomplete sequence, interpreted to represent changes in lake level through the LGIT (Cloutman, 1988a; b; Palmer *et al.,* 2015). Attempts to date these deposits however has resulted in limited success, with low abundances of terrestrial macrofossils preserved in the deposits (Day, 1996; Mellars and Dark, 1998; Dark *et al.,* 2006). The infill however is confirmed to have been deposited during the LGIT by the presence of the Vedde Ash in LFA 3 (12.02 ± 0.04 cal ka BP; Bronk Ramsey *et al.,* 2015), dating these deposits to the LLS (Palmer *et al.,* 2015).

Palaeoenvironmental signals through the LGIT are constructed principally via pollen assemblages from the PF infill, with specific focus upon the EH (Day, 1996; Dark, 1998; Cummins, 2003). These records show a similar pattern of vegetation succession to those identified in other NE English records (section 3.4.2). This demonstrates that sedimentary sequences in the eVoP have significant potential to record abrupt palaeoclimatic events through the LGIT, but these records have yet to be constructed, and sedimentary sequences from PF do not contain the material viable for constructing robust chronological records through the WI, limiting comparisons to

other regional palaeoclimatic records. Furthermore, whilst the sedimentary sequences from PF have alluded to significant changes in the lake level through the LGIT, potentially linked to changes in climatic regime (Palmer *et al.,* 2015), these changes have yet to be investigated, meaning their link to shifts in the hydrology of the eVoP, and regional hydroclimatic changes (e.g. Rach *et al.,* 2014) are unresolved.

Excavations from Wykeham Quarry to the west of PF, have uncovered a series of fine grained fossiliferous deposits which have been radiocarbon dated to the WI (Fraser *et al.,* 2009; Batchelor, 2009). These sedimentary sequences demonstrate: a) that further sedimentological and geomorphic evidence exists in the eVoP which can aid interpretations on the palaeoclimatic, and palaeoenvironmental evolution of the valley throughout the Last Termination, b) fossiliferous deposits such as those reported from Wykeham Quarry have the potential to circumvent the problem of chronological control on palaeoenvironmental sequences via the dating of preserved plant macrofossil remains (Lowe *et al.,* 2008). The palaeoenvironmental potential of these deposits have yet to be realised, meaning conclusive models of landscape development associated with deposits outside of PF remain equivocal (Fraser *et al.,* 2009).

Human occupation through the LGIT in the VoP

Since the discovery of exceptionally rich, and well-preserved archaeology at Flixton site 1 and Star Carr, by Moore (1950) and Clark (1954), 24 locations around the margins and islands of PF have been found to preserve evidence of Early Mesolithic activity (Taylor, 2011), making the eVoP the most important, and well documented Early Mesolithic site in Britain (Mellars and Dark, 1998; Gonzalez and Huddart, 2002). Further excavations around the palaeolake edge have also identified remains associated with human occupation during the earlier stages of the LGIT (Schadla-Hall, 1987; Conneller and Schadla-Hall, 2003; Conneller, 2007), suggesting that the eVoP was repeatedly utilised by human populations during the WI as well as the EH. In summary, the series of sites around PF can be subdivided into three periods of occupation based upon typological criteria (Conneller, 2007; summarised in Figure 3.15). These are: a) Final Palaeolithic sites at Seamer site K, which record occupation at some time between *ca* 13.8-13cal ka BP (Schadla Hall, 1987; Conneller, 2007) b) Terminal Palaeolithic sites, including a horse butchery site on Flixton Island, with 'Long blade' assemblages (Moore, 1954; Conneller, 2007; Conneller *et al.,* 2016), c) Early Mesolithic occupation at Star Carr which has been extensively radiocarbon dated and tightly chronologically constrained to the EH (Clark, 1954; Mellars and Dark, 1998; Conneller *et al.,* 2016). Much of the palaeoenvironmental work in the valley has therefore been focussed upon providing a palaeoenvironmental context to these remains, particularly with respect to the Early Mesolithic occupation at Star Carr during the EH (e.g. Walker and Godwin, 1954; Cloutman, 1988a; b; Mellars and Dark, 1998; Cummins, 2003; Candy *et al.,* 2015).

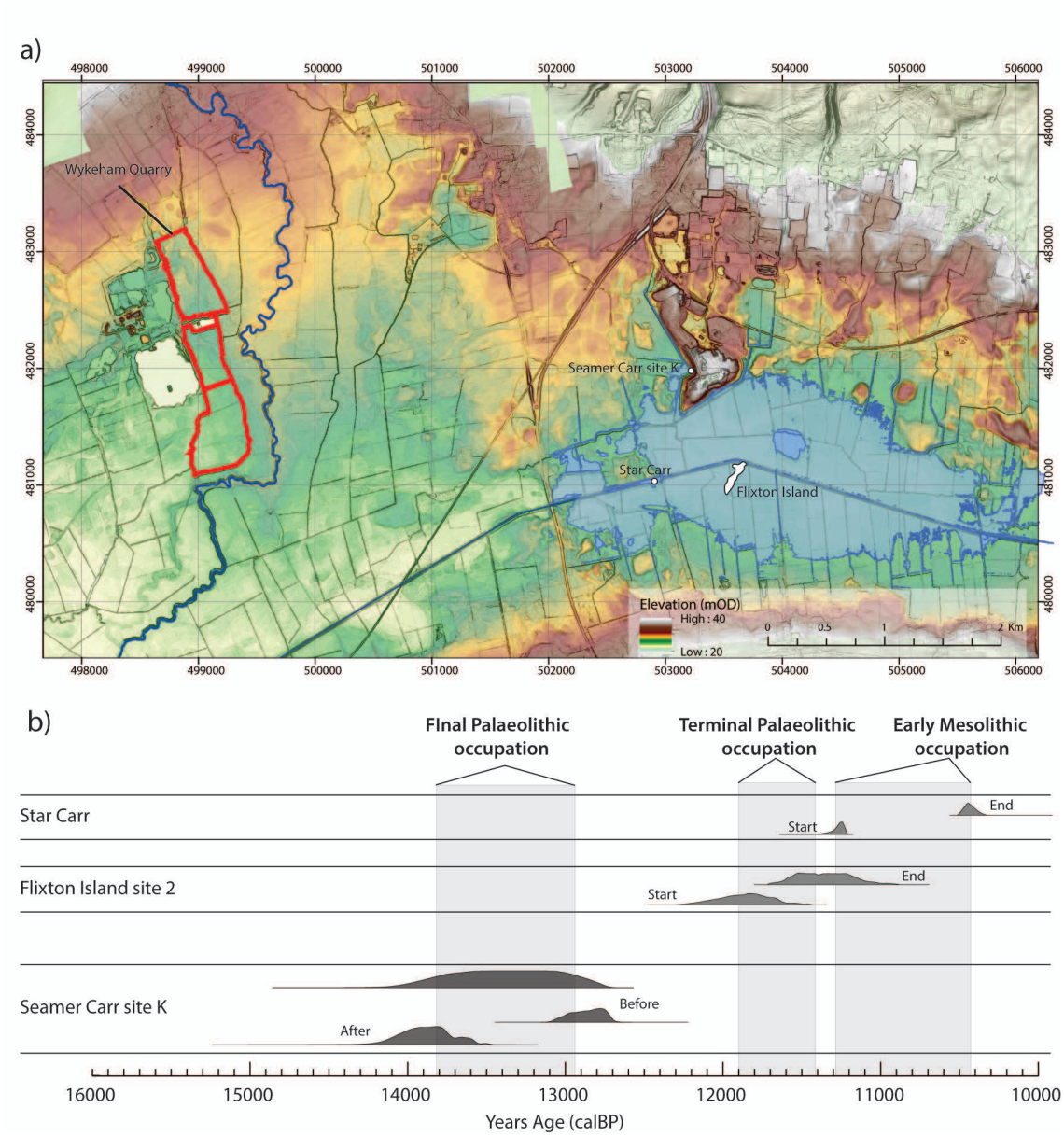

Figure 3.15. *a) Location map of archaeological sites in the eVoP mentioned in text. The mapped extent of Palaeolake Flixton (blue) and the location of Wykeham Quarry are shown for reference. b) Phases of occupation in the eVoP derived from combined radiocarbon ages on archaeological remains (shown as probability density functions) from the Final Palaeolithic at Seamer Carr, the Terminal Palaeolithic at Flixton Island, and the Early Mesolithic at Star Carr. The timing of Final Palaeolithic occupation is derived from the bracketing ages reported in Schadla-Hall (1987), whilst Flixton Island site 2 and Star Carr are from remodelled, and new ages on archaeological remains provided to the author by Alex Bayliss (POSTGLACIAL unpublished data; Conneller 2016).*

3.5.4. The VoP as a site of potential for palaeoenvironmental reconstruction

The geographic position of the VoP has significant potential with which to test previous models of palaeoclimatic evolution in the North Atlantic and surrounds during the Last Termination. The eVoP in particular has potential to obtain high resolution sedimentary records which can be used to reconstruct palaeoclimatic and hydrological regimes through the LGIT which can be directly compared to other regional sequences based upon the following criteria:

First, the advance and retreat of the NSIL in the eVoP through the Dimlington Stadial (Stages 2-4), provides the criteria with which to precondition the landscape for palaeolake formation.

Elsewhere in the lowland areas of northern England, the retreat of the BIIS led to the formation of a topographically irregular landscape, characterised by abundant dead-ice melt-out and palaeochannel incision which developed lake bodies in the topographic depressions through the LGIT (e.g. Livingstone *et al.,* 2010; Bridgland *et al.,* 2011; Chiverrell *et al.,* 2016). The infill of these palaeolake bodies have provided the most readily available sedimentary sources viable for high resolution palaeoenvironmental reconstructions through the LGIT in the British Isles (e.g. Jones *et al.,* 2002; Brooks *et al.,* 2012; Candy *et al.,* 2016). The presence of glacially formed topographic depressions is supported by the presence of PF in the eVoP (Palmer *et al.,* 2015). It is highly likely that further topographic depressions containing LGIT-aged deposits exist in the eVoP, although previous mapping has failed to locate any further palaeolake bodies in the valley, primarily due to a lack of focus upon these landforms.

The presence of fossiliferous deposits at Wykeham Quarry supports this, demonstrating that the eVoP contains sedimentary sequences that can be used to construct robust palaeoenvironmental and chronological records through the LGIT (e.g. Walker *et al.,* 2008; Lohne *et al.,* 2013), which is not possible at PF. Furthermore, the development of macrofossil assemblage data may also be possible, providing records of changes in local vegetation assemblages (Birks, 2003), as well as shifts in hydrological regimes through the LGIT (Digerfeldt, 1988; Magny and Ruffadi, 1995; Bos *et al.,* 2006), which although alluded to in the PF sedimentary sequences, has yet to be adequately reconstructed in NE England.

In summary, the eVoP provides an area of high potential with which to reconstruct chronologically constrained, high resolution multiproxy palaeoenvironmental records stretching through the LGIT. Such records would significantly improve understanding on the development of palaeoclimatic regimes in NE England, as well as the N. Atlantic region during the Last Termination. Uncertainties remain on the timing and mechanism/s responsible for glacial lake drainage in the VoP, most notably the relationship to drainage of Glacial Lake Humber (Fairburn and Bateman, 2016). This consequently affects understanding on the evolution, timing and mechanisms responsible for the evolution of post ice recession environments in the valley (Stages 4 and 5), demonstrating further work is required to improve models of landscape evolution through in the eVoP through the Last Termination.

4. Research Methodology

4.1. Introduction

This chapter describes the research methodologies used to address the aims and objectives of this research project outlined in Chapter 1, and these are split into three primary research phases:

- Phase 1: use GIS-based techniques to re-examine the geomorphic mapping of the VoP in order to supplement our understanding of the regional context to sediment accumulations in the eVoP whilst also identifying landforms formed during the LGIT (section 4.2).
- Phase 2: Understand the sedimentology and stratigraphy of deposits at Wykeham Quarry, to ascertain the context, and timing of sediment accumulation, and to identify sites viable for palaeoenvironmental reconstruction (section 4.3).
- Phase 3: Palaeoenvironmental reconstruction of climatic, geomorphic, and biotic regimes during the LGIT in the eastern VoP (section 4.4).

Phases 1 and 2 were completed to establish and target the preferred palaeoenvironmental sequences within the eVoP, whilst Phase 3 concentrates on palaeoenvironmental reconstruction. In each section a rationale for the use of the chosen methodologies is presented, followed by a description of the analytical tehcnqiue.

4.2. Phase 1: Geomorphic mapping of the VoP

4.2.1. Rationale

Geomorphic mapping of the Vale of Pickering was undertaken to provide regional context to sedimentological and palaeoenvironmental work undertaken in Phases 2 and 3 of this thesis (see section 4.3 and 4.4). As outlined in Chapter 3, the VoP has been directly affected by glacial activity from the British-Irish ice sheet (BIIS) during the Dimlington Stadial (Kendall, 1902; Evans *et al.,* 2016). The use of digital elevation models (DEM) and digital terrain models (DTM) to map glacial geomorphology has shown considerable potential (Clark *et al.,* 2004; Beckenbach *et al.,* 2014; Hardt *et al.,* 2015; Chiverrell *et al.,* 2016) owing to:

a) The ability to cover wide spatial distances at larger spatial scales than field and imagery based studies.
b) The ability to strip away superficial topography, such as vegetation and buildings (DTM), enabling the identification of landforms otherwise hidden in other forms of analysis.
c) A record of absolute elevations enabling quantitative mapping of identified features.

Consequently, using DTMs to map landforms in the VoP, which has had limited application to the Vale to date, has the potential to provide additional detail on the retreat of ice from the VoP during the Last Termination). The use of high-resolution airborne datasets such as, light detection and ranging (LiDAR), and interferometric synthetic aperture radar (IfSAR), also provides potential to identify features such as palaeochannels, and small palaeolakes (Challis, 2006; Jones *et al.,* 2007; Pieńkowski, 2008), formed through the LGIT and viable for palaeoenvironmental analysis (e.g. Marshall *et al.,* 2002; Tolksdorf *et al.,* 2013; Candy *et al.,* 2016).

4.2.2. Assessing the accuracy and precision of LiDAR and NEXTMAP DEMs

Geomorphological mapping for this project utilized two remote sensing datasets, the extents of which are shown in Figure 4.1:

a) 2 m resolution airborne light detection and ranging (LiDAR), digital terrain model (DTM), data for the eVoP and upper Derwent Valleys
b) 5 m resolution interferometric synthetic aperture radar (IfSAR) NEXTMAP DTM data for the areas of the Vale of Pickering not covered by the LiDAR.

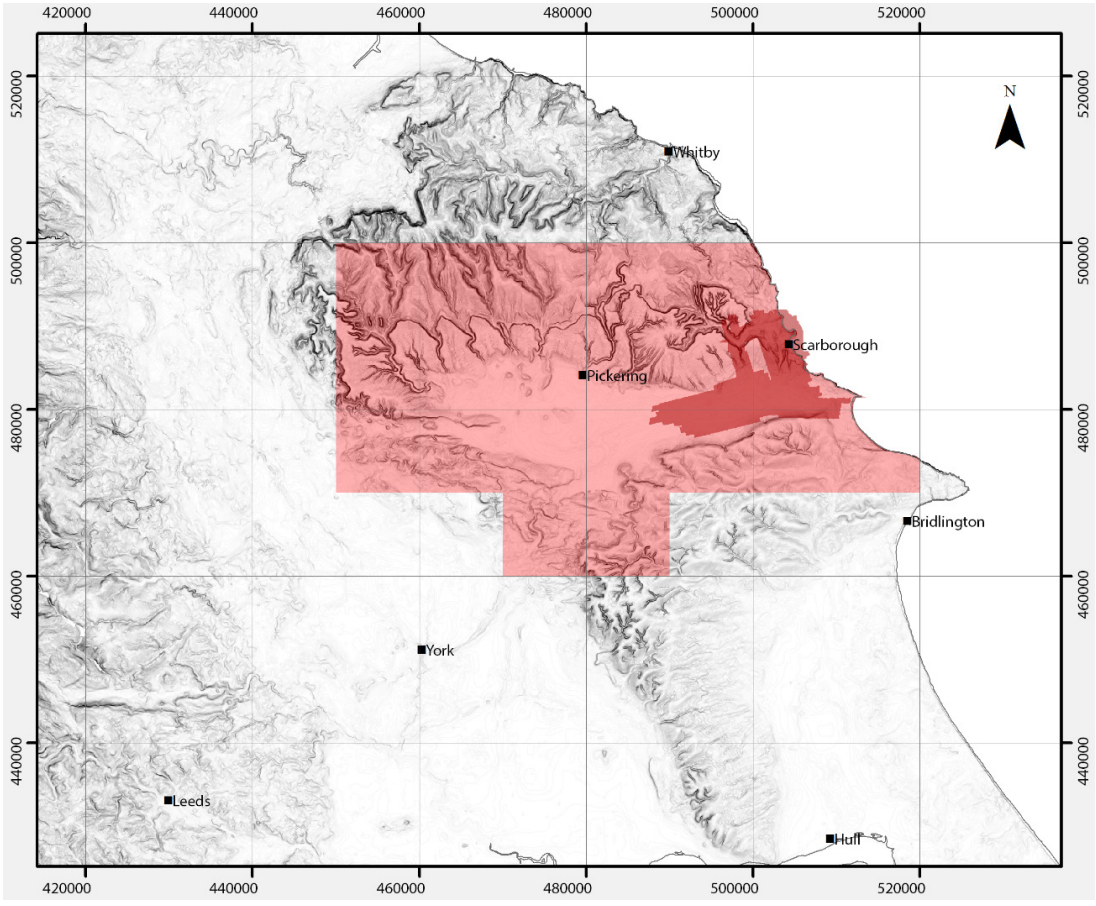

Figure 4.1. *Map showing the spatial extent of the LiDAR (dark red) and NEXTMAP (light red) datasets used in this thesis. The location of major towns (i.e. Scarborough, Pickering and York), and Wykeham Quarry are provided for reference.*

LiDAR data were obtained from the Environment Agency, and obtained using an Optech 2033 airborne laser terrain mapper (ALTM) flying at *ca.* 800 m OD with a surveying swathe width of *ca.* 600 m (Holden, 2004) processed to WGS84 projection and transformed to the British National Grid with elevation points in the OSGB36 datum. The NEXTMAP DTM was acquired from Intermap Technologies, and collected between 2002 and 2003, using airborne IfSAR with a 5 m post spacing, producing a quoted vertical root mean square error (RMSE) of 1 m (Intermap Technologies, 2007).

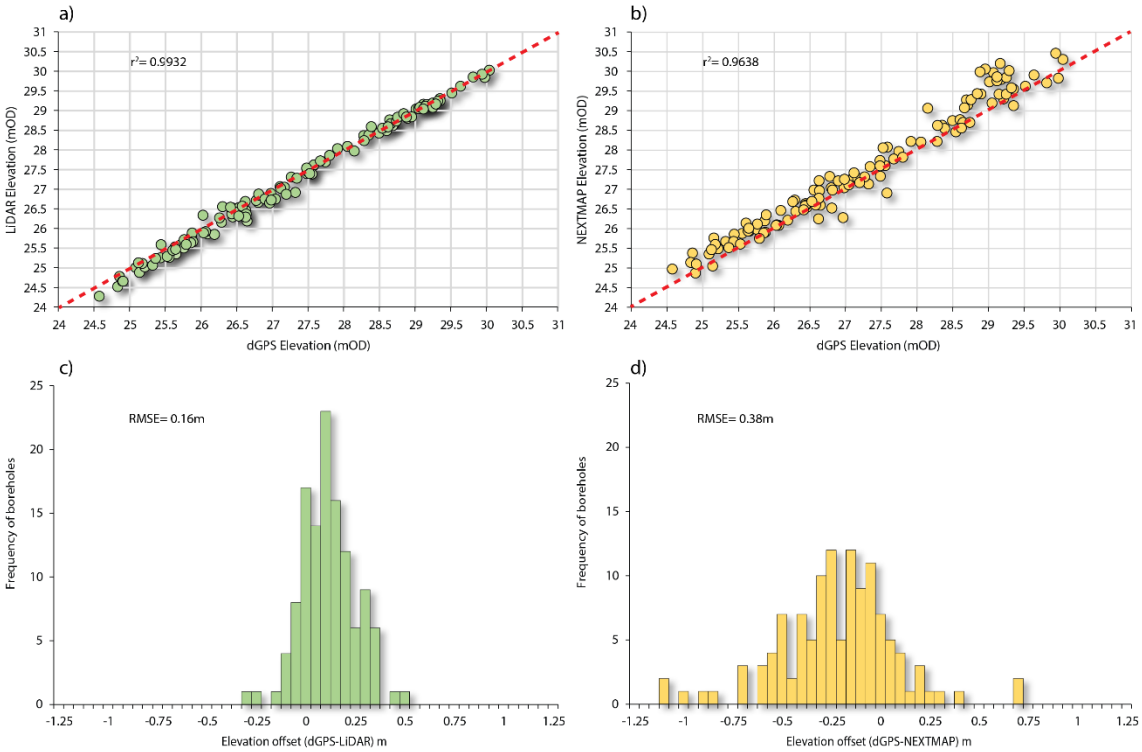

Figure 4.2. *Plots used to assess the accuracy of the GIS dataset elevations in relation to field measured dGPS measurements of the Hanson Borehole dataset at Wykeham Quarry. a) and b) scatter plots of the dGPS elevations of the Hanson Borehole dataset, plotted against the LiDAR (green) and NEXTMAP (yellow) derived elevations respectively. The red dotted line on each plot represents the 1:1 relationship. c) and d) are frequency plot histograms, representing of the offset of the LiDAR, and NEXTMAP derived elevations in relation to the dGPS measurements. The x axis for each plot is divided into 5 cm bins, with the frequency of boreholes falling within the error offset plotted on the y axis. Root mean square errors (RMSE) in the dataset are also presented.*

The accuracy of the LiDAR and NEXTMAP DTMs were tested against differential Global Positioning Satellite (dGPS) derived elevations of 114 boreholes from Wykeham Quarry, made available by Hanson Aggregates (section 4.3.2). dGPS measurements on these boreholes have a reported X,Y,Z accuracy of ± 0.02 to 0.03 m (Hanson pers. comm.), allowing GIS derived elevation values to be tested against the true landscape elevation. The LiDAR DTM-derived elevation of each borehole was compared to the field derived elevation (Figure 4.2). Where the land surface elevation had substantially changed between borehole extraction and LiDAR/NEXTMAP sampling, samples were removed (e.g. H-1992 18, 19 and 20 lie in areas quarried between 1992 and 2004). High correspondence was found between the LiDAR and

dGPS-derived elevations for the boreholes (r^2= 0.99, RMSE= 0.12 m), suggesting that the LiDAR derived elevations for the eVoP were on average, accurate with the dGPS measurements to ± 0.12 m (section 4.3.2, for raw data see Appendix A.).

The correspondence between the NEXTMAP and dGPS derived elevations was similarly high (r^2= 0.96), but with consistently larger offsets than the LiDAR (RMSE= 0.38 m; Figure 4.2). Therefore, the LiDAR DTM was used preferentially to the NEXTMAP DTM to assign elevations to mapped geomorphic landforms (section 4.2.3) and sedimentary deposits (see section 4.3.2), due to its higher X and Y resolution (2 m) and its more accurate derivation of Z values (± 0.12 m) for the eVoP.

4.2.3. Identifying landforms from DTMs

Manipulating remotely sensed data in ArcGIS enabled different types of raster surface to be displayed. These are summarized in Table 4.1. Combinations of these raster surfaces were used to map landforms, based upon the characteristics of the landform, and the capability of the raster surface to identify these features see Figures 4.3a-d. To visualize landform characteristics, output raster values for each raster surface were displayed in two ways: a) stretched values, and, b) classified values.

Table 4.1. *Summary table of the LiDAR/NEXTMAP raster surfaces used to map geomorphic landforms.*

Raster surface	Value definition	Description	Display grouping
Digital elevation model (DEM)	Elevation in metres above datum (m OD)	Identifies the elevation of a land surface. A DEM can be viewed either as unfiltered (Digital Surface Model DSM) or filtered, removing objects that extrude above terrain height, creating a 'bare land surface' (Digital Terrain Model DTM). For this work, a filtered DTM raster was used to map geomorphic landforms.	Classification
Slope	Degrees: 0°- flat slope 90°- vertical slope	Identifies the maximum elevation change between each grid cell to its neighbors (within a 3x3 cell grid). A higher the slope value therefore represents a steeper slope.	Stretched
Aspect	The raster surface values are recorded in compass direction in relation to North: e.g East facing= 90°	Identifies the downslope direction of the maximum rate of change in elevation value from each grid cell to its neighbors. The aspect raster surface therefore represents the direction of slope on a surface.	Classification
Hillshade	Shadow and light are displayed as shades of grey associated with integers from 0 to 255 (increasing from black to white)	Calculates a hypothetical illumination of a surface based on variation of relief, slope and aspect in relation to a light source (representative of the sun) set at a defined azimuth and altitude. This raster surface is used primarily as an overlay to the DEM to enhance visual output.	Stretched

Stretching assigns a continuous colour scale across the values of the entire raster dataset, which is stretched using statistical properties of the raster Z values to increase visual contrast. Stretching provides a means of covering a dataset with large ranges and displays continuous variations (e.g. hillshade raster surfaces). Classification enables the manual definition of class intervals into an ordinal range, assigning raster surface values into groups assigned by the user. The size interval of these groups was altered to span a varying range of intervals that are differentiated by a colour scale. This enabled increased control and precision when mapping subtle changes in raster surface values of geomorphic features such as palaeochannels, or features with a preferred orientation/ aspect. As such, the classification setting of the raster surface was used for the DEM raster surface when mapping geomorphic landforms.

Four types of landform were classified and mapped in this study: positive relief glacial topography (principally glacifluvial sands and gravels), palaeolake basins, meltwater channels, floodplain palaeochannels, glacially incised valleys and river/lake terraces. Topographic and spatial characteristics for each type of landform were classified prior to mapping, which provides criteria to identify and delineate features from the LiDAR and NEXTMAP datasets (Table 4.2; Figures 4.3a-d). Landforms were mapped as polygon/polyline shapefiles in ArcGIS.

Supplementary information in the form of aerial imagery and superficial geological maps were used to validate mapped landforms (Figure 4.3a-b; d). The raster datasets were overlain by aerial imagery from the Bing maps aerial imagery service (image resolution at 30 cm) for the eVoP. This provided a means to map landforms, particularly subtle features in the base of the valleys where the relative change in topography or slope was minimal (e.g. palaeochannels, former lake basins). The extent of palaeobasins, identified from the DTMs was corroborated by cropmarks in agrarian fields, indicative of a change in the underlying sediment (Figure 4.3b). Both the aerial imagery and the LiDAR mapping criteria are used to identify the majority of palaeochannels in the central VoP but a small number could only be delineated using a single dataset. Mapping the palaeochannels through a combination of aerial imagery and LiDAR therefore increased the potential of identifying landforms (Figure 4.3d). A 1:50000 map of the superficial geology from the British Geological Survey (BGS) was used when mapping positive topographic relief, to provide a sedimentological reference for elevated areas and also to provide a guide when accurate delineation of feature margins were difficult to identify (Figure 4.3a-d). Terrace mapping was undertaken following the method outlined in Figure 4.3c. To test the methods with potential to identify terrace forms, a trial was performed upon the well-established Hutton Buscel kame terrace, in the eVoP. The elevation of this landform is well constrained, and has repeatedly been used to reconstruct the elevation of Glacial Lake Pickering to between 60-70 m OD during Stage 2 (Kendall, 1902; Straw, 1979; Evans *et al.,* 2016; Figure 3.10). Clusters of terrace elevations were identified between 62 and 64 m OD, with secondary peaks identified between 67 and

Table 4.2. *Summary of the geomorphic landforms mapped in this study. The table includes a brief description of each type of landform, their morphology, and potential uncertainties encountered when mapping.*

Landform	Description of feature	Reasons for mapping	Datasets used	Shapefiles	Morphology	Uncertainties
Glacial sands and gravels and lineations	Sand and gravel complexes formed as a result of ice presence in proglacial, subglacial, and englacial environments. Landforms include kettle- kame units, glaciofluvial gravels, and lineations	Can be used to reconstruct landscape evolution of the VoP. Areas of potential for palaeobasins required for palaeoenvironmental reconstruction.	LiDAR/NEXTMAP DTM, Aspect Hillshade, Slope, BGS 1:50000.	Polygons and polylines	Comprised of laterally continuous areas of undulating topography, with irregular hills and hollows. Outcrops lie above the fine grained alluvium of the valley bases *ca.*>26 m OD.	Deposits span large areas, modified by postglacial sedimentation or anthropogenic activity, making it difficult to precisely define maximum limits for the deposits.
Palaeolake basins	Hollows in the glacial sediment complexes formed either by river channel avulsion (*see below*), or as a remnant of dead ice melt.	Sites with potential for palaeoenvironmental reconstruction through the Last Termination	LiDAR/NEXTMAP DTM & Hillshade, Aerial Imagery	Polygons	Topographic depression within glacial sediments, constrained on all sides by elevated topography, characterised by flat surfaces, suggestive of infill by lacustrine sediments and peat.	Hard to accurately map the full extent of palaeobasins on aerial imagery and LiDAR alone. Unclear how deep or expansive features may be without detailed field excavations.
Palaeochannels	Abandoned river channels formed by previous fluvial activity .	Can be used to reconstruct phases of fluvial activity through the Last Termination and provide potential sites for palaeoenvironmental reconstruction	LiDAR, DTM,& Hillshade, Slope, Aerial Imagery	Polygons	Sinuous-straight, linear depressions subtly depressed in relation to the surrounding landscape.	Channels are picked out on very subtle changes in the landscape, which may not be laterally continuous, meaning some channels may be either partially mapped, or missed entirely.
Terraces	Bench or step on the side of a valley or above a river floodplain, representing a former level of the valley floor prior to river incision or the former elevation of a palaeolake.	Can be used to reconstruct phases of fluvial activity, as well as former glacial lake limits	LiDAR/NEXTMAP DTM, Slope, Aerial Imagery, BGS 1:50000.	Polygons	Breaks in slope running parallel to the valley side, above contemporary lake or river elevations.	Decline in slope on valley sides may be geologically or anthropogenically controlled. Detailed field investigations would be needed to verify their classification as terraces.

a) Positive glacial topography

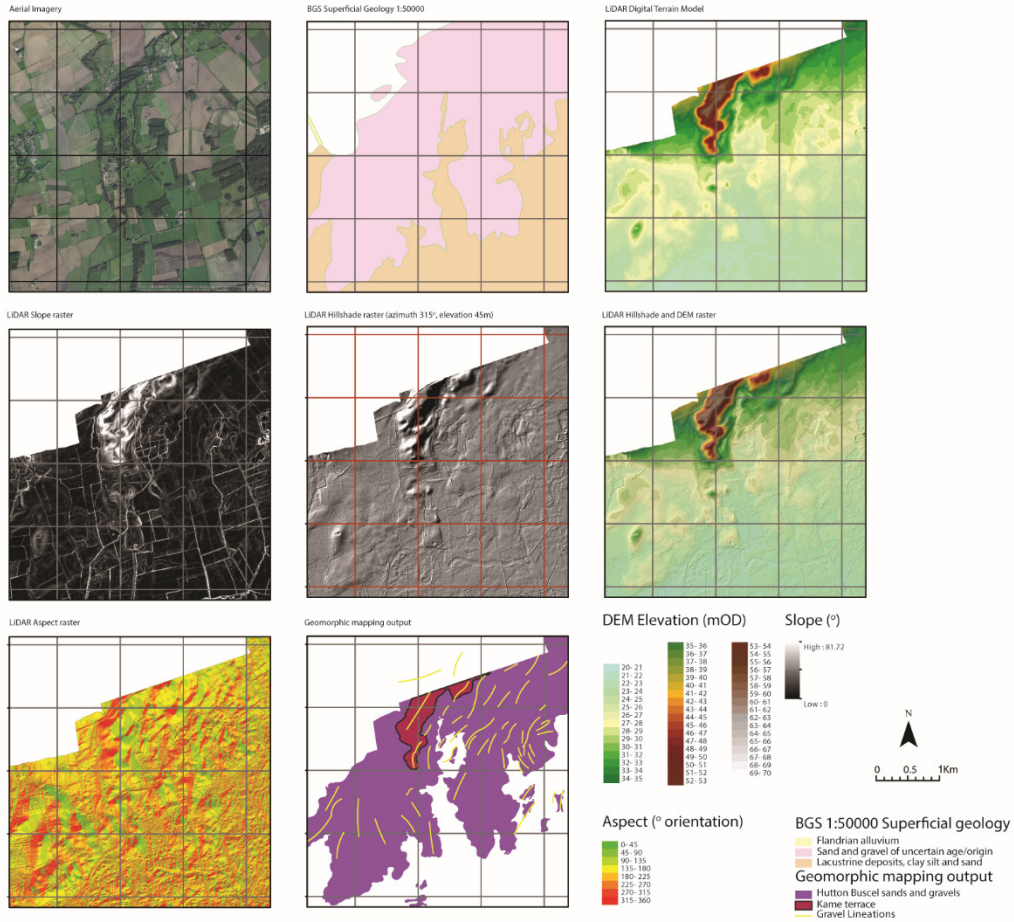

b) Potential palaeolake basins

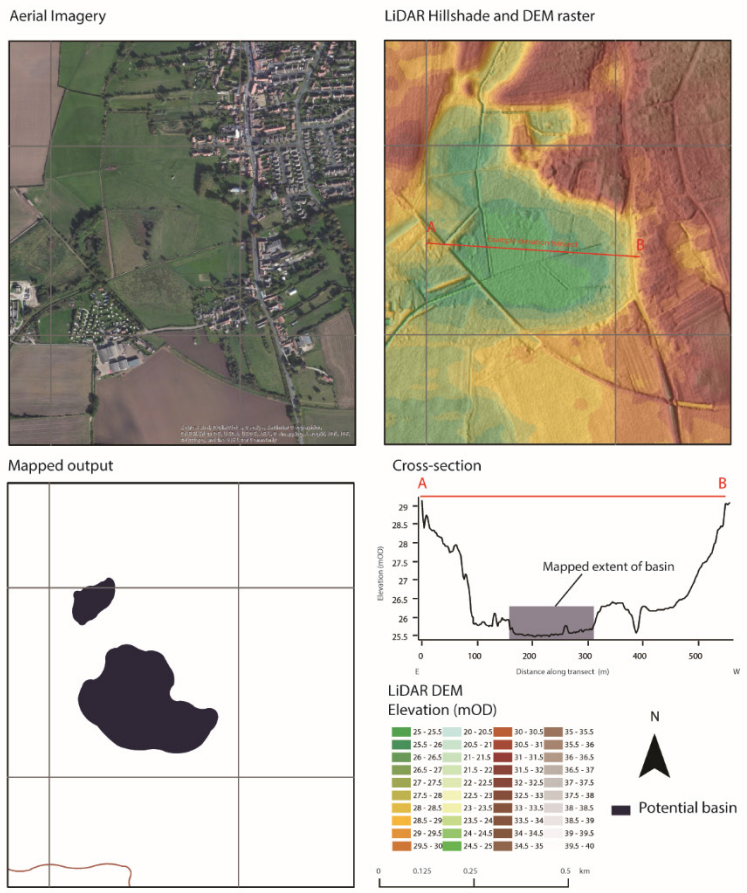

c) Terraces

1) Slope map for section of the eVoP

2) Classified cells with slope (degree) values of 0-1%

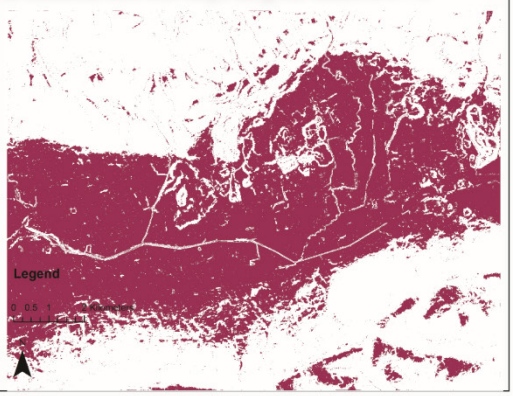

3) Plot cumulative graph of cells with slope values of 0-1% against at elevation to identify clusters

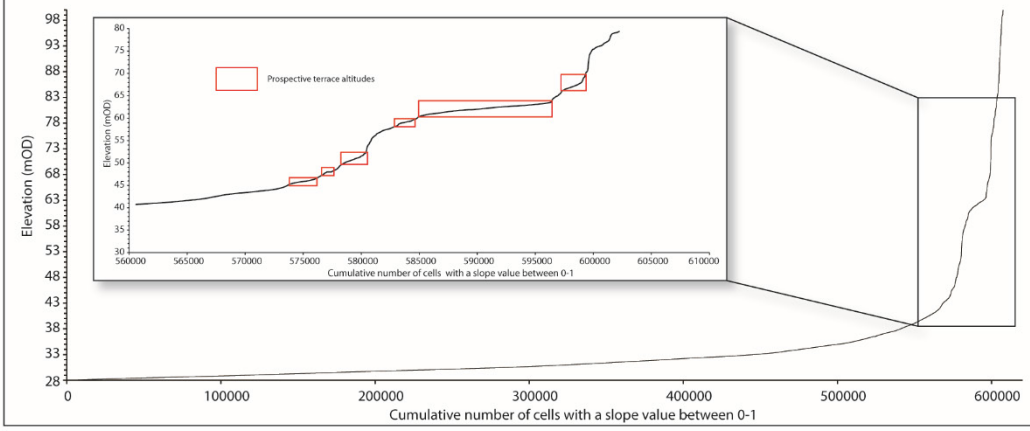

4) Draw contours on map at identified elevations in graph to investigate their potential as terraces

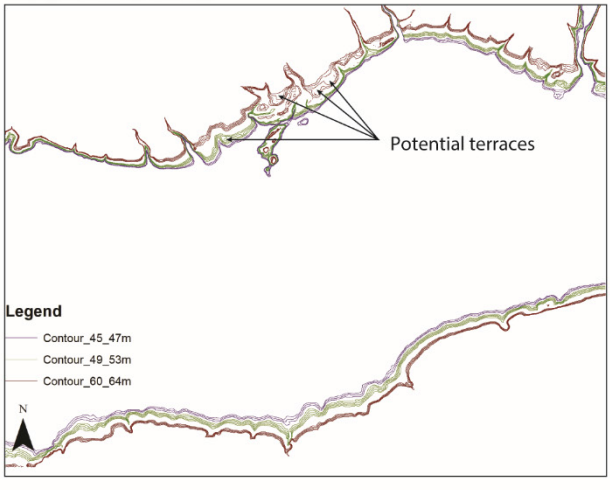

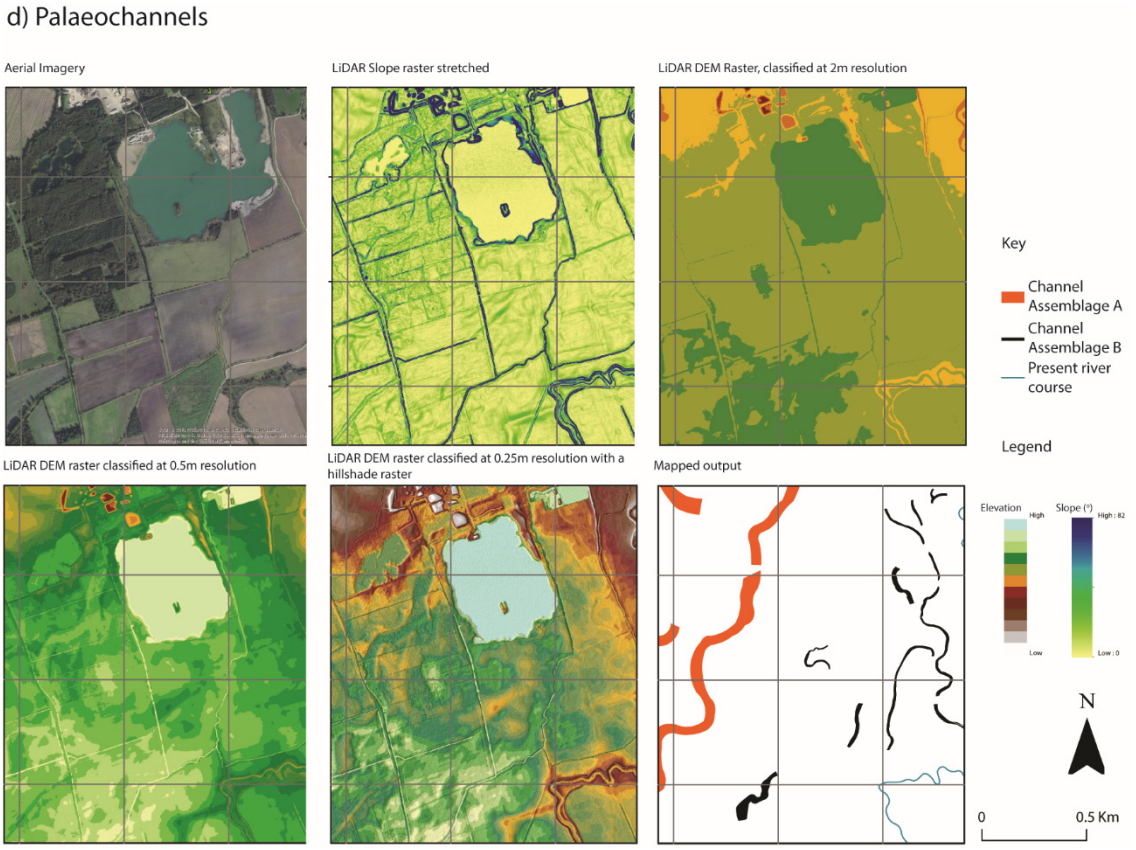

Figure 4.3. *Summary of the methods used to map landforms in the VoP via GIS DTMs.* ***a)*** *group of images from the same spatial plain showing the seven dataset outputs used to map the glacial topography. These datasets were used to best express subtle changes in positive relief, as well as linear trending features such as topographic ridges* ***b)*** *palaeolake basins were mapped using a combination of hillshade/slope and DEMs to identify level, flat areas showing potential of infill via water and/or peat. This was supplemented by aerial imagery which was used to identify changes in soil colouration and texture, potentially indicating wet conditions and peat development.* ***c)*** *Terraces were mapped using the extraction of low cell slope elevations to identify clusters of low slope values at specific elevations. Slope raster values were classified between 0-1° (indicative of flat surfaces depicted in 1) and 2). The elevation of these cells were extracted from the DTM, and plotted in Excel to identify elevation clusters (3). These graphs represent clusters of flat surfaces present at specific elevations in the valley which may represent terrace surfaces formed either by fluvial or glaciolacustrine activity. The elevation ranges of these low slope value clusters were plotted back onto the DTM to investigate their potential as terrace features (4).* ***d)*** *palaeochannels were mapped using a combination of aerial imagery, LiDAR Slope raster surfaces, and various classifications of DTM raster surfaces, ranging from 2 m resolution to 0.25 m overlain with hillshade surfaces. This identification technique optimised the potential to identify subtle palaeochannels, as well as larger, incised conduits.*

69 m OD, and *ca.* 65 m OD across the terrace surface. These results are identical to the findings of Kendall (1902) and Franks (1987), demonstrating that this method is able to confidently reproduce the elevation of landscape terraces identified via field based mapping. Areas of further potential for terrace formation were identified on the basis of the 5 stage landscape model of the VoP outlined in Chapter 3, and mapped following the same criteria as that performed on the Hutton Buscel kame terrace. All landforms were validated and mapped based upon the descriptions reported above, and are summarised in Table 4.2. The results of the geomorphic mapping are presented in Chapter 5.

4.3. Phase 2: Sedimentology and stratigraphy of the Wykeham Quarry deposits

4.3.1. Rationale

To develop an understanding of the nature and spatial extent of sediment deposition in Wykeham Quarry, and prospect sites for further palaeoenvironmental analysis, a modelling exercise was undertaken. Previous geomorphological and sedimentological analyses in the eVoP suggest that two distinct lithofacies are present in the area (Fraser *et al.,* 2009). These are:

a) Sediment units considered to be of glacifluvial origin, laid down during the Dimlington Stadial (Franks 1987; Palmer *et al.,* 2015; Evans *et al.,* 2016), termed as the Lower and upper gravels and the Interburden.
b) Complex sequences of fine grained sediments deposited on the floodplain of the River Derwent through the LGIT (Fraser *et al.,* 2009; Batchelor, 2009; Cloutman *et al.,* 2010). These deposits are collectively termed as the Overburden.

In order to identify sequences viable for palaeoenvironmental reconstructions, a model of the sedimentary characteristics and spatial extent in the quarry area was produced. This was necessary as a variety of different depositional environments could be preserved within the quarry sediments, covering different temporal and spatial extents, meaning further interrogation of the sedimentary sequences was required before selecting sedimentary sequences viable for palaeoenvironmental reconstruction.

4.3.2. Constructing the Wykeham Quarry stratigraphy

4.3.2.1. Data sources

Stratigraphic information previously recorded from the quarry is comprised of two types of dataset:

a) Field sediment logs from open sediment faces exposed during aggregate excavation between 2004-2013, by Northern Archaeological Associates (NAA), summarised in Fraser *et al.* (2009), and this project (Figure 4.4).
a) Stratigraphic data from boreholes excavated between 1992 and 2015 (Hanson, *pers comm*; Batchelor, 2009; this project; Table 4.3; Figure 4.4).

The borehole records, consist of six surveys that extracted a total of 244 boreholes from Wykeham Quarry and its surrounds (Table 4.3; Figure 4.4). Four of the surveys (Hanson-1992, Hanson-1997, Hanson-2007, and Hanson 2015), totalling 112 boreholes, were conducted by Hanson Aggregates, as a means to map the bathymetry of aggregate deposits for prospective

quarry expansion. The X, Y and Z coordinates of these boreholes were measured using dGPS, with an accuracy of ± 0.02 to 0.03 m (section 4.2.2).

***Table 4.3**. Summary of the borehole datasets used to construct the depositional model of deposits at Wykeham Quarry. Abbreviated locations in the quarry are as follows: Northern Extension (NE), Southern Extension (SE), Present Quarry (PQ).*

Dataset	Number of Boreholes	Degree of stratigraphic description	Location within Quarry
RHUL Boreholes	63	Detailed	NE
QUEST BHN	71	Detailed	NE
QUEST BHS	43	Detailed	SE
Hanson 2015	8	Basic	NE
Hanson 2007	53	Basic	NE and east of NE
Hanson 1997	28	Basic	NE
Hanson 1992	49	Basic	PQ and SE

Two other surveys conducted by Quaternary Scientific (QUEST) from the University of Reading were undertaken between 2007 and 2009 and focussed on the Northern (QUEST BHN, 71 boreholes) and Southern (QUEST BHS, 43 boreholes) Extension areas of the quarry (Batchelor, 2009). These surveys were undertaken to ascertain the thickness and characteristics of sedimentary units contained within the Overburden, and to identify areas of archaeological potential similar to the marshlands and lake shorelines of PF. X, Y, and Z coordinates of these boreholes were calculated using a total station measurements that were calibrated to a known spot height. These boreholes are spaced between 25 to 50 m in the Northern Extension, and 50 to 100 m in the Southern Extension and were logged until persistent coarse grained, unconsolidated sediments were recorded. Sediments were described using standard field logging techniques, characterising the physical properties, composition, and boundaries of identified units (Batchelor, 2009).

4.3.2.2. Assessing the reliability of borehole datasets

The construction of depositional models from Wykeham Quarry relied upon: a) the accurate measurement of the X, Y and Z coordinates of sedimentary sequences b) the exact description of lithofacies from sequences.

Field derived elevations for the Hanson borehole dataset has a reported accuracy of ± 0.02 to 0.03 m (section 4.2.2). The accuracy of the QUEST BHN and QUEST BHS datasets, was assessed by comparing the reported elevation of each borehole to the LiDAR derived elevations, calculated in this study (Figure 4.5). The reported elevations for the 43 boreholes in the QUEST BHS dataset showed a good correspondence with the LiDAR derived elevations (r^2=0.7269,

RMSE=0.20 m), suggesting the derived elevations were sufficiently accurate to use in the deposition model (Table 4.4).

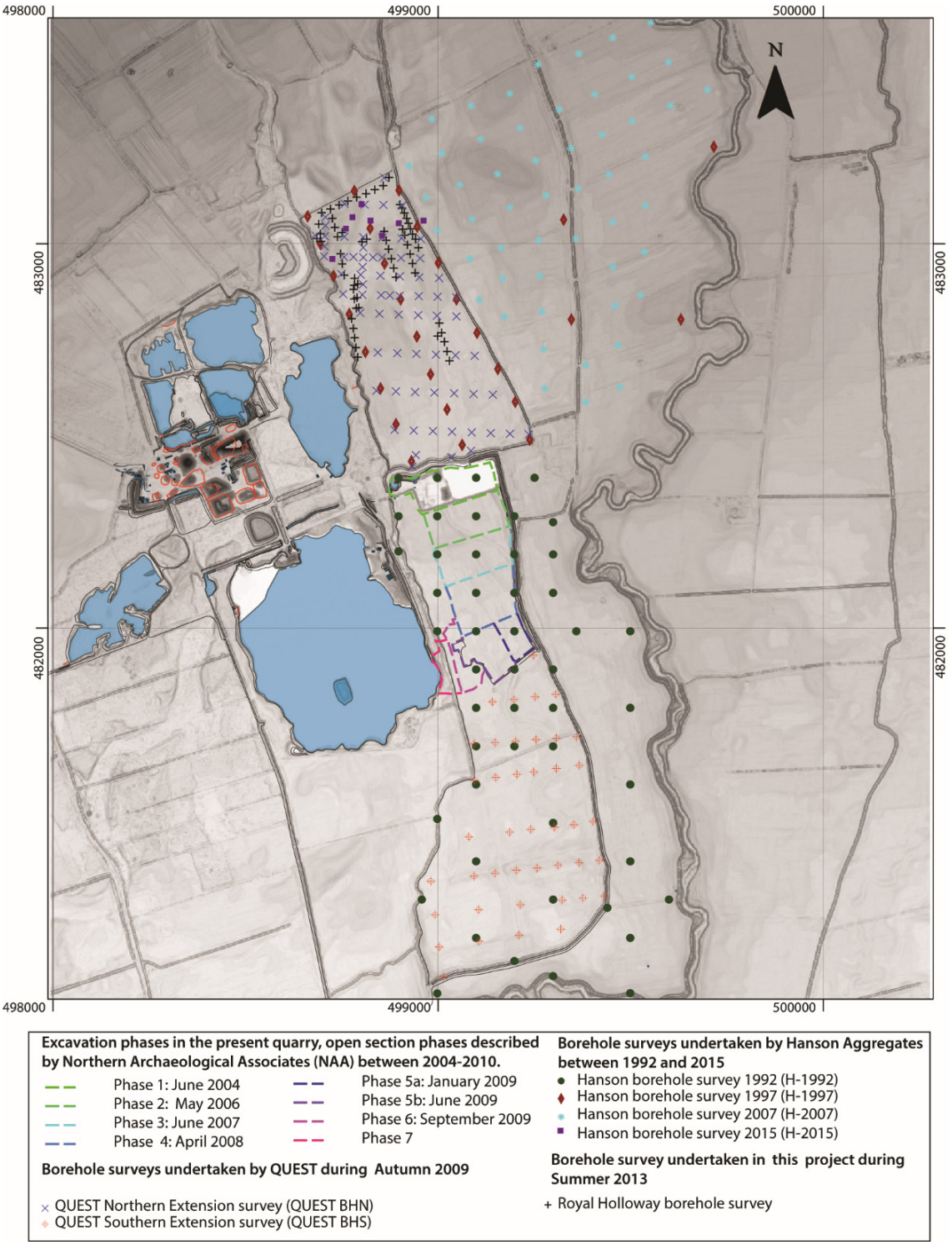

Figure 4.4. *Map of Wykeham Quarry, showing the location of open sections described in the NAA reports (Fraser et al., 2009; Cloutman et al., 2010), and borehole surveys (H-1992, H-1997, H-2007, H-2015, QUEST BHN, QUEST BHS, and RHUL), which were used to construct the deposition model of deposits at the site. The location of field outlines (black lines), marking the extent of the present quarry, Northern and Southern Extension areas, lakes (blue shading), and buildings (red outlines), associated with Wykeham Quarry, are included for reference.*

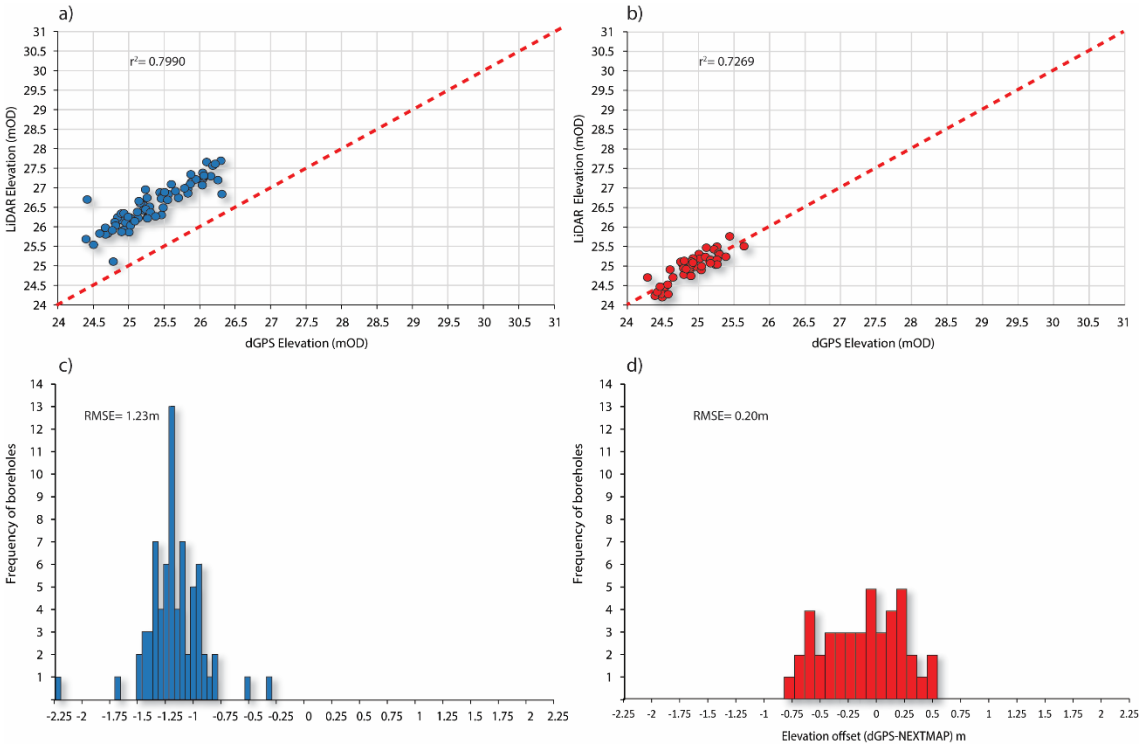

Figure 4.5. *Plots used to assess the accuracy of the QUEST borehole elevations in the Northern, and Southern Extensions of Wykeham Quarry. a) and b) are scatter plots of the total station elevations of the QUEST borehole datasets (QUEST BHN in a) and QUEST BHS in b)), plotted against the LiDAR derived elevation, which has a calculated accuracy of ±0.16 m (Figure 4.2). The red dotted line on each plot represents the 1:1 relationship for reference. c) and d) are frequency plot histograms, representing of the offset of the total station derived elevations for the QUEST BHN and QUEST BHS datasets (c, and d respectively) in relation to the LiDAR derived elevations. The x axis for each plot is divided into 5 cm bins, with the frequency of boreholes falling within the error offset plotted on the y axis. Root mean square errors (RMSE) in the dataset are provided for reference.*

The 71 boreholes in the QUEST BHN dataset also showed a good correspondence to the LiDAR derived elevation (r^2=0.7990), but contained a systematic offset, underrepresenting the point elevation by an average of 1.23 m (Figure 4.5; Table 4.4, for raw data see Appendix A). This offset likely relates to a miscalculation of the original spot elevation when calibrating absolute elevation values from total station measurements. To account for this, the LIDAR DTM derived elevations for the QUEST BHN dataset were used for the depositional modelling.

To corroborate the sedimentological descriptions of the QUEST dataset, 63 boreholes were drilled in the N1 and N3 sections of the Northern Extension in Summer 2013 (Figure 4.6). This area was considered important because it had the most variable stratigraphic assemblages in the QUEST surveys, including carbonate-rich deposits which warranted additional sampling for palaeoenvironmental reconstruction, and the greatest potential for archaeological remains to be recovered (Batchelor, 2009). Furthermore, the N1 extension was also the first area of the quarry due for extraction in 2015, making stratigraphic logging of the sequences important before they were excavated.

Table 4.4. *Summary table showing the correlation of the field derived elevations for the boreholes used in the depositional model compared to the LiDAR derived elevations.*

Dataset	Number of boreholes	LiDAR-Field elevation r^2	RMSE (m)	σ (m)	2σ (m)
RHUL BHN	63	0.93	0.32	0.18	0.35
QUEST BHN	71	0.80	1.23	0.26	0.52
QUEST BHS	43	0.73	0.20	0.20	0.40
Hanson 2007	51	0.99	0.08	0.08	0.16
Hanson 1997	28	0.98	0.15	0.12	0.24
Hanson 1992	41	0.95	0.23	0.15	0.31
Entire dataset	296	0.82	0.63	0.60	1.20
Entire dataset excluding QUEST BHN	225	0.98	0.22	0.19	0.39

Open gouge core samples (RHULBHN) were taken at *ca.* 50 m intervals across the N1 section of the Northern Extension (Figure 4.6). Where the Overburden deposits were absent, samples were taken using a hand screw auger to estimate the depth of topsoil (RHULGBHN; Figure 4.6). These boreholes were taken at *ca.* 10 m intervals to map the maximum elevation of Overburden deposits more precisely. Borehole elevations were determined from total station heights, measured in relation to a spot height, determined with a dGPS by Hanson Aggregates. Sediments were logged in the field with physical properties including colour (Munsell), composition (Troels-Smith), texture and stratigraphic -boundaries documented (raw data provided in Appendices B and C). The field derived elevation of these boreholes corresponded well to the LiDAR derived elevation (r^2= 0.93), with a RMSE of 0.32 m (Figure 4.7; Table 4.4), and were consistent with the stratigraphic information from the QUEST boreholes from similar localities.

4.3.2.3. Constructing stratigraphic models

The depositional model for deposits at Wykeham Quarry was constructed in two phases. First, the elevation and thickness of the stratigraphic units assigned to the Hanson borehole datasets were calculated. As described above, the stratigraphic units recorded by Hanson have been classified as four main facies: Clays, Overburden, Lower and Upper Gravels, and, Interburden. In order to allow correlation of these facies with the borehole datasets produced in this study, the Hanson facies were re-classified using the sedimentological criteria devised for discriminating lithofacies associations (Figure 4.8; Chapter 6).

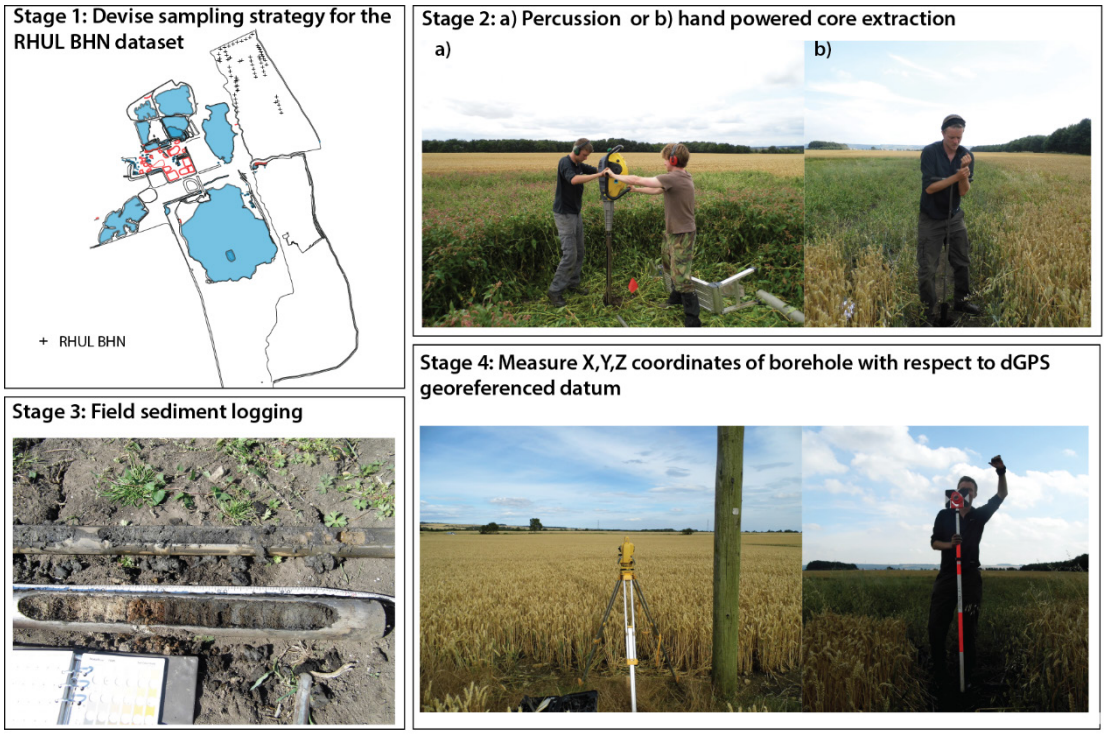

Figure 4.6. *Field methods used during the augering and sediment logging of the RHUL dataset. Boreholes were augered along croplines in the N1 to N3 extension areas of the quarry (Stage 1). 63 boreholes in total were excavated, using: a) percussion b) hand powered augering techniques (Stage 2). Samples were logged in the field to characterise their textural properties (Stage 3), before the location of each borehole was georeferenced in relation to a fixed spot datum, using a total station (Stage 4).*

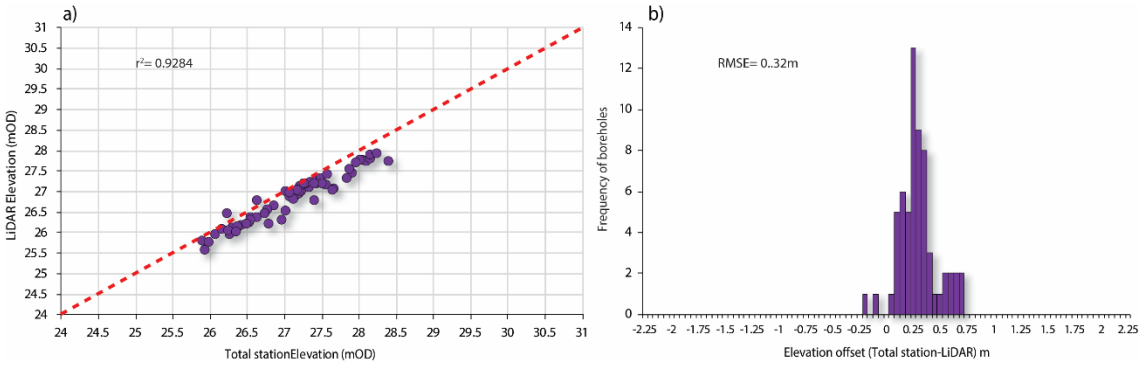

Figure 4.7. *Plots used to assess the accuracy of the RHUL borehole elevations. a) scatter plot of the total station elevations of the RHUL borehole dataset (RHUL BHN), plotted against the LiDAR derived elevation, which has a calculated accuracy of ± 0.16 m (see Figure 4.2). The red dotted line represents the 1:1 relationship for reference. b) frequency plot histogram, representing of the offset of the total station derived elevations for the RHUL BHN dataset, in relation to the LiDAR derived elevations. The x axis for each plot is divided into 5 cm bins, with the frequency of boreholes falling within the error offset plotted on the y axis. Root mean square error (RMSE) of the dataset are provided for reference.*

All of the boreholes classified the present land surface, and the Overburden-Upper gravel boundary, meaning they could be used to model the thickness of Overburden. The Hanson Borehole datasets also include stratigraphic records of the gravel sequences, which the QUEST, and RHUL datasets do not (Table 4.3). These units were used to estimate the extent and thickness of Interburden deposits across the quarry area.

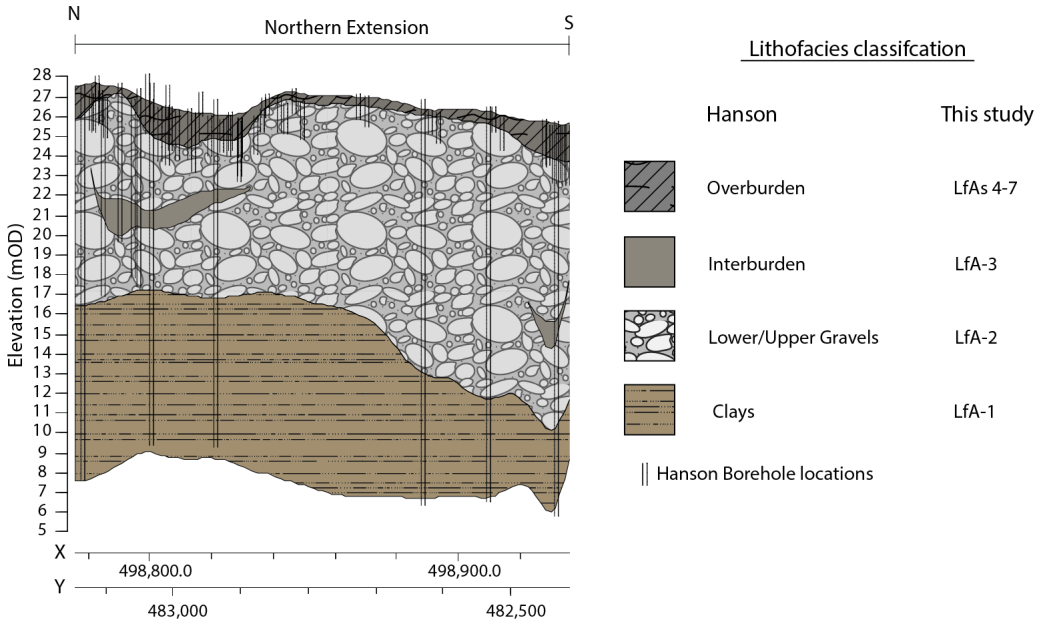

Figure 4.8. *Schematic cross-section of the Wykeham Quarry northern extension, showing the classification of stratigraphic units by Hanson and reclassification as LfAs as part of this study.*

Boreholes with sedimentological descriptions of Overburden deposits (QUESTBHN, QUESTBHS, and RHULBHN) were assigned into Lithofacies Assemblages (LfA) on the basis of stratigraphic and sedimentological charateristics. Seven LfAs were classified based upon sedimentological descriptions of 186 boreholes (Batchelor, 2009; this study) and open sections (Fraser *et al.,* 2009; Cloutman *et al.,* 2010; Figure 4.9).

Bathymetric elevation and thickness maps of lithofacies were modelled in Rockworks 2004 using 3-point high fidelity inverse distance weighted averaging with a weighting exponent of 0.25. Model performance was assessed using 5 point weighted, leave-one-out cross validation, to assess how accurately the model could predict the elevation of stratigraphic units (these data are reported in Appendix F).

To assess the timing of deposition for each LfA, spot samples for radiocarbon measurements were taken from key stratigraphic horizons, following the methods outlined in section 4.5. These dates were combined with those previously reported by Fraser *et al.,* (2009), to aid the reconstruction of the depositional history of the Overburden deposits.

4.3.3. Site selection for palaeoenvironmental reconstruction

The depositional modelling of sedimentary sequences highlighted two LfAs viable for palaeoenvironmental reconstruction at Wykeham Quarry. These were LfA-4, which consists of carbonate-rich, fine-grained deposits, and LfA-6, which consists of fossiliferous sands, silts and clays (Chapter 6). Similar lithofacies from sequences in Northern England are reported, and

contain sediments viable for palaeoenvironmental reconstruction and organic remains viable for radiocarbon dating (Walker *et al.,* 1993; 2003; Marshall *et al.,* 2002; Candy *et al.,* 2015).

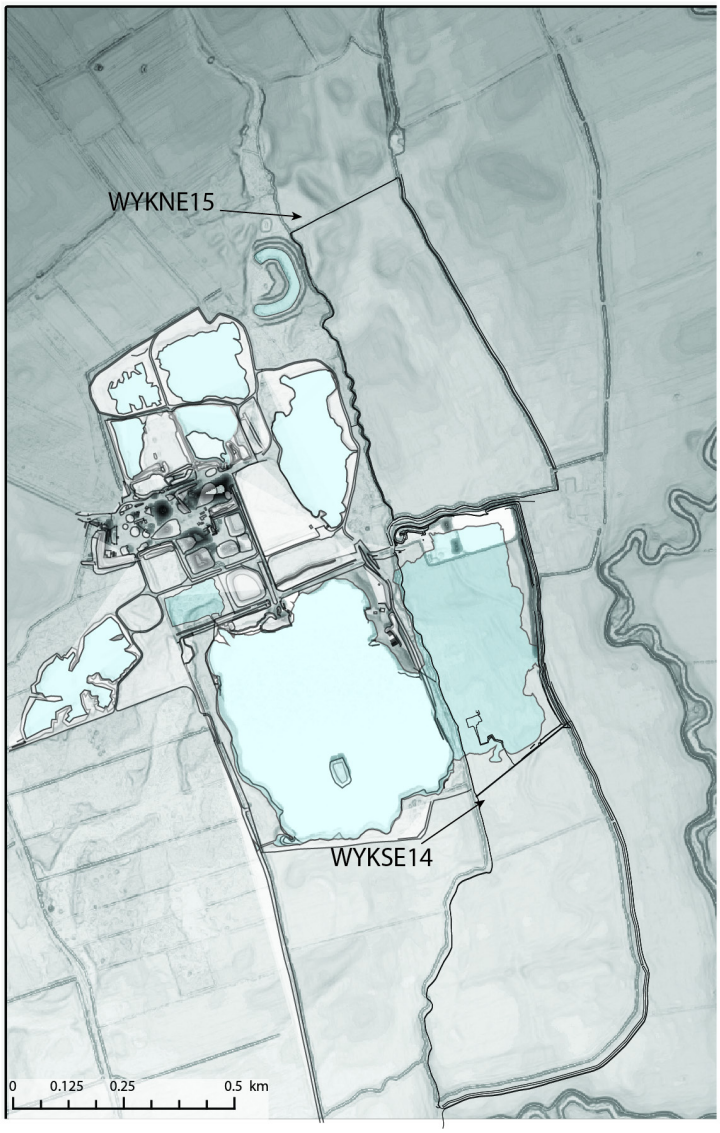

Figure 4.9*. Location of WYKSE14 and WYKNE15 at Wykeham Quarry*

The best representation of LfA-4 and LfA-6 records for palaeoenvironmental reconstruction at Wykeham Quarry were selected for palaeoenvironmental reconstruction based upon two principle criteria:

a) Deposited during the LGIT.
b) Contain evidence of sedimentological complexity, which may represent variability in climatic, landscape, and/or hydrological regimes through the LGIT (Lewis and Maddy, 1999; Schnurrenberger *et al.,* 2003).

To identify sequences that fulfilled these criteria, basins identified from the geomorphic mapping of the eVoP (section 4.2.3; Chapter 5), and the stratigraphic modelling of Wykeham Quarry

(section 4.3.2; Chapter 6) were assessed. For this project, two principal sites were selected for detailed palaeoenvironmental reconstructions, one from LfA-4 termed the Wykeham Northern Extension 2015 sequence (WYKNE15), and one from LfA-6 termed the Wykeham Southern Extension 2014 sequence (WYKSE14). The location of these sequences is shown in Figure 4.9. Further criteria used to select these sequences are discussed in Chapter 6.

4.4. Phase 3: Palaeoenvironmental reconstruction

4.4.1. Overview of techniques used

Methodologies used for palaeoenvironmental reconstruction from the Wykeham records can be divided into three main categories. First, sedimentological techniques employed to understand the nature of sediment deposition, and associated prevailing, environmental conditions. Second, biological and geochemical techniques used to reconstruct palaeoenvironmental conditions, identify periods of environmental variability, and enable correlation of sequences to other regional sites in NE England, (see Chapter 3). Third, stratigraphic and chronological techniques employed to assign absolute ages to sedimentary sequences, enabling robust correlations to palaeoenvironmental records across the N Atlantic region. The specific methods utilised in each sequence are summarised in Table 4.5 and are described in the following sections.

4.4.2. Sedimentological techniques

4.4.2.1. Rationale

Sedimentological analysis was undertaken on all of the lithological sequences reported in this project. This was done to develop understanding on the processes of sedimentation and infer depositional environments. For samples taken from open exposures, field and laboratory sediment logging were performed to characterise distinct sedimentary units (lithozones), within each sequence (Gale and Hoare, 1991; Jones *et al.,* 1999). Samples analysed from cores, were only subjected to laboratory analysis. Sediment descriptions were supplemented by the measurement of calcium carbonate content and organic content to provide an index of biological productivity of the sediments (Gale and Hoare, 1991; Heiri *et al.,* 2001), and siliclastic particle size to identify changes in the mode of depositional environment (Jones *et al.,* 1999; Lowe and Walker, 2014).

Table 4.5. *Summary of the palaeoenvironmental techniques undertaken on sediment sequences in this project. Red ticks show work undertaken by the author, blue ticks show samples prepared by the author but analysed by others, green ticks*

	Site	Sediment Description	Bulk sediments	Particle size	Thin sections	Magnetic susceptibility
Sedimentology	WYKNE15	✓	✓	✓	✓	✓
	WYKSE14	✓	✓	✓		

	Site	Plant Macrofossils	Pollen	Coleoptera	Stable isotopes
Palaeoecology and geochemistry	WYKNE15	✓	✓		✓
	WYKSE14	✓	✓	✓	

	Site	Radiocarbon dating	Tephra	SAR-OSL
Chronology	WYKNE15	✓	✓	
	WYKSE14	✓	✓	✓

Thin section micromorphology was undertaken on the WYKNE15 sedimentary sequence to understand the mode of sediment deposition (e.g. Bullock *et al.,* 1985), and supplement the interpretations of stable isotopic analysis (e.g. Candy *et al.,* 2015; section 4.4.4). Thin sections are regularly used to ascertain the mode of carbonate composition (e.g. Candy *et al.,* 2015; Tye *et al.,* 2016), as they provide a detailed insight into the processes associated with sediment deposition in sorted sedimentary sequences (e.g. Bullock *et al.,* 1985; Palmer *et al.,* 2008; Candy *et al.,* 2015), revealing sediment characteristics that may not be observable with the naked eye.

4.4.2.2. Sample collection

Percussion core sampling

Owing to the compacted and coarse nature of most of the sedimentary deposits at Wykeham Quarry, hand powered augering was impracticable for consistent sediment extraction (Batchelor, 2009). To record subsurface deposits in the quarry, an Atlas Copco Cobra 2-stroke percussion engine was fitted with Eijkelkamp 1 m long open gouge equipment (100 mm and 75 mm diameter), and incrementally driven into sediment at 1 m intervals. To record sedimentary deposits, the open gouge cores were extracted from the borehole every metre using a rod pulling extension system fitted with a ball clamp. The extracted sedimentary sequence was recorded using field based logging techniques.

Field logging of open sections

Logging of open sedimentary sequences was undertaken on sediment faces exposed at Wykeham Quarry, between 2013-2014. Lithostratigraphic boundaries were defined based upon textural and structural properties of the sediment, and recorded following standard techniques outlined in Jones *et al.* (1999). Lithozones were mapped across section using 10 cm^3 grids, in relation to a horizontal datum. The elevation of this datum was translated to m OD using a total station, calibrated to known elevation via dGPS with an X,Y,Z accuracy of 0.02-0.03 m. As access to most of these faces was only available for short amounts of time (<1 day), detailed logging and sampling of the sequences was not possible. For these sequences, field sketches were made of the stratigraphy, supplemented by detailed photographs of the sediment sections. Monolith tins were taken from sites of best potential for palaeoenvironmental analysis for more detailed laboratory description (section 4.4.2).

WYKSE14

Samples for analytical analysis were obtained in two stages between May and October 2014. As no open sections were available at the time of field sampling, stratigraphic sequences for palaeoenvironmental analysis were obtained using the Eijkelkamp open gouge and stitz coring system in May 2014. Methods used to auger the open gouge cores followed those described in section 4.3, with five replicate sequences taken within a 5 m radius. These cores were subsampled across key lithostratigraphic boundaries in the field, and combined for coleopteran analysis (Jarosz, 2014). A stitz coring system (60 mm core diameter), fitted with a core retainer to prevent the loss of sediment during extraction was used to obtain a composite stratigraphic sequence for analytical analysis. Three overlapping 1.10 m cores (0 to 1.10 m, 0.90 to 2.00 m and 1.63 to 2.73 m) were extracted from two neighbouring boreholes 0.5 m apart. This is termed as the $WYKSE14_{core}$ sequence.

To obtain further material for plant macrofossil, coleopteran, and OSL analyses, (sections 4.4.3 and 4.4.4), in October 2014, a 10 x15 x 3 m trench was excavated in four 0.5-1 m vertical steps from the land surface to the base of the Overburden from the same location as the core sequence. Sedimentary facies for the south face of the trench were logged following method outlined in section 4.4.2. 10 monolith tins, 3 OSL samples, and 54 contiguous bulk samples (taken at between 2 to 5 cm resolution) were sampled from the trench between 0.4 to 2.5 m in the site stratigraphy.

WYKNE15

The WYKNE15 sequence was initially sampled in November 2013 using two replicate cores *ca.* 20 m apart (WYKNE15 site A and site B) using 50 cm Russian chamber corers. Attempts to map the bathymetry of the basin using hand augered dutch gouge equipment proved unsuccessful, owing to the coarse particle size of the deposits, coupled with the thickness of the infill (>7 m). Sites for sample extraction were therefore chosen as close as possible to previously excavated areas, containing sedimentary sequences of known palaeoenvironmental potential. This was supported by geomorphic mapping of the site, and the characterisation of the LfA-4 deposits (section 4.3). The extruded sequences from sites A and B were incomplete, with only fragmentary sections of the lower 3.5 m of the stratigraphy successfully obtained. These cores were used to assess the potential of the site for palaeoenvironmental analysis. Between January and May 2015, the WYKNE15 site A sequence was re-cored using the Eijkelkamp stitz coring system, to obtain further material for plant macrofossil, thin section, and stable isotopic analyses.

4.4.2.3. Analytical Techniques

Laboratory based sediment logging

Macroscopic structural and textural properties of sediment sequences followed standard descriptive terminology outlined in Gale and Hoare (1991) and Jones *et al.* (1999). Sediment properties were used to identify key lithofacies associations in sequences. Individual cores were correlated using key marker lithofacies in overlapping borehole sequences. Where no such beds existed, correlations were made based upon the comparison of composite bulk sedimentological properties of individual cores.

Magnetic susceptibility

Magnetic susceptibility measurements were undertaken on the WYKNE15 and WYKSE14$_{core}$ sequences using a Barington MS2C core-scanning sensor. Each core was unwrapped and passed through the sensor with measurements obtained on a low frequency at 3 cm intervals, being corrected for drift following the method of Dearing (1999).

Calcium carbonate, organic carbon, and siliclastic content

Measurement of calcium carbonate content in sediment samples was determined complying with the standard protocol of the Department of Geography, Royal Holloway, University of London. Air-dried samples weighing between 0.1-0.25 g were powdered and immersed in an excess of 10% hydrochloric acid, with the volume of CO_2 liberated during the reaction, measured using a Bascomb calcimeter (Gale and Hoare, 1991). Repeat measurements were undertaken every 10

samples to check for measurement consistency. Carbonate content is expressed as the % dry weight of the sample, and expressed as $CaCO_3$ (%).

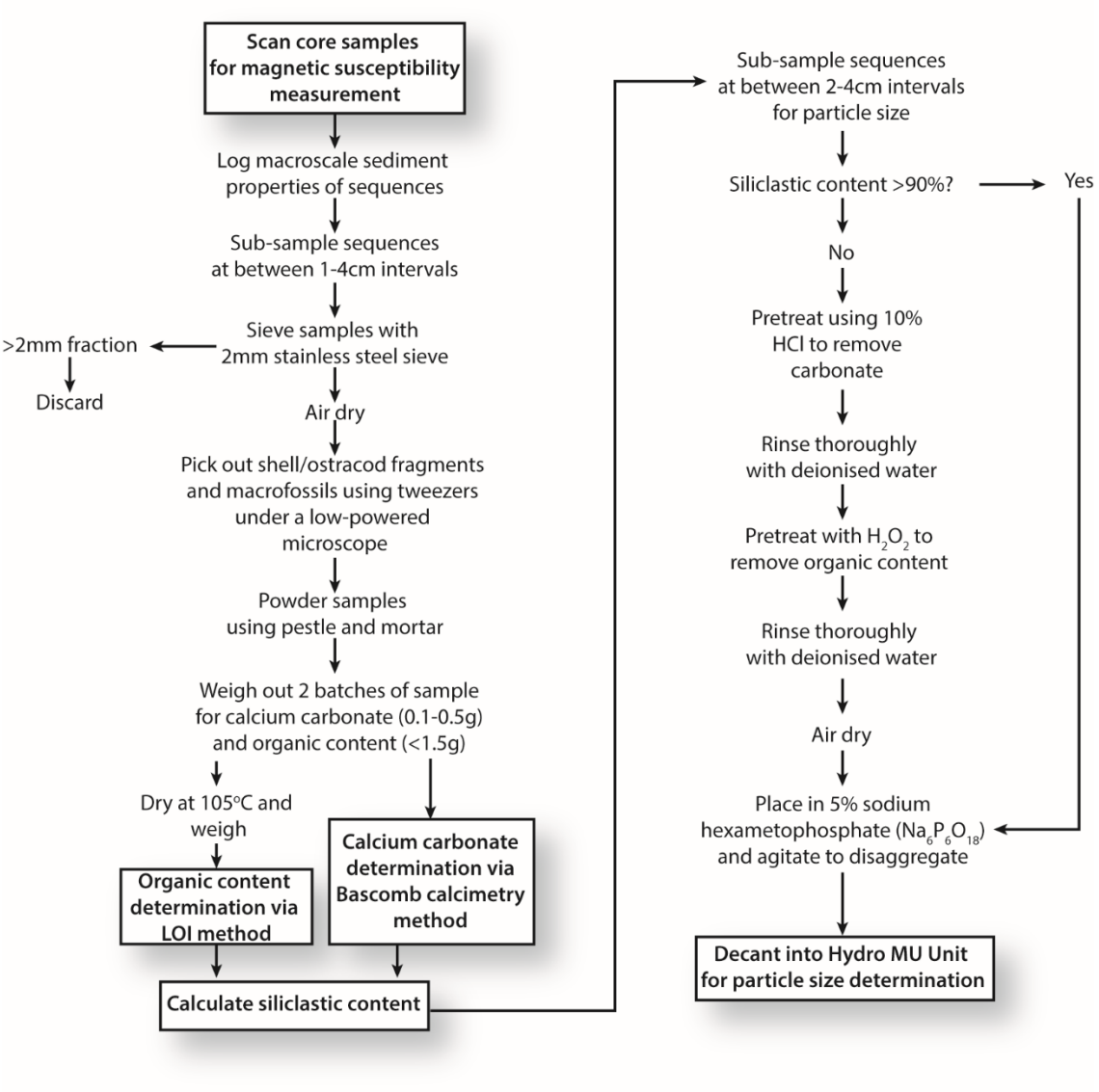

Figure 4.10. *Procedure followed for sampling and bulk sediment analysis from core based records.*

Organic carbon content was determined via the loss-on-ignition method (LOI) following standard procedure outlined in Dean (1974) and Heiri *et al.,* (2001). Samples were pre-treated following the methods outlined in Figure 4.10 before being ignited for 2 hours at 550 °C in a carbolite muffle furnace, and being reweighed to calculate the percentage of sample lost during ignition (Dean, 1974). Organic content is expressed as the % of the total sample dry weight hereafter. The percentage of siliclastic content of each sample was calculated using the following equation:

Siliclastic content (%)= 100- (carbonate content + organic content)

Particle size

Particle sizes were measured on the siliclastic fraction of sediment deposits following the method outlined in Figure 4.10. Where the siliclastic content of the sample was <90%, samples were pre-treated to remove residual carbonate and organic content. Carbonate was removed from samples using by sequentially adding 10% hydrochloric acid (HCl) to the sample until reaction ceased. 10% Hydrogen peroxide (H_2O_2) was incrementally added to samples to remove organic content until reactions ceased. Particle size determinations were carried out using standard laser granulometry protocol on the Malvern Mastersizer 2000 with a Hydro MU unit at the Department of Geography, Royal Holloway, University of London.

Thin section micromorphology

Eight thin section samples measuring 10 x 2 x 3 cm were taken from undisturbed core sediment through different lithofacies in the WYKNE15 sequence identified during sediment logging and bulk sediment analyses. Samples were prepared following the standard impregnation techniques of the Centre for Micromorphology at Royal Holloway, University of London (Palmer *et al.,* 2008b). Thin sections were vertically sub-divided, taking into account changes in facies for description. Full microscale descriptions were carried out in each area following terminology and protocol adapted from Bullock *et al.* (1985).

4.4.3. Biological techniques

Biological proxy techniques were applied to sedimentary records for two reasons. First, to strengthen the palaeoenvironmental interpretation of the records provided by sedimentological, and stable isotopic techniques, and second, to correlate and compare the sequences to other palaeoecological records from LGIT aged deposits in NE England.

4.4.3.1. Pollen analysis

Rationale

Pollen analysis was undertaken on selected sedimentary sequences, principally to reconstruct local-regional vegetation assemblages in the eVoP during the LGIT. The pollen records were also used to compare sequences to the other records in NE England, which show consistent trends through the LGIT (Chapter 3). Pollen analysis is one of the most common techniques applied to terrestrial LGIT records in NW. Europe (Bennet and Willis, 2002) to investigate past ecological and climatic changes in sedimentary sequences. Applying pollen analysis to the Wykeham sequences supplements the palaeoenvironmental reconstructions from other techniques, and

aids also comparisons to other palaeoenvironmental sequences at the local-regional scale (Birks and Birks, 2014).

Analytical Technique

The processing of all pollen samples in this project followed standard RHUL laboratory procedure. They were conducted by the author in all but two of the sequences. WYKSE14 samples were subsampled by the author and prepared by RHUL palaeoecology technician Marta Perez.

Pollen subsamples were prepared using a 1 cm^3 volumetric sampler, and deflocculated using 10% sodium pyrophosphate ($Na_4P_2O_7$). 2 exotic *Lycopodium* tablets (batch number 10031) were added to each sample, enabling estimates of pollen concentration to be calculated. Samples were wet sieved to between 125 µm and 10 µm, with the >10 µm fraction retained. To concentrate the pollen remains within each sample, 5 ml of 10% hydrochloric acid was added to remove carbonates. Samples were then floated with 5 ml of Sodium polytungstate ($Na_6(H_2W_{12}O_{40})$ at a specific gravity of 2.0 g/cm^3 to separate the pollen from the heavy mineral component of each sample. Erdtman's acetolysis with a ratio of 9:1 Acetic anhydride ($[CH_3CO]_2O$) and Sulphuric acid (H_2SO_4) was performed to remove residual biological cellulose from the samples. The remaining material was mounted onto slides using glycerol-jelly.

10 spot pollen samples were prepared from the WYKNE15 sequences to assess potential for palaeoenvironmental reconstruction. These were assessed by John Lowe, and Ian Matthews who deemed that pollen preservation in the sequence was poor and not reliable for an assessment of regional vegetation cover (John Lowe *pers comm.*). Therefore, no further pollen analysis was undertaken on this sequence.

4.4.3.2. Plant macrofossil analysis

Rationale

Plant macrofossil analysis was undertaken on the WYKSE14, and WYKNE15 sequences to reconstruct the development of local vegetation communities and provide supporting evidence for changes in relative lake levels through the LGIT (Harrison and Digerfeldt, 1993; Mortensen *et al.,* 2011). Macrofossil assemblages from lowland lake deposits can be used to assess relative lake level change over time (e.g. Digerfeldt, 1988; Harrison and Digerfeldt, 1993; Bos *et al.,* 2006; Taylor, 2011), potentially providing a means to assess relative changes in effective precipitation regimes through the LGIT (Bohncke and Wijmstra, 1988; Magny and Ruffadi, 1995; Birks, 2000; Hoek and Bohncke, 2002). Furthermore, the local presence/absence of vegetation can also be used to reconstruct palaotemperature regimes (e.g. Valiranta *et al.,* 2015). The use of probability

density functions in the derivation of Quaternary palaeoclimatic changes in botanical datasets has shown considerable potential in this analysis, principally because:

a) The technique is not dependant on modern analogue species assemblages (which are problematic when non-analogue assemblages are identified in palaeo-records), and can calculate summer and winter temperature ranges for single taxa (Kühl *et al.,* 2002).
b) The method relies on the presence/absence rather than relative abundance of taxa (e.g. pollen assemblages) meaning it can be used with macrofossil assemblage data (Kühl *et al.,* 2002; Aarnes *et al.,* 2012) which more confidently reflects the contemporaneous local presence of species in a sedimentary sequence (Birks, 2002; 2003).
c) By combining probability density function ranges of individual taxa from the same stratigraphic horizon, a mutual climatic range of summer and winter temperatures can be reconstructed from assemblage data. This technique has been demonstrated to be consistent with other palaeotemperature indicators such as chironomid-inferred temperatures during the LGIT (Aarnes *et al.,* 2012).

Analysis of macrofossil assemblages, coupled with sedimentological data therefore provide the potential to reconstruct palaeo-hydro-climatic regimes through the LGIT in the eVoP.

Analytical Technique

Plant macrofossil analysis followed methods outlined in Birks (2002). 20 cm^3 samples were subsampled at key stratigraphic horizons in the WYKNE15 and WYKSE14 sequences (2 cm thick samples from core material and 1 cm thick samples from monolith tins respectively) for the production of radiocarbon samples (section 4.4.5).

The sampling resolution was increased to between 4 and 16 cm, through intervals that showed higher sedimentological complexity. The volume of each sample was measured by displacement in water in a measuring cylinder (Birks, 2002). These measurements confirmed that sample volumes for both sequences were consistently *ca.* 20 cm^3. Sediments were disaggregated using sodium pyrophosphate ($Na_4P_2O_7$), diluted to 10% with deionised water for the WYKSE14 samples, and hydrochloric acid (HCl), diluted to 10% with deionised water for the WYKNE15 samples. The methods differed between the two sets of samples based upon the amount of $CaCO_3$ content present. Prior to treatment, samples from the WYKNE15 sequence were carefully disaggregated and examined under a low powered light microscope to obtain an abundance count of preserved charophyte thalli. HCl was then used to remove $CaCO_3$ from the WYKNE15 samples, which effectively dispersed the remaining sediment, circumventing the need to disperse further with sodium pyrophosphate.

Samples were placed over a 125 µm metal sieve mesh and gently washed with deionised water. The remaining residue (≥ 125 µm) was transferred to a glass beaker and kept in cold storage to await analysis. To pick macrofossils, small quantities of sample residues were dispersed in deionised water 2-3 mm deep on a glass petri dish, and systematically examined under a stereo light microscope at x 10 to x 40 magnification. Remains were picked with fine forceps into glass vials, filled with *ca.* 2 ml of 10 % HCl, and topped up with deionised water to prevent mould growth, which can contaminate radiocarbon dates from plant macrofossil material (Wohlfarth *et al.,* 1998). Macrofossils were identified using the reference collection at Royal Holloway and identification guides (Berggren, 1964; Birks, 1980; van Geel *et al.,* 1981; 1989; Watson, 1981; Smith, 2004; Cappers *et al.,* 2006; Mauquoy and van Geel, 2007). Incomplete and/or abundant remains such as mosses, broken leaves and wood fragments, *Chara* thalli, and charcoal were assigned a value on a 5 point, abundance scale (Birks and Matthewes, 1978; Birks, 2002; termed as ABUN), ranging from 0= absent, 1= present (n-=1-10), 2= rare (n=10-25), 3= frequent (n= 25-50), 4= abundant (n=50-100), 5= very abundant (n=>100). Moss taxa in the WYKNE15 sequence were identified by the analysis of leaf material under a high powered microscope and are reported via presence/absence. All other macrofossils are presented as numbers per 20 cm^3 of fresh sediment.

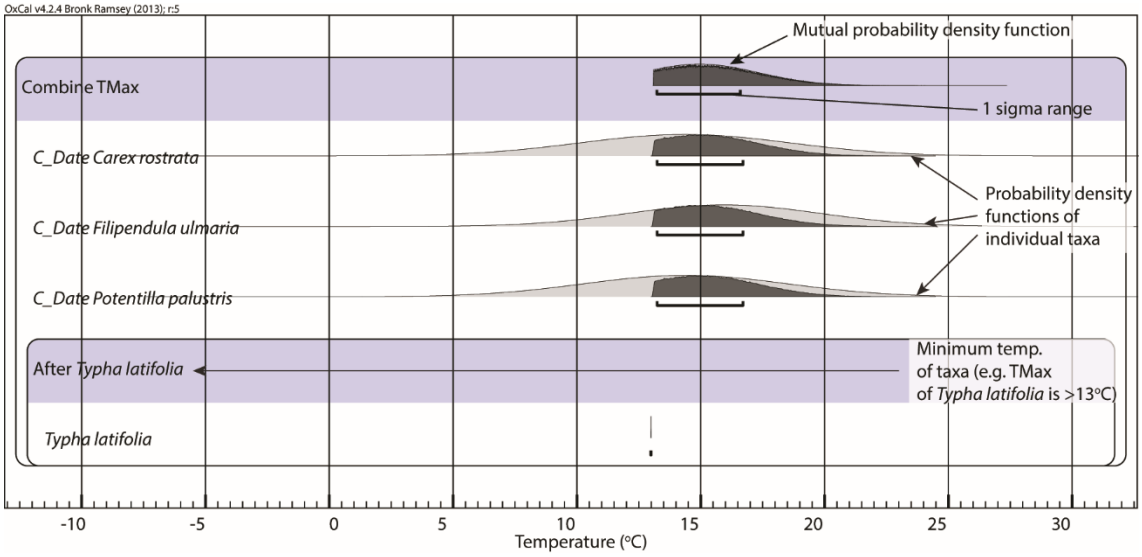

Figure 4.11. *Summary of the method used to construct a mutual climatic range from macrofossil assemblage data in OxCal v4.2 using the Combine function to create a mutual probability density function for taxa in each sample horizon.*

Calculating mutual climatic ranges from plant macrofossils

Summer and winter temperature estimates were reconstructed from the macrofossil assemblages in the WYKNE15 and WYKSE14 sequences using published TMax and TMin ranges (calculated from 1σ probability density functions of present day species distributions) for selected taxa reported in Aarnes *et al.* (2012) and minimum TMax temperatures reported in

Isarin and Bohncke (1999). To construct a mutual climatic ranges of temperature estimates from macrofossil assemblages, the Combine function in Oxcal v4.2 was used to overlap macrofossil probability density function ranges present in individual samples (Figure 4.11). The Combine function was used as it provided an easy and robust way of producing probability density functions from sigma range data, which are frequently used in radiocarbon research (Bronk Ramsey, 2009a). Individual taxa were inputted as C_Dates with the mean temperature inputted as a 'cal date' and the 1σ range as 'uncertainty'. Where only a minimum temperature is reported (i.e. *Typha latifolia* constrained by Isarin and Bohncke (1999) to TMax temperatures >13°C) values were inputted as an 'After' function in OxCal, which produces a probability density function after (above) the inputted value. The function works by calculating the entire probability distribution (sample temperature ranges) from a number of individual probability density functions (in this case TMax and TMin ranges from sample taxa) present in each sample. These temperature ranges are then presented as a 1σ range of the combined probability density function range (Aarnes *et al.,* 2012), which is the case for all temperature ranges reported in this study.

4.4.3.3. Coleoptera

Rationale

Coleopteran analysis was undertaken on the WYKSE14 sequence to supplement palaeoenvironmental reconstructions, and to develop a mutual climatic range estimate for the WI. At a local scale, fossil coleopteran assemblages provide detailed palaeoenvironmental reconstructions of past plant communities and landscape contexts for sedimentary sequences (Elias, 2001). Coleopteran assemblages can also be used to reconstruct climatic changes based upon the Mutual Climatic Range (MCR) method (Atkinson *et al.,* 1987; Coope and Lemdahl, 1996). This method has been successfully implemented on numerous LGIT records in Britain to reconstruct summer and winter temperature ranges for sedimentary sequences (e.g. Coope and Brophy, 1972; Atkinson *et al.,* 1988; Walker *et al.,* 1993; 2003). The organic and plant macrofossil rich characteristics of LfA-4 deposits at Wykeham Quarry, are ideal for coleopteran analysis (Elias, 2001; Fraser *et al.,* 2009), providing the potential to reconstruct regional climatic regimes during the LGIT.

Analytical technique

Coleopteran samples were prepared following standard protocol used at the Department of Geography, Royal Holloway, University of London. Mutual climatic ranges were calculated by Sophie Jarosz, and Professor Scott Elias using standard techniques in the BUGS programme (Buckland and Buckland, 2006).

4.4.4. *Bulk sediment stable isotopes ($\delta^{18}O_{bulk}$ and $\delta^{13}C_{bulk}$)*

4.4.4.1. Rationale

Stable isotopic analysis ($\delta^{18}O$ and $\delta^{13}C$) of freshwater carbonates has significant potential with which to reconstruct palaeoclimatic regimes in the British Isles through the LGIT. This is demonstrated by existing records from the British Isles which contain a number of fluctuations in $\delta^{18}O$ values that have been correlated with isotopic changes recorded in the Greenland GICC05 record (Marshall *et al.,* 2002; 2007; van Asch *et al.,* 2012; Whittington *et al.,* 2015; Candy *et al.,* 2015; 2016; Chapter 2). It is important however to review the primary controls on isotopic values in lake systems of NW Europe that provide a basis to derive palaeoclimatic signals from stable isotopic datasets (Figure 4.12).

$\delta^{18}O$ values obtained from lacustrine carbonates (hereafter termed $\delta^{18}O_{bulk}$) are a function of the $\delta^{18}O_{water}$ of the lake, which is in turn controlled by mean annual $\delta^{18}O_{rainfall}$ values and temperature in temperate, hydrologically-open lake basins (Leng and Marshall, 2004; Figure 4.9). In temperate, mid-latitude regions such as the British Isles, measured $\delta^{18}O_{rainfall}$ values are positively correlated to changes in air temperature (Dansgaard, 1964; Rozanski *et al.,* 1992; 1993; Darling, 2004). Consequently, in the absence of other modifications of the $\delta^{18}O$ signal, changes in the measured $\delta^{18}O_{bulk}$ values are likely to reflect changes in prevailing air temperatures.

$\delta^{13}C$ values obtained from lacustrine carbonates (hereafter termed $\delta^{13}C_{bulk}$) are a function of $\delta^{13}C$ of dissolved inorganic carbon (DIC) in the lake water, which is primarily controlled by vegetation development in the catchment (Cerling and Quade, 1993; Leng and Marshall, 2004). However, hydrological and catchment processes, such as the open and closed nature of water bodies, detrital contamination, and vital effects during precipitation, can modify the $\delta^{18}O_{bulk}$ and $\delta^{13}C_{bulk}$ signal prior to and during carbonate precipitation in the water body, and therefore need to be accounted for when interpreting stable isotopic signals (Leng and Marshall, 2004; Figure 4.12). A detailed review of all of these modifying sources is beyond the scope of this section. Two variables, namely shifts in basin hydrology, and detrital contamination however provide two likely sources of modification in $\delta^{18}O_{bulk}$ values, particularly in LGIT lacustrine sediments from western Europe (Hammarlund *et al.,* 2003; Candy *et al.,* 2015), and therefore warrant further discussion.

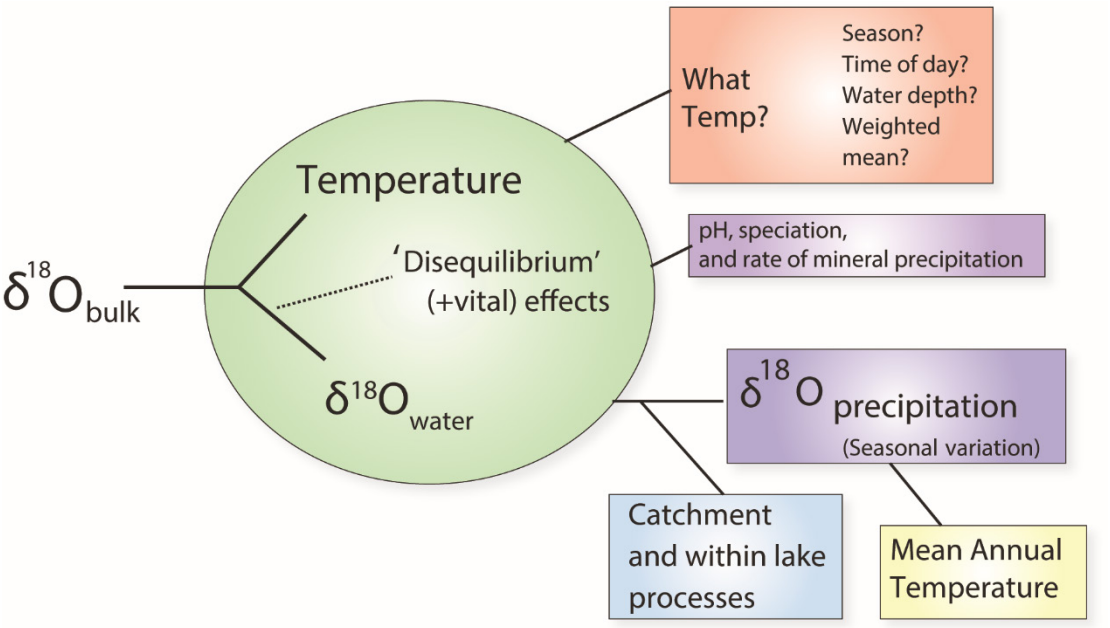

***Figure 4.12**. Major controls on the oxygen isotope composition of lacustrine carbonates ($\delta^{18}O_{bulk}$; modified from Leng and Marshall, 2004).*

In hydrologically-closed basins, water residence time is typically long, and stable isotopic values are principally controlled by the relationship between precipitation, and evaporation of the water body (Li and Ku, 1997; Hammarlund *et al.,* 2003). In hydrologically-open basins, residence time is shorter, resulting in $\delta^{18}O_{water}$ values that are more representative of $\delta^{18}O$ of precipitation, rather than the balance between precipitation and evaporation. In hydrologically-closed basins, $\delta^{18}O$ and $\delta^{13}C$ values often co-vary as a result of evaporitic processes which causes the preferential loss in ^{16}O, and the equilibration of DIC with atmospheric CO_2 which results in higher $\delta^{13}C_{bulk}$ values (Talbot, 1990; Leng and Marshall, 2004; Horton *et al.,* 2016). Co-variance in measured $\delta^{18}O_{bulk}$ and $\delta^{13}C_{bulk}$ values is therefore often used as an indicator to determine if the basin is hydrologically open, or closed (Li and Ku, 1997; Hammarlund *et al.,* 2003).

In lacustrine systems, bulk carbonate is derived from three sources: a) authigenic carbonates precipitated in the water body, b) biogenic carbonates such as gastropod shells and ostracod carapaces, c) detrital carbonates eroded from the catchment. These will all have different isotopic signals and it is important to identify and isolate specific carbonate fractions prior to analysis (Leng and Marshall, 2004). This is most readily achieved via detailed sedimentological work, including micromorphological analysis to identify the principle sources of carbonate within the sediment body (Candy *et al.,* 2015; Tye *et al.,* 2016; section 4.4.2). Comparisons of $\delta^{18}O_{bulk}$ and $\delta^{13}C_{bulk}$ values to local bedrock sources, which, if consisting of marine limestone and chalk (as in the eVoP; Chapter 3), also provides a method to confidently differentiate authigenic lacustrine carbonates from detrital carbonate sources (e.g. Leng and Marshall, 2004; Candy *et al.,* 2015).

On this basis, carbonates identified in the eVoP sequences, if demonstrated to represent authigenic precipitation in a hydrologically open basin, can be linked to $\delta^{18}O_{water}$ values of the lake, and in turn $\delta^{18}O_{rainfall}$ values and prevailing air temperature. Consequently, variations in measured $\delta^{18}O$ values of bulk carbonate can be used to infer past changes in temperature.

4.4.4.2. Analytical technique

0.5 cm thick bulk carbonate samples were taken from the WYKNE15 sequence at 8 cm resolution for the measurement of $\delta^{18}O$ and $\delta^{13}C$ values (termed $\delta^{18}O_{bulk}$ and $\delta^{13}C_{bulk}$ respectively hereafter). Resolution was increased to 4 cm where complexity was identified in the sediment stratigraphy, potentially being indicative of changes in climatic regime.

Contaminants including charophyte thalli, and biogenic carbonate (ostracod carapaces and gastropod shells) were handpicked from each sample using a stereo light microscope at 10x to 40x magnification. The remaining sample was rinsed over a 200 μm mesh to remove any further stem fragments, and a 64 μm mesh into plastic centrifuge tubes, to remove any remaining detrital material and biogenic carbonate fabrics. Sieved samples were treated with 10% hydrogen peroxide (H_2O_2) to remove organic material, rinsed and centrifuged three times with deionised water, before being air-dried. Dried samples were powdered with an agate pestle and mortar, and weighed to between 600-1200 μg using a Mettler Toledo XP6 microbalance. $\delta^{18}O_{bulk}$ and $\delta^{13}C_{bulk}$ values were determined by analysing the CO_2 liberated when reacted with phosphoric acid at 90 °C, using a VG PRISM series 2 mass spectrometer in the Earth Sciences Department at Royal Hollloway. Internal (RHBNC) and external (NBS19, LSVEC) standards were run every 4 and 18 samples respectively. All isotope values are expressed as ‰ V-PDB.

4.4.5. Chronological techniques

Construction of a robust chronostratigraphy for both the WYKSE14 and WYKNE15 sequences was essential to provide the palaeoenvironmental records constructed from these sequences with an independent absolute calendar timescale. This is imperative when comparing sequences, to other palaeoenvironmental records on a local, regional, and global scale (Björk and Wohlfarth, 2001) in the N Atlantic region (Chapter 2). Palaeoenvironmental responses to climatic fluctuations during the LGIT is known to be spatially variable (e.g. Lane *et al.,* 2013). Therefore, in order to compare palaeoenvironmental records constructed from Wykeham Quarry to other records, robust age models for the palaeoenvironmental sequences are required (Lowe *et al.,* 2008). Three geochronological techniques can be applied to the palaeoenvironmental sequences at Wykeham Quarry. These are a) Accelerator mass spectrometer (AMS) radiocarbon dating of terrestrial plant macrofossils, b) Single-aliquot-regenerative-dose optically stimulated

luminescence (SAR-OSL) dating of sand rich facies in the WYKSE14 stratigraphy, and c) cryptotephra analysis.

4.4.5.1. Radiocarbon dating

Rationale

Radiocarbon dating is the geochronological technique most widely used to date LGIT aged sediment sequences (Walker, 2001; Blockley *et al.,* 2004). Recent methodological advances have resulted in the ability to analyse increasingly small samples of organic carbon (<1 mg) with enhanced analytical precisions using an AMS (Lowe and Walker, 2000). This enables the routine dating of terrestrial plant macrofossil material rather than bulk limnic samples, which significantly reduce potential contaminants that produce erroneous age determinations (Lowe and Walker, 2000; Walker, 2001; Figure 4.13). Application of AMS radiocarbon dating techniques on terrestrial plant macrofossils therefore provides the most robust means to construct age models for the palaeoenvironmental records constructed from Wykeham Quarry.

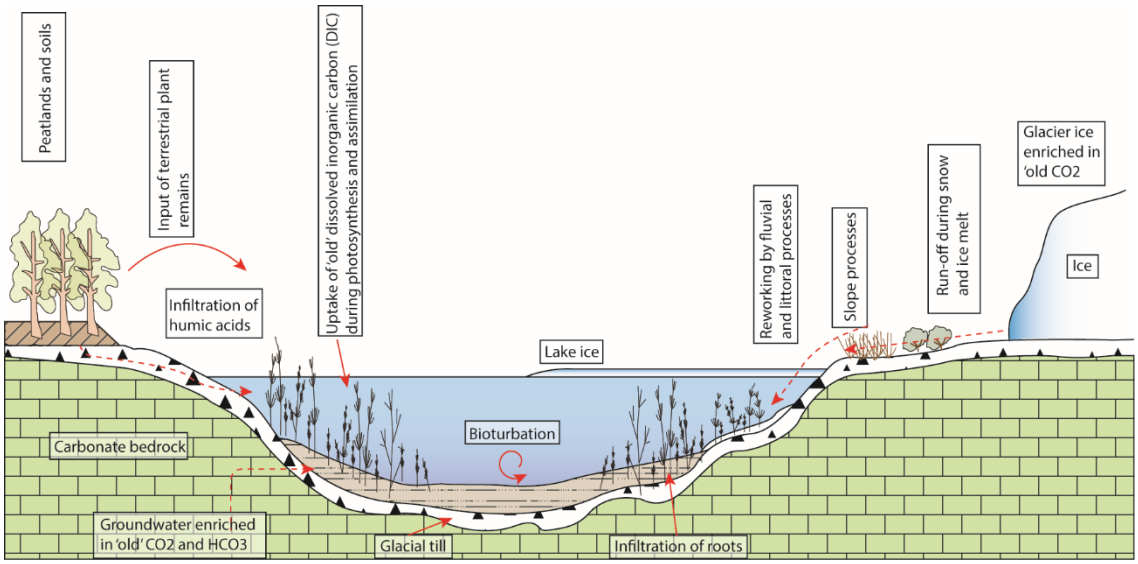

Figure 4.13. *Schematic cross-section of a hard water lake system showing a variety of potential error sources which can erroneously influence radiocarbon dates (modified from Björk and Wohlfarth, 2001). The analysis of carefully selected. terrestrially derived plant macrofossil samples is preferential to bulk sediment dates as the potential for contamination should be minimised, meaning the date is more likely to accurately reflect the age of sediment deposition (Lowe and Walker, 2000).*

Analytical technique

Radiocarbon samples were prepared by the author under the supervision of Richard Staff at the Oxford Radiocarbon Accelerator Unit (ORAU) Research Laboratory for Archaeology and the History of Art (RLAHA), University of Oxford. Terrestrial plant macrofossil samples were

repeatedly washed with ultra-pure (MillQ™ MILLIPORE) water to remove potential contaminants. Sample pre-treatment for accelerator mass spectrometry (AMS) radiocarbon dating followed standard acid-base-acid (ABA) methodologies (after de Vries and Barendsen, 1954) compliant with ORAU protocols for delicate macrofossil material (ORAU pre-treatment code 'VV', Brock *et al.,* 2010). This process was undertaken in three stages: 1) an initial acid wash (1 M HCl for 20 minutes at 80 °C) to remove sedimentary- and other carbonate based contaminants, 2) a base wash (0.2 M NaOH for 20 minutes at 80 °C) to remove organic acid contaminants; and 3) a second acid wash (1 M HCl for 1 hour at 80 °C) to remove any dissolved atmospheric CO_2 that may have been absorbed during the preceding base wash (Brock *et al.,* 2010). Samples were rinsed 3 times with ultra-pure (milliQ™) water in-between each wash to remove any residual acid or base in each sample.

Samples were freeze-dried overnight before being weighed into tin capsules (≤ 5 mg of material) and combusted in an elemental analyser (EA CARLO-ERBA NA 2000) at a temperature of 1000°C. The CO_2 and N_2 of each sample were siphoned from a gas chromatograph into an isotope ratio mass spectrometer (IRMS, SERCON 20/20) via a 50:1 splitter, where stable isotopic compositions ($\delta^{13}C$ and $\delta^{15}N$) were determined, alongside carbon and nitrogen quantities. The remaining 98% of the CO_2 gas was siphoned out of the IRMS and collected cryogenically with a reactor graphite rig (Brock *et al.,* 2010).

Following ORAU protocol, (Dee and Bronk Ramsey, 2000) the graphite rigs were heated to 560 °C for 6 hours, enabling the collected CO_2 to reduce into graphite over an iron catalyst (Vogel *et al.,* 1984). The residual pressure of the remaining gas contained within the graphite rigs was measured prior to disassembly in order to confirm that graphitisation of the sample had reached completion (≥ 95 % efficiency). Sample graphite was subsequently removed from the rig and pressed into aluminium targets for AMS at *ca.* 350 kgf for 20 seconds. Samples were analysed on a HVEE Accelerator Mass Spectrometry (AMS) system at ORAU. All radiocarbon dates reported in this thesis are calibrated to calendar age before AD 1950 (cal BP), using the IntCal13 calibration curve (Reimer *et al.,* 2013) in OxCal v4.2 (Bronk Ramsey and Lee, 2013).

4.4.5.2. SAR-OSL

Rationale

SAR-OSL dating is a well-established method used to determine the time elapsed since quartz grains were last exposed to light (Lian and Huntley, 2001; Roberts and Lian, 2015). The technique can be utilised in any sedimentary sequence, provided that quartz grains are suitably bleached prior to deposition (Figure 4.14). SAR-OSL is commonly applied to deposits where radiocarbon dating is not viable (e.g. Bateman et al., 2015), providing an alternate means to establish the age

of sedimentary sequences. Repeat SAR-OSL samples were applied to the WYKSE14 stratigraphy where insufficient macrofossil remains were preserved for radiocarbon dating. By utilising this multiproxy chronological approach, robust ages were able to be obtained from otherwise undateable sections of the sedimentary sequence.

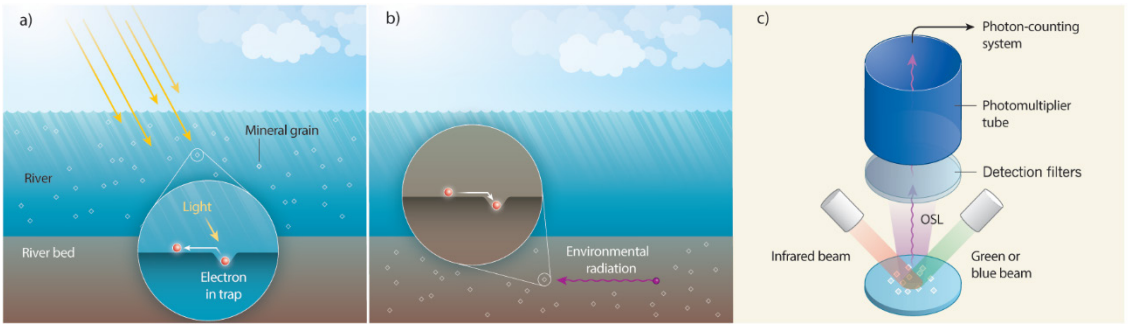

***Figure 4.14**.. Summary of the methodology used to obtain ages from mineral grains via OSL (from Roberts and Lian, 2015). a) Mineral grains are exposed to sunlight when transported by air and/or water. Electrons caught in traps in the crystal lattice structure of the mineral grains are evicted when exposed to light, returning to a normal atomic state (bleached). b) when mineral grains are deposited and buried they cease to be exposed to sunlight, enabling environmental radiation to be steadily transferred from the sediment body into traps in the crystal structure of the mineral grain. c) mineral grains collected from the sediment body (concealed from daylight), are illuminated in the laboratory, liberating stored electrons from the crystal lattice structure, giving rise to an OSL signal, which is amplified and measured via a photomultiplier tube and a photon-counting system. The amount of past radiation dose that the mineral grain was subjected to is calculated, allowing the burial age of the mineral grain to be determined.*

Analytical technique

Three optically stimulated luminescence samples were taken from the WYKSE14 stratigraphy. These samples were analysed by Simon Armitage following standard procedure at the Department of Geography, Royal Holloway, University of London.

Quartz was extracted from the bulk sample using standard laboratory techniques. Carbonates and organic matter were removed from the sample using 1.16 M HCl and H_2O_2 respectively, after which the residue was wet sieved to 90-125 µm. Quartz was extracted from this fraction using density separations at 2.62 and 2.70 g/cm^3 and a subsequent Hydrofluoric acid (HF) etch (23M HF for 50 minutes followed by a 10M HCl rinse). Etched samples were re-sieved at 60 µm, to remove partially dissolved grains, and stored in opaque containers prior to measurement. All OSL measurements presented in this study were carried out using a Risø TL/OSL-DA-20 dating system (Bøtter-Jensen et al., 2003). Single-aliquot equivalent doses were determined using the single-aliquot regenerative-dose (SAR) method (Galbraith et al., 1999; Murray and Wintle, 2000). Prior to measuring equivalent doses, the most appropriate preheating conditions for the samples was determined by performing a dose recovery test (Roberts et al., 1999; Wallinga et al., 2000) on sample WYK-OSL1. This sample shows a relatively weak dependence of equivalent dose upon preheating regime, resulting in the adoption of a 200 °C, 10 s PH1 (the preheat prior to measurement of the natural or regenerated luminescence intensity) and 160 °C, 0 s PH2 (the

preheat prior to measurement of the test dose luminescence intensity) for all subsequent measurements. Twenty-four aliquots of each sample were measured, and aliquots not yielding recycling (Murray and Wintle, 2000) or IR depletion (Duller et al., 2003) ratios consistent with unity were rejected.

Table 4.6. *Equivalent dose and dosimetry measurements from the WYKSE14 OSL samples.*

Sample (WYK-)	Dose rates (Gy/ka)				Equivalent dose (Gy)	Age (ka)
	Beta	Gamma	Cosmic	Total		
OSL1	1.31 ± 0.13	0.98 ± 0.09	0.17 ± 0.01	2.47 ± 0.15	30.5 ± 1.4	12.4 ± 1.0
OSL2	1.27 ± 0.12	0.88 ± 0.08	0.17 ± 0.01	2.33 ± 0.14	28.9 ± 1.2	12.4 ± 0.9
OSL3	1.35 ± 0.14	0.96 ± 0.09	0.17 ± 0.01	2.49 ± 0.16	29.4 ± 1.1	11.8 ± 0.9

For HF acid etched sand-sized quartz grains, the environmental dose rate consists of external beta, gamma and cosmic ray components. Uranium, thorium and potassium concentrations were calculated for each sample using thick-source alpha-counting and gas-flow Geiger-Muller beta counting (Bøtter-Jensen and Mejdahl, 1988). Beta and gamma dose rates were then calculated from these radioisotope concentrations, using the conversion factors of Adamiec and Aitken, (1998) and an assumed water content of 20 ± 7.5%. This assumed water content was chosen since samples are likely to have been located both above and below the water table at various points during their burial and the uncertainty value (quoted at 1σ) was chosen to cover, at 2σ, the driest (5 % - typical of freely drained sands) and wettest (35 % - approximately saturation water content) which conditions which these samples might have experienced. Cosmic dose rates were calculated using the sample location (latitude, longitude and altitude) and a burial depth of 1.12 ± 0.2 m (Prescott and Hutton, 1988). Equivalent dose and dosimetry data are presented in Table 4.6.

4.4.5.3. Cryptotephra analysis

Rationale

Tephra analysis was applied to the Wykeham sequences in an attempt to identify time-parallel marker horizons that could enable precise correlations to other regional LGIT records (Lane *et al.,* 2013; Davies, 2015). Cryptotephras of NW Europe during the LGIT are well characterised, and dated (Blockley *et al.,* 2012; Bronk Ramsey *et al.,* 2015), and sites proximal to Wykeham have shown that Icelandic eruptions reached the eVoP during the LGIT (e.g. the Vedde Ash dated to 12.121 ± 0.058 cal kaBP (Bronk Ramsey *et al.,* 2015) recovered from PF; Palmer *et al.,* 2015). The presence of tephra horizons in the sedimentary sequences at Wykeham would provide a further means to correlate to regional palaeoenvironmental records.

Analytical technique

Tephra sampling followed the stepped flotation procedure adopted by Turney *et al.* (1997); Turney (1998) with the modifications of Blockley *et al.* (2005). 5-10 cm 'scan' samples (0.3-1.2 g dry weight) were extracted from the host sediment, dried at 105 °C overnight and weighed. Samples were ashed at 550 °C for 2 hours, before being immersed in 10% HCl to remove residual organic and carbonate content respectively. Samples were wet sieved between 80µm and 15µm, and floated in sodium polytungstate ($Na_6(H_2W_{12}O_{40})$ at a density of 2.0g cm^3 to remove biogenic silicate. A float at 2.5 g cm^3 was used to separate heavy minerals from any rhyolitic tephra shards present within samples. The floated samples were mounted onto slides using Canada balsam heated to 85 °C and examined under a polarising light microscope at between x100 and x400 magnification.

4.4.5.4. Bayesian age modelling

Rationale

In order to assess the timing of palaeoenvironmental events identified in sedimentary sequences, and compare relative timing of palaeoenvironmental events between records, accurate and precise age-depth models are required (Blockley *et al.,* 2007; Bronk Ramsey 2008; Lowe *et al.,* 2008). Bayesian statistics provides the potential to generate robust depositional models from sedimentary sequences and is now widely employed in the development of age models in Quaternary stratigraphic studies (Blockley *et al.,* 2004; Wohlfarth *et al.,* 2006). This method is favoured for two reasons. First, it enables the inclusion of prior information obtained on the sedimentary sequence (i.e. superposition of dates, sedimentological characteristics, etc.), and can account for variations in sedimentation rates and hiatuses (Bronk Ramsey, 2009a; Bronk Ramsey and Lee, 2013), which are readily identified in LGIT sedimentary sequences (e.g. Walker *et al.,* 1993; Blockley *et al.,* 2004). Adopting this approach can substantially reduce uncertainty ranges of calibrated ages (Bronk Ramsey, 2008). Second, it provides criteria with which to statistically identify outliers, enabling down-weighting or exclusion of erroneous dates from age models (Bronk Ramsey, 2009b), which are also readily identified in LGIT records (Blockley *et al.,* 2004; Elias and Matthews, 2013). For these reasons, Bayesian age-modelling techniques were utilised in the construction of age-depth models for palaeoenvironmental sequences.

Analytical technique

To assess the age-depth relationship of the Wykeham stratigraphies, deposition models were constructed using the Bayesian-based *P_Sequence* function, with k_0 factors in OxCal v4.2 (Bronk Ramsey, 2008; 2009a; Bronk Ramsey and Lee, 2013). These criteria were chosen to account for

randomly variable deposition rates in sedimentary sequences (Bronk Ramsey, 2009), which are suggested by the sedimentological data from each sequence, and is characteristic of basin infill during the LGIT, in northern Europe (Blockley *et al.,* 2007). Detailed descriptions of the methods used to construct age models in the WYKNE15 and WYKSE14 sequences are discussed further in Chapter 6.

5. Developing a landscape model for the eastern Vale of Pickering through the Last Termination

5.1. Introduction

This chapter presents results of geomorphological mapping of the VoP, and the description, interpretation, and modelling of deposits at Wykeham Quarry in the eVoP with the aim of developing a model of landscape evolution through the Last Termination. This model is required to: a) better understand the phasing and mode of deglaciation in the eVoP, b) develop understanding of geomorphic activity through the LGIT, c) identify sites of optimum potential for palaeoenvironmental reconstruction. This chapter first describes and interprets new landforms identified from targeted GIS mapping of the VoP, before presenting the results of sedimentological work undertaken at Wykeham Quarry. The chapter concludes by presenting the model of landscape evolution constructed from these data.

5.2. Landforms identified by GIS mapping in the VoP

Three landform assemblages were critical for understanding the evolution of the VoP through Stages 2-5 (Chapter 3). These assemblages can be grouped into: a) terraces which are used to reconstruct former lake levels; b) palaeochannels, which are used to reconstruct the development of fluvial regimes, and; c) palaeobasins, which provide potential archives for palaeoenvironmental reconstruction. The following sections provide descriptions and interpretations of these landforms identified via GIS-based mapping (Chapter 4).

5.2.1. Terraces

Description

Terraces are classified as flat to gently dipping surfaces bounded on either side by higher sloped topography on valley sides. Terraces are often identified in previously glaciated terrain, sometimes associated with ice-marginal, glaciofluvial activity from decaying ice masses, forming kame terraces on valley sides (Sissons, 1979; Livingstone *et al.,* 2010; Benn and Evans, 2010), or as shorelines demarking former surfaces of proglacial lakes (Sissons, 1979; Breckenridge, 2015; Fairburn and Bateman, 2016).

Evidence for 70-60 mOD lake level for Glacial Lake Pickering is a kame terrace at Wykeham (Kendall, 1902; Penny and Rawson, 1969; Straw, 1979), and two outwash fans at Seamer and Newtondale, graded to 45 and 30 mOD respectively provide evidence of the lower two lake levels (Kendall, 1902; Penny and Rawson, 1969; Straw, 1979; Evans *et al.,* 2016). Alluvial inflows

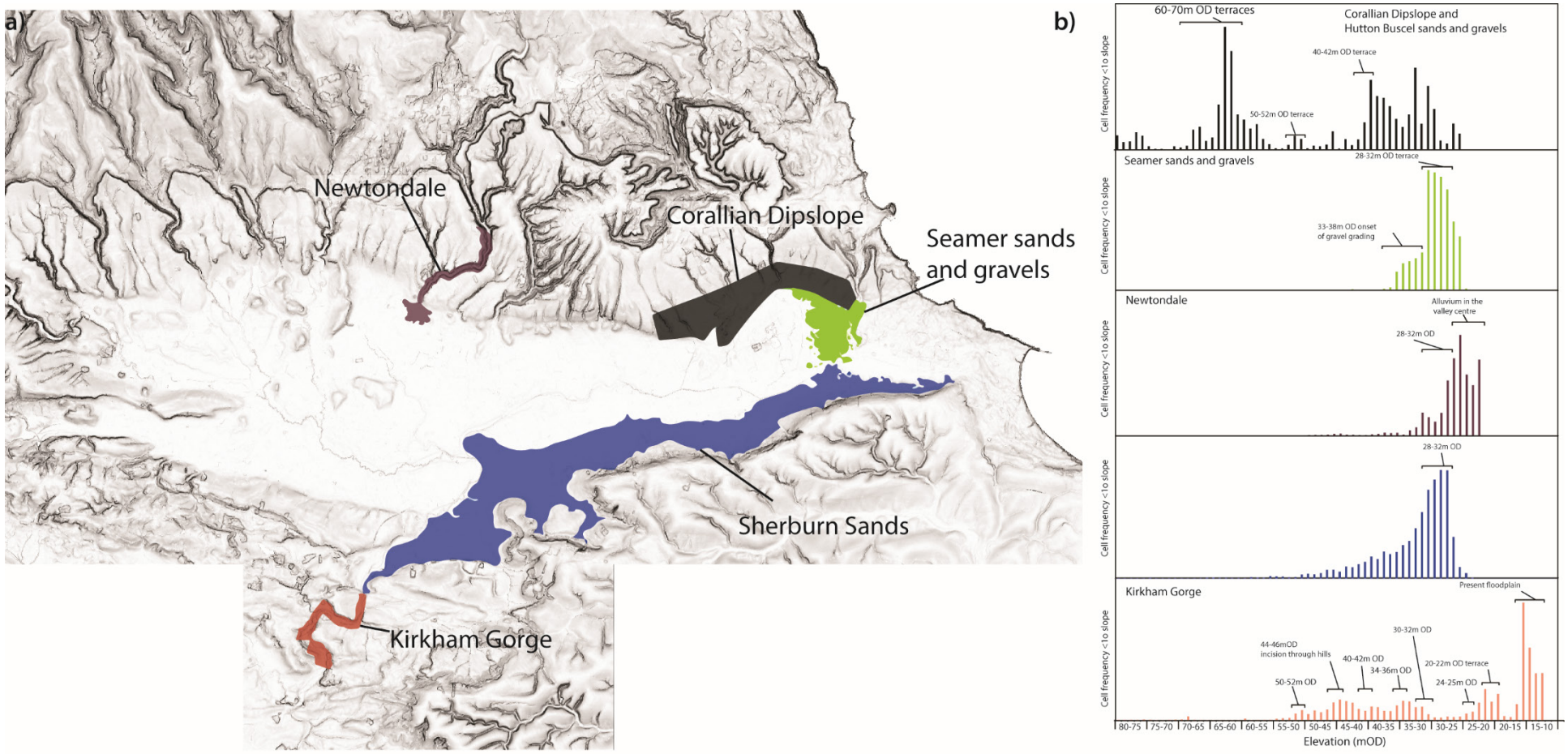

Figure 5.1. *a) Slope map of the VoP showing the areas assessed for terrace development. b) Histograms showing frequency of slope values <1° plotted against elevations (sectioned into 1 m bins). These graphs were used to identify elevation ranges with the potential to preserve terraces in each study area. Identified terrace forms discussed in text are labelled.*

to Glacial Lake Pickering such as those present on the Corallian Dipslope, the Sherburn Sands and Newtondale, have the potential to aggrade and incise terrace surfaces associated with former lake levels in the VoP (Livingstone *et al.,* 2012; Bateman *et al.,* 2015; Evans *et al.,* 2016).

Terrace mapping focussed upon five areas in the VoP: The Corallian dipslope in the eVoP, the Seamer sand and gravels, the Sherburn Sands, Newtondale, and Kirkham Gorge (Figures 5.1-5.4; Table 5.1). These regions were chosen as they either: a) have previously been interpreted as remnant lake shorelines, b) have been interpreted as inflow, or outflow conduits of Glacial Lake Pickering, c) are areas of constrained flow for the River Derwent. The Forge Valley and the Hunmanby channel were also assessed for terrace preservation, but the steep slope angles of the valleys limited the potential identification of terraces with the resolution of the LiDAR and NEXTMAP DTMs.

Table 5.1. *Summary of terraces identified in the Vale of Pickering. Black ticks represent large, laterally extensive aggradation terraces (based upon the position of the landform in the valley, and sedimentological analysis of these landforms by previous work). Orange ticks represent small terraces which are either not laterally extensive (< 100 m in length and < 40 m in width) and/or fragmented. The genesis of these terrace forms is discussed in text but remains equivocal without more extensive field analysis.*

Terrace elevation (mOD)	Seamer sands and gravels	Corallian dipslope	Sherburn sands	Newtondale	Kirkham Gorge
20-22					✓
24-25					✓
28-32	✓		✓	✓	✓
34-36	✓		✓		✓
40-42		✓			✓
44-46		✓			✓
50-52		✓			✓
60-70		✓			

Interpretation and synthesis

The terraces identified provide supporting evidence for the evolution of Glacial Lake Pickering, and demonstrate that the 3 stage model (70, 45, and 30 mOD) for the lakes evolution is too simplistic and/or erroneous. Terracing at *ca.* 30 mOD at Newtondale, Sherburn, and the Seamer sands and gravels all represent deltaic landforms graded to the elevation of a *ca.* 30 mOD lake in the VoP (Kendall, 1902; Evans et al., 2016). More fragmented terraces at 44-46 mOD on the Corallian Dipslope and in Kirkham Gorge are consistent with a 45 mOD level (Penny and Rawson, 1969). With the exception of the Hutton Buscel kame terrace on the Corallian Dipslope (which need not relate to the elevation of a proglacial lake), no supporting evidence of a 70 mOD lake is identified. If a lake did exist at this elevation in the VoP during the Late Devensian, the lake must have been controlled by ice in the Vale of York damming the Howardian Hills.

Kirkham Gorge would not have been the principal outflow for this waterbody as, a) the gorge is incised from a maximum elevation of > 76.2 mOD (Edwards, 1978), b) other outlets in the Howardian Hills (ranging between 50- 65 mOD; Eddey, *pers comm.*), demonstrate that this elevation would have been impossible to maintain, without some sort of blockage or obstruction at these points. The presence of the Vale of York ice lobe across the Howardian Hills provides the only realistic damming mechanism to form such a lake body (Evans *et al.,* 2016). If a lake at this elevation did exist in the Vale of Pickering during the Late Devensian, Kirkham Gorge would not have been utilised as the outflow, as it must have been incised to below the elevation of the other conduits in the Howardian Hills by the time the Vale of York ice had retreated northward.

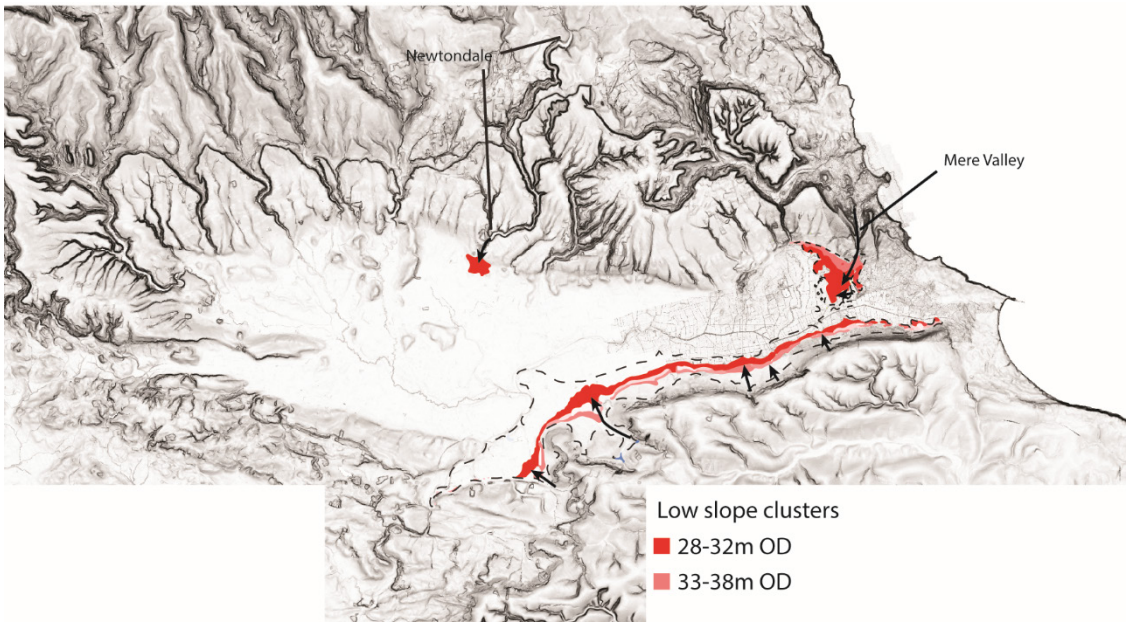

Figure 5.2. *Terrace cluster elevations identified in the Seamer sands and gravels, the Sherburn sands, and Newtondale.*

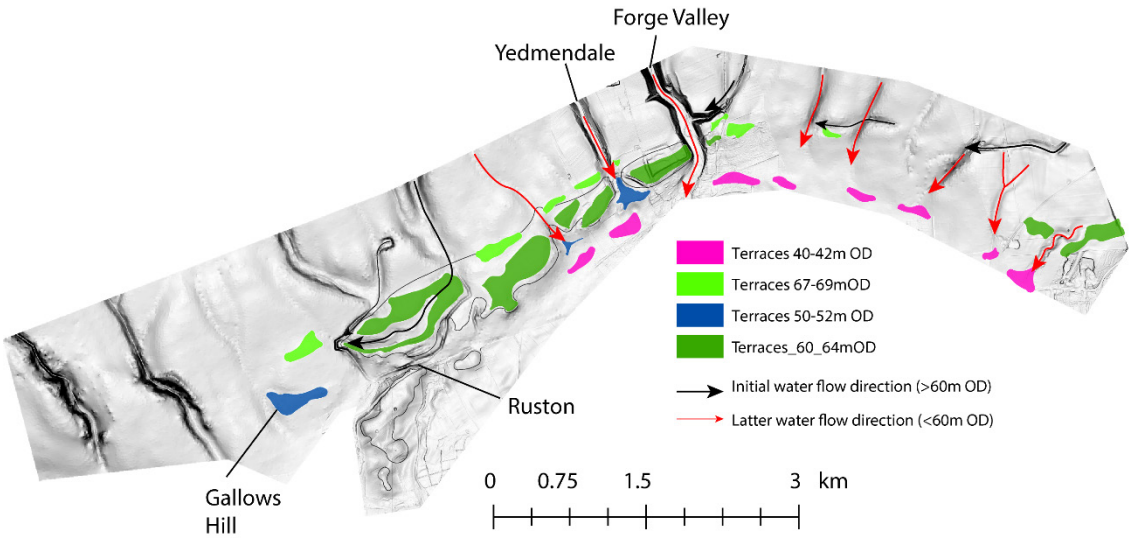

Figure 5.3*. Major terraces identified on the Corallian Dipslope. The extent of this Figure in relation to the VoP is shown in Figure 5.1.*

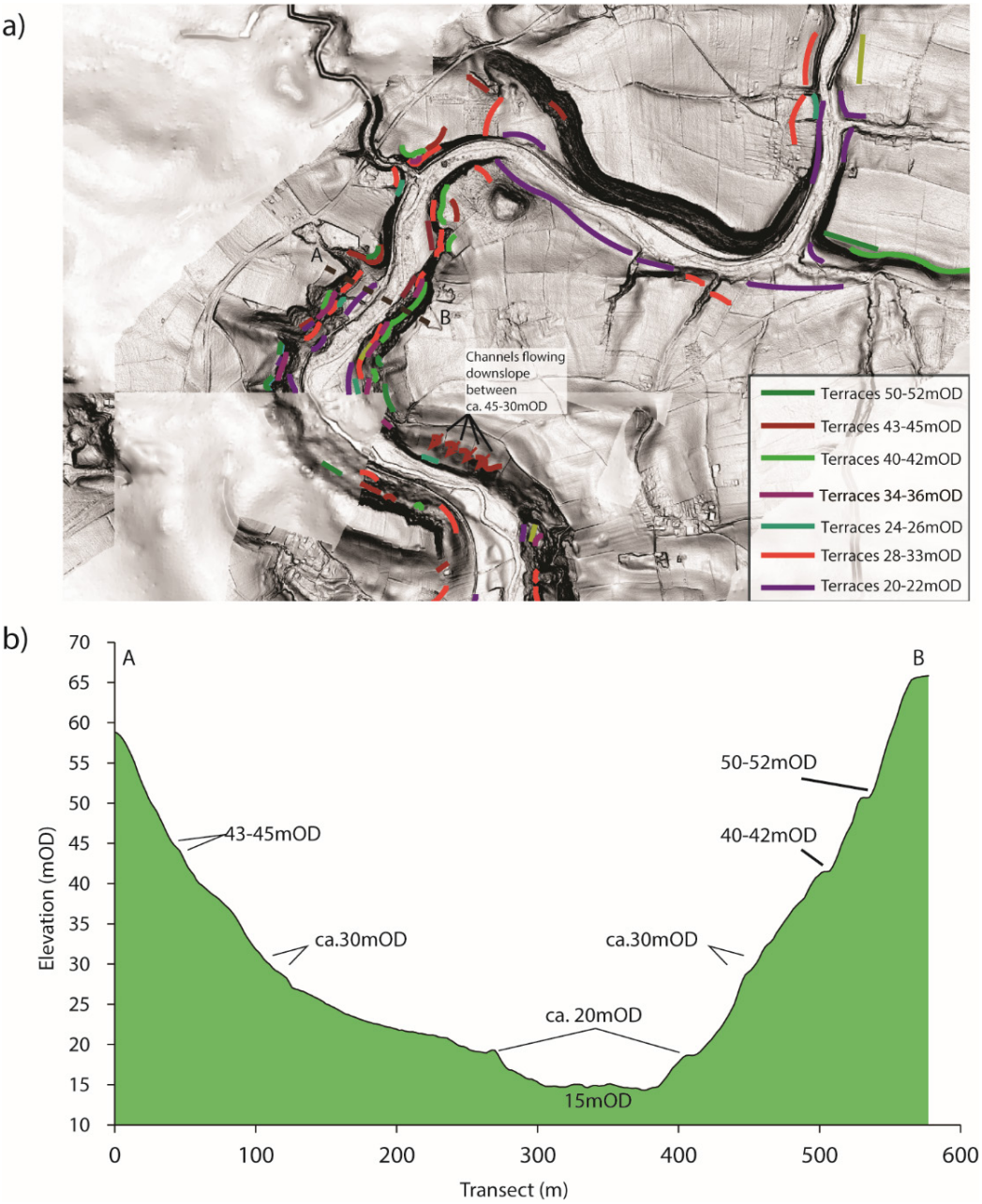

***Figure 5.4.**. a) Terraces identified in Kirkham Gorge. Note that LiDAR was used preferentially to NEXTMAP due to its higher X Y resolution, and more accurate Z values (Chapter 4). b) cross section across the gorge (location marked in a)) showing the presence of small terrace forms at the altitudes discussed in text.*

The 50-52 mOD terraces identified on the Corallian Dipslope, and in Kirkham Gorge provides evidence of a possible lake elevation during initial drainage through the col. This therefore supports that the formation of Kirkham Ggorge to an elevation below 60 mOD was initiated prior to the Late Devensian.

Further terraces identified in Kirkham Gorge provide the first supporting evidence for stepped down cutting of the valley during formation. This valley is interpreted to have been the principal outflow from the VoP during the Dimlington Stadial, transferring water from Glacial Lake

Pickering into the Vale of York (Kendall, 1902; Evans *et al.,* 2016). Small terraces identified between 20-22, 24-25, 30-32, and 40-42 mOD correspond well to the 20, 25, 30, 33, 40, and 42 mOD lake levels of Glacial Lake Humber (Fairburn and Bateman, 2016; Chapter 3), suggesting that phases of incision in Kirkham Gorge were likely related to changes in the base level in the Vale of York through the Dimlington Stadial. On this basis, the following model can be proposed for the formation of terraces in the VoP and Kirkham Gorge:

- **Stage 2 (*ca.* 21-18 ka BP):** Maximum lake levels in the VoP at altitudes $\leq$ 70 mOD, possibly fluctuating to *ca.* 50 mOD must be related to the damming of the valley by the position of ice dams to the east (NSIL) and west (VOYL).
- **Stage 2-4 (*ca.* 18-15 ka BP):** Lower elevation terraces at Seamer, Sherburn, and Newtondale suggest a fall in the lake level as the VOYL receded northward, allowing the lake to drain via Kirkham Gorge which was already incised to $\leq$ 50-52 mOD. The level of incision was constrained by the elevation of Glacial Lake Humber, which during this interval stood at 42 mOD (Fairburn and Bateman, 2016). The elevation of Lake Humber lowered in stages from <40-20 mOD, causing periodic incision and terrace formation in Kirkham Gorge, leading to progressively lower lake levels in the VoP.

5.2.2. Palaeochannels

The River Derwent

The River Derwent is the primary watercourse in the eVoP, draining the eastern North York Moors (upstream catchment *ca.* 110.7 km^2), before flowing westward and exiting the VoP (catchment *ca.* 1474.6 km^2) through Kirkham Gorge and eventually feeding west into the Ouse catchment (Vale of York; Figure 5.5). The river presently enters the eVoP *ca.* 22 km from its source, through the Forge Valley at (*ca.* 33.9 mOD) as a sinuous, single channel, meandering river (mean channel width 18.2 m, channel sinuosity=1.82; Figure 5.6). The river flows southwards for *ca.* 4 km, 250-600 m east of Wykeham Quarry, towards the centre of the eVoP, where the floodplain widens from 1 km, to *ca.* 3.5 km, south of Wykeham Quarry, 2.8 km downstream. The river flows westwards in the centre of the eVoP and becomes confluent with the canalised River Hertford north of Ganton on the southern margins of the valley at 24.2 mOD. Downstream of this confluence, the River is canalised (see below), reducing the sinuosity index to 1.11. The major focus of this study examines this *ca.* 10 km stretch of river, where the majority of palaeochannels have been identified.

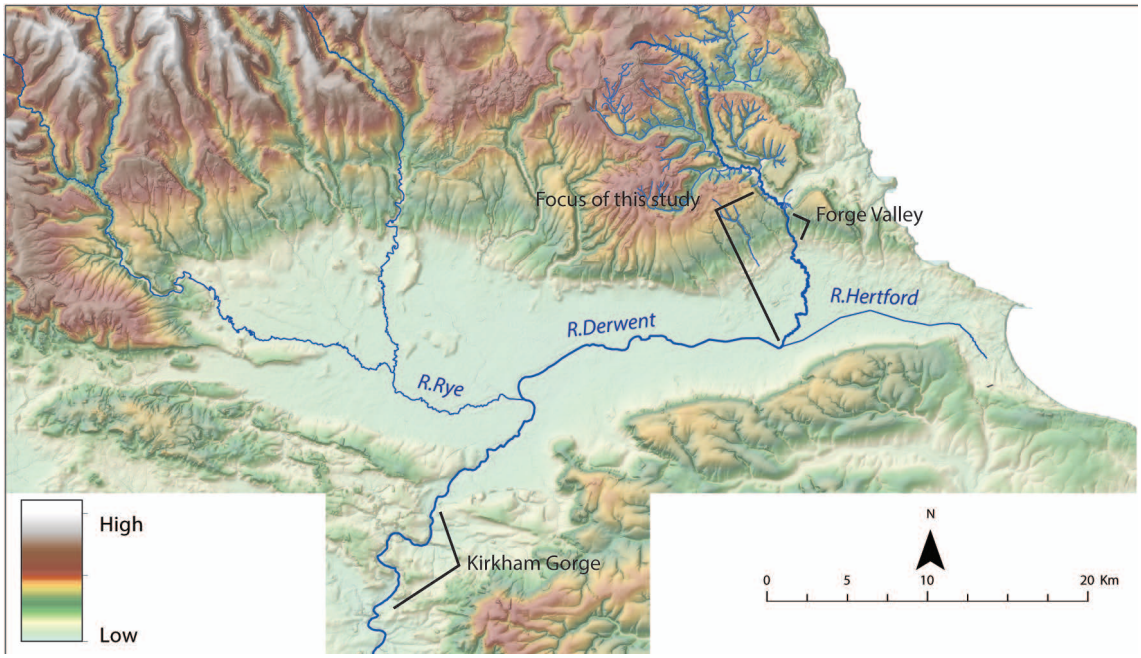

Figure 5.5. *Contemporary drainage routes of the VoP, showing the area of focus for this study.*

River sinuosity	1.38	1.54	1.15	1.82	1.11 (cannalised)	1.28 (cannalised)	1.24 (cannalised)	1.68	1.40
River gradient	0.0200	0.0019		0.0011	0.0016	0.0004	0.0005		0.0002

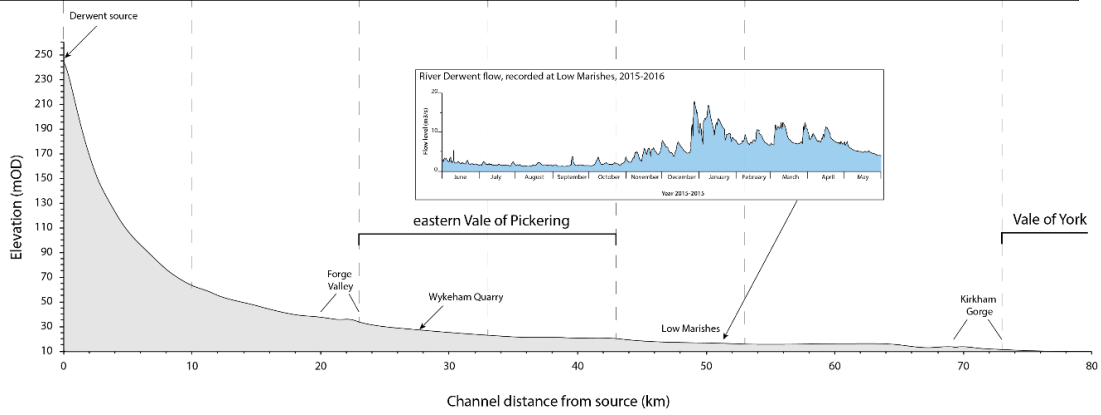

Figure 5.6. *Characteristics of the contemporary River Derwent, showing an elevation profile between the rivers source in the North York Moors, and its outflow into the Vale of York (Figure 5.5). the rivers sinuosity, gradient are summarised for 10 km sections of the river, highlighting the degree of modification in the VoP. A flow record from the central VoP is included to show the persistent low flow regime in the VoP. Note that this graphs covers a period of excessive flooding in the VoP during January 2016, and therefore most accurately portrays the River Derwent's optimum flow parameters excluding anthropogenic influence.*

Since 1800 AD, the River Derwent has undergone coordinated anthropogenic alteration, aimed at reducing flooding in the VoP, providing viable land for agriculture (Menuge, 2001). These alterations include the excavation of a drainage channel in the Seacut Valley, and straightening and canalisation of the River Derwent and River Hertford in the eVoP. The alterations, coupled with exploitation of groundwater resources from the Corallian Dipslope aquifer (Carey and Chadha, 1998; Brown *et al.,* 2013), have had a negative impact on the regional groundwater levels, and the peak flow discharges of the River Derwent (Menuge 2001).

Palaeochannels in the VoP

Palaeochannels previously identified in the VoP have all been associated with overflows, or subglacial-marginal drainage of the North Sea, and Vale of York Ice Lobes on the valley sides of the VoP, the Seacut Valley, The Coxwold-Gilling Gap, and Harwood Dale (Kendall, 1902; Straw, 1979). Previously identified channels in the eVoP are focussed in the upland areas of Seamer and Irton Moors, well above contemporary fluvial drainage. In this study, a further 288 channels are identified in the eVoP. These channels lie either within the glacial sand and gravel units, or across the lowland alluvial wetlands in the centre of the valley. The channels identified are split into three channel assemblages (Channel Assemblage A-C) based upon variations in geometry, sinuosity, and location within the valley (Table 5.2; Figures 5.7-5.8).

Table 5.2. *Measured characteristics of the three palaeochannel assemblages identified in the Derwent floodplain. All values are reported as means to 1 standard deviation.*

Channel Assemblage	Number of individual channels identified	Mean sinuosity (1σ)	Mean channel gradient (1σ)	Mean channel width (m; 1σ)
A	28	1.16 (0.22)	0.0039 (0.0021)	70.7 (17.7)
B	204	1.20 (0.24)	0.0031 (0.0027)	21.5 (6.9)
C	55	1.70 (0.55)	0.0029 (0.0028)	20.1 (4.1)

Description

Channel Assemblage A

Channel Assemblage A consists of channel widths ranging between 45 and 102 m, and an average sinuosity index of 1.12, representing primarily straight river planforms. Channels are located primarily outside, or at the margins of, the River Derwent floodplain in the eVoP, largely distal to the present day river, where they are incised into the Hutton Buscel-, and Seamer- sands and gravels.

Channel A1 is the best represented channel of Channel Assemblage A, traced from 200 m north of Wykeham Quarry (29.44 mOD). The channel is cut into the Hutton Buscel sands and gravels at Wykeham Quarry, before disappearing underneath the processing yard and reappearing in the west of the quarry. It can then be traced across the northwestern margin of the present floodplain, adopting a more sinuous planform (sinuosity index 1.38) for *ca.* 5 km, before terminating 2.4 km to the south of the Hutton Buscel terrace (at 22.8 mOD). Excavations in the Wykeham Quarry Silting Lagoon in November 2013, revealed the channel to be at least 7 m deep (Hanson Aggregates *pers comm.*), but no section through the channel infill was accessible

due to elevated water table levels during the excavation. Channel assemblage A channels are also identified more proximal to the contemporary River Derwent, but are highly fragmented (<400 m long), and cross cut by Channel Assemblages B and C (Figure 5.8).

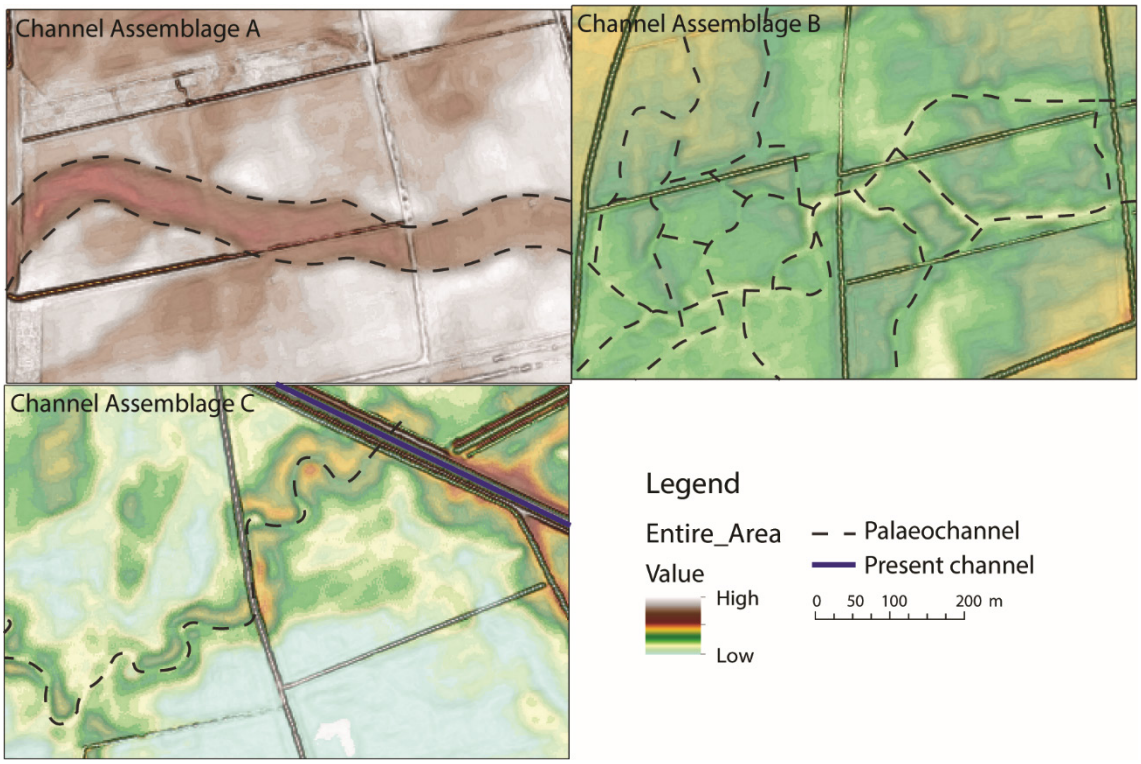

Figure 5.7. *Characteristics of the three types of palaeochannel identified in the eVoP. Dotted lines mark the mapped extent of each channel form.*

Channel Assemblage B

Channel Assemblage B is characterised by medium-low sinuosity channels (mean sinuosity index of 1.20), which have channel widths ranging between 11 and 30 m (mean= 21.5 m). Channels are the most widespread and are regularly interconnecting, separated by elongate- rounded bars forms *ca.* 50-200 m in length (Figure 5.7). In total, 204 channels are identified across the Derwent Floodplain, in the eVoP. Two channels in Channel Assemblage B are of particular interest. The first is channel B1, which comprises a series of interconnected palaeochannels, running from N-S for *ca.* 2.5 km, *ca.* 400 m west of the contemporary River Derwent, through Wykeham Quarry (Figure 5.8).

The second channel (B2) is mapped flowing E-W for *ca.* 1.7 km, through the lowest position of the Seamer sands and gravels. Channel B2 is the most easterly palaeochannel identified in the alluvial area of the eVoP, and ceases abruptly close to the mapped western extent of PF (Cloutman 1988a).

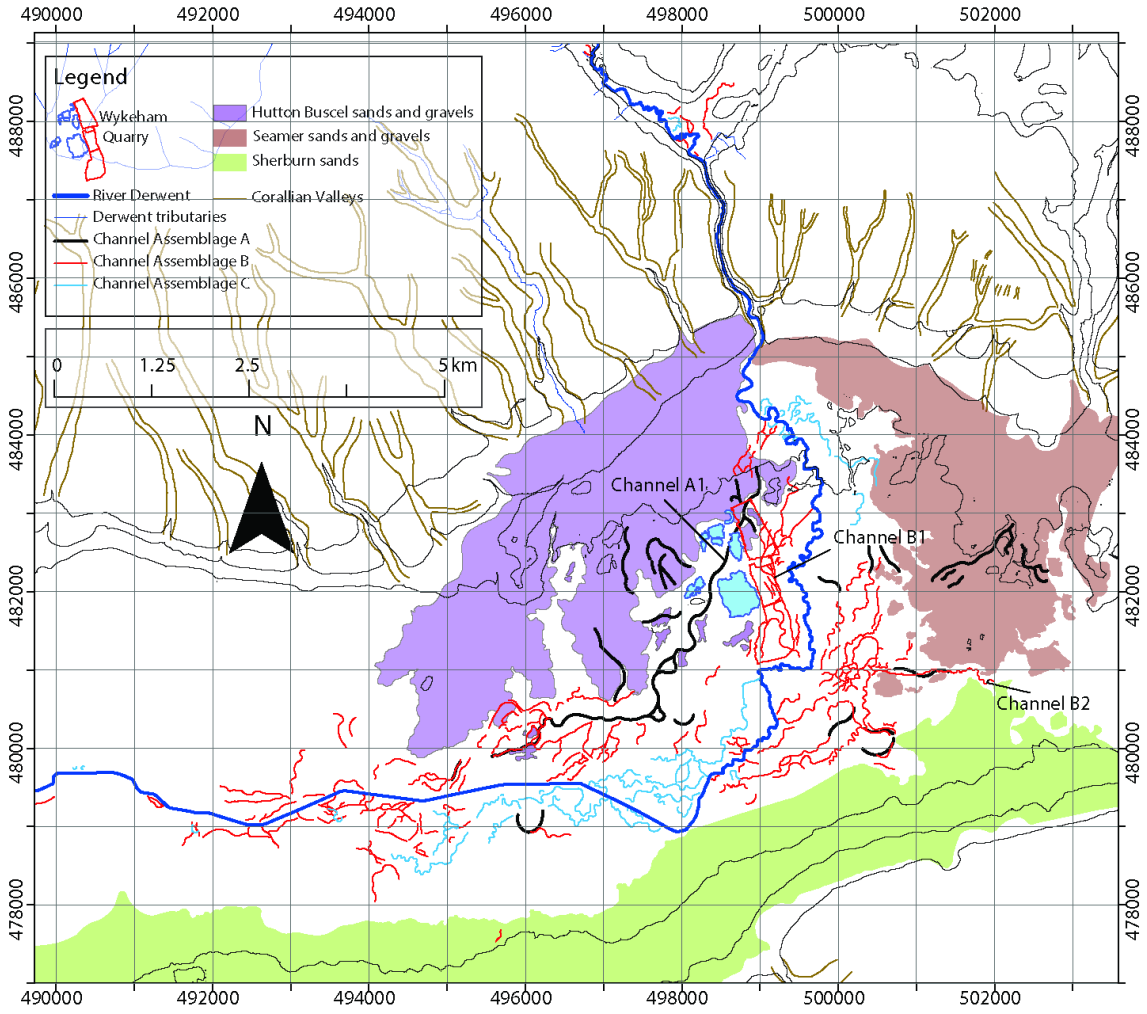

Figure 5.8. *Palaeochannel assemblages mapped in the eVoP. Topographic deposits which constrain the present floodplain (Hutton Buscel sands and gravels, Seamer sands and gravels, Sherburn sands) are included alongside the extent of the LiDAR DTM (black outline) used to map palaeochannels. Specific channels mentioned in text are also labelled.*

Channel Assemblage C

Channel Assemblage C is comprised of 55 sinuous (mean sinuosity index=1.70), meandering single channels, found flowing parallel, and frequently proximal to, the contemporary river with a mean channel width of 18.3 m (Table 5.2; Figure 5.7-5.8). The channels are mapped from the Everley Valley, and directly south of the Forge Valley in the eVoP, where they are comprised of regular to tortuous meander cut offs. A second cluster of Channel Assemblage C channels are identified in the valley centre of the eVoP, and are characterised by regular meandering planforms. These channels are found in close association with the canalised section of the River Derwent and match well with the course of the river prior to anthropogenic alteration in the 19th century (Menuge, 2001).

Interpretation

Channel Assemblage A

Large channel widths, isolation from the present floodplain in most instances, and straight, low sinuosity planforms, imply formation by high stream energy, comprising mixed-load to bedload dominated channels (Ferguson, 1987; Bridge, 2003). Whilst the channel characteristics do not discount a subglacial origin entirely (Greenwood *et al.,* 2007), their position, (incised into glacially derived sand and gravel landforms, interpreted to have been deposited proglacially (Franks 1987; Fraser *et al.,* 2009)), advocates that channel formation postdates ice recession from the Stage 2, and Stage 3 limits in the eVoP.

Channel Assemblage A is therefore interpreted as representing the presence of meltwater fed rivers, sourced either directly from the receding NSIL in the eVoP, or the North York Moors, flowing across the outflow gravels and kettle and kame topography of the eVoP during Stages 2 to 4. The orientation of the channels associated with the Hutton Buscel sands and gravels and the Seamer sands and gravels, suggest water may have been sourced from flow through the Corallian Dipslope via the Forge and Mere Valleys respectively.

Channel Assemblage B

The channel dimensions of Channel Assemblage B means that they can be interpreted as being formed by lower energy peak streamflows than those of Channel Assemblage A, but a similar to higher peak energy than those of the contemporary river systems of the VoP. It is difficult to determine whether the interconnecting channel systems in Channel Assemblage B were active contemporaneously based upon available evidence. If they were, the low width/depth (w/d) ratios (mean w/d ratio for channel B1 calculated at 16.64 from the sections of Fraser *et al.,* 2009), suggest that a braided river planform is unlikely (Nanson and Croke, 1992).

Sedimentological evidence from Wykeham Quarry suggests that the channels were abandoned and reoccupied repeatedly (Fraser *et al.,* 2009; see above) during their formation. The river system therefore, was likely to be laterally unstable (Schumm, 1985), characterised by frequent avulsion across the floodplain and at peak flow, reoccupying abandoned channels, potentially forming temporary anastomosing/anabranching planforms during high flow phases (Nanson and Croke, 1992; Makaske, 2001).

The slope values for the Channel Assemblage B are similar to those of the contemporary river, suggesting that the change in channel planform was most likely driven by changes in antecedent environmental conditions during formation (Rose *et al.,* 1980; Vandenberghe, 2002). The inability to trace channel assemblage B channel features east of the Seamer sands and gravels would

suggest that they were formed prior to the infilling of PF, and channel B2 therefore may be a remnant outflow of the former lake, into the River Derwent floodplain.

Whilst Channel Assemblage B includes palaeochannels with a moderate, and regular sinuosity (sinuosity index of *ca.* 1.3), the interconnecting channel forms imply a different fluvial planform to that of the present river. Such channel systems are most frequently found in ephemeral river systems, with higher peak discharges, required to shift the river system into a multi-channel planform (Bridge, 2003).

Channel Assemblage C

Channel Assemblage C were formed by low energy, sinuous rivers, similar to the contemporary River Derwent. These low energy river systems are typical of the temperate lowlands of the UK, where channel planform is invariably single channelled and meandering. The surrounding landscape for these rivers is characterised by high vegetation cover, resulting in reduced sediment supply and increased bank stability (Brown *et al.,* 1994). These rivers are laterally stable, have low stream power, and high suspended sediment loads, resulting in the deposition of fine grained silts and clays across floodplains (Nanson and Croke, 1992; Brown *et al.,* 1994).

5.2.3. Palaeobasins

Description

Palaeobasins are determined as topographic depressions formed either by river channel avulsion or as a remnant of dead ice melt during the Last Termination, and are potential sites for palaeoenvironmental reconstruction through this interval. 42 palaeolake basins are identified in the eVoP and Everley-Seacut Valleys (Figure 5.9). The mapped basins are all topographically constrained, having the potential to accumulate water and inhibit flow and currently have a flat surface, with slope values < 3°. They also provide evidence of infill by fine grained sediments in either a standing water body or via peat accumulation. Further criteria used include evidence for palaeo-inflow and outflow channels, including potential springline channel conduits, and aerial imagery evidence of waterlogged, peaty soils. commonly found capping infilled palaeolakes during hydroseral succession (e.g. Mellars and Dark, 1998).

All of the mapped palaeobasins lie within, or between the glacial sands and gravel units. They are circular to elliptical in shape, or elongated parallel to topographic ridges in the gravels, and with the exception of the Mere Valley basin, and Palaeolake Flixton (PF), < 400 m in diameter. Two of the landforms are identified in the Northern Extension of Wykeham Quarry and are termed as Depression A and B. To investigate the subsurface bathymetry and infill of the landforms, an auger survey (consisting of 13 boreholes) was performed on a basin identified within the Seamer sands

and gravels (termed the Seamer Basin; Figure 5.10). This basin is steep sided and in excess of 9 m deep (Figure 5.10b). The sediment infill was sampled from the deepest point and analysed in the laboratory to ascertain the bulk sedimentological properties. The basal 1 m is characterised by interbedded marls, and silty clays with pebbles. In clay-rich units, cold stenothermic chironomid taxa including *Micropsectra radialis* and *Orthocladus* sp. were identified (Figure 5.10c). Detailed maps, sediment logs and the raw data obtained from these deposits are reported in Appendices D and E.

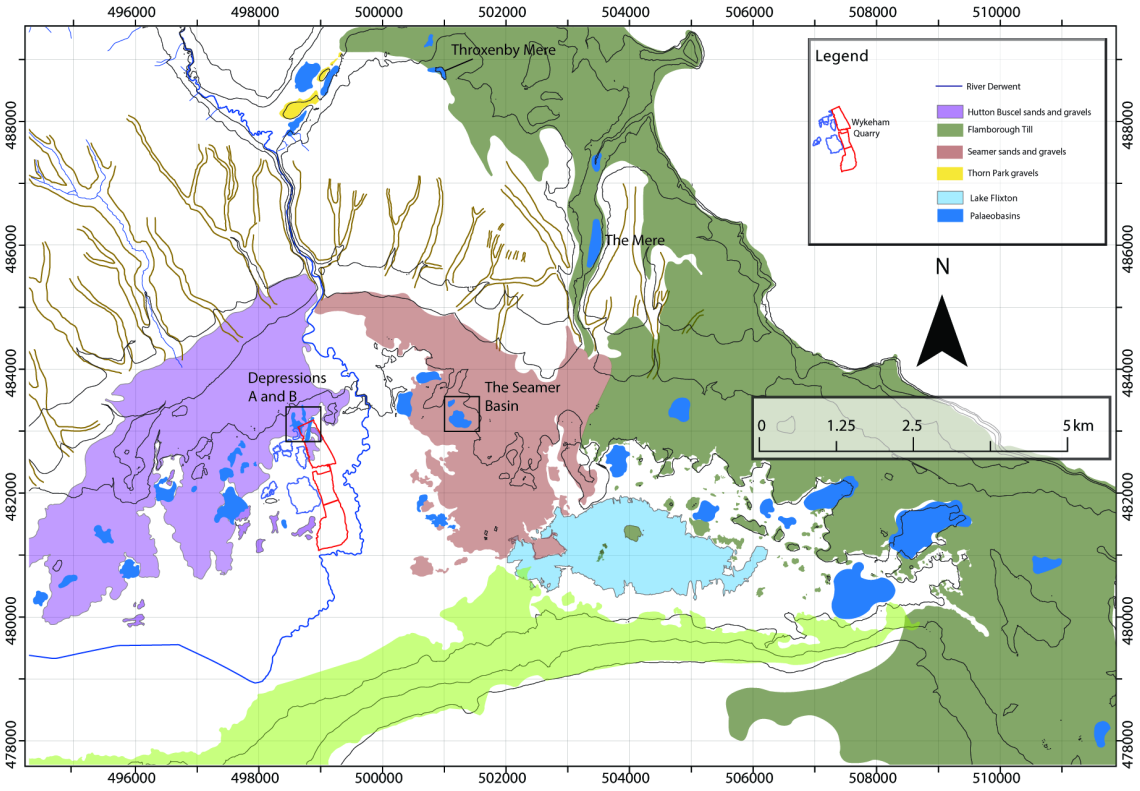

Figure 5.9. *Palaeobasins identified in the eVoP. Basins are focussed showing their affinity to the glacially derived sediments in the valley. The location of specific basins discussed in text are labelled.*

Interpretation

The emplacement of the basins within glacially derived sand and gravel units, suggest that they were formed at, or soon after deglaciation (Stages 2-4), either by the subaerial melt out of dead ice within outwash gravels, and till deposits (Fay, 2002; Livingstone *et al.,* 2010; Ben and Evans 2010), or within topographic depressions in abandoned meltwater channels, (section 5.2.2). The infill of the Seamer basin represents a tripartite sequence characteristic of LGIT infill in British lacustrine deposits (Lowe and Walker, 1986; Palmer *et al.,* 2015). This interpretation is supported by the presence of cold stenothermic chironomids in the clay rich beds, which are characteristic of LLS aged deposits in the British Isles (Brooks and Birks, 2000; Brooks *et al.,* 2016).

The bathymetric properties and infill of the basins are similar to PF (Cloutman, 1988; Palmer *et al.,* 2015), and therefore have significant potential for high-resolution palaeoenvironmental reconstructions through the LGIT using a variety of proxies. The presence of kettle-hole lakes

within sand and gravel bodies is consistent with formation in a proglacial outwash environment, where large bodies of ice become detached from the main body of the glacier, and melt-out in situ, forming a chaotically pitted surface (Bennett and Glasser, 2009). This is in accord with the model put forward by Palmer *et al.* (2015) for the bathymetry of the PF basin.

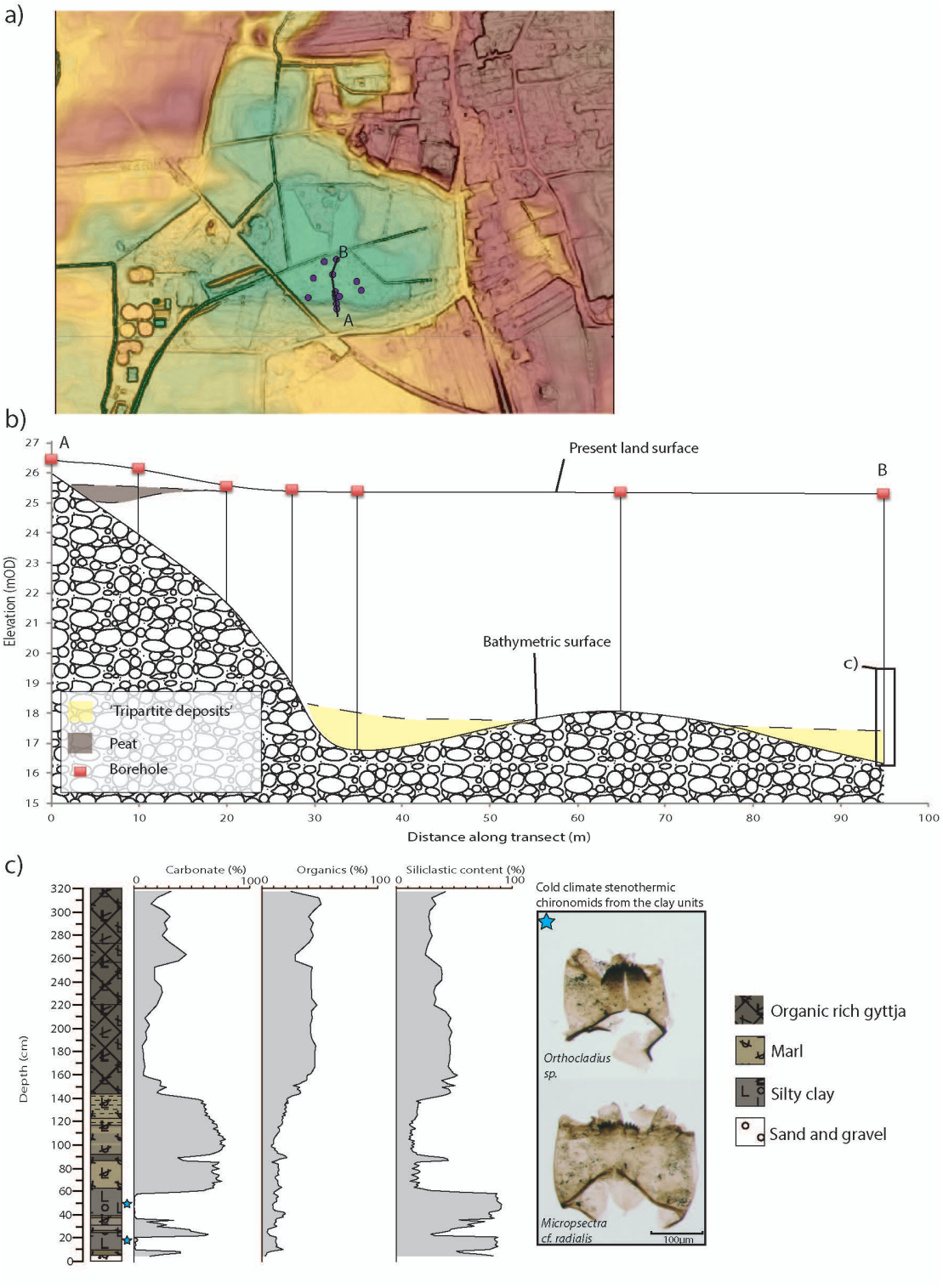

Figure 5.10. *a) DTM of the Seamer Basin showing the auger survey conducted in the southern margins of the depression (purple circles) b) Schematic S-N cross-transect through the basin demonstrating the steep incline at the margins, and the presence of 'tripartite sequence' type deposits in the basal infill. c) Sediment log and bulk sediment analyses on the basal infill of the palaeobasin (location marked on b)). Interbedded marls and clays at the base, coinciding with cold adapted chironomids in the clay units support deposition through the LGIT.*

5.3. Sedimentological and Stratigraphic data from Wykeham Quarry

The quarry at Wykeham (SE 98231 82344), *ca.* 1.5km from Wykeham village (Figure 5.11), produces dragline excavated, aggregate sand and gravel, for ready mixed concrete, and building contractors. The quarry is run by Hanson Quarry Products Europe Limited, and has been in operation since 1981. In 2004, permission was granted to extend mineral extraction to the east of the original quarry site. This excavation area (*ca.* 153,000 m^2 situated *ca.* 0.5km from the quarry processing yard), termed the present quarry, was excavated by Hanson in seven stages (Phases 1 to 7) between 2004 and 2013, with excavated areas being inundated by water, forming boating and fishing lakes. In 2012 permission was granted for a second extension phase, to the north, and the south of the present quarry site. These areas are designated as the Northern Extension (*ca.* 253,000m^2), and the Southern Extension (291,000m^2). Excavation of these areas, as with the present quarry, is/will be undertaken in stages (Extension phase N1 to N6 in the Northern Extension, and S1 to S5 in the Southern Extension), the extent of which are shown in Figure 5.11. Excavation of these areas began with Phase N1 in January 2015, with excavation estimated to continue for approximately 20 years based upon reserve estimates (Hanson *pers. comm.*).

5.3.1. Hanson Boreholes

138 boreholes have been recovered by Hanson Aggregates in four surveys in 1992, 1997, 2007, and 2015, (termed H-1992, H-1997, H-2007, and H-2015), using a reverse circulation drilling platform, to characterise the thickness, and extent of gravel deposits. The location of these borehole surveys are shown in Figure 5.12 with borehole elevations determined by dGPS.

The Hanson boreholes, consist of four stratigraphic units, from base to top termed: Basal Clay, Lower Gravel, Upper Gravel, and Overburden. The Upper and Lower gravels consist of similar deposits, and are divided, in order to place a subunit, termed as the Interburden, which lies stratigraphically within the gravels. The H-1992 survey consists of 49 boreholes drilled in transects, at 100 to 300m intervals in the present quarry, and Southern Extension regions of the study area (Figure 5.12.). The H-1997 survey comprised of 28 boreholes located within, and to the east of the Northern Extension. 53 boreholes in the H-2007 survey were focussed upon the region lying to the east of the Northern Extension and to the west of the River Derwent.A small survey of 8 boreholes makes up the H-2015 survey focussed upon the N1 extension phase, aimed to better characterise the thickness of the Interburden deposits.

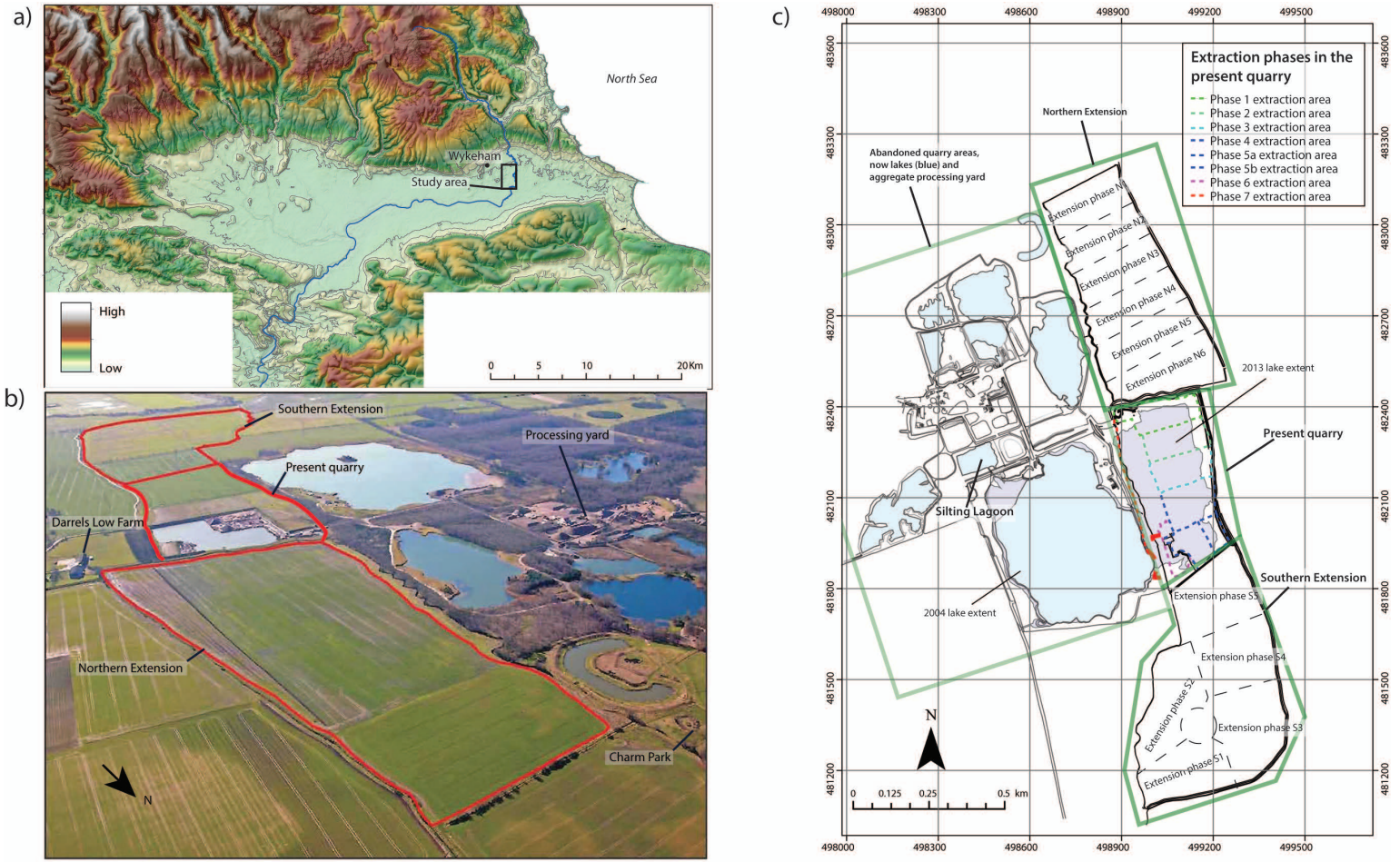

Figure 5.11. *a) Map of the VoP showing the location of the Wykeham Quarry study area in the eVoP. b) Aerial image of Wykeham Quarry looking southwest, taken ca. 2004 (after Josephs, 2010). during excavation of the Phase 1 extension area of the present quarry, showing the Northern and Southern Extensions, used as agricultural land prior to quarrying. c) Map showing the location of the quarry areas discussed in text. Extraction phases 1 to 7, excavated in the present quarry between 2004 and 2013, are outlined for context to the NAA records (section 5.3.2.), whilst the prospective extension phase N1 to N6 in the Northern Extension, and S1 to S5 in the Southern Extension are also marked.*

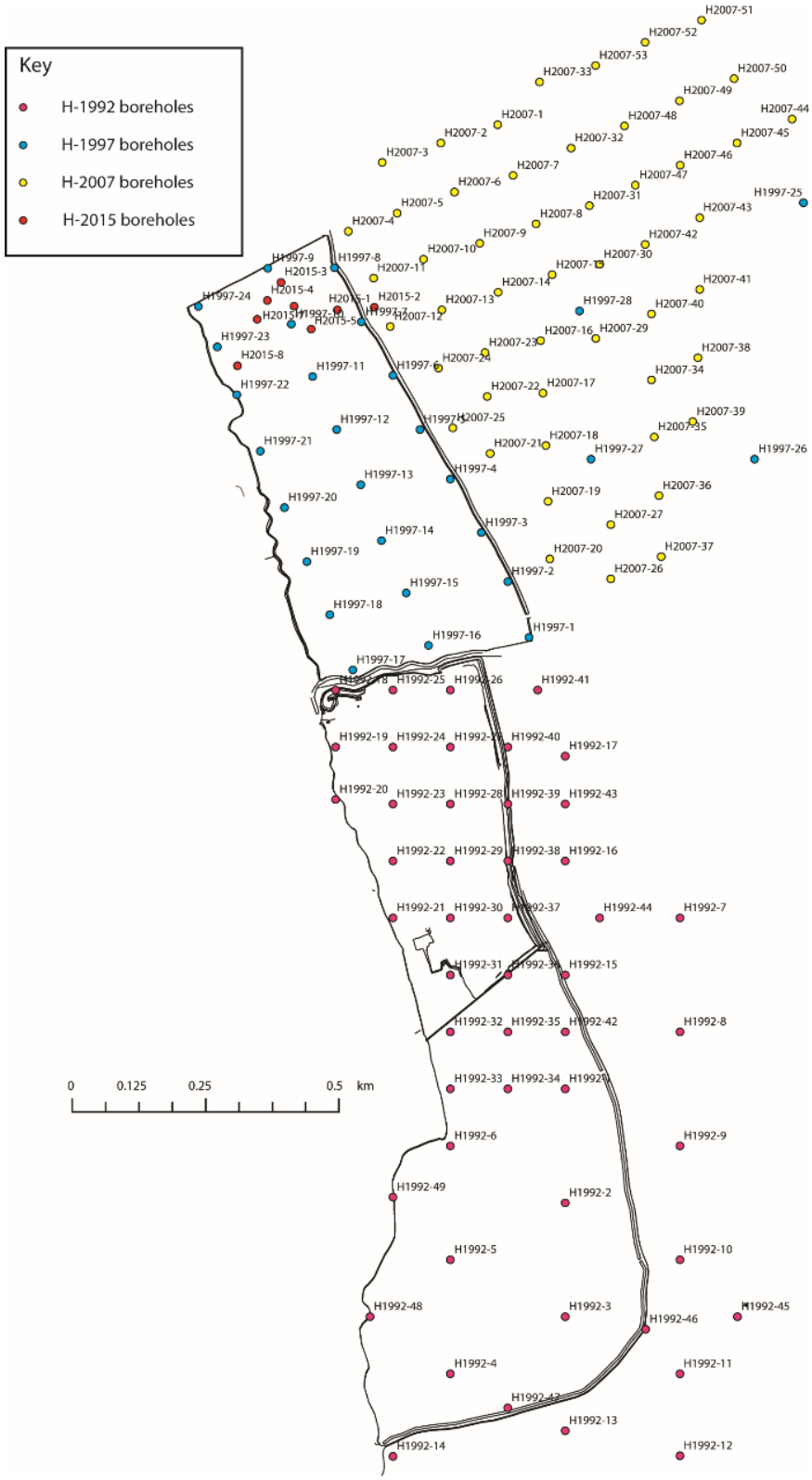

Figure 5.12. *Location of the four Hanson borehole surveys (H-1992, H-1997, H-2007, H-2015) at Wykeham Quarry, discussed in section 5.3.1.*

5.3.2. Northern Archaeological Associates (NAA)

Overburden deposits in Phase 1 to 6 extraction areas of the present quarry, were investigated between 2003 and 2009 by NAA (Fraser *et al.,* 2009; Cloutman *et al.,* 2010). Summaries of these

records are reported via photographs of sections (Figure 5.13a), and isolated logs of deposits (Fraser *et al.,* 2009). Seven records (Section C, Trench C1, Section G2, Trench Q1, Phase 1 south face section 3, Phase 1 north face, Phase 6a section 2) were field logged and subsampled for skeleton palaeoenvironmental proxy analysis (Figure 5.13b-c). These records were also radiocarbon dated at contacts between widespread stratigraphic units across the quarry. Whilst in isolation these records lack the required sedimentological information for thorough interpretation, they provide valuable context to the borehole records from the Northern and Southern Extensions (sections 5.3.3 and 5.3.4).

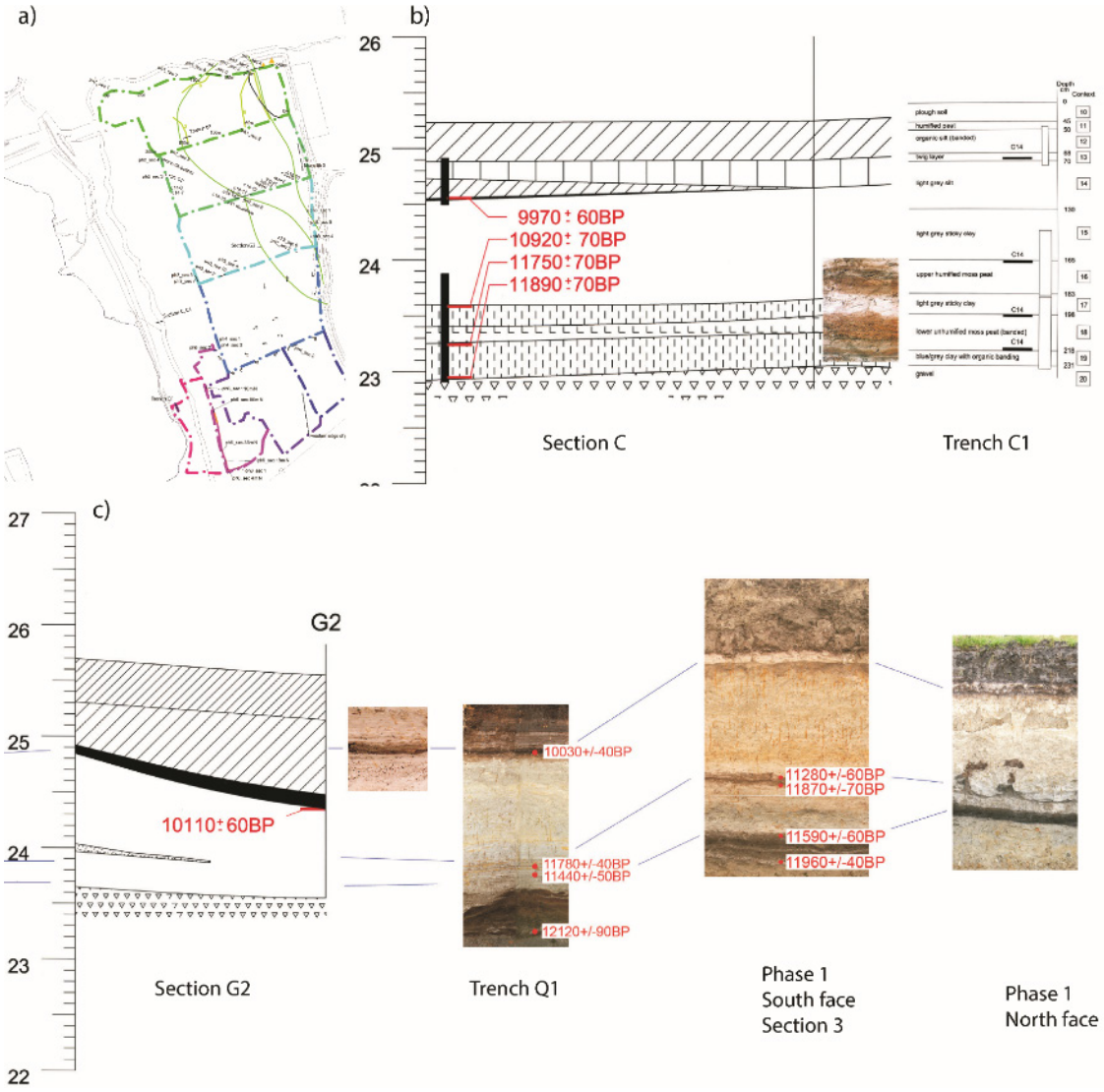

Figure 5.13. *Summary of the open section records described by the NAA between 2003-2009 (after Fraser et al., 2009). a) Map of the present quarry area, showing the locations of sites assessed by NAA. b) and c) show a summary of the key sites studied by NAA between 2003-2009. The vertical scale for these records is elevation (mOD), and the red labels are radiocarbon dates taken from stratigraphic contexts which are discussed further in section 5.4.*

5.3.3. QUEST Boreholes

A borehole survey undertaken by Quaternary Scientific (QUEST) from the University of Reading in September-October 2009, aimed to characterise the Overburden deposits in the Northern,

and Southern Extension areas of the quarry (Batchelor *et al.,* 2009; Figure 5.14). 114 boreholes, 71 located in the Northern Extension (BHN), and 43 in the Southern Extension (BHS) were spaced at 25-50m intervals, along four north-south, and nine east-west transects in BHN, and 50-100m intervals along two north-south and seven east-west transects in BHS. Borehole core samples were described following standard procedures for recording unconsolidated sediment, noting composition, physical characteristics, and colour and reported in Batchelor (2009). Stratigraphic logs from these records (Figure 5.14) are grouped by Batchelor (2009) into 5 types of sediments: a) Topsoil (black), b) Fine-grained waterlain sediments (blue), c) Organic rich/peat sediments (brown), d) Calcareous-rich marl sediments (green), and e) Sands and gravels (yellow).

5.3.4. Royal Holloway dataset (RHUL)

The main body of lithostratigraphic data in the Royal Holloway dataset (RHUL) is provided from 60 boreholes from the Northern Extension of the quarry area, taken in June 2013. The boreholes were exhumed along field croplines, using, a) percussion open gouge coring (RHULBHN 1 to 25; Figure 5.15), and b) hand screw augering (RHULGBHN 1 to 35; Figure 5.16). Retrieved sediment from each borehole was described in the field, with elevation calculated by a total station anchored to a dGPS georeferenced datum. Simplified stratigraphic logs of these boreholes are presented in Figures 5.15-5.16, and detailed sediment descriptions and X-Y co-ordinates are presented in Appendices B-C. A further 11 stratigraphic logs were made from open sections (RHUL S), either made available by Hanson during the course of quarrying between 2013 and 2014. The sections were logged in the north of the Phase 7 extraction in the present quarry (RHUL S1-3), the Silting Lagoon to the south of the quarry processing yard (RHUL S4), the quarry conveyor route in the Northern Extension, excavated in Summer 2014 (RHUL S5-10), and the northwestern corner of the S5 Extension Phase (RHUL S11). Sediment sequences were logged (see Chapter 4), and surface elevations calculated from 2m LiDAR data, with a vertical accuracy of ± 0.12m. The locations of these records are shown in Figure 5.14. In addition, three records excavated between 2014-2015, were described during the palaeoenvironmental reconstruction phase of this study (RHULPal 1-3). These records are situated in the west of the N1 Extension Phase (RHULPal 1-2), and the northwestern corner of the S5 Extension Phase (RHULPal 3).

5.3.5. Lithofacies associations at Wykeham Quarry

Seven lithofacies associations (LfA) are distinguished in the deposits at Wykeham Quarry (Table 5.3). A schematic representation of the deposits' distribution using a modelled cross section through these deposits presented in Figure 5.17. From this it can be seen that LfA 1-3 are distributed uniformly across the quarry area forming the lower part of the sediment sequences, whilst LfA-7 is distributed uniformly across the upper surfaces of all sequences.

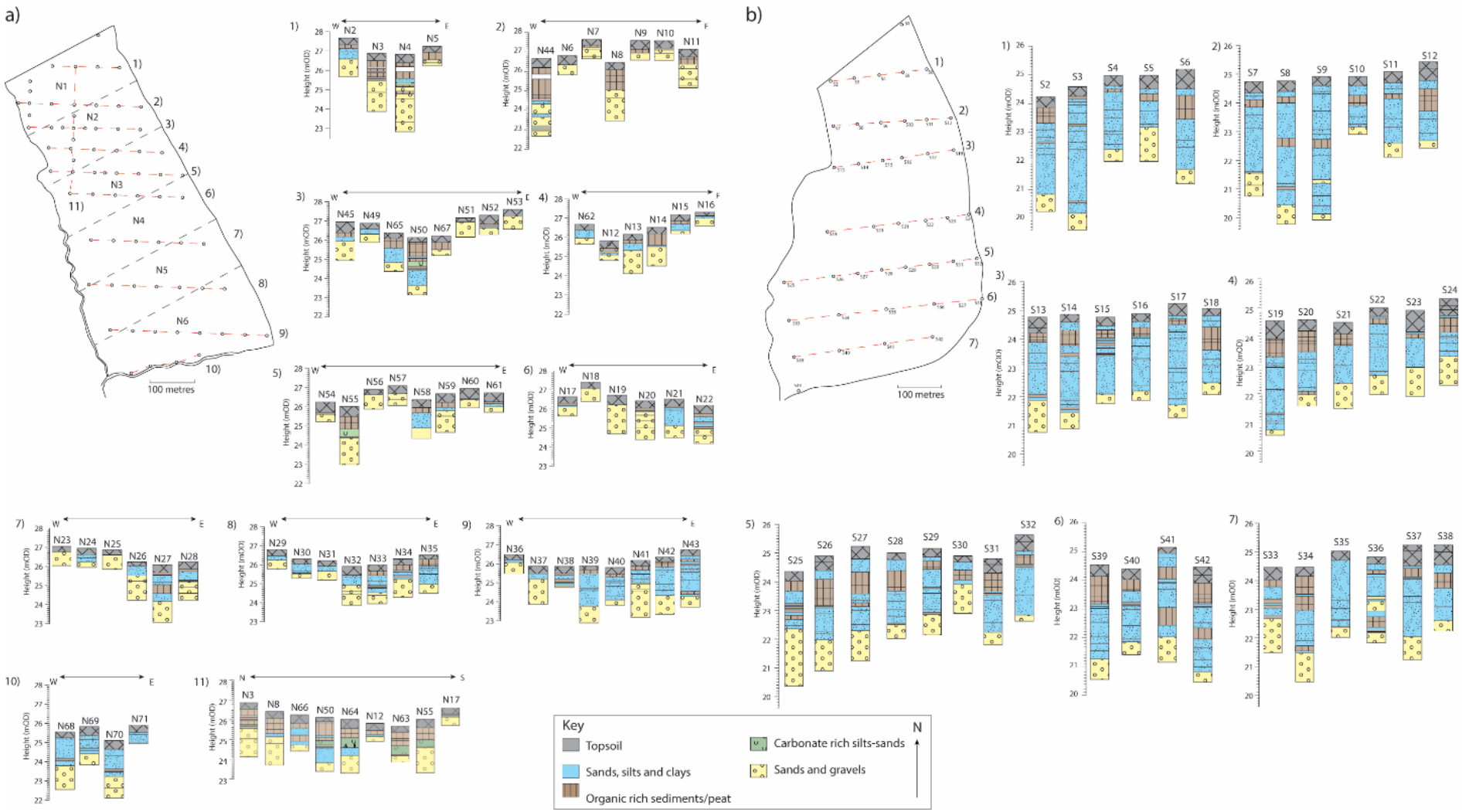

Figure 5.14. *Summary of the 114 boreholes excavated in the QUEST survey (after Batchelor, 2009) across the Wykeham Quarry extension areas. a) 71 boreholes excavated in the Northern Extension (BHN1 to 71) and b) showing the 43 boreholes excavated in the Southern Extension (BHS1 to 43). Boreholes are colour coded following the system adopted by Batchelor (2009) based upon each record's field descriptions.*

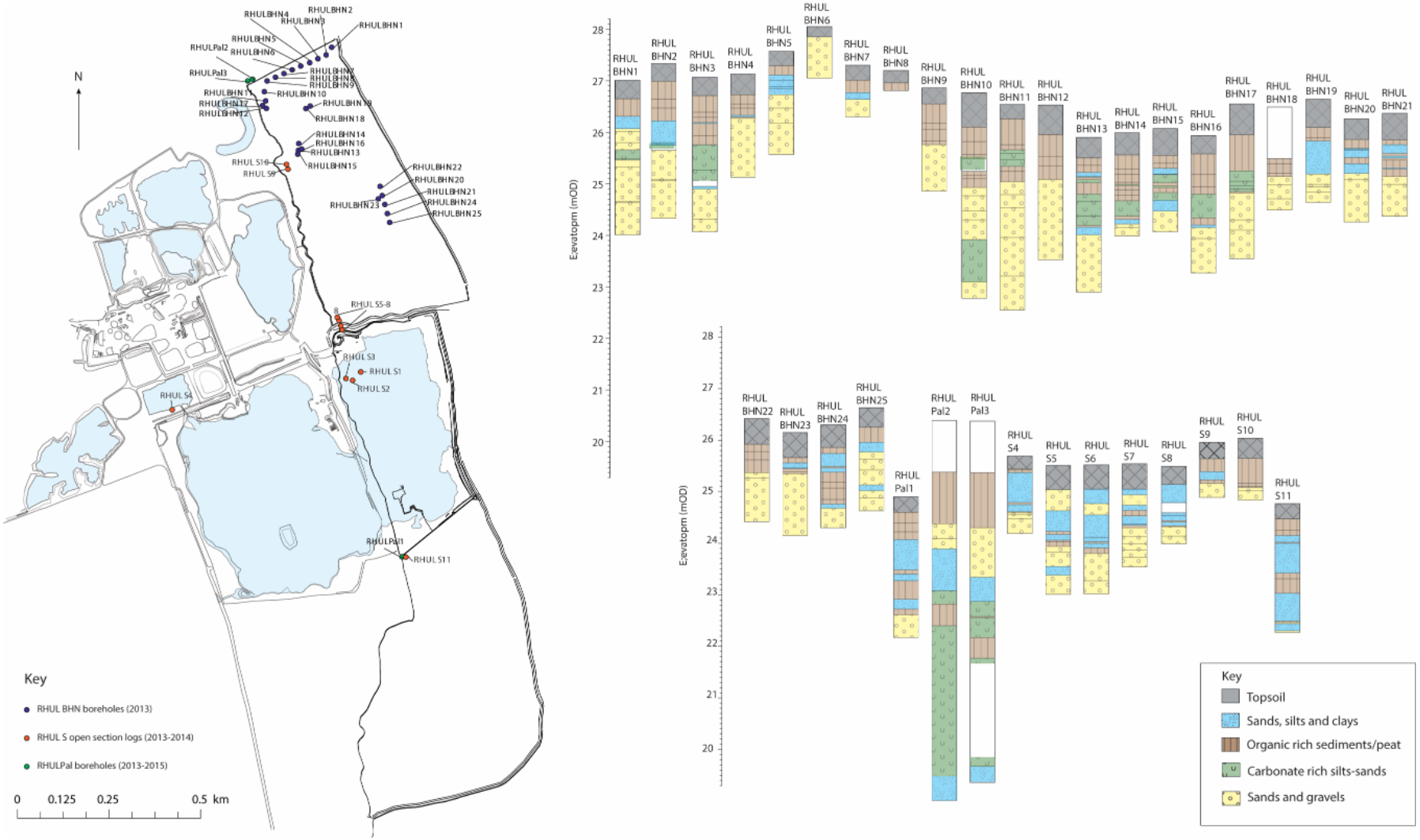

Figure 5.15. *Summary of the location, and basic stratigraphy of the sedimentological records exhumed at Wykeham Quarry by the author. Stratigraphic logs of the RHULBHN, RHULS, and RHULPal records are plotted against elevation, and colour coded following the same classification scheme as the QUEST records (Batchelor 2009, see Figure 4.6). Full sediment descriptions for these records are in Appendices B-C.*

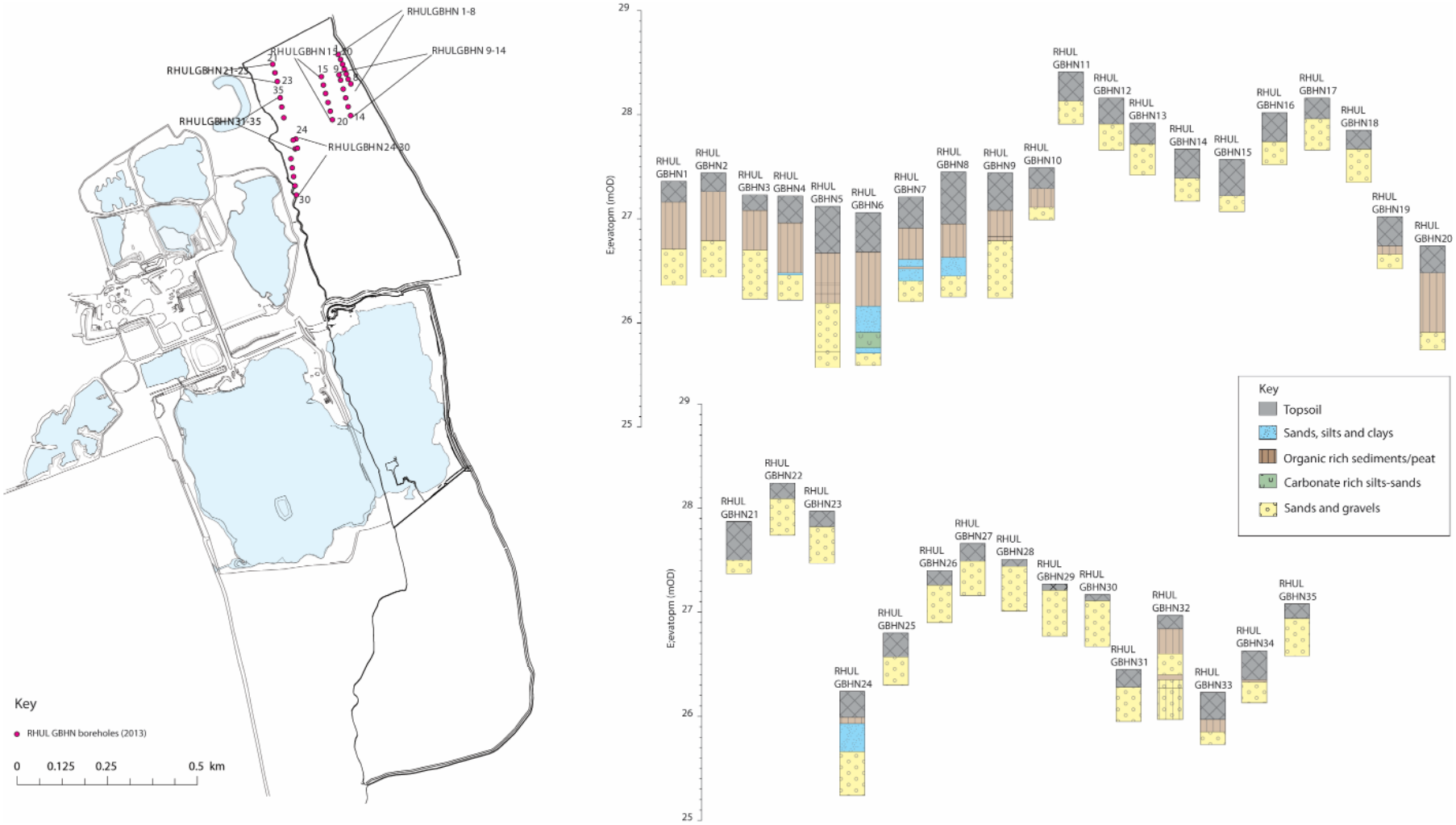

Figure 5.16. *Stratigraphic logs of the RHUL GBHN records, plotted against elevation. Description and classification of records follows the scheme adopted in Figures 5.14 (Sediment descriptions presented in Appendix B.*

Table 5.3. *Summary of the 7 lithofacies assemblages identified from the sedimentary sequences at Wykeham Quarry.*

Hanson Stratigraphy	LfA	Lithofacies codes	Further information	Process Interpretation	Depositional Environment
Overburden	7	Fr	Modern rootlets from the surface	Reworking of deposits by anthropogenic activity	Topsoil
	6C	Sm; Sh; Sr; (Gh)	Very fine to medium, massive and ripple cross laminated sands with vertical root inclusions	Variable low to moderate flow regimes in poorly vegetated catchments	Low-moderate energy overbank flows.
	6B	Fl, Fsm;	Silts and clays, finely interbedded (with LfA-5) and regularly organic-rich, containing frequent plant and woody material	Low energy suspension settling in poorly to well vegetated, shallow water-bodies and marshes.	Fluvial system dominated by overbank sedimentation in backswamp environments with occasional flood events.
	6A	Sm; Se; Sh; Sr; Sl; Ss; St	Medium-coarse sands and occasional gravels associated with scour features and larger channel forms, containing occasional rootlets and consistently found directly overlying LfA 2	Mid and high energy flows associated with mid-channel processes and/or high energy flood deposits.	Fluvial sedimentation either in midchannel, or proximal channel settings.
	5	C; Fm	Peat poorly to well humified, commonly interbedded with carbonate-rich deposits (LfA-4) and organic-rich sediments (LfA-6)	Marginal accretion of organic detritus either where peat is submerged for long periods (poorly humified), or at higher elevations, being predominantly sub-aerially exposed (well humified)	Terrestrial to eulittoral environments, representing marginal environs to water bodies
	4C	Fm; Sm; Gm	Siliclastic rich deposits interbedded with gravel lenses oolitic limestone, sand beds and massive fines.	Episodic higher energy flow events reworking deposits and diluting the authigenic carbonate production.	Flood events interrupting sedimentation or drop in lake water level allowing reworking of the lake margins into the lake basin.
	4B	Fm; Fl; Sm	Carbonate-rich deposits including authigenic marl and carbonate tests. Occasionally interbedded with peat	Fine-grained, still-water sediment in base rich waters and possibly some flowing water.	Freshwater lacustrine and spring deposits within a depression in the gravel surface.
	4A	Sm	Isolated gravel clasts within sands.	Gravity flows in shallow water	Unstable gravel margins on the sides of depressions causing gravity flows into shallow water bodies.
Interburden	3	Dmm	Matrix supported diamicton.	Slope and/or glacial processes, (debris flows).	Supraglacial-proximal proglacial slumping of melt-out deposits and/or reworking in topographically unstable environs
Lower and Upper gravels	2	Gm, Gh, Sm,	Gravels modally sub-angular to sub-rounded and of widespread, local and erratic lithologies.	High energy flows and lower energy sedimentation in channels. Mixed lithology suggests glacial input into Vale of Pickering but also evidence of increasingly significant input from the Forge Valley, to the north of the quarry.	Ice-proximal glaciofluvial outwash.
Basal clays	1	Fl(d); Fl; Sm	Well sorted, isolated gravels clasts interbedded, reverse graded at the top.	Distal glaciolacustrine with more proximal sediments toward the top.	Glaciolacustrine.

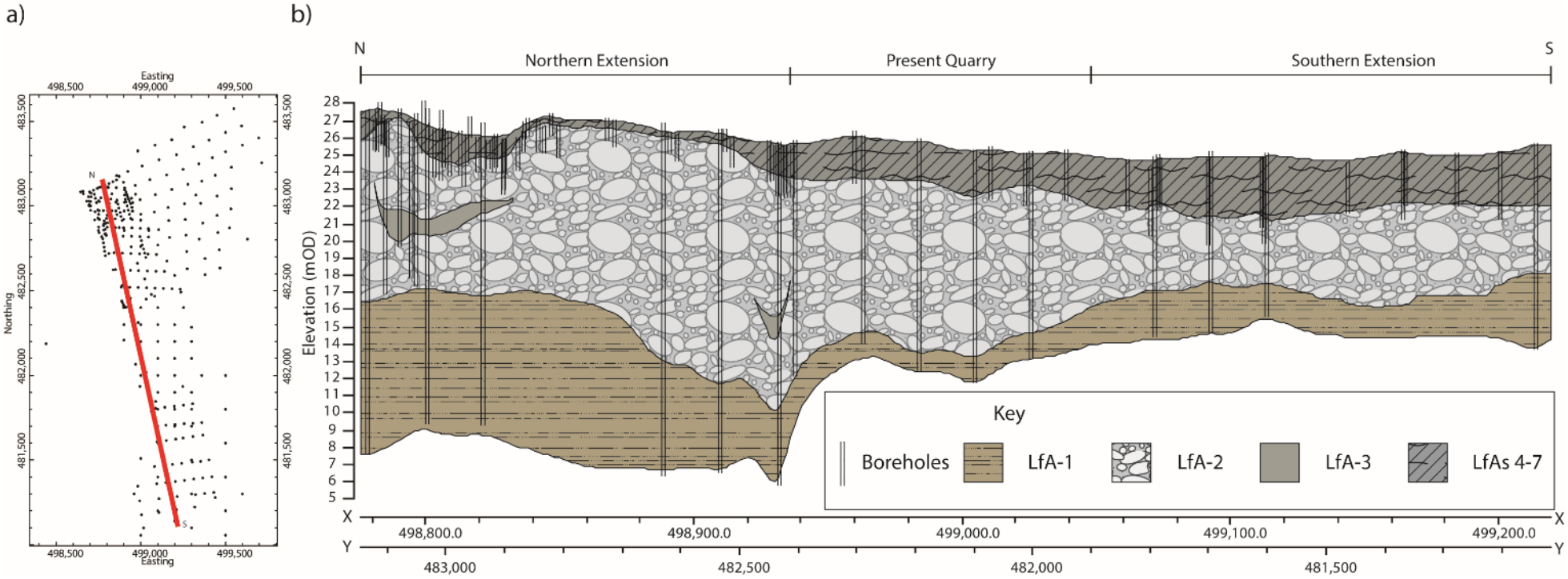

Figure 5.17. *a) Transect line used to construct the stratigraphic model. The distribution of stratigraphic records are marked by black dots. B) Stratigraphy of the 7 LfAs at Wykeham Quarry, modelled using a 5 point inverse distance weighted model, with a 50m swath width from the transect line depicted in a).*

Sedimentological information from LfAs 1-3 are based principally on borehole records from the Hanson dataset. Some open exposures were available to previous workers (Franks, 1987; Fraser *et al.,* 2009), and can be used to inform interpretations on the modes of sediment deposition. In LfAs 4-6 there is greater complexity in the properties and sediment architecture, which dominate the upper fill of the sediment sequences. These deposits were assessed via borehole records (QUEST BHN and BHS, RHULBHN, GBHN, RHULPal) as well as open section descriptions obtained in this study (RHULS) and the NAA reports (Fraser *et al.,* 2009).

LfA-1-Basal Clays

Description:

The basal sediment unit identified in the Hanson borehole datasets consist of grey to brown, stiff laminated silty clays. with occasional gravel clasts, and sands. In some instances these sediments are reverse graded to fine to medium, brown sands, interbedded with the clay-rich sediments. Sedimentological information for these units are provided only by field descriptions from the H-1997, and H-1992 logs, meaning sedimentary characteristics such as the Munsell colour, and nature of contacts are not reported. These deposits are widely distributed across the quarry area, consistently >10m from the present-day land surface (Figure 5.17).

Interpretation:

The fine grained and well sorted characteristics of LfA-1 indicate deposition via suspension settlement in a low energy lacustrine environment of sufficient depth to preclude substantial reworking via current flows (Ashley, 1975). The high minerogenic component of the deposits indicate low organic productivity in the lake waters or within the lake catchment (Hubbard and Glasser, 2005). The presence of isolated gravel clasts within the fine grained matrix is indicative of dropstones being transported via ice rafting across the lake surface and deposited by melt-out and/or overturn of icebergs (Thomas and Connell, 1985; Pickering *et al.,* 1986; Hubbard and Glasser, 2005). These characteristics are indicative of formation in a proglacial lake environment, in cold climatic conditions (Palmer *et al.,* 2008a; 2010). The coarser particle sizes reported towards the top of LfA-1 demonstrates an increase in depositional energy (Schilleref *et al.,* 2015). This indicates a more proximal source of sediment influx into the lake, either via a lowering of the relative lake level (pre-conditioning the basin margins for sediment delivery/slumping), and/or a more proximal ice frontal position in respect to Wykeham Quarry.

LfA-2- Sands and gravels

Description:

LfA-2 consists of moderately to poorly sorted, clast supported massive to horizontally bedded (Figure 5.18) gravels. In the present quarry, gravels with clasts in the 4 to 20mm size fraction are

composed of sub-angular to well-rounded, and moderately rough to smooth clasts, consisting of a wide range of lithologies. Sandstones, limestones and siltstones all constitute ≥10 % of the gravel assemblage (Table 5.4), which reflect the regional geology of the eVoP. Quartzite, dolomite, and mafic igneous clasts each constitute between 2 and 10% of the assemblage, the source rocks of which, are not present in the eVoP. This gravel assemblage is characteristic of the present quarry area and the Southern Extension of Wykeham Quarry (Hanson *pers comm*.). Excavations in the N1 extension phase by Hanson Aggregates during 2015, revealed a gravel assemblage, that subtly varies from that described above, being composed primarily of angular to rounded Limestone and Sandstone, with evidence of iron oxide staining (Hanson *pers comm*.; Table 5.5). Erratic lithologies are also present in these deposits (2-10% of mafic igneous clasts, <2% of basalt and chert). No open sections through LfA-2 were available at Wykeham Quarry through for this study, principally due to their submergence below the water table.

Table 5.4. *Characteristics of the 4-20 mm fraction of the aggregate deposits at Wykeham Quarry (provided by Hanson pers comm.). These measurements are derived from the boating lake area of the present quarry, and are representative of the aggregate assemblage across the present quarry area. Roundedness is abbreviated as follows: VA= Very angular, A= Angular, SA= Subangular, SR=Subrounded, R= Rounded, WR=Well rounded. Surface texture abbreviations are as follows: R= Rough, MR= Moderately rough, S=Smooth.*

Clast lithology		Roundedness	Surface texture	Coatings/Encrustations	Weathering
Major (≥10%)	Sandstone	SA to WR	R to S	None	None
	Limestone	SA to WR	MR to S	None	None
	Siltstone	SA to WR	MR to S	None	None
Minor (2 to <10%)	Quartzite	SA to R	MR to S	None	None
	Dolomite	SA to WR	MR to S	None	None
	Quartz	SR to WR	MR to S	None	None
	Igneous rock fragments	SR to WR	MR to S	None	None
Trace (<2%)	Chert	SA	MR	None	None
	Shell fragments	SR	S	None	None

Table 5.5. *Characteristics of the 4-20 mm fraction of the aggregate deposits from the N1 Extension Phase at Wykeham Quarry (provided by Hanson pers comm.). Roundedness is abbreviated as follows: VA= Very angular, A= Angular, SA= Subangular, SR=Subrounded, R= Rounded, WR=Well rounded. Surface texture abbreviations are as follows: R= Rough, MR= Moderately rough, S=Smooth.*

Clast lithology		Roundedness	Surface texture	Coatings/Encrustations	Weathering
Major (>10%)	Limestone	A to R	MR to S	Rare iron oxide staining	None
	Sandstone	SA to R	MR toS	Rare iron oxide staining	None
Minor (2-10%)	Mafic volcanics	SA to R	MR to S	Iron oxide staining	Moderate
	Vein quartz	A to R	MR to S	Iron oxide staining	None
Trace (<2%)	Basalt	VA	SR to S	None	None
	Mudstone	VA	SR to S	Iron oxide staining	None
	Chert	SR to R	S	Iron oxide staining	None

Interpretation:

The particle size, sorting, and roundedness data from LfA-2 are consistent with deposition via current flows in a high energy environment, with variations in depositional energy. The rounded, smoothed, and unweathered nature of the clasts also support direct transportation, and rapid deposition in a fluvial environment (Siegenthaler and Huggenberger, 1993; Miall, 1996). Additionally, the consistent presence of these deposits across the quarry area suggests the episodes of uniform, high energy flow across wide spatial areas, with most sediments transported as effective bedload material, and finer sand grains transported via saltation/suspension (e.g. Rose *et al.,* 1999).

The erratic lithologies in LfA-2 can also be used to indicate the provenance of sedimentary source material (Evans and Benn, 2004). Whilst the quartzite, and dolomite lithologies are hard to precisely provenance without more detailed investigation, the igneous clast assemblage can be attributed to the source region. The most proximal mafic, igneous outcrops to Wykeham Quarry, are the Cheviot Volcanic Complex (Busfield *et al.,* 2015), and the Carboniferous, and Devonian lava successions of NE England (Taylor, 1971), which are situated 175 to 200km north of the study site. For these clasts to be present in the gravel assemblage at Wykeham, a southerly transport of material is required prior to deposition. This pathway correlates well with erratic flow courses during the Dimlington Stadial (Clark *et al.,* 2004; Evans *et al.,* 2005; Livingstone *et al.,* 2012; Yorke *et al.,* 2012; Busfield *et al.,* 2015; Bateman *et al.,* 2015; Chapter 3). This is reinforced by analogous clast lithologies in both the Hutton Buscel sands and gravels which surround Wykeham Quarry (Franks 1987; Chapter 3), and the Skipsea Till by (Busfield *et al.,* 2015), supporting a close association between the sedimentary sources of these deposits. The higher proportion of more angular, and weathered clasts of local lithology in the N1 phase of the quarry is unclear, but would suggest a higher proportion of locally derived clasts in comparison to the rest of LfA-2, and might indicate a sudden influx of material from rivers systems draining the North York Moors, possibly as ice retreated.

LfA-3- Diamicton

Description:

LfA-3 is a matrix-rich diamicton composed of a very dark greyish brown (10YR 3/2) poorly to unsorted matrix supported sandy silty clay, interbedded with frequent fine to coarse, subangular-subrounded gravel clasts, which are randomly distributed through the matrix. These deposits form lenses and interbeds within LfA-2 (Figure 5.18).

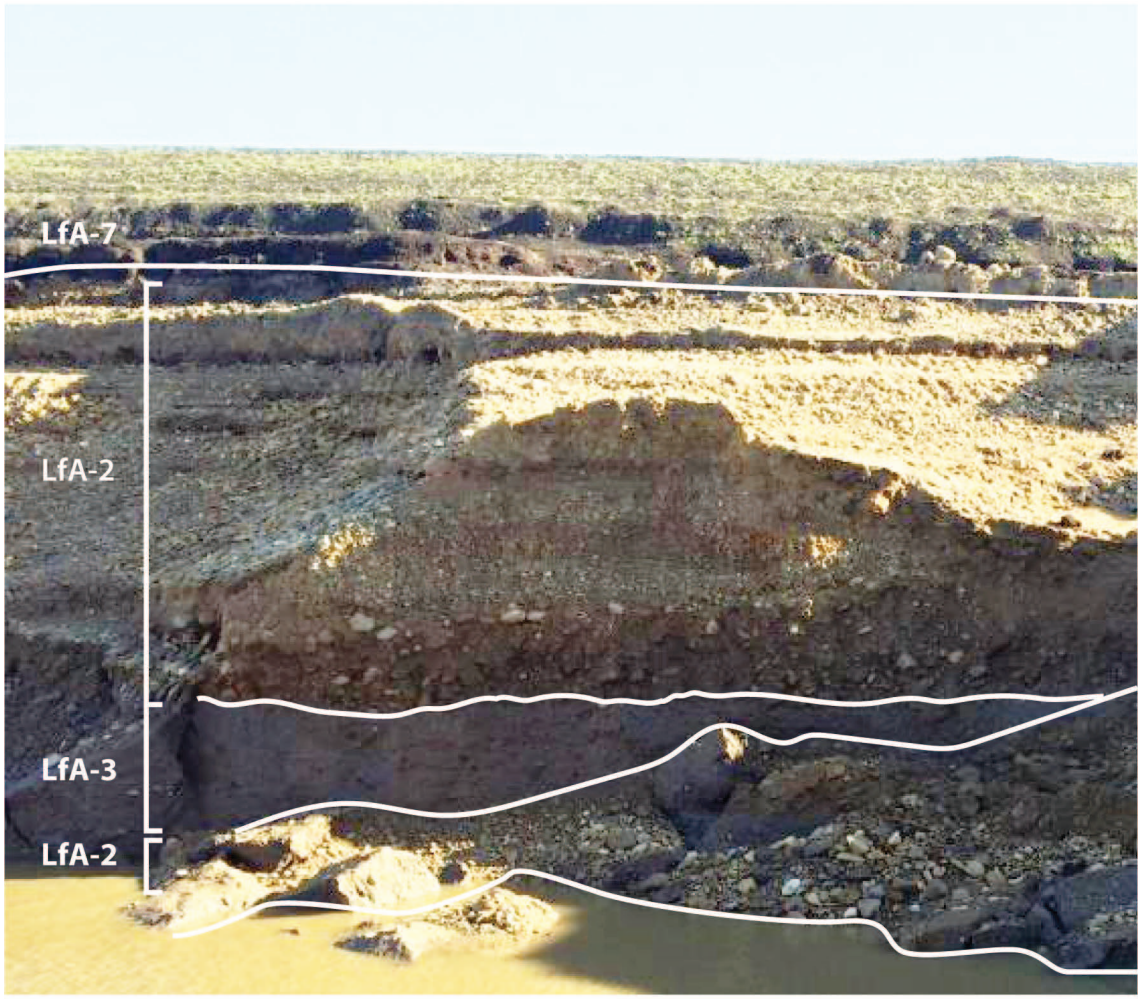

Figure 5.18. *Image provided by Hanson, during the initial excavation of the N1 phase of the Northern Extension in 2015, showing the interbedded nature of LfA-3 within LfA-2. Access to these deposits for detailed sediment logging was not possible due to the unconsolidated nature of the exposed deposits, and the high water table during excavation.*

Interpretation:

Unsorted sediment assemblages are formed by processes which shift rapidly in depositional energy. These processes most commonly occur either via gravitational mechanisms (debris flows) and/or glacial processes (subglacial or supraglacial tills). The presence of LfA-3 within deposits interpreted as being derived from ice-proximal glacifluvial outwash (LfA-2) suggest that formation via associated glacial processes is probable. These environments are highly susceptible to the interbedding of debris flows derived from supraglacial meltout till, formed via slumping from unstable gradients due to ice surface ablation during retreat (Bennett and Glasser, 2009). This mode of formation is supported by the analogous characteristics to the Skipsea Till across the NE Yorkshire Coast (dark greyish brown, matrix supported diamict; Busfield *et al.,* 2015), suggesting a similar sediment source for LfA-3. Without further sedimentological evidence however, confidently ascribing LfA-3 to a specific depositional process is difficult, meaning the formation of these deposits remains equivocal.

LfA-4- Carbonate-rich freshwater lacustrine facies including subfacies A-C

Description:

LfA-4 is are sub-divided into three subfacies termed LfA-4 A-C. The properties of these subfacies are outlined below. LfA-4A is the basal sedimentary unit of LfA-4, where it directly overlies LfA-2 deposits and consists of very dark greyish brown (10YR 3/2), medium to fine minerogenic rich sand, with isolated gravel clasts and a diffuse upper contact. LfA-4B consists of dark grey (10YR 4/1), homogeneous to faintly laminated silty, friable fine sand, with abundant calcium carbonate thalli casts of *Chara sp.,* isolated shell fragments and fine gravel clasts. These deposits are occasionally interbedded with black (2.5Y 2.5/1) poorly humified-telmatic peat (LfA-5) containing abundant herbaceous macrofossils, interdigitated with thin beds (0.02-0.05m) of carbonate rich sandy silts. LfA-4C is composed of dark grey (5Y 4/1) minerogenic sandy clayey silt, interbedded with laminations to beds (0.005-0.95m) of olive grey (5Y 5/2) fine-coarse sands and moderately to poorly sorted fine to medium gravels. Where LfA-4C is best expressed (e.g. RHUL-Pal 2-3), these laminations/beds coarsen, thicken and become more regular from the base to the top of the lithofacies. The coarsest gravel-rich beds range between 0.73 and 0.95m in thickness, and consist of clast supported, subangular to well-rounded clasts of varying lithologies including oolitic limestones, and sandstones within a medium to coarse sandy matrix. These beds exhibit reverse, and normal grading at their lower and upper contacts respectively.

Interpretation:

The sediment properties of LfA-4A (colour, minerogenic content, composition) invoke high volumes of allogenic inwash, similar to those of LfA-3 (interpreted as a cold climate debris flow of glacigenically derived diamicton), although the deposit is composed of a coarser modal particle size (sand) and is better sorted, suggesting formation via current flow. LfA-4A is therefore interpreted to represent re-deposition of glacigenic sediments in shallow waterlain environments via gravity flows from episodic slumping of these sediments. This interpretation is supported by the stratigraphic position of LfA-4A, directly overlying LfA-2 suggesting formation soon after the cessation of proximal glacifluvial outwash in the eVoP.

LfA-4B represents authigenic sedimentation within still to slow flowing, littoral, base rich water bodies (Murphy and Wilkinson, 1980; Treese and Wilkinson, 1982; Boreham and West, 1993). Shallow water depths of these deposits are supported by the presence of calcified *Chara* thalli (Anadón *et al.,* 2000; Apolinarska *et al.,* 2011) and interbedded, poorly humified peats (LfA-5), which possibly represent changes in water depth during deposition (Murphy and Wilkinson, 1980).

The high minerogenic composition of LfA-4C represents low organic productivity within water bodies and surrounding catchments, with silts and clays falling from suspension during periods

of limited turbulence in the water column (Palmer *et al.,* 2015). The introduction of coarser grained beds in LfA-4C is indicative of higher energy processes episodically delivering sediment into water bodies. This may either be as a result of a lowering in the level of the lake body, enabling the redistribution of lake margin deposits via slumping (Ashley, 1975), and/or episodic influx of high energy flood deposits (Schilleref *et al.,* 2015). The sorted and graded characteristics of LfA-4C, and presence of locally derived clast lithologies (oolitic limestones), supports formation via higher and lower current flows from the Corallian Dipslope, to the north of Wykeham Quarry.

LfA-5- Peats

Description:

LfA-5 consists of dark grey to black (10YR 4/1 to 2.5Y 2.5/1) poorly to well humified silty, mossy-, herbaceous-, and infrequent woody- peats. Poorly humified deposits (Th^{1-2}) are consistently identified episodically interbedded with LfA-4 and LfA-6B (Figure 5.19). These facies contain well preserved woody, and mossy macrofossil remains (Franks *et al.,* 2009). Well humified and friable remains (Th^{3-4}-Sh) are focussed into the uppermost sections of the overburden, consistently underlying LfA-7.

Interpretation:

Peatland formation in fluvial wetlands is closely associated with limited minerogenic influx in low flow velocity contexts (Rose *et al.,* 1980; Rose, 1995; Miall, 1996) and relative variability in water table elevations (Moore, 1989; Rodwell, 1995). This is supported by the interbedding of LfA-5 deposits within littoral lacustrine sediments in LfA-4 and LfA-6b, which demonstrates that variations in relative water levels were an important mechanism for the formation of these deposits (Digerfeldt, 1988; Harrison and Digerfeldt, 1993). These deposits are therefore interpreted as telmatic peats, formed in close association with the elevation of the water table. The high volumes of fine-grained, organic-rich material are also likely to accumulate in shallow, waterlogged pools and backswamps distal to high velocity flow regimes in floodplains (Miall, 1996). The high abundance of organic material demonstrates high organic productivity in catchments, in temperate environments (Rose, 1995; Tolksdorf *et al.,* 2013).

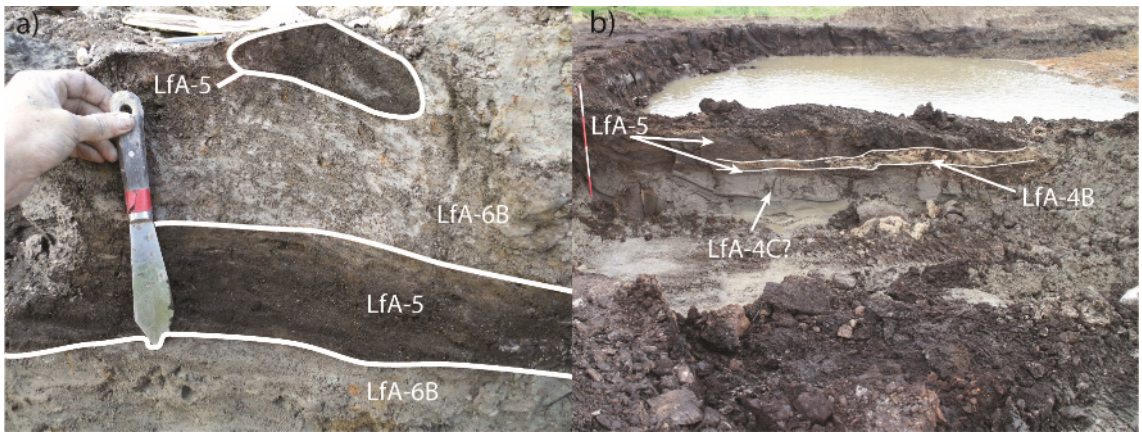

***Figure 5.19**. Examples of interbedding of LfA-5 with LfA-6 and LfA-4. a) is an image from the RHULS5 sequence taken by the author demonstrating the interdigitation of LfA-5 with LfA-6B, b) is an image provided by Oxford Archaeology (pers comm.) demonstrating LfA-5 deposits interbedded with LfA-4B and LfA-4C. This image was taken from the N1 excavation phase in the Northern Extension for which the author was not present.*

LfA-6- Fine-grained non-carbonate deposits

Description:

LfA-6 deposits consist of complex interbeds of moderately to well sorted silts, sands and clays. These deposits can be divided into three sub-facies termed LfA-6A, LfA-6B, LfA-6C. LfA-6A consists of grey to dark yellowish brown (10YR 5/1 to 10YR 10YR 4/6), massive, silty fine to medium sands, with isolated fine to medium gravel clasts, ranging between 0.91 to 0.04m in thickness, and detrital wood fragments. In most instances these deposits directly overlie LfA-2 across the quarry area. Lenticular outlines of small scour fills, are identified in the RHULS-5-7 records, as well as trough cross bedded forms which are identified in the NAA records from the present quarry area (Fraser *et al.,* 2009; Figure 5.20).

LfA-6B consists predominantly of well sorted grey to blueish grey (10YR 5/1 to Gley 2 5/1) silty clays. These deposits are interbedded with dark greyish brown to black (10YR 4/2 2.5Y 2.5/1), organic rich silty clays/ poorly humified telmatic peats (LfA-5), which contain well preserved mossy, herbaceous, and woody macrofossil remains (Fraser *et al.,* 2009; Cloutman *et al.,* 2010; Figure 5.20). Sub-fossilised annelid casts are also occasionally observed within these deposits (Batchelor, 2009). Contacts between organic and inorganic beds are sharp and in some instances involuted (these are observed only when directly underlying LfA-6C deposits; Figure 5.20).

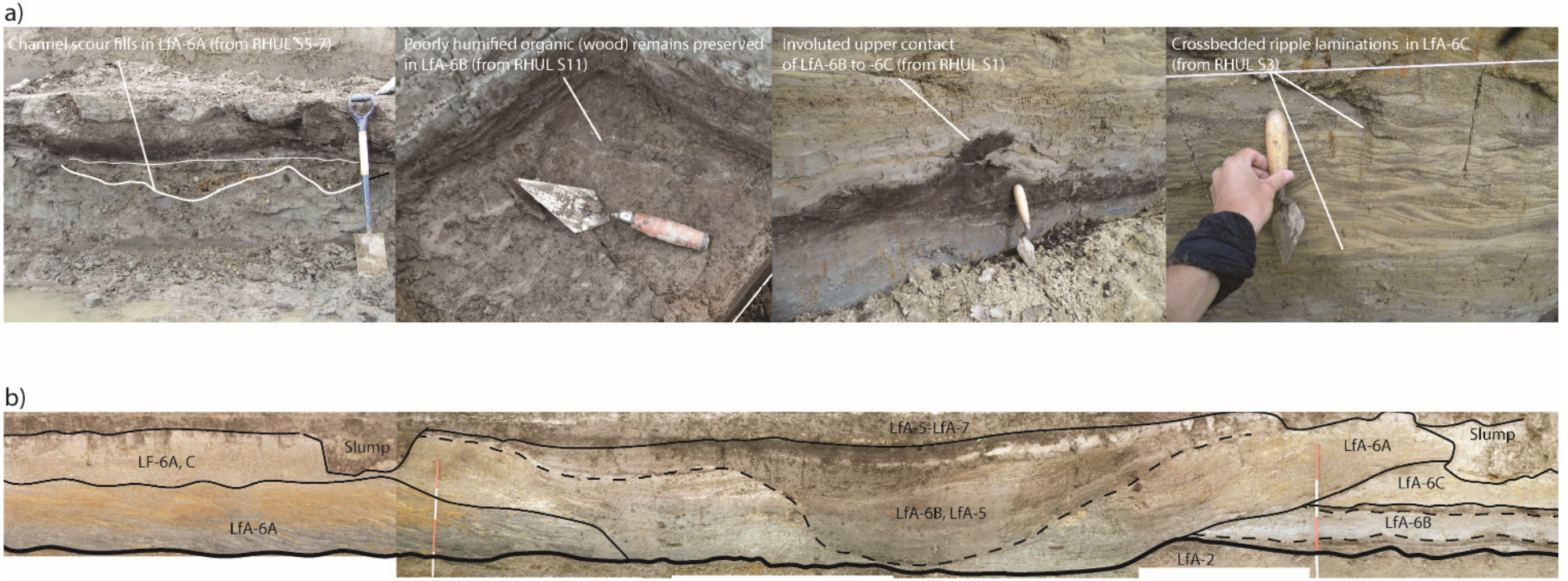

Figure 5.20. *Features identified in LfA-6 records from open sections (RHUL S), by the author and described in text b) An image of the south face of the Phase I excavation of the present quarry area, reported in Fraser et al., (2009), showing a palaeochannel form incised through LfA-6B deposits (to the right of the image). This demonstrates the complex lateral variability in LfA-6 deposits across the quarry.*

LfA-6C is composed of well sorted blueish grey to grey (Gley 2 5/1 to 10YR 5/1) massive, fine sandy silt to silty very fine to medium sands, with remnant iron stained, vertical rootlet inclusions. These beds are predominantly massive, but in some sections horizons of planar bedded, and cross bedded ripple laminations are identified (Figure 5.20). These laminations are identified principally via subtle variations in particle size.

Interpretation:

The coarse-grained characteristics, and presence of small scour fill channels and trough cross-bedding structures within LfA-6A strongly supports formation via moderate-high energy flows, associated with mid-channels, lateral accretion of channel forms, and/or high energy flood deposits proximal to active channel sources (Miall, 1985; 1996). Sediment architectural forms from the present quarry (Fraser *et al.,* 2009) demonstrates that these processes were capable of scouring pre-existing deposits from the landscape (LfA-6B) prior to aggradation (Rose *et al.,* 1999).

The well sorted, fine grained, and fossiliferous characteristics of LfA-6B demonstrates low energy sedimentation, with silts and clays settling from suspension in still-to-slow-flowing water bodies with limited turbidity (Miall, 1996). The high organic content and in some instances well preserved macrofossil remains support that deposition occurred in fluvial systems dominated by overbank sedimentation across well vegetated wetlands (Wing, 1985; Miall, 1996), which are ephemerally-perennially submerged (Rose, 1995; Gao *et al.,* 2007). This depositional environment is consistent with temperate lowland floodplains (Rose and Boardman, 1983; Rose, 1995; Lewis and Maddy, 1999), with the sediment assemblages conforming to those of floodplain fines (FF), deposited in backswamps and abandoned palaeochannels (*sensu* Miall, 1985; 1996).

The low organic content, and coarser particle size of LfA-6C invokes lower biological productivity and higher energy depositional processes those present in LfA-6B. This is supported by the presence of planar bedded, and cross bedded ripple laminations which demonstrate the presence of current flows and re-activation surfaces during deposition, and changes in flow intensity (e.g. Miall, 1996).

LfA-7 – Topsoil

Description

LfA-7 consists of greyish brown (10YR 5/2) highly compacted, and occasionally dessicated silty clay to silty sandy clay with vertically oriented modern rooting. The deposits consistently contain a sharp lower contact, with an upper contact representing the contemporary ground surface.

Interpretation

The highly-consolidated nature of these deposits, coupled with the presence of well-preserved roots, which can be traced to the contemporary land surface supports that LfA-7 is representative of topsoil, formed by anthropogenic activities (agriculture and aggregate extraction). The sharp lower contact of these deposits demonstrates that in large areas of the quarry, pre-existing deposits have been significantly altered or removed (e.g. LfA-5 deposits directly underlying LfA-7 are regularly either absent or highly humified (Batchelor, 2009; RHULS 5-8) as a result of anthropogenic activity in the quarry area.

Summary

The description and interpretation of the seven LfAs presented above allows for an understanding of the depositional processes occurring in the Wykeham Quarry area through the Last Termination. Using these LfAs and their suggested correlatives elsewhere in the eVoP, three different periods of deposition can be identified:

- ☐ LfAs 1-3 can be associated with glacial activity in the eVoP during the Dimlington Stadial, with differences in sedimentary properties associated with different periods of advance and retreat of the NSIL. LfA-1 represents the sedimentation in a glaciolacustrine setting distal from the ice margin, with evidence for migration of the ice margin to a more proximal position towards the top of the facies. LfA-2 represents high energy fluvial processes proximal to the NSIL ice margin, with LfA-3 likely representing deposition in a proximal location to the ice margin. These facies can be linked to Stages 2 and 3 of the 5-stage model of the landscape evolution.
- ☐ LfAs 4-6 represent low energy sedimentation associated with still to slow moving shallow water bodies, with differences in facies being related to flow regime, water depth and topography. Broadly these facies represent three different depositional environments: 1) low energy lacustrine sedimentation (LfA-4B), 2) low-high energy alluvial activity in a range of positions to active channels (LfA-6), and 3) peat formation (LfA)-5). These facies are frequently interbedded, representing variations in water level and flow regime across the Wykeham Quarry area. These facies overlie LfA 1-3, and therefore are likely to represent periods of sediment deposition during the LGIT. These can be linked to Stages 4 and 5 of the model of landscape evolution.
- ☐ LfA-7 can be associated with modern pedogenic and anthropogenic processes.

5.3.6. Modelled extent, elevation and thickness of LfAs

Using the LfA classifications, combined with XYZ values and depths from the borehole and open section datasets, the lateral extent, sub-surface elevation, and thickness of LfA 1-6 can be

modelled (Figures 5.21-5.24). This allows for a greater understanding of the stratigraphic relationship of these facies, allowing the optimal sites for palaeoenvironmental investigation to be identified.

LfA-1- Basal clays

Models for LfA-1 are constructed from 77 borehole records from the H-1992 and H-1997 records (Figure 5.21) which show that this lithofacies is widely distributed across the study site, where the transition to LfA-2 ranges between 9.93 and 21.23 mOD. The total thickness of the deposit is unknown, but is in excess of 10 m thick in the H-1997 dataset.

The widespread distribution, and consistent sedimentological properties support formation by an extensive water body. Whilst LfA-1 is not reported in the H-2007 records, there is no reason to doubt that these deposits underlie the entire quarry area. These deposits therefore fit with the model of proglacial lake development prior to ice advance to a setting more proximal to Wykeham Quarry.

LfA-2 – Sands and gravels

LfA-2 ranges between 2 and 16 m thick, with the thickest units located in the east of the study area (Figure 5.21). The surface elevation of LfA-2 is irregular, declining from *ca.* 30 to 18 mOD from north to south, and consisting of a series of topographic highs and lows. The maximum elevations of 29-30 mOD are confined to a linear feature, trending north to south, directly east of the Northern Extension. To the west of this feature, three less distinct areas of elevated topography, (*ca.* 27-27.5 mOD) are identified in the Northern Extension of the quarry, separated by elongated to circular depressions. Two of these depressions correlate to the landforms identified as potential basins (Depression A and Depression B; section 5.2.3), attaining elevations of *ca.* 24, and 19 mOD respectively (Figure 5.21). Further south, in the present quarry area, two shallow depressions (*ca.* 300 x 150 m) are identified (basal elevations between 23-22.5 mOD), separated by a linear, north-south oriented topographic high at *ca.* 24 mOD. The depressions continue past the eastern, and western margins of the borehole survey in the present quarry area, meaning their maximum extent is unquantified. The westernmost depression (Depression C) continues as a linear, northeast to southwest trending topographic low, reaching a minimum value of *ca.* 20 mOD (BHS-3) in the northwest of the Southern Extension.

The widespread extent, and undulating upper surface of LfA-2 supports the interpretation of deposition under a glacifluvial regime, with substantial bodies of stagnant ice emplaced during the formation of LfA-2. These processes provided the mechanism required to produce an undulating upper surface via stagnant ice melt, potentially significantly after initial emplacement.

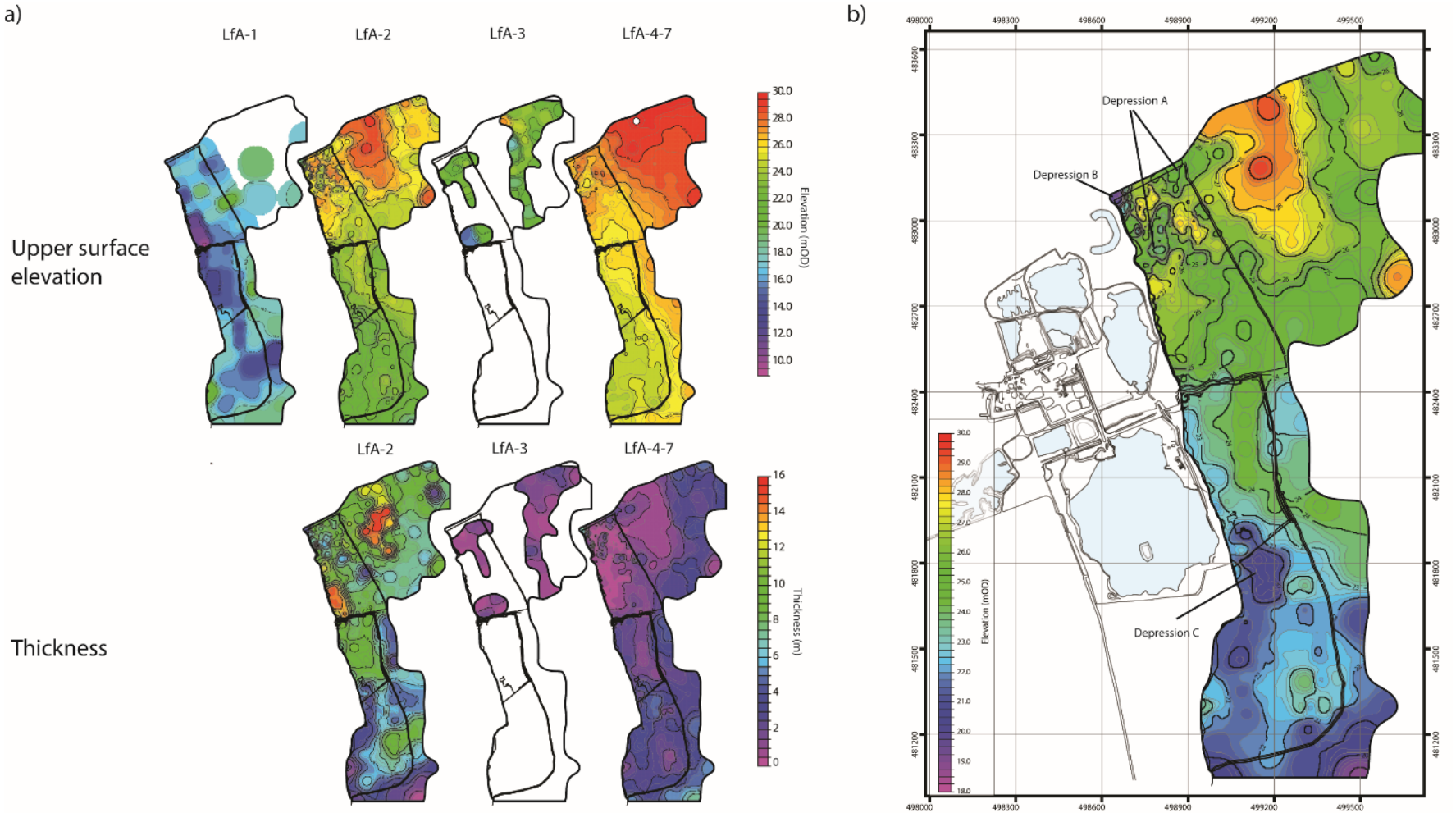

Figure 5.21. *a) Models of the lateral extent, upper surface elevation and thickness of LfA-1-3, and LfA-4-7, using 5-point inverse distance weighted models b) Enlarged image of the upper surface of LfA-2, listing the location of topographic depressions (Depressions A-C) discussed in text.*

LfA-2 is therefore interpreted as an extension of the Hutton Buscel sands and gravels, mapped directly to the north, west and east of Wykeham Quarry (Chapters 3 and 5; Franks, 1987; Evans *et al.,* 2016).

The higher proportion of more angular, and weathered clasts of local lithology in the N1 phase of the quarry may be attributed to deltaic outflow from the Forge Valley, *ca.* 2 km to the north of Wykeham Quarry, after ice recession (Franks *et al.,* 2009). This must have occurred whilst stagnant ice still remained within LfA-2/the Hutton Buscel sands and gravels, providing a means to form the topographic depressions after ice recession. Gravel deposits with similarly highly angular, limestone- and sandstone-rich components have been identified in sections of the Hutton Buscel sands and gravels (Franks, 1987), where they are also attributed to outflow from the Forge Valley by the River Derwent, during, and/or ice recession (Stages 3-4).

LfA-3 - Diamicton

LfA-3 ranges between 0.2 to 2.5 m in thickness, and is identified between 15-23 mOD. The deposit is only identified in the H-1997, H-2007, and H-2015 datasets, where it is located in three clusters in the north of the study site (Figure 5.21). Two of these clusters lie within the N1-N3 and N5 Extension phases of the quarry. The third cluster is identified directly to the east of the most elevated LfA-2 topographic high, to the east of the Northern Extension, where it is present as a linear N-S trending unit. Here, LfA-3 follows the gradient of the LfA-2 ridge, rising in elevation from E-W, reaching an optimum elevation of >26 mOD.

The sporadic presence of LfA-3 within LfA-2 deposits is consistent with the interpretation of formation via the redistribution of glacigenic diamicton via mass flow and slumping from a retreating ice mass, with flows preferentially concentrated into topographic lows preserved in the LfA-2 surface. This is most evident from the LfA-3 cluster to the east of Wykeham Quarry which is observed to follow the topography of LfA-2, suggesting formation via gravitational debris flow processes during deglaciation (Bennett and Glasser, 2009).

LfA-4 – Carbonate-rich freshwater lacustrine facies

LfA-4 deposits are situated within topographic depressions in the upper surface of LfA-2 (Depression A and Depression B). The models show that the upper surface elevation of LfA-2, over which LfA-4 is deposited, varies between these depressions, resulting in LfA4 deposits being substantially thicker in Depression B than Depression A (Figure 5.22).

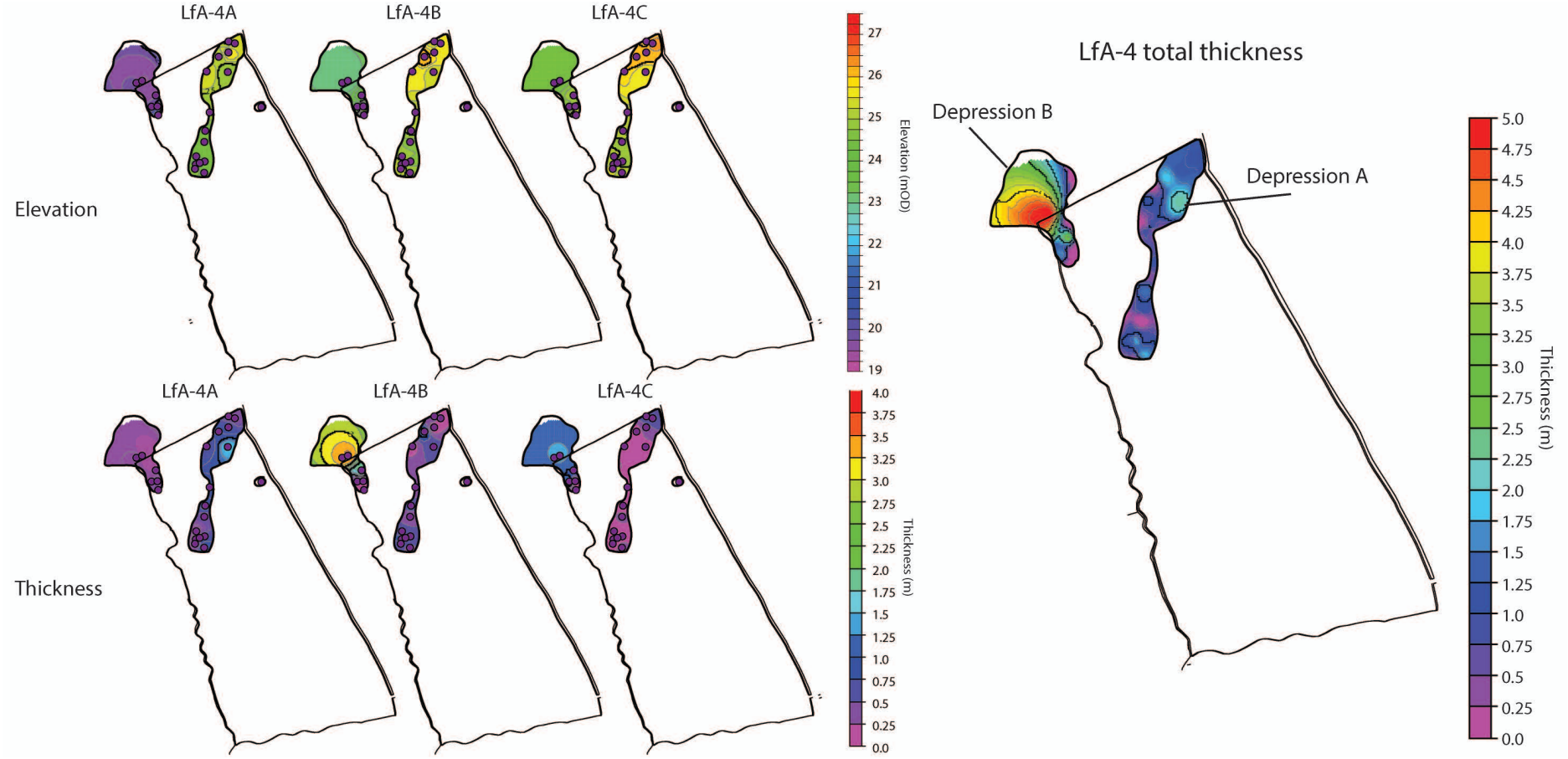

***Figure 5.22**. Modelled lateral extent (derived from the presence and absence of LfA-4 deposits in sediment records), upper surface elevation, and thickness of LfA-4 deposits (derived from 5-point inverse distance weighted modelling).*

LfA-4A is <1m in thickness, and lies at between 24.2 and 25.6 mOD in Depression A, and between *ca.* 19-20 mOD in Depression B. In the centre of Depression B (RHULPal-2-3), LfA-4B represents the thickest unit of LfA-4, infilling the basin by 3.2 to 3.4 m to an altitude of *ca.* 23.2 mOD (validated by BHN 44). In Depression A, LfA-4B reaches a maximum thickness of 1.1m, and a maximum elevation of 26.1 mOD in the northernmost region of the study area (RHUL BHN3), before steadily declining and thinning to the south, and west. A second thicker region of LfA-4B, focussed around RHULBHN 13 (thickness of 0.97 m, between 24.16 and 25.13 mOD), is identified in the N2 Extension Phase area. LfA-4C is located between 24.87 to 26.31 mOD in Depression A, varying between 0.65 and 0.02 m in thickness, and declining in elevation from NE to SW. In Depression B, LfA-4C is absent at the margins of the landform (RHUL BHN 11 and 12), but >1 m thick in more central positions, reaching an optimum thickness of 1.35m in BHN44.

The location of LfA-4 deposits represents infilling of lake bodies formed in topographic depressions in the LfA-2 surface, after the melt-out of stagnant ice and meltwater channels, emplaced during the recession of ice from the Wykeham Quarry area. The carbonate-rich characteristics of LfA-4B suggest formation within temperate climates, meaning deposition during the LGIT represents the most likely timeframe for their formation.

LfA-5 - Peats

LfA-5 deposits are widely distributed across the study site, frequently interbedded with LfA-4 and LfA-6 deposits, whilst also consistently capping records, and directly underyling the topsoil (LfA-7) to altitudes up to 28.13 mOD. Modelling these deposits is therefore unfeasible. A model of the uppermost beds of LfA-5 deposits across the quarry area (Figure 5.23) demonstrates that the thickest expression of these LfA-5 deposits are associated with topographic depressions in the LfA-2 surface (Depressions A-C, reaching up to 2 m) before consistently declining in elevation with increasing elevation. LfA-5 deposits are only absent from the uppermost LfA-2 surfaces in the Northern Extension.

The distribution and thicknesses of LfA-5 at the quarry is consistent with formation at the margins of topographic depressions in the LfA-2 surface in the Northern Extension, with the thickest deposits being focussed into topographic depressions after open water bodies (LfA-4) infilled (e.g. Cloutman, 1988a).

LfA-6 - Fine grained non-carbonate facies

The extent, elevation and thickness of LfA-6 are modelled as a single sediment body, encompassing LfA-6-A-C (Figure 5.24), due to the complex, interbedded nature of the deposits. These models demonstrate that with the exception of RHULS-9-10 at the western edge of the

Northern Extension, LfA-6 is entirely focussed into the mid-to southerly regions of the quarry area (i.e. the southerly limits of the Northern Extension, and throughout the present quarry and Southern Extension). Deposits decline steadily in elevation in association with the declining LfA-2 surface N-S, but also increase in thickness, with the lowest elevations, and thickest expression of LfA-6 (> 4 m) being focussed into Depression C in the Southern Extension (Figure 5.24).

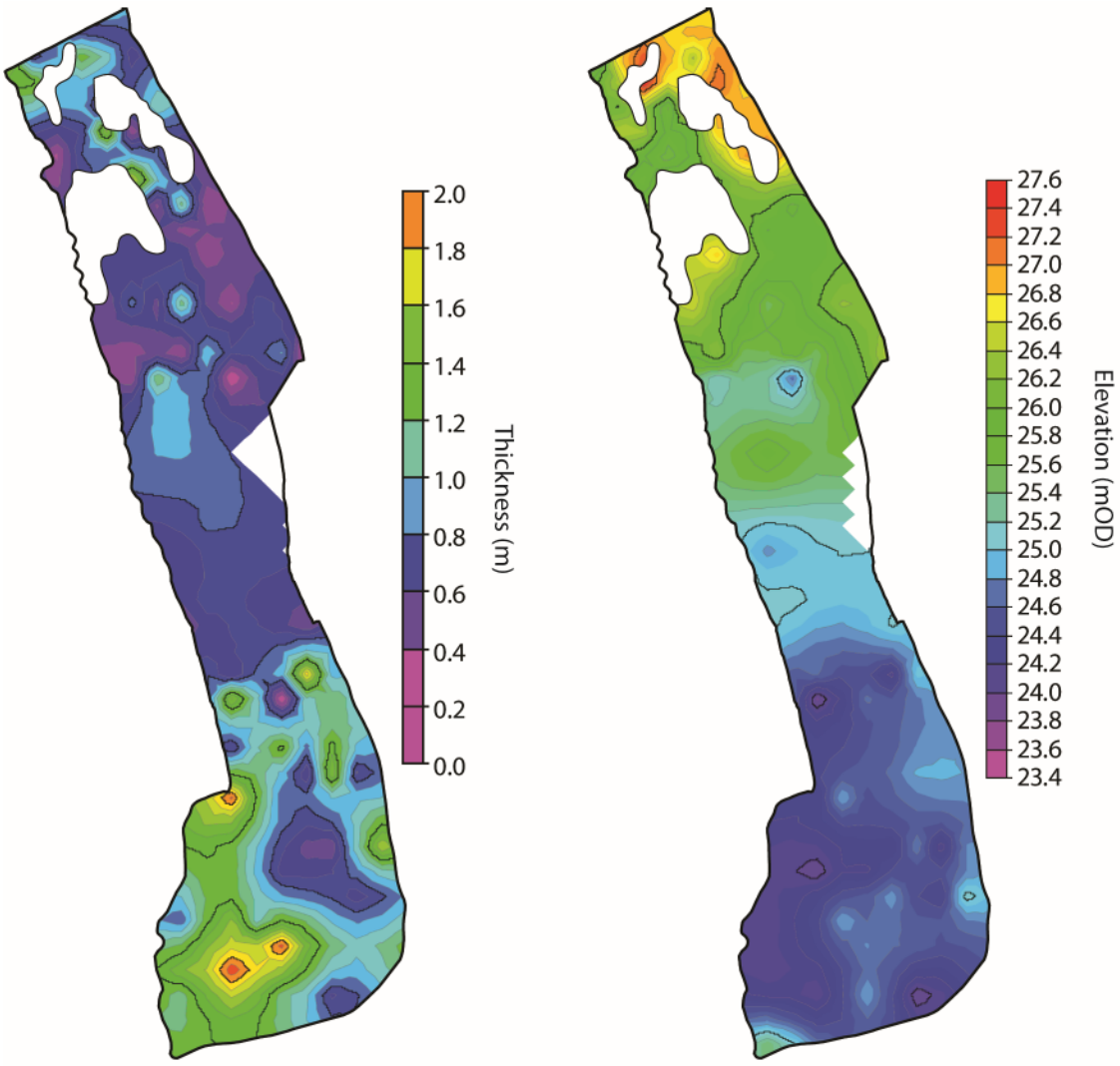

***Figure 5.23**. Modelled lateral extent, thickness and upper surface elevations of LfA-5 deposits at Wykeham Quarry. Records which demonstrably contain no LfA-5 records are clipped from the model output (three clusters in the Northern Extension).*

The distribution of LfA-6 deposits demonstrates the formation of a low energy, lowland floodplain environment in the mid-southerly sectors of Wykeham Quarry, persistently south of the LfA-2 topographic highs located in the northerly realms of the study site. These deposits are therefore not directly interbedded with LfA-4 deposits, supporting formation via different depositional processes, i.e. sediment sourced largely via phases of low-mid energy overbank flooding, mid-channel formation and other associated fluvial processes rather than authigenic, biochemical productivity within a water column (e.g. LfA-4B).

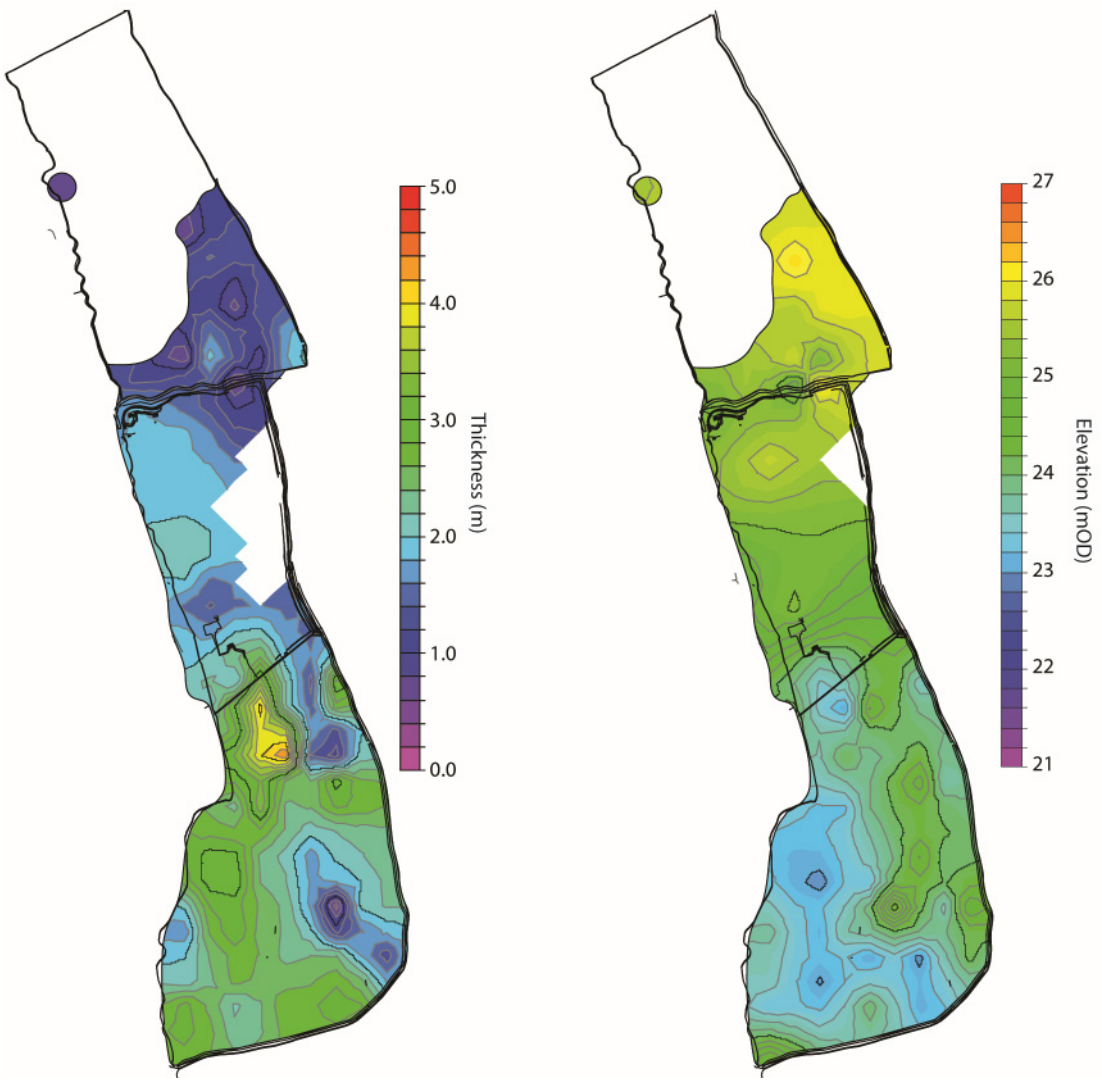

Figure 5.24. *Modelled lateral extent, thickness and elevation of LfA-6 deposits at Wykeham Quarry. These deposits are modelled as a single unit (incorporating LfA-6A-C) owing to the complexity and lateral variability of these deposits (see Figure 5.20).*

5.3.7. Stratigraphic assemblages

Description and interpretation:

Sedimentological descriptions and mapping of LfA 4-6 demonstrates that the thickness, elevation, and inter-relationship of these deposits is spatially variable, strongly associated, and frequently interdigitated (Figures 5.19-5.20). Developing an understanding on the stratigraphic context of the LfAs is therefore critical to comprehend spatial variability in sediment accumulation, which in turn, optimises the potential identification of sites for palaeoenvironmental reconstruction. LfA-4-6 can be sub-divided into five stratigraphic assemblages (stratigraphic assemblage A-E), termed as sequences containing sequences of LfAs in consistent stratigraphic order. These are established by the primary sedimentary features, and the relative superposition of LfAs in each record (Table 5.6). The characteristics, stratigraphy, and spatial distribution of the stratigraphic assemblages are presented in Table 5.6 and Figures 5.25-5.26.

Table 5.6. *Summary of the five stratigraphic assemblages identified via the stratigraphic association of LfAs 4-6 at Wykeham Quarry.*

Stratigraphic assemblage	No. of records	Stratigraphic summary (from base to top)	Interpretation
A	26	LfA-2→LfA-7	Dry land throughout the LGIT
B	59	LfA-2→LfA-5→LfA-7	Marginal deposits, at the edge of wetlands/ floodplains, and/ or open water bodies
C	22	LfA-2→LfA4→LfA-5→LfA-7	Small, base rich, open water bodies infilled via hydroseral succession through the LGIT
D	51	LfA-2→LfA-6A-C→LfA-5→LfA-7	Fluvial overbanks, and wetland deposits in the floodplain of the River Derwent
E	26	LfA-2→LfA-6AorB→LfA-5→LfA-7	Scour fills from river channels incised into LfA-4

Records containing fluvial facies (LfA-6 deposits), are differentiated into two stratigraphic assemblages (termed stratigraphic assemblages D and E) based upon the following lines of evidence:

a) Channels are scoured through overbank deposits (LfA-6B-6C; stratigraphic assemblage D) to the upper surface of LfA-2 (Figure 5.20) in the east of the study area. The channels are infilled by LfA-6A and LfA-6B deposits (Franks et al., 2009).
b) These channels can be confidently correlated to channel B1 (section 5.2.2), which extends *ca.* N-S across the eastern edges of the study area (Figure 5.25).
c) Open sections and boreholes show a linear, north-south trending strip of records showing similar evidence of scour of pre-existing deposits (either via interdigitated thin gravel seams, and/or the lack of a complete stratigraphic sequence consisting of LfA-2→LfA-6B→LfA-6C→LfA-6B/LfA-5→LfA-7 which is characteristic of stratigraphic assemblage D), and correlate to the mapped extent of channel B1 (Figure 5.25). These records are therefore separated from stratigraphic assemblage D on this basis.

Distribution:

Stratigraphic assemblage A, is located in three clusters in the north of the Northern Extension, on the three topographic highs identified in the upper surface of LfA-2 (elevations >26.3 mOD; Figure 5.26). Stratigraphic assemblage B records are located surrounding the same topographic highs of the sands and gravels as stratigraphic assemblage A, which are located in the northern phases (N1-N3) of the Northern Extension. The distribution of stratigraphic assemblage C records are identical to those described for LfA-4 deposits, being focussed into topographic depressions in the Northern Extension, fringed by stratigraphic assemblage B in more topographically elevated areas.

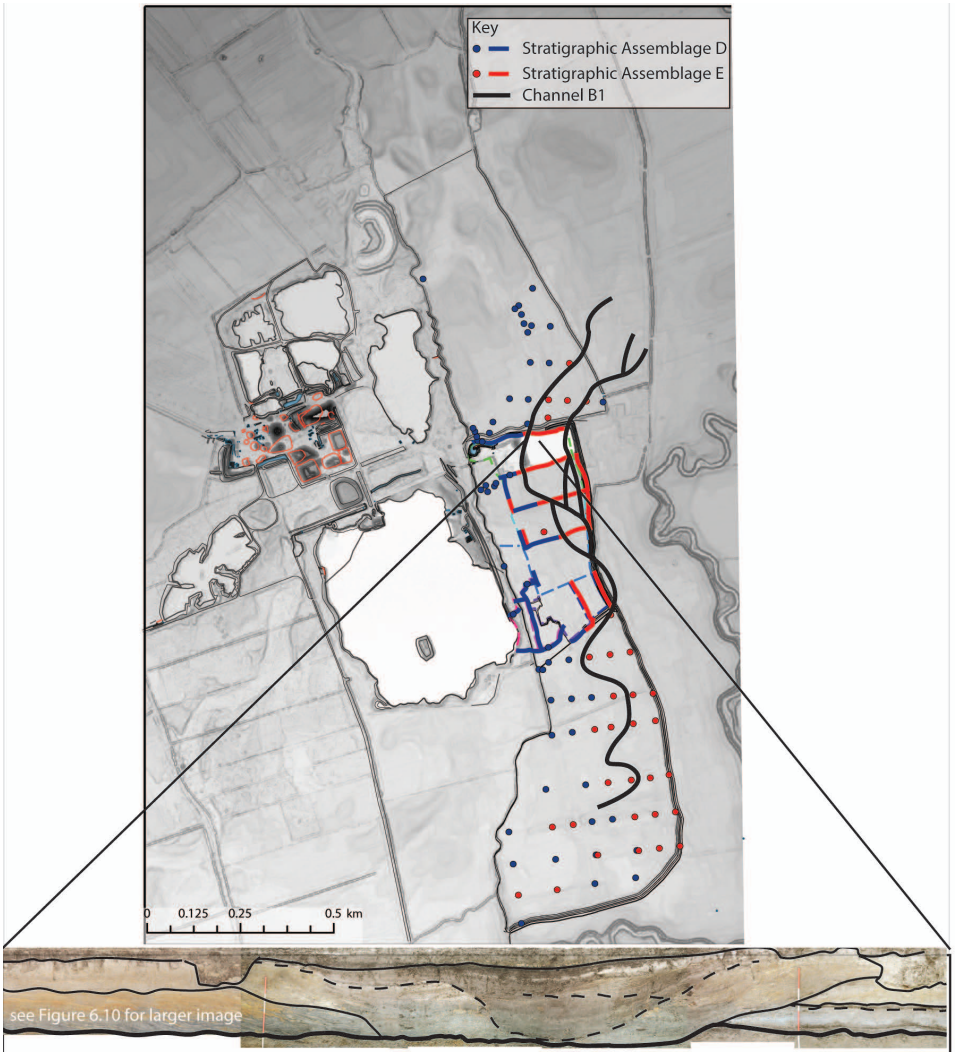

Figure 5.25. *Justification for sub-dividing LfA-6 into two stratigraphic assemblages, based upon the spatial consistency of stratigraphic records in association with mapped extent of channel B1 (black lines, Chapter 5), and the open section of a palaeochannel reported in Fraser et al. (2009; 5.20).*

Stratigraphic assemblage D records (LfA-2→LfA-6A-C→LfA-5→LfA-7) are situated in the west of the study area, extending from the southern margins of the Northern Extension (Phase N4), across the present quarry, and the Southern Extension, consistently south of the topographic highs in LfA-2 (Figure 5.26).

Stratigraphic assemblage E, records are situated the west of stratigraphic assemblage D, where they extend as a linear, assemblage of records *ca.* 100 to 250m wide and oriented *ca.* N-S, primarily in the eastern extent of the study area. These locations are consistent with the mapped extent of channel B1 (see above) and are interpreted to represent scour and fill of channel B1 through stratigraphic assemblage D.

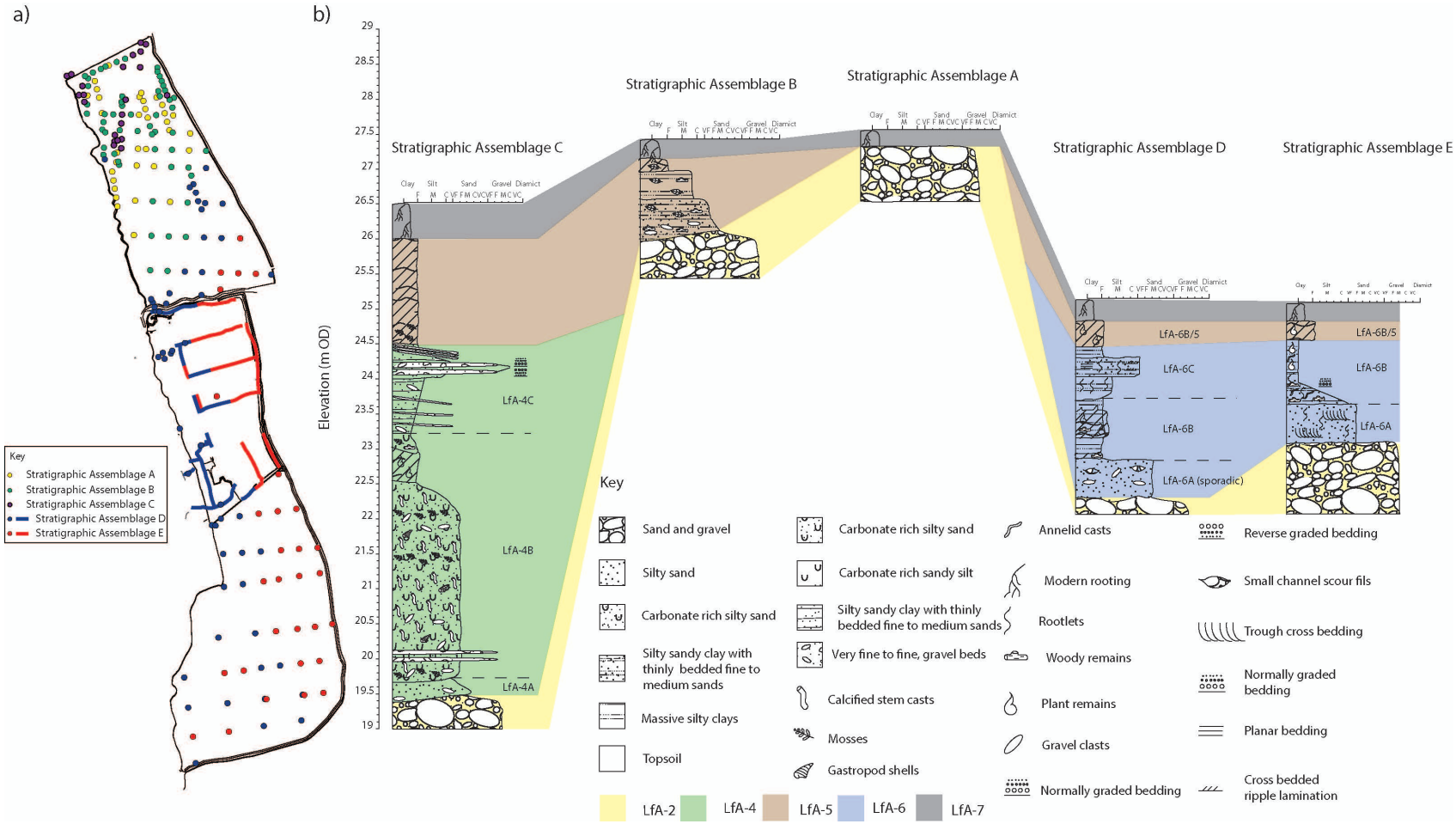

Figure 5.26. *Summary of the stratigraphic assemblages identified from LfAs 4-6 at Wykeham Quarry. a) shows the distribution of records assigned to each stratigraphic assemblage. b) presents a schematic correlation of the LfAs in each stratigraphic assemblage. The sediment logs for each assemblage are constructed either from sediment records chosen to best represent each assemblage (BHN-6, RHULBHN-6, RHULPal-2, for stratigraphic assemblaes A-C respectively) or from composites (sediment assemblage D represents a composite of RHULS-6 and S11, whilst stratigraphic assemblage E is based upon descriptions of the phase 1 open section by Fraser et al., 2009).*

5.4. Chronology of landforms and sediments

5.4.1. Palaeochannels

The timing of channel formation across the River Derwent floodplain in the eVoP is constrained by radiocarbon ages on channel infills at Wykeham Quarry, undertaken by Fraser *et al.,* (2009), and supported by dates in this study (Table 5.7). All radiocarbon ages are calibrated to calendar age before AD 1950 (cal BP), using IntCal13 (Reimer *et al.,* 2013), and reported as unmodelled age ranges to 2σ.

Channel Assemblage A

The infill of channel A1 was radiocarbon dated from excavations on the RHULBHN13, and RHULS-10 records. Two dates were obtained from the channel infill, and were sampled from the base of sedimentary sections, as close as possible to the transition from coarse grained sediment, interpreted to best represent the point of abandonment. These ages demonstrate that Channel Assemblage A began to infill by 14.58-14.00 cal ka BP, during the Early Windermere Interstadial (E-WI; *ca.* 14.7-14 ka BP).

Channel Assemblage B

Ages from the infill of channel B1 are derived from LfA-6A and LfA-6B deposits and range from 12.34 to 11.41, continuing to 11.17 to 10.45 cal ka BP (Fraser *et al.,* 2009). These dates show that channel infilling overlaps with the timing of climatic amelioration from GS-1 into the Early Holocene (Walker *et al.,* 2009; Rasmussen *et al.,* 2014; Figure 5.27).

Channel Assemblage C

No dates exist from Channel Assemblage C, but their association with the contemporary river suggest that they most likely represent low energy, stable fluvial activity during the Holocene. This is supported by regional models of fluvial development in lowland rivers during the LGIT (Antoine *et al.,* 2003; Brown *et al.,* 1994). The overlap of channel characteristics between Channel Assemblage B and C suggests that the channels were likely formed across a continuum, with the lower sinuosity B channels transitioning into C type channels during the EH and maintaining this planform until the present day.

Table 5.7. *Radiocarbon dates from palaeochannel infills at Wykeham Quarry. The Channel Assemblage A dates come from channel A1, taken from RHULBHN13 and RHUL S10 in the Northern Extension of the quarry (Chapter 6). Channel assemblage B ages are from palaeochannel bases and infill in Channel B1 reported in Fraser et al., (2009).*

Laboratory ID code	Channel Assemblage	Context	Sample composition	Radiocarbon age (^{14}C a BP)	1σ error	δ^{13}C	Calibrated age range (95.4%) (ka BP)	Study
OxA-32439	A	Base of RHULBHN13	Twigs	12315	55	-27.13	14.58-14.04	This study
OxA-32438	A	Base of subsidiary palaeochannel in RHUL S10	Twigs	11180	50	-27.76	13.15-12.93	This study
Beta-195999	B	Palaeochannel infill	Wood	9980	50	-29.3	11.69-11.25	Fraser *et al.,* (2009)
Beta-196000	B	Palaeochannel infill	Organic sediment	9600	40	-28.1	11.19-10.82	Fraser *et al.,* (2009)
Beta-196001	B	Palaeochannel base	Wood	9860	50	-27.5	11.39-11.20	Fraser *et al.,* (2009)
Beta-214583	B	Palaeochannel base	Wood	9780	90	-26.8	11.60-10.87	Fraser *et al.,* (2009)
Beta-214584	B	Palaeochannel base	Wood	10150	80	-24.0	12.00-11.33	Fraser *et al.,* (2009)
Beta-214585	B	Palaeochannel base	Wood	10090	70	-21.3	11.92-11.29	Fraser *et al.,* (2009)

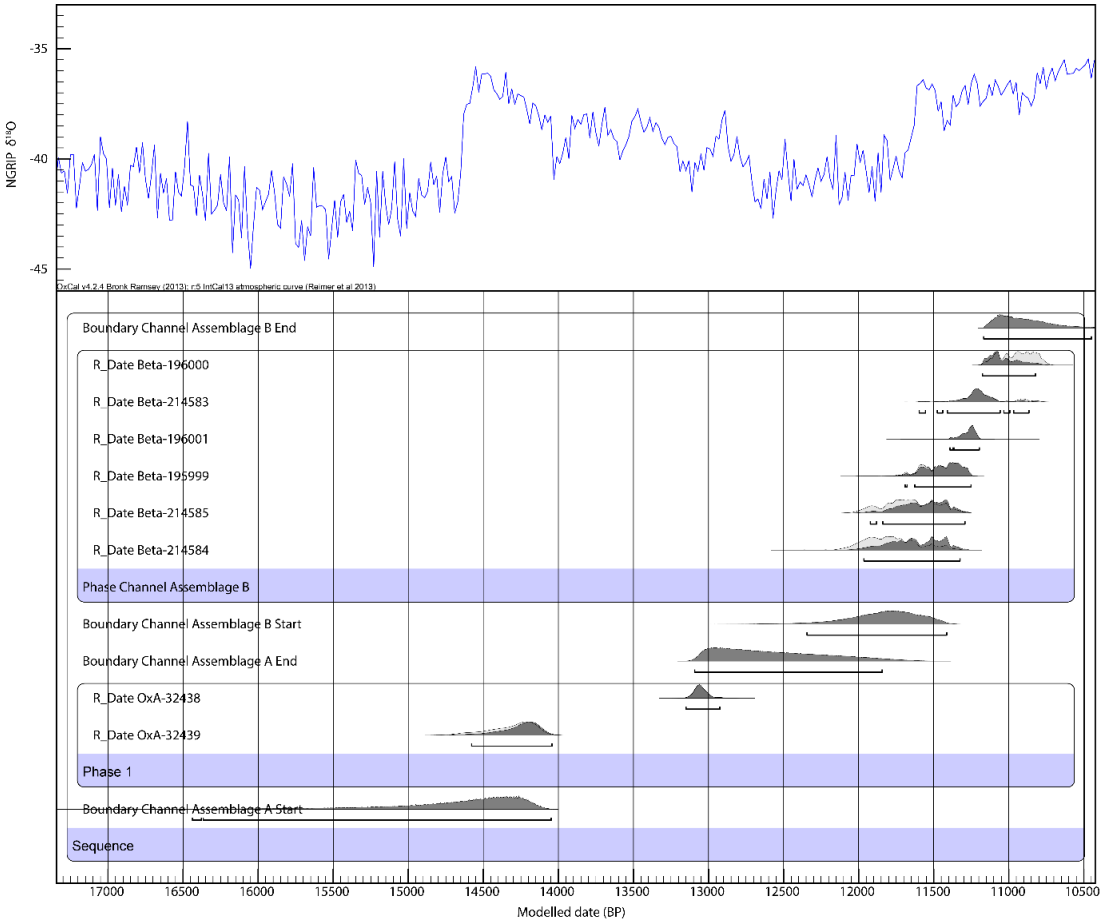

Figure 5.27. *Phase model of ages obtained on the infill age of Channel Assemblage A and B (Table 5.7).*

5.4.2. Sediments and palaeobasins

Twenty radiocarbon ages exist from six sites in the present quarry area (Fraser *et al.,* 2009). These ages are focussed upon LfA-6 deposits in stratigraphic assemblage D (Phase 1 section 3, Trench Q1, Trial pit C1) and stratigraphic assemblage E (Phase 1 north face section 8, Trench B5). Where the radiocarbon dates are analysed in stratigraphic sequence, a series of age reversals are identified (Fraser *et al.,* 2009). To address this, the NAA ages reported from records in stratigraphic sequence have been deposition/sequence modelled following the methods outlined in Chapter 4 to identify outliers. The output of these analyses are summarised in Table 5.8.

Twenty-four dates (twenty-one radiocarbon ages on terrestrial plant macrofossils, and three SAR-OSL ages from the same stratigraphic horizon in LfA-6C deposits) were obtained from lithofacies in LfA-4, LfA-5/6B, and LfA-6C, (summarised in Table 5.9). All but two of these measurements were sourced from two records used for palaeoenvironmental analysis (Figure 5.28; Chapter 6). A summary of the ages obtained on deposits a Wykeham Quarry are presented in Figure 5.29.

Table 5.8. *Summary of the radiocarbon dates reported in Fraser et al., (2009). Each date is labelled by a lab code assigned by Beta Analytic, and listed with the record the date was taken from in the quarry, and its lithostratigraphic context. To assess validity, all dates were deposition, or sequence modelled in Oxcal. Ages are reported as an unmodelled age range, and assigned into a period of the chronostratigraphic framework for the British Isles: WI- the Windermere Interstadial, LLS- the Loch Lomond Stadial, and EH- The Early Holocene.*

Lab Code	Age	Error	Depth	$\delta^{13}C$	Sample type	Method	Record	LfA-	Strat. Assemblage	Accepted/rejected	Calibrated age range (95.4%) (kaBP)	Chronostratigraphy
Beta-214579	11280	60	71	-29.0	Bulk organics	AMS	Phase 1 south face section 3	$6B_{(lower)}$	D	Accepted Dep. model	13.27-13.04	WI
Beta-214580	11870	70	75	-28.0	Bulk organics	AMS	Phase 1 south face section 3	$6B_{(lower)}$	D	Rejected Dep. model		WI
Beta-214581	11590	60	118	-27.7	Bulk organics	AMS	Phase 1 south face section 3	$6B_{(lower)}$	D	Accepted Dep. model	13.60-13.33	WI
Beta-214582	11960	40	135	-27.8	Bulk organics	AMS	Phase 1 south face section 3	$6B_{(lower)}$	D	Accepted Dep. model	13.95-13.56	WI
Beta-191686	10030	40	36	-27.3	Bulk organics	AMS	Trench Q1	$6B_{(upper)}$	D	Accepted Dep. model	11.80-11.32	EH
Beta-191687	11780	40	123	-27.7	Bulk organics	AMS	Trench Q1	$6B_{(lower)}$	D	Rejected Dep. model		WI
Beta-191688	11440	50	129	-27.2	Bulk organics	AMS	Trench Q1	$6B_{(lower)}$	D	Accepted Dep. model	13.40-13.12	WI
Beta-191685	11850	80	174	-27.1	Wood	AMS	Trench Q1	$6B_{(lower)}$	D	Rejected Dep. model		WI
Beta-191684	12120	90	177	-27.4	Bulk organics	Radiometric	Trench Q1	$6B_{(lower)}$	D	Accepted Dep. model	14.22-13.73	WI
Beta-178506	9970	60			Bulk organics	Radiometric	Trial Pit C1 north face	$6B_{(upper)}$	D	Accepted Dep. model	11.70-11.24	EH
Beta-178507	10920	70			Bulk organics	Radiometric	Trial Pit C1 north face	$6B_{(lower)}$	D	Accepted Dep. model	13.02-12.72	WI
Beta-178508	11750	70			Bulk organics	Radiometric	Trial Pit C1 north face	$6B_{(lower)}$	D	Accepted Dep. model	13.70-13.39	WI
Beta-178509	11890	70			Bulk organics	Radiometric	Trial Pit C1 north face	$6B_{(lower)}$	D	Accepted Dep. model	13.95-13.58	WI
Beta-214583	9780	90		-26.8	Wood	AMS	Phase 1 north face section 8	6B	E	Accepted Dep. model	11.59-10.78	EH
Beta-214584	10150	80		-24.0	Wood	AMS	Phase 1 north face section 8	6A	E	Accepted Seq. model	12.03-11.40	LLS-EH
Beta-214585	10090	70		-21.3	Wood	AMS	Phase 1 south face section 8	6B	E	Accepted Seq. model	11.99-11.35	LLS-EH
Beta-195999	9980	50		-29.3	Wood	?	Trench B5 Phase 1	6B	E	Accepted Seq. model	11.69-11.28	EH
Beta-196000	9600	40		-28.0	Bulk organics	?	Trench B5 Phase 1	6B	E	Accepted Seq. model	11.19-10.84	EH
Beta-196001	9860	50		-27.5	Wood	?	Trench B5 Phase 1	6B	E	Accepted Seq. model	11.32-11.19	EH

Table 5.9. *Summary of the radiocarbon, and SAR-OSL dates produced in this study. Each radiocarbon date is labelled by a lab code assigned by the Oxford Radiocarbon Accelerator Unit (ORAU), and listed with the record the date was taken from in the quarry, and its lithofacies context. Ages are calibrated using OxCal 4.2, and assigned into the chronostratigraphic framework for the British Isles discussed in Chapters 2-3.*

Lab Code	Age	Error	13C	Sample type	Method	Record	LfA	Stratigraphic Assemblage	Calibrated age range (95.4%) (kaBP)	Chronostrat.
OxA-32336	9850	60	-25.31	*Carex sp.* seeds and twigs	AMS	WYKSE14 (RHUL-S11)	6B	D	11.59-11.17	EH
OxA-32337	9870	65	-27.11	*Urtica dioica* seeds	AMS	WYKSE14 (RHUL-S11)	6B	D	11.602-11.18	EH
OSL 3	11800	900	N/A		SAR-OSL	WYKSE14 (RHUL-S11)	6C	D	N/A	LLS
OSL2	12400	1000	N/A		SAR-OSL	WYKSE14 (RHUL-S11)	6C	D	N/A	LLS
OSL1	12400	1000	N/A		SAR-OSL	WYKSE14 (RHUL-S11)	6C	D	N/A	LLS
OxA-32338	10805	45	-27.56	Brassicaceae sp. seed and twigs	AMS	WYKSE14 (RHUL-S11)	6B	D	12.76-12.66	LLS
OxA-32339	10695	50	-29.8	*Betula nana* leaf fragments	AMS	WYKSE14 (RHUL-S11)	6B	D	12.72-12.57	LLS
OxA-32340	11640	55	-26.7	*Carex sp.* seeds	AMS	WYKSE14 (RHUL-S11)	6B	D	13.58-13.35	WI
OxA-32433	12080	50	-26.38	*Carex sp.* seeds	AMS	WYKSE14 (RHUL-S11)	6B	D	14.09-13.77	WI
OxA-32341	12070	60	-27.92	*Betula nana* leaf fragments	AMS	WYKSE14 (RHUL-S11)	6B	D	14.09-13.76	WI
OxA-32440	12120	50	-28.24	Twigs (undiff.)	AMS	WYKSE14 (RHUL-S11)	6B	D	14.14-13.80	WI
OxA-32342	12145	60	-27.23	*B.nana* leaf fragments	AMS	WYKSE14 (RHUL-S11)	6B	D	14.18-13.80	WI
OxA-32343	9925	50	-29.5	*Betula sp.* leaf fragments	AMS	WYKNE15 (RHULPal-2)	3E	C	11.60-11.23	EH
OxA-32397	10205	45	-29.13	Twigs (undiff.)	AMS	WYKNE15 (RHULPal-2)	3D	C	12.11-11.75	LLS
OxA-30541	11210	140	-27.13	*Carex sp.* seeds	AMS	WYKNE15 (RHULPal-2)	4B	C	13.32-12.75	WI
OxA-32434	11520	45	-28.1	*Carex sp.*, and *Betula sp.* seeds	AMS	WYKNE15 (RHULPal-2)	4B	C	13.45-13.28	WI
OxA-32441	11540	50	-28.59	Twigs (undiff.)	AMS	WYKNE15 (RHULPal-2)	4B	C	13.49-13.28	WI
OxA-32401	11420	50	-27.92	Twigs (undiff.)	AMS	WYKNE15 (RHULPal-2)	4B	C	13.39-13.14	WI
OxA-30030	11475	45	-28.92	*Carex sp.* seeds	AMS	WYKNE15 (RHULPal-2)	4B	C	13.44-13.22	WI
OxA-32436	11895	50	-26.45	Juniperus sp. needles, leaf frags. (undiff.)	AMS	WYKNE15 (RHULPal-2)	4B	C	13.81-13.56	WI
OxA-32437	12320	55	-27.24	*B.nana* leaf frags and twigs (undiff.)	AMS	WYKNE15 (RHULPal-2)	4B	C	14.67-14.08	WI
OxA-32400	12530	75	-30.17	*B.nana* leaf frags and twigs (undiff.)	AMS	WYKNE15 (RHULPal-2)	4B	C	15.13-14.31	WI
OxA-32438	11180	50	-27.76	Twigs (undiff.)	AMS	RHUL-S10	6B	E	13.15-12.91	WI
OxA-32439	12315	55	-27.13	Twigs (undiff.)	AMS	RHULBHN-13	4B	C	14.66-14.07	WI

Stratigraphic assemblage C- (LfA-2→LfA-4→LfA-5→LfA-7)/ Palaeobasins/Channel Assemblage A

Ten radiocarbon dates were obtained from RHULPal-2, (named WYKNE15 site A), from Depression B in the Northern Extension. These measurements provide age ranges for the deposition of stratigraphic assemblage C in the palaeobasins formed in Depressions A and B. The radiocarbon ages show that the LfA-4 deposits in Depression B (LfA-4A to C) span between the Early Windermere Interstadial (E-WI; *ca.* 14.7-14 cal ka BP), and the Early Holocene (EH; *ca.* 11.7-11 cal ka BP). The basal age from the sequence, sampled from LfA-4B provides an age range of 15.13-14.31 cal ka BP (OxA-32400), placing the initiation of carbonate rich sedimentation across the transition from the Dimlington Stadial into the E-WI. A date from the base of the infill of Depression A/Channel A1 (RHULBHN 13), produces an age of 14.66-14.07 cal ka BP (OxA-32439), suggesting that the initiation of carbonate rich lake sedimentation in these basins (LfA-4), and the cessation of Channel Assemblage A formation occurred during the E-WI.

Five ages obtained from an LfA-5 interbed in LfA-4B (OxA-30030, 32434, 32401, and 32441), span between 13.47 and 12.75 cal ka BP, placing them within the Mid-Late Windermere Interstadial (M-L-WI; *ca.* 14-13 cal ka BP). An age from a secondary, peat filled channel infill within channel A1 (Figure 5.28) suggests smaller scale channel reactivation and abandonment, (LfA-5 deposits in RHULS-10) at 13.15 to 12.93 cal ka BP during this interval.

A single age from LfA-4C in Depression B of 12.11-11.75 cal ka BP (OxA-32397), places deposition into the Loch Lomond Stadial (LLS, *ca.* 13-11.7 cal ka BP). An uppermost age from stratigraphic assemblage C is provided by OxA-32343, which is located at the base of LfA-5 deposits in WYKNE15 site A, and provides an age of 11.60-11.23 cal ka BP, constraining deposition to the EH.

Stratigraphic assemblage D- (LfA-2→~LfA-6A→LfA-6B→LfA-6C→LfA-5→LfA-7) and Channel Assemblage B

Ages on organic-rich laminae in LfA-6B range between 14.18-13.80 cal ka BP (OxA-32342), and 12.76-12.66 cal ka BP (OxA-32338), spanning the transition into-, and out of-, the M-LWI. Radiocarbon ages on LfA-6B deposits overlying LfA-6C (Beta, 178506, 191686, OxA-32336, 32337), range between 11.75-11.33 cal ka BP (Beta-191686), and 11.59-11.17 cal ka BP (LF4E top, OxA-32336), placing deposition into the transition from the LLS, to the EH. By implication therefore, LfA-6C, which is interbedded between these facies was deposited during the LLS. This is supported by three SAR-OSL dates from the same stratigraphic horizon in the WYKSE14 sequence, providing a combined age of 13.23-10.99 cal ka BP. Where present, LfA-6A deposits

consistently underlie the lowermost LfA-6B deposits, demonstrating that they must have formed prior to *ca.* 14.18-13.80 cal ka BP.

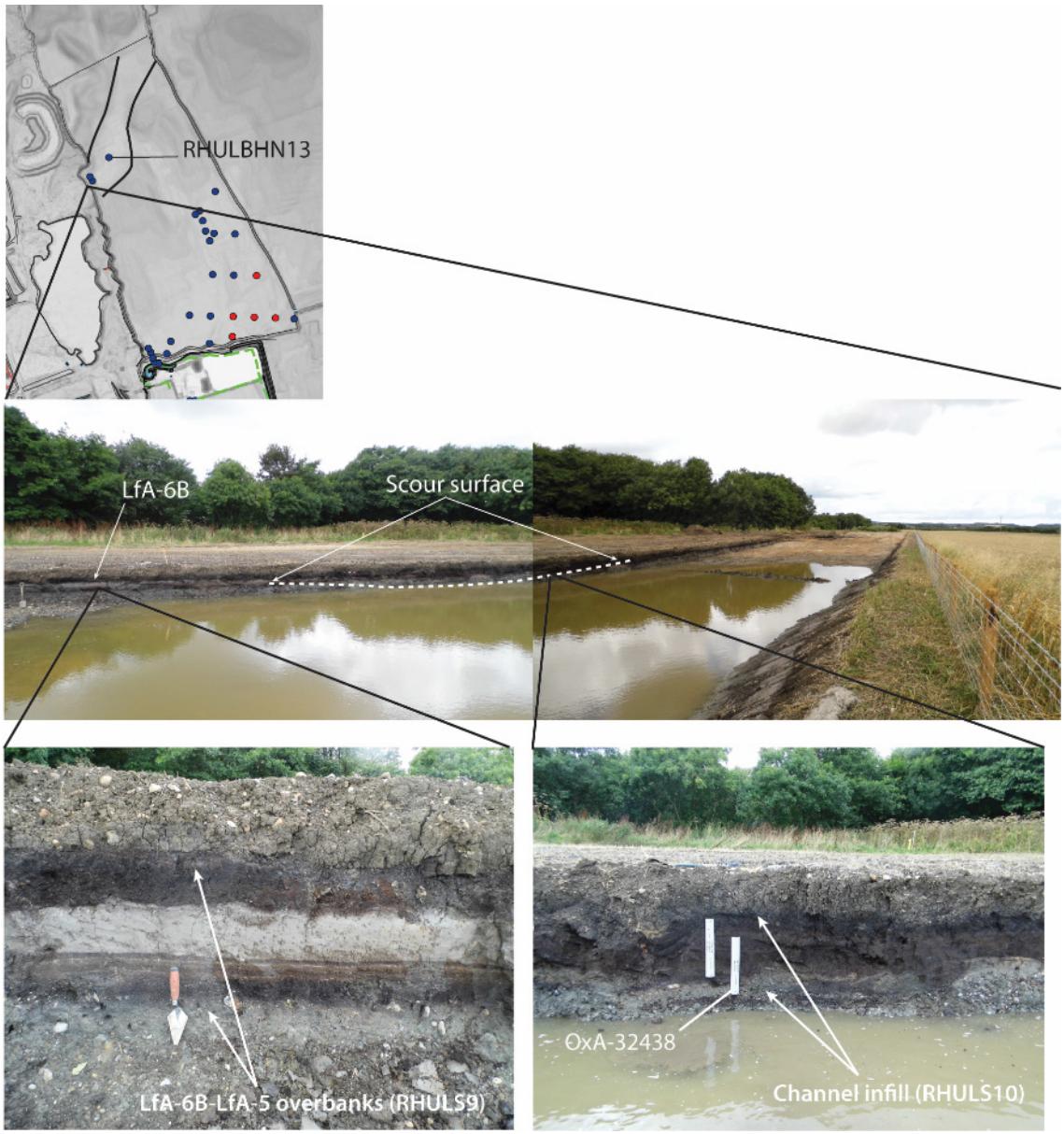

Figure 5.28. *Context for the OxA-32438, and 32439 radiocarbon ages obtained from the RHULS10 and RHULBHN13 records respectively. The figure shows the locations of the RHULBHN13, and RHULS10 records upon which, ages were obtained. These sequences were chosen for dating as they could securely be associated with phases of channel abandonment in channel A1/Depression A (marked by black lines in the map), which was identified in the mapping stages of this thesis (Chapter 5). The initial infill of Depression A is constrained by OxA-32439, sampled by the basal infill of the sequence (LfA-4B). A smaller-scale scour-fill palaeochannel, at the western mapped margins of channel A1 identified incising through LfA-6B deposits was targeted during logging of excavations by the author in 2014. The figure above demonstrates the criteria used to identify the channel form, namely via a scour surface, overlain by LfA-6B-LfA-5 deposits which differed substantially from those recorded to the north and south of this feature. The RHULS10 sequence was sampled from the infill of this feature, whilst the OxA-32438 date was obtained from the lowest possible organic deposits (ca. 8cm from the base of the monolith tins).*

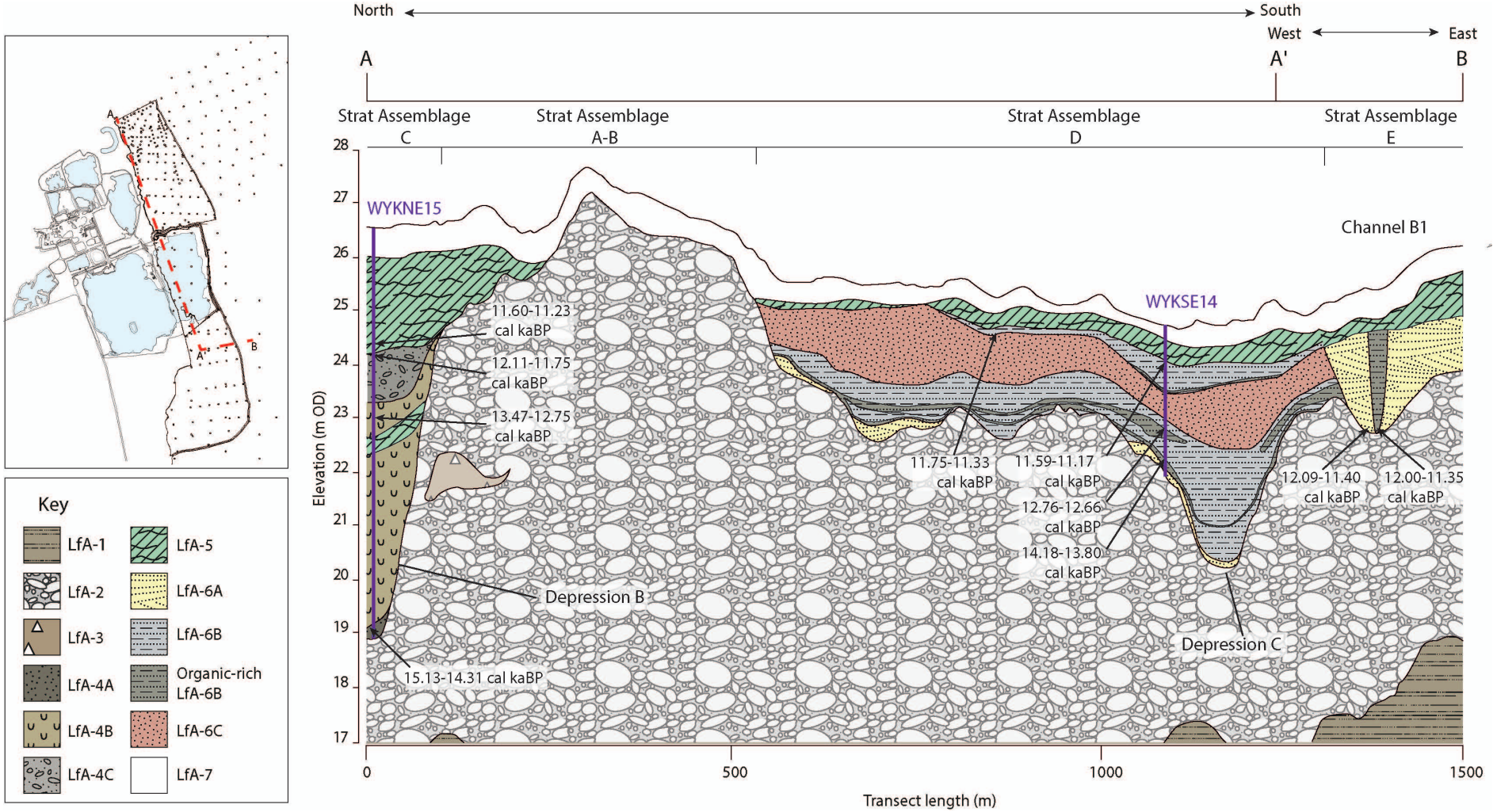

Figure 5.29. *Revised inverse distance weighted model of deposits at Wykeham Quarry showing the distribution of LfAs- 1-7 and associated age constraints on these deposits. The locations of the WYKNE15 and WYKSE14 records designated as those with optimum potential for palaeoenvironmental reconstrctuons are illustrated in purple.*

Stratigraphic assemblage E- (LfA-2→LfA-6A and/orB→LfA-5→LfA-7)

A single age from LfA-6A deposits, provides a range of 12.09-11.40 cal ka BP, placing it's deposition across the transition between the LLS, and the EH. An age on the basal infill of channel B1 (LfA-6B, Beta-214585), which is incised into LfA-6A deposits, provides a similar age range of 12.00-11.35 cal ka BP (Figure 5.29). Similar ages are provided by subsidiary palaeochannel infills (Trench B5 (LfA-6A-6B)), supporting that the formation, and abandonment of these landforms occurred during the end of the LLS, and into the EH.

5.5. Landscape model for the eastern Vale of Pickering

Using the mapped landforms in the VoP and the sedimentology, stratigraphy, and chronology of deposits at Wykeham Quarry, a landscape model can be constructed through the Last Termination for the eVoP.

5.5.1. The Dimlington Stadial (LfA-1-3, Channel Assemblage A)

Evidence from the GIS mapping of the VoP, enables a re-evaluation of the model of ice presence in the eVoP. This is based upon: a) terraces, used as evidence for palaeolake levels, of Glacial Lake Pickering, b) the reconstruction of an outwash plain (LfA-2-3), and high energy palaeochannels (Channel Assemblage A), and dead ice palaeolake depressions in the eVoP. This model is discussed below and summarised in Figure 5.30.

A 5-stage model of glacial occupancy of the eVoP through the Last Termination is constructed using previously published geomorphological interpretations from the valley (Kendall, 1902; Kendall and Wroot, 1924; Penny and Rawson, 1969; Straw, 1979; Foster, 1985; Franks, 1987; Evans *et al.,* 2005; 2016; Chapter 3). This model consists of:

a) Stage 1: Pre-Late Devensian glacial activity identified in the western VoP, interpreted as a plateau ice field advance from the North York Moors into the valley during a cold stage after MIS 12 but before MIS 2, possibly MIS 8 (Powell *et al.,* 2016).

b) Stage 2: Maximum ice advance into the eVoP, the Thornton-le-Dale/Wykeham Stage, leading to the formation of a proglacial lake in the VoP to an elevation of up to 70 mOD, controlled by the presence of ice in the Vale of York. This occurred between *ca.* 21-18ka BP (Bateman *et al.,* 2015; Evans *et al.,* 2016).

c) Stage 3: Retreat of the eVoP ice margin towards Filey Bay and stabilisation east of Seamer, leading to the formation of the Seamer sands and gravels. Proglacial lake levels interpreted to lower in response to ice retreat in the Vale of York (Evans *et al.,* 2016). Termed as the 'Cayton-Speeton Stage' by Straw (1979).

d) Stage 4: Ice recession from the eVoP at *ca.* 17.3 ± 1 kaBP (Evans *et al.,* 2016), leading to a decline in Glacial Lake Pickering to *ca.* 30 mOD.

e) Stage 5: Initiation of the LGIT and the formation of PF in the eVoP (Bateman *et al.,* 2015).

The geomorphological mapping, and sedimentological data obtained from the VoP enables a subtle re-evaluation of Stages 2-5 of this model to be undertaken. No additional information can be provided for pre-Dimlington Stadial glaciation associated with Stage 1, which therefore remains unmodified. The evidence associated with the timing of ice advance and retreat in the eVoP is considered below and charts a transition from a glacial lake system to an open landscape with many depressions and hollows that could form small lake water bodies in a developing fluvial network.

Stage 2: Ice advance into the eVoP during the LGM, ca. 21-18ka BP

<u>The inception of Glacial Lake Pickering:</u>

Sedimentological evidence from Wykeham Quarry provides new information on the extent of Glacial Lake Pickering and a more complex record of glacial advance and retreat in the VoP. The new borehole data from the area around the quarry indicates that there is a substantial thickness of LfA 1, glaciolacustrine silts and clays, below 20 mOD and with a thickness of greater than 10 m at the base of the sequences. These lake sediments formed as a result of ice advance in the North Sea, and the Vale of York, blocking drainage conduits out of the VoP and leading to the formation of a proglacial lake termed Glacial Lake Pickering (Kendall, 1902; Foster, 1985; Franks, 1987; Evans *et al.,* 2016). Previously these deposits have been identified as being concentrated in the western end of the VoP, with coarser grained facies dominating in the east (Kendall, 1902; Foster, 1985; Franks, 1987; Evans *et al.,* 2016*).* The fine-grained characteristics of LfA-1 would suggest that during initial stages of lake formation, ice presence was either relatively distal to Wykeham Quarry or formed away from major meltwater portals that were supplying sediment to the lake basin. Therefore it is possible that the deposits formed as ice advanced into the eVoP, or after initial ice retreat. It is interesting to note that the sediments gradually coarsen upwards and are succeeded by the coarser glaciofluvial gravels of LfA-2. This could indicate that either the ice re-advanced into the Wykeham area or that the ice was stationary and the glacial lake system progressively shallowed. Currently it is not possible to resolve this issue without further analysis of LfA-1 to examine whether there is evidence of subglacial deformation of the lake sediments (indicative of ice presence; e.g. Evans and Thomson, 2010), or establish where the ice front was during the advance and retreat of the NSIL into the eVoP (Phillips and Auton, 2000; Livingstone *et al.,* 2015b). The initial advance of the NSIL onto Holderness, to the south of the eVoP is constrained by Bateman *et al.* (2015) to *ca.* 20.5 ± 0.51ka BP. Therefore, this provides a constraining maximum age for the formation of LfA-1, as the presence of this ice mass enabled

ponding of water in the VoP to an altitude set by the outflow cols in the topographic elevations surrounding the VoP, and possibly to a maximum at Thornton-le-dale or at the Hutton-Buscel kame terrace/'Wykeham Moraine'. Although it was beyond the scope of this thesis to develop the sedimentological data further, it remains an interesting area of future research as the record of ice dynamics during advance and retreat is probably retained within this sedimentary archive.

Stage 3: Ice recession from the 'Wykeham to Cayton-Speeton Stage' limits, ca. 18 – 17 ka BP

The lower lake levels of Glacial Lake Pickering, and the transition to a subaerial depositional environment:

The eastward retreat of the ice margin from the Hutton Buscel kame terrace to the Flamborough Moraine led to the deposition of outwash gravels in the Wykeham area (associated with LfA-2 and correlated to the Hutton Buscel sands and gravels). The high erratic content indicates a glacial origin for these deposits, coupled with outwash from the rivers emerging from the North York Moors. The high clast content suggests that the ice remained proximal to the site during deposition. Occasionally these sediments contain LfA-3 deposits which may represent reworking of glacially derived diamicton via debris flows either directly from the ice, or mass flow events emerging from the Forge valley. Clearly the ice was in retreat from Wykeham to Flamborough, occurring between *ca.* 18 ka and 17 ka BP (Evans *et al.,* 2016). There is evidence that the lake waters also fell from *ca*. 70 mOD, to 45 mOD and then to at least 30 mOD during this 1000-year period. In this study, the GIS mapping only identifies the Hutton Buscel kame terrace as being consistent with a 70 mOD lake, meaning this landform and the channel at Hunmanby remain the only evidence for this lake level. This could reflect the inability of the lake body to form or preserve shorelines at this elevation, the inefficiencies of the techniques used to identify shorelines, or possibly the lack of a 60-70 mOD lake level in the VoP. Further field based mapping and levelling of landforms would be required to test this. The mapping across the basin does identify terraces associated with the lower lake levels between 45 and 30 mOD, which perhaps indicate that these terraces are more spatially extensive than previously thought.

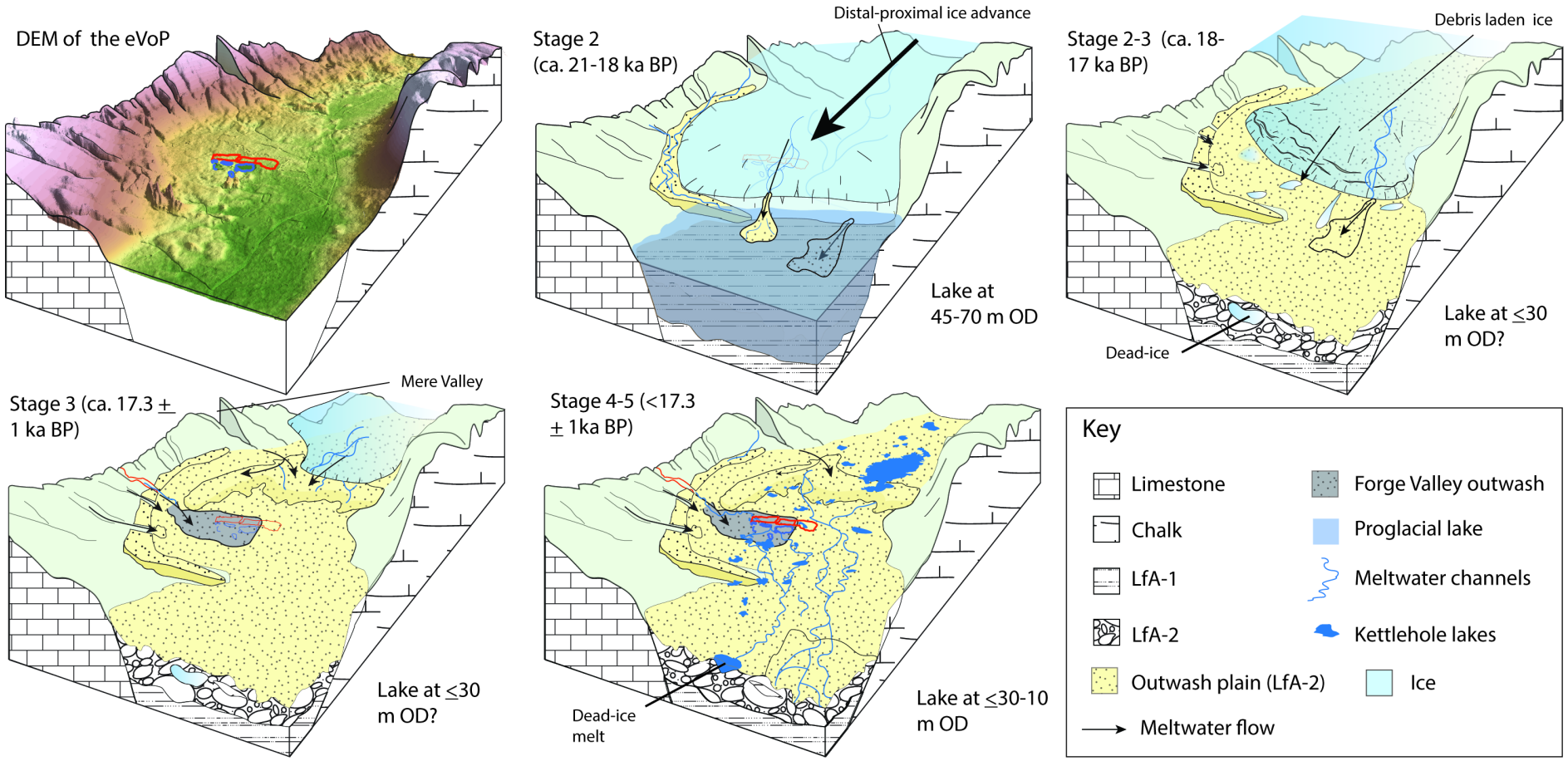

Figure 5.30. *Summary of the revised model of deglaciation of the eVoP between ca. 20.5 and 17.3 ka BP discussed in text. The stages follow those discussed in Chapter 5 with Stage 2 representing ice presence at the 'Wykeham Stage', Stage 3 representing ice present at the 'Cayton-Speeton Stage', and Stages 4 and 5 representing ice evacuation from the eVoP and the climatic amelioration at the start of the WI. Stage 2 represents the formation of glaciolacustrine deposits (LfA-1) at an early stage of ice presence. Recession from the Hutton Buscel kame terrace (Stages 2-3) was characterised by high discharge of sediment laden subglacial, englacial, and supraglacial meltwater depositing glacifluvial sediments across an outwash plain into or above a progressively lowering proglacial lake, which was controlled by the elevation of Glacial Lake Humber in the Vale of York. After ice receded from the eVoP at ca. 17.3 ±1 ka BP (Stage 4), Glacial Lake Pickering progressively diminished in size from 25-10 mOD, subaerially exposing the outwash plain, enabling kettlehole lakes, and high energy channels (Channel Assemblage A) to form. The abrupt climatic amelioration at onset of the WI (Stage 5) led to the melt-out of any residual dead ice, including that in the Flixton basin.*

However, it is more difficult to associate these lake levels to the formation of the Hutton Buscel sands and gravels in the vicinity of Wykeham Quarry, as the sediment properties of LfA-2 alone, cannot be used to confidently differentiate between a subaerial and subaqueous depositional environment. The high concentration of kettle-holes in this part of the eVoP would suggest however that deposition occurred in a subaerial environment (Brodzikowski and van Loon, 1991). However, the elevation of LfA-2 at Wykeham Quarry which ranges between *ca.* 10 and 30 mOD, would have been below the lake surface level of Glacial Lake Pickering if it existed at its previously reported elevations of 70 or 45 mOD. Additionally, the outwash deposits of the Seamer sands and gravels are graded to *ca.* 30 mOD, supporting that the lake had fallen to approximately this elevation by the time that ice had receded to the east of the Mere Valley in the eVoP (Stages 3-4). Therefore, this evidence points toward the lake having fallen to at or below 30 mOD by the time ice had retreated from the Wykeham area with the ice in the Vale of York having retreated to allow the Kirkham Gorge to be open and allow drainage to Glacial Lake Humber. Evans *et al.* (2016) suggest that this ice retreat was initiated around 17.6 ± 1 ka BP using evidence around East Heslerton in the VoP (Evans *et al.,* 2016), with lake water levels progressively falling to *ca.* 30 mOD by 17.3 ±1 ka BP.

As ice receded east of the Forge Valley, outflow from a dammed lake in the Seacut Valley is interpreted to have incised through the Corallian Dipslope, forming an alluvial fan across the outwash plain (Kendall, 1902; see Figure 5.30). This is supported by the higher proportions of angular, and weathered clasts of local lithology in the N1 phase of Wykeham quarry, and Ings Bridge (Franks, 1987) demonstrating a more localised source of aggregate than the outwash deposits. A similar depositional process is envisaged for the Seamer sands and gravels, which were formed via outflow of the Mere Valley (see Figure 5.30) as ice temporarily stabilised in the Filey Bay area (Kendall, 1902; Palmer *et al.,* 2015). Final ice recession out of the eVoP (Stage 3-4) led to the deposition of an analogous sequence of deposits in the PF basin as at Wykeham Quarry, forming a chaotically pitted kettle and kame topography formed by high volumes of sediment laden meltwater which covered residual dead ice (Palmer *et al.,* 2015).

It should also be noted that other potential terraces and consequently lake levels at 50-42, 40-42, 38-35 mOD have been identified, suggesting further complexity in the manner of lake level falls between 70 m and 30 mOD. Furthermore, there is a relationship between certain lake level elevations in the VoP, including lower terraces, and the terrace fragments in the Kirkham Gorge. The elevation ranges of 40 to 42, 30 to 32, 26 to 25, and 20 to 22 mOD provide consistent evidence for terrace development at similar altitudes to proglacial lake shorelines mapped by Fairburn and Bateman (2016) in the Vale of York. Additionally, dates obtained upon the lake levels of Glacial Lake Humber suggest that it lowered from 42-40 mOD to 33-30 mOD between

ca. 17.01 ± 1.33 and 16.6 ± 1.2 ka BP (Fairburn and Bateman, 2016) which is consistent within uncertainties to the inferred lowering of Glacial Lake Pickering to *ca.* 30 mOD (by 17.3 ± 1 ka BP; Evans *et al.,* 2016). This demonstrates that Glacial Lake Pickering and Glacial Lake Humber were consistently hydrologically connected through the Kirkham Gorge during the time of the lower lake levels between 42 and 10 mOD levels. As such, the evolution of Glacial Lake Pickering can be sub-divided into two lake systems: the upper Glacial Lake Pickering (60-70 and 45 mOD) controlled by the ice lobes; and as ice retreated, a series of lower lake levels controlled by the level of Glacial Lake Humber through the connection in the Kirkham Gorge. This would suggest that the 30 mOD lake level was attained prior to ice recession from the Stage 2 limit. The implication is that the initial ice recession phase in NE England may well have been diachronous, with the VOYL, retreating prior to the NSIL. This enabled Glacial Lake Pickering to drain into Glacial Lake Humber through the Kirkham Gorge. However, the age uncertainties placed upon the timing of these changes (frequently ≥ 1 ka BP; Bateman *et al.,* 2015; Fairburn and Bateman, 2016) means that the precise timing and phasing of lake level changes in the valleys during this interval remain equivocal.

Stages 4-5: Recession of ice from the eVoP, ca. 17-15 ka BP

<u>The transition from a glacial to a paraglacial landscape:</u>

Ice is interpreted to recede from the eVoP by *ca.* 17.3 ± 1 ka BP (Evans *et al.,* 2016) coinciding with NSIL retreat from Holderness (Bateman *et al.,* 2015), but remained adjacent to the contemporary Yorkshire coast until 14.9 ± 0.44 ka BP (Bateman *et al.,* 2015). However, with the ice front in a more distal position it is unlikely that glacier meltwater was directly depositing sediments from the glacier, with more active fluvial systems emanating from the North York Moors providing the major supply of sediment to the eVoP (see previous section).

The presence of the NSIL, which deposited the Withernsea Till on Holderness, maintained an ice dam ensuring the Glacial Lake Humber still existed (Fairburn and Bateman, 2016) at this time. During this interval, Glacial Lake Humber had declined to between 25 and 10 mOD (Fairburn and Bateman, 2016), meaning that if the two lakes were hydrologically connected through Kirkham Gorge, the outwash plain surface in the eVoP became subaerially exposed between 17.3 ± 1ka BP and 14.9 ± 0.44 ka BP. This time interval reflects the formation of meltwater and/or nival-fed subaerial channels (Channel Assemblage A) across its surface, and the melting of residual dead ice blocks within LfA-2, leading to the development of kettle-hole lakes.

5.5.2. The Last Glacial-Interglacial Transition (LfA-4-6, Channel Assemblage B)

In the topographic depressions formed in LfA-2 in the north of Wykeham Quarry (stratigraphic assemblage C), base-rich water bodies developed, likely fed by spring-lines from the Corallian

Dipslope aquifer (Brown *et al.,* 2013). Initially these water bodies were inundated by gravity flows (LfA-4A) sourced from the unstable margins of LfA-2 slopes (stratigraphic assemblage A), but as climate ameliorated at the start of the LGIT (*ca.* 14.7 cal ka BP), authigenic deposits formed in shallow, low energy water-bodies (LfA-4B), whilst peatland formed around the basin margins possibly increasing slope stability (stratigraphic assemblage B). The sporadic preservation of LfA-6A deposits underlying LfA-6B in stratigraphic assemblage D would suggest the presence of erratic fluvial activity, characterised by small scale scour and fill channels formed prior to *ca.* 14.18-13.80 cal ka BP (Channel Assemblage A). The limited preservation of fluvial deposits in this period remains unclear, but would support that the River Derwent was not consistently aggrading sediments during the E-WI. LfA-6B formation during the M-L-WI (<14.10 cal ka BP) demonstrates the formation of low energy flow regimes, and backswamps across large areas of the floodplain. These conditions were perturbed during the LLS by phases of enhanced flow regimes in both lacustrine- (LfA-4C), and fluvial systems (LfA-6C), culminating in the incision of palaeochannel forms through the floodplain deposits across the LLS-EH transition (*ca.* 11.7 cal ka BP; stratigraphic assemblage E; Channel Assemblage B). In the EH Channel Assemblage B channels were permanently abandoned, and fine-grained siliclastic, and telmatic deposits (LfA-6B, LfA-5) formed in stratigraphic assemblages C-E, demonstrating a consistent decline in the energy of depositional processes and the infilling of open water bodies via hydroseral succession (Taylor, 2011).

5.6. Selection of sites for palaeoenvironmental investigation

To meet the research aims, sequences viable for palaeoenvironmental reconstruction had to meet the following criteria:

- Deposited during the Last Termination/LGIT.
- Demonstrate evidence of sedimentological complexity, potentially representing variability in climatic, hydrological, and/or geomorphic regimes.
- Contain sediments viable for radiocarbon dating via terrestrial plant macrofossil remains.

LfA-4, and LfA-6 deposits in stratigraphic assemblages C and D provide the best potential for palaeoenvironmental reconstruction as: a) they have been demonstrated to have been deposited during the LGIT, and contain deposits (e.g. interbedded poorly humified LfA-5 peats) representing varying modes of sedimentation, possibly driven by shifts in climatic, and hydrological regimes , b) they contain deposits viable for palaeoenvironmental reconstructions using a variety of techniques. Most notably, the carbonate-rich characteristics of LfA-4 deposits in stratigraphic assemblage C have potential for bulk sediment stable isotopic analysis (Leng and Marshall, 2004), whilst interbedded, organic rich deposits in stratigraphic assemblage D (LfA-6B) demonstrate significant potential for palaeoclimatic and palaeohydrological reconstructions using

palaeoecological techniques such as coeloptera, pollen, and plant macrofossils (e.g. Walker *et al.,* 1993; 2003; 2008; Bos *et al.,* 2006).

The best expressed record for stratigraphic assemblage C is identified from the deepest augered locality in Depression B (RHULPal 1 and 2), where LfA-4 deposits are in excess of 7m thick, and contain sedimentological complexity, potentially indicating sensitivity to climatic events through the LGIT. Stratigraphic assemblage D is best expressed in the phase 6 area of the present quarry (Cloutman *et al.,* 2010), which lies at the margins of Depression C. This area contains thick units of WI, and EH aged, organic rich, LfA-6B deposits, with well-preserved macrofossil, and invertebrate remains (Cloutman *et al.,* 2010), interdigitated with LfA-6C, indicative of deposition during the LLS. These records are therefore confidently interpreted to represent a tripartite sequence through the LGIT with minimal evidence for proximal fluvial activity capable of eroding pre-existing deposits. Chapter 6 presents palaeoenvironmental reconstructions from these selected sequences.

6. Palaeoenvironmental reconstructions from Wykeham Quarry

6.1. Introduction

This chapter presents palaeoenvironmental reconstructions through the LGIT from two sequences (one in stratigraphic assemblage C and one in stratigraphic assemblage D) at Wykeham Quarry. These records were chosen as they represent the sites of optimum potential to reconstruct palaeoenvironmental and palaeoclimatic regimes through the LGIT, constrained by a high-resolution chronology. This chapter first reviews the sedimentological, chronological, and palaeoenvironmental reconstructions from each record, before synthesising the proxy data used to reconstruct palaeoenvironmental regimes through the LGIT.

6.2. Stratigraphic Assemblage C: the Wykeham Northern Extension 2015 (WYKNE15) sequence.

Stratigraphic assemblage C represents a complex palaeoenvironmental sequence through the LGIT, consisting of sediments representing deposition within still-to-slow flowing, shallow, and base rich water bodies (LfA-4A-4C), capped by peats (LfA-5). These deposits are focussed into two topographic depressions (termed as Depression A and Depression B), in the basal sands and gravels (LfA-2) of the Northern Extension area at Wykeham Quarry (Figure 6.1), where they are interpreted as small kettlehole lakes, and palaeochannel infills, formed soon after ice recession. The depositional context of the deposits are similar to those found within Palaeolake Flixton (PF), *ca.* 3km to the east of Wykeham Quarry (Day, 1996; Mellars and Dark, 1998), providing the potential to directly compare palaeoenvironmental signals between sites. The primary focus for palaeoenvironmental reconstructions for stratigraphic assemblage C, is the deepest modelled infill of Depression B, most likely to provide the most complete, and highest resolution palaeoenvironmental record.

Sequences were obtained from two sites in the centre of Depression B, spaced *ca.* 20 m apart (RHULPal-2 and RHULPal-3, termed hereafter as Wykeham Northern Extension 2015, site A and site B (WYKNE15 sites A and B) Figure 6.1; 6.2)). Sites were initially sampled in November 2013, using hand powered augering equipment, and overlapping 50 cm Russian cores, from two parallel boreholes at each site. A complete stratigraphy through the LfA-4B deposits could not be obtained from these records due to the presence of sand and gravel beds in the sequence, and the consolidated and friable characteristics of the sediment matrix (Figure 6.2b). The basin was re-sampled in January 2015, and May 2015, using percussion augered stitz cores from 3 overlapping boreholes from site A, in order to replicate the stratigraphy, and fill gaps left in the sequence, from the original sampling. 22 cores were excavated from site A during these visits (Figure 6.2). A further 10 x 50 cm Russian cores, sampled from WYKNE15 site B were also

subsampled for bulk sedimentological properties, providing a correlative to the site A stratigraphy. The correlation of these records is outlined in Figure 6.2c.

6.2.1. Composite stratigraphy

A composite stratigraphy was constructed from the WYKNE15 site A record using the presence of key marker horizons, and patterns in the bulk sedimentological records between individual cores. Below 450 cm from the land surface, the friable nature of the carbonate deposits in LfA-4B prevented the consistent capture of sediments in situ, particularly in the percussion augered records, where the upper sections of cores were consistently disturbed, and slumped, preventing reliable cross correlations using the methods outlined above. In these records, supplemental palaeoenvironmental, and chronological data were used to provide supporting evidence of the exact positioning of the cores. These correlations are supported by all other palaeoenvironmental, and sedimentological evidence gathered from the records, and the depths from which they were sampled. The composite stratigraphy therefore represents the most complete sedimentary sequence recorded from the core sequences extracted from Depression B. When the composite stratigraphy is constructed, two gaps are present between 76-82 cm (Gap 1) and 160-172 cm (Gap 2) from the base of the sequence, (Figure 6.3 and Figure 6.4). Both gaps are artefacts of disturbed, and/or slumped sediments from the core sampling, and cannot be reliably utilised for palaeoenvironmental reconstruction. From the WYKNE15 composite stratigraphy, 6 lithozones are identified (termed WN-L1 to 6 from base to top; Table 6.1, and Figures 6.3 and 6.4), which can be correlated to the Wykeham lithofacies associations (LfA-4A-4C, LfA-5).

6.2.2. Bulk sedimentology

Carbonate, organic, and siliclastic content were obtained at 2-4 cm intervals whilst magnetic susceptibility values were obtained at 3 cm intervals. Siliclastic particle size measurements were also obtained from WN-L4 and 5, while low siliclastic yields in WN-L1, 2, 3, and 6 prevented particle size measurements, owing to the limited amount of available sediment, and the series of proxy data required from the core material. All bulk sediment values are reported as percentages of the total sediment matrix < 2 mm. Sand, silt and clay values in WN-L4 and 5 are reported as the % of the siliclastic component of the entire sediment matrix. A summary of the bulk sedimentology is presented in Table 6.1, and Figure 6.5 with raw values presented in Appendix G.

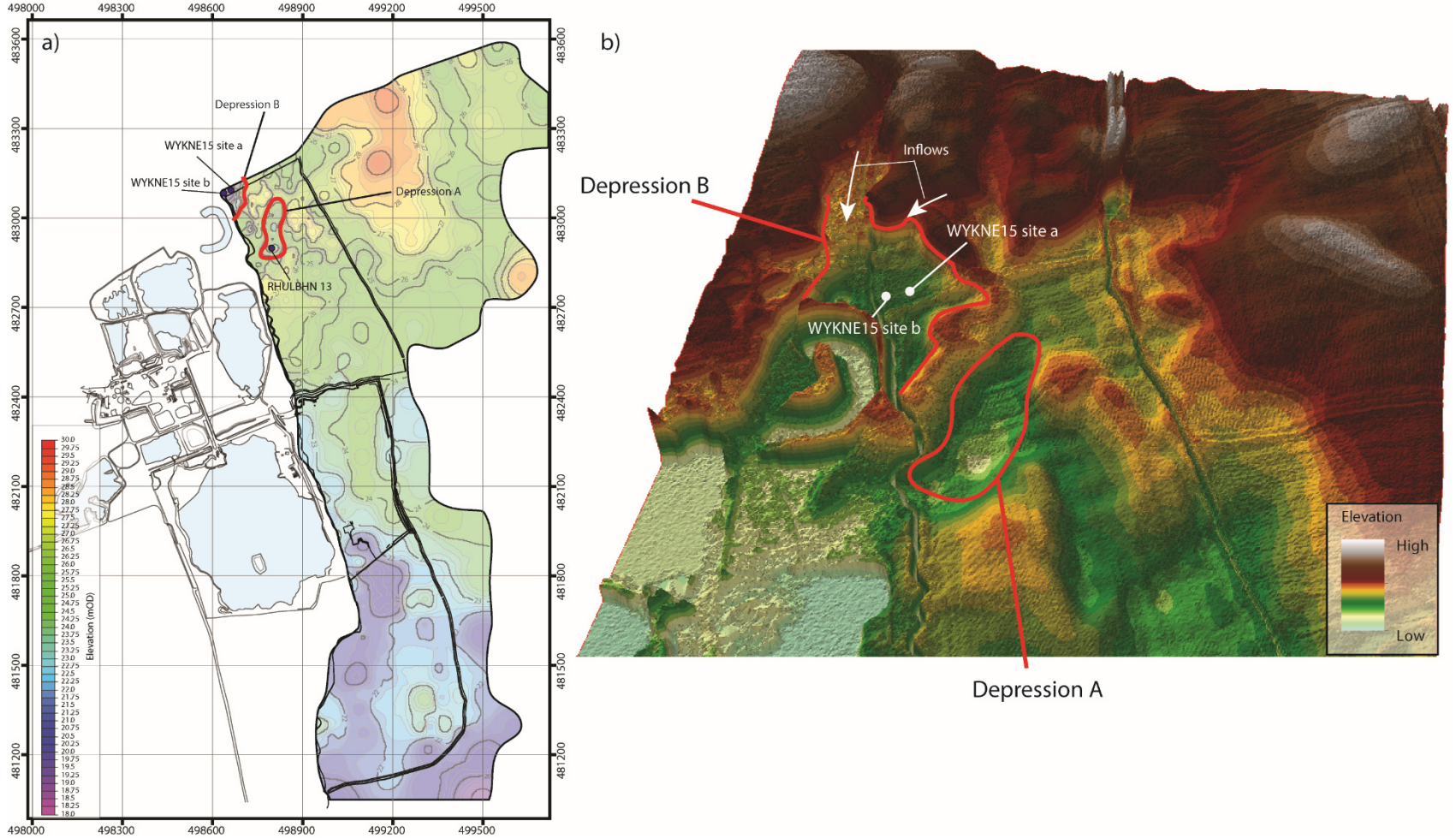

Figure 6.1. *a) Map showing the location of sites sampled for palaeoenvironmental reconstructions in the Northern Extension of Wykeham Quarry. The location of Depression A and B (marked in red), alongside records described in text are displayed in relation to the inverse distance weighted model of the surface elevation of LfA-2. b) A LiDAR 3D elevation model, highlighting the palaeoinflows into Depression B (white arrows). The location of borehole records are marked for reference.*

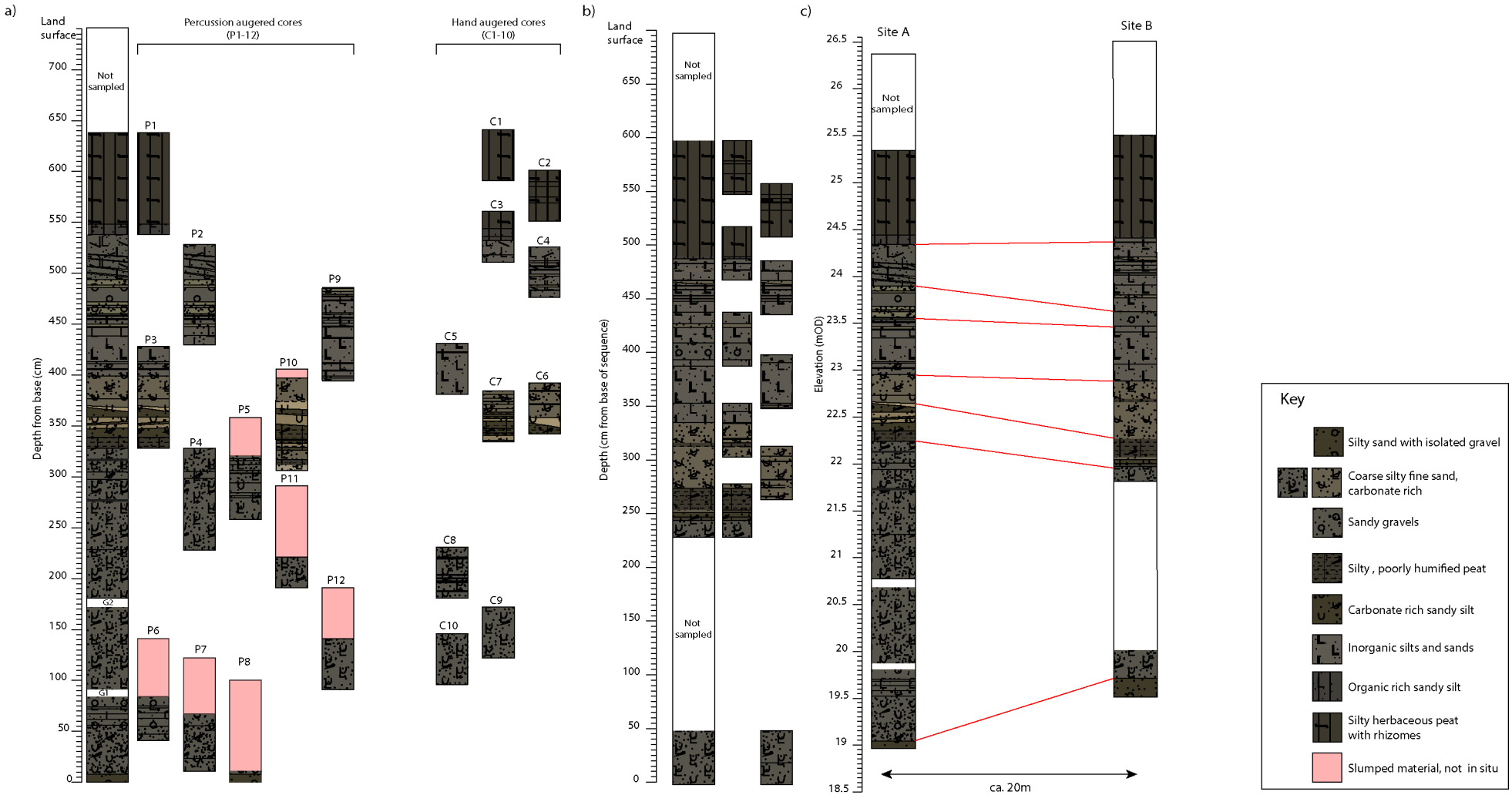

Figure 6.2. *a-b) composite logs from the WYKNE15 site A and site B sequences respectively. c) Correlation between the site A and site B stratigraphies. The sequences display identical stratigraphies, with only slight offsets in elevation.*

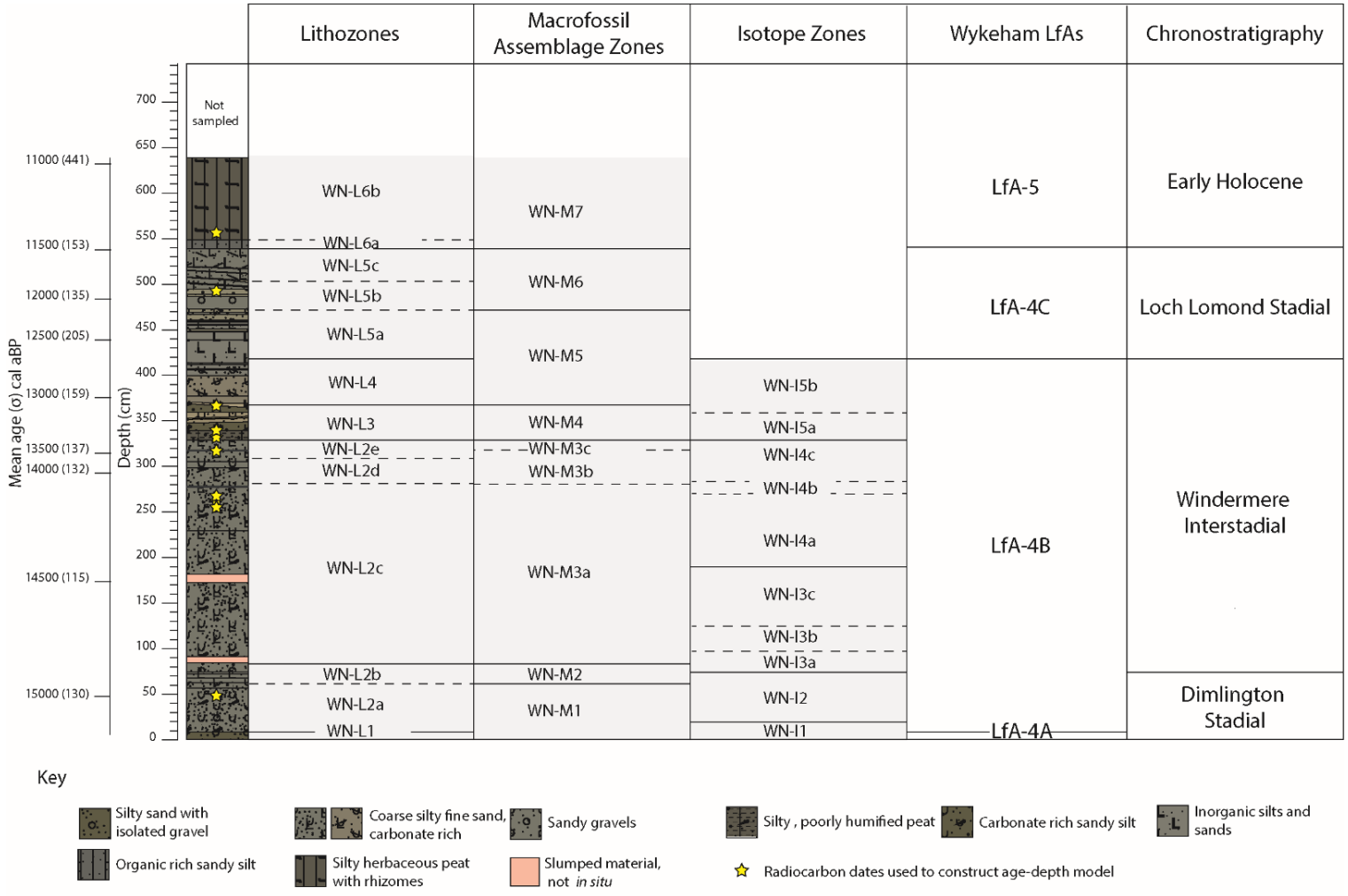

Figure 6.3 *Correlation between the lithozones, macrofossil assemblage zones, and isotope zones through the WYKNE15 stratigraphy discussed in text. These zones are compared to the Wykeham Lithofacies associations (summarised in Chapter 6), and the chronostratigraphic framework for the British Isles. The stratigraphy is plotted against depth (cm) from the base of the sequence, and median age ranges (2σ) derived from the P_Sequence model described in section 6.2.4.*

Table 6.1. *Summary of the lithozones in the WYKNE15 sequence. Colour and texture descriptions follow the Munsell, and Troels-Smith classification schemes respectively. Depths for each unit are recorded as cm from the base of the stratigraphy.*

Lithozone	Depth (cm)	Description
1	0-8	Very dark greyish brown (10YR 3/2) silty medium to fine sand, with isolated gravel clasts (Ga3,Ag1,Gg+).
2a,c,e	8-328	Olive to dark grey (5Y-10YR 4/1), massive, to weakly laminated, carbonate rich, coarse silty fine sand, with abundant remains of horizontal-sub-horizontally bedded, calcified charophyte thalli casts (Lc4,Ag+,Ga+,Dg+).
2b	58-76	Dark grey (5Y 4/1) fine sandy silt with mossy remains and gravel clasts (Ag2,Ga1,Sh1,Gs+).
2d	280-306	Dark grey to very dark grey (10YR 4/1 to 2.5Y 3/1) fine sandy, silt, with isolated gravel clasts and moss remains (Lc2,Ag1,Ga1,Dg+)
3	328-366	Dark olive grey to black (5Y 3/2 to 2.5Y 2.5/1), organic rich coarse silty, clayey, poorly humified peat, with isolated fine to medium sand grains (Th3,Ag+,Dg+,Ga+), interbedded with dark greyish brown (2.5Y 5/3 to 2.5Y 3/2), carbonate rich, fine sandy silts (Lc2,Dg2,Ag+,Ga+).
4	366-417	Light yellowish brown, to dark grey (2.5Y 6/3 to 2.5Y 4/1), massive, to weakly laminated (2-4 mm), carbonate rich, fine sandy coarse silt (Lc3,Ag1,Dg+).
5a,c	417-537	Dark grey (5Y 4/1), fine sandy coarse silt (Ag2,Ga2) interbedded with thin beds of olive grey (5Y 5/2), fine to medium sand (Ga4-Gs4, 0.1 to 2 cm thick).
5b	471-505	Normally graded (lower contact) and reverse graded (upper contact), medium to coarse sandy fine to medium gravel beds (Gg3,Gs1), interbedded by dark grey (5Y 4/1) silty medium to coarse sands (Gs3,Gg1).
6a	537-548	Dark to very dark grey (5Y 4/1 to 2.5Y 3/1), fine silt with herbaceous remains (Ag2,Dg2,Sh+,Th+).
6b	548-624	Black (2.5Y 2.5/1), poorly to moderately humified, fine silty herbaceous peat ($Th4_{(h2)}$,Ag+,Dg+,Sh+) with preserved *Phragmites australis.*

Microsedimentology

The macroscale sedimentology, demonstrates that there is variability in the type of sediment deposition through the sequence. The style of carbonate deposition is of particular interest, owing to the potential that authigenically precipitated lacustrine carbonates have for reconstructing palaeoenvironmental regimes (Marshall *et al.,* 2002; Leng and Marshall, 2004).

To develop understanding on the modes of carbonate deposition through the sequence, 8 thin sections were produced from WN-L2-5 (TS-1-8). These were used to: a) develop understanding of the mode of deposition within these zones, b) clarify the style of carbonate deposition for prospective bulk sediment isotopic analysis. The positions that these thin sections were taken in the stratigraphy is shown in Figure 6.4. Descriptions follow Bullock (1985), with summaries presented in Appendix G, and images of key features presented in Figures 6.6-6.7. A summary of the microscale characteristics of WN-L2-5 is presented in Table 6.2.

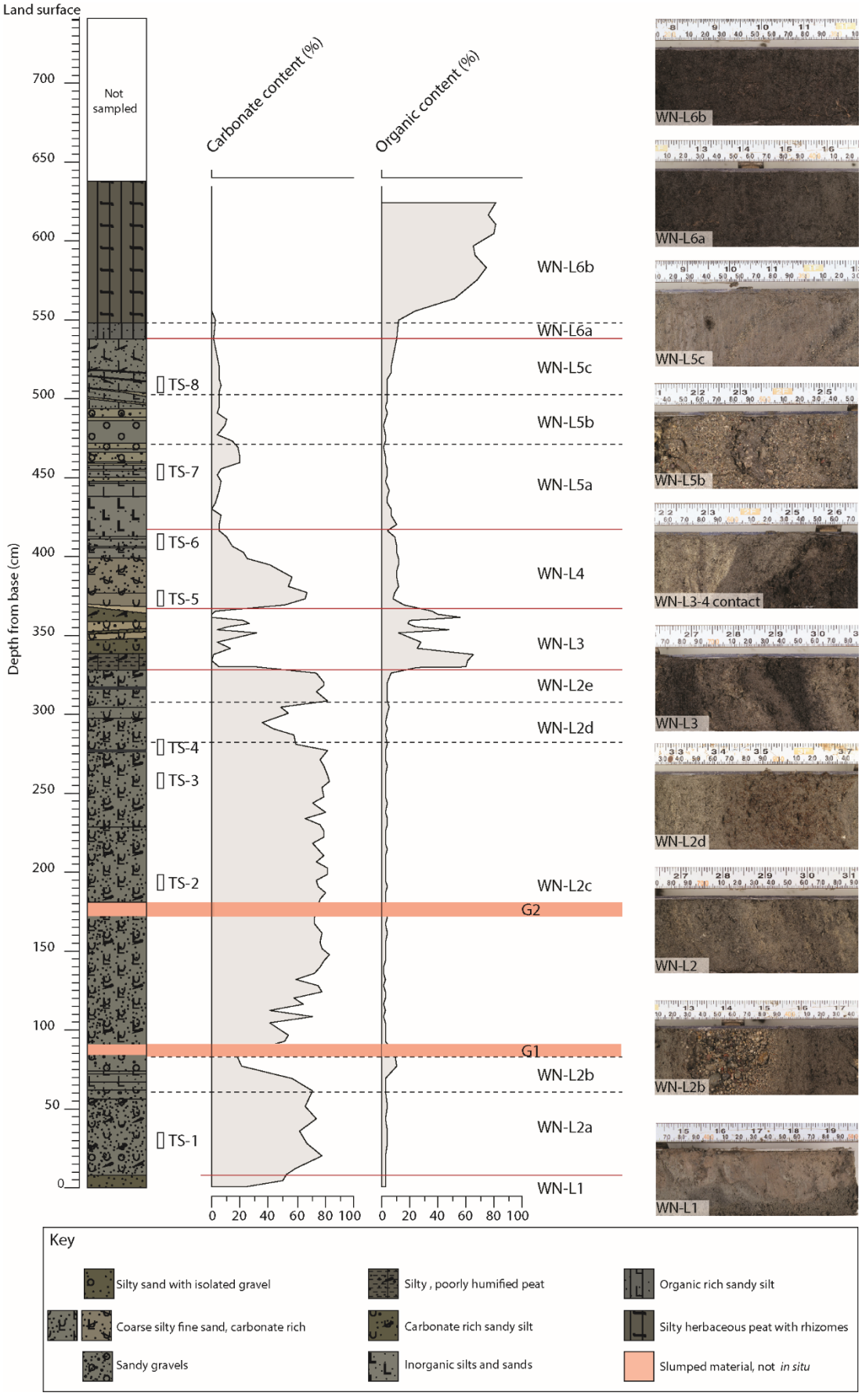

***Figure 6.4**. Summary diagram of the WYKNE15 stratigraphy, highlighting the sedimentological variability in the sequence. The location of thin section samples (TS-1-8), discussed in text are shown, alongside images showing the sedimentological characteristics of the lithozones discussed in text.*

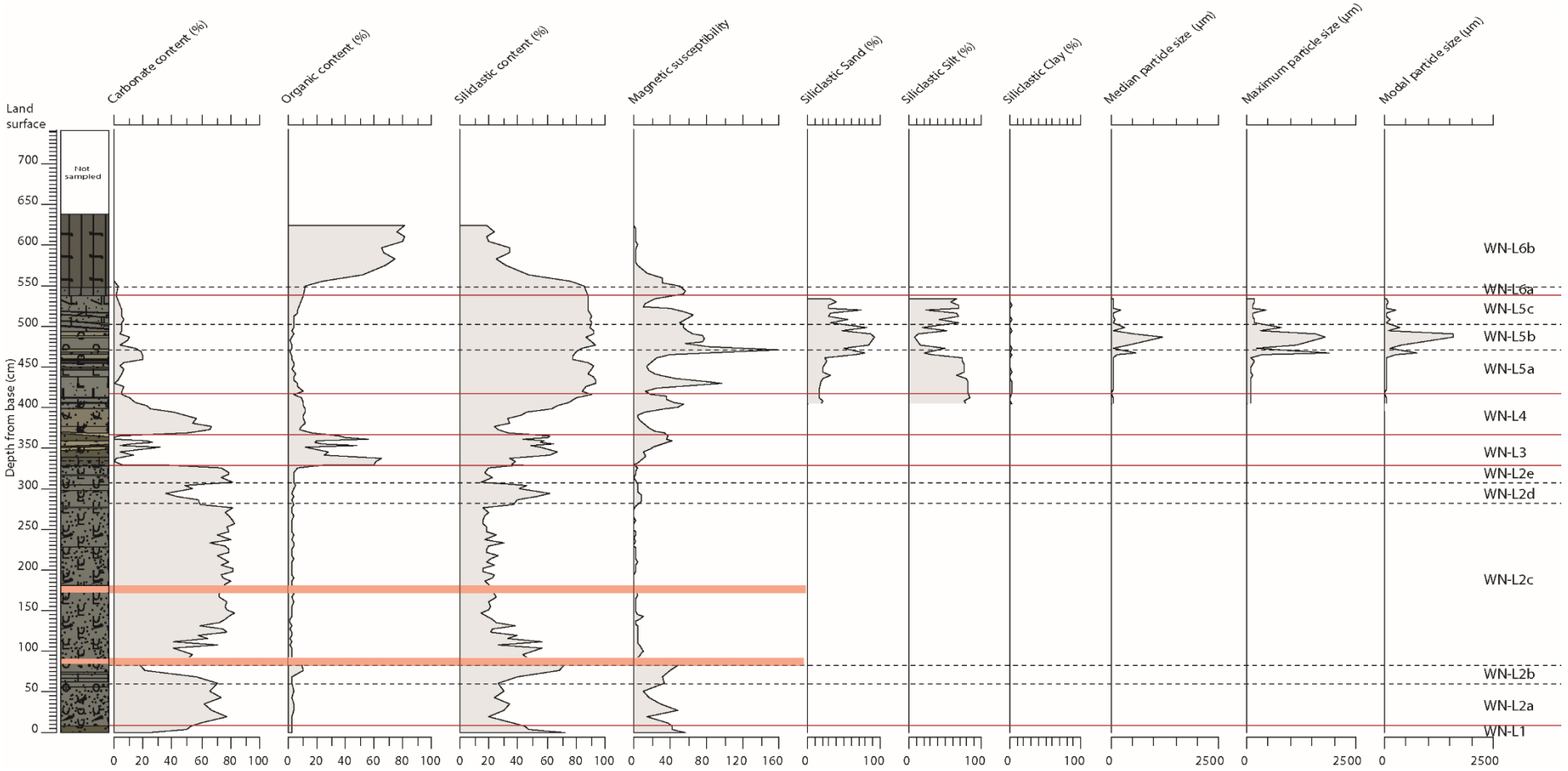

***Figure 6.5**. Summary of the bulk sediment properties of the WYKNE15 sequence.*

Table 6.2. *Summary of microscale characteristics of the WYKNE15 sequence. Descriptions follow Bullock (1985).*

WN-L	Thin section (TS)	Micromass	Porosity and voids	Sediment matrix	Carbonate	Non-carbonate
2a	1	Carbonate: mineral ratio 1:1	Irregularly spaced planar voids (5-20%), and packing voids (5-20%), ranging between 20 and 200 μm, and spherical/channel voids associated with charophyte thalli (5-20%).	Carbonate-rich granular microfabric associated with charophyte precipitation, comprised of equant-subhedral crystals of platy to blocky microspar and spar (20 and 80% of carbonate micromass respectively; Figure 6.6 a-d).	High frequency (20-30% of slide cover) of charophyte thalli casts, which have an identical crystal structure to the microfabric (Figure 6.6a). They can be distinguished from the microfabric on the basis of their shape and concentric structure. Molluscan shell and ostracod valves present (<2 % slide cover).	Mineral fraction consists of randomly distributed, sand sized sub-angular quartz and oolitic limestone grains, with rare occurrences of very coarse sand to granule sized grains. Organic material focussed into weakly developed horizontal laminations (250μm; 10 % slide cover).
2c	2,3,4	Carbonate: mineral ratio 4:1	Irregularly spaced spherical and channel voids (100-1000 μm), associated with calcite precipitation around charophyte thalli, and complex packing voids (20-600 μm), both within, and between the microfabric and charophyte thalli casts (*ca.* 10-20% of slide cover; Figure 6.6c and f).	Carbonate-rich, micrite and equant-subhedral, platy-blocky microspar (*ca.* 80%), and spar (*ca.* 20%), crystals (≤68 μm), forming a granular texture (40-60 % of particles; Figure 6.6 c-h)	High amounts of spar-microspar calcite, matching the description of the matrix is also precipitated in association with charophyte thalli. Skeletal carbonate (<1% of slide cover), includes whole, and broken gastropod shells, and ostracod valves (Figure 6.6e and g). No oncoids or peloids are identified.	5-10 % slide cover. Mineral grains, herbaceous, and amorphous organics and charcoal focussed into irregularly spaced, horizontal-sub-horizontally bedded laminations, ranging between 10 and 1900 μm in thickness. Minerals are sub-angular to sub-rounded fine silt to very fine sands (10-70 μm) of varying lithologies
2d	4	Carbonate:mineral ratio 1:1	Porosity *ca* 50-60 % primarily packing voids	Clast supported matrix consisting of moderately to well sorted mineral clasts (modally very fine to medium sand (120-300 μm); Figure 6.6h). Carbonate matrix correspond to those outlined for WN-L2a and c.	Carbonate consists principally of *Chara* remains which are frequently broken and incomplete (>60% of charophyte thalli casts)	Mineral grains and organics focussed into laminations ranging from very fine to fine sand (60-250 μm), and increased abundances of charcoal. These zones coincide with macroscale charcoal lenses above, and below WN-L2d. Increasing frequencies of mineral clasts randomly positioned within the sediment matrix is also noted directly below the transition into WN-L2d.

3	5	Minerogenic-organic-carbonate microfabric, consisting of a minerogenic, organic, carbonate, ratio 2:1:1.	Porosity *ca* 20% of the slide cover, which consist of complex packing voids, planar voids, and spherical/channel voids associated with charophyte thalli casts which are frequently broken (80% of Chara remains)	Massive, granular microfabric, consisting of equant and subhedral crystals of microspar and spar (80 and 10% of carbonate micromass respectively), and micrite (10% of carbonate micromass).	Charophyte thalli casts (10% of slide cover, focussed into subhorizontally bedded lenses) frequently incomplete or broken (80% of charophyte remains).	Mineral silts consistently distributed through the microfabric, and isolated subangular-subrounded quartz grains (25-130 μm), irregularly distributed, comprising <5% slide cover in total. Organic fraction, represents up to 40% of the slide cover, and is composed of amorphous organic material, and subhorizontally bedded bryophyte and herbaceous remains (≤80 μm).
4	5, 6	Weakly laminated carbonate-minerogenic microfabric, consisting of a carbonate: mineral ratio of 1:1. Increasing mineral content at top of zone	Porosity accounts for between 30-40% of the slide cover, consisting of spherical and channel voids formed from charophyte thalli casts (80-90% of voids), small packing voids (20-80 μm), and vughs (≤370 μm).	Similar in composition to WN-L2 and 3, being comprised of platy to blocky, equant and subhedral-anhedral microspar and spar crystals (70-20% of carbonate composition). Top of zone is a silt dominated microaggregate.	Charophyte thalli casts (30-40 % of carbonate cover) which are frequently incomplete or broken (>90% of thalli casts; Figure 6.7a). No charophytes are found at the top of the zone.	Mineral particles increase in abundance through the zone. organic fraction (*ca.* 10% slide cover), consists of amorphous organic material, and herbaceous and bryophyte fragments (Figure 6.7d), which contain pyrite framboids, and are randomly distributed within the microaggregate, and focussed into subrounded-rounded intraclasts (<5% slide cover; Figure 6.7c).
5	7, 8	Matrix consists of a minerogenic-organic, intergrain microaggregate, with a mineral:organic ratio of 2:1.	Porosity ranges between 10% (slide cover) in finer grained beds to 20% (slide cover) in coarse beds, where pores are composed of simple intergrain packing voids.	Horizontal laminations to thin beds (450-10000 μm), of well sorted, clast supported aggregate, with a clast:matrix ratio of 3:1. A minerogenic-organic, intergrain microaggregate, Low abundances of carbonate are present within the microaggregate (<5% of slide cover), where they consist of isolated, and irregularly distributed, equant, microspar-spar crystals.	Carbonates within the microaggregate comprise <5% of slide cover, and consist of individual spar and microspar crystals irregularly distributed within the microaggregate.	Minerogenic fraction of the matrix consists of medium to coarse silts, whilst the organic fraction (5-10% slide cover) is composed of amorphous organic material, and vertically oriented herbaceous stem remains, which are consistently transformed to pyrite framboids (Figure 6.7h; Wilkin and Barnes 1997).

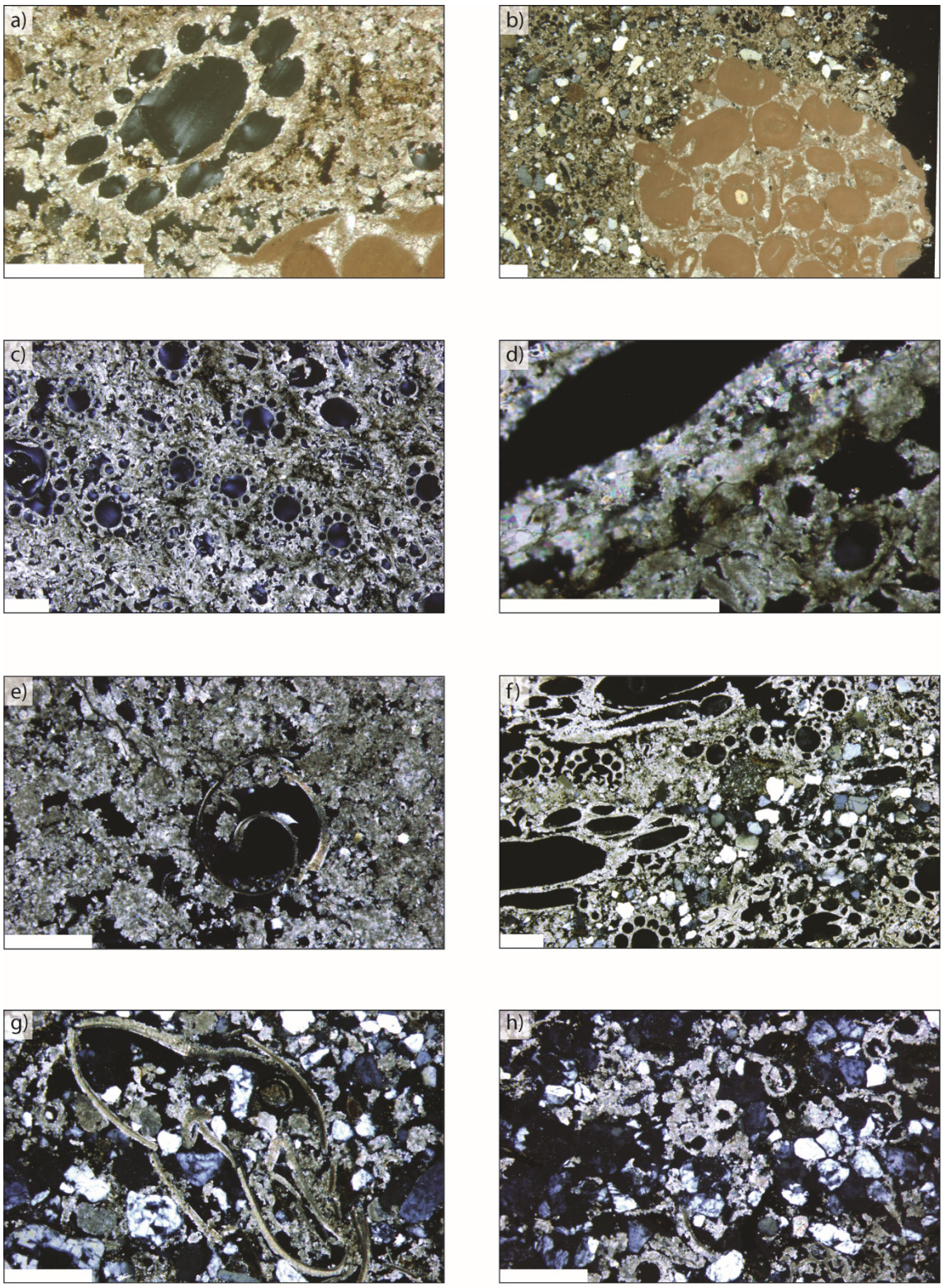

Figure 6.6. *a) to g) Photomicrographs of key microsedimentological features identified in WN-L2. The white bar at the base of each image represents 500 µm. All images with the exception of those labelled PPL (plane polarised light) were taken using cross polarised light (XPL). For descriptions of features refer to text.*

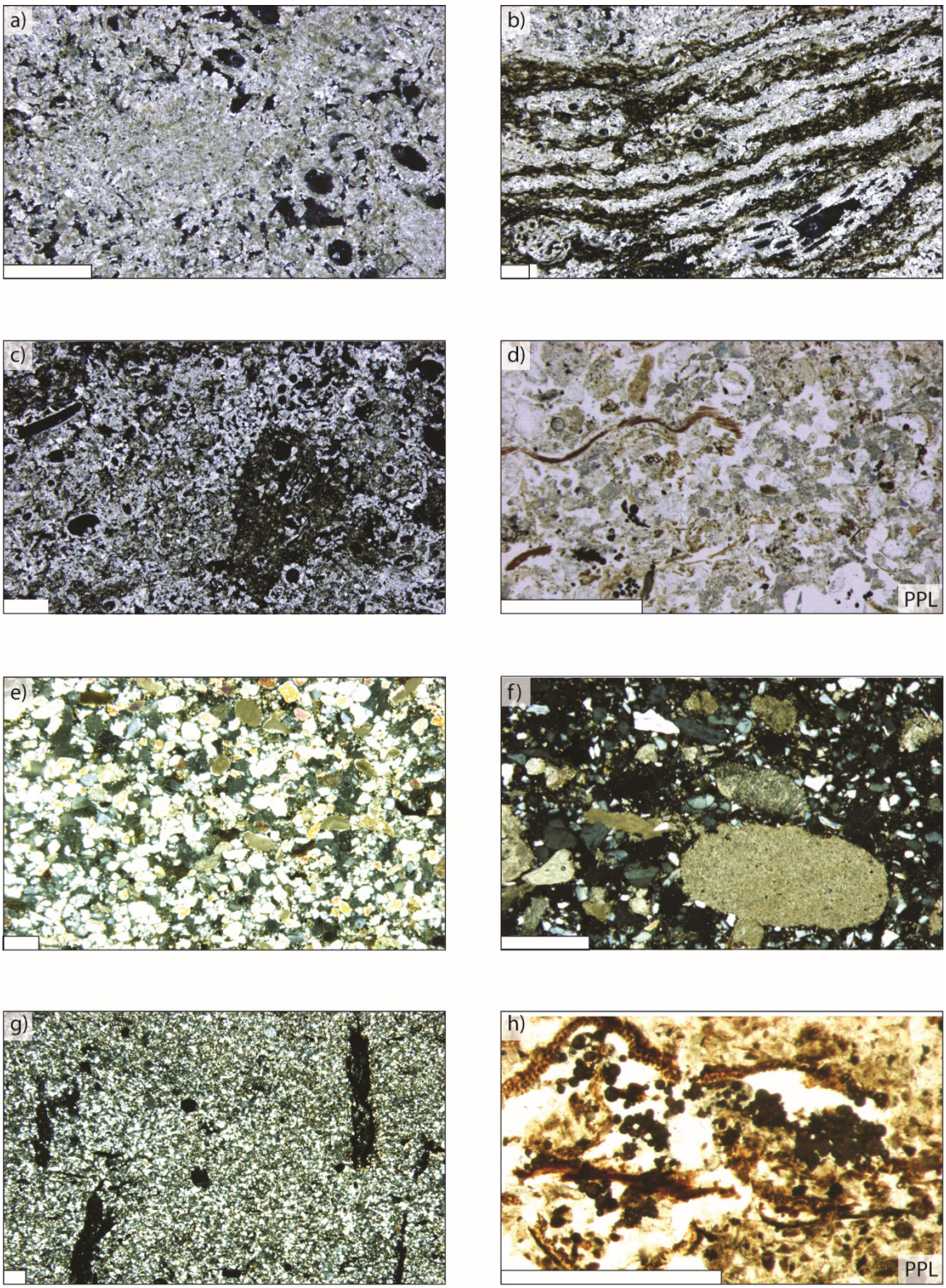

Figure 6.7. *a) to h): Photomicrographs of key microsedimentological features identified in WN-L3-5. The white bar at the base of each image represents 500 μm. All images with the exception of those labelled PPL (plane polarised light) were taken using cross polarised light (XPL). For descriptions of features refer to text.*

6.2.3. Sedimentological interpretation

WN-L1 represents the initial infill of the depression. The sorted, characteristics of the zone, imply formation within a water body. High siliclastic content and magnetic susceptibility values indicate a depositional regime dominated by inwashed, allogenic material. Low carbonate and organic values infer minimal organic productivity, either in the lake body, and/or the surrounding catchment.

Similar deposits are identified at the base of PF, in the eVoP, where they are attributed to lacustrine environments, formed soon after deglaciation of the eVoP, with sediment sourced either directly from the glacier, or via the reworking of glacigenic till deposits near the lake basin, which was perennially frozen (Palmer *et al.,* 2015). The coarser characteristics of the sediments in comparison to those in PF may either represent a more proximal position to the lake edge, and a slightly higher energy depositional regime, potentially driven by increased through-flow from meltwater bodies during deglaciation.

WN-L2a represents the first instance of authigenically dominated sedimentation (calcium carbonate precipitation) in the WYKNE15 sequence. High frequencies of mineral grains, and isolated gravel clasts suggest a high allogenic component, coupled with authigenic carbonate accumulation. This is also reflected in the low, but rising $CaCO_3$ values, and high magnetic susceptibility measurements.

At the microscale, sparite, and microsparite crystals, precipitated around charophyte thalli, indicate that increasing $CaCO_3$ content is largely driven by calcite precipitated as a consequence of photosynthesis in *Chara* sp. algae (McConnaughey, 1991; Hammarlund *et al.,* 2003). Similar characteristics in the carbonate-rich matrix, suggests that a significant proportion of the carbonate matrix derives from calcite detached from charophyte thalli, either by wave action, or inflow events into the water body (Jones *et al.,* 2002; Apolinarska *et al.,* 2010).

The lack of oncoidal or peloidal features within the WN-L2a-e microfabric, indicative of flowing water bodies (Arenas-Abad *et al.,* 2010), and the persistent preservation of the fragile *Chara* sp. thalli casts, suggest persistently low energy conditions during deposition (Apolinarska *et al.,* 2011; Boreham and West, 1993), in a littoral lacustrine environment populated by charophyte meadows (Treese and Wilkinson, 1982; Anadón *et al.,* 2000; Freytet and Verraechia, 2002).

Minerogenic material, most abundant in the base of WN-L2a-b and d, reflects periodic allogenic inwash from the catchment. These deposits are persistently focussed into thin laminations, with mineral particle sizes being moderately to well sorted, representing phases of inwashing. The primary inflow for the basin is thought to be a spring, mapped to the north of the basin, emanating from the Corallian Dipslope (Figure 6.1). Periodic flushing of this spring, provides a

means to produce the microscale laminations, and clastic-rich beds (e.g. WN-L2b). Spring-flow from the Corallian Dipslope also accounts for the presence of oolitic limestone clasts identified at the base of the lithozone.

WN-L2b and 2d represent periods of enhanced siliclastic inwash into the basin from the catchment, diluting authigenic carbonate formation, reflecting increased catchment instability. Charcoal bands identified in WN-L2d-e reflect phases of burning in the catchment, that may be linked to the enhanced allogenic component in WN-L2d.

WN-L3 represents a shift in the style of deposition in the sequence. The basal 14 cm of WN-L3 is characterised by silty peat, capped by a sand bed, with increases in organic content, and magnetic susceptibility. Carbonate is virtually absent, from this interval (<1 %), replaced by organic and siliclastic material. In order to form this deposit, the water level must have been close to the elevation of the sediment infill, forming a telmatic environment. This was either due to a temporary cessation in spring-fed waters into the basin, and/or a drop in the water table, leading to the subaerial exposure of the littoral areas of the water body.

It is unlikely that the transition between WN-L2 and 3 was driven by hydroseral succession as: a) the transition is sharp, and b) lacustrine sediments overlie WN-L3, implying that accommodation space was not filled, making a decline in the water level of the lake the most likely explanation for the formation of the silty peat at the base of WN-L3.

Overlying the peat, WN-L3 is characterised by interbedded carbonate-rich deposits, and organic rich remains, with *Chara* sp. stem casts, implying temporary periods of subaqueous inundation, enabling calcite precipitation around charophyte thalli. The depression was not continually flooded during this stage, as repeated transitions between organic, and carbonate rich beds imply variations between a littoral and a telmatic environment (Murphy and Wilkinson, 1980).

The sedimentological properties of WN-L4 are similar to those of WN-L2, representing the re-emergence of a littoral lake environment in the sequence, but characterised by progressively higher siliclastic content, and magnetic susceptibility values (similar to WN-L2b). This is interpreted as allogenic input into the basin, either from small-scale fluvial action, and/or inwash of organic and siliclastic material from the surrounding slopes. At the microscale, charophyte thalli casts are present in the sequence, suggesting that authigenic precipitation remained the primary source of carbonate in the sediment body. Thalli casts are frequently broken, or incomplete, suggesting increased disturbance within the charophyte meadow, either by allogenic inflow, or wave action, during the deposition of WN-L4 (Apolinarska *et al.,* 2011). Isolated, clastic sand grains, contained within the microfabric probably represent locally wind-blown material (Bateman, 1998), deposited either directly into the lake body, or onto a frozen lake surface during the winter months (Lamoreux *et al.,* 2002; Palmer *et al.,* 2010).

The sedimentary data presents evidence for a more unstable depositional environment than that recorded through WN-L2, with declining organic productivity both within the lake body, and in the catchment, likely related to a deterioration in climate. The sediments shift from a carbonate (authigenically precipitated material) dominated sequence at the base of the zone, to a siliclastic (inwash of allogenic material) dominated sequence at the top, which inhibited authigenic carbonate formation.

Siliclastic content dominates the sediments in WN-L5, representing allogenic inwash into the basin from the catchment. The landscape was therefore unstable, and organic productivity in, and around the basin remained low. Siliclastic sediment would have been deposited either from suspension in the water body, during periods of minimal turbulence, from periodic inflows of physically eroded coarser material from the basin margins (Palmer *et al.,* 2015), and from the sporadic influx of wind-blown particles. Organic material preserved within TS-7 and TS-8 is consistently pyritized, reflecting the early stages of low temperature diagenesis, in weakly reducing conditions (Wilkin and Barnes, 1997; Cavalazzi *et al.,* 2014).

Carbonate is present in very low abundances, which mostly derives from allogenic material, including limestone and intraclasts, inwashed from the basin margins, and the catchment (e.g. Jones *et al.,* 2002). The lack of preserved charophyte thalli in the microscale descriptions represents either that charophytes were not present in the water body during deposition of WN-L5a-c, and/or conditions were not conducive to form, or preserve thalli casts.

Graded gravel beds in WN-L5b represent a phase of higher depositional energy, either from high-velocity inflows into the basin, or via sediment flow from higher gravel slopes (LfA-2). These reflect high energy modes of the same depositional process that deposited the sand interbeds in WN-L5a and 5c, and most likely relate to ephemeral high energy inwash and/or flood events (Schilleref *et al.,* 2014). Low organic productivity across the catchment invokes decreased soil stability, and enhanced erosive potential of unconsolidated sediment bodies. The unconsolidated glacifluvial sediments which bound the basin, would therefore have also been prone to continued weathering, erosion, and slumping during the deposition of WN-L5.

WN-L6 represents the transition from a littoral lake environment, to reedswamp/fenland, during a stage of hydroseral succession (Cloutman, 1988a;b; Cloutman and Smith, 1988), resulting from the infilling of the lake body. Rising organic values, and decreasing siliclastic content, and magnetic susceptibility values in WN-L6a, reflect increasing organic productivity in the basin, and declining allogenic input. The lack of carbonate within WN-L6 suggests that although organic productivity had increased, littoral lacustrine conditions similar to WN-L2 and 4, were not attained in WN-L6. At the transition between WN-L5 and 6 the water level in Depression B was close to the elevation of the sediment infill in the WYKNE15 record, producing a telmatic

environment, with water depths too shallow for subaqueous carbonate formation around charophytes. In WN-L6b, peat formation, containing *Phragmites* remains is indicative of the development of a eulittoral reed swamp environment, which is readily identified elsewhere in the eVoP (Cloutman, 1988a;b; Day, 1996; Palmer *et al.,* 2015).

6.2.4. Chronology

11 dates were obtained from the WYKNE15 stratigraphy, all of which consist of AMS radiocarbon ages derived from terrestrial plant macrofossils (Table 6.3; Figure 6.8). The ages are used to construct a P_Sequence deposition model following the criteria outlined in Bronk Ramsey (2008; 2013). All radiocarbon ages are calibrated to calendar age before AD 1950 (cal BP), using the IntCal13 calibration curve (Reimer *et al.,* 2013) in OxCal v4.2 (Bronk Ramsey and Lee, 2013).

Table 6.3. *Summary of the age model runs (Unconstrained Sequence, Unconstrained Sequence excluding outliers, and P_Sequence with boundaries at lithostratigraphic intervals), used to create an age-depth model for the WYKNE15 sequence. All ages are reported as 2σ ranges with the calculated agreement index (A).*

Date	z (cm)	Unmodelled range (cal ka BP)	Sequence		Sequence_excluded		P_Sequence with boundaries	
			2σ age range (cal ka BP)	A	2σ age range (cal ka BP)	A	2σ age range (cal ka BP)	A
OxA-32400	51	15.13-14.31	15.05-14.29	91.2	15.07-14.31	94.8	15.19-14.71	102.3
OxA-32437	265	14.67-14.08	14.66-14.16	93.5	14.67-14.16	91.6	14.36-14.09	131.8
OxA-32435	274	14.69-14.10	14.46-14.08	113.2	14.47-14.08	113.3	14.31-14.07	100.9
OxA-32436	320	13.81-13.56	13.81-13.56	100	13.81-13.56	99.8	13.78-13.56	96.3
OxA-32401	329	13.39-13.14	13.45-13.32	22.4	13.43-13.23	73.3	13.39-13.14	62.7
OxA-30030	338	13.44-13.22	13.42-13.30	105.7	13.38-13.18	86.7	13.44-13.22	104
OxA-32441	365	13.47-13.28	13.40-13.28	96.3	Excluded as outlier		Excluded as outlier	
OxA-30541	365	13.32-12.75	13.38-13.22	37.6	13.27-12.79	105.1	13.30-12.80	103.7
OxA-32434	396	13.45-13.28	13.35-13.19	47.6	Excluded as outlier		Excluded as outlier	
OxA-32397	494	12.11-11.75	12.11-11.75	100	12.11-11.75	100.1	12.10-11.75	101.9
OxA-32343	560	11.60-11.23	11.69-11.23	82.5	11.62-11.23	86.1	11.60-11.24	94.7
A_{model}			30.1		75.5		88.9	

The deposition model was constructed in two stages. Firstly, an unconstrained Sequence model was run with all ages, to identify outliers. The Sequence model identified age reversals through dates obtained in the upper section of WN-L3 and 4, with OxA-32441 and OxA-32434 statistically older than OxA-30030, OxA-32401, and OxA-30541. The age discrepancies are attributed to reworking of older *Carex* achenes, and twigs into the sequence during the upper stages of WN-L3 and WN-L4. This interpretation has previously been envisaged for other erroneously old radiocarbon ages containing *Carex* achenes and wood during this period (Turney *et al.,* 2000; Walker *et al.,* 2003), and is supported by the sedimentological data, which shows increased erosion from the catchment during the deposition of these lithozones. When OxA-

32441 and OxA-32434 are excluded from the Sequence model, the agreement index improves significantly, with all ages surpassing the 60% threshold (Table 7.3), indicating no further samples needed to be removed from further model runs.

The age model was refined by running a *P_Sequence* function with a k_0 of 1, enabling variation of k by 2 orders of magnitude (i.e. 100-0.001; Bronk Ramsey and Lee, 2013), and boundaries inputted at lithostratigraphic subdivisions in the sequence. This accounts for variable sedimentation rates, and the low number of dated horizons within the sequence. The base of the record is constrained to occur after the OSL age (Shfd-15056) from East Heslerton, reported by Evans *et al.* (2016), which constrains the lowering of Glacial Lake Pickering to below 45 m OD. The initiation of littoral sedimentation in Depression B cannot have occurred until after this event, and this age therefore provides a maximum age constraint for the initiation of the sequence. The model exhibits good model agreement, in both the entire run, as well as for the individual dates. Model outputs are summarised in Table 6.4 and Figure 6.8. The age model shows that the sequence was deposited between 15.69-14.82, and <11.60-11.24 cal ka BP (0 cm and 650 cm respectively). This model is used to provide calendar age ranges for the litho- (Table 6.4) and palaeoenvironmental zones identified in the WYKNE15 sequence which are described in sections 6.2.5-6.2.10.

Table 6.4. *Summary of the depth, elevation, and bounding ages of the lithozones in the WYKNE15 sequence.*

Lithozone	Depth from top (cm)	Depth from base (cm)	Elevation (m OD)	Start (cal ka BP)	End (cal ka BP)	Wykeham Lithofacies
1	742-734	0-8	18.96-19.04	15.69-14.82	15.61-14.80	4A
2a-e	734-414	8-328	19.04-22.24	15.61-14.80	13.66-13.24	4B
2b	684-666	58-76	19.54-19.72	15.17-14.68		4B
G1	-650	84-92	-19.88			
G2	560-572	170-182	20.66-20.78			
2d	462-436	280-306	21.76-22.02	14.30-13.88	14.08-13.81	4B
3	414-376	328-366	22.24-22.62	13.66-13.24	13.30-12.80	4B
4	376-325	366-417	22.62-23.13	13.30-12.80	13.01-12.20	4B
5a-c	325-205	417-537	23.13-24.33	13.01-12.20	11.82-11.26	4C
5b	271-237	471-505	23.67-24.01	12.46-11.82	12.05-11.54	4C
6a	205-194(150)	537-548	24.33-24.44	11.82-11.26	11.70-11.25	5
6b	194-118	548-624	24.44-25.20	11.70-11.25	11.49-10.04	5

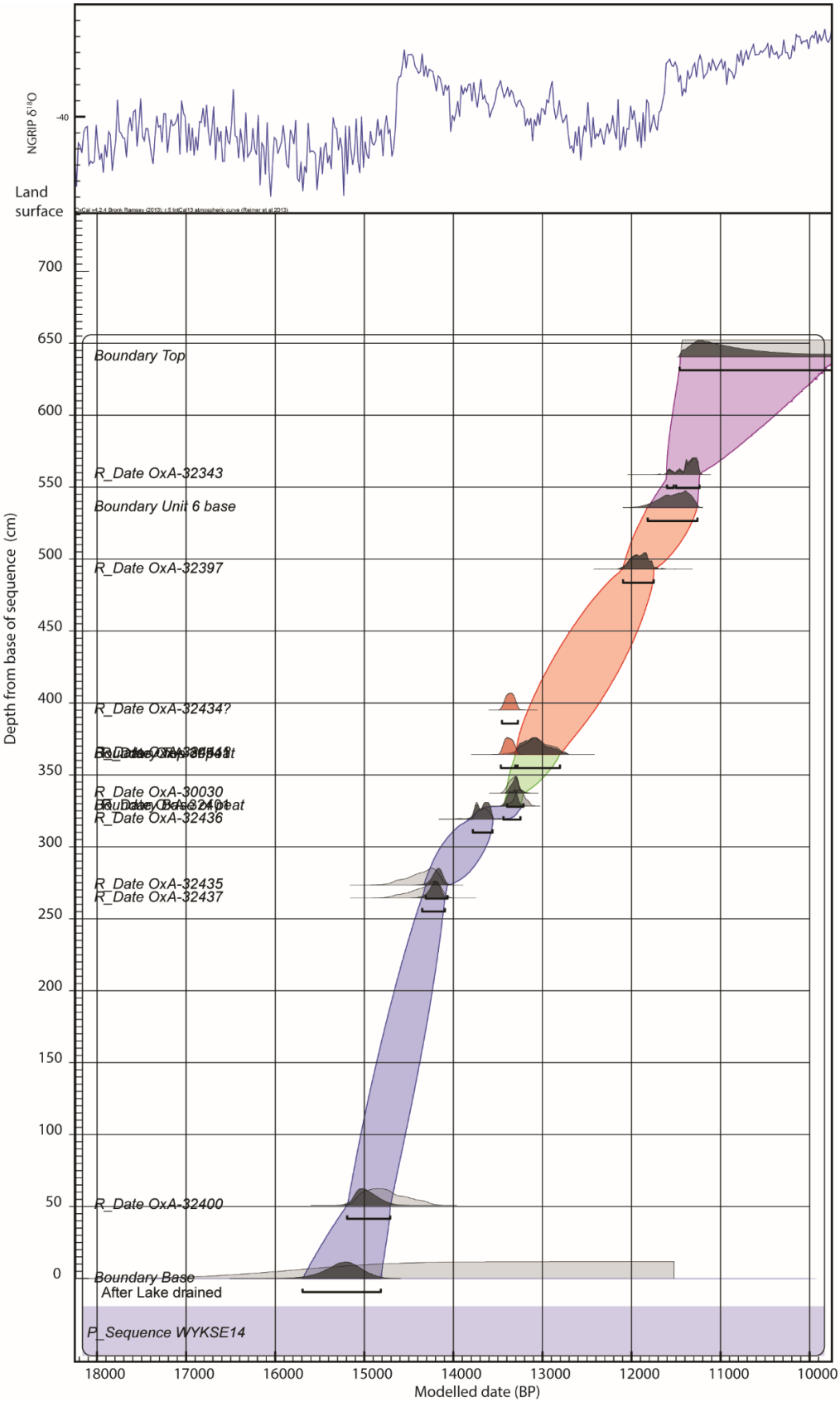

Figure 6.8. *Age-depth, P_Sequence model for the WYKNE15 stratigraphy, with age uncertainties plotted at 2σ. The model utilises a k_0 factor of 1 and boundaries at lithostratigraphic boundaries. The base of the sequence is constrained to be after the OSL age Shfd13056, on proglacial lake sediments from Glacial Lake Pickering (Evans et al., 2016).*

Tephrostratigraphy

In an attempt to provide further chronological tie-points, cryptotephra analysis, was undertaken on the sequence. Owing to time constraints, this was only performed on WN-L2d, 4 and 5, which were interpreted as the stratigraphic intervals most optimal for the preservation of the Penifiler tephra, and the Vedde Ash, which have previously been identified in PF (Palmer *et al.,* 2015; Matthews *et al.,* unpublished data).

A single tephra horizon was identified between 292-294 cm in the stratigraphy (termed WN-T 292-294), consisting of large, blocky-fluted, and microlitic shards (<1 shard per g; Figure 6.9). Samples were prepared twice for geochemical analysis but shards could not be successfully recovered due to low abundance, and loss of material during sample preparation. The stratigraphic position of the WN-T 292-294, allows an age range to be assigned, using the age depth model, which ranges between 14.07-13.58 cal ka BP (2σ). This is consistent with the prior age distribution of the Penifiler tephra (14.06-13.81 cal ka BP), reported by Bronk Ramsey *et al.* (2015; Figure 6.9). The analogous age range, correspondent shard morphology, and locally preserved deposits (at PF), all support that WN-T 292-294 correlates with the Penifiler tephra. Further work is needed however to verify this, and inferences made upon this discovery are limited (this tephra is not included in the deposition model).

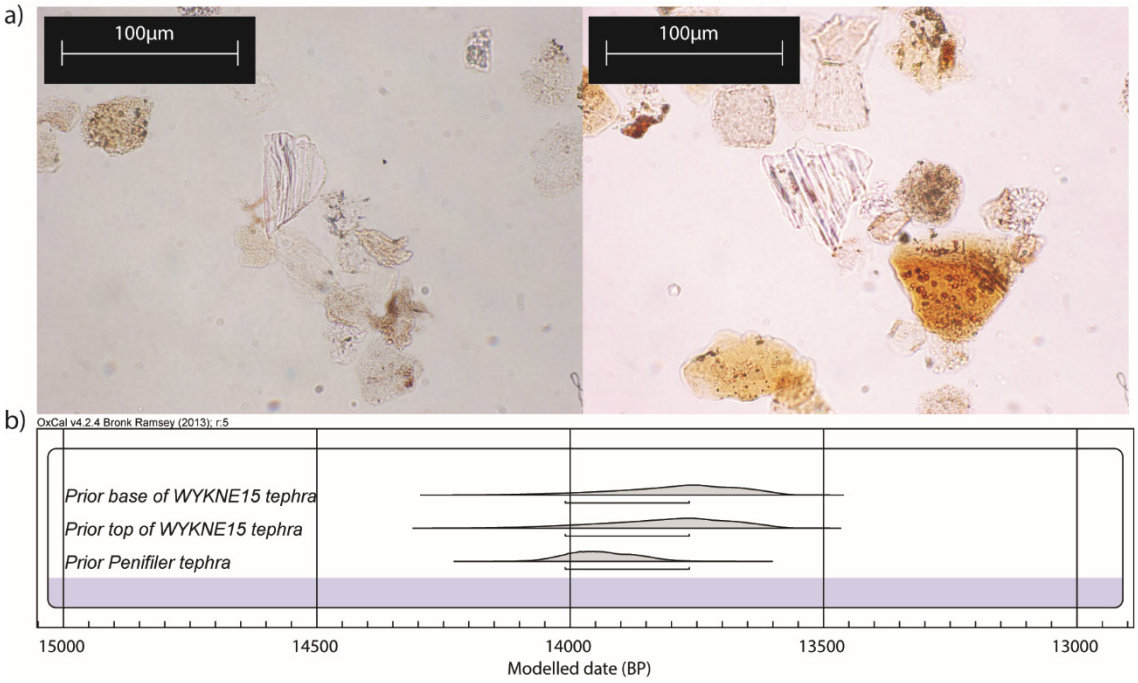

Figure 6.9. *a) Images showing the fluted, and microlitic shard characteristics of the WN-T 292-294 tephra. b) Comparison of the age ranges of the top and base intervals of the WN-T 292-294 tephra, and the Penifiler Tephra. The similar age ranges,, coupled with analogous stratigraphic positions of the Penifiler tephra in other records (e.g. Matthews et al., 2011; Candy et al., 2016) support the correlation of the WN-T 292-294 tephra to the Penifiler Tephra.*

6.2.5. Macrofossils

Macrofossil analysis was undertaken on 46, 2 cm thick samples from the WYKNE15 stratigraphy, with a volume of 20 cm^3, following the methods outlined in Chapter 4. As the record is primarily recording the presence and absence of taxa, the assemblage is zoned visually, picking out characteristic trends in the vegetation assemblage. The record is split into 7 macrofossil assemblage zones (WN-M1-7). The trends identified in each zone are summarised in Table 6.5, and presented in Figure 6.10.

6.2.6. Macrofossil interpretation

The macrofossil record resembles other datasets from LGIT aged sediments in the British Isles (e.g. Sheldrick 1997; Walker *et al.,* 2003), and NW Euzrope (e.g. van Geel *et al.,* 1989; Birks, 2003; Bos *et al.,* 2006; Mortensen *et al.,* 2011), and supports the sedimentological interpretation of the sequence.

WN-M1 is indicative of the development of open water, fringed by mats of pleurocarp mosses, surrounded by an open landscape, characterised by low concentrations of vegetation cover. Open water conditions are interpreted from the presence of charophyte thalli casts, and aquatic fauna including Chironomidae, and, *Plumatella* sp. *Plumatella* sp. and *Chara* sp. are readily identified as pioneering taxa, living in littoral regions of lakes, with low trophic status, high visibility, a high calcium content, and with water depths <10 m (Wade, 1990; Apolinarska *et al.,* 2011).

In the catchment, perennial herbaceous communities (consisting of Poaceae, *Primula* sp., *Saxifraga* sp., and *Caryophyllaceae* sp.), and scrubland (characterised by *B.nana*, and *Empetrum nigrum*) grew on exposed the glacifluvial gravels in the eVoP, and base-rich bedrock of the Corallian Dipslope. Increasing vegetation cover reduced the amount of clastic inwash of allogenic material into the basin, enabling the preservation of slow flowing-stationary conditions in the water body, required for thalli cast formation, and preservation (Apolinarska *et al.,* 2011; Pelechaty *et al.,* 2013).

WN-M2 represents the disappearance of *Chara* sp. from the sequence, and the introduction of emergent, and telmatic taxa into Depression B, either as a result of a temporary decline in water level, and/or increased instability in the catchment. Sphagnum, *Juncus* sp., *Phragmites australis,* and trigonous *Carex,* are all characteristic of shallow, standing waters, at the margins of lakes, or within fens/reed swamps (Rodwell, 1995). The presence of disturbed ground indicator *Rumex crispus*, coupled with the presence of gravel beds in WN-L2b, suggest periods of increased catchment instability during this phase. The presence of *Salix herbacea,* and *Selaginella selaginoides* at the base of WN-M3, suggest periods of extended snow lie within the catchment (Birks and van Dinter 2010; Wheeler *et al.,* 2016).

Table 6.5. *Summary of the depth, age and description of the 7 macrofossil assemblage zones in the WYKNE15 sequence.*

WN-M	Depth (cm)	Age (cal ka BP)		Description
1	0-58	15.69-14.82 15.17-14.68	to	Open ground and herbaceous taxa such as Poaceae, *Saxifraga* sp., Caryophyllaceae,, and *Primula* sp., and *Betula nana* remains (including fruits, catkin scales, and leaves). *Chara sp.* gyrogonites, initially present in high abundances steadily decline and are replaced by calcified *Chara sp.* thalli. Mosses including *Scorpidium scorpioides* and *Drepanocladus* sp. are recorded between 12 and 20 cm where, from macroscale, and microscale descriptions they are found to be focussed into thin, horizontal-sub-horizontally bedded laminations. Littoral aquatic fauna *Plumatella sp.* and *Chironomidae sp.,* are recorded with *Plumatella* becoming absent above 46 cm.
2	58-84	15.17-14.68 15.09-14.60	to	Low but rising macrofossil concentrations characterised by the appearance of emergent taxa including *Juncus* sp. *Selaginella selaginoides*, and *Phragmites australis* (remains of stem material). Higher macrofossil concentrations at 84 cm are coupled with an increase in wood fragments and the appearance of perennial herbaceous taxa including *Papaver* sp. and *Rumex crispus*. *Betula nana* remains continue to be recorded in low abundances alongside remains of *Salix* undiff., including leaf remains of *S. herbacea. Polytrichium* sp., and *Barbula recurvirostra* mosses are recorded for the first time at 84 cm, alongside *Scorpidium scorpioides* and *Drepanocladus* sp. which continue to be present from WN-M1. Littoral aquatic fauna including *Chironomidae* sp. head capsules continue to be present alongside *Daphnia epphipia.*
3a	92-280	15.07-14.57 14.30-13.87	to	Emergent and wetland taxa including *Phragmites australis*, *Juncus* sp., and Sphagnum are each recorded in single samples between 108 and 140 cm, with trigonous achenes of *Carex* occurring sporadically throughout. Poaceae seeds are recorded intermittently), alongside single seeds of other perennial herbs such as *Saxifraga* sp. and *Silene* sp. *B.nana* remains including fruits, leaves, and catkin scales are consistently recorded in low abundances between 156-256 cm. *Betula* undiff. fruits are recorded sporadically. These seeds were unidentifiable to species owing to their poor state of preservation. Undifferentiated terrestrial leaf fragments are consistently recorded in low to moderate abundances.
3b	280-316	14.30-13.87 13.92-13.56	to	Differentiated by the introduction of littoral aquatic flora, coupled with the decline in the abundance of calcified *Chara* thalli. Small Potamogeton seeds (<5000x2000 µm) are present between 287-305 cm. Moss stem, and leaf abundances (including *Scorpidium scorpioides*, *Drepanocladus* sp., and *Barbula recurvirostra* leaves), also increase in abundance. *Selaginella selaginoides* megaspores are identified in low abundances for the first time since WN-M2.
3c	316-328	13.92-13.56 13.66-13.24	to	*Chara* sp. thalli increase in abundance between 305 and 312 cm. Charred needles of *Juniperus communis* are identified coinciding with small and large charcoal fragments, and charred moss stems, leaves, and wood fragments, which are subsampled from visual charcoal beds in the stratigraphy. *Saxifraga* sp. and *Caryophyllaceae* seeds are present alongside *Betula* sp. remains and low abundances of *B.nana* leaf fragments. Telmatic-aquatic taxa including trigonous *Carex* achenes and *Chara* sp. oospores are also identified in the sequence.
4	328-366	13.66-13.24 13.30-12.78	to	Characterised by an increase in macrofossil concentration, and the transition towards emergent and wetland adapted taxa dominated by trigonous *Carex* achenes, including *C. rostrata*. Other taxa are limited to low numbers of *Betula* undiff. fruits, Poaceae seeds, *Selaginella selaginoides* megaspores (2 per 20 cm^3 at 359 and 365 cm), and moss remains (including *Scorpidium scorpioides*. At the top of the zone (365 cm), single seeds of open ground taxa *Silene* sp., and *Caryophyllaceae* sp. are identified.
5	366-471	13.30-12.78 12.46-11.82	to	Characterised by the expansion of disturbed, and open ground taxa and the re-emergence of aquatic faunal remains. Macrofossil concentrations initially increase before declining through the upper sections of the zone. Terrestrial leaf fragments are recorded in high numbers, and include *Salix herbacea,* and *Salix polaris, B.nana* (fruits, and catkin scales also identified), and ericad leaves. Open, and disturbed ground taxa including Poaceae, *Saxifraga* sp., *Silene* sp., *Caryophyllaceae* sp., *Gentianella* sp., *Asteraceae* sp. (including perianths), *Thalictrum alpinum*, and *Rumex acetosella* are identified. Aquatic faunal remains increase in abundance, with *Daphnia* sp., *Diaptomus castor* and Chironomidae consistently present.
6	471-537	12.46-11.82 11.82-11.26	to	Characterised by low macrofossil concentrations, and the absence of identifiable terrestrial macrofossil remains. Wetland and aquatic species diversity is low, with only *Selaginella selaginoides* and *Chara* recorded, alongside small, and poorly preserved terrestrial leaf fragments. Fungal mycelium persist through the zone, coupled with a persistent presence of poorly preserved wood fragments and small charcoal fragments. Large charcoal fragments (>0.5 mm and >0.5 cm) are also present in the sequence above 517 cm.
7	537-624	11.82-11.26 11.49-10.04	to	Characterised by the re-emergence of a vegetation assemblage, consisting primarily of wetland and emergent taxa with low species diversity. Macrofossil concentrations increase from the base of the zone driven principally by higher abundance of trigonous *Carex* achenes. wetland adapted *Typha latifolia* and *Phragmites australis* (rhizomes) are also present between 570-591 cm, and 615-620 cm respectively. *B.nana* remains are also recorded between 549-560 cm. Open ground adapted taxa are confined to Poaceae seeds, which are recorded sporadically, and in low abundances through the zone.

Melting of this snow mass during the summer months would have led to periods of enhanced allogenic inwash into Depression B, eroding telmatic sediments deposited at the margins of the depression, and depositing them in the littoral regions of the water body, alongside course grained allogenic material (WN-L2b). These inflows also explain the disappearance of charophyte thalli casts from the sequence, which are poorly preserved in high energy environments (Anadón *et al.,* 2000). This evidence supports a continually open environment with low vegetation cover. The consistent presence of amorphous charcoal through WN-M2 likely derives from the reworking of glacial deposits exposed in the catchment which contain coal (Catt, 2007; Busfield *et al.,* 2015).

WN-M3a represents the re-emergence of a stable, low-energy, oligotrophic, lacustrine environment in Depression B, similar to the environment in WN-M1. Charophyte meadows re-expanded in the littoral regions of the basin, depositing high abundances of oospores at the base of WN-M3a, followed by the re-emergence of charophyte thalli, which monopolised littoral lake waters.

Vegetation cover in the lake margins remained persistently low throughout WN-M3. Only in WN-M3b are other shallow aquatic taxa consistently recorded (*Myriophyllum* sp., and small *Potamogeton* sp.). In the catchment, *Betula nana* and *Salix sp.* continued to occupy ruderal soils, developed on the higher ground surrounding the lake,

WN-M3b represents the expansion of mosses and littoral aquatics with low species diversity and the absence of *Chara* sp. thalli casts. This is interpreted to represent a period of instability in the catchment, leading to allogenic inwash from the basin margins (WN-L2b), and surrounding slopes. Re-emergence of herbaceous taxa including *Saxifraga* sp., *Silene* sp., Asteraceae sp., at the base of WN-M3a, point toward open conditions in the catchment, whilst *Salix herbacea* and *Selaginella selaginoides* imply the formation of late lying snowbeds. The expansion small *Potamogeton* sp. types, which are most readily found in shallow waters (<1 m deep), may indicate a decline in the nutrient status, and potential shallowing of the lake (Sheldrick, 1997; Walker *et al.,* 2003). A deterioration in climate through this interval is indicated by stable isotopic analysis of the sediments (section 6.2.8), supporting the trends observed at the top of WN-M3a.

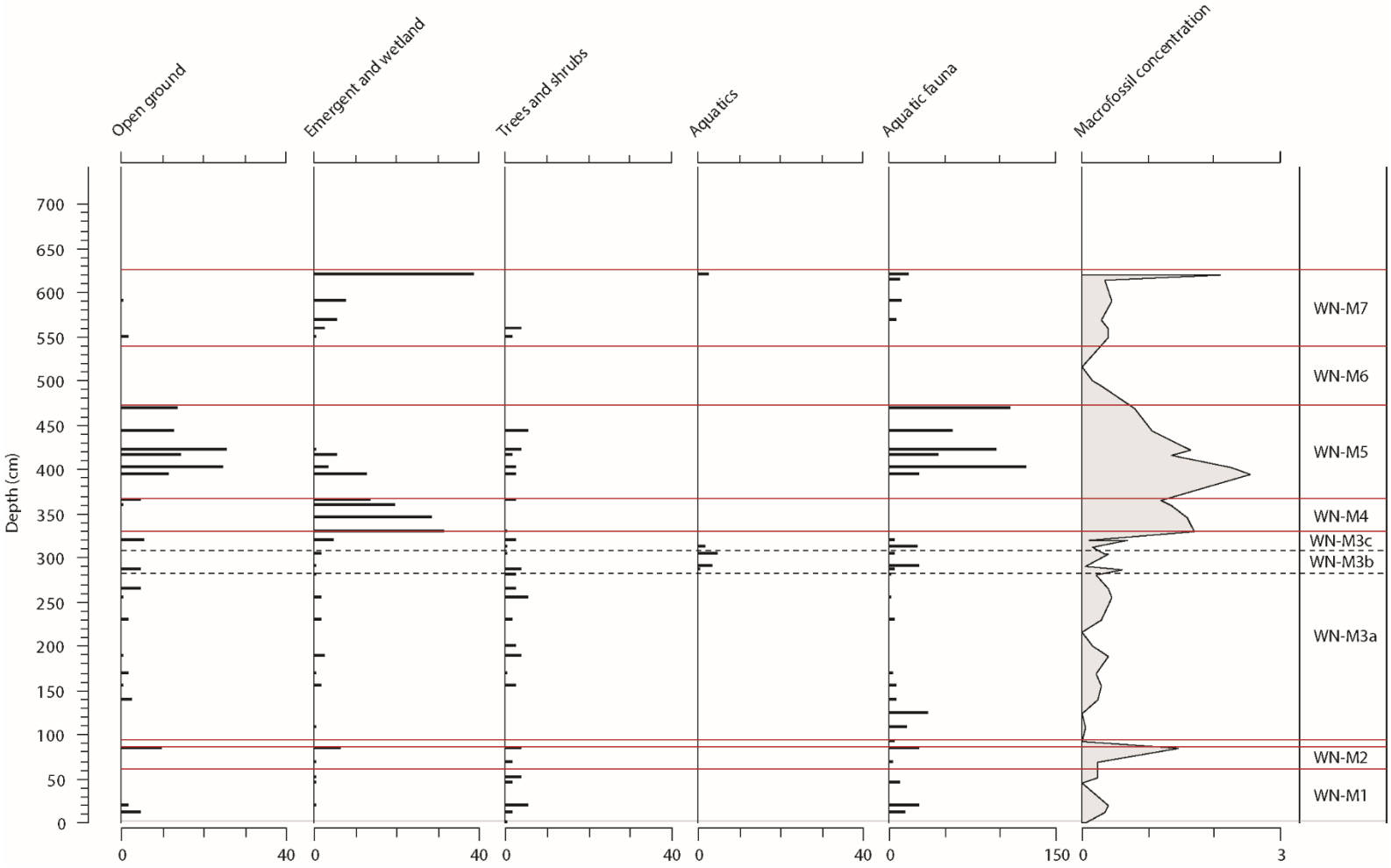

Figure 6.10. *Summary plant macrofossil diagram from the WYKNE15 stratigraphy. All macrofossil counts are reported as numbers per 20 cm³. Charophyte stem casts and oopsores which monopolise the assemblage in WN-M1-3 are excluded from the aquatic counts.*

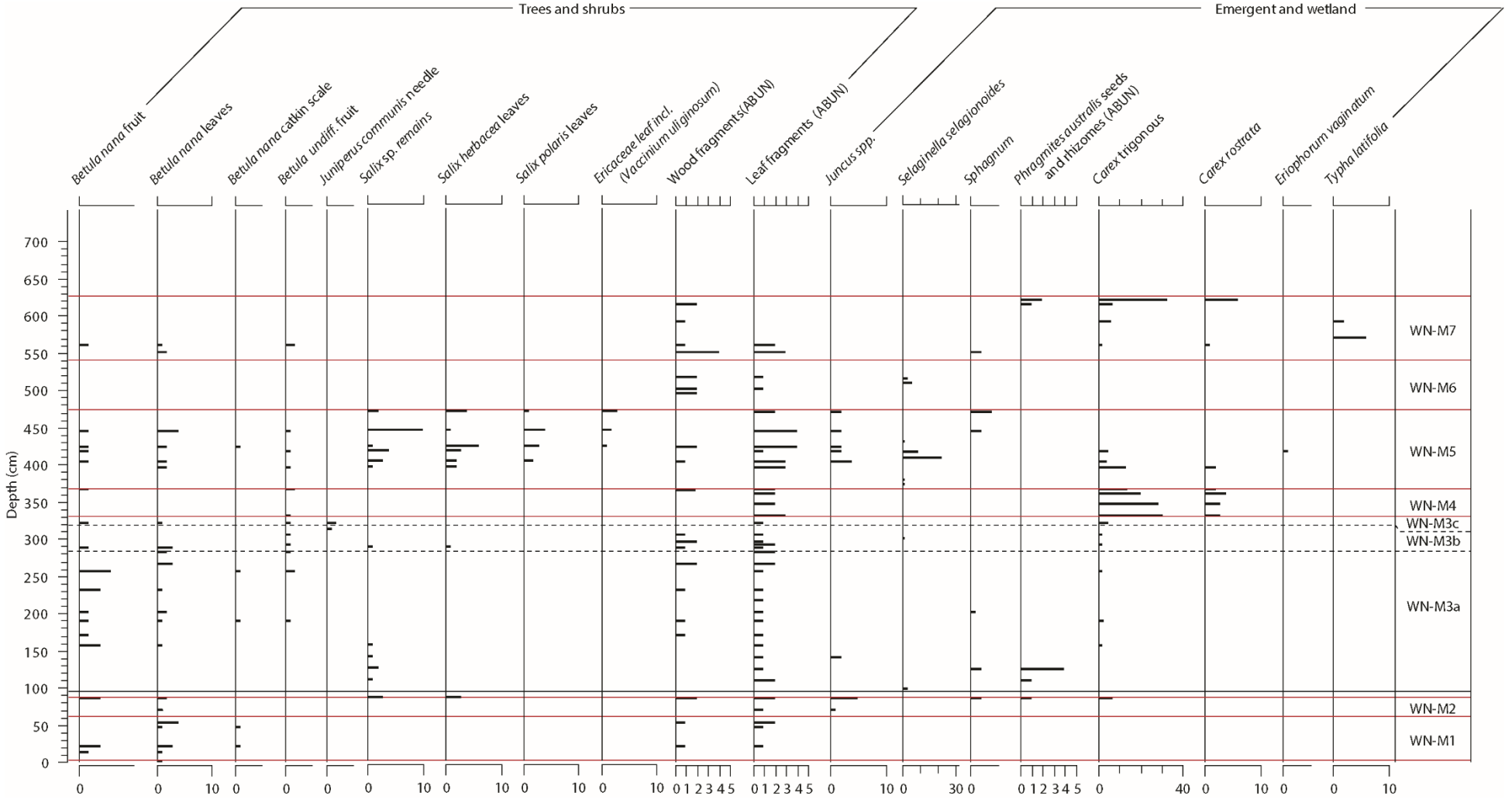

Figure 6.10. *contd.*

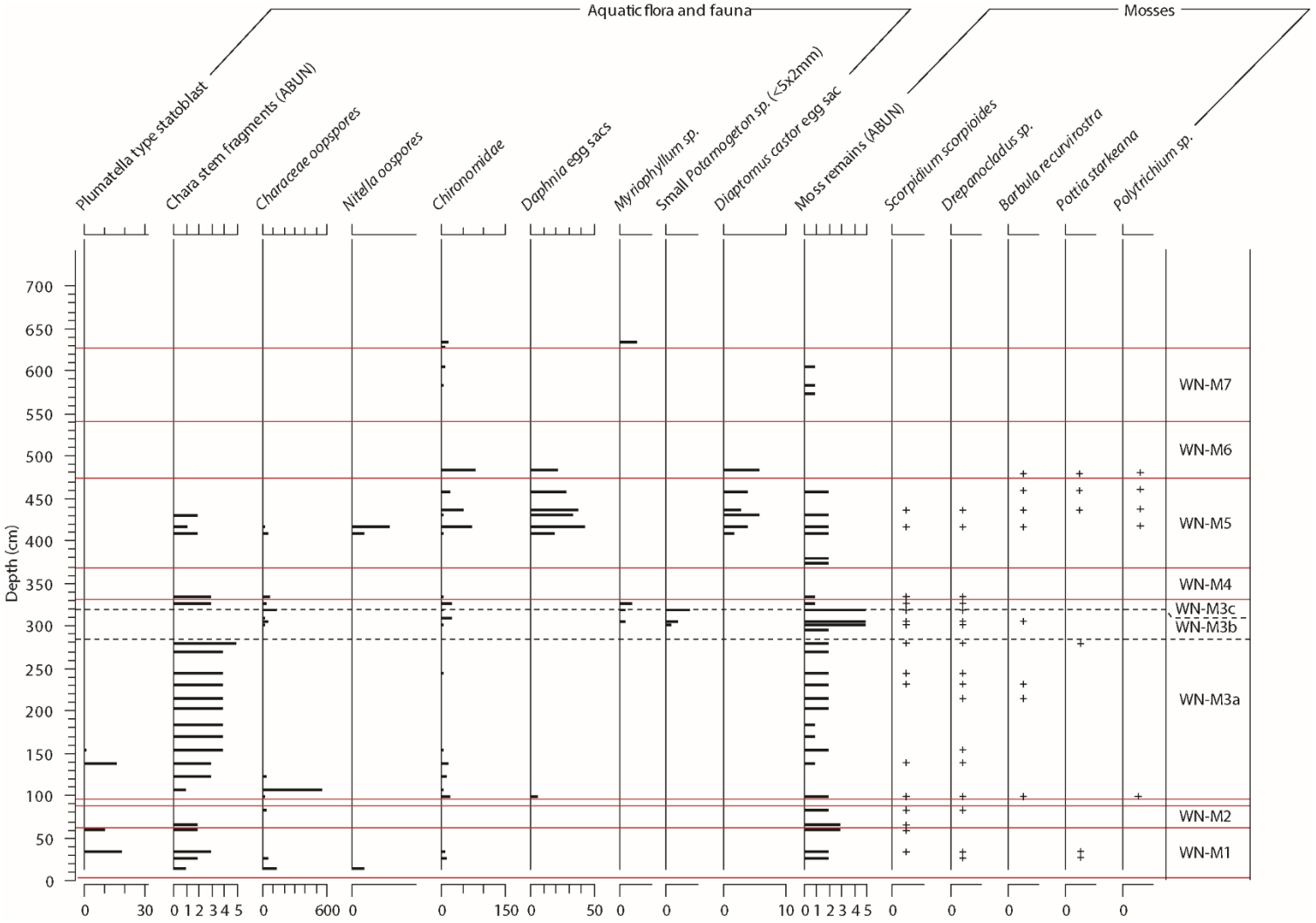

Figure 6.10. *contd. + indicates the presence of this moss taxa. No counts of abundance were made on these remains*

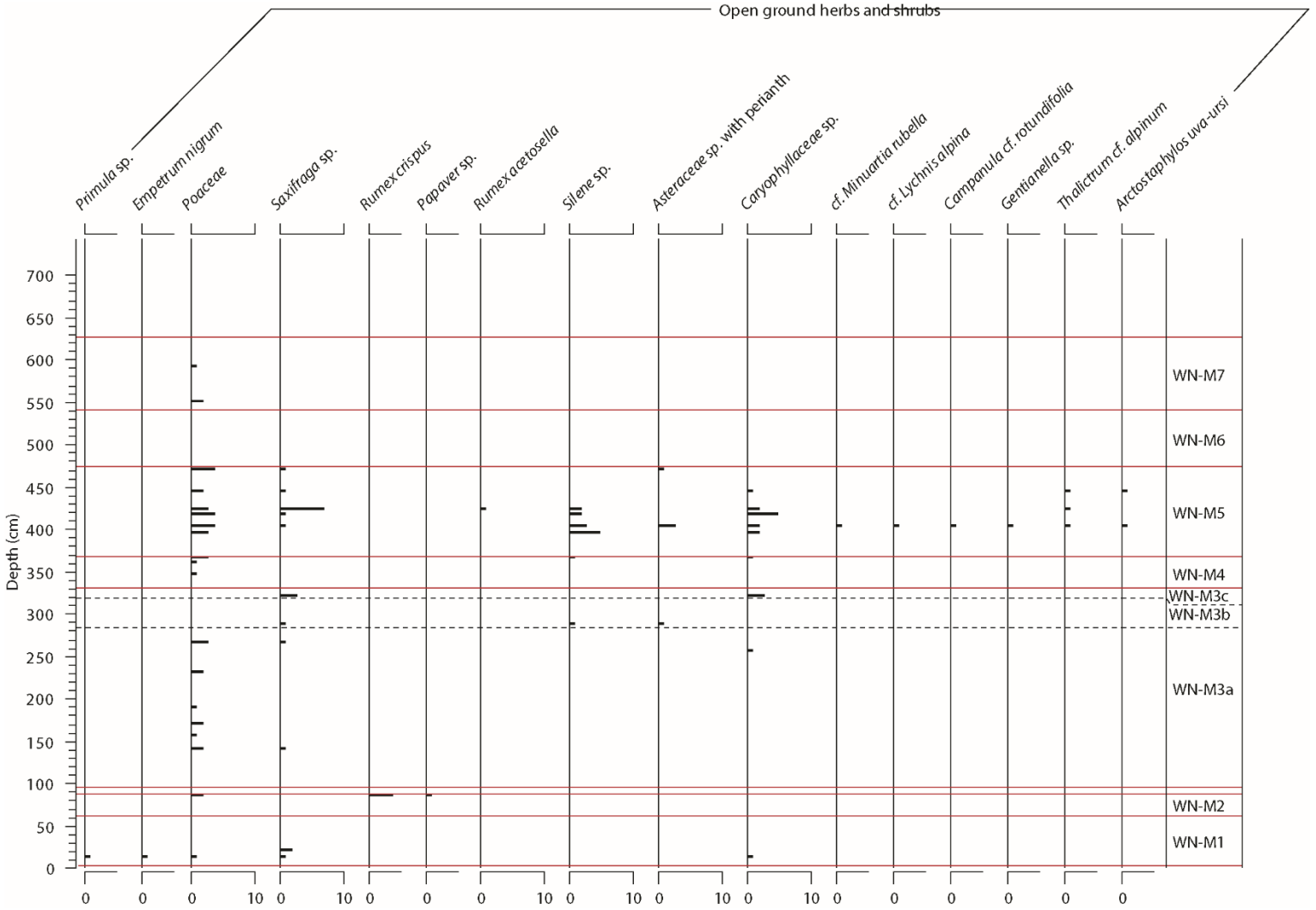

Figure 6.10. *contd.*

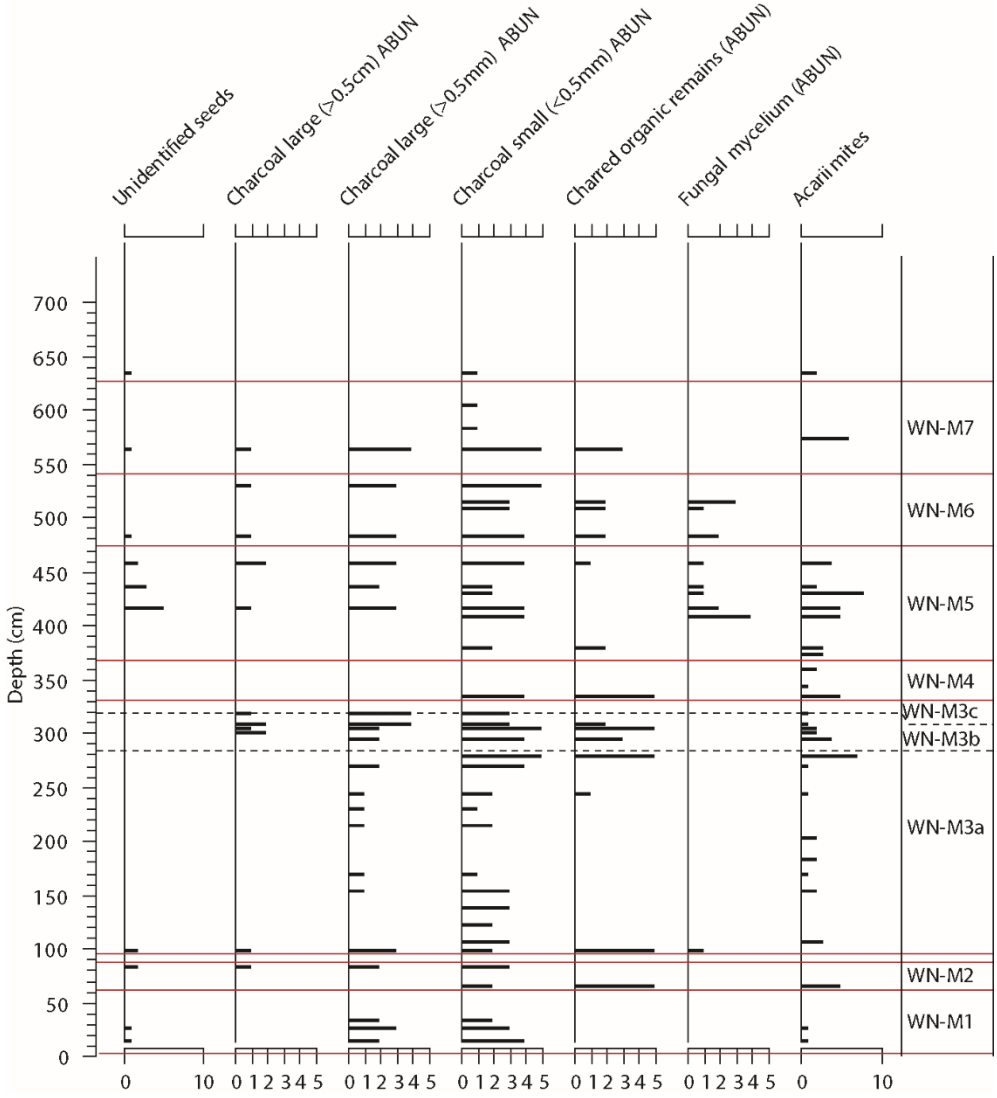

***Figure 6.10**. contd.*

Together these conditions resulted in a decline in charophyte calcite formation/preservation, either due to periodically turbid waters within the basin, or a decline in lake level, impeding calcite formation in the littoral section of the lake. Charophyte oospores are recorded in the zone. Unlike aquatic macrofossil remains which are not readily transported long distances, charophyte oospores can be widely dispersed in shallow lakes, potentially long distances from their vegetative source (Zhao *et al.,* 2006). This suggests that the macrophyte was still present in the lake basin, but not forming thalli casts in the position of the WYKNE15 record. A decline in lake level, during a phase of unstable climate therefore provides the most likely explanation for the trends observed in WN-M3b.

In WN-M3c, the lake system described for WN-M3a was re-established, characterised by the re-establishment of charophyte meadows in the littoral regions of the lake. Significant increases in macrocharcoal abundances, and charred plant material, including *Juniperus communis,* indicate periods of increased burning in the catchment. Elsewhere in the eVoP, a similar trend is identified in pollen records, where a short expansion in *Juniperus* pollen coincides with high abundances of

micro-charcoal (Day, 1996). The short-lived dominance of *Juniperus* in WI records in the eVoP, suggest that the analogous trends identified in these records represent a period of enhanced regional fire frequency/intensity, potentially fuelled by high abundances of dead, and dry organic material across the landscape (Veblen *et al.,* 2006; Hardiman *pers comm.*).

WN-M4 represents an expansion of emergent and wetland taxa in the littoral regions of the water body, coinciding with the formation of peat in the stratigraphy (WN-L3). The emergence of well preserved, trigonous *Carex* sp. achenes represents the establishment of semi-aquatic to fully terrestrial conditions (marsh-fenland), either as a result of a lowering of the water level, or a cessation of inflow from the catchment. The absence of aquatic macrofossils in WN-M4 suggests that permanently standing water was absent or confined only to the deepest parts of the basin.

The decline in water levels reduced the influx of macrofossils from the catchment, resulting in the observed declines in shrub remains. Low abundances of *Betula* undiff. remains, and terrestrial leaf fragments however suggest that Depression B was well vegetated during WN-M4.

WN-M5 is indicative of the re-establishment of open water in Depression B, and an increasingly open landscape in the catchment, related to a decline in vegetation cover, and a deterioration in temperatures. In the lake body, littoral conditions in the WYKNE15 sequence are reflected by the re-emerence of calcified charophyte thalli, reflecting the transition to an oligotrophic, littoral lake body. The decreased abundance of these casts in relation to WN-M3a and 3c is interpreted to be an artefact of decreased preservation (noted in TS 5). The lake was inhabited by a faunal assemblage consisting of Chironomidae, *Diaptomus castor*, and *Daphnia* sp., fringed by stands of pioneering macrophyte taxa *Nitella* sp. and *Chara* sp. *Daphnia* sp. and *Diaptomus castor* advocate cool and clear lake waters, potentially freezing to base during winter (*Diaptomus castor* are most readily identified from ephemeral ponds in Greenland (Bennike, 2000)). Populations of *Daphnia* sp. are consistently identified in records, soon after climatic deteriorations in the LGIT (Sheldrick, 1997; Birks, 2000), representing a decline in the nutrient status of the water body. Similar trends in aquatic fauna and flora are identified in WS-M4 of the WYKSE14 sequence (section 6.3).

The rise in macrofossil concentration in WN-M5 coincides with high abundances of fungal mycelium, which point toward soil instability in the catchment (Anderson *et al.,* 1984). The macrofossil assemblage consists *of Carex* sp.*, Juncus* sp, *Sphagnum*, which would have subsisted in wet open meadows. These meadows were fringed by dwarf shrub communities (*B.nana, S.polaris, S.herbacea*), on higher ground, and perennial open ground herbs (including Poaceae, *Saxifraga* sp. *Silene* sp. *Caryophyllaceae, Thalictrum alpinum*), on mineral-rich soils, persistently occupied by late lying snow. The increase in macrofossil concentration in WN-M5 is therefore interpreted to

reflect an increase in allogenic macrofossil delivery into the basin via soil erosion, rather than increased vegetation cover in the catchment.

Low macrofossil concentrations in WN-M6 suggest sparse vegetation cover in the catchment of Depression B, and a clear, oligotrophic water body, characterised by sporadic stands of *Chara* sp. and *Selaginella selaginoides*. The increase in particle size in WN-L5b, invokes a decline in sedimentation rate in the sequence. Any standing water in Depression B through this interval was therefore likely to be ephemeral, fed from seasonal snow melts, and high fluvial discharges which temporarily produced a shallow water body during the summer months.

WN-M7 is characterised by the development of a reedswamp in Depression B, representing the infilling of the lake basin via hydroseral succession. The re-introduction of *Betula* undiff. and *Betula nana* remains, coupled with wood fragments, at the base of the zone reflect increasing vegetation cover in the catchment, driven by ameliorating temperatures (with summer temperatures >13 °C indicated by the presence of *Typha latifolia* (Isarin and Bohncke, 1999). The landscape remained open, with herbaceous communities consisting of *Poaceae*. As the basin infilled, open water diminished, and a telmatic environment formed, dominated by *Carex* sp. and other eulittoral taxa. The introduction of reeds and rushes including, *Typha latifolia*, and *Phragmites australis*, indicates progressively shallower water depths (<1 m), and an increasingly eutrophic environment (Hannon and Gaillard, 1997). This is interpreted to occur prior to the development of closed *Betula* woodland in the eVoP (Day, 1996).

6.2.7. $\delta^{18}O$ and $\delta^{13}C$ stable isotopic analysis of lacustrine carbonates

Lacustrine carbonates in WN-L2-4 provide potential to reconstruct a palaeoenvironmental signal using bulk sediment oxygen and carbon isotope ratios ($\delta^{18}O_{bulk}$, and $\delta^{13}C_{bulk}$). This is based upon the following criteria:

a) The lake in Depression B remained hydrologically open for much of its history, being fed predominantly by spring waters draining the Corallian Dipslope, during the WI.
b) Carbonates in the sequence consist primarily of authigenic material, formed within the water body.
c) The sediment model of lake conditions during the WI invokes low energy, and stable conditions, with minimal inwash of allogenic material.
d) There is no micromorphological evidence of post-depositional diagenesis of the lake carbonates, indicating that measured isotopic values reflect the isotopic composition of the carbonate at the time of initial deposition.

Authigenic carbonate precipitation is interpreted to derive primarily from the precipitation of calcite around charophyte thalli (section 6.2.2). Stable isotopic measurements from similar deposits have been utilised in numerous lacustrine sequences, providing information consistent

with known past climatic oscillations during the LGIT and Holocene (Drummond *et al.,* 1995; Hoek, 1997; Yu and Eicher, 1998). However, it has been suggested that in shallow eutrophic water bodies, charophyte calcite does not precipitate in isotopic equilibrium with the host water body (Pentecost *et al.,*, 2006). On this basis, a pilot study was carried out upon the hand augered cores sequences (Figure 6.2), prior to undertaking stable isotopic analysis through the full sequence. This was undertaken to test the consistency of measured $\delta^{18}O_{bulk}$ and $\delta^{13}C_{bulk}$ values from a single stratigraphic horizon, and make an assessment as to whether measured $\delta^{18}O_{bulk}$ and $\delta^{13}C_{bulk}$ values are indicative of precipitation in, or out of isotopic equilibrium. Three repeat samples taken from 12 horizons through the sequence (2 samples from WN-L1, 5 samples from WN-L2, 1 sample from WN-L3, 4 samples from WN-L4, see Figure 6.11) show consistent $\delta^{18}O_{bulk}$ and $\delta^{13}C_{bulk}$ values through WN-L2-4. Furthermore, all isotopic values plot within the range for LGIT, authigenic carbonates in PF, as reported in Candy *et al.,* (2015). This strongly supports that the carbonates preserved within the WYKNE15 basin, are authigenic, and precipitated close to isotopic equilibrium with the host water body.

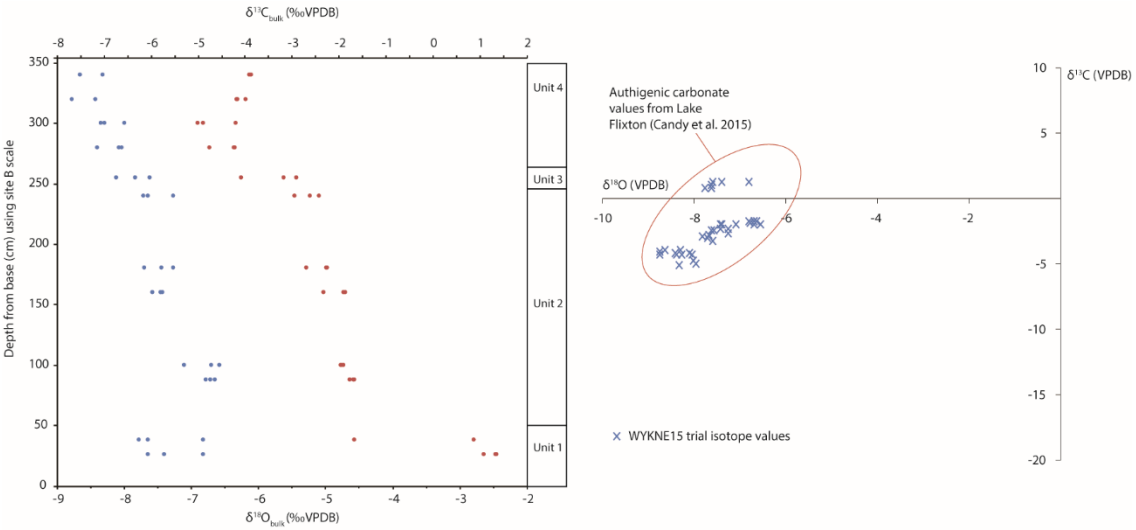

Figure 6.11. *Summary diagrams of the trial bulk isotope dataset, showing the consistent values at the same stratigraphic horizon through units 2-4. The values from the WYKNE15 sequence also overlap with values from regional authigenic carbonates reported in Candy et al. (2015), supporting that bulk sediment isotopes from the WYKNE15 sequence are precipitated in isotopic equilibrium.*

6.2.8. Summary of $\delta^{18}O$ and $\delta^{13}C$ datasets

59 0.5 cm thick samples were subsampled from the sequence and analysed for $\delta^{18}O_{bulk}$ and $\delta^{13}C_{bulk}$ measurements on bulk carbonate <63 μm in WN-L1-4, the results of which are presented in Figure 6.12.

Measured $\delta^{18}O_{bulk}$, and $\delta^{13}C_{bulk}$ values range between -5.71 to -8.66‰, and 1.64 to -4.90‰ respectively, with mean values of -7.44 ± 0.62‰ (1σ), and -2.10 ± 1.36‰ (1σ) respectively.

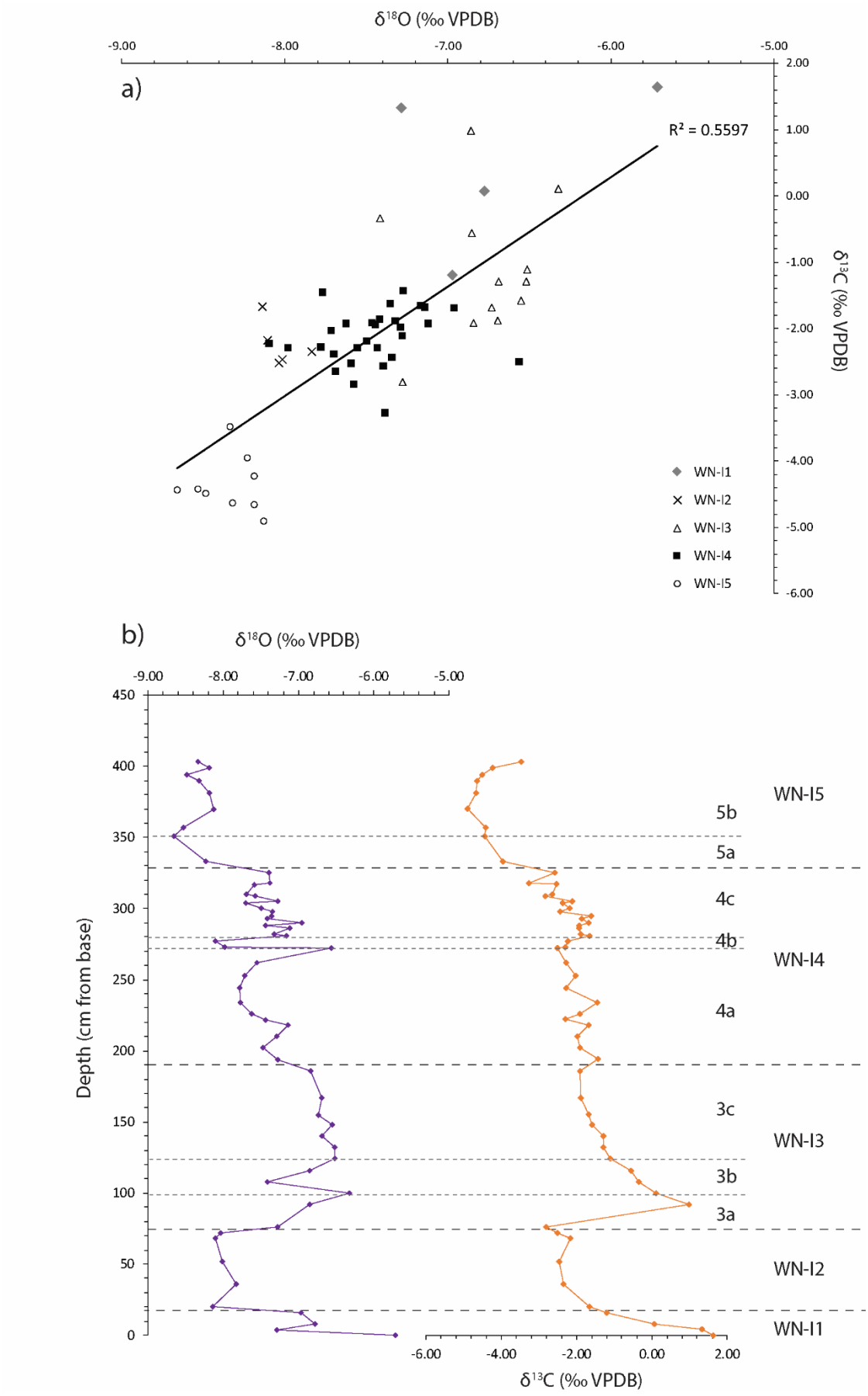

***Figure 6.12**. a) Comparison of the $\delta^{18}O_{bulk}$ and $\delta^{13}C_{bulk}$ values from the WYKNE15 sequence. b) $\delta^{18}O_{bulk}$ and $\delta^{13}C_{bulk}$ values plotted in relation to depth. Isotope zones, and events discussed in text are labelled for reference.*

Measurement uncertainties based upon the three standard calibration in the sequence range between 0.00 and 0.11‰ (1σ) for $\delta^{18}O_{bulk}$, and between 0.00 and 0.06‰ (1σ) for $\delta^{13}C_{bulk}$ (raw values are presented in Appendix G). The stable isotopic dataset can be sub-divided into five isotopic zones, based on observed variations in $\delta^{18}O_{bulk}$ values. $\delta^{18}O_{bulk}$ values were used to zone the dataset as shifts in $\delta^{18}O$ in lacustrine carbonates in western Europe, yields the clearest palaeoenvironmental signal (Leng and Marshall, 2004). These zones are termed as WYKNE15 isotope zones (WN-11-5; Table 6.6).

Table 6.6. *Summary of the depth, elevation and bounding ages of the 5 isotope zones in the WYKNE15 sequence.*

WN-I	r^2	Sub-zones	Depth (cm)	Age (cal ka BP)	$\delta^{18}O$ description
1	0.50		0-18	15.69-14.82 to 15.53-14.77	High values (-6.69 ± 0.68 ‰ (1σ)) decreasing through the zone
2	0.30		18-74	15.53-14.77 to 15.12-14.62	Low values (-8.03 ± 0.12 ‰ (1σ))
3	0.26	3a	17-100	15.12-14.62 to 15.04-14.54	Sharp rise to high values (to -6.32 ‰)
		3b	100-124	15.04-14.54 to 14.96-14.46	Oscillation (minimum = -7.41 ‰)
		3c	100-190	14.96-14.46 to 14.71-14.26	High values (-6.65 ± 0.12 ‰ (1σ))
4	0.03	4a and c	190-328	14.71-14.26 to 13.66-13.24	Decreasing values (from -6.93 to -7.28 ‰)
		4b	272-282	14.32-14.07 to 14.29-13.84	Oscillation (minimum = -8.10 ‰)
5	0.01	5a	328-351	13.66-13.24 to 13.37-12.96	Sharp decline to low values (to -8.66 ‰)
		5b	351-417	13.37-12.96 to 13.04-12.24	Low values (-8.34 ± 0.18 ‰ (1σ))

6.2.9. Controls on stable isotopic values in WYKNE15 lacustrine carbonates

Authigenic lacustrine carbonate $\delta^{18}O_{bulk}$ values are a function of the $\delta^{18}O_{water}$ of the lake, which is in turn, controlled by mean annual $\delta^{18}O_{rainfall}$ values in temperate, hydrologically open lake basins (Leng and Marshall, 2004). $\delta^{13}C_{bulk}$ values are a function of $\delta^{13}C$ of dissolved inorganic carbon (DIC) in the lake water, which is primarily controlled by vegetation development in the catchment (Cerling and Quade, 1993; Leng and Marshall, 2004). Covariance between, $\delta^{18}O_{bulk}$ and $\delta^{13}C_{bulk}$ values is low in WN-11-5, supporting that the Depression B lake body remained an open system, constantly recharged by spring- and groundwaters during the deposition of WN-L2-6 (Talbot, 1990; Leng and Marshall, 2004).

The principal source of recharge for Depression B through the LGIT is thought to be via a groundwater fed spring, inflowing into the northern extent of the basin (Figure 6.1). Therefore, it can be suggested that the $\delta^{18}O_{water}$ value of the host water in which the carbonate was precipitating is a reflection of mean annual $\delta^{18}O_{rainfall}$ values, which are demonstrated to have a

positive linear relationship with mean annual air temperatures (Dansgaard, 1964; Rozanski *et al.*, 1992; 1993). Consequently, in the absence of other modifications of the $\delta^{18}O$ signal, changes in the measured $\delta^{18}O_{bulk}$ values in the WYKNE15 sequence will reflect changes in prevailing mean annual air temperatures.

However, detrital contamination from biogenic and geological carbonate also needs to be considered when interpreting the $\delta^{18}O_{bulk}$ and $\delta^{13}C_{bulk}$ signal of lacustrine carbonates (Leng and Marshall, 2004; Leng *et al.,* 2010; Mangili *et al.,* 2010). Geological carbonate in the eVoP could be derived from a number of geological sources within the eVoP, including the Speeton, Oxford and Kimmeridge clays, and the marine limestone and sandstone of the Corallian group.

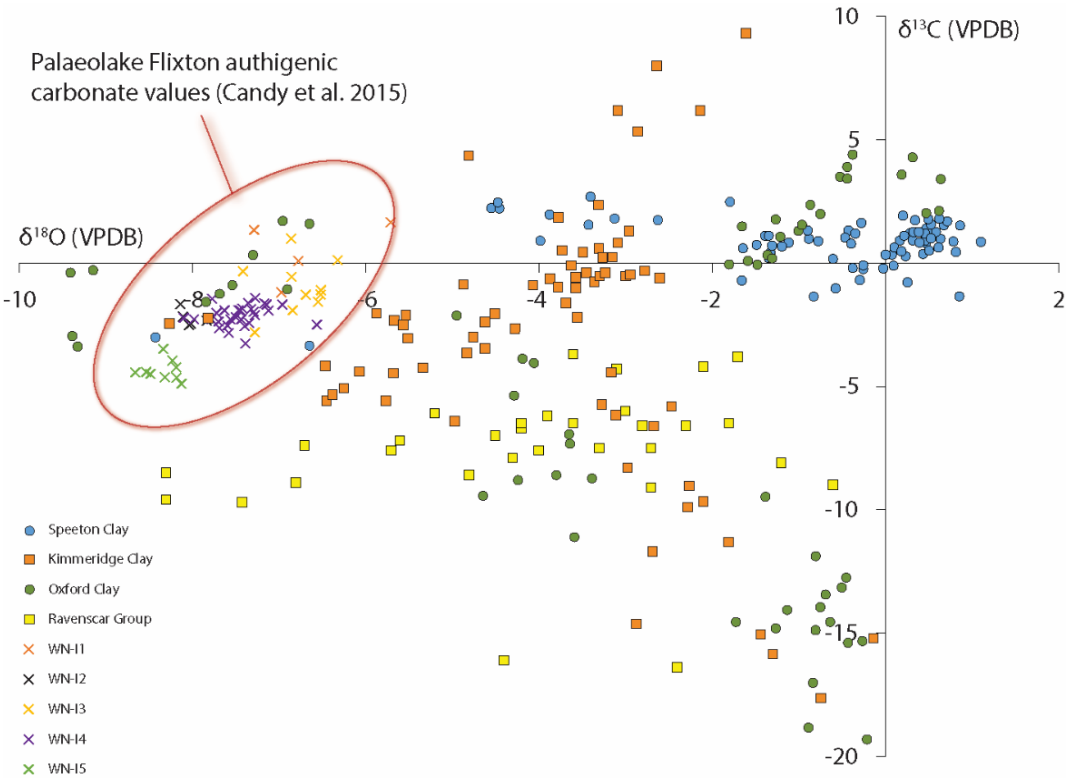

***Figure 6.13**. Comparison of the WYKNE15 stable isotope dataset (crosses) with previously published data on geological carbonate in the eVoP.*

In order to remove any detrital contaminants, samples were sieved at 63 µm to remove sand-sized material prior to isotopic analysis. Micromorphological analysis of the sediments was also undertaken to determine if detrital carbonate contributed significantly to the carbonate groundmass. These results suggest a negligible amount of geological carbonate grains and biogenic material in the sediments (section 6.2.2). In order to assess any potential contamination, $\delta^{18}O_{bulk}$ and $\delta^{13}C_{bulk}$ values from the WYKNE15 sequence are compared to isotopic values from regional bedrock geologies (Irwin *et al.,* 1977; Hudson, 1978; Astin and Scotchman, 1988; Kantorowicz, 1990; Price, 1998; Price *et al.,* 2000), and authigenic values from LGIT marl in Palaeolake Flixton (Candy *et al.,* 2015; see Figure 6.13). The WYKNE15 dataset shows minimal overlap with either the Ravenscar Group, or the Speeton Clays, which dominate the catchment geology. Furthermore, isotopic values consistently overlap with the PF isotopic dataset, which

are interpreted as authigenic lacustrine carbonates, precipitated during the LGIT (Candy *et al.,* 2015).

Values in WN-I1 however are sampled from a minerogenic-rich zone at the base of the sequence, and contain low amounts of carbonate (WN-L1). Detrital contamination is deemed to affect these results based upon the following criteria: a) Negligible charophyte remains are identified within these zones, indicating minimal authigenic carbonate precipitation within the lake body b) samples taken from sediment with a low carbonate content (<30 %) have $\delta^{18}O_{bulk}$ and $\delta^{13}C_{bulk}$ values that outlie from the rest of the dataset, and appear to trend towards isotopic values of the Speeton Clay matrix, which lies within the basin catchment (Price, 1998).

On this basis, with the exception of values in WN-I1, it is determined that detrital contamination from geological, and biogenic carbonates is not causing the variations observed in the isotopic record in the WYKNE15 sequence.

6.2.10. Palaeoenvironmental interpretation of the $\delta^{18}O_{bulk}$ and $\delta^{13}C_{bulk}$ records

Given $\delta^{18}O_{bulk}$ values from the WN-I2 to-5 reflect authigenic carbonate precipitation within a hydrologically open lake body with minimal influence of contamination from detrital carbonate sources, the $\delta^{18}O_{bulk}$ record is indicative of the $\delta^{18}O$ value of water recharging the lake body, moderated by the mean annual air temperature (Marshall *et al.,* 2002; Leng and Marshall 2004; Candy *et al.,* 2015).

In temperate mid-latitude regions, a 1 °C increase in air temperature equates to a + 0.58 ‰ increase in values of $\delta^{18}O_{water}$. Conversely, a 1 °C increase in water temperature results in a 0.34-0.38 ‰ decrease in measured $\delta^{18}O_{bulk}$ values, dampening the effect of changes in air temperature. The relationship between changes in measured $\delta^{18}O$ values and temperature can be equated at *ca.* + 0.3 ‰ per 1 °C rise in temperature (Leng and Marshall, 2004). An increase in mean annual air temperature would therefore result in an increase in $\delta^{18}O_{bulk}$ values, and a decrease in mean annual air temperatures would have the opposite effect. If the $\delta^{18}O_{bulk}$ values are interpreted purely in terms of temperature shifts, the following patterns are identified:

1. Low $\delta^{18}O_{bulk}$ values in WN-I2 associated with cold temperatures between 15.51-14.76 and 15.13-14.64 cal ka BP (20-72 cm respectively).
2. A sharp rise in $\delta^{18}O_{bulk}$ values in WN-I3a, indicating rising temperatures between 15.13-14.64 and 15.04-14.54 cal ka BP (72 and 100 cm respectively). High $\delta^{18}O_{bulk}$ values are maintained through WN-I3, with the exception of a sharp decline between 15.04-14.54 to 14.96-14.46 cal ka BP (100-124 cm; WN-I3b).
3. Steadily declining $\delta^{18}O_{bulk}$ values in WN-I4, reflecting persistently deteriorating temperatures between 14.66-14.24 and 13.74-13.27 cal ka BP (194-325 cm), perturbed by a sharp cooling event between 14.32-14.07 and 14.32-13.95 cal ka BP (273 and 277 cm), in WN-I4b.

4. A sharp decline in $\delta^{18}O_{bulk}$ values in WN-I5a indicating cooling between 13.66-13.24 to 13.37-12.96 cal ka BP, which is maintained until the cessation of authigenic carbonate formation in the sequence at 13.04-12.24 cal ka BP (WN-I5b).

Other environmental factors including the amount effect, changes in atmospheric circulation, and seasonality must also be considered when interpreting the $\delta^{18}O_{bulk}$ signal (Leng and Marshall, 2004; Candy *et al.,* 2015; Chapters 7-9).

In lake systems, the $\delta^{13}C$ of authigenic carbonate reflects the $\delta^{13}C$ of dissolved inorganic carbon (DIC), which is in turn relates to the DIC of recharging spring and groundwater, biological activity within the lake basin, and the equilibration of CO_2 between the lake waters and the atmosphere (Talbot, 1990; Leng and Marshall, 2004; Candy *et al.,* 2016). The $\delta^{13}C_{bulk}$ values in the WYKNE15 sequence exhibit 2 key trends:

1. Low $\delta^{13}C_{bulk}$ values, sharply rising in WN-I3a
2. Steadily declining $\delta^{13}C_{bulk}$ values through WN-I3 to -5

Unlike $\delta^{18}O$, the fractionation of $\delta^{13}C$ is weakly temperature dependant, and therefore doesn't represent changes in temperature (Leng and Marshall, 2004). The decreasing trend through WN-I3-5 is interpreted to reflect increasing vegetation cover, and landscape stabililty in the catchment, resulting in a decreasing influence of geological carbonate on the DIC signal, and an increase of soil derived CO_2, which is isotopically lighter than geological carbon sources (Leng and Marshall, 2004; Candy *et al.,* 2016).

The low $\delta^{13}C_{bulk}$ values in WN-I2 are more difficult to explain, as these values are associated with low $\delta^{18}O_{bulk}$ values, indicating a cooler climate, less vegetation cover in the catchment, and more geological carbonate within the lakes DIC signal, resulting in relatively higher $\delta^{13}C$ values.

Two factors can be invoked to account for the values observed in WN-I2. First, the low $\delta^{13}C$ values may be a function of low aquifer residence time of groundwater and spring water prior to entering the water body, potentially due to a higher or more seasonal rainfall regime. A decrease in aquifer residence time would have resulted in: a) less equilibration between CO_2 in the groundwater, and atmospheric CO_2, and b) reduced dissolution of geological carbon from the bedrock. Both of processes would result in low $\delta^{13}C$ values of DIC entering the water body.

Second, cool conditions may have been characterised by low biological productivity in the water body. Biological productivity results in the preferential removal of ^{12}C, resulting in relatively higher $\delta^{13}C$ values in the water body DIC. A decrease in productivity, caused by either cool climates, or a change in the trophic status of the lake, would have resulted in low $\delta^{13}C_{bulk}$ values, as observed in WN-I2. Further work is needed however, to differentiate between factors,

potentially via trace element analyses (Garnett *et al.,* 2004), or terrestrial-aquatic biomarker ratios (e.g. Sasche *et al.,* 2012).

6.3. Stratigraphic Assemblage D: the Wykeham Southern Extension 2014 (WYKSE14) sequence.

LfA-4 deposits in Stratigraphic Assemblage D represents low energy floodplain aggradation, and wetland formation, in small pools, during the LGIT (section 5.4). Sediments from similar depositional contexts have previously been utilised to reconstruct palaeoenvironmental regimes using a variety of proxy data (e.g. Rose *et al.,* 1980; Walker *et al.,* 1993; Bridgland *et al.,* 2011; Mortensen *et al.,* 2011). Areas of optimum potential for palaeoenvironmental reconstruction were identified using the inverse-distance weighted models constructed for LfA-4 (Chapter 5) and reports from the present quarry area (Fraser *et al.,* 2009; Cloutman *et al.,* 2010; Figure 6.14).

The western margins of Depression C are identified as an area of optimum potential, where the thickest accumulations of LfA-6 deposits (Figure 5.29), which contain material viable for palaeoenvironmental reconstruction, and chronology (e.g. pollen, terrestrial plant macrofossils and coleoptera, Fraser *et al.,* 2009; Cloutman *et al.,* 2010; Figure 6.14) are found. The linear form and ca. N-S orientation of Depression C suggest that this feature represents a palaeochannel, incised directly into the outwash plain (LfA-2; Figure 6.15).

Figure 6.14. *Image showing the stratigraphy of the south face of the Phase 6a extension after Cloutman et al. (2010) with the lithofacies and correlated chronostratigraphic units marked by the author. This assemblage was determined as the site with optimum potential for palaeoenvironmental reconstruction from stratigraphic assemblage D due to the thick, and fossiliferous LFA-6B deposits.*

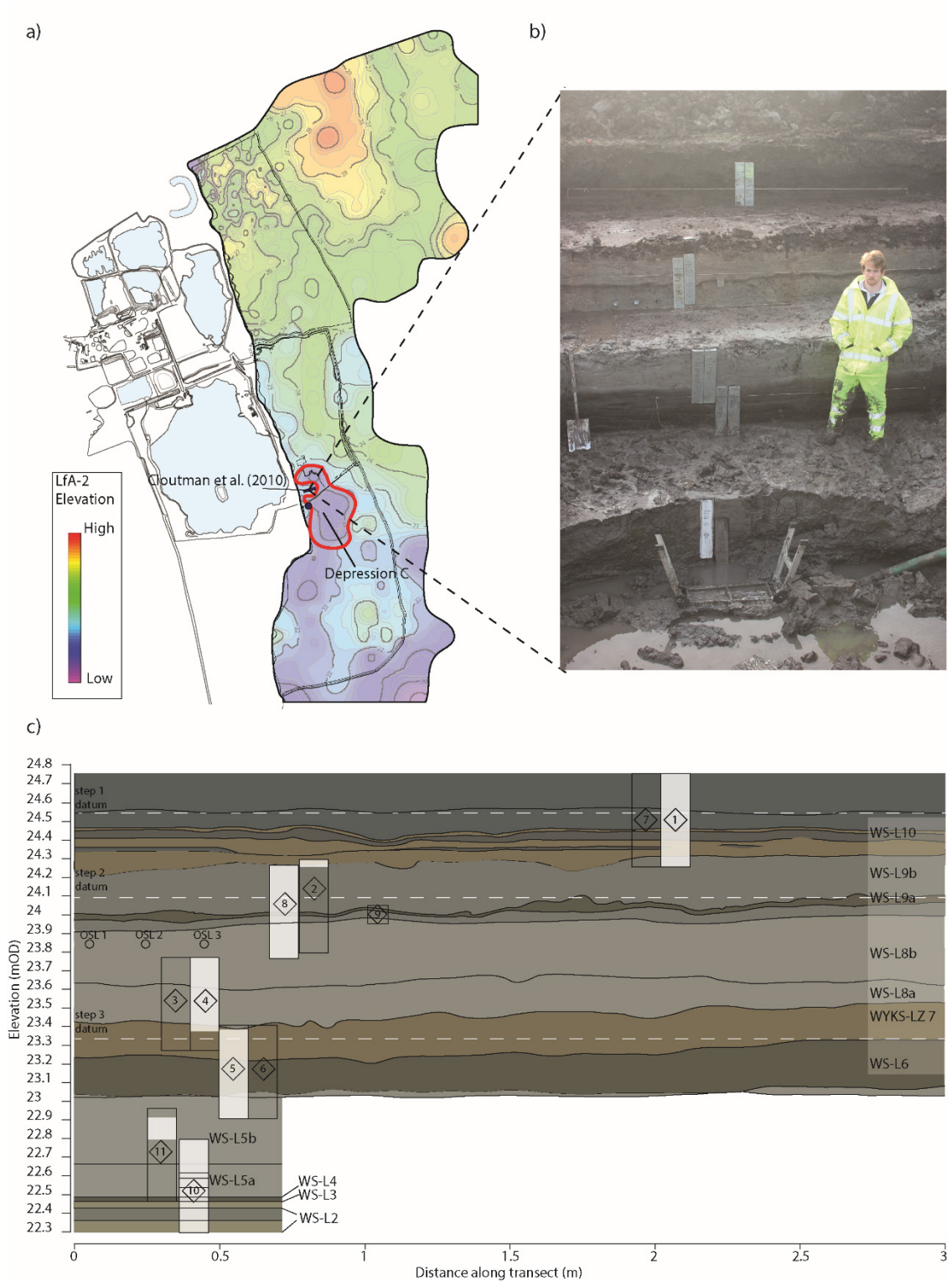

Figure 6.15. *a) Location map showing the location of Depression C identified from the upper surface elevation of LfA-2, and the position of the Cloutman et al. (2010), and WYKSE14 sequences. b) Image of the WYKSE14 excavation in September 2014 (R. Timms for scale). The sequence was excavated in four steps logged to a georeferenced datum on each step. c) Composite diagram of the stratigraphy logged from the WYKSE14 sequence, showing the distribution of the lithozones in the sequence, plotted against elevation. The locations of the 11 monolith/kubiena tins (labelled 1-8, 10-11 and 9 respectively) taken from the sequence are listed, alongside the position of 3 SAR-OSL samples (OSL 1-3). The whitened areas in the monolith tins represents the depths used to create the composite stratigraphy.*

Excavations in the Phase 6 area of the present quarry have shown that at the northern margins of Depression C, deposits consist of organic-rich, and very poorly humified remains (LFA-6B), which were determined by Cloutman *et al.* (2010) as providing the best potential for palaeoenvironmental reconstruction in the present quarry area. Cores from the QUEST-BHS survey showed that towards the centre of Depression C, the organic rich deposits taper out, being replaced by inorganic silts, sands and clays (Figure 5.29). The margins of the depression were therefore favoured for the purposes of palaeoenvironmental reconstruction.

A site directly to the south of the area logged by Cloutman *et al.* (2010), in Extension Phase S5 of the Southern Extension was identified as the area of optimum potential for palaeoenvironmental reconstruction from stratigraphic assemblage D (Figure 6.15). The study site, termed as the Wykeham Southern Extension 2014 record (WYKSE14) lies in a similar marginal position in relation to Depression C to that of the Section Q1 record, and the Phase 6a S. face reported in Cloutman *et al.* (2010), where organics are best preserved.

WYKSE14 was excavated in two stages: Firstly, repeat open gouge cores, and three stitz cores (RHULPal-1, termed WYKSE14$_{core}$), were taken in May 2014, to investigate the sedimentary sequence, and to construct a skeleton coleopteran record through the sequence, as part of a preliminary investigation by S. Jarosz (Jarosz, 2014).

Secondly, a machine excavated trench (RHUL-S11, termed WYKSE14$_{trench}$), was excavated in September 2014, *ca.* 10-20 m to the east of the WYKSE14$_{core}$ to further investigate the sedimentary sequence, and to obtain larger samples for plant macrofossil, radiocarbon, and coleopteran samples for analysis. 10 monolith tins, and 1 kubiena tin were extracted from the exposed sediment sequence from the south face of the trench, 7 of which were used for analysis.

6.3.1. Composite stratigraphy

The composite WYKSE14 records are presented in Figure 6.16. A description of the lithozones that comprise the WYKSE14$_{core}$ and WYKSE14$_{trench}$ records are presented in Tables 6.7-6.8. The WYKSE14$_{core}$ sequence can be correlated to the trench stratigraphy following the presence of key marker horizons and patterns in the bulk sedimentological records identified in both sequences (Figure 6.17-6.18; Table 6.9).

From this correlation, it is apparent that the WYKSE14$_{core}$ is a more marginal sequence and does not record the full sedimentary sequence (as observed in the WYKSE14$_{trench}$). On this basis, palaeoenvironmental reconstructions are focussed upon the WYKSE14$_{trench}$ stratigraphy.

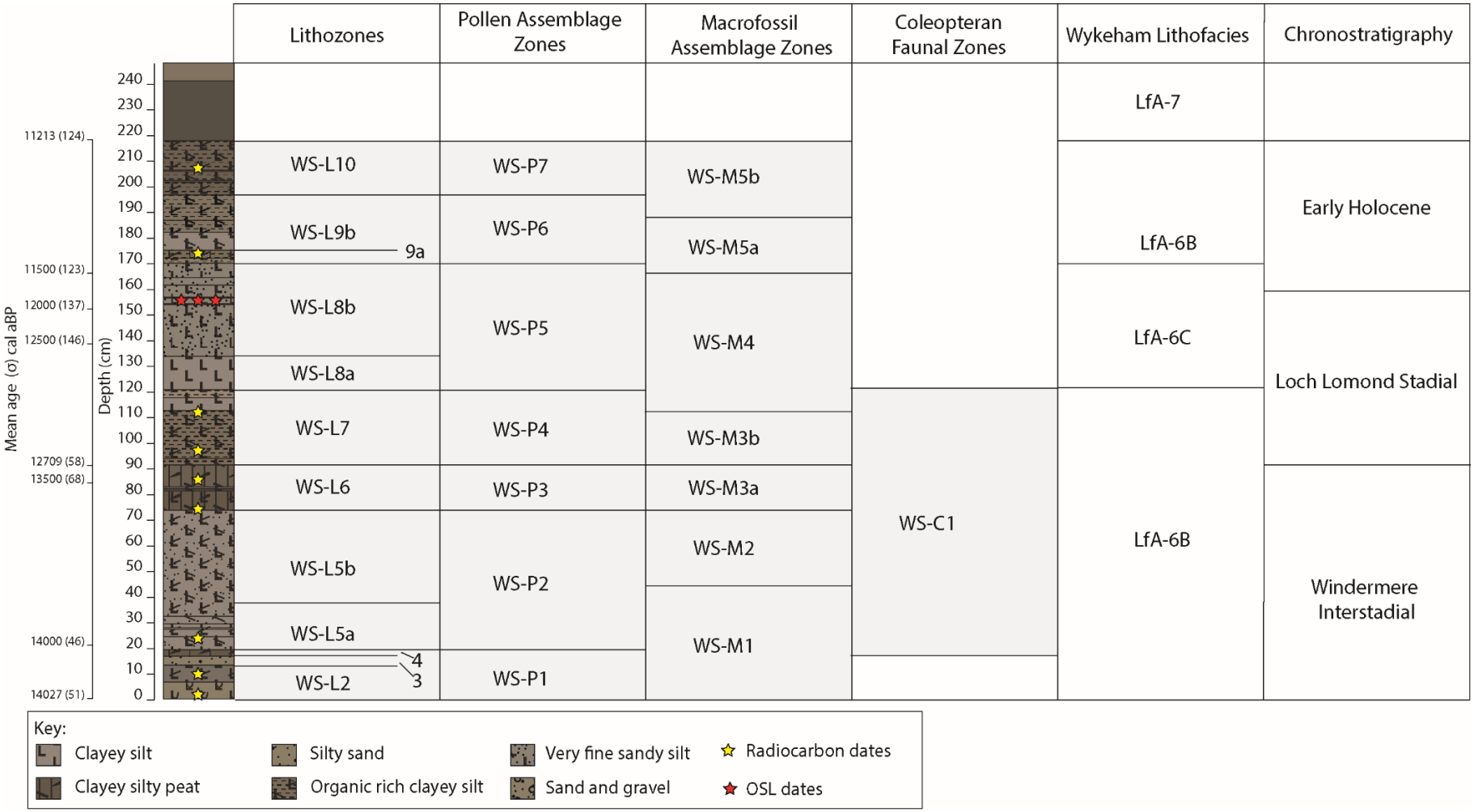

Figure 6.16. *Correlation between the sediment units, pollen, coleopteran and macrofossil assemblage zones through the WYKSE14 stratigraphy. These zones are compared to the Wykeham Lithofacies (reported in Chapter 5), and the chronostratigraphic framework for the British Isles. The stratigraphy is plotted against depth (cm), and mean age ranges (2σ) are derived from the P_Sequence model described in section 6.3.4.*

6.3.2. Bulk sedimentology

Sediment descriptions of the WYKSE14 stratigraphy are based upon bulk sedimentological descriptions, loss-on-ignition organic content, carbonate content, and siliclastic particle size analyses from the WYKSE14$_{trench}$ sedimentary sequence. The bulk sediment descriptions of the WYKSE14 stratigraphy is subdivided into 10 lithozones (WS-L1-11) observed in WYKSE14$_{trench}$ (Table 6.8).

***Table 6.7**. Summary of the lithozones identified in the WYKSE14$_{core}$ sequence. Descriptions include colour (Munsell) and texture which follow the Munsell, and Troels-Smith classification schemes respectively. Depths for each zone are recorded as cm from the base of the stratigraphy.*

Lithozone	Depth (cm from base of record)	Description
1	0-44	Well-rounded to sub-angular gravelly coarse sand (Gs2Gg2Ga+), graded.
2	35-44	Black (2.5Y 2.5/1) organic rich silty clay with poorly humified wood fragments and small seams (<0.5 cm) of very fine sand (As3Ag1Dg+Ga+). Sharp upper contact
3	44-60	Massive, grey (2.5Y 5/1) sandy fine to medium silty clay (As3Ag1Ga+Dg+), with interbeds of very fine to medium sand (Gs2Ga2Dh+, 0.1 to 2 cm thick). Diffuse upper contact
4	60-110	Thinly bedded dark greyish brown to grey (10YR 4/2 to 10YR 5/1) clayey very poorly humified herbaceous peat (Th3(h1)As1Dg+), laminated with grey (2.5Y 2.5/1) clays (As4) 0.2 to 0.3 cm in thickness between 64 and 65 cm. Upper 4 cm highly abundant with *Menyanthes trifoliata* seeds. Sharp upper contact
5	110-122	Massive, to weakly laminated, dark greyish brown (10YR 4/2) organic rich silty clay (As4Dg+ to As3Dh1Ag+) with black (2.5Y 2.5/1), horizontally bedded clayey, poorly humified herbaceous peat (Th3As1Dg+, 2 to 5 cm in thickness), and grey (2.5Y 5/1) silty clay (As3 Ag1 Dg+ 1 to 2 cm in thickness), with vertically oriented yellowish brown (10YR 5/6), oxidised rootlet casts,
6a	122-180	Massive, matrix supported, grey (Gley 2 5/1 to 2.5Y 5/1) sandy silty clay, with yellowish brown (10YR 5/6), oxidised rootlet casts oriented vertically through the unit. Matrix abruptly coarsens to grey (10YR 5/1) very fine sandy coarse silt (Ag3Ga1As+Dh+), where it is thinly bedded, by very fine sands (Ga4, 0.5 to 3 cm thick). Sharp upper contact.
7a	180-180.5	Greyish to dark greyish brown (10YR 5/2 to 10YR 4/2), organic rich sandy silty clay to clayey, poorly humified herbaceous peat (As3Ga1Sh+Dg+ to Th2Dg1As1Sh+Dg+ (h2)). Sharp, irregular upper contact.
7b	180.5-191	Massive, grey to greyish brown (10YR 5/1 to 10YR 5/2 from the base upward), silty clay (As3Ag1Dg+), with herbaceous remains, vertically oriented yellowish brown (10YR 5/6), oxidised rootlet casts, thinly bedded sandy clays (0.5 to 3 cm), and thin seams of grey (10YR 5/1) fine silty sand (Ga3Ag1). Diffuse upper contact.
8	191-204	Very dark grey to black (2.5Y 3/2 to 2.5Y 2.5/1) organic rich silty clay (As3Sh1Dg+Ag+), interbedded with poorly to moderately humified clayey herbaceous peat (Th2As2Dg+Ag+, 0.5 to 1 cm thick). Sharp upper contact.

Table 6.8. *Summary of the lithozones (WS-L) in the WYKSE14$_{trench}$ sequence. Colour and texture descriptions follow the Munsell, and Troels-Smith classification schemes respectively. The lithozones are correlated to the Wykeham Quarry lithofacies discussed in Chapter 5.*

Lithozones (WS-L)	Sub-zones	Depth (cm)	Age (cal ka BP)	Description	Wykeham Lithofacies
1		<0	> 14.13-13.92	Olive brown (2.5Y 4/3) matrix supported, well rounded to sub-angular gravels with a sharp upper contact	2
2		0-13	14.13-13.92 to 14.10-13.91	Olive dark grey (5Y 5/2 to 5Y 4/1), clayey silt with poorly humified, herbaceous plant remains and charcoal fragments (Ag3, As1, Dg+). Small carbonate content (<20%). Sharp upper contact	6B
3		13-16.5	14.10-13.91	Dark grey (5Y 4/1), silty fine to medium sand containing isolated herbaceous remains and charcoal fragments (Gs4, Dg+, Ag+).	6C
4		16.5-19	14.10-13.91 to 14.10-13.90	Black (2.5Y 2.5/1), very poorly humified herbaceous remains (primarily leaf fragments) and wood fragments (Dg4, Th+,(h1)).	5
5	5a	19-37	14.10-13.90 to 14.07-13.88	Grey (2.5Y 5/1) sandy clayey fine to medium silt, interbedded with very fine to medium sand beds (Gs2, Ga2, Dh+) 0.5 to 3 cm in thickness, similar to WS-L3.	6B
	5b	37-73	14.07-13.88 to 14.05-13.81	Grey (2.5Y 5/1), massive clayey fine to medium silt (Ag3, As1, Dg+).	6B
6		73-90.5	14.05-13.81 to 13.53-12.92	Very dark greyish brown (2.5Y 3/2) clayey, poorly humified peat, with plant and woody remains (Th4, As+, Dg+ (h1)), laminated with grey (2.5Y 2.5/1) clays (As4). Upper contact is determined to represent a hiatus in the sequence.	6B
7		90.5-120	13.53-12.92 to 12.74-12.48	Dark greyish brown (2.5Y 3/2 to 2.5Y 4/2) massive, to weakly developed laminated, organic-rich silty clay, with poorly humified herbaceous remains (As4, Dg+ to As3, Dh1, Ag+).	6B
8	8a	120-134	12.74-12.48 to 12.74-12.33	Grey (Gley 2 5/), massive sandy silty clay, with vertically oriented oxidised rootlets (As3, Ag1, Ga+, Dh+)	6B
	8b	134-170.5	12.74-12.33 to 11.63-11.22	Grey (10YR 5/1) very fine sandy, coarse silt (Ag3, Ga1, As+, Dh+), thinly bedded, with very fine sands (Ga4, 0.5 to 3 cm thick).	6C
9	9a	170.5-173.5	11.63-11.22 to 11.60-11.22	Dark greyish brown (10YR 4/2), organic-rich sandy silty clay (As3, Ga1, Sh+, Dg+)	6B
	9b	173.5-182	11.60-11.22 to 11.52-11.21	Greyish brown (10YR 5/2), clayey fine to medium silt (Ag3, As1), interbedded with herbaceous remains and horizontally bedded, grey (10YR 5/1) silty fine sands.	6B
10		182-218	11.52-11.21 to 11.36-11.05	Dark grey (2.5Y 2.5/1) organic-rich, clayey fine silt (Ag3, Sh1, Dg+, Ag+), interbedded with poorly to moderately humified fine silty, herbaceous peat (Th2, Ag2, Dg+, Ag+)	6B

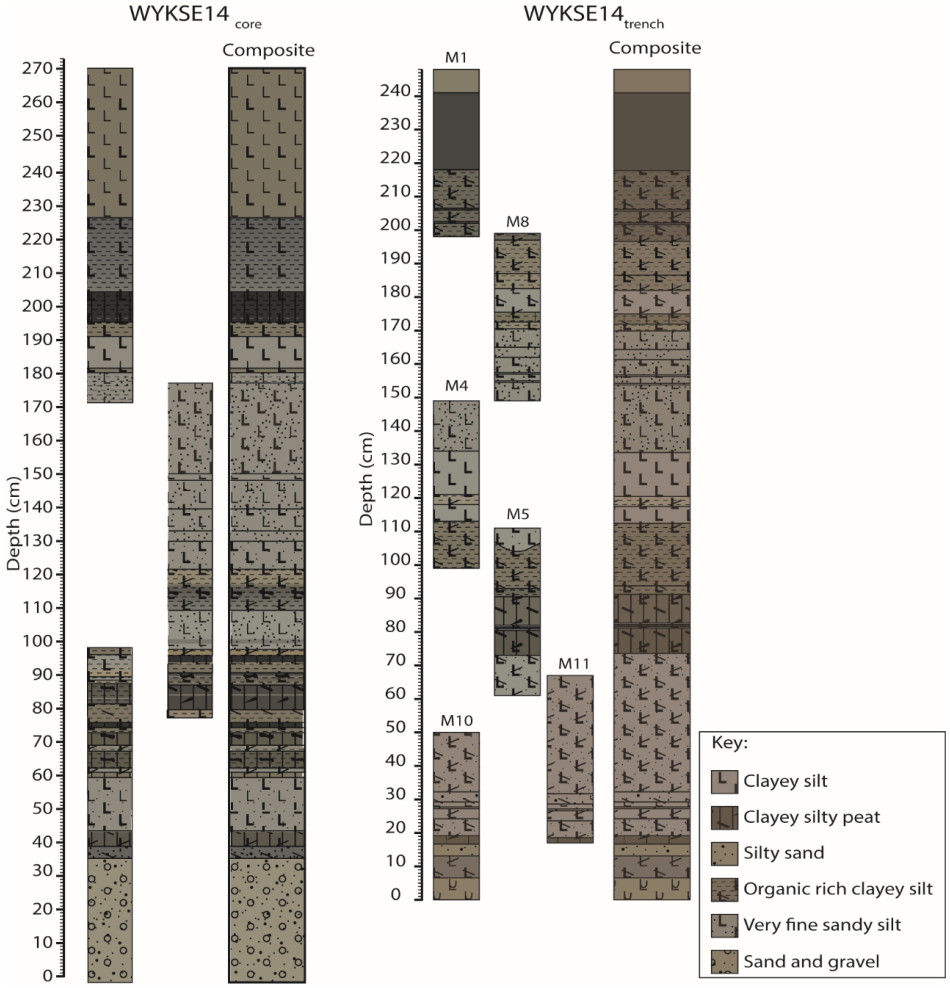

Figure 6.17. *Composite logs from the WYKSE14$_{core}$, and WYKSE14$_{trench}$ records, correlated using key marker beds between individual cores/monoliths.*

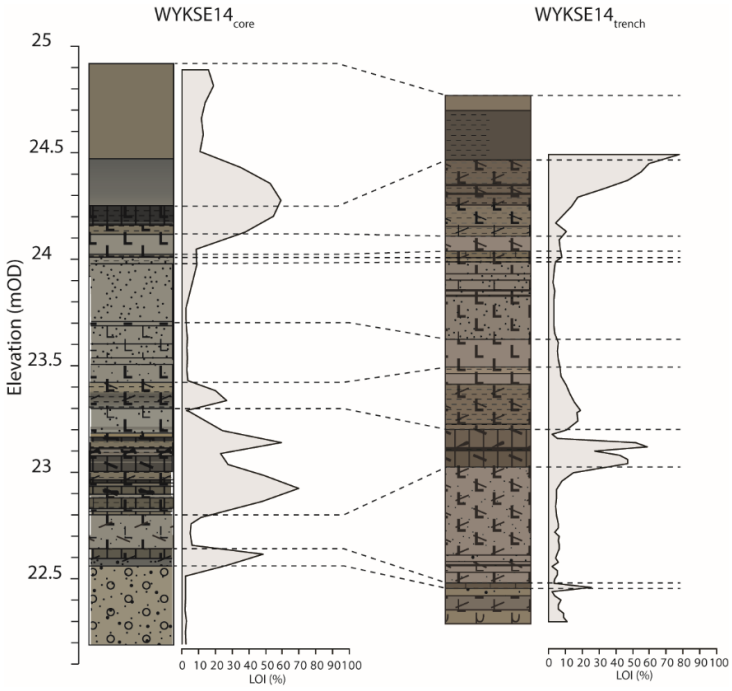

Figure 6.18*. Correlation of the WYKSE14$_{core}$ and WYKSE14$_{trench}$ records using key marker beds in conjunction with trends in the organic content of each record. Correlation points between the sequences are marked by dashed lines.*

Table 6.9. *Lithozone correlation of between the WYKSE14$_{trench}$, and WYKSE14$_{core}$ stratigraphies to form the composite lithozone classifications for the WYKSE14 stratigraphy, which utilises the unit depths from the WYKSE14$_{trench}$ stratigraphy. These lithozones are correlated to the Lithofacies (-6B to -6C and 5) identified across Wykeham Quarry.*

Composite WYKSE14 lithozone	**Composite depth (cm)**	**WYKSE14$_{trench}$ lithozone**	**WYKSE14$_{core}$ lithozone**	**Wykeham Lithofacies**
1	<0 cm	1	1	LfA-2
2	0-13	2		LfA-6B
3	13-16.5	3		LfA-6C
4	16.5-19	4	2	LfA-5
5	19-73	5	3	LfA-6B
6	73-90.5	6	4	LfA-6B
7	90.5-120	7	5	LfA-6B
8	120-170.5	8	6	LfA-6C
9	170.5-182	9	7	LfA-6B
10	182-218	10	8	LfA-5

6.3.3. Sedimentological interpretation

The interbedded, fine-grained, and in some instances fossiliferous deposits and peats (WS-L2; WS-L4; WS-L6-7; WS-L9-10; WS-L10), represent low energy suspension settling in shallow, organic rich water bodies; and telmatic peat development associated with decreasing abundance of allogenic inwash into Depression C, likely during stable, and temperate environments (Rose, 1995). Low abundances of carbonate in WS-L2 represent the formation of a shallow, base-rich water body, in Depression C. The lack of carbonate throughout the rest of the sequence show that these conditions did not persist, with consistently high volumes of siliclastic particle delivery into the basin, and shallow, possibly ephemeral open water minimising authigenic carbonate formation, and favouring the formation of telmatic deposits. The coarser grained lithozones (WS-L5a; WS-L8b), are characterised by low organic values, representing low organic productivity in the water body and the catchment. Additionally, the sorted characteristics of the deposits represent deposition via currents, during phases of higher energy flows into the basin, either via a lowering of relative lake level (Harrison and Digerfeldt, 1993) or enhanced transport capacities/more proximal relative position of the river system, inwashing coarser sediments during flood phases (Schillereff *et al.,* 2014). The sequence is capped by a return to fine-grained and organic rich sediments, representative of the reformation of a low energy wetland (WS-L10).

6.3.4. Chronology

12 dates were obtained from the WYKSE14$_{trench}$ stratigraphy, 9 of which are radiocarbon dates derived from terrestrial plant macrofossils, and 3 are single aliquot regenerative, optically

stimulated luminescence (SAR-OSL) dates from the same stratigraphic horizon in WS-L8 (155 cm). Tephra analysis was conducted on WS-L8 of the $WYKSE14_{trench}$ and $WYKSE14_{core}$ stratigraphy, but no tephra shards were identified between 120 and 170 cm.

These dates are used to construct a *P_Sequence,* deposition model for the WYKSE14 stratigraphy, following the criteria outlined in Bronk Ramsey (2008) (Figure 6.19; Table 6.10). All radiocarbon dates are calibrated to calendar age before AD 1950 (cal BP), using the IntCal13 calibration curve (Reimer *et al.,* 2013) in OxCal v4.2 (Bronk Ramsey and Lee, 2013).

Table 6.10*. Summary of the 3 age model runs (Unconstrained Sequence, P_Sequence, and P_Sequence with boundaries at lithostratigraphic intervals) used to create an age-depth model for the WYKSE14 sequence. All ages are reported as 2σ ranges with the calculated agreement index (A). The Sequence model shows all dates are above the 60% threshold, supporting the inclusion of all dates into the P_Sequence model runs (Bronk Ramsey 1995; 2008). The agreement index for each model run (A_{model}) is also reported.*

Date	**z (cm)**	**Unmodelled range (cal ka BP)**	***Sequence***		***P_Sequence***		***P_Sequence with boundaries***	
			2σ age range (cal ka BP)	**A**	**2σ age range (cal ka BP)**	**A**	**2σ age range (cal ka BP)**	**A**
OxA-32342	0	14.18-13.80	14.20-13.94	113.4	14.17-13.94	123.1	14.13-13.92	129.5
OxA-32440	9	14.14-13.80	14.10-13.87	117.7	14.12-13.90	122.7	14.11-13.91	126.8
OxA-32341	24	14.09-13.76	14.04-13.81	113.2	14.08-13.83	105.7	14.09-13.90	96.8
OxA-32433	76	14.09-13.77	13.97-13.76	97.9	13.97-13.42	74.5	14.00-13.75	94.5
OxA-32340	85	13.58-13.35	13.58-13.35	100	13.58-13.33	100.1	13.59-13.35	101.3
OxA-32339	95	12.72-12.57	12.74-12.66	74.5	12.86-12.61	73.7	12.77-12.61	76.2
OxA-32338	109	12.76-12.66	12.73-12.64	73.8	12.74-12.63	82.2	12.74-12.58	70.1
OSL3	155	13.55-9.96	12.68-11.44	124.8				
OSL2	155	14.35-10.36	12.68-11.44	128.6				
OSL1	155	14.35-10.36	12.68-11.44	128.6				
Combine OSL	155		12.68-11.44	134	12.38-11.32	113.3	12.23-11.58	133.9
OxA-32337	173	11.60-11.18	11.60-11.22	85.9	11.69-11.23	61.7	11.60-11.22	86.6
OxA-32336	205	11.59-11.17	11.38-11.18		11.39-11.17	111.7	11.39-11.17	113.8
A_{model}			**107.6**		**80**		**108**	

The deposition model was constructed in three stages. First, an unconstrained *Sequence* model was run with all dates to identify obvious outliers. Second, a *P_Sequence* model was run, incorporating depth information for all dates, and third, a second *P_Sequence* model was run, including boundaries at lithostratigraphic subdivisions, to account for variable sedimentation rates, and hiatuses in the WYKSE14 stratigraphy.

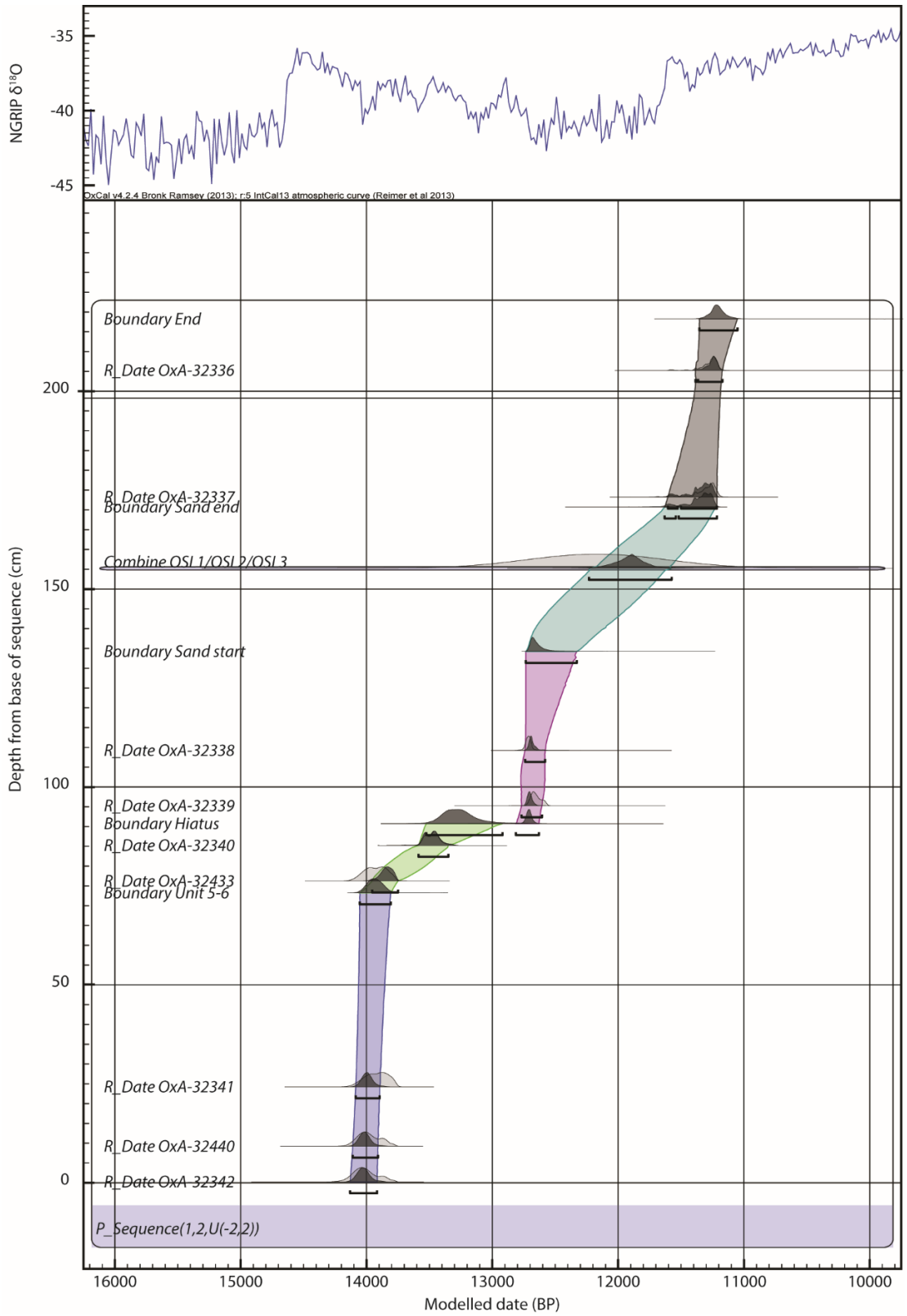

***Figure 6.19**. Age-depth, P_Sequence model for the WYKSE14 stratigraphy, with age uncertainties plotted at 2σ. The model utilises a k_0 factor of 1, and includes boundaries at 73, 90.5, 134, and 170.5 cm, at changes in the lithostratigraphy. The model output is presented in Table 6.10.*

The unconstrained *Sequence* model, used to identify outliers (Blockley *et al.,* 2007; Bronk Ramsey, 2009b), showed that all dates passed with an agreement index above the 60% threshold (between 73.8, and 134; Table 6.10). The model agreement index was also above the 60% agreement threshold (=107.6), indicating that no samples needed to be removed from the age-depth model runs. Automatic outlier detection was not used as it was found to produce anomalous results due to the hiatuses recorded within the sequence, and the sharp contrast in lithostratigraphies encountered. The model was refined using the *P_Sequence* function in OxCal v4.2 (Bronk Ramsey, 2013). 0.5 cm interpolations were used to account for the sub-centimetre division of the lithostratigraphy, and a k_0 factor of 1 was used to account for the variable nature of sediment deposition, and the low number of dated horizons within the sequence (Bronk Ramsey and Lee, 2013). The age model was further refined by the inclusion of boundaries at lithostratigraphic horizons, representing sedimentological changes in the stratigraphy, either by the mode of sediment deposition (e.g. the transition between WS-Ls 3 and 4 at 73 cm), or by shifts in particle size (e.g. the transition from WS-L8a to 8b, and 8b to 9 at 134 cm and 170.5 cm respectively).

The characteristics of the sediments in the WYKSE14 sequence have the potential for sedimentary hiatuses to exist. This is based upon: a) the variable particle size through the sequence demonstrating highly variable sedimentation rates (*see above*), b) organic-rich lacustrine/telmatic deposits which are known to be highly responsive to small fluctuations in groundwater variability (Harrison and Digerfeldt, 1993), especially during climatically unstable periods (Magny and Ruffadi, 1995; Bos *et al.,* 2006). This is most evident between WS-Ls 6-7 (at 90.5 cm), where the following lines of evidence demonstrate the presence of a sedimentary hiatus:

- A sharp bedding plane which often results from erosion, or a shift in depositional process, developing an unconformity (Schnurrenberger *et al.,* 2003).
- In the $WYKSE14_{core}$ stratigraphy, this transition is marked by a thin (1-2 cm), fine sand bed, with sharp upper and lower contacts. These beds can be associated with sedimentary hiatuses in lacustrine records (e.g. Palmer *et al.,* 2015).
- The transition between WS-L6-7 is representative of different depositional, and environmental regimes, below, and above 90.5 cm, which is supported by sedimentological and palaeoecological evidence (sections 6.3.2-6.3.8.)

The presence of a hiatus is supported by the initial *P_Sequence* model run, which shows a phase of very low sedimentation rates across this transition (between OxA-32340 and OxA-32339). This is unlikely to result from erroneous radiocarbon ages as the material used for OxA-32339, and OxA-32340 (terrestrial seeds and leaves), should be almost contemporaneous with sediment deposition, owing to their fragile nature, and minimal potential for cross contamination

(Turney *et al.,* 2000; Oswald *et al.,* 2005). Based upon these criteria, a double boundary is placed at 90.5 cm to represent a sedimentary hiatus.

6.3.5. Pollen

From the pollen counts from the WYKSE14 sequence, seven pollen assemblage zones (WS-P 1-7) are identified from the stratigraphy by constrained hierarchical clustering analysis, the boundaries of which match well with WS-L2-10 (Table 6.11). A summary pollen diagram is presented in Figure 6.20, and the raw data from these counts are presented in Appendix I.

Table 6.11. *Summary of the depth, elevation, and bounding ages of the 7 pollen assemblage zones in the WYKSE14 stratigraphy. Ages are reported as 2σ ranges from the base and top of each zone.*

WS-P	Depth (cm)	Age (cal ka BP)	Description
1	0-19	14.13-13.92 to 14.09-13.90	Decreasing *Betula* and *Juniperus* through the zone. Rises in disturbed ground indicators *Artemisia,* Asteraceae and *Rumex*. TLP declining from 53 to 11 k/cm^3
2	19-73	14.09-13.90 to 14.05-13.81	Herbaceous taxa such as *Artemisia, Galium,* Asteraceae, and *Thalictrum* all present between 1-8%, *Betula* and *Salix* present between 10-30%, *Juniperus* absent. Low TLP (<11 k/cm^3)
3	73-90.5	14.05-13.81 to 13.53-12.92	Heliophyte shrubs *Prunus* and *Sorbus* present for the first time, alongside tall herbs including *Apiaceae*. Photophillic taxa Helianthemum and *Saxifraga* also present in low percentages. *Betula* and *Salix* present although *Pinus* is absent through zone. High TLP (107-205 k/cm^3).
4	90.5-120	12.81-12.63 to 12.73-12.48	*Prunus* and *Sorbus* replaced by *Filipendula* (rising from 3-28%) and *Typha* in low abundances. Rises in herbaceous taxa including Caryophyllacee, *Epilobium,* and *Cirisium*. *Betula* increasing in abundance. Moderate TLP (23 $\pm$ 3 k/cm^3).
5	120-170.5	12.73-12.48 to 11.63-11.22	When *Cyperaceae* and *Poaceae* are excluded, assemblage is dominated by *Betula* (between 21-57%). High abundances of *Pteridium* and *Pteropsida* spores and charcoal between 136-168 cm. Low TLP declining from 57 to 9 k/cm^3.
6	170.5-196	11.63-11.22 to 11.41-11.19	Sequential rises in *Filipendula* and *Typha* (0% at 168 cm to 53.52% at 176 cm, and 2.82% at 176 cm to 23.81% at 192 cm). Decline in *Betula* and *Filipendula* between 176-192 cm coincident with small increases in herbaceous taxa Helianthemum, *Heracleum,* and *Cirisium*. Fluctuating TLP from 9 to 49 k/cm^3.
7	196-218	11.41-11.19 to 11.36-11.05	*Filipendula* and *Typha* both decline in abundance (48.15% at 200 cm to 12.24% at 212 cm and 22.22% at 200 cm to 0% at 212 cm respectively), being replaced by *Betula* and *Salix* (rising from 3.70% at 200 cm to 30.61% at 212 cm, and 3.70% at 200 cm at 200 cm to 20.41% at 212 cm respectively). Rising TLP from 67 to 99 k/cm^3.

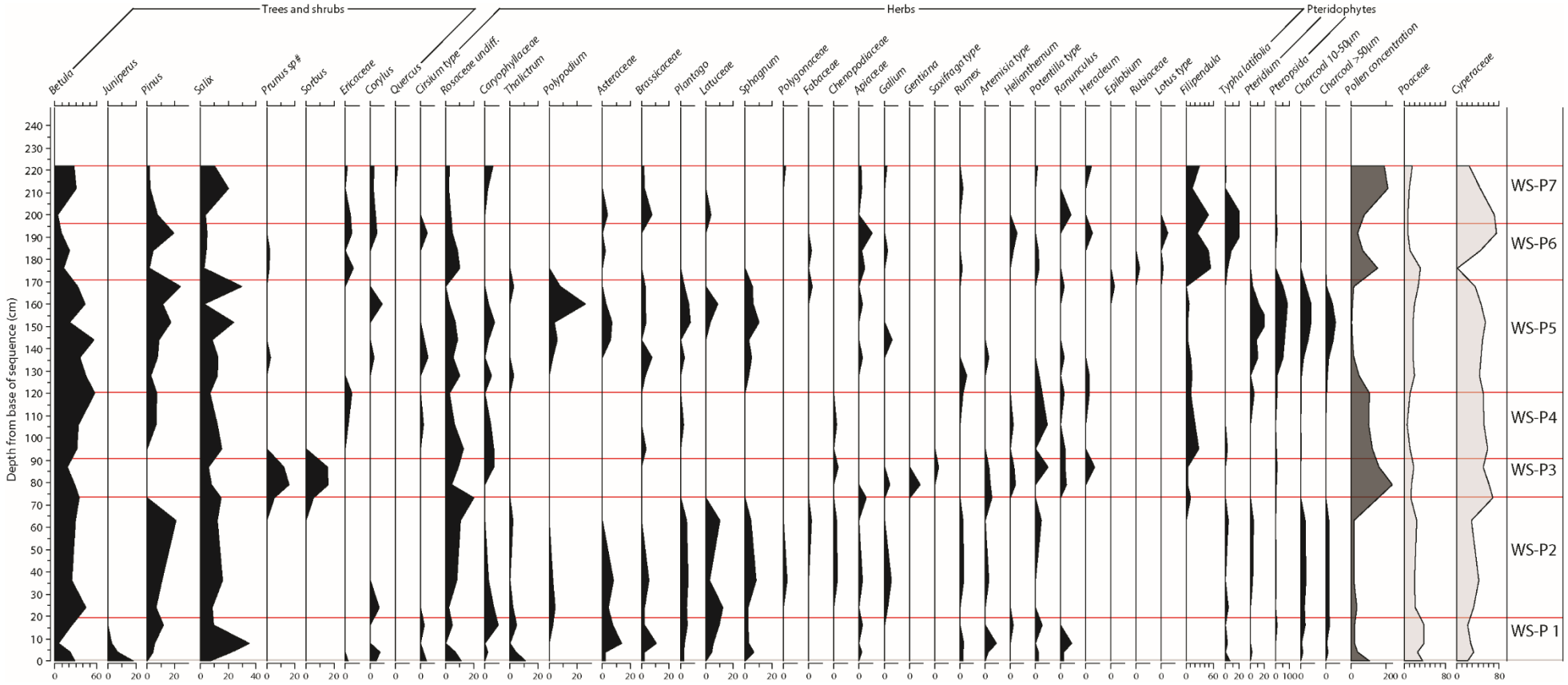

Figure 6.20. *Percentage pollen diagram from the WYKSE14 stratigraphy highlighting the 7 assemblage zones (WS-P1-7) discussed in text. Poaceae and Cyperaceae (grey), excluded from the percentage diagram are also presented as % of total land pollen (TLP)*

Reported percentages represent totals excluding *Cyperaceae* and *Poaceae* from the total land pollen sum, unless stated. These taxa dominate the assemblage (values exceeding 68 and 35 % of total land pollen respectively) and are excluded in order to identify more subtle trends within the assemblage. The record is presented as percentages to correspond to other pollen records constructed in the eVoP (Cloutman 1988a; b; Day, 1996; Mellars and Dark, 1998; Cummins, 2003), and Holderness (Walker *et al.,* 1993; Tweddle, 2001; Gearey, 2008). Pollen sample concentrations are also reported as thousand grains per cm^3 (k/cm^3) to determine pollen influx into the sedimentary sequence (Maher, 1981; Bennett and Willis, 2001).

6.3.6. Macrofossils

The macrofossil record is split into 5 macrofossil assemblage zones (WS-M), identified by variations in taxa presence and abundance. As the record is primarily recording the presence and absence of taxa, it is zoned visually, picking out characteristic trends in the vegetation assemblage. Macrofossil concentrations are reported as the number of macrofossil remains identified (excluding spores, and remains calculated according to the abundance scale), divided by the sample volume ($seeds/cm^3$). All macrofossil abundances are reported as the number of remains per 20 cm^3 of sediment. The major trends identified in the assemblage are summarised in Table 6.12, and Figure 6.21. The raw data from these analyses are presented in Appendix I.

6.3.7. Vegetation interpretation

The pollen and macrofossil records from the WYKSE14 sequence are consistent, and resemble other vegetation datasets from LGIT-aged sediments in NE England (e.g. Bartley, 1962; Walker *et al.,* 1993; Day, 1996; Sheldrick, 1997; Gearey, 2008).

WS-M1 is indicative of the development of shallow open water in Depression C fringed by *Carex* fen with small stands of *Selaginella selaginoides* and *Juncus*. Based upon the presence of *Daphnia* sp., and *Chara* sp., the trophic status of the lake water would have been oligotrophic-mesotrophic. *Juniperus communis* macrofossils demonstrate that the basin margins were unshaded, and also occupied by *Poaceae, B.nana* and *Salix herbacea,* the latter of which invoke late lying snow cover existing throughout winter and into the spring months (Walker *et al.,* 2003; Birks and Birks, 2014). The high volume of ericaceous leaf litter, and wood fragments indicate a very shallow lake body prone to repeated inwash from the basin margins. Unstable margins are supported by the presence of disturbed ground indicator *Rumex acetosella* and fungal mycelium, indicative of soil inwash from the catchment (Andersen *et al.,* 1984). These remains coincide with the sand-rich beds in WS-L3-5a supporting high energy inwash and/or a fluctuating water table in the basin through this interval.

Table 6.12. *Summary of the 5 macrofossil assemblage zones in the WYKSE14 stratigraphy. Ages are reported as 2σ ranges from the base and top of each zone.*

WS-M	Depth (cm)	Age (cal ka BP)	Description
1	0-48	14.13-13.92 to 14.07-13.86	Littoral and emergent taxa such as *Ranunculus subgen. Batrachium*, *Hippuris vulgaris*, and *Chara* sp., leaf litter and wood remains characterise the assemblage. *Juniperus communis* needles consistently present above 4 cm, some of which, alongside other macrofossil remains, show evidence of partial burning (Figure 6.22).
2	48-73	14.07-13.86 to 14.05-13.81	Very low macrofossil concentrations and no discernible trend in species assemblages. Chironomid head capsules in low abundances, *Carex undiff.* and *Rumex acetosella* present at 52 cm, poorly preserved. *Selaginella selagionoides* spores, fungal mycelium, and *Sphagnum* undiff. sporangia are identified throughout the zone and *Cristatella mucedo* statoblasts are identified at 63 cm
3a	73-90.5	14.05-13.81 to 13.53-12.92	Wetland and emergent taxa including *Carex undiff., Menyanthes trifoliata, Potentilla palustris, Lotus cf. glaber*, and *Lythrum salicaria* appear in the record at 79 cm, alongside Brassicaceae *undiff.*, and Poaceae. Single seed of small *Potamogeton undiff.* is recorded at the top of the zone (87 cm), which is absent from the other samples.
3b	90.5-112	12.81-12.63 to 12.74-12.56	Trigonous *Carex* achenes (including *C.rostrata*) continue to be the most abundant macrofossil identified in the assemblage although *Betula undiff.* and *Betula nana* fruits and leaves into the assemblage between 94 and 111 cm, possibly hybrids. *Potamogeton* undiff. seeds, including *Potamogeton pussilus* and *Nitella flexilis* oospores are recorded alongside Remains of aquatic taxa, *Daphnia* and *Diaptomus castor* reappear between 95 and 111 cm
4	112-165	12.74-12.56 to 11.82-11.33	No identifiable terrestrial macrofossils recorded. assemblage is dominated by charcoal fragments (small and large), which are present throughout, and increase in relative abundance. Fungal mycelium is consistently present. *Diaptomus castor* present between 113 to 128 cm. These taxa replace *Daphnia*, which are absent from WS-M4. *Diaptomus* egg casings are absent from the record above 128 cm, coinciding with the increase in siliclastic particle size in WS-L8b. The transition in particle size also coincides with the loss of *Nitella flexilis* oospores from the record, which are present in low abundances between 113 and 136 cm, becoming absent above 136 cm.
5a	165-188	11.82-11.33 to 11.47-11.20	Reappearance of herbaceous taxa including *Typha latifolia,* Poaceae, and *Aster undiff.* at 168 cm. Terrestrial leaf fragments also return to the assemblage in low abundances. At 170.5 cm, there is a sharp increase in *Urtica dioica* (from 1 to 91 seeds per 20 cm^3 between 168 and 170.5 cm), which disappear in the overlying sample at 176 cm. Poaceae, *Aster* type, and *Rumex acetosella* also recorded from this horizon.
5b	188-218	11.47-11.20 to 11.36-11.05	Emergent taxa *Carex undiff., Typha latifolia, Filipendula ulmaria, Potentilla palustris, Lythrum salicaria,* and *Juncus* undiff. decline in abundance and are replaced by woody remains and *Menyanthes trifoliata. Phragmites australis* stems are recorded for the first time in the record from 204 cm.

Low macrofossil concentrations in WS-M2 demonstrate low catchment vegetation cover, and/or rapid sedimentation rates. The sporadic presence of *Rumex acetosella* and *Selaginella selaginoides* suggest that high sedimentation rates may result from high amounts of allogenic inwash, sourced from the poorly vegetated basin slopes, and potentially driven by late lying snowmelt.

WS-M3a represents an expansion of emergent and telmatic taxa into the record, indicative of a eulittoral environment, characterised by a sedge rich fenland, formed in close association with the water table. High macrofossil concentrations invoke a substantial increase in vegetation development in the catchment in this interval. Small stands of shallow water are inferred from the continued presence of *Chara* sp. oospores, whilst the influx of taxa such as *Carex* sp., and *Menyanthes trifoliata* support the development of mestrophic conditions, and a decrease in the pH of the lake system, possibly due to the development of acidic soils in the catchment. Whilst vegetation cover in the landscape was high, the basin catchment was not extensively wooded, with no arboreal taxa recorded in the macrofossil record.

As outlined in section 6.3.4, a sedimentary hiatus exists between WS-M3a and WS-M3b. The macrofossil assemblage in WS-M3b demonstrates the reformation of a sedge fenland in a telmatic environment. Shallow standing water was occupied by small *Potamogeton,* littoral macrophytes (*e.g. Nitella flexilis*), *Daphnia* sp. and *Diaptomus castor,* which invoke relatively clear and cool lake waters (Bennike *et al.,* 2000), and a decreasing nutrient status of the water body (oligotrophic-mesotrophic; Birks, 2000). *Rumex acetosella* remains and fungal mycelium identified towards the

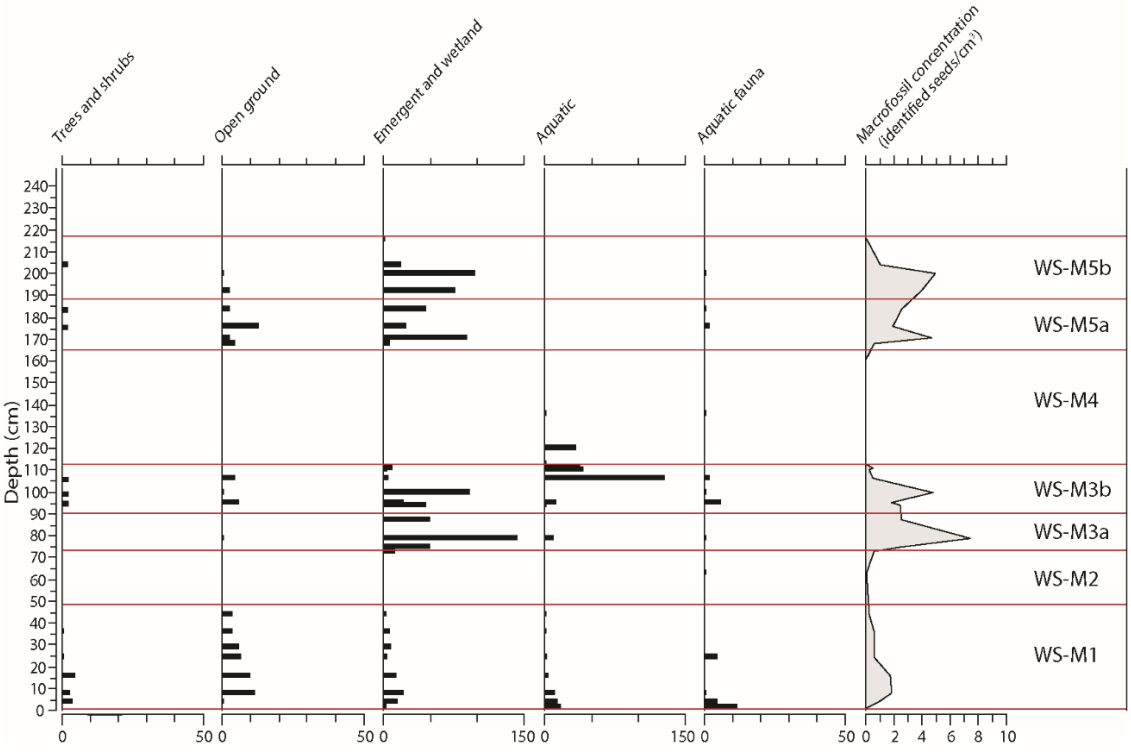

Figure 6.21. *Plant macrofossil diagram from the WYKSE14 stratigraphy. All macrofossil counts are reported as numbers per 20 cm³, whilst taxa counted according to the abundance scale are labellaed (ABUN). The 5 macrofossil assemblage zones discussed in text are marked in red.*

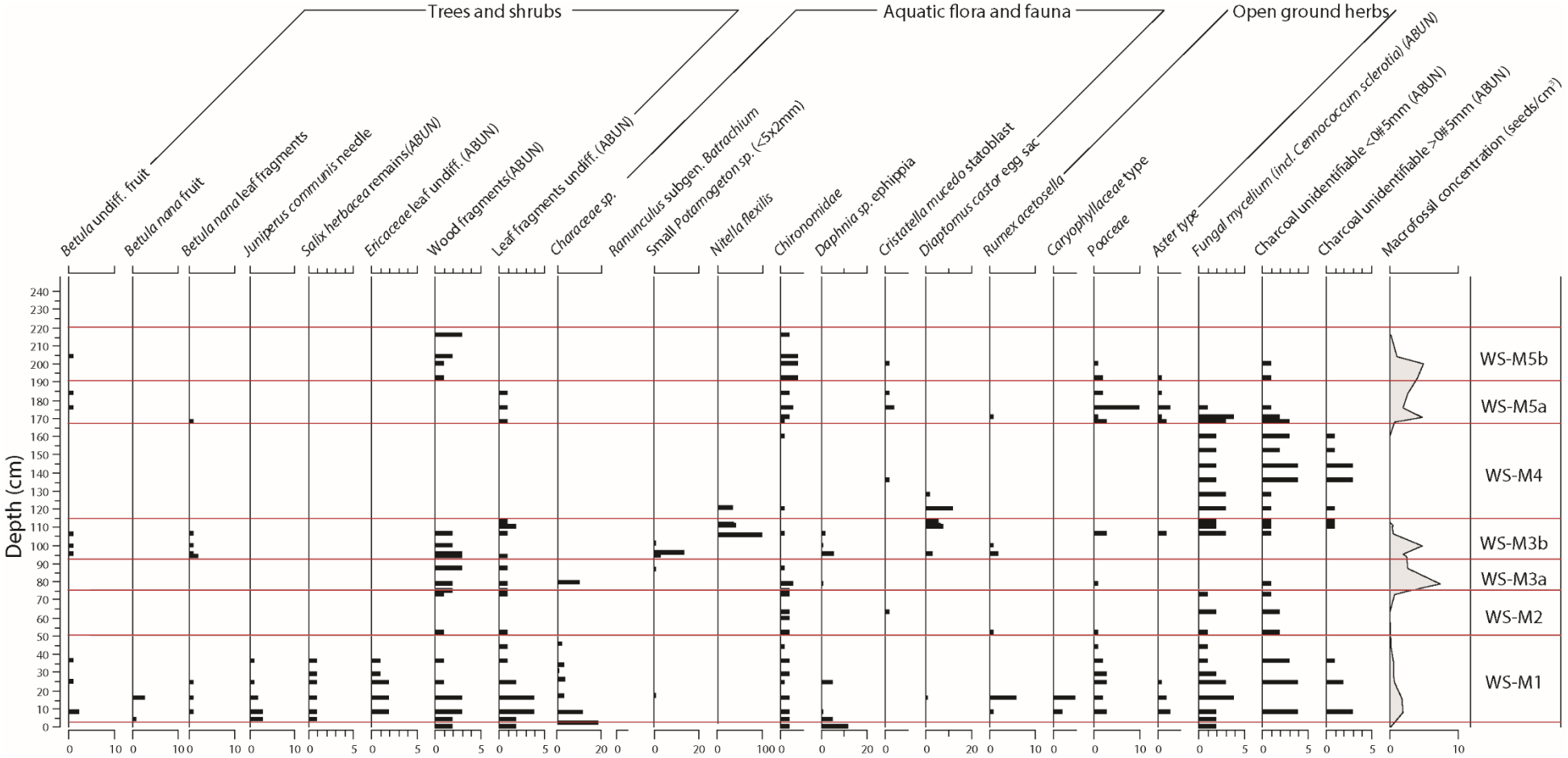

Figure 6.21 *contd.*

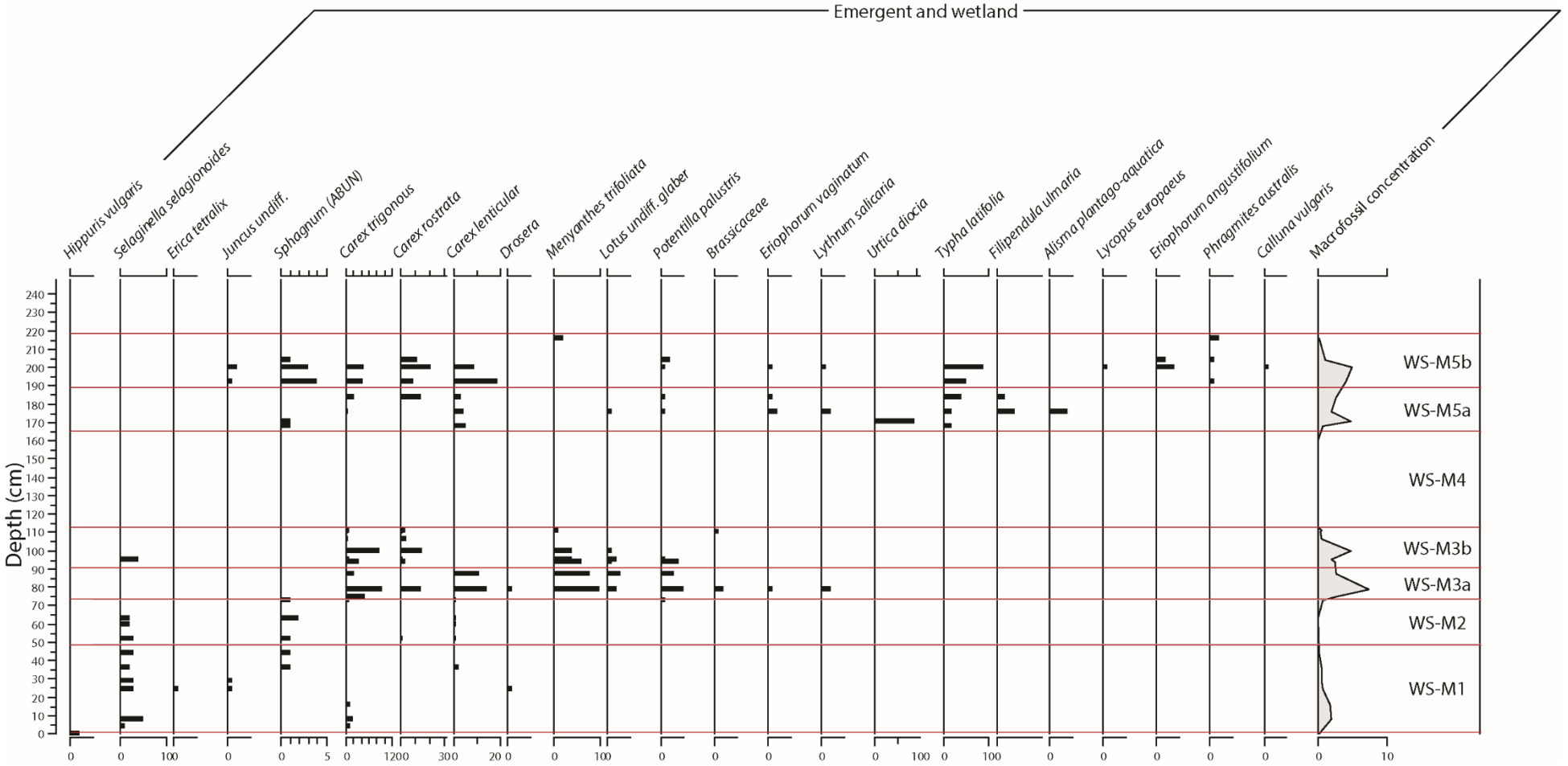

Figure 6.21. *contd.*

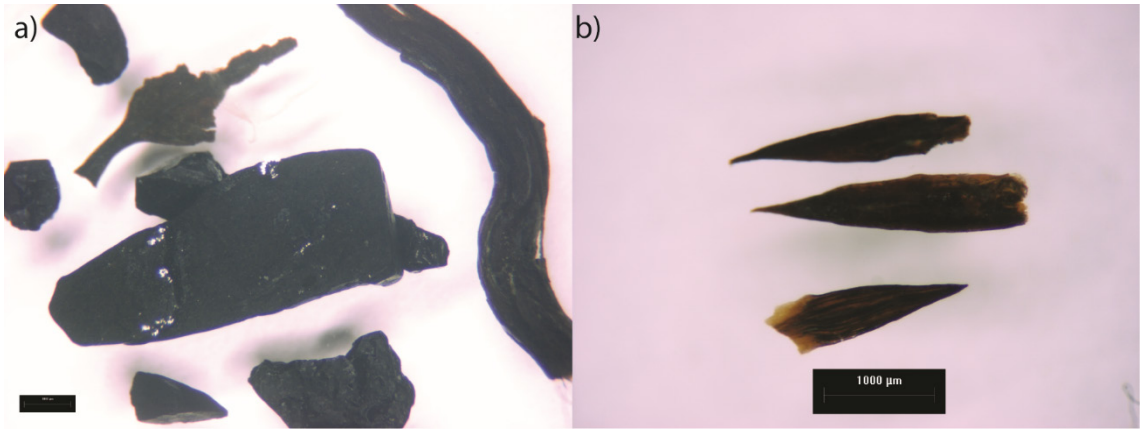

Figure 6.22. *Images of: a) macrocharcol (large), and charred leaf, and woody material from MFAZ-1, b) Partially charred Juniperus communis needles from WS-M1.*

top of the zone demonstrate that the basin margins became increasingly unstable, with the inwash of soils from the catchment (Anderson *et al.,* 1984; Walker *et al.,* 2003). The fine-grained siliclastic particle sizes through WS-L7 demonstrate that these remains were sourced from relatively low energy inwash events.

The absence of any identifiable terrestrial macrofossils in WS-M4 point toward sparse vegetation cover in the catchment of Depression C. This is supported by the low pollen concentrations in WS-P5. The loss of aquatic of telmatic taxa from the record are interpreted to represent the lack of open water at the sampling point of the WYKSE14 sequence. This interpretation is supported by the coincident rise in siliclastic particle size in WS-L8b, indicative of lower lake levels.

WS-M5a, and WS-P6-7 are characterised by the redevelopment of a eulittoral fenland environment, with by shallow stands of open water, surrounded by wet floodplain meadows. Tall herb fens consisting of *Typha latifolia* and *Filipendula ulmaria* developed at the margins of Depression C, with the holarctic bryozoan *Cristatella mucedo*, subsisting in open water. There is a temporary absence of *Typha latifolia* from the macrofossil assemblage at 170.5 cm (WS-L9a), where it is replaced by *Urtica dioica.* This may reflect a temporary lowering of the water level within the basin, and/or a decline in TMax temperatures, with *Typha latifolia* failing to subsist below 13°C but *Urtica dioica* subsisting in temperatures as low as 8°C (Isarin and Bohncke, 1999).

WS-M5b is characterised by the continued development of a fenland at the margins of the depression. Wood remains are identified through the zone, alongside *Betula undiff.,* fruits which were unidentifiable to species due to their poor preservation (van Dinter and Birks, 1996). This coincides with the decline in herbaceous remains such as *Aster*, and *Poaceae*, as arboreal taxa encroached upon the floodplain, outcompeting the tall herbs and wetland plants. WS-M5b therefore represents the infilling of Depression C via hydroseral succession coupled with the

development of higher vegetation, potentially including tree *Betula* remains close to the depression.

6.3.8. Coleoptera

10 coleopteran samples were focussed upon WS-Ls 4 to 8a of the WYKSE14 stratigraphy, collected from five repeat open gouge cores (<0.5 m horizontal spacing), subsampled at 5 cm intervals from analogous depths derived from field logging, and combined to produce the coleopteran sample. These samples can be directly correlated to the WYKSE14 composite stratigraphy, using the tie-points presented in Figure 6.18.

The following section briefly reviews the taxa identified in these samples. Further descriptions, and interpretation of the assemblage are presented in Jarosz (2014), and a full species list is presented in Appendix J.

83 taxa were identified in the WYKSE14 sequence, alongside one caddis fly (*Trichoptera*), and one true bug (*Hemiptera*). Of the coleopteran taxa, 58 were identified to species level. The assemblage in all samples is relatively consistent, and is therefore grouped into a single assemblage zone termed as Coleopteran Zone 1 (WS-C1).

Aquatic beetle fauna, commonly found in shallow, still to slow flowing pools are persistently present throughout the zone. Terrestrial coleopteran taxa (e.g. the family *Staphylinidae*) are also consistently present, implying a landscape consisting of shallow oligotrophic-mesotrophic ponds, with drier areas covered by leaf litter, and woody detritus (Jarosz, 2014).

Species confined to standing open water such as *Rhantus exsoletus* and *Agabus congener* (Merritt, 2006; Nilsson, 1995), are also found consistently, alongside caddis fly larvae (Trichoptera) in the family Limnephilidae, which are indicative of still water bodies (Williams, 1988). Dense emergent covers reeds, sedges, and/or rushes are implied by the presence of ground beetles (*Pterostichus minor* and *Agonum thoreyi*), and marsh beetles, which are consistently found through the sequence. The coleopteran assemblage is therefore consistent with the other proxy data from the WYKSE14 sequence, demonstrating the formation of fenland conditions with shallow standing pools of water through WS-L5b-7.

6.3.9. Coleopteran Mutual Climatic Range (MCR)

Coleopteran assemblages from LGIT sedimentary sequences in Britain have been successfully utilised to reconstruct summer and winter temperature estimates using the mutual climatic range (MCR) of taxa (e.g. Coope and Brophy, 1972; Atkinson *et al.,* 1988; Walker *et al.,* 1993; 2003). The coleopteran assemblage from the WYKSE14 stratigraphy can also be used to reconstruct summer and winter temperatures through the deposition of the sequence, using the MCR of recorded taxa. The following descriptions of MCR output, derive from Jarosz (2014),

with depths transferred to the WYKSE14$_{trench}$ stratigraphy by the author. A summary of the coleopteran MCR is presented in Table 6.13 and Figure 6.23.

Table 6.13. *Coleopteran MCR estimates from the 10 samples in WS-C1, calculated in BugsCEP (Buckland et al., 2006) after Jarosz (2014).*

Depth (cm)	TMaxLo (°C)	TMaxHi (°C)	TMinLo (°C)	TMinHi (°C)	TRangeLo (°C)	TRangeHi (°C)	NSPEC	Overlap (%)
16.5-19	13	17	-13	4	13	28	12	91.67
19-73	13	15	-17	-6	20	30	8	100
73-77	10	17	-18	4	13	30	4	100
77-81	15	17	-13	2	14	28	9	100
81-83	13	16	-17	-5	21	30	11	100
83-87	10	17	-17	4	13	30	9	100
87-91	10	19	-15	5	11	29	6	100
91-95	10	19	-15	6	11	29	6	100
95-100	13	25	-26	7	10	44	3	100
100-120	9	17	-28	1	15	37	3	100

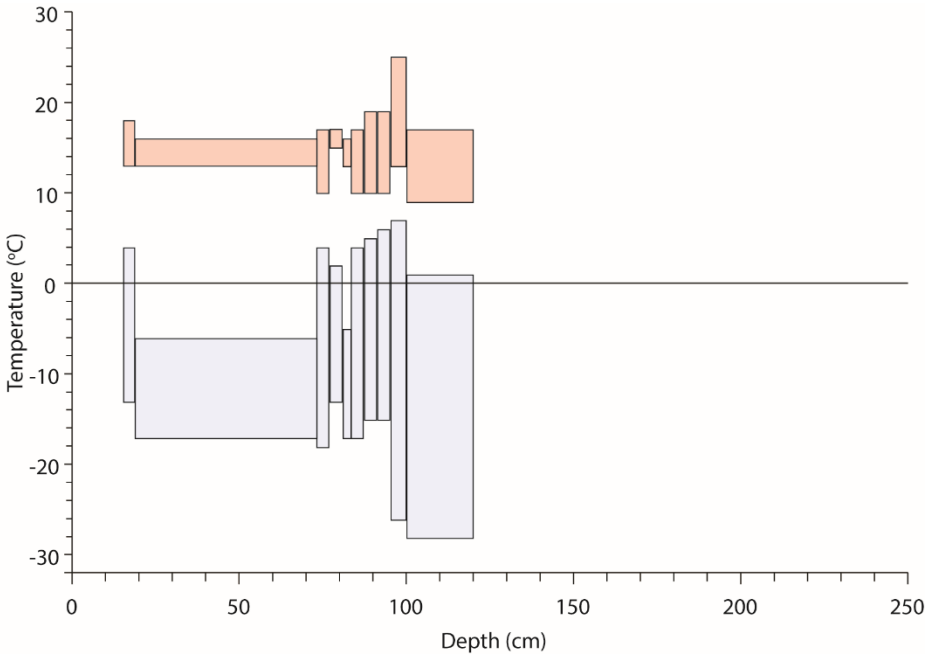

Figure 6.23. *TMax, and TMin, mutual climatic range plots for the coleopteran assemblage (light red and blue respectively) from the WYKSE14 stratigraphy. The output for these plots is provided in Table 6.13.*

The WYKSE14 beetle fauna are presently distributed across northern, and central Europe, indicating summer temperatures (TMax °C) as warm as, or slightly cooler those of the present day. The maximum TMax range in the assemblage, is between 9 and 25°C, with all but one sample constrained to an upper limit of 19°C. The temperature ranges between individual TMax estimates, are between 2 and 12°C, with the highest values identified in WS-L7). The assemblage represents little variation in the TMax values, with the range of each sample overlapping adjacent ranges. Winter temperature estimates (TMin °C), range between -28 and 7 °C, and are more poorly constrained than the TMax estimates (ranging between 11 and 33°C). As with the TMax, the widest ranges between minimum and maximum temperatures are found in WS-L7, and correspond to the low number of taxa used to develop the MCR.

In the uppermost sample in the record, the presence of the cold adapted, arctic and alpine rove beetle, *Pycnoglypta lurida*, which is currently not found in Britain, provides supporting evidence low winter temperatures at the top of WS-L7 (Coope *et al.,* 1972; Walker *et al.,* 1993). Enhanced continentality is reconstructed from these zones, with similar summer temperatures to surrounding values, but much cooler winters.

6.4. Macrofossil temperatures

Summer and winter temperature estimates can be reconstructed through the macrofossil assemblages from the WYKNE15 and WYKSE14 sequences. Temperature ranges are constructed using the reported temperature ranges for common LGIT macrofossils, presented in Aarnes *et al.,* (2012) and minimum TMax temperatures reported in Isarin and Bohncke (1999; Table 6.14).

Table 6.14. *TMax, and TMin temperature ranges used to reconstruct mutual temperature ranges for the macrofossil dataset. All ranges are from those reported in Aarnes et al. (2012), whilst the minimum Tmax for Typha latifolia and Urtica dioica follows (Isarin and Bohncke, 1999). Although taxa such as Juniperus communis also have a minimum TMax (>8 °C) in Isarin and Bohncke (1999), they are not included in the temperature ranges as they fail to further constrain the calculated TMax range.*

Taxa	TJan °C	σ °C	TJul °C	σ °C
Filipendula ulmaria	-5.5	9.3	15.86	3.88
Typha latifolia			>13	
Urtica dioica			>8	
Rumex acetosella	-6.91	9.66	11.46	4.88
Calluna vulgaris	-3.6	7.85	15.33	4.07
Carex rostrata	-28.99	17.15	14.28	4.27
Selaginella selaginoides	-6.13	7.99	11.83	3.38
Betula nana	-8.89	7.6	11.65	3.53
Salix polaris	-26.32	13.18	9.03	3.7
Salix herbacea	-8.55	7.9	7.91	4.85
Potentilla palustris	-18.41	14.82	14.3	4.12
Vaccinium uliginosum	-18.41	14.82	14.3	4.12

6.4.1. WYKNE15

Macrofossil mutual climatic ranges are reconstructed from 38 samples in the WYKNE15 sequence, using the ranges of between 1 and 5 taxa per sample (Appendix G). Temperature range estimates through the sequence are consistent, with little variability in either summer or winter ranges. Summer values are between 7.58 and 15.43 °C, with ranges between 4.18 and 8.56 °C (Figure 6.24). Winter values are between 1.69 and -21.53 °C with ranges between 6.95 and 34.3 °C. Lower TMax temperatures are consistently identified in WN-M5, reaching a minimum range of 7.58-12.36 °C at 469 cm. Higher TMax temperatures are identified in between 570-591 cm driven by the presence of *Typha latifolia* which has a minimum TMax of > 13 °C (Isarin and Bohncke, 1999; Table 6.14).

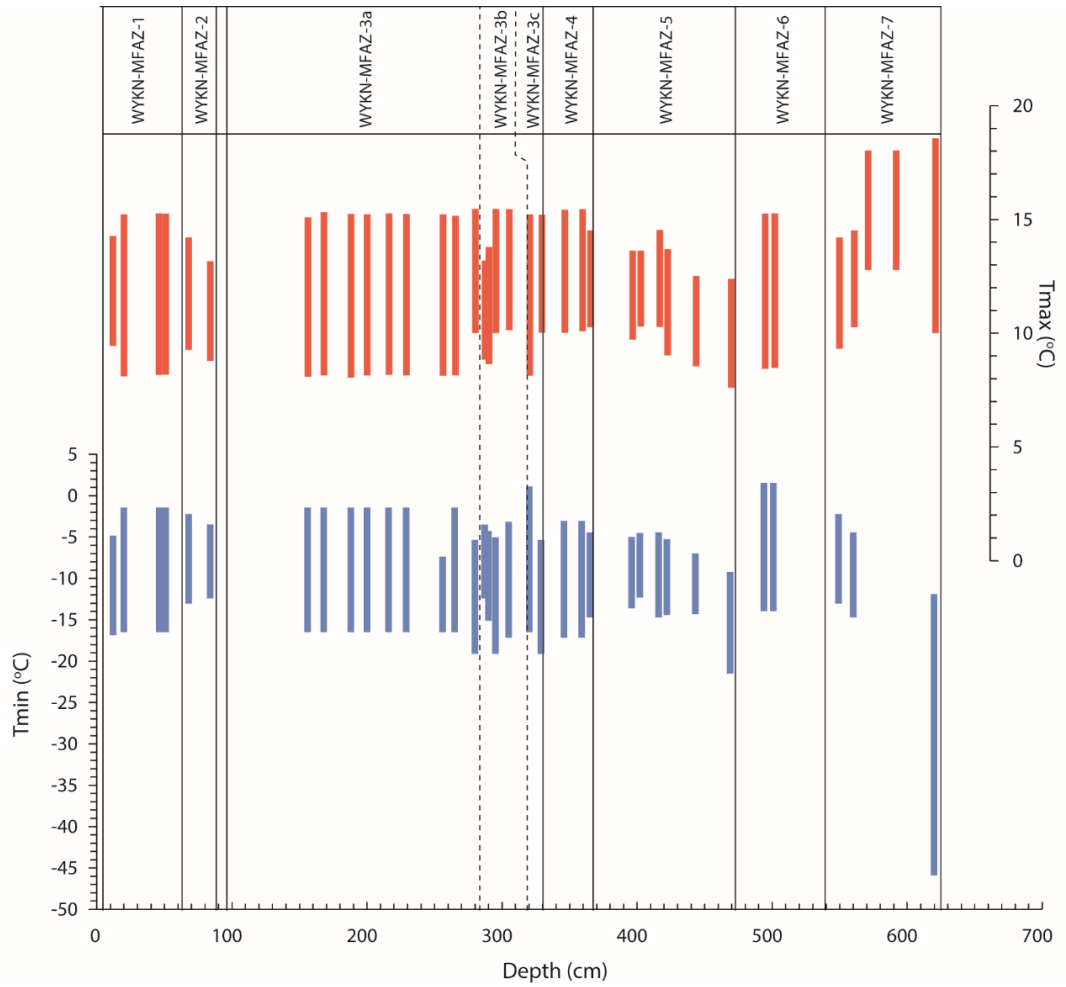

Figure 6.24. *TMax, and TMin, mutual climatic range plots for the plant macrofossil datasets from the WYKNE15 stratigraphy.*

The lack of variability through the rest of the sequence is assigned to: a) the low number of stenothermic macrofossils through the sequence, b) the low number of taxa with assigned temperature ranges.

6.4.2. WYKSE14

27 macrofossil MCRs are reconstructed from the WYKSE14 sequence. The macrofossil mutual temperature ranges enable the following temperature trends to be recognised (Figure 6.25).

In WS-M1, minimum, and maximum summer temperatures are consistently low, ranging from 8.15 to 9.72 °C, and 13.10 to 15.28 °C respectively, with ranges between 3.88 and 6.83 °C. With the exception of 44 cm (which has a maximum winter temperature of 1.89°C), optimum winter temperatures during WS-M1 are below 0°C, ranging between -2.39 and -4.96 °C. In WS-M2, summer temperatures are reconstructed between 10.1 and 17.26 °C, with consistently higher minimum estimates than those found in WS-M1. Optimum potential winter temperatures also increase (>-4 °C), coinciding with the loss of various arctic and alpine taxa from the assemblage.

In WS-M3a, only two species (*Carex rostrata*, *Potentilla palustris*) are used to reconstruct temperatures (Tables 8.9-8.10). As both of these taxa have wide ecological niches, the ranges

on temperature estimates are similarly wide (summer = 15.95-8.99 °C, winter= -12.56 to -34.30 °C).

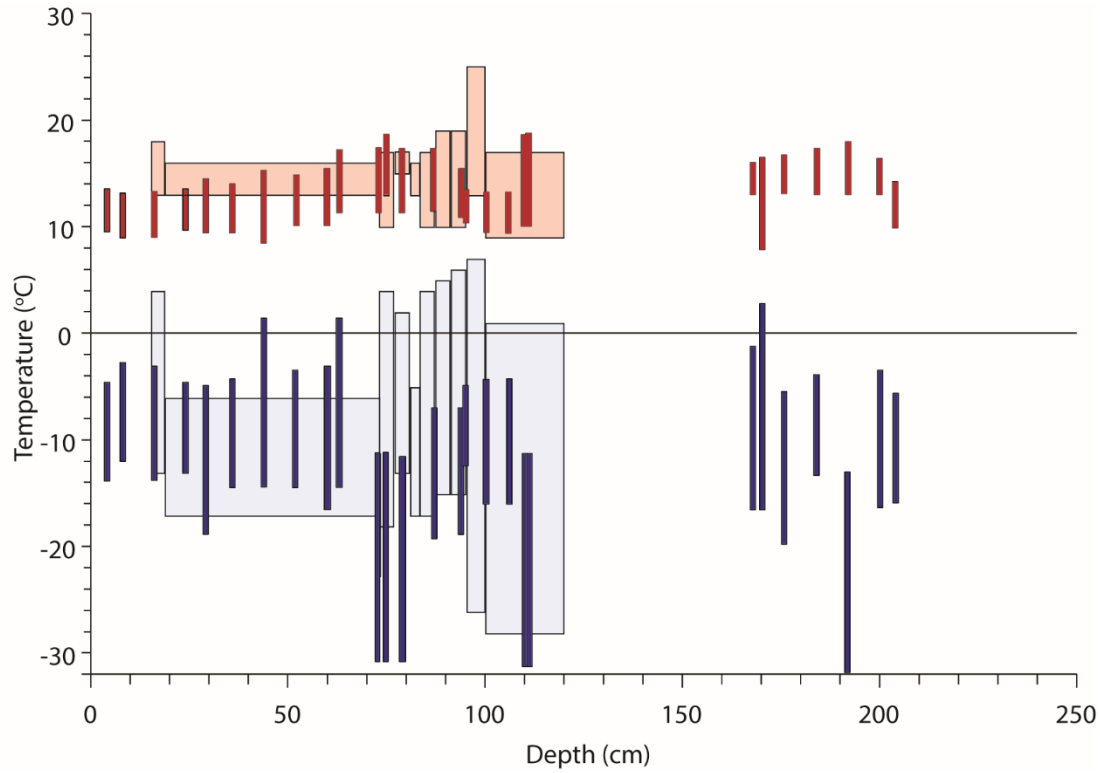

***Figure 6.25**. TMax, and TMin, mutual climatic range plots for the plant macrofossil (dark red and dark blue respectively) datasets compared to the coleopteran MCRs (light red and blue respectively; Figure 6.23) from the WYKSE14 stratigraphy. The output for these plots is provided in Tables 8.8 and 8.9.*

The low winter temperatures reconstructed during this stage derive from the temperature range from *Carex rostrata* (between -46.14 and -11.84°C), are treated with caution, as the wide ecological tolerance of the taxa imply that winter temperature is likely not a limiting factor in its distribution. The coleopteran MCR in these intervals implies that winter temperatures were warmer than -11.84 °C during WS-M3a, and the present distribution of *Carex rostrata,* almost down to sea-level in the British Isles (Rodwell, 1995), suggests that it is readily able to subsist in winter temperatures well exceeding -11.84 °C.

In WS-M3b, optimum (minimum) summer temperatures decline from 15.46 (10.91) to 13.24 (9.41)°C between 94 and 106 cm respectively. Between 110 and 111 cm *Carex rostrata* is again the only macrofossil used for temperature range. In contrast to WS-M3b however, the low macrofossil concentrations, and introduction of arctic and alpine coleopteran taxa into the assemblage at this stage suggest that the extreme winter temperatures reported by Aarnes *et al.* (2012) (between -46.14 and -11.84°C), are more likely.

The absence of macrofossil material precludes the reconstruction of temperatures in WS-M4. In WS-M5, the presence of *Typha latifolia* constrains minimum summer temperatures to >13 °C in Britain (Isarin and Bohncke, 1999), meaning that, with the exception of 170.5 cm, where *Typha latifolia* is absent, summers are in excess of 13 °C (optimum limits between 16.01 and 17.98 °C),

between 168 and 200 cm. Above this horizon, in the uppermost sample used for temperature estimates, the lack of *Typha latifolia* depresses minimum summer temperature to 9.88, with an upper limit reconstructed at 14.24 °C. Where more than *Potentilla palustris* and *Carex rostrata* are used for winter temperature reconstructions, (e.g. 192 cm), calculated ranges are between -1.29 and -19.76 °C.

6.4.3. Mutual MCR from the WYKSE14 sequence

There is consistent overlap between the macrofossil and coleopteran MCRs in the WYKSE14 record (Figure 6.25-6.26). When these MCR ranges are combined, a combined MCR consisting of macrofossil MCRs (MCR_{mac}) and coleopteran MCRs (MCR_{col}) can be constructed (Figure 6.26). This enables the TMax and TMin ranges to be better constrained, allowing for more precise reconstructions of summer and winter temperatures (Langford *et al.*, 2004; Holmes *et al.*, 2011). This dataset is hereafter termed as the WYKSE14 mutual MCR (MCR_{mut}). From this record, four MCR zones are identified. These are termed as MCR-A to D (Figure 6.26; Table 6.15) and when combined with the MCR_{mac} records from WYKNE15, they can be used to produce a composite MCR record through the LGIT (Figure 6.27).

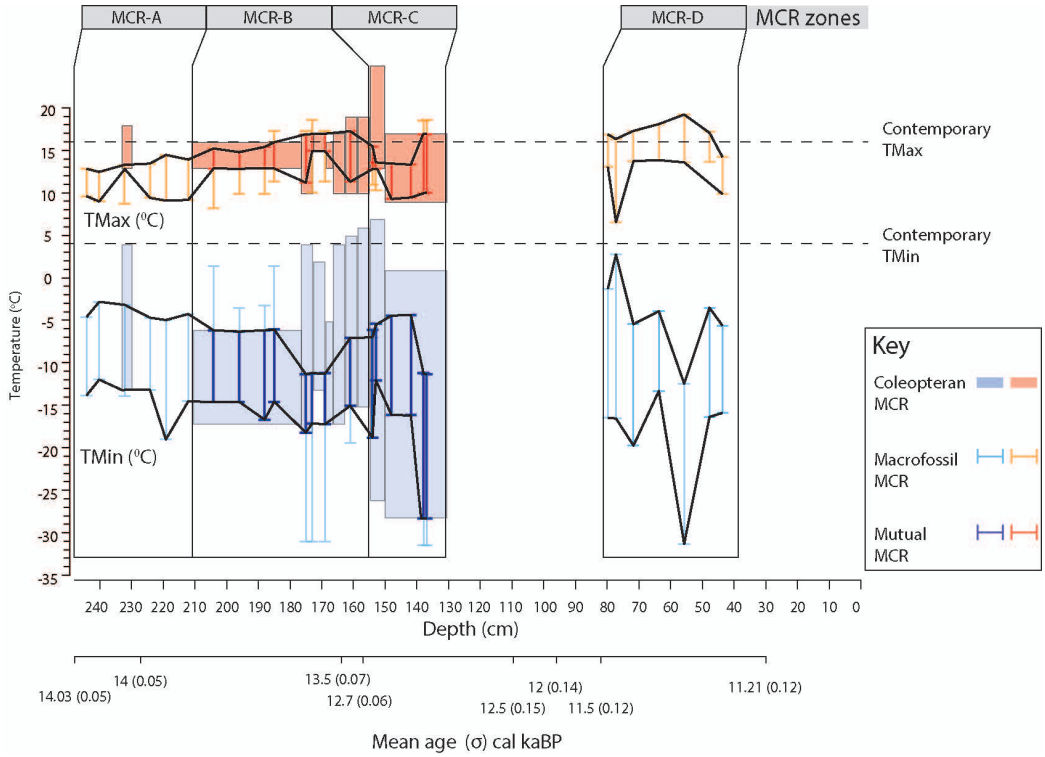

***Figure 6.26**. Summary of the TMin and TMax records from the WYKSE14 sequence, including the MCR_{mut} values constructed from the overlap of the MCR_{col} and MCR_{mac} between 14.01 ± 0.05 and 12.65 ± 0.09 cal kaBP. Black lines represent the upper and lower limits of the combined MCR output.*

Table 6.15. *Summary of MCR zones identified in the WYKSE14 MCR_{mut} record.*

MCR-	Depth (cm)	Age (cal ka BP)	Description
A	4-36	14.15-13.9 to 14.05-13.75	Low TMax (9-13 °C).
B	36-87	14.05-13.75 to 13.58-13.19	Rise in TMax to 13-15 °C, reaching optimum values of between 15-17 °C.
C	87-111	13.58-13.19 to 12.74 to 12.57	Decline in TMax (to 9.5-13.3 °C) and TMin (from -7 to -15 °C to -11 to -28 °C).
D	168-204	11.71-11.27 to 11.39-11.18	Rise in TMax to >13 °C.

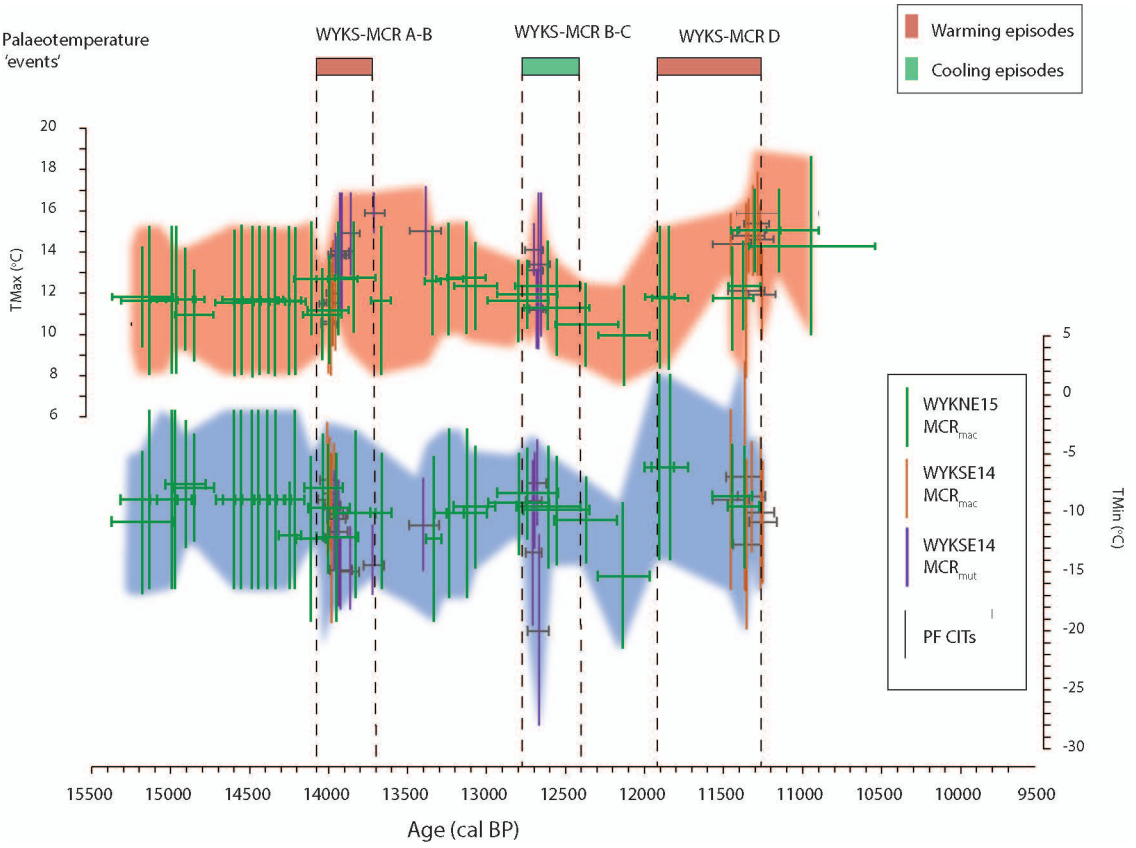

Figure 6.27. *Summary of MCRs reconstructed from the Wykeham Quarry records.*

6.5. Palaeoenvironmental reconstructions

The sedimentological, palaeoecological and geochemical data from the Wykeham records can be used to reconstruct past environmental regimes of the eVoP through the LGIT. The following sections describe the palaeoenvironmental evolution of the eVoP reconstructed from these records (Figure 6.28). The summary is split into five time-slices with all ages being reported as 2σ ranges.

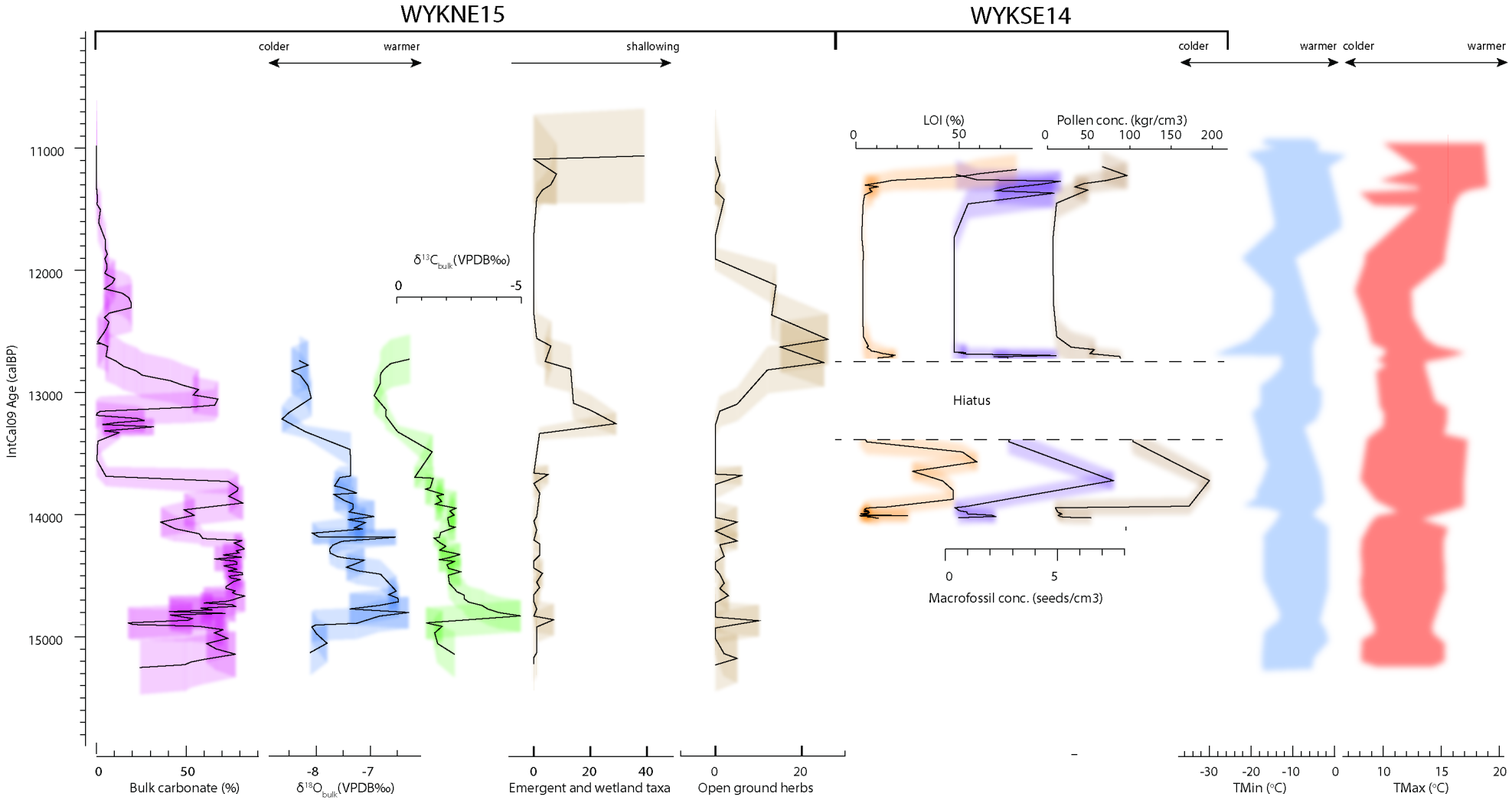

Figure 6.28. *Synthesis of environmental reconstructions from the Wykeham Quarry sequences. Shading represents σ age ranges from the mean value (black line). TMax and TMin ranges represent the MCRs presented in Figure 6.27.*

6.5.1. The Stadial to Interstadial transition and the Early-Windermere Interstadial ca 15.5-14.3 cal ka BP

Palaeoenvironmental reconstructions between *ca* 15.5-14.3 cal ka BP are derived entirely from the WYKNE15 sequence as no sediments were recovered from the WYKSE14 record through this interval. At the onset of sediment accumulation in WYKNE15 (15.69-14.82 cal ka BP), temperatures were cool (WN-I2), the landscape was open (WN-M1), and allogenic material dominated sedimentation within the lake (WN-L1, WN-I1). Charophyte meadows quickly colonized the basin, and initiated the formation of authigenic carbonate in the water body (WN-L1 to 2). At 15.12-14.62 cal ka BP, an abrupt rise in mean annual air temperatures (WN-I3a) led to an initial lowering of the lake level and inwash of sands and gravels from the unstable surrounding slopes (WN-L2b).

As climate ameliorated, a littoral lake body was formed, inundated by charophyte meadows (WN-L2c; Treese and Wilkinson, 1982). Optimum mean annual air temperatures were reached early in this phase (WN-I3a,c), but were briefly perturbed by a climatic oscillation between 15.04-14.54 to 14.96-14.46 cal ka BP (WN-I3b). Mild temperatures promoted catchment stability, driven in part by increasing vegetation cover, and soil development (WN-M3), although the low macrofossil abundances suggest that the landscape remained relatively sparsely vegetated with *Salix sp.* and *Betula nana* growing in the Depression B catchment. The re-emergence of calcified charophyte thalli and high carbonate values (WN-L2c), demonstrates that sedimentation in the basin was dominated by authigenic processes in a stable, shallow lake system, with limited allogenic inwash from the catchment. At 14.66-14.24 cal ka BP mean annual air temperatures began to steadily decline (WN-I4a), although the mode of sedimentation in WYKNE15 remained consistent.

6.5.2. Transition from the Early to Mid-Late Windermere Interstadial ca 14.3-13.9 cal ka BP

The transition from the Early to Mid-Late Windermere Interstadial (E-WI, M-LWI respectively) is characterised by unstable climatic regimes and the initiation of the WYKSE14 sequence. A sharp deterioration in temperatures between 14.32-14.07 and 14.32-13.95 cal ka BP (WN-I4b), initiated lower lake levels in Depression B, and potentially enhanced fire frequency in the catchment (high charcoal abundance in WN-M3a). The WYKSE14 sequence initiated infill at 14.13-13.91 cal ka BP as a small, shallow lake in Depression C (WS-L1). Soon after formation, the water body was occupied by the cladoceran taxa *Daphnia* sp. (WS-M1) which readily colonise recently formed water bodies during the LGIT (e.g. Birks, 2000; Sarmaja-Korjonen *et al.,* 2006), and subsist in open water bodies, with minimal competition. The basin was initially open and base rich, colonised at the margins by aquatic and emergent taxa such as *Chara* sp. and *Hippuris vulgaris*. The catchment was also relatively stable, and populated by shrub/arboreal communities

consisting of *Juniperus communis, Salix undiff.,* and isolated stands of *Betula undiff.* (WS-P1, WS-M1). Carbonate in WS-L1, is interpreted as being derived from authigenic precipitation within the basin on two criteria: firstly, the presence of charophyte oospores imply the presence of macrophyte stands in the littoral regions of the basin, which are known to occur readily in association with, and enhance, authigenic carbonate precipitation (Pelechaty *et al.,* 2013). Secondly, the lack of carbonate elsewhere in the stratigraphy advocates that the allogenic material deposited from the catchment, contains a negligible carbonate content.

Above WS-L1, carbonate precipitation declines, coinciding with phases coarser grained allogenic inwash into Depression C (WS-Ls 3 to 5). Vegetation abundance also declines, corresponding to the development of base-rich open grassland in the catchment, characterised by open, and disturbed ground, herbaceous taxa such as Poaceae, Caryophyllaceae, Asteraceae, *Chenopodium, Rumex acetosella,* and *Selaginella selaginoides* (WS-P1-2 and WS-M1-2). Increases in macro-, and microcharcoal abundances coincide with charred macrofossil remains of *Juniperus* (WS-M2) suggesting enhanced fire activity in the catchment. Remains of burnt *Juniperus* needles, and other organic remains dating to the same period are also identified in the WYKNE15 record, suggesting that these fires were widespread, possibly clearing the landscape of arboreal and shrubby taxa.

These trends invoke a phase of decreased landscape stability, with periods of higher energy deposition across the floodplain, inwashing organic (e.g. WS-L4) and inorganic material (e.g. WS-L3 and 5) into basins, during a phase of deteriorated temperatures (MCR-A, WN-I4b). Well-sorted, coarse grained beds in WS-L 3-5 invoke high energy deposition in Depression C, and could be related to two mechanisms:

a) Avulsion of the primary river channel, resulting in The River Derwent moving to a more proximal position to Depression C.
b) An enhancement in peak flow regimes of the river, resulting in increase in energy and transport of bedload material.

The position of the River Derwent during the WI is not known, making estimates on the proximity of the river channel to Depression C difficult to assess. Trends in the sedimentological and palaeoecological records however provide support for phases of enhanced flow regimes. Winter temperature estimates are persistently below freezing (MCR A) during this interval, which would have led to increased snow-bed accumulation within the catchment (supported by the presence of *S.herbacea* remains), coupled with a decline in vegetation abundance. Enhanced peak river flows, driven by snowmelt during spring and summer, would follow, transporting coarser grained sediment from readily erodible sediment archives in the catchment. This in turn

would lead to the flushing of overbank sediments consisting of fine to medium sands, rather than silts across the floodplain, and into Depression C.

The decline in siliclastic particle size (WS-L5b), invokes either a shift in the river's position, decreasing peak flood flow energy or a phase of incision (Rose 1995; Kasse *et al.,* 2003), but vegetation abundance in the WYKSE14 record remains low. The low pollen concentrations, coupled with the continued presence of perennial herbaceous taxa such as *Galium, Rumex, Artemisia, Asteraceae* (WS-P2), and *Selaginella selaginoides* (WS-M2), invoke the persistence of open grassland in the vicinity of Depression C.

6.5.3. The Mid-Late Interstadial ca 13.9-13 cal ka BP

The sedimentation rate in the WYKSE14 sequence declined at 14.05-13.81 cal ka BP (175 cm), and was coincident with an increase in organic content, pollen, and macrofossil concentrations (WS-L6, WS-P3, WS-M3a respectively), and a rise in TMax temperatures to 15-17 °C (MCR-B, WN-I4c). The palaeoecological data represents the development of mesotrophic, neutral, to base-rich sedge fenland, characterised by shallow, well vegetated pools, peatlands and backswamps (Rodwell, 1995) in the vicinity of Depression C. In Depression B, sedimentation rates also declined significantly between 14.08-13.81 and 13.66-13.24 cal ka BP as a low energy, littoral lake system, inundated by charophyte meadows and fringed by *Carex* sp. fen (WN-M3c), developed. These conditions limited allogenic inwash into the basin, promoting authigenic carbonate precipitation (WN-L2e).

In WS-P3, increases in *Cyperaceae*, and a coincident reduction/absence of *Poaceae*, and perennial herbs (*Thalictrum,* and *Asteraceae*), reflect the transition to a wetland environment, dominated by sedge fen. At this stage, Depression C existed as a shallow lake, with stagnant, to slow moving waters, which were colonised by various aquatic, and emergent taxa.

Alongside *Carex* sp.*,* the appearance of *Menyanthes trifoliata*, (which typically grows either as a grounded mass, or floating mats in shallow pools), *Potentilla palustris,* and *Lotus cf. glaber* macrofossils in WS-M3a, suggests that the water table during this phase was at, or just below the infill elevation of the WYKSE14 sequence for much of the time (Rodwell, 1995; Wheeler *et al.,* 2009). Based upon the presence of oligophagous coleopteran taxa such as *Tanysphyrus lemnae* and *Donacia crassipes* (WS-C1), further aquatic taxa such as *Lemna* spp., *Spirodela* spp., *Nymphaea alba,* and *Nuphar lutea*, not represented in the macrofossil record, were also likely existing at more central locations in the basin. The higher ground was covered by *Betula* sp., and *Salix* sp.*,* with small accumulations of *Prunus* and *Sorbus* shrubs.

At this stage, the River Derwent is interpreted to have been a very low energy river system, with backswamps formed across large swathes of the perennially submerged floodplain. These

conditions were driven by a high water table, and a regular flow regime (Rose 1995; Kasse *et al.,* 2003), which are common in low relief environments, characterised by high infiltration, small discharge variation, and limited bedload transport (Rose *et al.,* 1980). These trends all demonstrate a transition to a stable landscape in the eVoP between *ca* 13.9-13.5 cal ka BP.

Whilst the trends point towards significant increases in vegetation cover, there is limited evidence for the development of birch woodland, with only *Betula nana* remains and undifferentiated *Betula* fruits identified. Some of these fruits show evidence of hybridization, suggesting cross-pollination between multiple *Betula* taxa, supporting that multiple taxa of *Betula* were growing in the catchment (van Dinter and Birks, 1996; Birks and Birks, 2014), potentially including *Betula pubescens* (Day, 1996; Dark, 1998). The lack of tree-type *Betula* in the macrofossil records however, suggests that dense birch woodland did not develop in the eVoP. This is consistent with other northern British, and NW European macrofossil records which demonstrate that the local introduction of tree-*Betula* did not occur until *ca.* 13.6 cal ka BP (Walker *et al.,* 2003; 2004; Birks, 2003; Mortensen *et al.,* 2011). By this time, a eulittoral environment had developed in Depression B, and a hiatus had developed in the WYKSE14 sequence, meaning that any tree-*Betula* macrofossils in the landscape, were unlikely to have been incorporated into either of the Wykeham records. The macrofossil data either supports that the initial rise in *Betula* pollen in the latter stages of the WI represents enhanced influx of long distance transport into northerly localities (Birks, 2003), or that *Betula nana* was an important taxon at this time.

Between 13.52-12.90 and 12.80-12.63 cal ka BP, a hiatus formed in WYKSE14 and a telmatic environment developed in WYKNE15 (WN-L3, WN-M4). Hiatuses in wetland sedimentary records are commonly attributed to shifts in water levels, associated with climatic variability, especially effective changes in precipitation (Birks, 1980; Magny, 2012). In a fluvial environment, erosion from channel reactivation may also provide a means to produce unconformities in sediment sequences (Miall, 1996).

The water body in Depression C was shallow, and characterised by the onset of hydroseral succession between 14.06-13.81 to 13.52-12.90 cal ka BP. Only a slight drop in the lake level would be required, to starve the basin of the sediment and moisture, and cessate fenland development. The telmatic environment in Depression B supports a phase of lower lake levels at 13.66-13.24 cal ka BP. Whilst phases of channel activity are identified in the Northern Extension of the quarry during this interval, there is no direct evidence for palaeochannel incision in the stratigraphy. The hiatus in WYKSE14 is therefore interpreted to represent a decline in water table elevation. The decline in water level is coincident with a deterioration in mean annual temperatures declined between 13.66-13.24 to 13.37-12.96 cal ka BP (WN-I5a), although the

timing of this event is poorly constrained owing to uncertainties in the age model (due to insufficient dated horizons and changes in sedimentation rates) through this interval.

6.5.4. The Loch Lomond Stadial ca 13-11.7 cal ka BP

At the onset of the Loch Lomond Stadial (LLS), littoral lacustrine sedimentation resumed in Depressions B and C (at 13.30-12.78 and 12.80-12.63 cal ka BP respectively), characterised by rapidly accumulating silts sourced from allogenic inwash into the basin (WN-L4, WS-L7) under cold and more continental conditions (WN-I5a), with minimum winter temperatures reaching -15 to -28 °C (MCR-C). The water bodies were nutrient rich and shallow, similar to those formed during the M-LWI. The presence of *Daphnia* sp.*,* in both lakes supports open and species poor littoral waters. *Nitella flexilis* gyrogonites, indicative of shallow (Haas, 1994; Väliranta *et al.,* 2011), highly transparent water bodies (Coops, 2002), are present in both sequences, suggesting that the lakes remained relatively clear. These conditions likely resulted from decreased littoral vegetation cover, potentially due to increased allogenic inwash, negating the formation of dense mats of aquatic vegetation (WN-M4, WS-M3b). The presence of shallow aquatic, and emergent taxa including small *Potamogeton*, *Menyanthes trifoliata* in WS-M3b however demonstrates that at least initially, the water bodies were mesotrophic, and fringed by *Carex* sp. and *Juncus* sp. fen.

Open ground taxa such as *Rumex acetosella, Caryophyllaceae,* Poaceae, *Saxifraga* sp. *Silene* sp. *Caryophyllaceae, Thalictrum alpinum* and *Helianthemum* (WN-M5, WS-M3b, WS-P4), reflect the deterioration in vegetation cover across the catchment, transitioning to an open landscape characterised by open grassland and perennial herbaceous communities, coupled with late lying snow, and perennially frozen ground. Spring to summer melting of this snow, increased allogenic inwash into the basin, eventually leading to the cessation of authigenic carbonate formation in WYKNE15 (WN-L4-5a).

Between 12.5 and 11.8 cal ka BP, coarse silts and fine sands were deposited in Depression C (WS-L8b), and clastic gravel beds were inwashed into Depression B (WN-L5b), representing ephemeral phases of increased depositional energy separated by quiescent phases of sedimentation. The decline in aquatic organisms, which can subsist in severe temperatures (e.g. *Diaptomus castor* and *Daphnia* sp.), suggest that open water was either ephemeral or absent in both records during this time. In Depression C, these sediments were delivered either by enhanced transport energy of the River Derwent, or an avulsion of the channel to a more proximal position to the basin. Sediment logs from elsewhere in the floodplain demonstrate an analogous evolution of coarse-grained deposits, overlying finer grained alluvium (LfA-6C). This would suggest that the coarsening trend in particle size between WS-L8a to 8b most likely reflects a shift in river process, driven by a decrease in vegetation cover, and a decline in water table elevation. The gravels in Depression B are interpreted to represent periodic high energy influx either via slumping or inflow from the basin margins. An enhanced component of aeolian

derived sands, which are recorded from NE England, during the Loch Lomond Stadial (Gaunt *et al.,* 1971; Bateman *et al.,* 1998; Bateman, 2001; Hoare *et al.,* 2002) may also have contributed coarser particle sizes to these deposits.

In the catchment, low concentrations of pollen (WS-P5), and the absence of terrestrial macrofossils (WN-M5, WS-M4) point toward an open landscape, characterised almost entirely by herbaceous communities and *Pteridophytes*. The persistent presence of fungal mycelium (Anderson *et al.,* 1984)), and macrocharcoal in the records suggest high levels of erosion into the depressions.

Quantitative palaeoclimatic reconstructions from the Wykeham records are not possible, owing to: a) the lack of authigenic carbonate required for $\delta^{18}O_{bulk}$ measurements, b) large siliclastic particle sizes demonstrating higher energy deposition (WN-L5b, WS-L8b), precluding macrofossil deposition/preservation. Sedimentation during this phase was most likely discontinuous in both records.

6.5.5. Early Holocene ca 11.7-11 cal ka BP

Gravel inwash ceased in WYKNE15 at 12.05-11.54 cal ka BP, and a water body re-formed, initiating fine-grained deposition, perturbed by the ephemeral inwash of sand beds, likely via floods during the spring-summer melt seasons (WN-L5c). Siliclastic particle size also declined in WYKSE14 at 11.63-11.22 cal ka BP (WS-L9), although organic productivity initially remained low, with lake sedimentation dominated by allogenic influx of minerogenic material in both records.

The introduction of *Typha latifolia* and *Filipendula ulmaria* in the records at *ca* 11.8-11.35 cal ka BP (WN-M7, WS-M5) demonstrates an increase in TMax to >13°C (MCR-D). These species were joined by tall herbaceous fenland taxa, which are persistently recorded in pollen and macrofossil forms from both records (WN-M5a-5b, WS-P6-7 and WS-M5a-b). Around the margins of the depressions, fenland developed, fringed by wet floodplain meadows including *Filipendula ulmaria, Typha latifolia, Urtica dioica, Carex* sp. At deeper localities, shallow open water bodies re-emerged, occupied by taxa such as *Potentilla palustris.*

The presence of the holarctic bryozoan *Cristatella mucedo,* commonly found in lowland, oligotrophic-mesotrophic water bodies (Økland and Økland, 2000) in WYKSE14, support temperate conditions between 11.58-11.21 and 11.39-11.19 cal ka BP. In Norway, the expansion of *Cristatella*, closely corresponds to the introduction of *Betula pubescens*, in the Early Holocene (EH), slightly preceding its arrival in sites such as Kråkenes (Birks and van Dinter, 2010). This also appears to be the case in the eVoP, where the presence of *Cristatella* coincides with *Betula*

undiff. remains and woody fragments, reflecting the local expansion of shrubby and/or arboreal taxa from 11.44-11.20 cal ka BP (192 cm; WS-M5).

Herbaceous remains such as *Aster* type, and *Poaceae* decline as shrub and arboreal taxa encroached, outcompeting the tall herbs and wetland plants. In Depression C, hydroseral succession continued, as accommodation space in the basin filled. The re-emergence of *Menyanthes trifoliata,* and *Phragmites australis* near the top of the sequence reflect a shallowing water body and the development of peatland between 11.44-11.20 and 11.36-11.07 cal ka BP (192 to 216 cm).

At 11.82-11.26 cal ka BP, rapid hydroseral succession was initiated in Depression B as a eutrophic, tall herb fen developed at the WYKNE15 sampling site (WN-L6a-7). A similar sequence of hydroseral infill is recorded in Depression C as the WYKSE14 record transitioned from a littoral water body to a telmatic environment. The re-emergence of *Menyanthes trifoliata,* and *Phragmites australis* near the top of the sequence (WS-M5a-b) reflect a shallowing water body and the development of peatland between 11.44-11.20 and 11.36-11.07 cal ka BP.

7. Developing an LGIT palaeoclimatic event stratigraphy for the eastern Vale of Pickering

7.1. Introduction

In the North Atlantic stratotype for the LGIT, the GICC05 composite ice-core stratigraphy, abrupt climatic events are well understood and chronologically constrained, forming the North Atlantic event stratigraphy (Björk *et al.,* 1998; Chapter 2). However, in terrestrial records, the sequence is less well understood, with uncertainties regarding the timing. duration and magnitude of abrupt climatic events during this period (Lowe *et al.,* 2008; Brooks *et al.,* 2012). The Wykeham sequences provide excellent evidence for climatic and hydrological changes in the eVoP through sedimentological, geochemical ($\delta^{18}O$ and $\delta^{13}C$ stable isotopes) and biological (macrofossil and coleopteran) proxy reconstructions.

This chapter synthesises the evidence for palaeotemperature and palaeohydrological changes in the eVoP, which are used to construct a palaeoclimatic and palaeohydrological event stratigraphy through the LGIT. Data is also presented from the unpublished lacustrine sequence from Palaeolake Flixton (PF) located 2-3 km west of Wykeham, demonstrating that the hydrological changes identified at Wykeham reflect extra-local influences. This provides a climatic framework for the area which is compared to other regional records and the Greenland event stratigraphy (Chapter 8).

7.2. Comparing LGIT palaeotemperature reconstructions from the eVoP

This section summarises the palaeoclimatic data obtained as part of the POSTGLACIAL Project from Core B at PF (Palmer *et al.,* 2015; Candy *et al.,* 2015). Palaeotemperature records from this sequence (Figure 7.1) are used as comparative datasets to the Wykeham palaeotemperature records (Figures 7.2-7.3).

7.2.1. Palaeolake Flixton

PF is a former water body situated *ca.* 2-3km east of Wykeham Quarry from where quantitative palaeotemperature records including $\delta^{18}O_{bulk}$ values and chironomid-inferred temperatures (C-ITS) have recently been constructed from LGIT-aged, carbonate-rich deposits (PF Core B; Palmer *et al.,* 2015; Candy *et al.,* unpublished data). The Core B stratigraphy consists of two lithozones of marl separated by a sand horizon which is interpreted to represent a sedimentary hiatus during the LLS, meaning no LLS aged sediments are sampled (Palmer *et al.,* 2015). The lower marl lithozone is confirmed to date to the WI by the presence of the Penifiler Tephra at 428 cm (Figure 7.1).

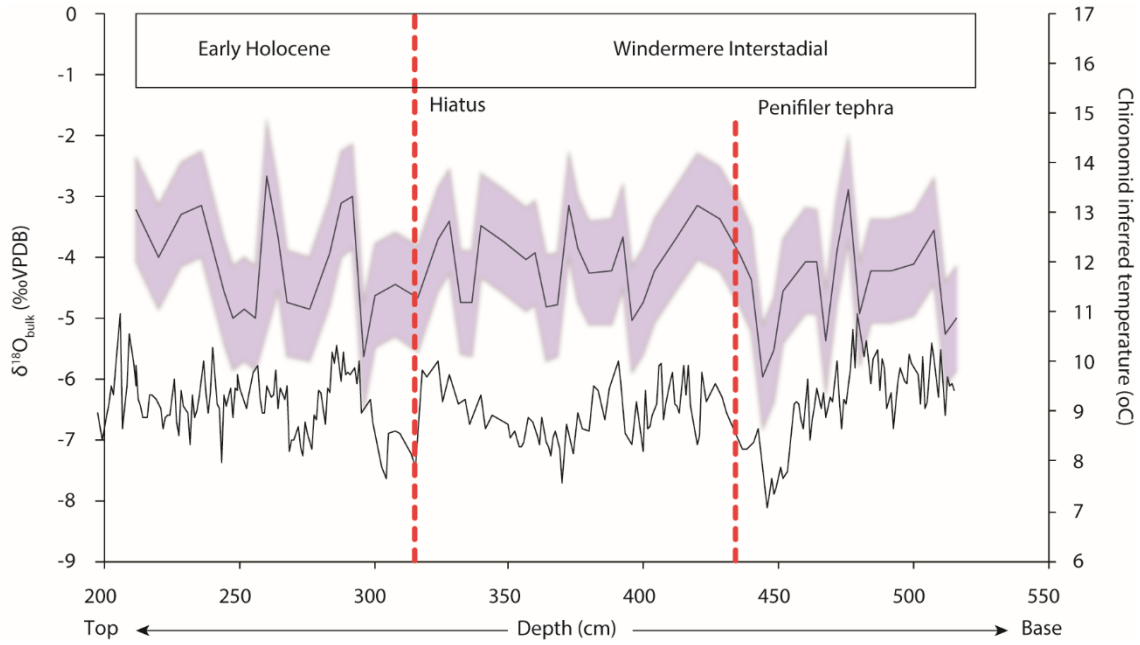

Figure 7.1. *Bulk lacustrine carbonate $\delta^{18}O$ values and C-ITs from Core B Palaeolake Flixton (Candy et al., unpublished). No age-depth model exists from these records, but the presence of the Penifiler Tephra confirms that deposition occurred during the LGIT.*

7.2.1.1. Lacustrine carbonate $\delta^{18}O_{bulk}$ values

The $\delta^{18}O_{bulk}$ record from PF consists of 244 samples taken at 1-3 cm intervals from carbonate-rich deposits in Core B (Figures 7.1-7.2). $\delta^{18}O_{bulk}$ values range between -4.94 and -8.12 ‰ and are characterised by initially high values (-4.94 to -6.81 ‰) between 516 and 480 cm, which then steadily downtrend, towards the location of the Penifiler Tephra (*ca.* 14.0 cal ka BP). Two distinct oscillations are present in the sequence prior to the Penifiler Tephra, which are located between 499-489 and 458-442 cm, with $\delta^{18}O_{bulk}$ values lowering to -6.81 and -8.12 ‰ respectively. Above the Penifiler tephra, $\delta^{18}O_{bulk}$ values become progressively higher and stabilise between 427 and 384 cm, before declining again to a minimum value of -7.70 ‰ at 370 cm. Above this interval, values steadily rise between 366 and 318 cm, before abruptly lowering between 318-315 cm, where a hiatus is present in the record (Palmer *et al.,* 2015). Above this interval, $\delta^{18}O_{bulk}$ values are constrained in time by a radiocarbon based age-depth model (Matthews *et al.,* unpublished data), being deposited between *ca.* 11.4 cal ka BP and 9.7 cal ka BP. The values in this interval remain low before rising to -5.55 ‰ at 289 cm (*ca.* 11.4-11.1 cal ka BP). A further oscillation is identified between 289-264 cm (*ca.* 11-10.8 cal ka BP) before the signal stabilises at the top of the sequence. The $\delta^{18}O_{bulk}$ values from PF are interpreted to be controlled primarily by mean annual air temperatures (Candy *et al.,* 2015; unpublished data) and therefore represent an analogous proxy to the WYKNE15 $\delta^{18}O_{bulk}$ values.

7.2.1.2. Chironomid-inferred temperatures (C-ITs)

The C-ITs are calculated from chironomid assemblages and are representative of mean July temperatures (i.e. TMax °C; Brooks *et al.,* 2012). The C-ITs are calculated from the same core (core B) as the $\delta^{18}O_{bulk}$ record, and can therefore be compared (Figure 7.3). C-ITs range between 14.81 and 8.64°C, with one prominent downturn, identified prior to the Penifiler tephra between 464 and 444 cm, where temperatures decline by between 2-4.5 °C to a minimum value of 8.64 °C. This downturn corresponds to the largest $\delta^{18}O_{bulk}$ depletion in the sequence where values reach -8.12‰ (section 7.2.1.1). Apart from this oscillation, the C-ITs record a series of lower amplitude oscillations prior to the sedimentary hiatus which range between 1-2°C in amplitude, reaching minimum temperatures >10 °C. Above the hiatus, values continue to fluctuate, broadly corresponding with the trend in $\delta^{18}O_{bulk}$ values (Figure 7.1).

7.2.2. Comparison of PF and Wykeham palaeotemperature records

7.2.2.1. Lacustrine carbonate $\delta^{18}O_{bulk}$ values

The $\delta^{18}O_{bulk}$ record from WYKNE15 can be compared to $\delta^{18}O_{bulk}$ records from PF (Figure 7.2). With the exception of EH, the $\delta^{18}O_{bulk}$ values from PF do not contain an age-depth model to directly compare records upon a common timescale. The $\delta^{18}O_{bulk}$ record from Core B in PF, is validated as LGIT in age, based upon: a) detailed sedimentological analysis of the basin infill (Cloutman, 1988 a; b; Palmer *et al.,* 2015), b) the presence of the Penifiler tephra in the Core B sequence at 428 cm, which has a modelled 2σ age range of 14.05-13.8 cal ka BP (Bronk Ramsey *et al.,* 2015). A tephra horizon in the WYKNE15 record (WN-T 292-294), is tentatively correlated to the Penifiler tephra based upon: a) shard morphology (Pyne-O'Donnell, 2007), b) an analogous age range calculated from the WYKNE15 age-depth model (Chapter 6). By using these horizons as tie points, the $\delta^{18}O_{bulk}$ values for each sequence can be correlated as follows.

The PF $\delta^{18}O_{bulk}$ record can be sub-divided into four zones (PF-I1-4) which show similar trends to WN-I3 to 5 (Figure 7.2). Values are initially high (PF-I1) but steadily decline (PF-I2-4), and are interrupted by 3 distinct zones of low $\delta^{18}O_{bulk}$ values (PF-I1b, 2b, 3a, 4a), which are correlated to WN-I3b, 4b and 5a (Figure 7.2). A further event is identified in the PF sequence where $\delta^{18}O_{bulk}$ values steadily increase (PF-I3b) before abruptly lowering again (PF-I4). This sequence is not represented in the WYKNE15 sequence. The reasons for this are thought to relate to the presence of a hiatus in the WYKNE15 record in WN-L3.

It is therefore apparent that the first major isotopic shift in the WYKNE15 record (WN-I3a, 15.1-14.6ka BP) is not present in the PF sequence, whilst PF-I4 is absent from the WYKNE15 sequence. The absence of the initial rise in $\delta^{18}O_{bulk}$ values in the PF sequence is attributed to an increased period of time for the PF depression to become a competent lake basin, able to sustain

authigenic carbonate formation (Chapter 11). The WYKNE15 sequence therefore contains the earliest palaeoenvironmental signal in the eVoP, and represents the earliest sediment record identified post ice recession from the valley.

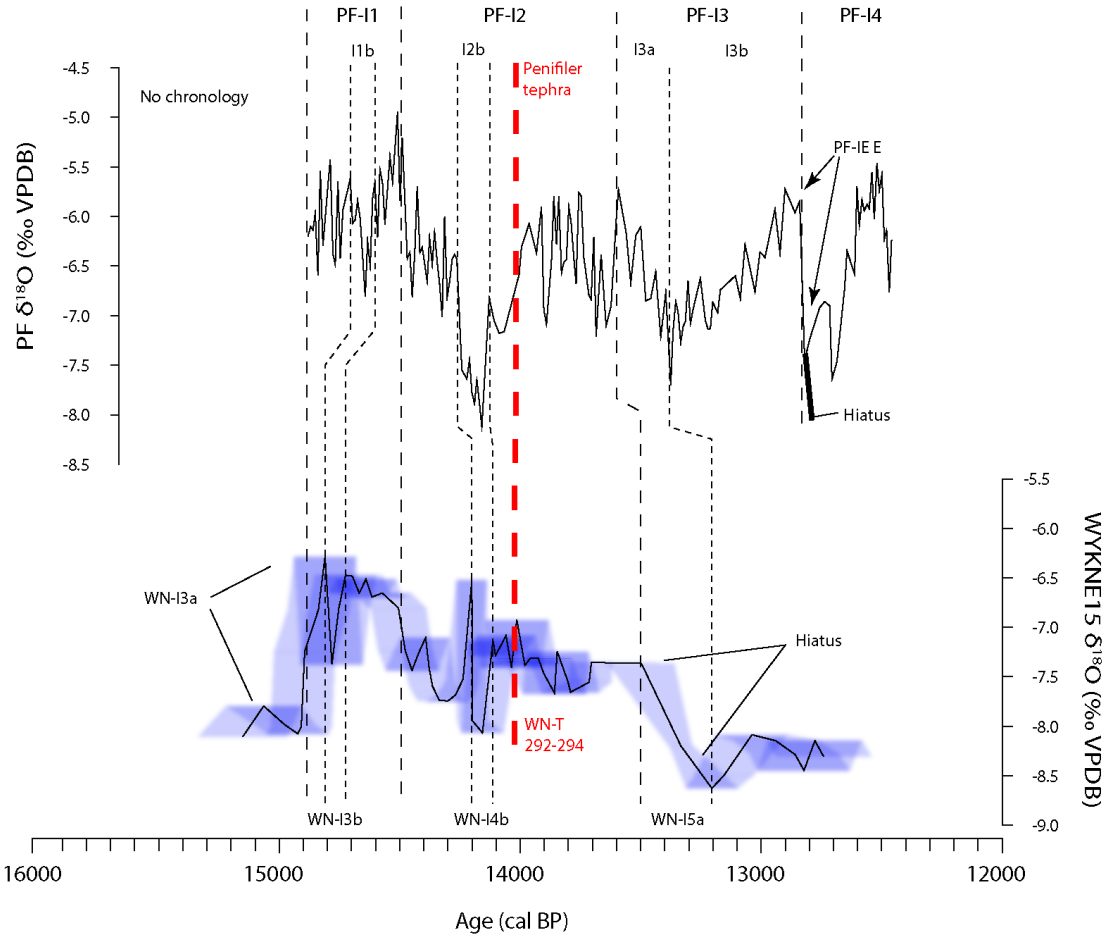

Figure 7.2. *Correlation of the $\delta^{18}O$ records from PF to the WYKNE15 $\delta^{18}O_{bulk}$. Trends are correlated based upon the structure and magnitude of the $\delta^{18}O$ values, coupled with the location of the Penifiler Tephra and the WN-T 292-294 tephra in the PF, and WYKNE15 sequences respectively.*

Although the $\delta^{18}O_{bulk}$ records have a similar structure, there is an offset in absolute values between the two datasets, with the WYKNE15 record containing lower $\delta^{18}O_{bulk}$ values (*ca.* 1-1.5 ‰), than the PF sequence. This is attributed to the carbonate from the WYKNE15 record deriving primarily from calcite precipitated in association with charophyte photosynthesis, which has been shown to result in lower $\delta^{18}O$ values than other lacustrine carbonates (Hoek *et al.,* 1999), due to kinetic effects during carbonate precipitation (Andrews *et al.,* 2004; Leng and Marshall, 2004). Comparable trends identified in the WYKNE15 and PF $\delta^{18}O_{bulk}$ records support that abrupt shifts in $\delta^{18}O_{bulk}$ values relate to regional climatic changes. Furthermore, the similar magnitude of isotopic events in the two records demonstrate that although there is an offset in absolute values between the two records, the offset is relatively uniform, and therefore the trends in the WYKNE15 record cannot be explained by varying sources of carbonate

composition through the sequence, or vital effects during carbonate precipitation (Leng and Marshall, 2004).

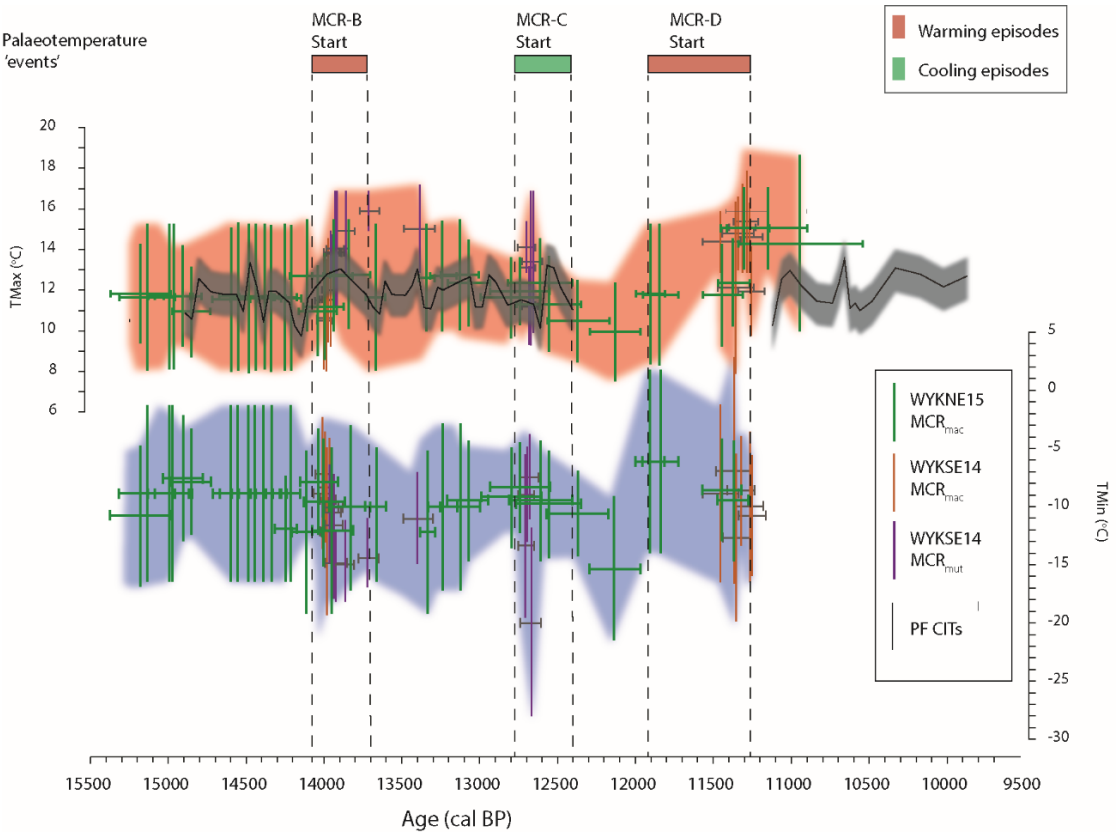

Figure 7.3. *Comparison of the Wykeham MCR record (Figure 6.27) to the PF C-IT reconstructions, showing a consistent overlap.*

7.2.2.2. Reconstructed $MCR_{mut,}$ TMax and C-ITs

The TMax values from macrofossils, coleopteran, and mutual-mutual MCRs from the Wykeham records can be compared to C-ITs from PF (Figure 7.3). This indicates that the TMax ranges from the Wykeham records are consistent with the C-ITs from PF. This strongly suggests that throughout the LGIT, variations in TMax in the eVoP were of a low amplitude, ranging between *ca.* 10-15 °C. Furthermore, lower TMax values recorded in Wykeham can also be identified in the C-IT record from PF. This is best expressed between 14.3-13.9 cal ka BP, where the most prominent deterioration in C-ITs of *ca.* 2-4.5 °C occurred in association with PF-I2b/WN-I4b, indicating this decrease in temperature is expressed in all of the eVoP records. Furthermore, this excursion indicates that decreases in $\delta^{18}O_{bulk}$ values during 14.3-13.9 cal ka BP can confidently be attributed to a deterioration in temperatures. This represents the most pronounced TMax oscillation through the WI, although the shift is still relatively muted in comparison to the change in $\delta^{18}O_{bulk}$ values (Figure 7.4). This can be attributed to the different temperature signals that the two datasets are recording, with the TMax and C-ITs recording changes in summer temperatures, and the $\delta^{18}O_{bulk}$ values recording variations in mean annual air temperatures. By implication, changes in winter temperatures must also have occurred through these events, and were of a higher amplitude than changes occurring during the summer. Further

correlations between these datasets are limited by the lack of chronological control in the PF record, but the consistent trends identified after the deposition of the Penifiler tephra in both of the sequences, demonstrate these records likely record changes in temperature through the eVoP, rather than local air temperature variations or hydrological changes (Figures 7.2-7.4).

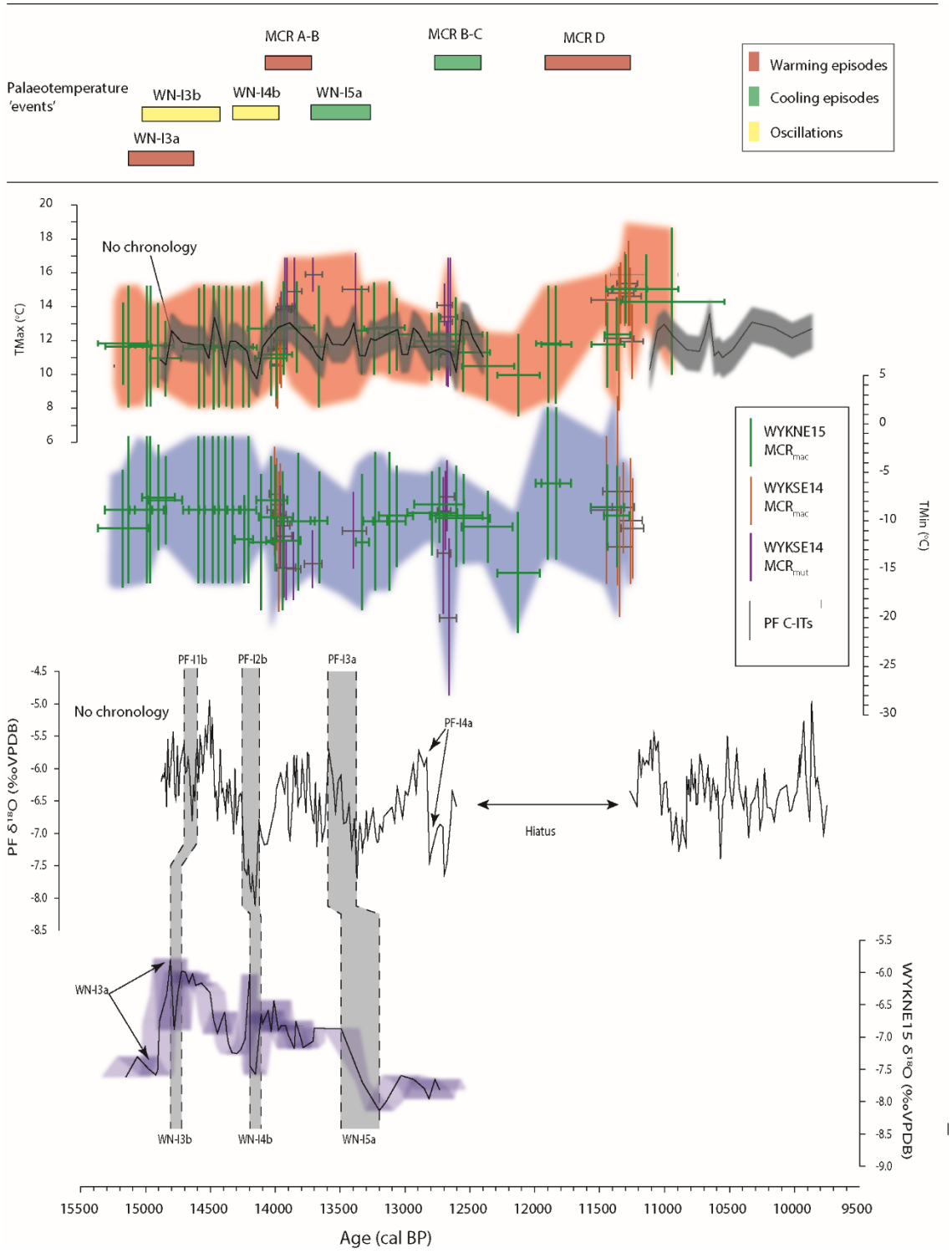

Figure 7.4. *Synthesis of measured $\delta^{18}O$ and MCR data from the eVoP. Also shown are palaeotemperature 'events' as described in main text*

7.3. Reconstructed LGIT Palaeohydrological variations in the eVoP

In lowland lake bodies, lake level variability can be reconstructed using variations in the sedimentological and palaeoecological characteristics of sedimentary sequences (Schnurrenberger *et al.,* 2003; Bos *et al.,* 2006; 2013; Jones *et al.,* 2011). This is based upon the assumption that changes in water depth affect a variety of biological, limnological, and sedimentological processes in the lake system (Cloutman, 1988a;b; Harrison and Digerfeldt, 1993; Hannon and Gaillard, 1997; Palmer *et al.,* 2015; Figure 7.5). The major source of information used to reconstruct changes in past water depths are derived from changes in sedimentological characteristics and local vegetation cover (plant macrofossils) of littoral lake sediments, which reflect the horizontal displacement of the littoral zone resulting from changes in water level (Harrison and Digerfeldt, 1993). Changes in water levels can be caused by various local factors including the opening and blockage of outflow streams, vegetation growth, or landslides; yet regionally synchronous changes in lake levels can be assumed to be driven by changes in the hydroclimate regime (Bohncke and Wijmstra, 1988; Magny, 2007; Charman *et al.,* 2009).

The sedimentological and palaeoecological data obtained from the Wykeham records show evidence of changes in relative lake levels. This is best demonstrated by the development of fen peat characterised by an increasing abundance of telmatic taxa such as *Carex sp.* in the WYKNE15 sequence between 13.65-13.25 and 13.3-12.8 cal ka BP (22.24-22.63 mOD; WN-L3, WN-M4). As these deposits are under- and overlain by littoral lacustrine sediments (WN-L2 and WN-L4; 19.04-22.24 and 22.62-23.13 mOD respectively), the lake level in Depression B must therefore have temporarily lowered during the deposition of WN-L3. The following sections outline evidence from the Wykeham records for changes in relative lake-level through the LGIT.

7.3.1. Palaeohydrological reconstructions from WYKNE15 (18.96-25.20 mOD)

The lithozones (WN-L1 to 6), and macrofossil zones (WN-M1 to 7), summarised in Table 7.1 enable the reconstruction of relative changes in lake level, in the WYKNE15 sequence. The sequence reflects the persistence of littoral lacustrine to eulittoral conditions between 18.96-25.20 mOD. The aquatic vegetation is monopolised by charophyte thalli casts between 15.6-14.8 and 13.65-13.25 cal ka BP and 13.3-12.8 to 13-12.2 cal ka BP (WN-M1-3; 18.96-22.24 mOD, and WN-L4; 22.62-23.13 mOD respectively), which are characteristic of shallow lacustrine environments, in water depths of up to 10 m (Hannon and Gaillard, 1997; Apolinarska *et al.,* 2011; Pelechaty *et al.,* 2013), but most commonly between 0-2 m (Hannon and Gaillard, 1997; Bos *et al.,* 2006). A shallow depth range for these charophyte meadows is supported by the presence of *Chara globularis* oospores in the sequence which most readily occupy shallow water bodies <4 m deep (Haas, 1994).

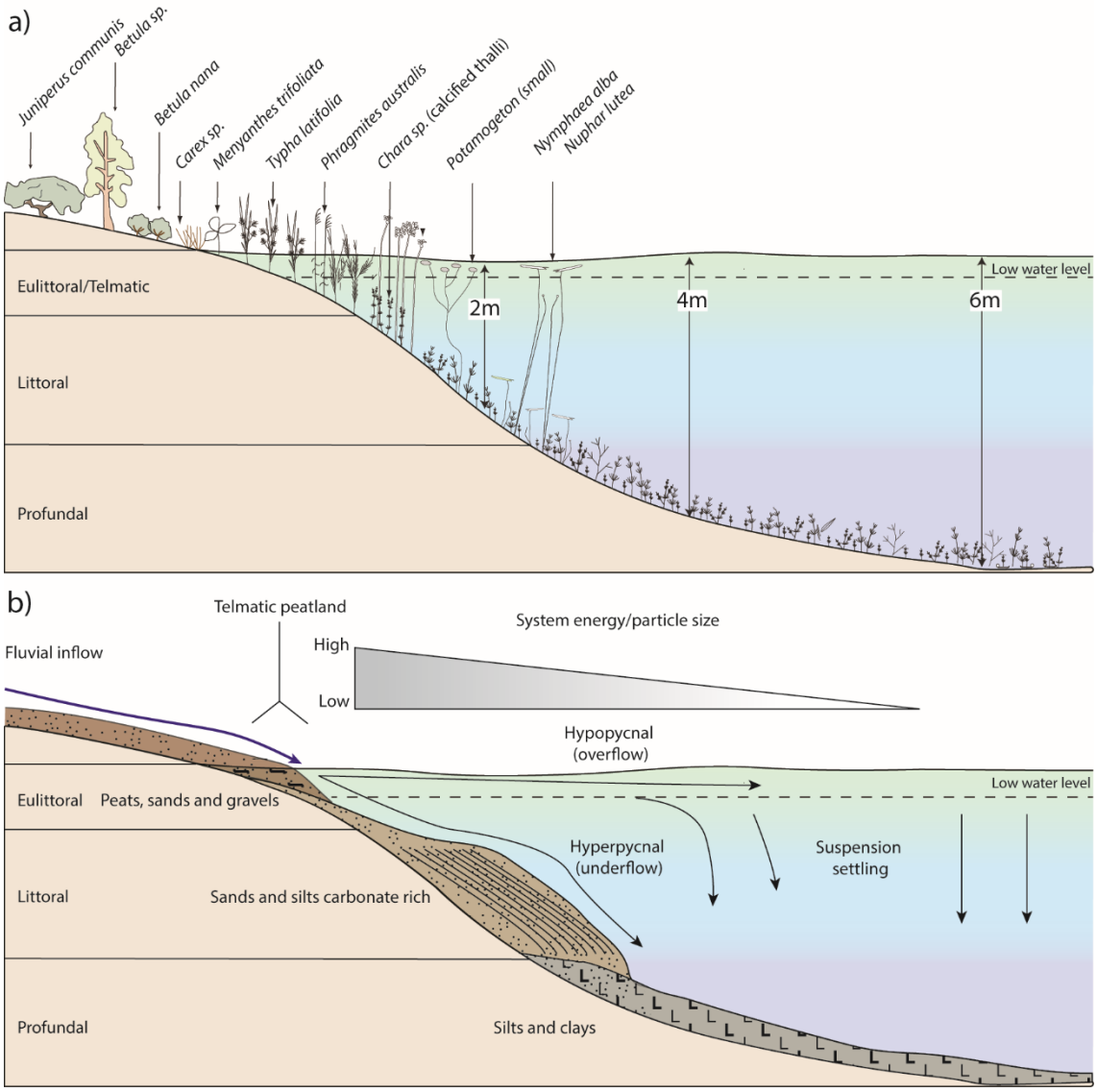

Figure 7.5. *a) Schematic lake showing the relationship between different plant taxa and water level in an idealised lacustrine system (adapted from Wiik et al., 2015), b) simplified schematic presenting the modes of clastic sediment dispersal in lake systems. The model demonstrates consistently coarser particle sizes in shallow sections of lake bodies, associated with high energy processes. The model also depicts the formation of telmatic peatland in the eutlittoral section of the lake (after Treese and Wilkinson, 1982; Harrison and Digerfeldt, 1993; Schilleref et al., 2014).*

Additionally, no other aquatic macrofossils characteristic of deeper water (e.g. large *Potamogeton*, *Myriophyllum spicatum, Nuphar lutea,* or *Nymphaea alba* seeds; Figure 7.5; Hannon and Gaillard, 1997; Sheldrick, 1997) are identified through WN-M1-3. Eulittoral taxa are also sparse through WN-M1-3 supporting that the WYKNE15 coring site remained submerged during deposition. Depths between *ca.* 1-2 m therefore represent the most likely range during the deposition of WN-M1-3, although it is acknowledged that the water body may have been lower (i.e. 0.25-1 m) or higher (2-4 m) through intervals.

Shifts from these conditions reflect changes in the hydrology of the lake body, typically relative shallowing, represented by the absence of thalli casts, and increasing abundances of shallow aquatics between 15.2-14.7 to 15.1-14.6 cal ka BP (WN-M2; 19.54-19.80 mOD) and 14.3-13.9 and 14.1-13.8 cal ka BP (WN-M3b; 21.76-22.02 mOD), or telmatic taxa/and peat development

Table 7.1. *Summary of the criteria used from the litho- and macrofossil assemblage zones to construct the hydrological model for the eVoP presented in Figures 7.6-7.7. These data are combined with lake level data from PF to construct lake level variability through the LGIT*

Zone	Elevation	Constraining criteria	Minimum (mOD)	Maximum (mOD)	References
WYKNE15					
WN-M1	18.96-19.54	*Chara sp.* thalli (most likely *ca.* +1-2 m), potentially 0.25-4 m	19.96 to 20.54	20.96 to 21.54	Hannon and Gaillard (1997); Bos *et al.,* (2006); Apolinarska *et al.,* (2011)
WN-M2/WN-L2b	19.54-19.72	*Juncus sp., Phragmites australis,* Gravel inwash, loss of *Chara sp.* (*ca.* <0-1 m)	<19.54 to <19.72	20.54-20.72	Hannon and Gaillard (1997)
WN-M3a	19.88-22.24	Initial continuation of *Phragmites,* then *Chara sp.* thalli (*ca.* +0-1 rising to *ca.* +1-2 m)	19.88-23.24	20.88-24.24	Boreham and West (1993); Hannon and Gaillard (1997); Bos *et al.,* (2006); Apolinarska *et al.,* (2011)
WN-M3b	21.76-22.02	Small *Potamogeton,* pleurocarps, loss *of Chara* thalli (*ca.* <+1 m)	<22.76-<23.02		Hannon and Gaillard (1997); Sheldrick (1997); Walker *et al.,* (2003)
WN-M4	22.63-23.13	Peat formation, telmatic taxa (+<1 m)	<22.63-<23.13	<23.63-<24.13	Hannon and Gaillard (1997)
WN-L5b	23.67-24.01	Sand and gravel deposition (<)	<23.67-<24.01	<23.67-<24.01	
WN-M7	24.33-25.20	Hydroseral succession, rise in telmatic taxa			Cloutman (1988a; b); Rodwell (1995)
WYKSE14					
WS-L3-5a	22.43				
WS-M3a	23.03-23.21	*Menyanthes trifoliata,* (<1 m)	>23.03->23.21	<24.03-<23.21	Hannon and Gaillard (1997); Rodwell (1995)
WS-M3a-3b	23.21	Hiatus (<)	<23.21	<23.21	
WS-M3b	23.21-23.42	*Menyanthes trifoliata, Carex rostrata.* (>*ca.* 0.25-<1 m)	Ca. 23.5-23.67	<24.21-<24.42	Hannon and Gaillard (1997); Rodwell (1995)
WS-M5a-5b	23.95-24.48	*Typha latifolia, Carex rostrata* (<1 m)	>23.95->24.48	<24,95-<25.48	Van Geel *et al.,* (1980); Hannon and Gaillard (1997)

between 13.65-13.25 to 13.3-12.8 cal ka BP (WN-M4/WN-L3; 22.24-22.62 mOD) and <11.8-11.2cal ka BP (WN-M7/WN-L6; 23.67-24.33 mOD). When compared to the palaeotemperature variations, it is evident that hydrological changes through the WYKNE15 sequence are closely linked to variations in regional temperature regimes.

7.3.2. Palaeohydrological reconstructions from WYKSE14 (22.30-24.48 mOD)

In the WYKSE14 sequence, the lithozones (WS-L1 to 10), and macrofossil zones (WS-M1-5), reflect deposition in a wetland/shallow lacustrine environment. Sedimentation initiates in the sequence at 22.30 mOD at 14.15-13.9 cal ka BP. Soon after this, the deposition of well sorted sands and organic rich beds (WS-L3-5a; 22.43-22.47 mOD) interbedded with fine-grained deposits (WS-L2 and WS-L5b), suggests that the lake level temporarily lowered. The deposition of the coarse-grained beds between 14.1-13.9 and 14.05-13.85 cal ka BP is closely associated with the lower lake levels reconstructed in the WYKNE15 sequence (WN-M3b). A similar transition in the record between 12.475-12.35 and 11.65-11.2 cal ka BP (WS-L8b; 23.64-24 mOD) is also interpreted to represent lower lake levels.

The expansion of eulittoral taxa in WS-M3a-3b represents an environment of in <1 m water depth (Hannon and Gaillard, 1997). The presence of *Menyanthes trifoliata* substantiates that sedimentation occurred in very close association with the water table (Rodwell, 1995) from 14.05-13.8 to 13.55-12.9 cal ka BP (WS-M3a; 23.03-23.21 mOD). A hiatus in the sequence between 13.55-12.9 to 12.8-12.65 cal ka BP (WYKS-MFAZ 3a to 3b; 23.21 mOD) represents lower lake levels during this interval (Chapter 6). This occurs at a similar time to the deposition of peat in the WYKNE15 sequence (WN-M5/WN-L3; 22.24-22.62 mOD) and therefore represents a regional lowering of the groundwater table. A rise in relative lake levels are reconstructed between 12.8-12.65 cal ka BP (WS-M3b; 23.21-23.42 mOD), and 11.65-11.2 cal ka BP (WS-M5a; 23.95-24.18 mOD) based upon the occurrence of eulittoral and aquatic taxa into the sequence, representing sequential hydroseral succession (Cloutman, 1988a; b). This final rise appears to have been temporarily perturbed at 11.65-11.2 cal ka BP (24-24.04 mOD), which is indicated by the temporary expansion of *Urtica dioica* in WS-L9a. The WYKSE14 sequence infills via hydroseral succession between 11.44-11.2 and 11.35-11 cal ka BP (24.18-24.48 mOD; WS-M5a).

7.3.3. Palaeohydrological reconstructions from PF

Previous attempts to reconstruct lake levels in the eVoP have focussed upon EH littoral-eulittoral lake sediments at the margins of PF, associated with Early Mesolithic occupation at Star Carr (Cloutman *et al.,* 1988a; b; Taylor, 2011). These records demonstrate that water levels steadily rose in PF (from *ca.* 23-25 mOD), during the EH before infill via hydroseral succession between 22-24 mOD at *ca.* 10.75-10.5 cal ka BP (Taylor, unpublished data).

WI lake levels have been reconstructed to a level of *ca.* 23 mOD by Palmer *et al.,* (2015), based upon the distribution and elevation of marl and peat within the basin. This reconstruction is limited in the following ways: first, the lack of detailed analysis on littoral WI-aged sediments preclude the development of a detailed model of relative lake level change. Second, the lack of any robust chronology limits the comparison of this reconstruction to that from the Wykeham records. The data from Wykeham Quarry suggest that it is highly unlikely that PF existed as a stable lake system at 23 mOD throughout the WI, particularly considering the high amplitude climatic oscillations during this period, which are shown to alter lake levels at Wykeham.

Changes in lake levels during the late WI and early LLS are, in part, constrained by four radiocarbon dates (CAR-874, CAR-880, CAR-883, CAR-1027) obtained on littoral lake sediments at 23 mOD by Cloutman (1988a; b). These deposits demonstrate a rise in relative lake levels between *ca.* 13.05-12.7 cal ka BP. Little emphasis was placed upon these ages however as it was not the main focus of the project and the potential that these ages had for hard water error (Cloutman, 1988a; b). The consistent age ranges however provide supporting evidence for a rise in PF lake levels during this interval.

7.3.4. Comparison of palaeohydrological datasets from the eVoP

The hydrological datasets from the eVoP show consistent trends in relative lake level changes, with coincident episodes of lower (*ca.* 14.1-13.9 cal ka BP, *ca.* 13.55-12.8 cal ka BP, *ca.*12.65-11.8 cal ka BP) and higher (*ca.* 12.8-12.65 cal ka BP, *ca.* 11.8-11.3 cal ka BP) lake levels. Two of these relative changes (i.e. rising levels between *ca.* 12.8-12.65 cal ka BP, and 11.8-11.3 cal ka BP) are also represented in PF records. Furthermore, these shifts occur in close association with changes in palaeotemperatures in the eVoP which supports that the lake level changes recorded in these records are: a) consistent across the eVoP, b) linked to changes in local-regional palaeoclimatic regimes through the LGIT.

7.4. Developing a hydroclimatic event stratigraphy for the eVoP during the LGIT

MCRs between 15.5-14 cal ka BP in the WYKNE15 sequence show consistent summer and winter temperature ranges through a period where the WYKNE15, and PF stable isotopic datasets show variability. This can be attributed to: a) the low number of macrofossils used to create the MCRs (mostly *Betula nana* in isolation), b) the lack of supporting coleopteran MCR estimates, resulting in wide TMax and TMin ranges, c) a lag in the response time of thermophilous vegetation colonising the eVoP after WN-I3a (15.1-14.6 cal ka BP), d) different palaeotemperature signals recorded in the two datasets. On this basis, measured $\delta^{18}O$ values of lacustrine carbonates are used preferentially as a proxy for temperature changes in the eVoP, and form the basis for the LGIT stratigraphy of the area.

Changes in relative lake levels across the eVoP sequences record similar trends through the LGIT. By combining the evidence for water level changes in WYKNE15, and WYKSE14, and using the derived elevation for these changes within each sequence, a model of the elevation range of the water table in the eVoP can be constructed (Figures 7.6-7.7). This model uses the water depth ranges reported in Hannon and Gaillard (1997) and Bos *et al.,* (2006) alongside the radiocarbon ages for specific lake levels of PF reported in Cloutman (1988a; b), and Taylor (2011) allowing for a more robust reconstruction.

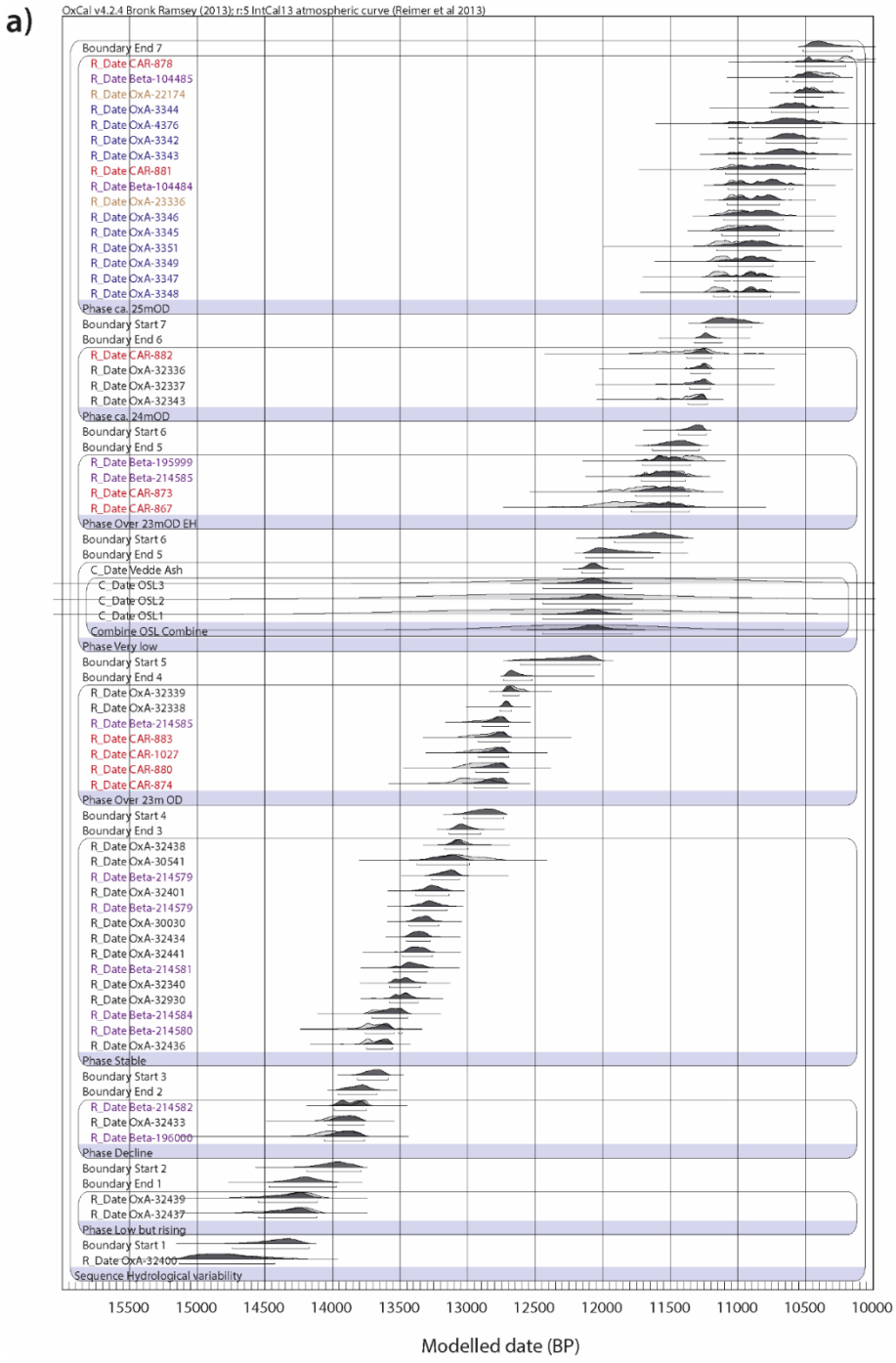

Figure 7.6. *Phase model of radiocarbon, OSL, and tephra ages used to constrain the elevation of the water table in the VoP. Purple ages are those from Franks et al. (2009), red dates are from Cloutman (1988) and black dates are from this study.*

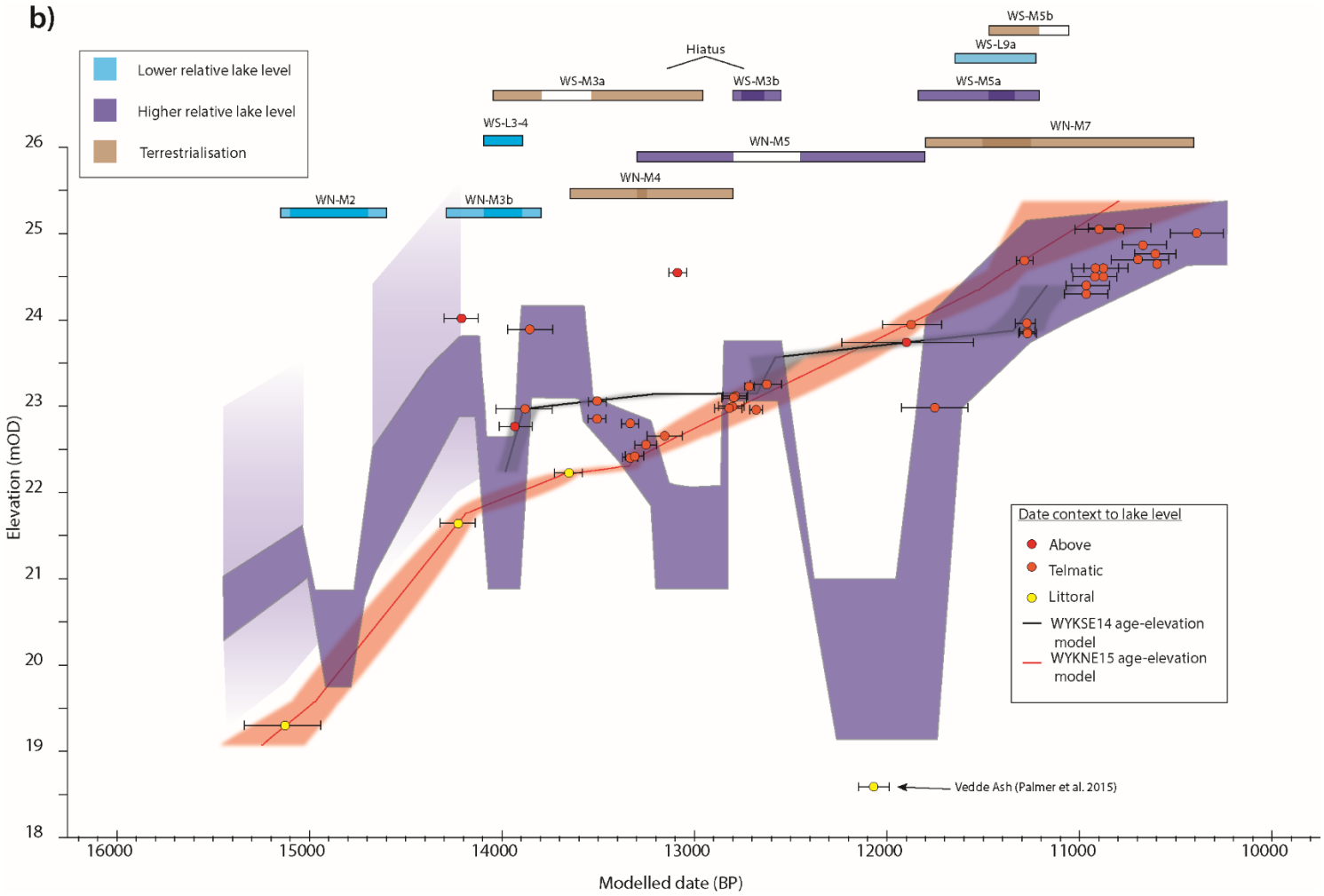

Figure 7.7. *Model of water table variability in the eVoP during the LGIT (dark blue ribbon represents most likely range), using the dates presented in Figure 7.6. The model uses the ecological niches of preserved macrofossils in the WYKNE15 and WYKSE14 sequences (Hannon and Gaillard, 1997; Rodwell, 1995) to estimate the elevation of the water table at the time of deposition. Light blue shading represents potential water depths associated with the presence of charophyte thalli in the WYKNE15 sequence. The rationale for this range is discussed in text.*

Both the WYKSE14 and WYKNE15 sequences are derived from the littoral section of small lake systems which would have been sensitive to variations in lake level (Bos *et al.,* 2006; Jones *et al.,* 2011). The principal controlling factor on the lake levels in Depression B (WYKNE15), and Depression C (WYKSE14) would have been changes in groundwater availability, which is primarily determined by rates of catchment precipitation and evaporation (Cohen, 2003). This is also true of PF, which was fed by local groundwater during the LGIT (Candy *et al.,* 2015; Palmer *et al.,* 2015). All three lake bodies would have been sourced by the same aquifer (Atkinson, *pers. comm.*), and therefore, local changes in the hydrology of the eVoP should have been recorded in a similar manner in all basins, probably relating to net changes in effective precipitation (Harrison and Digerfeldt, 1993; Magny, 2007). The radiocarbon dates obtained on deposits by Fraser *et al.* (2009) can also help verify the observations made from these studies as they are sampled LfA-5 deposits (fen peats), which must have been sensitive to groundwater variability (Rodwell, 1995). The relative depth ranges for shallow aquatic and telmatic taxa are well established (e.g. Harrison and Digerfeldt, 1993; Rodwell, 1995; Hannon and Gaillard, 1997), and have been frequently used to assign water depth ranges to palaeolake bodies (van Geel *et al.,* 1989; Harrison and Digerfeldt 1993; Magny *et al.,* 1995; Sheldrick 1997; Bos *et al.,* 2006; Magny *et al.,* 2006; Jones *et al.,* 2011; Bos *et al.,* 2013; Wiik *et al.,* 2015). Using these depth ranges, coupled with the lithozone changes and the age models constructed for each record, a composite model of groundwater elevation change in the eVoP can be constructed (Figure 7.7).

7.4.1. Uncertainties in palaeotemperature and palaeohydrological reconstructions

7.4.1.1. Palaeotemperature reconstructions

Uncertainties in the MCR_{mac} records can be attributed principally to: a) the low number of macrofossil taxa used to reconstruct TMax and TMin ranges (Isarin and Bohncke 1999; Aarnes *et al.,* 2012), and the lagged response time of vegetation to climatic events (Pennington, 1986; Walker *et al.,* 1993). Furthermore, TMax and TMin ranges reported by Aarnes *et al.* (2012) are calculated via the present distribution of taxa in relation to contemporary climates. It is noted that temperature is only one environmental variable that controls floral migration and growth, with other criteria such as soil development, light availability and catchment hydrology also affecting the distribution of vegetation (Birks and Birks, 2014). This is also true for the other biological proxies including chironomids which are known to respond to variables such as pH, substrate morphology, salinity and food availability (Brooks *et al.,* 2007). The consistent temperature ranges reconstructed in all palaeoecological datasets however, demonstrate that changes in temperature were a dominant control on the distribution of taxa. The changes in summer temperatures are relatively subdued throughout the LGIT, which invoke significantly larger shifts in winter temperatures during the isotopic oscillations, that reflect changes in mean

annual air temperature. The TMin ranges however are too wide to ascertain any significant shifts in winter temperature change.

In order to improve these temperature estimates, larger numbers of stenothermic macrofossils with specific warm or cold tolerances are required. Furthermore, TMax and TMin ranges on a larger number of taxa than those reported in Aarnes *et al.* (2012) are also required to further constrain the temperature ranges through these records.

7.4.1.2. Palaeohydrological reconstructions

It is accepted that the absolute values of the hydrological model are likely to contain systematic errors associated with: a) the depth ranges assigned to taxa, b) the potential for macrofossil reworking, c) elevation offsets between the water bodies in the eVoP, d) short intervals of lake level changes not detected by the sampling resolution of the macrofossil datasets. This is most prevalent in the early stages of the record (i.e. > *ca.* 14 cal ka BP) where the water table elevation is reconstructed principally using the presence of *Chara* thalli. These macrofossils can be confidently placed into a subaqueous depositional environment (Magny, 2012), but are known to occupy wide depth ranges (Haas, 1994; Magny and Ruffadi, 1995; Hannon and Gaillard, 1997). Further evidence (e.g. transect cores from the margins of the basin to the centre; Bos *et al.,* 2006; Jones *et al.,* 2011) would be required to constrain the model through these intervals further.

The water table model (Figure 7.7) is therefore a smoothed guide to the variation in hydrological regimes in the eVoP that best explains the observed trends in all datasets and provides a testable model for the evolution of groundwater through the LGIT (Palmer *et al.,* 2015).

7.4.1.3. Chronological uncertainties

Chronological uncertainties are derived principally from the integrity of the age-depth models constructed for the palaeoenvironmental sequences. Uncertainties include: a) the integrity of dated material (Turney *et al.,* 2000), coupled with site-specific factors such as hard-water error which is common in catchments consisting of carbonate-rich bedrock b) a lack of precision in calibration curves used to convert radiocarbon ages to calendar time (Guilderson *et al.,* 2005; Blockley *et al.,* 2007; Reimer *et al.,* 2013) c) variability in sedimentation rates not captured by the sampling resolution of radiocarbon ages. Here, terrestrially derived macrofossils were used, which are least prone to hard water error, and should most accurately reflect the age of sediment deposition (Wohlfarth *et al.,* 1996; Blockley *et al.,* 2007; Lowe *et al.,* 2008). Uncertainties also derive from in the IntCal13 calibration curve, particularly >14 cal ka BP where standard deviation ranges for the calibration curve are significantly larger than <14 cal ka BP, increasing age uncertainties (Reimer *et al.,* 2013). The ages of the palaeoclimatic reconstructions

are presented as 2σ calibrated age ranges to best express the statistical uncertainties present in the age modelling approach (Bronk Ramsey, 2008; Lowe *et al.,* 2008).

The variations in variations in particle size and organic content of the WYKNE15 and WYKSE14 sequences demonstrate evidence for variable sedimentation rates and hiatuses through the LGIT. To account for these shifts, *P_Sequence* models were run with a k_0 factor and boundaries at lithostratigraphic horizons to best account for changes in sedimentation rate and hiatuses (Bronk Ramsey, 2013).

Outlier ages in WN-L3-4 (OxA-32441 and OxA-32434) however produce large uncertainties between *ca.* 13.4-12 cal ka BP in the WYKNE15 sequence, and these uncertainties therefore limit the correlation of the hydrological and palaeotemperature models. The hydrological model demonstrates that a hiatus likely exists in the WYKNE15 sequence between ca. 13.2-12.8 cal ka BP (Figure 7.7). This is supported by the WYKNE15 and PF $\delta^{18}O_{bulk}$ datasets which diverge across this interval, with $\delta^{18}O_{bulk}$ values steadily rising in the PF record whilst $\delta^{18}O_{bulk}$ values in the WYKNE15 record remaining low.

If a hiatus does exist in the WYKNE15 record in WN-L3, and the rise in water levels between the two basins is synchronous, then the lower $\delta^{18}O_{bulk}$ values in WN-I5 would reflect climatic conditions between *ca.* 12.8 and 12.65 cal ka BP (Figure 7.7) rather than 13.7-13.4 cal ka BP, as is shown in the present age model. As with the WYKSE14 sequence, the rise in the water table (WN-M5) is reconstructed during colder climatic conditions (reflected by low $\delta^{18}O_{bulk}$ values in WN-I5) in the WYKNE15 record. Constraining these events relied upon radiocarbon samples consisting of *Carex sp.* achenes, which have been shown to produce erroneously old ages (Turney *et al.,* 2000).

Leaf fragments of *Salix herbacea, S.polaris,* and *Betula nana* in WN-M5, identified after the production of the radiocarbon samples, would in the future, provide a means to address the chronological uncertainty through this stage of the sequence. These remains are more fragile, and therefore less likely to have been physically transferred or reworked from older deposits in the catchment than *Carex* sp. achenes (which were used in OxA-32441 and OxA-32434), which are more likely to represent secondary deposition into the lake body in WN-M5 (Turney *et al.,* 2000).

7.5. Synthesis of palaeotemperature and palaeohydrological variations in the eVoP during the LGIT

A summary of the palaeoenvironmental reconstructions from the VoP is presented in Figures 7.8 and 7.9 and discussed below.

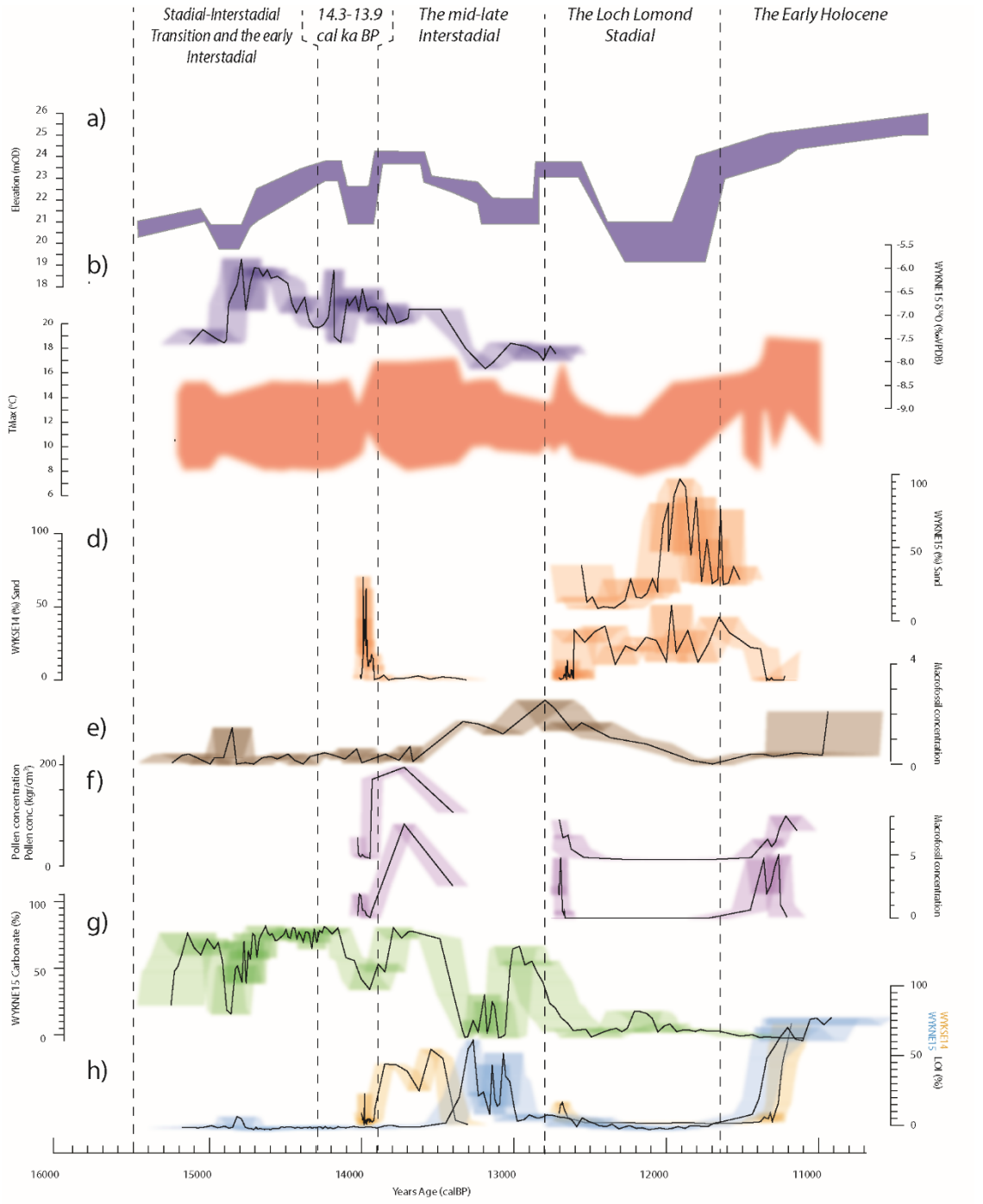

Figure 7.8. *Summary of the palaeoenvironmental datasets and models developed from the eVoP in this thesis. a) water table elevation model for the eVoP, b) $\delta^{18}O_{bulk}$ record from the WYKNE15 sequence, c) TMax MCR reconstructions from the Wykeham records, d) siliclastic sand (%) of the WYKNE15 and WYKSE14 sequences, e) Macrofossil concentration (per 20 cm³) from the WYKNE15 sequence, f) pollen and macrofossil concentrations from the WYKSE14 sequence, g) Calcium carbonate (%) in the WYKNE15 sequence, h) LOI (%) from the WYKNE15 (blue) and WYKSE14 (yellow) sequences. The time-slices discussed in section 7.5 are labelled for reference.*

7.5.1. The Stadial to Interstadial transition and the Early-Windermere Interstadial ca. 15.5 – 14.3 cal ka BP

At 15.5-14.8 cal ka BP, regional temperatures had ameliorated sufficiently to enable the formation of a shallow (*ca.*1-2 m deep) lake body in Depression B occupied by high volumes of calcified charophyte thalli (WN-L2). For these structures to form, a lake body must have existed in during this interval, meaning that the infill of the WYKNE15 sequence occurred consistently below the water table (Jones *et al.,* 2011).

The North Sea Ice Lobe may still have been in the vicinity at this time (Bateman *et al.,* 2015; Evans *et al.,* 2016), suggesting mean annual temperatures were low, and permafrost may have persisted in the eVoP. This is supported by the low $\delta^{18}O_{bulk}$ values in WN-I1, although remains of *Betula nana* found in this interval, imply summer and winter temperatures were no lower than 8 and -17°C respectively (Aarnes *et al.,* 2012), and the formation of authigenic carbonate in the WYKNE15 sequence support that temperatures were warm enough for a springline to form.

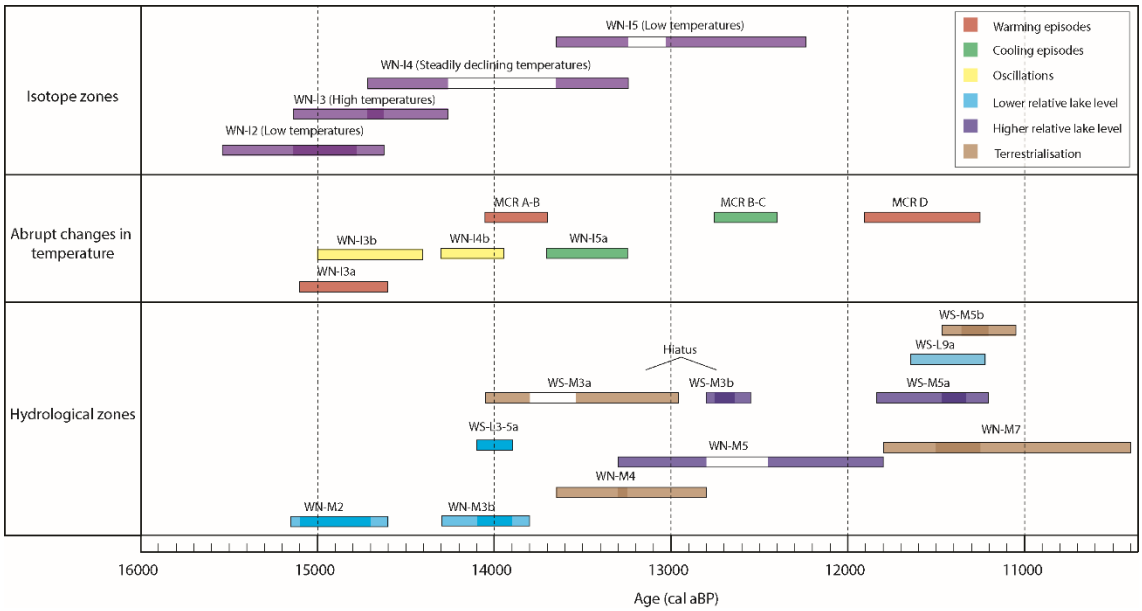

Figure 7.9. *Summary of the palaeoclimatic zones identified in the Wykeham Quarry sequences. Bars represent the 2σ age ranges for the start and end of each interval, with darker bands representing overlap between the start and end ages.*

At 15.1-14.6 cal ka BP, mean annual air temperatures rose abruptly (WN-I3a), and there was an associated drop in the relative lake level in Depression B (WN-M2). This is supported by the absence of calcified charophyte thalli, and the presence of eulittoral and terrestrial taxa in WN-M2 (19.54-19.72 mOD), coupled with the deposition of sorted gravels in WN-L2a (Harrison and Digerfeldt, 1993) between *ca.* 15.15-14.7 cal ka BP. Eulittoral taxa consist of *Phragmites australis* remains and *Juncus* sp., which indicate that lake levels ranged between 0-1 m above the infill of the WYKNE15 sequence during this interval (Hannon and Gaillard, 1997).

The drop in lake level is interpreted to represent the melting of permafrost, and buried ice in the eVoP outwash plain (LfA-2), as temperatures ameliorated, allowing water to freely drain through the substratum of glaciofluvial sediments (Hoek, 1997). This abrupt amelioration marks the onset of the WI in the VoP. Optimum mean annual air temperatures were attained between 15.1-14.6 and 14.7-14.25 cal ka BP (WN-I3), which melted residual dead ice in the PF depression, leading to increases in effective precipitation, raised water levels (Bos *et al.,* 2013), and authigenic carbonate formation in PF and Depression B. This occurred prior to the isotopic downturn at 15-14.5 cal ka BP (WN-I3b), which is recorded in both the PF and WYKNE15 records, and is interpreted as an abrupt climatic oscillation during the E-WI (Brooks and Birks, 2000; Marshall *et al.,* 2002). At 14.7-14.25 cal ka BP, mean annual air temperatures began to steadily decline

(WN-I4a). During this phase, the water levels in Depression B remained consistently above the infill elevation of the WYKNE15 sequence, with charophyte thalli casts being consistently preserved.

This depth range is interpreted to have remained no more than *ca.* 2 m above the infill of the WYKNE15 sequence, as no aquatic macrofossils which are characteristic of deeper water (e.g. large *Potamogeton, Nuphar lutea,* or *Nymphaea alba* seeds; Hannon and Gaillard, 1997) are present through WN-M1-3. Furthermore, the lack of lacustrine deposits of this age elsewhere at Wykeham Quarry support relatively low lake levels during this period, preventing the formation of lake bodies in the shallower depressions of the quarry area. The basal radiocarbon age in Depression A (RHULBHN-13; OxA-32439; Chapter 6) at *ca.* 24 mOD produces an age of 14.65-14.05 cal ka BP, which is significantly after the infill of Depression A. These ages confirm that a lake was formed in Depression B earlier than Depression A. The most likely explanation for this offset is that the water table was not high enough during the E-WI to form a lake body in Depression A, and the radiocarbon date obtained from the base of the RHULBHN-13 sequence represents the first instance of stable conditions in the depression. This radiocarbon date was derived from twigs with no evidence of aquatic or telmatic material which would suggest that even at this interval, open water did not persist >24 mOD in Depression A. For these reasons, the lake level during the deposition of WN-L2 (19.04-22.24 mOD) is interpreted to range from between *ca.* 1-2 m above the infill of the WYKNE15 sequence on the basis of *in situ* calcified charophyte thalli, and supporting evidence outlined above.

7.5.2. Transition from the Early to Mid-Late Windermere Interstadial ca. 14.3-13.9 cal ka BP

Between 14.3-14.1 and 14.3-13.85 cal ka BP an abrupt oscillation in mean annual air temperatures is reconstructed from the eVoP $\delta^{18}O_{bulk}$ records (WN-I4b), as well as the PF C-ITs and MCR_{mut} temperatures from WYKSE14 (MCR A-B). This centennial-scale climatic deterioration led to a decline in groundwater levels. The decline in temperature and lake levels in Depression B were offset during this event, with the temperature deterioration leading the hydrological shift, which occurs after $\delta^{18}O_{bulk}$ values have risen out of WN-I4b. Lake levels must have initially been sufficiently high to form standing water in Depression C (WYKS-LZ2; 22.30-22.43 mOD; 14.15-13.9 cal ka BP), enabling the deposition of fine grained deposits with authigenic carbonate content. Soon after this, the deposition of well sorted sand beds and organic rich beds (WYKS-LZ 3-5a; 22.43-22.47 mOD), in the WYKSE14 sequence demonstrate shallower relative lake levels (Harrison and Digerfeldt, 1993) in comparison to WS-L2 and WS-L5b (Figure 7.8).

A shift in relative lake level and/or chemistry reconstructed through WN-M3b/WN-L2d (21.76-22.02 mOD;14.3-13.9 to 14.1-13.8 cal ka BP) in the WYKNE15 sequence is characterised by the loss of charophyte thalli, the influx of littoral aquatic taxa (e.g. small type *Potamogeton* seeds and pleurocarp mosses), and the decrease in bulk carbonate content. The aquatic taxa in WN-M3b

have wide depth tolerances (Harrison and Digerfeldt, 1993; Hannon and Gaillard, 1997), but *Potamogeton* small type seeds reflect shallower water depths <1 m (Sheldrick, 1997; Walker *et al.,* 2003), supporting a lower relative lake level in the WYKNE15 sequence during this interval.

The timing of these events in the Wykeham records overlap, which suggests a consistent decline in the groundwater levels between 14.3-13.9 cal ka BP, probably due to a decline in effective precipitation and enhanced aridity. Enhanced aridity can favour frequent natural fires in temperate environments (Veblen *et al.,* 2006), and this accounts for increased abundances of macrocharcoal, and burnt organic remains including *Juniperus communis* needles in WS-M1 (22.3-22.78 mOD) and WN-M3b-3c (22.02-22.24 mOD).

7.5.3. Mid-Late Interstadial ca. 13.9-13 cal ka BP

After the temporary decline in relative groundwater elevation between 14.3-13.9 cal ka BP, lake levels in the Wykeham records rise and remain stable between *ca.* 13.9-13.6 cal ka BP. This is based upon the reintroduction of charophyte thalli-rich deposits in the WYKNE15 sequence (WN-M3; WN-L2; 22.02-22.24 mOD), and organic-rich silts, clays and peats in WYKSE14 (WS-M3a; WS-L6; 23.03-23.21 mOD). The presence of telmatic, eulittoral taxa such as *Menyanthes trifoliata,* and *Carex* sp., and wood fragments show that the groundwater elevation was close to the WYKSE14 infill elevation during this interval (<1 m, *ca.* >23.2-<24.1 mOD).

Between 13.65-13.25 and 13-12.25 cal ka BP, mean annual air temperatures declined (WN-5a), and groundwater lowered to levels that created a hiatus in the WYKSE14 sequence (WS-M3a-3b; at 23.21 mOD), and the development of fen peat in the WYKNE15 record (WN-L3/WN-M4 at 22.4-22.62 mOD). Based upon these criteria, the groundwater level must have lowered to below 22.63 mOD, although the minimum level obtained is poorly constrained as no dated deposits exist from below the water table during this period. Low lake levels are best expressed in the WYKSE14 sequence by the hiatus between *ca.* 13.5-12.8 cal ka BP (WS-M3a-3b).

The PF and WYKNE15 $\delta^{18}O_{bulk}$ records diverge across the formation of WN-L3, further supporting the interpretation of a hiatus in the WYKNE15 record and/or an alternative control on the PF isotopic values. The lower water table reconstructed between *ca.* 13.5-12.8 cal ka BP (Figure 7.7-7.8) provides a means to produce a hiatus in the WYKNE15 sequence, and a more evaporitic signal in the isotopic dataset in PF (Leng and Marshall, 2004). These trends support lower amounts of effective precipitation reaching the eVoP groundwater table during the latter stages of the WI. The rise in the in PF and WYKSE14 lake levels between 12.8-12.65 cal ka BP (WS-M3b) is therefore considered to correspond to the rise in lake levels in the WYKNE15 sequence in WN-L4/WN-M5.

The $\delta^{18}O_{bulk}$ records through this period are less reliable, primarily due to the ambiguity of sedimentation rates (see above). On the criteria outlined above, WN-I5a is interpreted to

represent the decline in temperatures across the WI-LLS transition, with a sedimentary hiatus in the WYKNE15 record in the fen peats of WN-L3 (Figure 7.9).

7.5.4. Loch Lomond Stadial ca. 13-11.7 cal ka BP

Cold temperatures (MCR B-C), coupled with a rise in lake levels are reconstructed from the WYKSE14 sequence between 12.8-12.4 cal ka BP (WS-L7/WS-M3b; 23.21-23.42 mOD) with minimum TMin ranges reaching -20°C. $\delta^{18}O_{bulk}$ values from the WYKNE15 sequence also reflect cold temperatures through this interval, although the age model through is more poorly constrained. The timing of this rise is well constrained by two radiocarbon dates in WS-L7 (OxA-32339 and OxA-32338), showing that sedimentation rates during this interval were high. Therefore, this high lake level stage is interpreted to have been short-lived, finishing at *ca.* 12.6-12.65 cal ka BP. This is supported by radiocarbon dates from PF (CAR-874, CAR-880, CAR-883, CAR-1027; Cloutman 1988a), which demonstrate the presence of groundwater at, or above 23 mOD at a similar interval to that reconstructed in WS-M3b.

Between *ca.* 12.5 and 11.9 cal ka BP, the quantitative palaeoclimatic reconstructions from the eVoP are not possible, owing to: a) the lack of authigenic carbonate required for $\delta^{18}O_{bulk}$ measurements, b) increased siliclastic particle sizes, demonstrating higher energy deposition, precluding macrofossil deposition/preservation. Sedimentation during this phase was most likely discontinuous (Palmer *et al.,* 2015), with hiatuses in records reflecting low organic productivity, and low effective precipitation regimes.

These trends demonstrate a consistent drop in eVoP lake levels through the LLS. In PF, levels are reconstructed to a maximum elevation of *ca.* 21 mOD on the basis of LLS-aged sedimentary infill, and the presence of the Vedde Ash (12.02 $\pm$ 0.04 cal ka BP; Bronk Ramsey *et al.,* 2015) at 18.66 mOD in core C (Palmer *et al.,* 2015). This ash layer must have been deposited sub-aqueously (Palmer *et al.,* 2015), meaning that PF must have been above this elevation during the deposition of the tephra. Vedde Ash shards are reworked to a maximum altitude of 20.54 mOD in 'Core C', which invokes lake levels at *ca.* 21 mOD after its deposition. This is supported by the sediments in 'Core B' in PF where no LLS-aged sediments are present, at an altitude of ca. 22.50 mOD. Prior to the Vedde Ash however constraining lake level elevations are absent in PF.

A drop in lake levels through the LLS is also reconstructed from the WYKNE15 and WYKSE14 records on the basis of the loss of littoral aquatic macrofossils in WN-M6 (23.67-24.33 mOD) and WS-M4 (23.42-23.95 mOD), and the deposition of coarser grained sediments in both records (WN-L5a, WS-L8b), which is indicative of relatively lower water levels in lakes (Harrison and Digerfeldt, 1993). No radiocarbon dates are obtained from these intervals in either record due to the lack of available material for dating, with the only chronologically constrained horizon being the combined SAR-OSL ages from WS-L8b. The Vedde Ash is also absent from the Wykeham sequences. The absence of this ash horizon in these records is unlikely to result from

taphonomic processes operating in each basin as the peak shard abundance (1565 shards/gm) is high in PF 'Core C' (Palmer *et al.,* 2015), meaning that large abundances of tephra shards would have been deposited by primary airfall across the landscape. The WYKNE15 and WYKSE14 sequences were infilled to a minimum altitude of 23.67, and 23.42 mOD respectively during this interval, *ca.* 5 m above the infill of PF Core C where the Vedde Ash is preserved. Its absence in these records is therefore more likely to represent either the lack of sediment deposition in these other depo-centres, and/or the coarse-grained mode of deposition, incapable of preserving tephra shards. Both criteria support lower lake levels across the eVoP by the time the Vedde Ash was deposited, with it only being preserved in the deepest bathymetric depressions (infilled to under *ca.* 20.5 mOD at the time of ashfall), capable of containing water bodies throughout this stage of the LLS. The consistent drop in lake levels demonstrates a decline in effective precipitation reaching the eVoP during the mid-stages of the LLS and an increase in aridity.

7.5.5. Early Holocene ca. 11.7-11 cal ka BP

The introduction of *Typha latifolia* and *Filipendula ulmaria* at Wykeham at *ca.* 11.8-11.35 cal ka BP (WS-M5, WN-M7) demonstrate both an increase in TMax to >13°C (MCR-D; Isarin and Bohncke, 1999), as well as a rise in relative lake levels (Hannon and Gaillard, 1997), suggesting an increase in effective precipitation in the eVoP (Magny *et al.,* 2006). A deterioration in temperatures at 11.65-11.2 cal ka BP is suggested by the local replacement of the warm stenotherm *Typha latifolia*, by *Urtica dioica* (which can exist with a lowermost TMax limit of 8°C; Isarin and Bohncke, 1999) in WS-M5a. $\delta^{18}O_{bulk}$ records are present only from PF which show an initial rise at *ca.* 11.4-11.1 cal ka BP, followed by a climatic deterioration at *ca.* 11-10.8 cal ka BP.

Whilst the chronological uncertainties on these trends are relatively large (driven principally by the plateau in the radiocarbon calibration curve during this interval; Björk *et al.,* 1997; Reimer *et al.,* 2013), the influx of thermophilous stenothermic macrofossil taxa occurs prior to the re-initiation of organic, and carbonate-rich sediments in the WYKNE15 (WN-M7), WYKSE14 (WS-M5b) and PF sequences. This demonstrates a short phase lag in climatic amelioration and the associated environmental response.

Palaeohydrological changes in the eVoP during the EH are best constrained by work on littoral deposits at the margins of PF (Cloutman, 1988a; b; Cloutman and Smith, 1998; Dark, 1998; Taylor, 2011). Here, the water level is interpreted to steadily rise through the EH, with littoral deposits (marl) being formed to an elevation of *ca.* 23 mOD before transitioning into detrital muds and peat where lake deposits (marls) are overlain by sediment indicative of terrestrialisation via hydroseral succession between *ca.* 11.15-10.3 cal ka BP (Dark, 1998; Taylor, 2011). This is recorded up to an elevation of *ca.* 24.5 mOD (Cloutman, 1988a;b; Cloutman and Smith, 1988; Palmer *et al.,* 2015; Figure 7.8).

In the WYKNE15 and WYKSE14 sequences, a rise in lake level is also identified based upon the expansion of telmatic taxa and peat in WN-M7/WN-L6 (24.33-25.20 mOD), and WS-M5a-5b/WS-L9-10 (23.95-24.48 mOD) respectively, representing sediment accumulation in close association with the water table between *ca.* 11.8-11.25 to 11.5-10 cal ka BP and 11.65-11.2 and 11.4-10.6 cal ka BP respectively. Superimposed upon the steadily rising trend is a temporary lowering of the lake level in Depression C, reconstructed by the rise of organic content and expansion of *Urtica dioica* in WS-L9a/WS-M5a, at 11.65-11.2 cal ka BP (24-24.04 mOD), suggesting a temporary phase of water table lowering and the development of a land surface. Further data are needed however to support this correlation.

The WYKNE15 and WYKSE14 records were infilled prior to PF as a result of accommodation space being filled during the LLS. This is supported by unpublished data from PF which demonstrate that marl was not formed in 'Core B' (at *ca.* 22 mOD) until *ca.* 11.4-11.1 cal ka BP, by which time the Wykeham records had largely infilled. This is interpreted to reflect the variable infill rates of the basins during the LLS, with the WYKNE15 and WYKSE14 sequences largely infilled up until *ca.* 24 mOD prior to the initiation of the EH. In contrast, in PF, infill had only reached *ca.* 21-22 mOD (Palmer *et al.,* 2015), meaning that as the water table steadily rose through the EH, open water reformed in PF, but not in the Wykeham sequences. These data therefore further support analogous lake levels existing between basins in the eVoP throughout the LGIT.

8. Regional comparisons to the eastern Vale of Pickering palaeoclimatic event stratigraphy

8.1. Introduction

The palaeoclimatic records from the eVoP developed in this study represent one of the best records of: a) the climatic structure of the LGIT in NW Europe, b) the manifestation of abrupt climatic events during the LGIT in the British Isles. The eVoP event stratigraphy improves the understanding of the hydroclimatic evolution of the LGIT in Britain in four specific criteria.

First, the reconstruction of summer and winter temperature estimates provides quantitative temperature estimates, which can be compared to local and regional sequences (Walker *et al.,* 1993; Elias and Matthews, 2013). These records are a valuable addition to the British climatic reconstructions in the LGIT, which are sporadic in NE England, and allow an examination into factors such as longitudinal climatic gradients in NW Europe, which have been hypothesised, but have lacked supporting evidence (Brooks and Langdon, 2014). Second, $\delta^{18}O_{bulk}$ values from the WYKNE15 sequence provides a high-resolution and sensitive proxy record for past mean annual air temperature, extending into the earliest stages of the LGIT. Unlike palynological records, from which most palaeoenvironmental reconstructions in NE England are derived, $\delta^{18}O_{bulk}$ values in lacustrine sequences are highly sensitive to climatic change (Leng and Marshall, 2004), responding rapidly to abrupt climatic oscillations (Marshall *et al.,* 2002; Candy *et al.,* 2016). These records therefore provide a more sensitive signal of palaeoclimatic evolution than has previously been available east of the Pennines. The $\delta^{18}O_{bulk}$ record from the WYKNE15 sequence is the first of its type from NE England, and is one of the highest resolution palaeoclimatic records through this interval, with an average resolution of < 40 years per sample. Third, the multiproxy reconstruction of lake level change in the eVoP provides a novel assessment on relative shifts in effective precipitation regimes in the eVoP (Bos *et al.,* 2006). This is the first hydroclimatic reconstruction through the LGIT in the British Isles, and in combination with the palaeotemperature reconstructions, allows the phasing of environmental/hydrological responses to temperature changes to be assessed in previously unobtainable detail. Fourth, the age-depth models from the Wykeham sequences enable quantitative assessments into the age and duration of palaeoclimatic events in the eVoP. These age-models are of sufficient precision to confidently compare these records to other high-resolution, multiproxy climatic records across the North Atlantic seaboard, which has not been possible with many other British palaeoenvironmental records that lack a chronology. By adopting this approach, insights into the timing, phasing, magnitude, and forcing mechanisms of abrupt climatic events through the LGIT can be better quantified (Lowe *et al.,* 2008).

8.1.1. Comparisons to regional records

Ideally, inter-site comparisons should be undertaken between records containing independent, and quantified palaeotemperature/palaeohydrological estimates, and age models consisting of radiocarbon-dated terrestrially-derived plant macrofossils and/or robustly-dated tephra layers (Lowe *et al.,* 2008). Doing so, enables records to be directly compared to other palaeoclimatic reconstructions, including the Greenland GICC05 $\delta^{18}O$ record on a common timescale (Lowe *et al.,* 2008; Rasmussen *et al.,* 2014). Therefore, in this section the eVoP records are preferentially compared to other regional records that: a) reconstruct the same palaeoclimatic parameters as those from the eVoP; b) record events that are potentially analogous to those in the eVoP; and c) have a robust chronology. It is acknowledged that for periods during the LGIT, (particularly those covering the transition into the WI), few, if any records meet these criteria, principally due to the lack of a reliable chronology. Therefore, high-resolution records which utilise analogous proxies to those in the eVoP are used for comparison, with the assumption that regional records with analogous climatic intervals are occurring in phase across the British Isles (Lowe *et al.,* 1995). Five sites are used for comparison to the eVoP datasets in the British Isles (Figure 8.1):

a) Coleopteran MCR ranges from Gransmoor (Walker *et al.,* 1993; Elias and Matthews, 2013), used as the local stratotype for palaeoclimatic change during the LGIT in NE England, containing an age model terrestrial plant macrofossils.
b) Abernethy Forest in the Grampian Highlands of Scotland (Matthews *et al.,* 2011; Brooks *et al.,* 2012), which contains a robust chronology, quantitative palaeotemperature estimates from C-ITs (TMax) and the Penifiler tephra, which can be directly tied to records in the eVoP.
c) Fiddaun in western Ireland (van Asch *et al.,* 2012), which contains a quantitative temperature reconstructions from analogous proxies to the eVoP records (C-ITs and $\delta^{18}O_{bulk}$), and a skeleton radiocarbon based chronology upon terrestrial plant macrofossils.
d) Hawes Water in the Lake District, which contains high-resolution quantitative temperature reconstructions ($\delta^{18}O_{bulk}$ values and C-ITs; Marshall *et al.,* 2002 and Bedford *et al.,* 2004; Lang *et al.,* 2010 respectively), covering the entire Lateglacial period, albeit without an independent chronology.
e) Whitrig Bog in southern Scotland (Brooks and Birks, 2001), which records C-ITs through the entire LGIT period and has both the Borrobol and Vedde ash tephra layers, providing a skeleton chronology for the sequence.

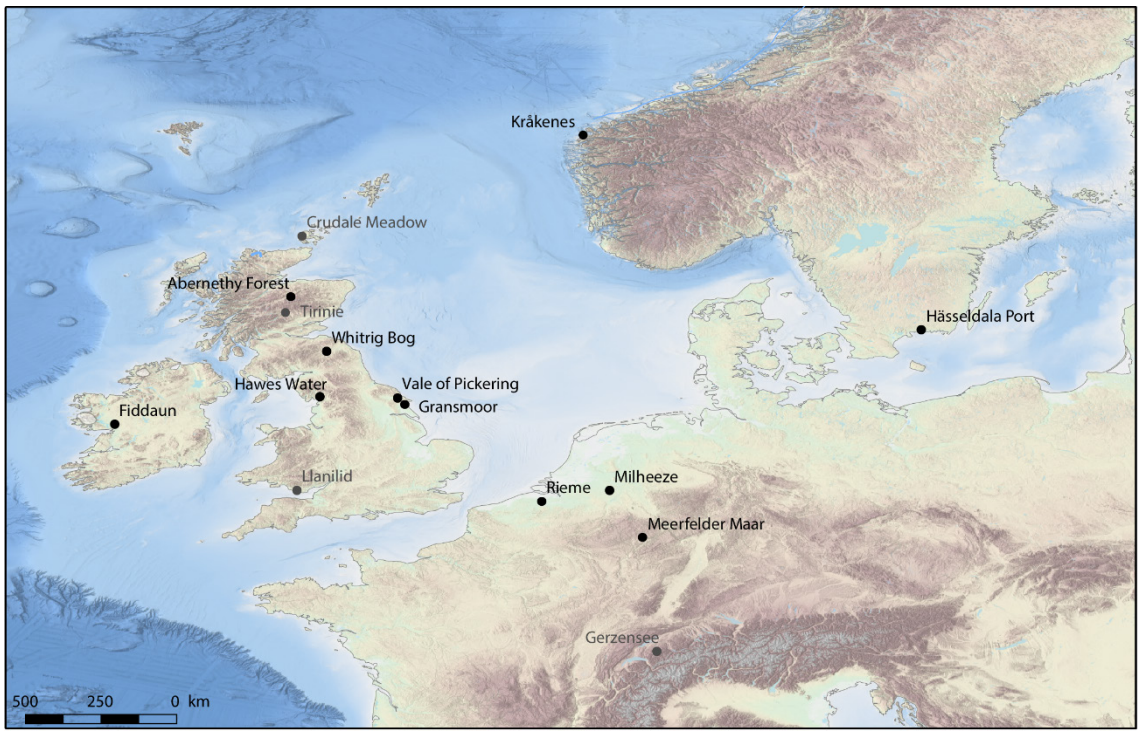

Figure 8.1. *Map of LGIT sequences in the British Isles and western Europe compared to the eVoP records in this chapter.*

Further comparative records are also identified from western Europe and Greenland which can be used as further correlation points through different intervals of the LGIT (Figure 8.1). These sites include:

a) The North Atlantic Event stratigraphy ($\delta^{18}O$ record on the GICC05 timescale Rasmussen *et al.,* 2006; 2014) from the Greenland ice cores, which provide the highest resolution and best constrained palaeoclimatic record through the Last Termination in the North Atlantic and surrounds (Björk *et al.,* 1998; Lowe *et al.,* 2008).
b) Hässeldala port in southern Sweden which contains C-ITs and leaf-wax derived hydrogen isotopes for terrestrial and aquatic plants, providing a proxy for hydroclimatic change ($\Delta\delta$Dterr-aq; Muschitiello *et al.,* 2015b; Wohlfarth *et al.,* 2016). These records are chronologically constrained by 40 radiocarbon dates on terrestrial macrofossils which provide a robust chronology for the palaeoclimatic datasets between *ca.* 14.2-9.7 cal ka BP (Wohlfarth *et al.,* 2016).
c) Kråkenes in western Norway (Brooks and Birks, 2000; Bakke *et al.,* 2009; Lohne *et al.,* 2014) which contains C-ITs (TMax), and high resolution palaeoclimatic proxy data from annually laminated sediments (Bakke *et al.,* 2009) that are constrained by 118 dates on terrestrial plant macrofossils (Lohne *et al.,* 2013; 2014). Kråkenes also contains detailed records of changes in aquatic macrofossil assemblages through the LGIT (Birks, 2000; Birks *et al.,* 2000) which provide a valuable correlative to the datasets obtained in the eVoP.
d) Meerfelder Maar (MFM) in western Germany (Brauer *et al.,* 2008; Rach *et al.,* 2014), which contains a high resolution (annually-laminated) record of abrupt climatic transitions during

the latter stages of the LGIT (Brauer *et al.,* 2008; Rach *et al.,* 2014), which are constrained by 69 radiocarbon dates from terrestrial plant macrofossils (Brauer *et al.,* 2000). MFM also contain a $\Delta\delta$Dterr-aq record (Rach *et al.,* 2014) which provides a correlative both to the record from Hässeldala Port (Muschitiello *et al.,* 2015b; Wohlfarth *et al.,* 2016), as well as the hydroclimatic model from the eVoP.

e) Milheeze and Rieme in the southern Netherlands, (Bos *et al.,* 2006), and NW Begium (Bos *et al.,* 2013). These records provide the most proximal models of littoral lake level variations through the LGIT. These records are well constrained by radiocarbon dates on terrestrial macrofossils enabling comparisons between sites upon a common timescale.

8.2. Comparison of the eVoP event stratigraphy to palaeoclimatic records from the British Isles

8.2.1. Comparison of the eVoP event stratigraphy to Gransmoor

The coleopteran MCR from Gransmoor (Walker *et al.,* 1993), *ca.* 25km southeast of the eVoP (Figure 8.1) represents the most proximal LGIT record of quantitative palaeoclimatic change, supported by an independent chronology (Elias and Matthews, 2013). The MCR shows a structure of low temperatures at the base of the sequence, which abruptly rise to an early optimum, before steadily declining through the WI (Atkinson *et al.,* 1987; Walker *et al.,* 1993). Figure 8.2 shows the comparison of the Gransmoor TMax to the TMax from the eVoP. These records correspond well between *ca.* 13.9-11.7 cal ka BP, with consistently overlapping ranges between *ca.* 15-10 °C. Between 15.5-13.9 cal ka BP however, the MCR_{mut} record from the eVoP invoke consistent summer and winter temperature ranges through a period where the Gransmoor MCR, WYKNE15 and PF $\delta^{18}O_{bulk}$ datasets show a structure of an initial rise in mean annual temperatures (WN-I3a) to optimum values early in the WI (WN-I3), which steadily lower between *ca.* 14.5-13 cal ka BP (WN-I4).

The offset between these records can be attributed to two mechanisms. Firstly, the low number of taxa used to create the eVoP MCR between 15.5-13.9 cal ka BP (mostly *Betula nana* in isolation from the WYKNE15 sequence), and the lack of supporting coleopteran MCRs, result in wide TMax and TMin ranges, meaning temperature changes within these ranges cannot be distinguished. Secondly, a lag in the response time of stenothermic, thermophilous vegetation colonising the eVoP after WN-I3a (15.1-14.6ka BP), meaning the warmest temperatures during the E-WI are not recorded in the vegetation data. This can be related to the delayed development of shrub and woodland taxa in Britain during the early stages of the WI (Pennington, 1986; Birks and Birks, 2014), resulting in discordant palaeoenvironmental/palaeoclimatic signals between coleopteran MCR ranges and palynological signals at Gransmoor (Walker *et al.,* 1993).

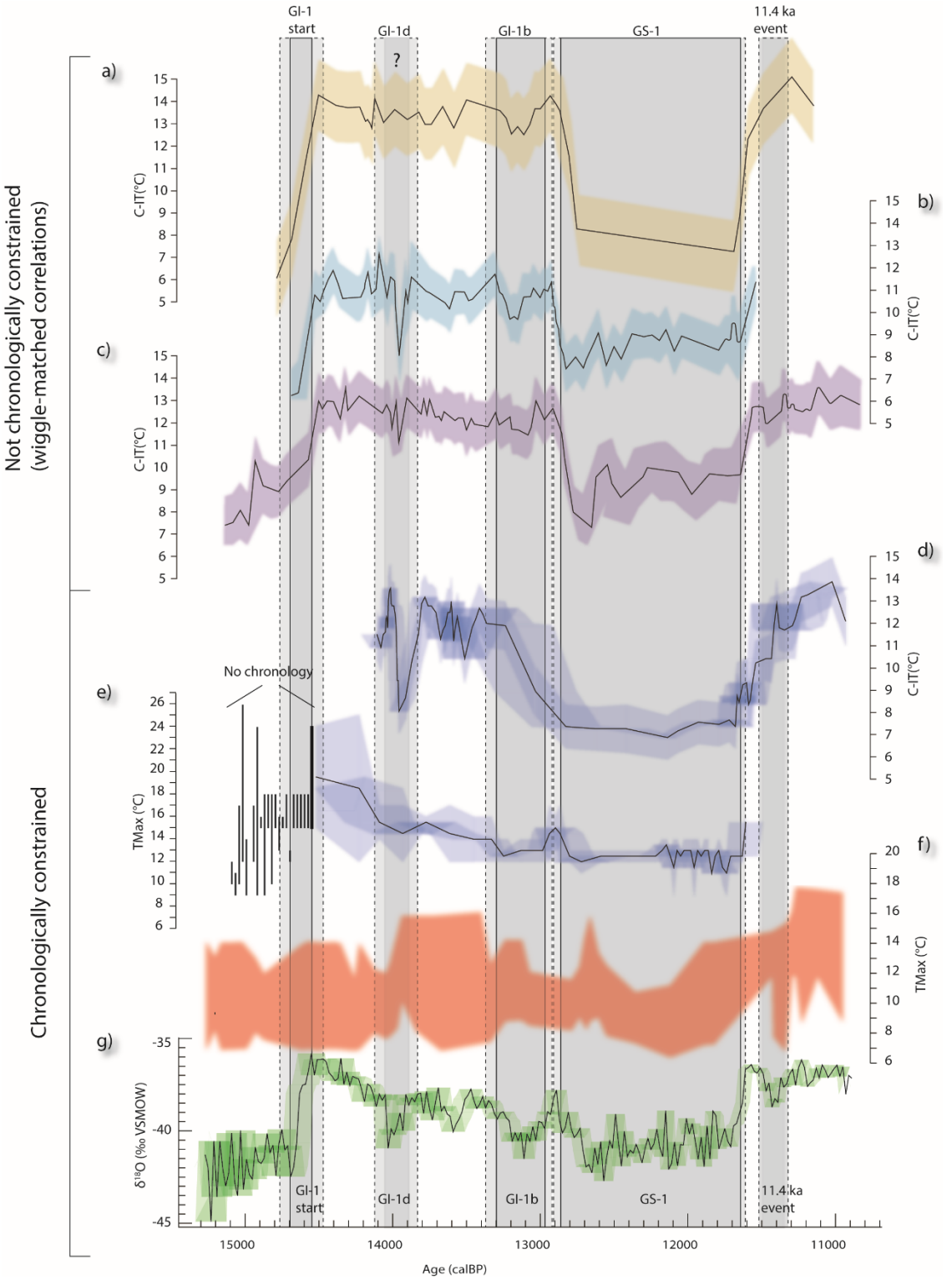

Figure 8.2. *Comparative regional summer temperature ranges to the eVoP and Greenland: a) chironomid-inferred temperatures (C-ITs) from Fiddaun (van Asch et al., 2012), b) C-ITs from Whitrig Bog (Brooks and Birks, 2000), c) C-ITs from Haweswater (Bedford et al., 2004), d) C-ITs from Abernethy Forest (Brooks et al., 2012), blue ribbons represent 1σ age and proxy uncertainties e) Coleopteran MCR TMax from Gransmoor (Walker et al., 1993), blue ribbons represent 1σ age and proxy uncertainties, f) eVoP mutual MCR TMax, g) NGRIP $\delta^{18}O$ on the GICC05 timescale (Rasmussen et al., 2006) converted to cal BP. Of these records only d), e), and g) contain a robust age-depth model with which to compare the timing of events to the eVoP event stratigraphy. Records a)-c) show a similar climatic structure to the N Atlantic event stratigraphy and are wiggle-matched to this record. This is done only for illustrative purposes, as without a robust chronology the timing and phasing of the climatic trends in these records cannot be reliably compared to the eVoP, or to Greenland.*

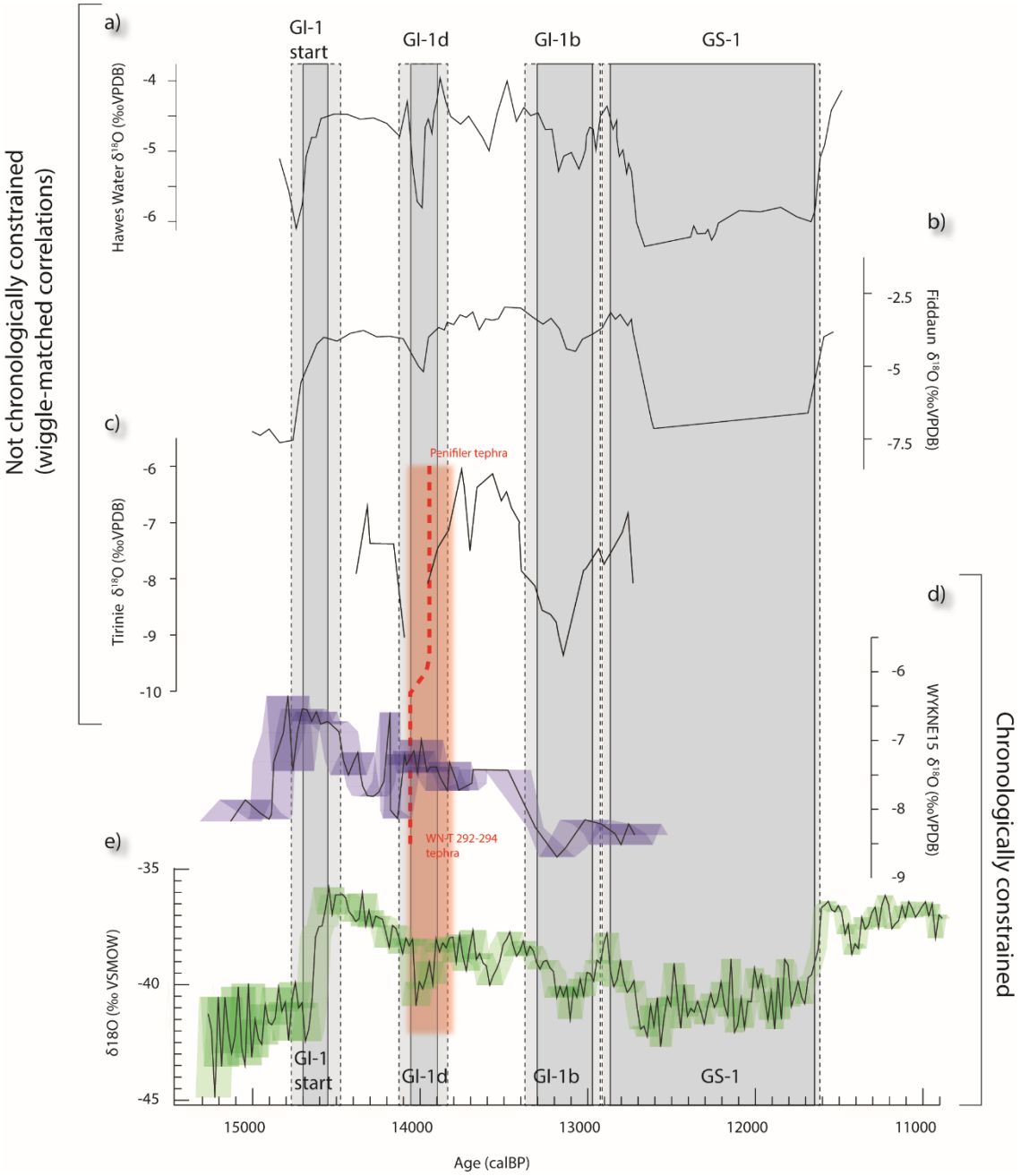

Figure 8.3. *British $\delta^{18}O$ records compared to the eVoP records in text: a) $\delta^{18}O_{bulk}$ record from Hawes Water (Marshall et al., 2002), b) $\delta^{18}O_{bulk}$ record from Fiddaun (van Asch et al., 2012), c) $\delta^{18}O_{bulk}$ record from Tirinie (Candy et al., 2016), d) the $\delta^{18}O_{bulk}$ record from Wykeham Quarry (this study), blue ribbons represent 1σ age uncertainties, e) NGRIP $\delta^{18}O$ on the GICC05 timescale (Rasmussen et al., 2006) converted to cal BP. Intervals discussed in further detail are shaded between records. Of these datasets, only the GICC05, and WYKNE15 sequences contain an independently derived age-depth model, whilst the Tirinie records can be tentatively correlated to the WYKNE15 sequence based on the presence of the Penifiler and WN-T 292-294 tephras. This summary demonstrates the regional importance of the WYKNE15 $\delta^{18}O$ record as it is the only terrestrial $\delta^{18}O$ sequence with a robust chronology, enabling direct comparison to the Greenland ice-core records upon a common timescale. The other records, as with Figure 8.2, have been wiggle-matched to the climatic events in the GICC05 record for illustrative purposes only. It is important to note that no assessment on the leads and lags of climatic events between these sites can be made without robust chronological information.*

Not until the decline of *Juniperus* on Holderness between *ca.* 14.3-13.9 ka BP (Lowe and Walker, 1986) are concordant climatic signals recorded in coleopteran, and vegetative remains (Walker *et al.,* 1993). This is also the case for the eVoP and Gransmoor MCRs, where TMax ranges are consistent after 14 cal ka BP.

This demonstrates that the 'stable' MCR ranges between *ca.* 15.5 and 14ka BP in the eVoP are not reflective of the climatic regime during the transition into, and during the early WI (E-WI). This results from a lagged vegetation response to the climatic amelioration, coupled with low macrofossil abundances in the Wykeham sequences. Consistent climatic signals between coleopteran, macrofossil, and chironomid TMax estimates during the latter half of the WI (*ca* 14-13 ka BP) between the eVoP and Gransmoor, show that these temperature ranges were concordant across NE England during these intervals.

8.3. Comparison of the eVoP event stratigraphy to other palaeoclimatic records from the British Isles

8.3.1. Stadial to Interstadial transition and the early Interstadial ca. 15.5-14.3 cal ka BP

The earliest signal of climatic amelioration in the eVoP is identified in the WYKNE15 sequence where authigenic carbonate is precipitated around charophyte thalli in WN-L2. This occurs at 15.6-14.8 cal ka BP, prior to the rise in $\delta^{18}O_{bulk}$ values (climatic amelioration) at the onset of the WI. In order to form authigenic carbonates, firstly the water table must have risen sufficiently to form subaqueous conditions, and secondly the spring, feeding the basin must have become resurgent during this period. Therefore, by the time the WYKNE15 sequence began to deposit authigenic sediments at 15.6-14.8 cal ka BP, temperatures must have risen sufficiently to melt permafrost and enable spring flow into the basin. The presence of *Betula nana* remains in this interval demonstrate that TMax and TMin were no lower than 8 and -17°C respectively (Aarnes *et al.,* 2012), supporting significantly warmer conditions than those reconstructed during the Last Glacial Maximum (LGM; Renssen and Vandenberghe, 2003). Initial warming in the British Isles prior to the WI is also supported by C-ITs from Hawes Water, where a rise of *ca.* 3 °C (from *ca.* 7- to 10 °C) is recorded. This is consistent with that in the eVoP prior to the transition into the WI (Figure 8.2; Bedford *et al.,* 2004).

To explain these trends, both a rise in effective precipitation, and mean annual air temperatures are required to melt permafrost (Renssen and Vandenberghe, 2003), and produce a subaqueous environment in topographic depressions (Depression B) in which authigenic carbonate precipitation could occur. This may reflect two possible forcing mechanisms: (1) the retreat of the North Sea Ice Lobe during this interval (Bateman *et al.,* 2015) which possibly led to locally warmer conditions prevailing in the eVoP; and (2) a low amplitude strengthening of AMOC prior to the abrupt transition into the LGIT. The first mechanism fails to explain the regional warming trend shown during this period, favouring a strengthening in AMOC as the driving factor. A low amplitude increase in AMOC strength prior to the onset of the LGIT has been proposed (Clark *et al.,* 2002; Wilson *et al.,* 2014; Thiagarajan *et al.,* 2014). These findings are consistent with the

palaeoclimatic records from the eVoP and Hawes Water, and provides a mechanism with which to explain the low amplitude warming signals in the British Isles prior to the LGIT.

The onset of the WI in the eVoP is characterised by a + 1.72 ‰ rise in $\delta^{18}O_{bulk}$ values (WN-I3a) in the WYKNE15 sequence at 15.1-14.6ka BP (Figure 8.4). This signal represents the first chronologically constrained proxy record of this climatic amelioration in the British Isles, and, when coupled with the hydrological evidence from the Wykeham records, enables the timing and phasing of climatic change in the E-WI to be assessed, which has yet to be achieved in any other record in the British Isles/NW Europe.

The lakes in Depression B and PF are now extinct, meaning that the rates of lake recharge, and the relationship between the $\delta^{18}O$ of the lake water and rainfall can no longer be quantified. As such, the changes in the $\delta^{18}O_{bulk}$ values of the WYKNE15 record can only be used to assess the magnitude of climatic changes, and not the absolute values of mean annual air temperature (Marshall *et al.,* 2002; Leng and Marshall, 2004). In order to assess the absolute magnitude of the isotopic shift in terms of temperature, the event must be compared to other regional sequences in which independent temperature reconstructions are present. Few palaeoclimatic records in the British Isles contain a record of the transition into the WI, and those which do, lack ample chronological control to be directly compared upon a common timescale. This is likely due to the time taken for glacially-derived lacustrine basins to become competent to accumulate authigenic sediments in recently deglaciated localities at the end of the Dimlington Stadial.

Four sites in the British Isles have sequences in which climatic intervals can be considered as correlatives to WN-I3a. These are the coleopteran MCR ranges from Gransmoor (Walker *et al.,* 1993*),* C-ITs from Whitrig Bog (Brooks and Birks, 2000), Hawes Water (Bedford *et al.,* 2004; Lang *et al.,* 2010), and Fiddaun (van Asch *et al.,* 2012), and $\delta^{18}O_{bulk}$ values from Hawes Water (Marshall *et al.,* 2002; Figures 8.2-8.3). These records represent the best resolved quantitative palaeoclimatic records for comparison and can be correlated based upon the assumption that major palaeoclimatic changes in the British Isles occurred broadly in phase (Lowe *et al.,* 1995).

The + 1.72 ‰ rise in WN-I3a closely corresponds to a rise of + 1.7 ‰ in authigenic $\delta^{18}O_{bulk}$ values in event 'A' at Hawes Water (Marshall *et al.,* 2002). C-ITs from the same basin, record a rise in summer temperatures of *ca.* 6 °C (from 7.4 °C to 13.4 °C) through this interval (Bedford *et al.,* 2004; Lang *et al.,* 2010), which is identical to the C-IT rise at Whitrig Bog, (6 °C rise from 6 to 12 °C; Figure 8.2). If the isotopic values are accepted to reflect calcite precipitation in isotopic equilibrium with the water body, then a *ca.* + 0.3 ‰ rise in the $\delta^{18}O_{bulk}$ values can be equated to a 1 °C rise in temperature (Leng and Marshall, 2004). The + 1.72 ‰ rise in $\delta^{18}O_{bulk}$ values would therefore reflect a 5.7 °C increase in temperature through WN-I3a, which corresponds to the magnitude of temperature changes identified elsewhere in the British Isles.

These comparisons therefore strongly support that: a) the transition into the WI in Britain was characterised by a high amplitude and relatively rapid amelioration in summer and mean annual air temperatures across northern Britain, b) the robust age-model from the WYKNE15 record, and the spatial consistency of the climatic trends suggest that the amelioration would have occurred closely in phase across Britain between 15.1-14.6 cal ka BP.

The decline in $\delta^{18}O_{bulk}$ values identified in the eVoP sequences (WN-I3b) indicates an abrupt deterioration in mean annual air temperatures, soon after the onset of the WI (Figure 8.3). The small magnitude of this isotopic depletion, and the fact that it cannot be identified in the TMax estimates for either the Wykeham records or PF, strongly suggests that the magnitude of this event was relatively small. It is important to note a similar low amplitude oscillation in C-ITs of *ca.* 1-2 °C is identified in Whitrig Bog, *ca.* 200 km north of the eVoP, occurring soon after the onset of the WI (Brooks and Birks, 2000a). However, no correlatives of this event are identified in C-IT or $\delta^{18}O_{bulk}$ records from Hawes Water or Fiddaun, further to the west. This either suggests that the amplitude of this climatic deterioration was not spatially consistent across the British Isles, or the climatic reconstructions elsewhere in Britain are not of a high enough resolution, or not sufficiently sensitive enough to record this event.

8.3.2. Transition from the Early to Mid-Late Windermere Interstadial ca. 14.3-13.9 cal ka BP

Between 14.3 and 13.9 cal ka BP, an abrupt climatic oscillation is observed in the Wykeham sequences (WN-I4b; MCR A-B; Figure 8.2-8.3), coupled with evidence for temporarily lower lake levels (WS-L2-5a; WN-M3a). This is of local significance as it coincides with the initiation of stratigraphic assemblage B deposits (organic rich LfA-6B) at Wykeham Quarry, including the WYKSE14 sequence in Depression C, and of regional importance, as it is consistently identified as the period of most pronounced climatic variability during the WI in Britain (Brooks and Birks, 2000; Marshall *et al.,* 2002; Brooks *et al.,* 2016).

The timing of this event is best resolved at Abernethy Forest, where it is constrained by an age model consisting of radiocarbon dates on terrestrially derived plant macrofossils, and the Borrobol and Penifiler tephra horizons (Aber-Ch2; Matthews *et al.,* 2011; Brooks *et al.,* 2012). C-ITs from these sequences exhibit a high amplitude cooling occurring in close association with GI-1d in the GICC05 ice core chronology. The presence of the Penifiler tephra in PF, associated with the $\delta^{18}O_{bulk}$ values confirm that WN-I4b/PF-I2b, is directly comparable to Aber-Ch2, and allows for the structure and duration of event to be compared upon a common timescale. In the

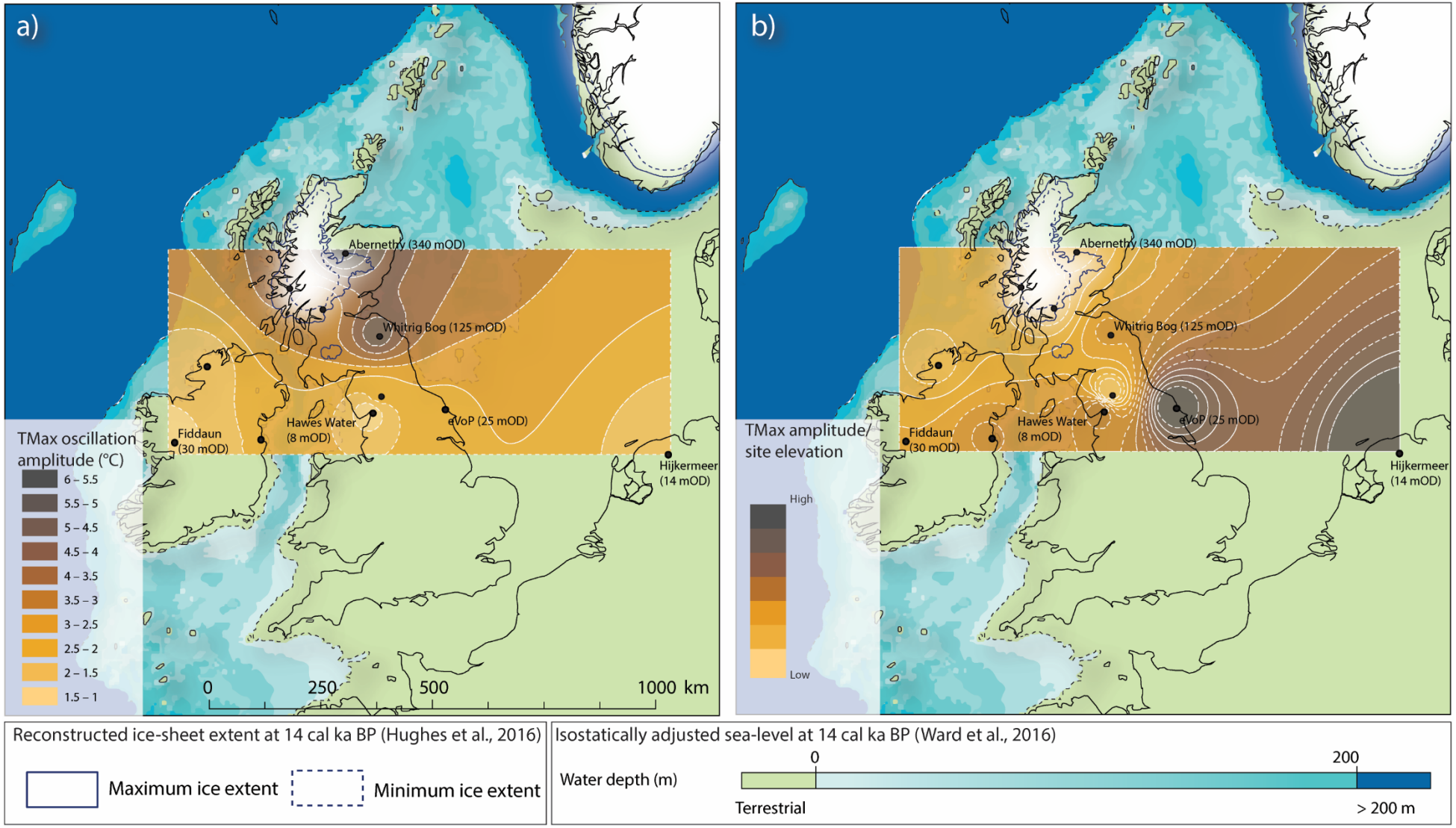
a)
b)
Abernethy (340 mOD)
Whitrig Bog (125 mOD)
Fiddaun (30 mOD)
Hawes Water (8 mOD)
eVoP (25 mOD)
Hijkermeer (14 mOD)
TMax oscillation amplitude (°C)
6 – 5.5
5.5 – 5
5 – 4.5
4.5 – 4
4 – 3.5
3.5 – 3
3 – 2.5
2.5 – 2
2 – 1.5
1.5 – 1
0
250
500
1000 km
TMax amplitude/ site elevation
High
Low
Reconstructed ice-sheet extent at 14 cal ka BP (Hughes et al., 2016)
Maximum ice extent
Minimum ice extent
Isostatically adjusted sea-level at 14 cal ka BP (Ward et al., 2016)
Water depth (m)
0
200
Terrestrial
> 200 m

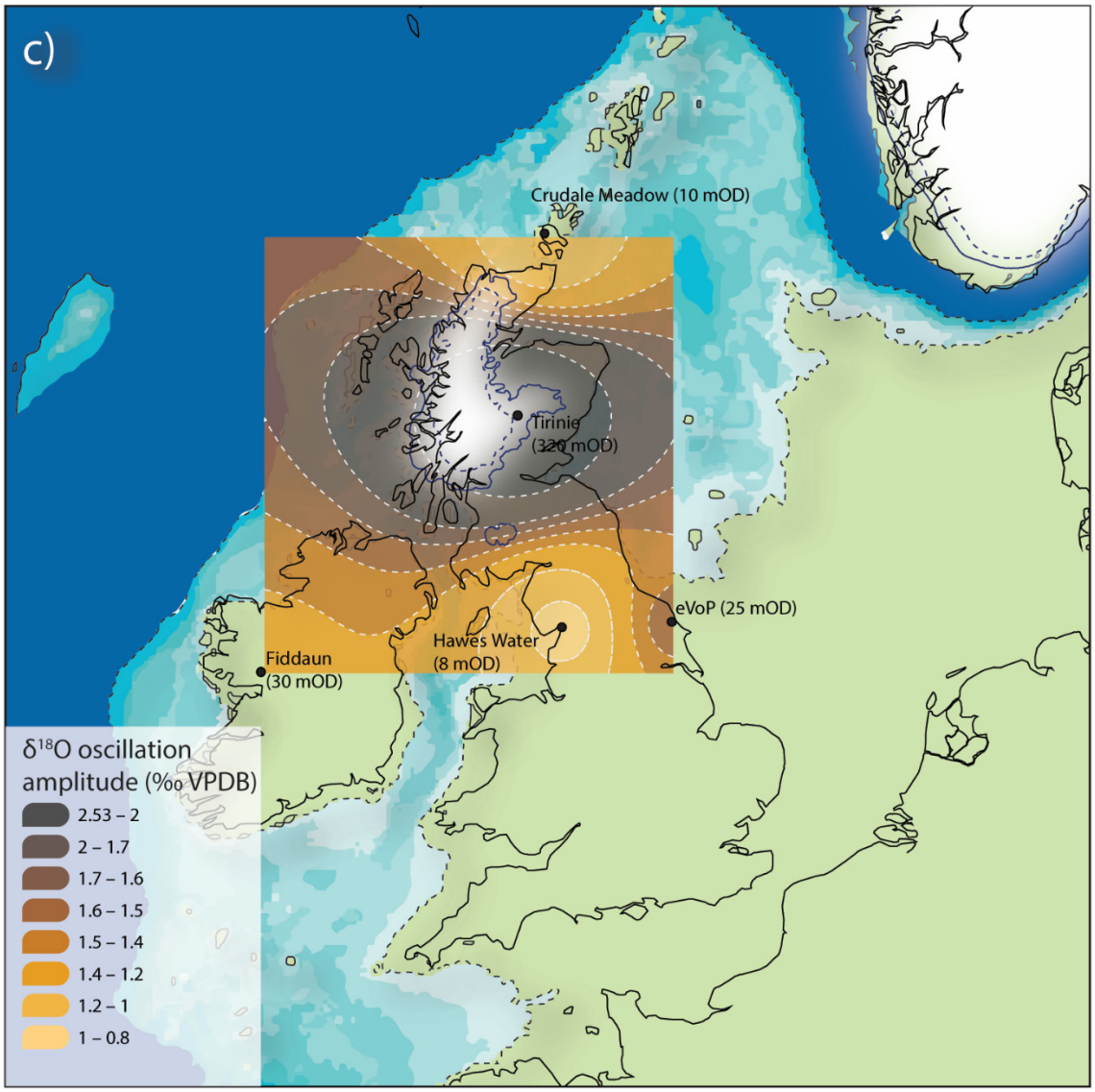

Figure 8.4. *Inverse distance weighted models of the amplitude of climatic oscillations correlated to GI-1d in the GICC05 ice-core chronology in the British Isles. The British-Irish, and Fennoscandian ice-sheet extents are derived from the 14 cal ka BP timeslice in Hughes et al. (2016), and the palaeoshorelines are derived from the isostatically adjusted sea-level models of Ward et al. (2016). Sites used to construct each model are displayed in each figure, and are referred to in text. a) The amplitude of TMax (C-IT) oscillations. These are most pronounced in the Scottish sites which all lie at higher elevations to the eVoP, and possibly more proximal to residual ice masses, b) Inverse distance weighted model of TMax/site elevation, attempting to discount elevation of each site as a variable. This trend shows a pronounced longitudinal gradient, with larger changes in the eastern UK (the eVoP) than the west. The C-IT record from Hijkermeer in the Netherlands (Heiri et al., 2007) supports this gradient, showing that higher amplitude climatic oscillations in TMax occurred at more distal positions to the North Atlantic, c) Inverse distance weighted model of $\delta^{18}O_{bulk}$ trends which, as with the C-ITs are most pronounced in the Scottish Highlands (Tirinie; Candy et al., 2016) which may also have still been affected by proximal ice masses. The plot shows that the oscillation in the eVoP is more pronounced than at Fiddaun, Hawes Water, and Crudale Meadow in the Orkneys (Whittington et al., 2015), which all lie more proximal to the palaeoshorelines of the N. Atlantic. For these reasons, it is suggested that sites relative proximity to the warming influence of the N. Atlantic was a key driver in the heterogeneous manifestation of abrupt climatic oscillations in the British Isles.*

WYKNE15 sequence, the climatic deterioration occurs slightly earlier than at Abernethy Forest (Figure 8.2). This may reflect inconsistencies with the IntCal13 calibration curve through this interval (section 8.4), but is more likely to result from the low number of dated intervals, and shifts in sedimentation rates associated with lake level changes. Lower lake levels and bulk carbonate percentages after WN-I4b overlap well with the timing of the climatic deteriorations at Abernethy Forest and Greenland.

The climatic oscillation can also be compared to other records in the British Isles to assess the regional magnitude, and spatial manifestation of the event (Figure 8.4). $\delta^{18}O_{bulk}$ values decrease by between -1.69 ‰ and -1.54 ‰ in the eVoP records (WN-I4b/PF-I2b respectively), whilst C-ITs at PF decline by -2.4 °C (from 12.2 to 9.8 °C) in the same interval, reflecting a concordant deterioration in summer and mean annual air temperatures. A rise in TMax values from 11 ± 1.7 °C to 14 ± 1 °C at 14.05-13.7 cal ka BP reflects the amelioration out of the event in the Wykeham records (MCR-A-B), coinciding with a 2.8 °C rise in C-ITs in PF, and an increase of +0.98 and +1.3 ‰ in the WYKNE15 and PF $\delta^{18}O_{bulk}$ records respectively.

The magnitude of the $\delta^{18}O_{bulk}$ shift is larger in the eVoP than at Hawes Water (-0.93 ‰), and Fiddaun (-1.36 ‰), (Figure 8.3-8.4), whilst the C-ITs from both sites show a less pronounced deterioration (1-2 °C) than in the eVoP (Bedford *et al.,* 2004; Lang *et al.,* 2010; van Asch *et al.,* 2012). In the highlands of Scotland however, the magnitude of the temperature changes are larger than in the eVoP (decrease of -2.53 ‰ in $\delta^{18}O_{bulk}$ values at Tirinie (Candy *et al.,* 2016; Figure 8.3); decreases in C-ITs of -5.8 °C and -4.9 °C at Abernethy Forest (Brooks *et al.,* 2012) and Whitrig Bog (Brooks and Birks, 2000) respectively) reflecting a disparity in the amplitude of the cooling event across the British Isles. The high resolution of the palaeotemperature reconstructions from these sites (sub-centennial scale for the $\delta^{18}O_{bulk}$ records from the eVoP, Hawes Water and Tirinie), coupled with the locally consistent magnitudes of temperature oscillations, support that the inter-site variations reflect a true spatial offset in the magnitude of the climatic oscillation, and not a sampling bias. Factors such as latitude, longitude, and elevation could all account for this regionally heterogeneous signal.

Latitude alone is unlikely to have been the driver for the variable amplitudes. This is supported by comparisons to the most northerly $\delta^{18}O_{bulk}$ record in the British Isles at Crudale Meadow in the Orkney Islands (Whittington *et al.,* 2015). If the variable magnitudes of this event were driven by a latitudinal gradient alone, it would be expected that the Crudale record would show a significantly larger decrease in $\delta^{18}O_{bulk}$ values than those in northern England. An oscillation of *ca.* -1 ‰ at Crudale which is correlated to the GI-1d oscillation in Greenland (Whittington *et al.,* 2015), suggests that the magnitude of this event is lower than in eastern England.

The relative elevation of sites may also account for the different magnitudes, as altitudinal lapse rates govern that cooling events would be of a higher magnitude at higher elevations. With the exception of Crudale Meadow (*ca.* 10 m OD), the Scottish sites are all located at higher elevations than the eVoP records. Whilst this may explain the higher relative magnitude of the oscillation in these records, it fails to account for the disparity between Fiddaun and the eVoP, which both lie at low altitudes (*ca.* 30 and *ca.* 25 m OD respectively). Elevation in isolation therefore does not explain the trends seen in the British records. The proximity of sites to cooling and warming bodies therefore must be considered further. At *ca.* 14 ka BP, the BIIS

and/or residual snow masses have been reconstructed to have still been present in the Grampians and Western Highlands (Hughes *et al.,* 2016; Figure 8.4). These masses would have exerted a significant cooling effect on the Scottish Highland basins via meltwater influx from the catchment, and rainout effects which would starve sites of moisture on the lee side of any remaining ice masses. By this time however, lowland England (the eVoP), and Ireland (Fiddaun), had long since deglaciated (Clark *et al.,* 2012; Bateman *et al.,* 2015), meaning these sites were not affected by the presence of large proximal ice masses. These factors also influenced records in NW Europe, where the Fennoscandian Ice Sheet still covered large expanses of the land mass (Coope *et al.,* 1998; Brooks and Langdon, 2014; Mangerud et *al.,* 2016; Hughes *et al.,* 2016). The larger climatic deteriorations observed in Scotland therefore may be attributed to a) higher elevation in relation to the eVoP, and b) relative proximity to the decaying BIIS at *ca.* 14ka BP.

The disparity between the eVoP and Fiddaun may be explained by the sites relative proximity to the North Atlantic. At 14 cal ka BP, global sea-level was *ca.* 100 m lower than the present day (Lambeck *et al.,* 2014), leaving large sections of the continental shelf, including the North Sea subaerially exposed (Ward *et al.,* 2016; Figure 8.4). The principal driver for abrupt climatic events during the LGIT in Europe is largely accepted to be caused by changes in the release of latent heat and moisture into the atmosphere via AMOC. Therefore, the relative proximity to this heat source would have influenced both the absolute temperature values, and the relative magnitude of temperature change and moisture availability when oscillations in AMOC strength occurred through the WI.

Palaeoclimatic records from the eVoP, Hawes Water (Marshall *et al.,* 2002; Bedford *et al.,* 2004; Lang *et al.,* 2010), and Fiddaun (van Asch *et al.,* 2012), provide a means to test the variability of cooling from West-East across the British Isles. All sites lie at similar latitudes (53-54 °N), but Fiddaun, and Hawes Water are closer to the North Atlantic margin than the eVoP, which is topographically separated from these sites by the Yorkshire Dales and Pennines (Figure 8.1). The magnitude of the $\delta^{18}O_{bulk}$ and C-IT shift is larger in the eVoP than at Hawes Water (Marshall *et al.,* 2002), or Fiddaun (van Asch *et al.,* 2012; Figure 8.3). These sites are at similar altitudes to the eVoP, meaning disparities in elevation can be discounted as a controlling factor in the magnitude of $\delta^{18}O_{bulk}$ changes. The fact that the amplitude of the oscillation is consistently lower in the western records than the east, demonstrates that the climatic deterioration was more pronounced in the eVoP than in the western British Isles. The variability in the magnitude of cooling oscillations can therefore be explained by a combination of latitudinal and longitudinal gradients (Coope and Lemdahl, 1995; Coope *et al.,* 1999), relative elevation (Candy *et al.,* 2016); and/or the relative proximity to cooling or warming masses (e.g. ice sheets and/or AMOC, Coope and Lemdahl, 1995; Brooks and Langdon, 2014) between sites in the British Isles.

In summary, these data support that a deterioration in AMOC strength between *ca.* 14.3 and 13.9 cal ka BP, led to a southerly displacement of the polar front (Ruddiman and McIntyre, 1981; Brauer *et al.,* 2008; Hogg *et al.,* 2016) and a decrease in NADW formation in the high seas of the North Atlantic. This in turn diminished the transfer of latent heat and moisture to the British Isles, with sites most distal to the N. Atlantic being most severely starved. Lags in mean annual air temperature and effective precipitation declines in the eVoP potentially reflect the time-lag associated with sea-ice build-up in the N. Atlantic, which modified wind patterns through this interval, and diminished moisture transport to NE England (Brauer *et al.,* 2008; Rach *et al.,* 2014). Higher resolution chronological data however are required to test this hypothesis. Similar trends are also noted in the other decadal-centennial scale oscillations during the LGIT, suggesting that the moderating influence of the North Atlantic, during periods of reduced AMOC strength, had less impact on the maritime climatic regime in the west, but developed an enhanced continental climatic regime in the east of the British Isles. These spatial gradients led to more severe changes in temperature, and enhanced aridity in the eastern British Isles, driven by the decreased latent heat, and moisture availability supplied by westerly winds.

8.3.3. Mid-Late Interstadial ca. 13.9-13 cal ka BP

The onset of the mid-late Interstadial (M-L-WI) in the eVoP is characterised by a rise in TMax temperatures (MCR-B 14.05-13.7 cal ka BP), and the rise, and stabilisation of the water table >23 m OD (Figure 8.2). These trends demonstrate an increase in effective precipitation delivery and heat transfer to the eVoP between *ca.* 13.9-13.65 cal ka BP. From *ca.* 13.6 cal ka BP the water table in the eVoP is interpreted to decline, forming hiatuses in the WYKSE14 record and terrestrialisation in the WYKNE15 record.

In other British records, C-ITs and $\delta^{18}O_{bulk}$ records are characterised by two distinct oscillations (Figures 8.2-8.3) representing temporary declines in summer, and mean annual air temperatures, respectively. As with the other oscillations through the WI where these proxies are coupled, the downtrend in C-ITs is consistently more muted than the amplitude of $\delta^{18}O_{bulk}$ decline, suggesting more pronounced shifts in mean annual/winter temperatures than summer temperatures. Furthermore, these shifts are demonstrated to be significantly amplified by geographic location and elevation (Candy *et al.,* 2016), supporting a reduction in NADW formation in the North Atlantic and reduced release of latent heat into the atmosphere. The lack of precise chronologies in other British sequences, and hiatuses in the Wykeham records from *ca.* 13.5 cal ka BP preclude precise comparisons to these events. Analogous shifts in the PF $\delta^{18}O_{bulk}$ record however demonstrate continued periods climatic instability after the hiatuses in the Wykeham records, which is in accord with the other palaeoclimatic datasets (Figure 8.2). The lack of littoral palaeohydrological records from the British Isles during this interval preclude direct comparisons to the lower lake levels recorded in the eVoP.

Aside from these oscillations, relatively consistent temperatures through the mid-latter stages of the WI are reconstructed in both C-ITs and $\delta^{18}O_{bulk}$ values in the British Isles compared the values during the E-WI. Whilst this is also the case for the TMax values in the eVoP, which show little variation (Figure 8.2), the $\delta^{18}O_{bulk}$ values are consistently lower (WN-I4) than during the E-WI (WN-I3). This offset is unique in $\delta^{18}O_{bulk}$ records from the British Isles (Candy *et al.,* 2016), and discussed further in section 8.3.3.

8.3.4. Loch Lomond Stadial ca. 13-11.7 cal ka BP

Palaeoclimatic records through the LLS are sporadic in the eVoP, as a result of the low water tables prior to the onset of the event (WS-M3a-3b) and also during its mid- latter stages, which formed hiatuses in both the Wykeham sequences, and all but the deepest bathymetric depressions in PF (Palmer et al., 2015). The short return to higher lake levels at the start of the LLS demonstrate colder TMax and a deterioration in TMin temperatures (MCR-C). The lowest $\delta^{18}O_{bulk}$ values through the entire WYKNE15 sequence are also reconstructed through this interval (WN-I5), supporting lower mean annual air temperatures (driven by significantly colder winters) through this interval, although the timing of the transition into these conditions (WN-I5a) is less secure.

As with the WYKNE15 sequence, the precise timing, and phasing of climatic deterioration into the LLS is not well resolved in many British sequences due to the lack of reliably dated records, and tephras (Watson *et al.,* 2010; Matthews *et al.,* 2011; Walker *et al.,* 2003), coupled with potential hiatuses in sequences. In contrast, the rise in Depression C lake levels between 12.8 and 12.65 cal ka BP (WS-M3b), and a decrease in TMax, and particularly minimum TMin temperatures (MCR-C) in the WYKSE14 sequence is well resolved and discussed further in section 8.3.4.

8.3.5. Early Holocene ca. 11.7-11 cal ka BP

Climatic amelioration, in the eVoP during the EH is inferred from the local presence of warm stenothermic flora, e.g. *Typha latifolia,* and, *Filipendula ulmaria* (Day, 1996; Cummins, 2003), at 11.7-11.25 cal ka BP (MCR-D), coupled with a steady rise in lake levels (Cloutman, 1988 a; b; Taylor *et al.,* 2011). These trends were punctuated by a short interval of lower relative lake level in the WYKSE14 sequence and a decrease in minimum MCR_{mut} temperatures (WS-L9a, at 11.65-11.2 cal ka BP). A chronologically constrained $\delta^{18}O_{bulk}$ record from PF shows a rise in values at 11.4-11.1 cal ka BP, followed by lower values at *ca.* 11-10.8 cal ka BP (Candy *et al.,* unpublished data, Figure 8.3), which demonstrates that formation of authigenic carbonate in PF core B needed for $\delta^{18}O_{bulk}$ analysis, occurred after the initial influx of warm stenothermic plants, and the reformation of marl in the eVoP.

The evidence for palaeoclimatic change at the Pleistocene–Holocene boundary in the eVoP is not recorded quantitatively, with evidence being limited to palaeoecological evidence (Chapter 7) and palynological signals from PF (Cloutman, 1988a; b; Cloutman and Smith, 1988; Day, 1996; Mellars and Dark, 1998). The introduction of stenothermic flora into the eVoP (MCR-D), provides the earliest signal of warming at 11.7-11.25 cal ka BP, and is likely to have occurred soon after the abrupt warming event occurred (Pennington, 1986; Birks and Birks, 2014; Walker *et al.,* 1993; Chapter 11), reflecting the rapid distribution rates of these taxa (Rodwell, 1995).

Across the Pleistocene-Holocene boundary, the water table is modelled to rise substantially in the eVoP, reflecting higher effective precipitation rates and progressively wetter conditions (WN-M7, WS-M5a). Furthermore, the influx of warm stenothermic plants into the valley in MCR-D demonstrates a sufficient increase in TMax temperatures to >13 °C which is warmer than any of the C-IT ranges reconstructed through the LLS in Britain (Figure 8.2). Changes in summer temperatures through the LGIT are demonstrated to be consistently smaller than changes in mean annual, and therefore winter temperatures (Denton *et al.,* 2005). Therefore, the rise in TMax values in MCR-D may also have been accompanied by a substantial rise in winter temperatures.

Hawes Water, Abernethy Forest, Whitrig Bog, and Fiddaun, all record a sharp rise in summer- (C-IT) and mean annual- temperatures, at the transition into the Holocene, corresponding to substantial climatic amelioration at the Pleistocene–Holocene boundary (Walker *et al.,* 2009; Figures 8.2-8.3). The sharp rise in C-ITs precedes the rise in LOI (reflecting the development of vegetation cover within the basin, and the surrounding catchment), by *ca.* 300 years (Brooks *et al.,* 2012). Furthermore, C-ITs above the initial rise show a short climatic oscillation occurring during rising LOI, reflecting periodically lower summer temperatures (Brooks *et al.,* 2012). A similar low amplitude C-IT deterioration is also identified at Hawes Water (Bedford *et al.,* 2004), demonstrating a consistent structure in palaeotemperature transitions into the EH, consisting of an initial high amplitude rise in C-ITs followed by at least one temporary oscillation in summer temperatures prior to *ca.* 11 cal ka BP. The palaeotemperature trends in the C-ITs from Abernethy Forest are therefore analogous to the trends identified in the eVoP.

In order to account for these changes, firstly an increase in moisture availability is required, the principal source of which is derived from the North Atlantic, transported via westerly winds. These trends therefore reflect the resumption of warmer and wetter air masses reaching the eVoP by 11.7-11.25 cal ka BP. For this to occur, sea ice cannot have been present in the moisture source areas, enabling evaporation and westerly heat transfer. These conditions therefore demonstrate the resumption of NADW formation and the sufficient strengthening of AMOC to redistribute heat and moisture to the eVoP.

8.4. Comparison of the eVoP event stratigraphy to palaeoclimatic records from the North Atlantic region

8.4.1. Stadial to Interstadial transition and the Bølling/GS-2-GI-1e ca. 15.5-14.3 cal ka BP

The stadial-interstadial transition is best recorded in the GICC05 $\delta^{18}O$ ice core stratigraphy. In this sequence, an abrupt rise in $\delta^{18}O$ values of 4 to 6 ‰ at 14.65 cal ka BP, occurred in under 3 years (Steffensen *et al.,* 2008; Figure 8.2-8.3), and corresponded to a warming of 9 ± 3 °C on the summit of the ice sheet (Severinghaus *et al.,* 1999), marking the transition from GS-2 to GI-1e, (Rasmussen *et al.,* 2014). The sharp rise in $\delta^{18}O_{bulk}$ values recorded in the eVoP is similar in structure to the event in Greenland, strongly suggesting that the amelioration in temperature was also abrupt in the eVoP. Whilst the 2σ age range of this amelioration (15.1-14.6 cal ka BP) overlaps with the range in the GICC05 chronology, the 1σ range may reflect a slightly earlier amelioration in temperatures in the eVoP in relation to Greenland (Figure 8.3). This is supported by other palaeoclimatic records in Britain (e.g. Coope and Brophy, 1972; Walker *et al.,* 2003), reflecting either deficiencies in site chronologies or palaeoclimatic records across this interval; or a genuine temporal lead between amelioration in the British Isles, in comparison to Greenland (Figure 8.2). A temporal offset of such an abrupt climatic event between Greenland and Britain is difficult to envisage (Lowe *et al.,* 1999), particularly as this event occurred on at least a hemispheric scale (von Grafenstein *et al.,* 1999; Rosen *et al.,* 2014), and the principal driving factor of the climatic system between the two sites is the same. Evidence exists for lower amplitude warming, and hydrological change prior to the onset of the LGIT, in the eVoP (section 8.3). This however isn't sufficient to explain the magnitude of temperature changes in this interval in the coleopteran records, which are shown to be at their highest recorded values prior to the warming signal in Greenland (Walker *et al.,* 2003; Elias and Matthews, 2013).

Furthermore, for the rest of the LGIT, palaeoclimatic regimes in the British Isles and Greenland have been shown to be broadly in phase (Lowe *et al.,* 1995; Benson *et al.,* 1997; Matthews *et al.,* 2011; section 8.3), meaning that for a significant temporal offset to exist during this period, a different explanation for palaeoclimatic forcing would be required. The offset therefore more likely reflects uncertainties in the palaeoclimatic, or chronological datasets of one or more of the records.

The palaeoclimatic datasets recording a temperature change across the transition into the LGIT are consistent in magnitude, showing that a warming signal of similar amplitude is recorded across the British Isles, supporting the integrity of these records. Deficiencies in chronological data can explain temporal offsets in terrestrial sequences, particularly those with beta counted dates on bulk limnic sediments, which have been shown to produce erroneously old ages (Lowe, 1991; Turney *et al.,* 2000; Walker *et al.,* 2001). Prior to the development of AMS techniques for

radiocarbon age determinations, datasets spanning this transition were regularly dated using this method, meaning the timing of climatic amelioration in these records must be treated with caution (Walker *et al.,* 2003). Whilst more reliable dates may be obtained from AMS dates on terrestrial plant macrofossils, these can also produce aberrant ages, particularly in periods such as the onset of the LGIT, where lake catchments were prone to enhanced sedimentary reworking, and the inwash of allogenic remains, significantly older than the age of the host sediment (Turney *et al.,* 2000). This is unlikely to be the case for the WYKNE15 sequence however, as sedimentary evidence from the basal dated horizon invokes a relatively stable lake system.

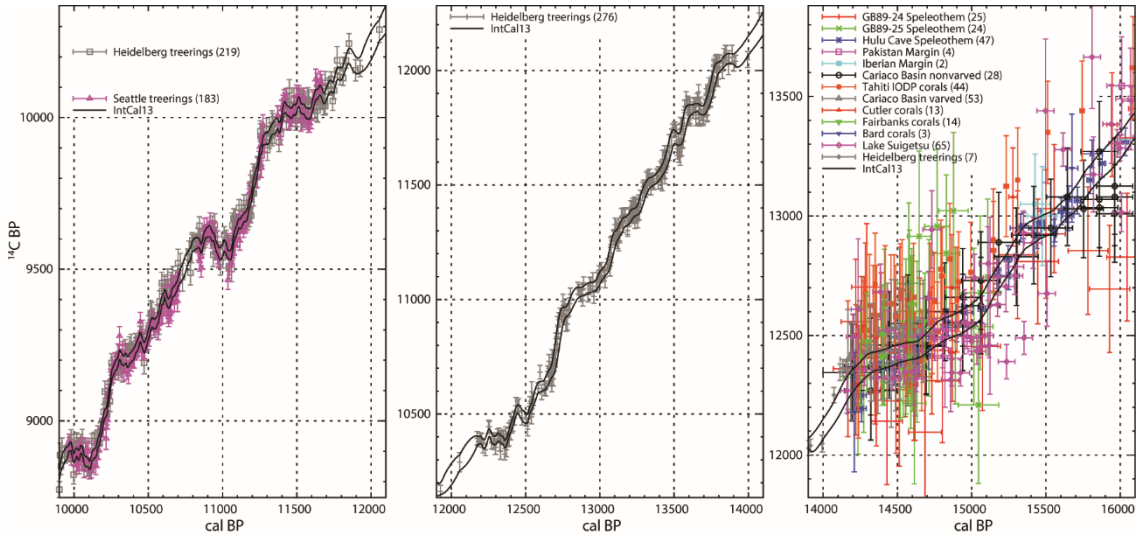

Figure 8.5. *Calibration curves of IntCal13 after Reimer et al. (2013) showing the datasets used to construct the calibration curve. Dendrochronological samples used curve between 10 and 14 cal ka BP are well resolved in comparison to the curve >14 cal ka BP which contains significa.ntly larger statistical errors.*

Allied to the problems of sample integrity, are uncertainties in radiocarbon calibration > 14 cal ka BP using the IntCal13 calibration curve (Reimer *et al.,* 2013), which relies upon a series of floating coral, speleothem, and varve records that contain significantly larger degree of scatter than the dendrochronological samples used <14 cal ka BP (Figure 8.5). These uncertainties are larger still on chronologies calibrated using previous calibration curves, which contain even larger sample scatter through this period (e.g. Reimer *et al.,* 2009). This provides the most likely explanation for the offset between the eVoP and Greenland during this interval. The warming in the British Isles and Greenland can therefore be interpreted to occur nearly simultaneously, within dating errors. Temporal offsets between the records reflect uncertainties derived from the IntCal13 calibration curve, and the low number of dated horizons in the WYKNE15 age-depth model, at the base of the sequence.

The palaeoclimatic reconstructions from Wykeham have produced supporting evidence that the onset of the WI (WN-I3a), was characterised as an abrupt climatic amelioration of *ca.* 6-7 °C in summer temperatures, occurring across the British Isles and NW Europe synchronously (within

age errors) with the onset of Greenland Interstadial 1 (GI-1), in the GICC05 regional stratotype (Rasmussen *et al.,* 2014). This is the most robust comparison of the phasing of climatic signals between the British Isles and Greenland and demonstrates the need for robust chronologies allied with quantitative palaeoclimatic reconstructions to assess the regional phasing of abrupt climatic oscillations (Blockley *et al.,* 2004).

8.4.2. 14.3-13.9 cal ka BP

The centennial scale climatic deterioration between 14.3 and 13.9 cal ka BP identified across the British Isles (WN-I4b; section 8.2) is also well documented across the North Atlantic and surrounds (Benson *et al.,* 1997; Yu and Eicher, 1998). In Fennoscandia, a vegetation response during this interval (14.2-13.7 ka BP) is termed as the Older Dryas in the Nordic Model (Mangerud *et al.,* 1974; Wohlfarth *et al.,* 2006), and a decline in $\delta^{18}O$ values in the GICC05 record between 14.15-13.95 cal ka BP, is termed as GI-1d (Rasmussen *et al.,* 2006; Lowe *et al.,* 2008). Consistent identification of a climatic deterioration between these intervals suggests that this was a near synchronous cooling event of significant magnitude, to be consistently recorded in terrestrial records, across a wide spatial extent (Yu and Eicher, 1998).

In the eVoP, the climatic oscillation also coincided with variations in lake levels, recognised in both of the Wykeham sequences (WN-M3b and WS-L3-5a). Using other records of littoral lake level variability, the regional expression of this temperature deterioration on palaeohydrological regimes can be assessed. Similar lake level declines are identified through the Older Dryas in the Netherlands, and Northern Belgium (Bohncke and Wljmstra, 1988; Hoek and Bohncke, 2002; Bos *et al.,* 2013) demonstrating a concordant hydrological signal to the eVoP. At *ca.* 14 cal ka BP these regions occupied similar medial positions to the North Atlantic. A decline in AMOC strength during this interval would therefore have led to decreased heat and moisture transfer to these regions, developing a progressively more continental precipitation regime from west-east in NW Europe. This would have led to local groundwater tables being insufficiently recharged, resulting in a consistent lowering of lake levels. To test the spatial manifestation of this signal, further data are required from sites more proximal (e.g. Fiddaun and Hawes Water) and more distal (e.g. Meerfelder Maar) to the North Atlantic. It would be expected that between 14.3-13.9 cal ka BP, lake level changes progressively increase in magnitude further east, as sites become more distal to the effects of weakening AMOC driven precipitation regimes. In contrast, depending on the magnitude of AMOC weakening, sites at the western fringes of NW Europe would be expected to show lower amplitude shifts, as they are positioned more proximal to the source precipitation reservoir and would therefore be expected to maintain a more maritime climate through this interval.

8.4.3. The Allerød ca. 13.9-13 cal ka BP

Between *ca.* 13.9-13 cal ka BP, lake levels initially rose in the eVoP, and subsequently declined, leading to the formation of hiatuses between *ca.* 13.65-13.25 cal ka BP (WN-M4, WS-M3a-3b). This occurred during a period of stability in TMax MCRs (MCR-B), but steadily lowering $\delta^{18}O_{bulk}$ values (WN-I4). Few sites exist from the British Isles with which to test the uniformity of these trends, especially in relation to lake level changes.

In other records from Northern Europe, decreases in lake levels are reconstructed at similar times to the eVoP (i.e. between 13.65-13.2 cal ka BP; Bohncke and Wijmstra, 1988; Hoek and Bohncke, 2002; Bos *et al.,* 2013). The most precisely dated of these records at Rieme in Northern Belgium, shows that organic sedimentation ceased between 13.65 and 13.3 cal ka BP, corresponding to a drop in regional water levels and a deteriorating climate (Bos *et al.,* 2013). Furthermore, at sites as far south as Gerzensee (northern Alps), a significant temporary lowering of lake levels is also identified at *ca.* 13.5 cal ka BP (Magny, 2013). This demonstrates that the hydrological trend identified in the eVoP at *ca.* 13.65-13.2 cal ka BP corresponds to a phase of lake level lowering across NW and central Europe during the mid-latter stages of the Allerød, which must reflect a decrease in effective precipitation or an increase in evaporation across large expanses of the European continent.

In the North Atlantic event stratigraphy two oscillations in $\delta^{18}O$, representing deteriorations in temperature occur between *ca.* 13.61-13.55 cal ka BP (GI-1c2) and *ca.* 13.25-13.05 cal ka BP (GI-1b). Correlatives of both of these oscillations have been consistently identified in the British Isles (e.g. Brooks and Birks, 2001a; Marshall *et al.,* 2002; Candy *et al.,* 2016; see Figure 8.3), and across the European continent (e.g. von Grafenstein *et al.,* 1999; 2013), demonstrating that they can be interpreted to represent temporary decreases in NADW formation, and reduced AMOC strength in the N. Atlantic (von Grafenstein *et al.,* 1999). The lowering of lake levels in the eVoP, are best dated in the WYKSE14 sequence, where they occur between *ca.* 13.5-12.9 cal ka BP. This demonstrates that lake level lowering in the eVoP occurred at similar intervals to:

a) lowering lake levels across Europe at *ca.* 13.5 cal ka BP, including the northern Alps (Magny *et al.,* 2006; Magny, 2013), and at Rieme in NW Belgium, where sediment hiatuses, similar to those in the eVoP are formed (Bos *et al.,* 2013),
b) Increases in $\Delta\delta D_{terr\text{-}aq}$ at Hässeldala Port, reflecting increased terrestrial evapotranspiration (i.e. drier conditions) between *ca.* 13.7-13.5 cal ka BP (Muschitiello *et al.,* 2015b),
c) Steadily lowering $\delta^{18}O$ values perturbed by an oscillation in the GICC05 event stratigraphy (GI-1c2; Rasmussen *et al.,* 2014)

d) Fennoscandian ice sheet expansion (at *ca.* 13.6 cal ka BP; Mangerud *et al.,* 2016), invoking the lowering of equilibrium line altitudes and the cooling of temperatures in NW Europe, which are required for ice sheet growth.

The hiatus in the WYKSE14 record is *ca.* 600yr long, meaning lake levels did not rise sufficiently during this interval to reform open water in Depression C during the latter stages of the WI/Allerød. This may relate to steadily decreasing temperatures through the latter stages of the Interstadial, as indicated in the North Atlantic event stratigraphy (Rasmussen *et al.,* 2014), although this is difficult to test at Wykeham itself due to the lack of preserved sediment. Prior to the hiatus, TMax ranges in the eVoP remain broadly stable within uncertainties, however $\delta^{18}O_{bulk}$ values steadily decline (WN-I4), demonstrating deterioration in mean annual air temperatures (Figure 8.3). This trend is also supported by the North Atlantic event stratigraphy, which shows steadily lowering $\delta^{18}O$ through GI-1c (Rasmussen *et al.,* 2014), as well as other continental $\delta^{18}O$ signals, which demonstrate that mean annual air temperatures were steadily declining (von Grafenstein *et al.,* 1999; van Raden *et al.,* 2013). These lines of evidence suggest an increasingly continental climatic regime between *ca.* 13.9-12.9 cal ka BP, with relatively stable summer temperatures but progressively cooler winters. The regional nature of this change indicates that at the onset of the M-L-WI/Allerød (*ca.* 13.9 cal ka BP), NADW formation strengthened, which increased heat and moisture transport to NW Europe. In the eVoP, lake levels stabilised and vegetation cover increased, coinciding with a rise in water table levels in Belgium (Bos *et al.,* 2013), and the establishment of maximum Interstadial vegetation cover across NW Europe (Hoek and Bohncke, 2002; Mortensen *et al.,* 2014). At *ca.* 13.65 cal ka BP AMOC strength began to weaken as a result of enhanced freshwater influx into the North Atlantic from Northern Hemisphere ice sheets. This in turn led to reduced heat and moisture transfer to NW Europe, reducing effective precipitation, lowering groundwater and preferentially decreasing winter temperatures, creating a more continental climate (Denton *et al.,* 2005).

These conditions were favourable for ice sheet expansion (Mangerud *et al.,* 2016) which would have provided enhanced potential for catastrophic outflow into the North Atlantic, further weakening AMOC during the latter stages of the Interstadial. The abrupt climatic events correlated to GI-1c2 and GI-1b likely result from large scale drainage events from the expanding ice masses, temporarily diminishing NADW formation (Broecker *et al.,* 1989).

8.4.4. The Younger Dryas/GS-1 ca. 13-11.7 cal ka BP

Palaeoclimatic records through the LLS are sporadic in the eVoP, due to hiatuses formed in palaeoenvironmental sequences < *ca.* 12.6 cal ka BP (Palmer *et al.,* 2015). Furthermore, most sequences are characterised by coarser grained sediments which are of limited potential for preserving organic remains. These trends reflect the variable position of the water table which

is initially interpreted to rise between 12.8-12.65 cal ka BP before falling to below the infill altitude of all but the deepest bathymetric depressions in the eVoP. The LLS is representative of the Younger Dryas (YD) in NW Europe, and GS-1 in the GICC05 timescale (Lowe *et al.,* 2001).

The onset of GS-1 in the ice cores occurs at 12.85 ± 0.15 cal ka BP, and is characterised by a rapid (< 1-3 year) shift in δD, reflecting a change in polar circulation, and the source of precipitation in Greenland (Masson-Delmotte *et al.,* 2005; Steffensen *et al.,* 2008; Figure 8.6). This is followed by a decline in $\delta^{18}O$ values over the subsequent *ca.* 200 years (from 12.85-12.65 cal ka BP; Steffensen *et al.,* 2008; Figure 8.6).

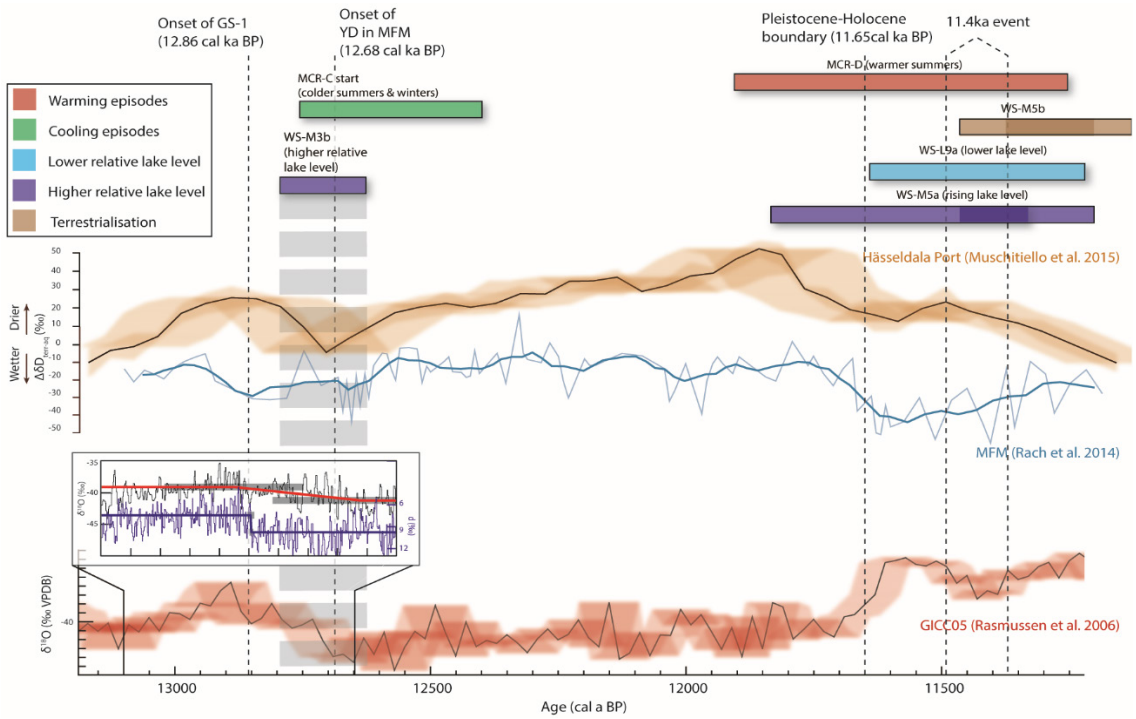

Figure 8.6. *Hydroclimatic d terr-aq datasets from Meerfelder Maar (Rach et al., 2014) and Hässeldala Port (Muschitiello et al., 2015) which are compared to the GICC05 record (Rasmussen et al., 2006; Steffensen et al., 2008), and the palaeoclimatic stratigraphy from the eVoP. The rise in lake levels in WS-M3b occurs after the transition into GS-1 in Greenland, and is correlated to a regional increase in effective precipitation in Northern Europe, during the atmospheric reorganisation between 12.9 and 12.6 ka BP. The rise in lake levels in the eVoP (WS-M5a) also occurs during a phase of progressively wetter conditions in Northern Europe across the Pleistocene-Holocene boundary. This evidence supports that the local hydrology in the eVoP relates to regional precipitation regimes in Northern Europe during the LGIT.*

The temporary rise in lake levels observed in the eVoP at 12.8-12.65 cal ka BP (WS-M3b), therefore occurs after the shift in δD at the onset of GS-1 in the GICC05 timescale, showing that the transition towards wetter conditions in the eVoP were occurring after the initiation of cooling in Greenland (Steffensen *et al.,* 2008). Cooler conditions in the eVoP during this interval are supported by the presence of stenothermic coleopteran taxa such as *Pycnoglypta lurida*, in the WYKSE14 sequence, which reflect the coolest MCRs of the entire dataset, particularly in minimum TMin values, which are lower than -25 °C (Figure 8.2). Whilst the magnitude of cooling at the onset of the LLS cannot be quantified in the eVoP due to the hiatuses in the palaeoenvironmental records during the latter phases of the WI, temperatures associated with

the rise in water levels in the eVoP are clearly cooler than the preceding sections of the WYKSE14 sequence, where these taxa are absent from the coleopteran assemblage. Furthermore, TMin ranges below -20°C are only identified in LLS-aged deposits at Gransmoor, supporting deposition after the transition into this cold interval.

This trend can be identified in other sites in NW Europe which, although not precisely dated, also record rising lake levels at the onset of the LLS/YD (Bohncke and Wijmstra, 1988; van Geel *et al.,* 1988; Magny and Ruffadi, 1995; Bos *et al.,* 2006; Magny *et al.,* 2006). This is further supported by $\Delta\delta D_{terr\text{-}aq}$ hydroclimatic records from Meerfelder Maar in Germany (Rach *et al.,* 2014), and Hässeldala Port in southern Sweden (Muschitiello *et al.,* 2015; Wohlfarth *et al.,* 2016), where decreased evapotranspiration rates, inferred as an increase in effective precipitation regimes (represented by a decrease $\delta D_{terr\text{-}aq}$ values), are recorded at an analogous time to the rising water levels in the eVoP (Figure 8.6). The rise in the water table between 12.8-12.65 cal ka BP in the eVoP is therefore interpreted to represent a rise in effective precipitation regimes across Europe after the rapid switch in δD at the onset of GS-1 (Steffensen *et al.,* 2008).

The YD/LLS/GS-1 is widely considered to result from catastrophic meltwater influx into the North Atlantic, fed either from the North American (e.g. Broecker *et al.,* 1989; Teller *et al.,* 2002; Murton *et al.,* 2010; Rayburn *et al.,* 2011) and/or Fennoscandian ice sheets (Bodén *et al.,* 1997; Muschitiello *et al.,* 2015b), which diminished NADW formation and heat flux into NW Europe (Broecker *et al.,* 1989). This explanation however is insufficient in isolation to explain the rise in water tables in NW Europe, as the decrease in temperatures associated with the decline in AMOC strength would have resulted in decreased moisture flux. Two alternative scenarios can account for these changes:

a) Reduced evapotranspiration as demonstrated from the $\delta D_{terr\text{-}aq}$ records (Rach *et al.,* 2014; Muschitiello *et al.,* 2015b) led to rainfall becoming more effective at recharging groundwater between 12.65-12.8 cal ka BP (e.g. Haynes, 2008).
b) The abrupt shift in polar circulation at 12.85 cal ka BP (Steffensen *et al.,* 2008) led to a temporary shift in atmospheric circulation and especially precipitation bearing westerly winds across NW Europe, leading to a temporary increase in moisture availability via precipitation.

Both scenarios provide a viable mechanism to temporarily raise water tables in NW Europe during the initial stages of the stadial. If the rise in the eVoP water table between 12.8-12.65 cal ka BP is assumed to be broadly in phase with the evapotranspiration records from Meerfelder Maar and Hässeldala Port (Figure 8.6), then these conditions lasted for *ca.* 200 years. The transition towards lower regional water-tables after 12.65 cal ka BP, reflects the increase in catchment evapotranspiration, which decreased the effectiveness of precipitation in recharging

groundwater aquifers. The increase in evapotranspiration in the Meerfelder Maar and Hässeldala records is attributed the time taken for sea-ice to expand in the North Atlantic (Brauer *et al.,* 2008; Rach *et al.,*2014; Muschitiello *et al.,* 2015b). When sufficiently far south (at *ca.* 12.68 cal ka BP), it led to cold air masses, devoid of moisture to be focussed from the North Atlantic, across Northern Europe as high intensity winds (Isarin *et al.,* 1998; Brauer *et al.,* 2008). The influx of these air masses explains the sharp increase in evapotranspiration and decreased moisture availability in NW Europe, which would have led to increased aridity and lower lake levels.

This mechanism would have been exacerbated by the development of deep frozen ground which would have limited the efficiency of available moisture transfer to groundwater bodies. Discontinuous permafrost formed across northern England during the LLS (Isarin *et al.,* 1998), and its presence in the eVoP is supported by periglacial involuted structures in the upper surface LfA-6B sediments at Wykeham Quarry (Figure 5.20). These structures demonstrate the development of deep frost under mean annual air temperatures ≤1 °C (Huijzer and Isarin, 1997; Renssen and Vandenberghe, 2003; Kasse *et al.,* 2003). Deep frozen ground would have further decreased the efficiency of precipitation recharging groundwater masses, with any precipitation during summer months dissipated as surface runoff (Vandenberghe and Woo, 2002).

In summary, palaeoclimatic reconstructions from the eVoP have demonstrated a complex hydrological response to decreasing palaeotemperatures during the LLS. A shift in atmospheric circulation, and a decline in temperatures across the North Atlantic between 12.9 and 12.6 ka BP, led to an initial rise in regional lake levels, associated with the southerly shift of the westerlies and the storm track (Brauer *et al.,* 2008; Lane *et al.,* 2013; Rach *et al.,* 2014; Muschitiello *et al.,* 2015), and the increasing efficiency of groundwater recharge. As temperatures decreased, sea ice expanded southward, focussing cold and dry air masses across the British Isles and NW Europe, causing enhanced evapotranspiration and aridity, leading to decreased moisture availability and lower lake levels.

8.4.5. Early Holocene ca. 11.7-11 cal ka BP

In the GICC05 record, the onset of climatic amelioration in the Holocene is placed at 11.65 ± 0.1 cal ka BP (Walker *et al.,* 2009; Rasmussen *et al.,* 2014), where it is characterised by a 2–3 ‰ shift in δD, followed by a rise in δ^{18}O, representing a rapid change in atmospheric circulation (northward shift of the polar front), and a subsequent increase in temperature (of *ca.* 10 ± 4 °C Severinghaus *et al.,* 1998) respectively (Steffensen *et al.,* 2008; Walker *et al.,* 2009). Lower amplitude climatic oscillations, after the Pleistocene–Holocene boundary, determined via perturbations in δ^{18}O, and accumulations rates are also identified (e.g. Vincent and Cwynar, 2016), the most pronounced of which occurs at 11.55-11.45 ± 0.1 cal ka BP, and is termed the

11.4 ka event in Greenland (Rasmussen *et al.,* 2007; 2014), and the Preboreal Oscillation (PBO) in NW Europe (Björk *et al.,* 1997).

Warming signals correlated to the Pleistocene-Holocene boundary in the British Isles are also abrupt, and reflect a similar structure to the GICC05 record, with an abrupt rise in C-ITs and $\delta^{18}O_{bulk}$, before a temporary decline in temperatures. These oscillations can be correlated to the 11.4 ka event/PBO, and are interpreted to represent a short deterioration in NADW formation, via freshwater influx from Northern Hemisphere ice melt (Björk *et al.,* 1997). The hydrological records from the eVoP correspond well to hydrological reconstructions in NW Europe, throughout the LGIT. Therefore, the regional $\delta D_{terr\text{-}aq}$ records, reconstructed from Hässeldala Port and Meerfelder Maar (Rach *et al.,* 2014; Muschitiello *et al.,* 2015b) should also be reflected in the local hydrology in the eVoP at this time. These records are both characterised by low but rising $\delta D_{terr\text{-}aq}$ values, reflecting progressively lower rates of evapotranspiration from *ca.* 11.8-11.6 cal ka BP (Rach *et al.,* 2014). The rise in the water table from *ca.* 21-24 m OD in the eVoP can therefore be correlated to this decline in evapotranspiration, which may reflect the cessation of high intensity winds across NW Europe, and the gradual northward shift of atmospheric circulation cells, bringing progressively higher abundances of heat and moisture to NE England, NW Germany, and S Sweden (Rach *et al.,* 2014; Muschitiello *et al.,* 2015b). These changes would have led to the break-up of any residual permafrost in the landscape, increasing the efficiency of groundwater recharge via higher volumes of effective precipitation.

By implication therefore, the lack of an episode of rising temperatures which can be correlated the Pleistocene-Holocene boundary in the eVoP, is interpreted to represent low water tables, meaning that by *ca.* 11.65 cal ka BP, open, stable water bodies required for marl formation were not present in the eVoP. The initial rise in $\delta^{18}O_{bulk}$ values in the PF record are therefore most likely to represent the climatic amelioration after the 11.4 ka event/PBO, rather than the Pleistocene-Holocene boundary.

Finally, it is important to explain the mechanisms leading to heterogeneous palaeoclimatic proxy data identified across the two major warming episodes during the LGIT. The transition into the WI is recorded in the WYKNE15 sequence by a sharp rise in $\delta^{18}O_{bulk}$ values corresponding to an increase in mean annual air temperature, and recorded in authigenic carbonate (Figure 8.3). Similar amelioration signals are demonstrated across the North Atlantic region during the transition into the EH, but are not seen in the eVoP. This is interpreted to relate to the changing water table alongside the amount of preceeding infill in the studied palaeolake basins at Wykeham. The hydroclimatic response to the WI amelioration, was sufficient to form an open water body in Depression B at >19 m OD. However, it was insufficient to produce standing water in the Depression >*ca.* 24 mOD (where the WYKNE15 sequence had infilled to by this time) by *ca.* 11.65 cal ka BP. This also applies to the PF Core B sequence which had filled to an

altitude of *ca.* 22 m OD by this time (Palmer *et al.,* 2015). Therefore, by the time marl began forming in PF Core B at *ca.* 11.4-11.1 cal ka BP, (Candy *et al.,* unpublished data), the Wykeham records had already begun terrestrialising via hydroseral succession (WN-M7, WS-M5b).

9. Reconstructing landscape responses to hydroclimatic changes in the eVoP during the Last Termination

9.1. Introduction

Previously, the understanding of landscape evolution in the VoP through the Last Termination has been limited, principally due to the lack of detailed geomorphic evidence in the valley, and robust, locally derived palaeoclimatic datasets. New data obtained from the Wykeham area (Chapters 5-7; Figure 9.1) allows the climatic evolution and environmental responses of NE England to be understood in greater detail than before. These data demonstrate that the broad climatic structure of the LGIT in the eVoP is comparable to other regional records, including the GICC05 stratotype (Chapter 8). Furthermore, they demonstrate that hydrological changes in the eVoP, in the main, closely corresponded to changes in regional climatic regimes and, most notably, variations in effective precipitation and temperature in Northern Europe. The combination of the palaeoenvironmental data with the GIS mapping of the eVoP and sedimentological data obtained from Wykeham Quarry provide further evidence that allow the reconstruction of the phasing of landscape development through the LGIT. These models can be used to provide valuable context to the timing of human occupation in the eVoP, allowing an integrated model of landscape evolution through the Last Termination to be constructed. This chapter presents a landscape model for the eVoP, using reconstructions of vegetation, hydrological, fluvial development through the LGIT, and a synthesis of how these reconstructions can be used to assess the leads and lags of the landscape to climatic forcing. The chapter then assesses how these landscape response signals can be used to better assess the factors responsible for the timing and manner of human occupation in the valley through the LGIT.

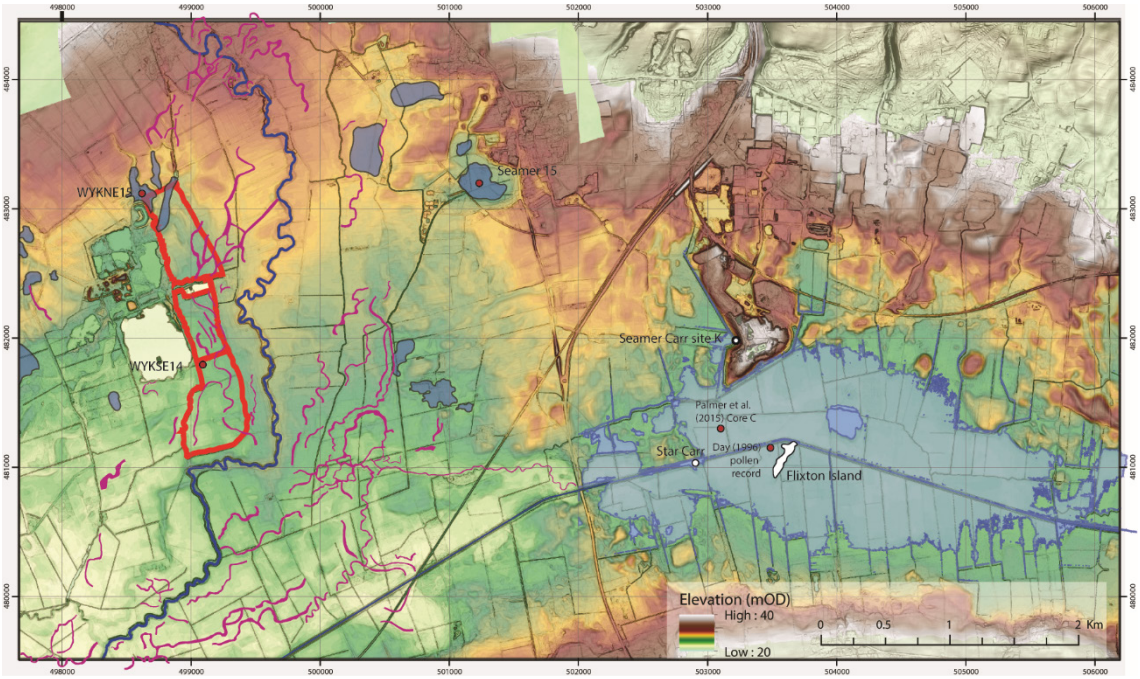

Figure 9.1. (previous page). *Location of sites used to construct the landscape model for the eVoP (WYKNE15 and WYKSE14 from Wykeham Quarry, Seamer 15 and PF). The location of the archaeological sites around the margins of PF are also displayed alongside Channel Assemblage B channels (purple), and other potential basins (dark blue).*

9.2. Re-interpretation of the deglaciation of the eVoP

The data obtained in this study represents the most detailed examination of the landforms and sediments in the eVoP, and demonstrates that the VoP sees the transition from a glacial lake system to a subaerial landscape, dominated by isolated lakes and a developing fluvial system over a period of *ca.* 2000 years (from *ca.* 17-15 cal ka BP). Whilst it is accepted that there are substantial uncertainties on the ages that constrain this activity, it would appear that ice advance into the VoP had occurred by *ca.* 18 ka and ice retreat began at *ca.* 17.6 ka BP, with the glacial lake systems lowering relatively quickly during this interval (Evans *et al.,* 2016). Assuming that Kirkham Gorge remained the principal outflow from the VoP after ice recession, the progressively lowering lake levels of Glacial Lake Humber (25-10 m OD between *ca* 15.9-<15.5 ka BP; Fairburn and Bateman, 2016), continued to inundate the western VoP, but developed a subaerial landscape by *ca.* 15.6 ka BP in the eVoP, with fluvial activity occurring in the Wykeham area (Channel Assemblage A channels). Critically the sedimentary sequences at Wykeham allow the connection of Dimlington Stadial deposits with LGIT deposits from the eVoP. There are still areas which require further litho-, morpho-, and chronostratigraphic detail, but that potential is demonstrated to lie in the eVoP.

9.3. Developing a landscape model for the eVoP through the LGIT

Datasets that can be used to reconstruct the development of the landscape in relation to climatic parameters through the LGIT, derive from the mapping of landforms in the eVoP, the development of the sedimentology, stratigraphy, and chronology of deposits at Wykeham Quarry (Chapter 5), and the palaeoenvironmental reconstructions selected sequences (Chapter 6). Using these datasets, the evolution of the landscape with respect to changes in vegetation, hydrology, river activity, and landscape stability can be reconstructed, in order to develop a landscape model for the eVoP (Figure 9.2). These reconstructions are discussed in the following sections.

9.3.1. Vegetation development

Vegetation development during the E-WI is not well constrained in the Wykeham records, limited to the macrofossil record obtained from the WYKNE15 sequence. Macrofossil concentrations during this interval are low, with terrestrial remains consisting principally of *Betula nana* and *Poaceae* (WN-M2). This demonstrates that vegetation cover in the eVoP was low, and limited to open ground, and dwarf shrub taxa.

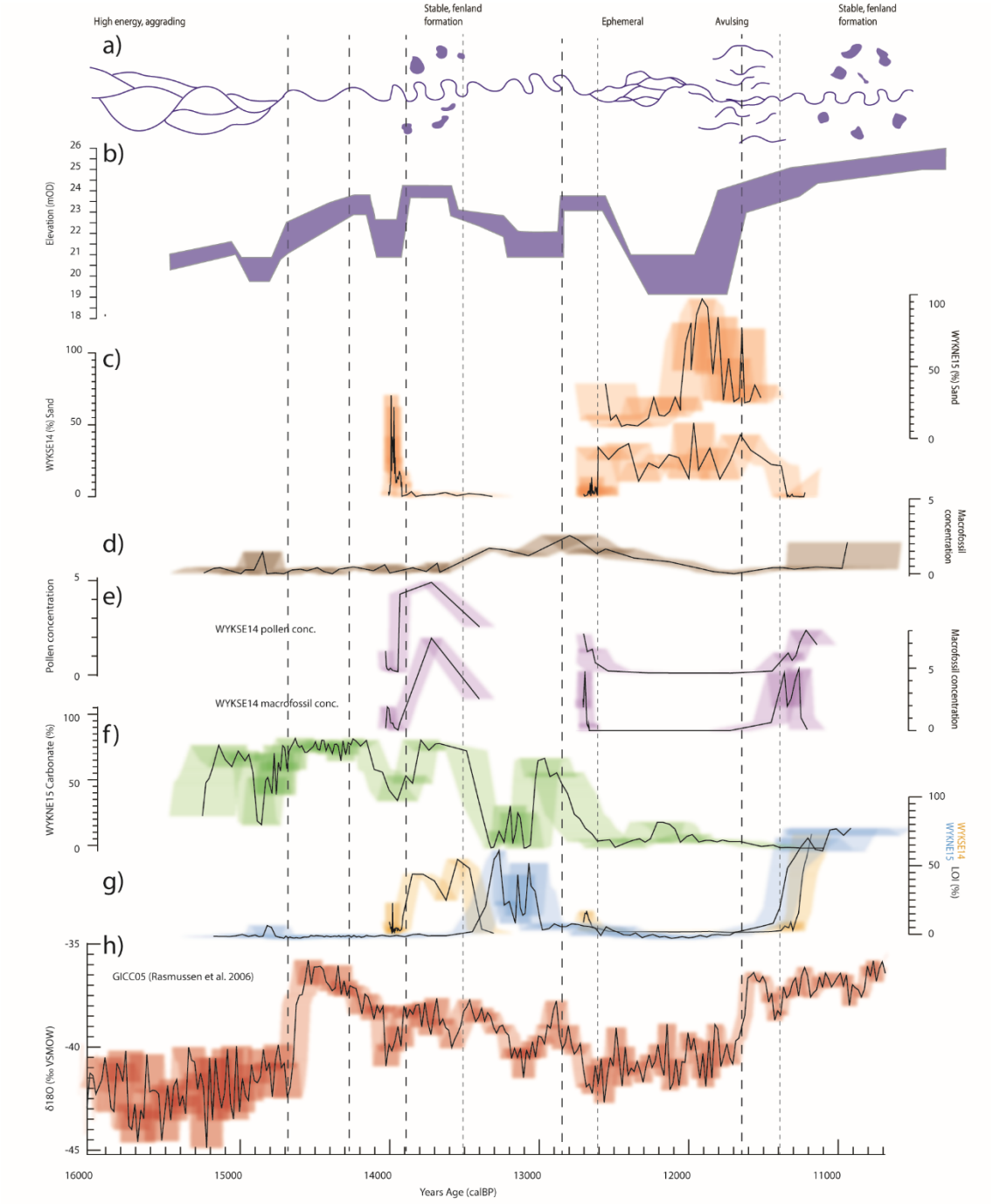

Figure 9.2. *Summary of the landscape models and palaeoenvironmental datasets from the Wykeham records: a) Model of fluvial activity of the River Derwent presented in Figure 9.4, b) water table elevation model for the eVoP (Chapter 7), c) siliclastic sand (%) of the WYKNE15 and WYKSE14 sequences, d) Macrofossil concentration (per 20 cm³) from the WYKNE15 sequence, e) pollen and macrofossil concentrations from the WYKSE14 sequence, f) Calcium carbonate (%) in the WYKNE15 sequence, g) LOI (%) from the WYKNE15 (blue) and WYKSE14 (yellow) sequences, h) NGRIP $\delta^{18}O_{bulk}$ record plotted on the GICC05 timescale (Rasmussen et al., 2006).*

This reconstruction is supported by other vegetation records from England which show that vegetation development lagged climatic amelioration at the onset of the LGIT (Pennington *et al.*, 1986; Walker *et al.*, 1993) either due to the migrational delay of taxa from glacial refugia, or local delays in the maturation of soils and the establishment of high and stable water tables (Birks and Birks, 2014). Therefore, although optimum mean annual air temperatures through the WI were achieved during the initial stages of the WI (WN-I3), terrestrial vegetation cover lagged the

palaeotemperature signal, demonstrating that this was not the principal control on distribution (Birks and Birks 2014). *Betula nana* in WN-M3 support that much of the *Betula* pollen abundances in other records is derived from the dwarf shrub taxa rather than tree remains (Bartley, 1962; Day, 1996; Walker *et al.,* 1993; Innes 2002) prior to the rise of *Juniperus.* This is supported by macrofossil records in Scotland, Ireland, and Northern Europe which demonstrate the local absence of tree-*Betula* until at least 14 cal ka BP/the Allerød/M-L-WI (van Geel *et al.,* 1989; Mortensen *et al.,* 2011; van Asch *et al.,* 2012; Birks and Birks, 2014).

Juniperus communis macrofossils, are present in the Wykeham records between *ca* 14.2-13.9 cal ka BP, and represent the expansion of *Juniperus* shrubs during the latter stages of- and soon after the WN-I4b climatic oscillation. The influx of *Juniperus communis* is diagnostic of this interval, where it is present in macrofossil and pollen form in the WYKSE14 and WYKNE15 records, and correlated to the S-2 pollen zone in Day (1996) from PF. This correlation is supported by a coincident rise in microcharcoal abundance, where it is interpreted to represent a short-lived deterioration in climate (Day, 1996). In the Wykeham records, high abundances of macrocharcoal are identified in association with charred and partially burnt plant remains, including *Juniperus communis* needles.

This correlation raises two discussion points. Firstly, how does the expansion of *Juniperus* in the eVoP compare with other regional signals where its presence has previously been interpreted to represent early vegetation expansion during the climatic optimum of the WI (Innes, 2002; Watts,1977; Bridgland *et al.,* 2011)? Secondly, what is the correlation between its local presence in the eVoP and the increase in local fire regimes?

Juniperus communis is a drought and cold tolerant shrub that subsists in unshaded habitats (Birks and Birks, 2014). Therefore, its presence in LGIT pollen records is often interpreted to represent initial biotic response to climatic amelioration, acting as a precursor to the development of open woodland into Northern Britain (Pennington *et al.,* 1977; Innes, 2002). The eVoP presents an opportunity to link the vegetation signals recorded with local climatic data. This link shows that the expansion of *Juniperus* in the eVoP occurs *ca* 500-800 years after the climatic amelioration at the start of the WI (WN-I3a), suggesting that either its expansion is not a good indicator of climatic amelioration during the WI, or its spread was spatially diachronous across the British Isles, driven by parameters other than temperature (Bush, 1993). Other dated palynological signals from Holderness (Walker *et al.,* 1993; Gearey, 2008), also illustrate a multi-centennial scale biotic lag to climatic amelioration, with *Juniperus* not declining until *ca* 14 cal ka BP, broadly coincident with the decline in the eVoP.

The manner of *Juniperus* decline also merits further discussion as its coincidence with rises in micro- and macrocharcoal, including charred *Juniperus* macrofossils support widespread burning

of *Juniperus* shrubs in the landscape. The role of fire in landscape development during the LGIT is poorly resolved (Edwards *et al.,* 2000), but is principally attributed to natural, or anthropogenic ignition. The microcharcoal peak from this interval in PF has previously been interpreted to relate to Upper Palaeolithic human activity in the eVoP (Day, 1996). This is thought to be unlikely, as the deposition of micro- and macrocharcoal occurs prior to the development of the most stable landscape conditions in the eVoP in which Upper Palaeolithic cultures in Northern Europe have been demonstrated to favour (Mortensen *et al.,* 2014). Additionally, the repeated ignition of high intensity fires across the eVoP is not seen again through the remaining phases of the WI, when humans are known to be present (Schadla-Hall, 1987; Day, 1996; Conneller, 2007). This supports that the macro- and microcharcoal around *ca.* 14 ka is unlikely to derive from anthropogenic burning. The burning signal occurs in close association with the WN-I4b climatic oscillation. This oscillation led to colder, and more arid conditions in the eVoP (WS-L5a, WN-M3b), coupled with a decline in the growth of *Betula* and an expansion of herbaceous communities (Day, 1996). These conditions would lead to an abundance of dead and dry wood in the catchment, providing an extensive fuel source which would have been susceptible to ignition via lightning strikes (van der Hammen and van Geel, 2008; Abatzoglu *et al.,* 2016). The macro- and microcharcoal presence during this interval is therefore interpreted to represent the initiation of repeated high intensity wildfires which were fuelled by the abundance of dead and dry wood and organic remains left in the catchment, as a result of the cold and arid climatic conditions through the WN-I4b climatic oscillation. The presence of these burning signals at both Wykeham and in PF suggests this event impacted the vegetation and potentially landscape stability of the entire eVoP.

Rises in pollen and macrofossil concentrations, and organic content between *ca.* 13.9-13.5 cal ka BP in the WYKSE14 sequence, soon after the decline in *Juniperus*, point towards a significant increase in biomass in the eVoP. This is supported by the high concentration of woody remains in LfA-6B at Wykeham Quarry, demonstrating that the Derwent floodplain was well vegetated during this interval.

Plant macrofossil, and pollen analysis from the Wykeham sequences correspond with other northern British records (e.g. Innes, 2002; Walker, 2005; Bridgland *et al.,* 2011) showing that the latter half of the WI represents the period of maximum vegetation development during the Interstadial. Pollen and macrofossil concentrations reach peak values, and the water bodies in the Derwent floodplain became meso-eutrophic, occupied by high abundances of aquatic and eulittoral vegetation, indicating high levels of biological productivity, and more acidic conditions, reflecting soil maturation (van Geel *et al.,* 1989; Rodwell, 1995; Ampel *et al.,* 2015). This is supported by pollen records from PF which show that after the peak in *Juniperus* pollen, *Betula* percentages increase to *ca* 50 % of total land pollen (S-3a, Day, 1996), reflecting the expansion of vegetation cover < 14cal ka BP in the eVoP (Figure 9.3). This trend occurs in pollen records

in NE England, with rises in *Betula* (Walker *et al.,* 1993; Gearey, 2008), and peat formation containing *Betula* twigs across coastal exposures in Filey Bay, at 11.38 ± 0.26 ^{14}C yr BP (Edwards, 1978; calibrated by author to 13.75-12.75 cal ka BP).

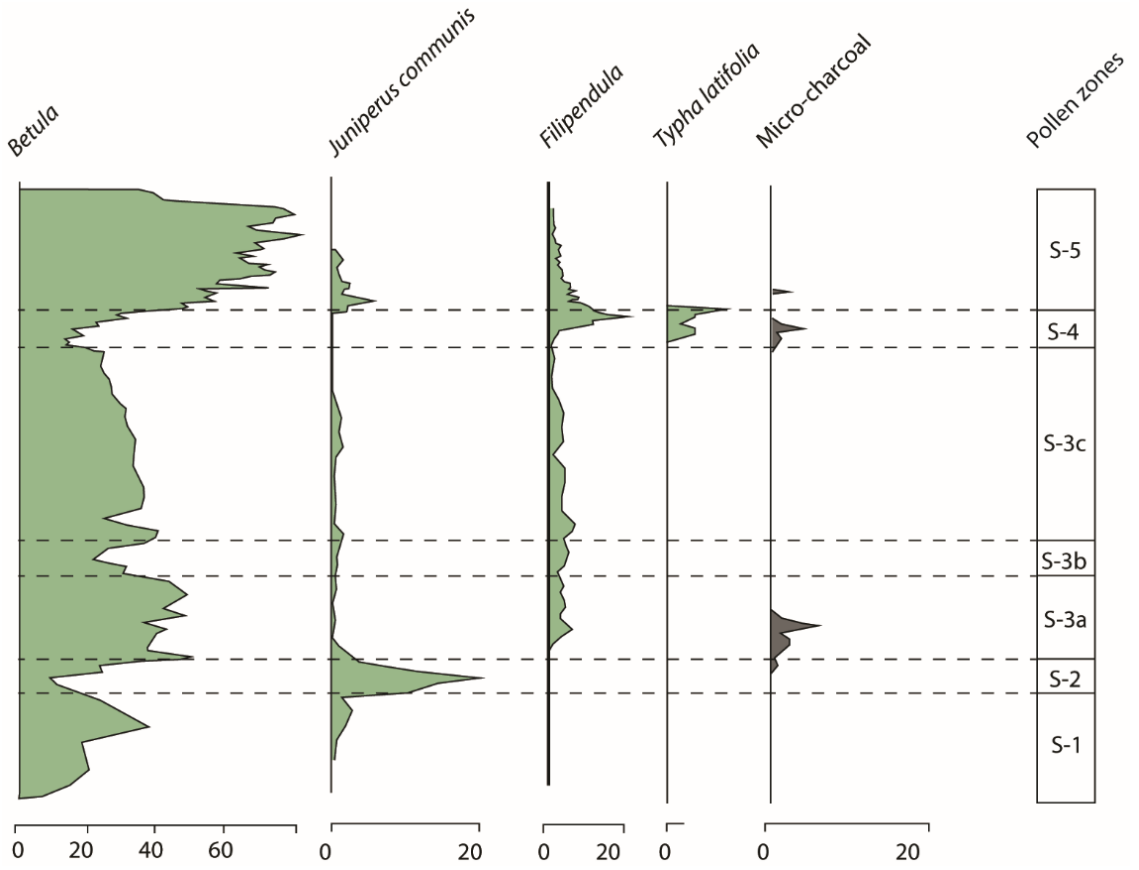

Figure 9.3. *Pollen diagram of selected taxa through the LGIT, discussed in text from PF (Day, 1996).*

In NW Europe, this transition is attributed to the final melting of residual permafrost (Hoek, 1997; Bos *et al.,* 2006), and/or the maturation of deep soils viable for vegetation development. The role of moisture is also posited for the lagged expanse of *Betula pubsescens* in NW Europe (Mortensen *et al.,* 2014; Birks and Birks, 2014). This may also apply in the eVoP where the optimum period of vegetation development in NE England (Day, 1996; Sheldrick, 1997; Bridgland *et al.,* 2011) occurred during the period of maximum water table elevation in the eVoP, when residual soils developed through the early Interstadial would have been sufficiently moist and mature to provide favourable conditions for growth (Hoek and Bohncke, 2002). The lack of tree *Betula* macrofossils in the Wykeham records however demonstrate that the eVoP was not extensively wooded between *ca.* 13.9-13.6 cal kaBP. This is supported by macrofossil records from Denmark and South Wales where macroremains of tree *Betula* were not present until *ca.* 13.6 cal ka BP (Mortensen *et al.,* 2011; 2014; Walker *et al.,* 2003 respectively), by which time sedimentation into the WYKSE14 and WYKNE15 sequences was characterised by eulittoral development and hiatuses, which would have diminished macorofossil influx into these records.

Between *ca.* 12.8-12.65cal kaBP, macrofossil and pollen concentration data demonstrate that considerable vegetation cover was still present in the eVoP (WS-M3b, WS-P4, WN-M5), but was characterised primarily by open ground shrubs and herbaceous taxa, demonstrating a relative deterioration in comparison to the mid-late Interstadial (*ca* 13.9-13.5cal ka BP). These changes would have been driven principally by the crossing of ecological thresholds, for a number of taxa, with declines in winter temperatures to *ca.* -20 °C (MCR C; Walker *et al.,* 1993) producing conditions unviable for growth. Furthermore, the decrease in effective precipitation in the eVoP after *ca.* 12.65 cal ka BP, coupled with enhanced wind intensity (Brauer *et al.,* 2008) would have further limited growth of most taxa subsisting in the valley prior to the onset of the LLS. This is supported by the LLS aged sediments in the eVoP, which are characterised by low organic/carbonate contents, and low pollen and macrofossil concentrations, representing low organic productivity, and minimal vegetation cover during the LLS (Day, 1996).

As climate ameliorated during the initial stages of the EH (*ca.* 11.65-11.4 cal ka BP), vegetation in the Wykeham records was characterised by open ground herbs and fenland taxa such as Poaceae, *Typha latifolia*, *Filipendula ulmaria,* and *Urtica. dioica* representing pioneering vegetation development. This phase can be confidently correlated to the S-4 pollen zone of the Day (1996) record, which shows a rise in *Filipendula* pollen prior to the rise in *Betula* and pollen concentration in S-5 (Figure 9.3; Cummins, 2003). The presence of *Typha latifolia* and *Filipendula ulmaria* support that temperatures had ameliorated sufficiently by this time (MCR-D), whilst the influx of aquatic fauna such as *Cristatella mucedo* and *Chironomidae sp.* support the presence of at least temporary standing water in the floodplain by *ca.* 11.4 cal ka BP. Biomass across the catchment is interpreted to have remained low however, primarily due to the low bulk organic contents in the Wykeham sequences, demonstrating low organic productivity. These conditions existed for *ca.* 200 years after the initial amelioration at the onset of the EH, reflecting another environmental lag to abrupt climatic change similar to that seen during the E-WI.

The influx of *Urtica. dioica* macrofossils in WS-L9a is interpreted to represent a temporary decline in TMax temperatures and relative lake level. This is correlated to the abrupt climatic oscillation termed as the 11.4 ka event (Rasmussen *et al.,* 2014). Soon after this interval, increasing abundances of wood fragments in the WYKSE14 macrofossil record, coupled with rises in pollen, macrofossil and organic content demonstrate the development of eutrophic conditions across the Derwent floodplain. In pollen records from PF, a sharp rise in *Juniperus* followed by *Betula* in S-5 demonstrates a distinct increase in vegetation cover coinciding with the decline in *Filipendula* and *Typha latifolia* (Day, 1996).

9.3.2. Hydrology

The hydrological reconstructions for the eVoP have been described and discussed previously in Chapters 7 and 8. Here, the effect that the shifts in the water table had on the landscape are briefly reviewed. The Wykeham records demonstrate that the LGIT water table was initially low, forming water bodies in only the deepest topographic depressions (Depression B) before steadily rising through the initial stages of the WI, eventually reaching an altitude required to initiate sediment accumulation in the shallower topographic depressions in the eVoP (Depressions A and C).

This trend conflicts with the palaeoclimatic reconstructions which demonstrate progressively declining mean annual temperatures during the latter stages of the E-WI (WN-I4). Based on this model, the water table would be expected to rapidly increase to an optimum elevation when temperatures were warmest (WN-I3), reflecting maximum AMOC strength, and therefore high moisture delivery. Climate models through this interval however show no discernible change in effective precipitation delivery to NW Europe across the climatic amelioration (Renssen and Isarin, 2001). This delayed response may relate to high summer insolation regimes, and high wind strengths which would enhance evaporation, and diminish precipitation supply to groundwater reservoirs (Renssen and Isarin, 2001; Birks and Birks, 2014). Additionally, effective moisture supply may initially have been lower during the early stages of the LGIT due to the lower sea-levels in the North Atlantic, and the North Sea (Lambeck, 1995; Ward *et al.,* 2016), which would have diminished groundwater recharge. As vegetation cover developed, soils stabilised, sea levels rose, and water percolation into reservoirs increased in efficiency, the water table elevation rose through the WI.

This trend was briefly perturbed by the abrupt climatic oscillation (WN-I4b), which led to a decline in the water table elevation. This can be attributed to a decrease in effective precipitation as a result of a weakening in AMOC strength. These conditions would have developed a more arid environment in the VoP, potentially crossing the ecological niches of moisture requiring terrestrial taxa (Birks and Birks, 2014), being replaced by open ground herbs (e.g. *Saxifraga sp.* and *Carophyllaceae sp.* in WN-M3a to 3b) and taxa tolerant to aridity (e.g. *Artemisia* in WS-P1 to -P2).

The water table reached its optimum elevation in the WI between *ca.* 13.9-13.65cal kaBP (WS-M3a; Figure 9.2), demonstrating increased efficiency in groundwater recharge after the WN-I4b oscillation. This interval is also coincident with a decline in the sedimentation rate in the Derwent floodplain (stratigraphic assemblage D), and siliclastic content of deposits, indicating that the rise in the water table was coincident with an increase in landscape stability under mild summer temperatures (MCR-B). This interval lasted for *ca.* 400-500 years before a decline in the

elevation of the water table at *ca.* 13.6-13.5 cal ka BP (WN-M4, WS-M3a-3b), which was maintained until the early stages of the LLS.

At the transition into the LLS (between 12.8-12.65 cal ka BP), the water table elevation rose (WS-M3b), representing an increase in effective precipitation under cold climatic conditions (MCR-C, WN-I5). These conditions lasted for *ca.* 100-200 years before the water table lowered below the infill of the Wykeham sequences (between *ca.* 12.6-11.7 cal ka BP), reflecting a decrease in effective precipitation and enhanced evapotranspiration.

The combination of low temperatures and high moisture availability would have developed snowbeds persisting late into the year in the eVoP (supported by the presence of *Salix herbacea* and *Selaginella selaginoides* in WN-M5), coupled with discontinuous permafrost (Isarin and Bohncke, 1999). As effective precipitation decreased through the LLS, this trend would have been reversed as less precipitation/snowfall reached the eVoP and a more continental climatic regime developed.

9.3.3. Fluvial activity

Using the GIS map of the River Derwent floodplain in the eVoP, and the sedimentological data from Wykeham Quarry (Chapter 5), a model of the fluvial modes of the River Derwent can be constructed through the LGIT (Figure 9.4). This model is constructed principally using observed changes in the sedimentological characteristics of LfA-6 deposits at Wykeham Quarry which provide viable evidence with which to differentiate fluvial regimes in lowland river systems (Miall, 1978; 1996; Rose, 1995). These reconstructions are supported by the 3 channel types identified across the eVoP (Channel Assemblage A-C). Using the radiocarbon dates obtained from these landforms and deposits (Fraser *et al.,* 2009), the timing of the shifts in river activity can be assigned. This model is discussed below.

There is limited sedimentological evidence available from Wykeham Quarry to reconstruct river activity > *ca.* 14 cal ka BP. Lowland British rivers are interpreted to have been incising during the E-WI, due to the low base level (sea level) and reduced sediment transfer upstream leading to an excess in river energy (Rose, 1995). This may also apply to the River Derwent in the eVoP, explaining the lack of aggradation in the floodplain, although no palaeochannels can readily be attributed to this phase of incision, likely as they have subsequently been infilled and hidden from the present-day topography. The elongated N-S geometry of Depression C in the upper surface of the outwash plain provides a candidate for such a channel incised into the glacial outwash sediments (LfA-2), which has been subsequently infilled by LfA-6 deposits. Furthermore, a 12 m deep section at the southernmost extent of the survey area in the quarry shows that significantly deeper palaeochannel remnants may be present elsewhere in the floodplain, outside the confines of Wykeham Quarry. The fact that no sediments in the floodplain can be confidently attributed

to aggradation prior to *ca* 14 cal ka BP demonstrates that the river was most likely incising at this time, driven by: a) increased moisture availability from enhanced AMOC conditions, and the melting of permafrost b) relatively low water table elevations in the eVoP c) decreasing sediment load, driven by the development of vegetation in the catchment (Day, 1996) d) high levels of glacial isostatic adjustment soon after BIIS recession (Bradley *et al.,* 2011).

Between 14.2-13.8 and 12.75-12.65 cal ka BP, the deposition of fossiliferous silts, clays and peats across the River Derwent floodplain at Wykeham Quarry (LfA-6B) are indicative of overbank sedimentation, and backswamp fen formation (Rose *et al.,* 1980; Miall, 1985; Rose, 1995). This demonstrates a transition to low energy and stable conditions in the River Derwent floodplain. Similar transitions are identified in almost all lowland river systems across the British Isles during the M-L-WI (e.g. Brown *et al.,* 1994; Rose, 1995), and many Northern European records during the Allerød (e.g. Kasse *et al.,* 2005; Tolksdorf *et al.,* 2013), suggesting that the driving factor for this transition was most likely a change in regional climatic and/or environmental controls, rather than local controls within individual river catchments. Furthermore, it demonstrates that the transition toward river systems characteristic of temperate lowlands occurred *ca* 500-700 yr after the initial climatic amelioration at the onset of the LGIT.

Two variables reconstructed here can help explain the transition of the Derwent to a low energy river system: a) higher groundwater levels in the eVoP, minimising the river energy, b) increased vegetation cover in the catchment, stabilising lateral movement of the channel. The higher water tables during this interval infer stable precipitation regimes, which would have in turn supported a more stable fluvial regime with minimal fluvial energy in the lowland regions.

This is supported by deposits in the floodplain (LfA-6B) which are characteristic of formation within standing water, with a high proportion of sediment being transported as suspended loads (Rose *et al.,* 1980). The increase in vegetation cover in the catchment would have resulted in decreased sediment yields from the river, resulting in a decline in sedimentation rates (WS-M3a). The regular discharge of the river and the lower sediment yields prevented the winnowing of silts and clays during peak flood events. These sediments would have formed cohesive banks that favoured river channel meandering (Rose, 1995; Kasse *et al.,* 2005).

Deterioration in mean annual temperatures and a decline in the water table is reconstructed in the Wykeham palaeoenvironmental sequences by *ca.* 13.5 cal ka BP. The only data for fluvial activity in the eVoP during this period comes from a radiocarbon date on a subsidiary palaeochannel infill in Channel A1 of 13.2-12.95 cal ka BP (OxA-32438; RHUL S10), which demonstrates that river channels were re-activated and subsequently abandoned in the floodplain during the period of low lake levels in the eVoP between *ca.* 13.5-12.8 cal ka BP. In

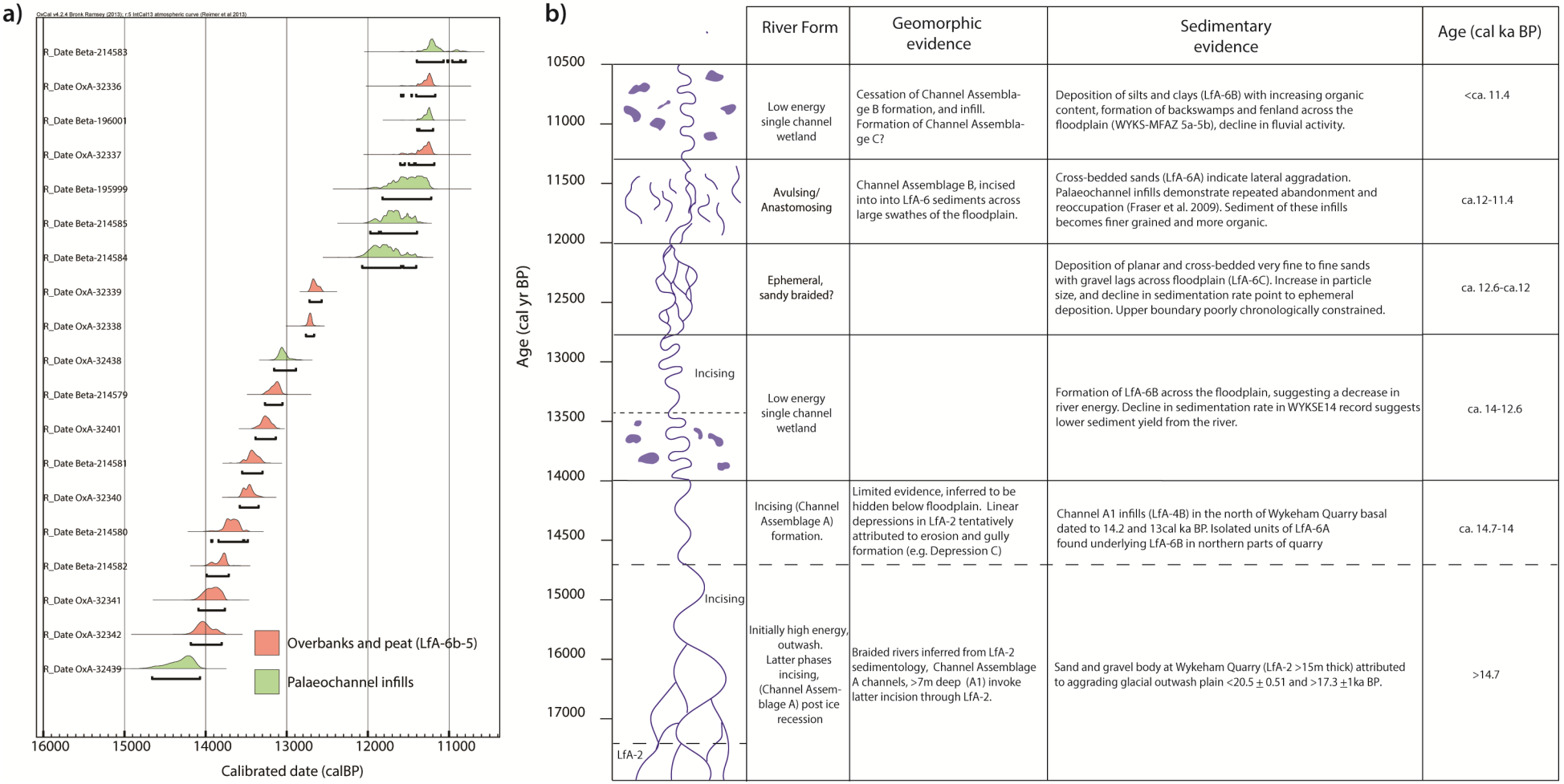

Figure 9.4. *Reconstruction of fluvial activity at Wykeham Quarry through the Last Termination. a) The radiocarbon dates used to chronologically constrain fluvial activity. These dates are derived from this work (OxA dates) and previous work by NAA at Wykeham Quarry, reported in Fraser et al. (2009). b) Schematic model of river activity at Wykeham Quarry. Supporting geomorphic and sedimentary evidence obtained for each stage is listed alongside age ranges.*

other British lowland rivers such as the River Gipping, incision was manifested in the form of large scale discontinuous gullies, rapidly eroding the cohesive bed material of the floodplain during periods of excessive river energy during this interval (Rose and Boardman, 1983). For such features to form, a more erratic flow regime is required characterised by higher relative peak discharges. Deteriorating temperatures would have led to a more ephemeral river flow regime, producing higher peak discharge nival fed flows during the early spring and summer months, but minimal flow during winter. During the hiatuses in the Wykeham sequences, sediments were continuously accumulating in PF (Day, 1996; Palmer *et al.,* 2015). Pollen signals from these deposits demonstrate that vegetation cover continued to remain relatively high on the landscape during this interval (Day, 1996).

The model of river formation between *ca.* 13.5 to 12.9 cal ka BP is therefore interpreted to mirror that of the River Gipping, with incision through the cohesive bed material deposited in the floodplain during the M-L-WI (LfA-6B; Rose, 1995). The lack of confidently identifiable gully forms in the floodplain is attributed to subsequent alluvial infill during the LLS and EH (Rose and Boardman, 1983), although deeper stratigraphic assemblage D sequences at Wykeham Quarry, which lack organic rich LfA-6B deposits may be evidence of erosion via channel incision during this interval. More data from these features during later excavation phases in Wykeham quarry will provide further information on these landforms and their infill.

At the start of the LLS (between 12.8-12.65 cal ka BP), fine-grained sediments continued to be deposited across the Derwent floodplain (WS-L7-8a; LfA-6B), demonstrating: a) low energy sedimentation regimes and b) a high relative water table. The fluvial activity during the initial LLS is therefore interpreted to have continued to have been low energy and similar in form to that reconstructed between *ca* 13.9-13.5 cal ka BP, although higher sedimentation rates through this interval demonstrate an increase in available sediment. This is interpreted to have been driven in part by the re-emergence of standing water bodies in the eVoP, which would have dissipated river peak flow discharges in the valley lowlands (Rose, 1995). Macrofossil and pollen concentration data demonstrate that considerable vegetation cover was still present in the eVoP at this time, which also would have preserved the cohesive banks of the river system, limiting the potential for avulsion (Brown *et al.,* 1994; Howard, 2005).

The transition to coarser particle sizes in LfA-6C, demonstrates increasing depositional energy of the river system during later stages of the LLS. However, from the age-depth model obtained from the WYKSE14 sequence, it is evident that sedimentation rate also declines significantly through this interval. A more ephemeral sedimentation regime is therefore required to explain these changes. Evidence of river activity during this period is derived principally from LfA-6C deposits at Wykeham Quarry. These deposits show evidence of horizons of planar bedded, and

cross bedded ripple laminations, demonstrating formation via flows from the N to NE of the quarry area (Fraser *et al.,* 2009). Vegetation cover through this interval was minimal and any river flow therefore would have had relatively low lateral constraint, and during periods of peak flows would have been spread across large areas of the floodplain. These features are therefore interpreted to derive from an ephemerally braided river planform (e.g. Kasse *et al.,* 2003), fed by high peak flow velocities from nival snowmelt. Transitions to braided river planforms are commonly attributed to lowland floodplains during the LLS/YD (e.g. Rose *et al.,* 1980; Rose and Boardman, 1983; Rose, 1995; Kasse *et al.,* 1995; 2003), driven by an increased availability of sediments/declining biomass cover, and increasing surface run off driven by the development of periglacial conditions (Vandenberghe, 2003; Vandenberghe and Woo, 2002).

Whilst the lower water table and minimal vegetation cover in the eVoP would have decreased the bank stability of the River Derwent, the lower sedimentation rates are indicative of a more continental climatic regime, which diminished river discharge and created a deficit in river energy. This would have led to a higher availability of sediment to be transported to the river channel (Rose and Boardman, 1983). Aggradation in the floodplain from ephemerally fed nival discharges during summer months therefore provides a valid explanation of the river development (LfA-6C- LfA-6A; Rose, 1995). The floodplain during this interval would therefore have had long quiescent phases through the year, which would have made the floodplain sediments (LfA-6) susceptible to erosion and re-deposition via strong windstorms during the Autumn and Winter months (Brauer *et al.,* 2008). These processes also transported and deposited aeolian sediments across large areas of Northern Britain (Gaunt *et al.,* 1971; Bateman *et al.,* 1998; Bateman, 2001).

During the latter stages of the LLS and the initial stages of the EH, fluvial activity in the River Derwent floodplain increased as laterally unstable and avulsive rivers channels were formed (Channel Assemblage B; stratigraphic assemblage E). Radiocarbon dates on the basal infill of these channels at Wykeham Quarry, range between 12.35-11.2 to 11.15-10.45 cal ka BP (Fraser *et al.,* 2009; Figure 9.4). This age range overlaps with the Pleistocene-Holocene boundary (Walker *et al.,* 2009), indicating that their formation was at least in part driven by antecedent climatic conditions. Increasing seasonal temperature and precipitation regimes at the end of the LLS (Rach *et al.,* 2014; Muschitiello *et al.,* 2015; Chapter 8) would have led to high volumes of stored snow, and permafrost melting slightly prior to, and across the Pleistocene-Holocene boundary. Low vegetation cover in the floodplain meant bank stability during peak flow discharges was low, and therefore the potential for lateral aggradation and avulsion was high, with channels being repeatedly abandoned and reoccupied during periods of peak discharge (Brown *et al.,* 1994). These conditions fit with the model of a northward shift of the polar front, and break-up of North Atlantic sea ice during the unstable latter half of the YD/LLS (Bakke *et al.,* 2009; Lane *et al.,* 2013). The spasmodic introduction of warmer and wetter conditions into

NE England, would have produced phases of snow build-up and melt in the Derwent catchment, feeding ephemeral high energy discharges into the eVoP.

The persistence of channel formation into the EH, reflects the lag in the water table rise and vegetation development, meaning unstable and poorly vegetated river banks would have persisted in the floodplain, leading to low interception and infiltration rates. Higher than contemporary discharges would also have been required to facilitate avulsion. The ameliorating climate (MCR-D) would have enhanced the seasonal melting of catchment snowpacks and residual permafrost, which would have fed ephemeral, high energy peak discharges. These events, coupled with the high erosive potential of the unconsolidated sediments in the floodplain enabled the river to continue laterally aggrade, and avulse after the EH climatic amelioration. This continued until *ca.* 11.4 cal ka BP (*ca.* 250 years after the climatic amelioration), when sufficient vegetation had developed in the catchment to increase interception, reduce peak discharge and stabilise bank sediments (Brown *et al.,* 1994), and/or the river discharge had declined due to the exhausting of available stored energy sources in the catchment (snowpacks and permafrost).

After this interval, palaeochannels became permanently abandoned and began to infill with fine grained alluvium (Fraser *et al.,* 2009; LfA-6B). This coincided with the re-formation of organic rich silts and peats in the floodplain (Figure 9.4), as a more stable fluvial regime formed, initiated via rising water table levels, and increasing vegetation cover across the floodplain. The re-formation of fine-grained deposits across the floodplain are indicative of rivers with small discharge variation, high infiltration, and negligible bedload transport, which is typical of EH lowland rivers in Britain (Rose *et al.,* 1980; Rose, 1995). The change in river form fits well with the model of Brown *et al.* (1994), demonstrating that the development of catchment vegetation cover initiated the stabilisation of the banks of the river channels, which limited avulsion. As outlined previously, the rise in the water table during the EH must have also played a role in enhancing the trophic status of the floodplain, and diminishing optimum stream power.

9.4. Driving factors of landscape stability through the LGIT

The data presented here shows that the landscape was sensitive to abrupt climatic events during the LGIT. The landscape trends in the eVoP can be closely associated with the abrupt climatic oscillations during the WI, LLS, and EH. What is most striking is that the land systems seem to be strongly responsive to changes in mean annual air temperatures and the consequent hydrological adjustments. Measures of summer temperature indicate little variability and seemingly have little influence on the landscape. Therefore, winter temperature variations are thought to be driving the mean annual variability in temperatures, and these are seemingly more important throughout the LGIT.

Colder winter conditions in the British Isles most likely results from enhanced seasonal sea-ice in the North Atlantic, which in turn disrupted atmospheric circulation, particularly during the winter months (Ruddiman and McIntyre, 1981; Brauer *et al.,* 2008; Rach *et al.,* 2014). Certainly, the data gathered from the eVoP suggest hydrological changes occurred alongside shifts to colder conditions (Hoek and Bohncke, 2002; Magny *et al.,* 2006). These changes appear to, at least in part, drive changes in fluvial and biological systems, although these are also interdependent (Vandenberghe, 2002). The other driving factor of landscape stability and vegetation change appears to be climatically-induced wildfires (reconstructed from charcoal in the Wykeham records), although it may be suggested that this too relates back to the seasonal variations in temperature and aridity, with cold and dry conditions providing a ready fuel source (e.g. dead and dry wood) for combustion (Edwards *et al.,* 2000).

Landscape signals can also be identified within these climatic oscillations, which may represent complexities in the climatic structure of these events. This is most evident through the LLS, where the sediments in the eVoP are consistently partitioned into siliclastic coarse grained deposits (sands and/or gravels) overlying fines (silts and clays), which reflect a uniform change in depositional energy during this interval. The limited chronological constraints on these transitions prevents inter-basin correlation, but the patterns in the eVoP records invokes a consistent change in the mode of sedimentation during the latter stages of the LLS, towards higher energy, and more variable regimes.

A northward shift of the westerly wind belt across Northern Europe during this interval, is reconstructed from varved sediments at Kråkenes, and Meerfelder Maar (Brauer *et al.,* 2000; 2008; Bakke *et al.,* 2009; Lane *et al.,* 2013; Figure 9.5), This shift has been shown to be time transgressive, shifting north at a rate of *ca.* 10 km/yr at *ca.* 12.15 cal ka BP, associated with the strengthening intensity of AMOC, leading to the periodic break-up of sea-ice in the North Atlantic, and the northward shift of zonal jet streams (Bakke *et al.,* 2009; Lane *et al.,* 2013). Similar 'mid-YD' signals are also recorded in the Alps (von Grafenstein *et al.,* 1999), and Iberia (Baldini *et al.,* 2015), indicating that the event affected wide areas of the European continent. The eVoP lies between the latitudes of Kråkenes and Meerfelder Maar and would therefore have also been affected by these atmospheric changes, with slightly warmer and potentially wetter conditions being brought back to northeast England at *ca.* 12.15 cal ka BP. The influx of coarser sediments in the eVoP records can therefore be interpreted to relate to a landscape response to this mid-stadial transition, based upon the following evidence:

a) The Vedde Ash, was deposited *ca.* midway through the LLS/YD in Northern Europe (Lowe and Turney, 1997; Lane *et al.,* 2013; Bronk Ramsey *et al.,* 2015), meaning that if the sedimentation rate was consistent in basins, it should lie roughly midway through the sediments deposited during the LLS. In core C in PF however it lies 42 cm from the base of

the lithostratigraphic LLS boundary, and 140 cm from the top of the lithostratigraphic LLS boundary (Palmer *et al.,* 2015) showing an increase in sedimentation rate after the deposition of the Vedde Ash.

b) The influx of coarse-grained deposits into the WYKNE15 sequence (WN-L5a), and overlying interbeds of coarse sands and silts, demonstrate the ephemeral deposition of high energy deposits, most likely sourced from catchment snow- and permafrost melt in spring-summer months.

c) The deposition of fine planar- and cross-bedded sands in the River Derwent floodplain (LfA-6C), represent flow regimes, most likely from ephemerally aggrading braided rivers (Rose and Boardman, 1983), followed by the development of anabranching river activitys.

Further work is needed to precisely constrain the timing of the transition to higher energy sediment deposition during LLS, but the climatic transition during the mid-YD in Northern Europe (Bakke *et al.,* 2009; Lane *et al.,* 2013), provides a viable mechanism to explain these shifts, and is supported by corresponding sediment signals in other well dated basins across Northern Europe (Bakke *et al.,* 2009; Lane *et al.,* 2013; Figure 9.5). These trends illustrate the sensitivity of the landscape to abrupt temperature and hydrological shifts through the LGIT.

Two exceptions to these landscape trends are the periods directly after deglaciation (*ca.* 17-14 cal ka BP) and during the very earliest Holocene (*ca.* 11.65-11.4 cal ka BP). During these intervals, landscape response does not directly follow climatic variation. During the E-WI, the landscape was characterised by a low water table, high sedimentation rates, and poorly developed soils and vegetation cover (open ground herbs and grasses). Furthermore, the outwash plain in the eVoP (LfA-2) may have continued to be extensively ice-cored, meaning the melting of these masses under a warmer climatic regime would have led to laterally and vertically unstable masses of unconsolidated sediment being readily available. The melting of permafrost within these sediment bodies, would have initially provided high volumes of sediment to erode and redistribute across the landscape via high intensity seasonal meltwater fluxes. These conditions persisted for *ca.* 500-700 years after the initial climatic amelioration (until *ca.* 14 cal ka BP), where declines in sedimentation rates, increases in organic content, macrofossil concentrations (including *Juniperus communis*), a rise in water table elevation, and a shift in the planform of the River Derwent (to a low-energy meandering system) are recorded. These reconstructions indicate a rapid increase in landscape stability very soon after very soon after climatic amelioration (MCR-B) out of the WN-I4b climatic oscillation. The mechanisms responsible for this temporal lag to warming at the onset of the WI likely relates to paraglacial readjustment processes, as residual sediment bodies, and dead-ice cores re-arranged in response to climatic amelioration, and soils matured, allowing higher vegetation communities to colonise.

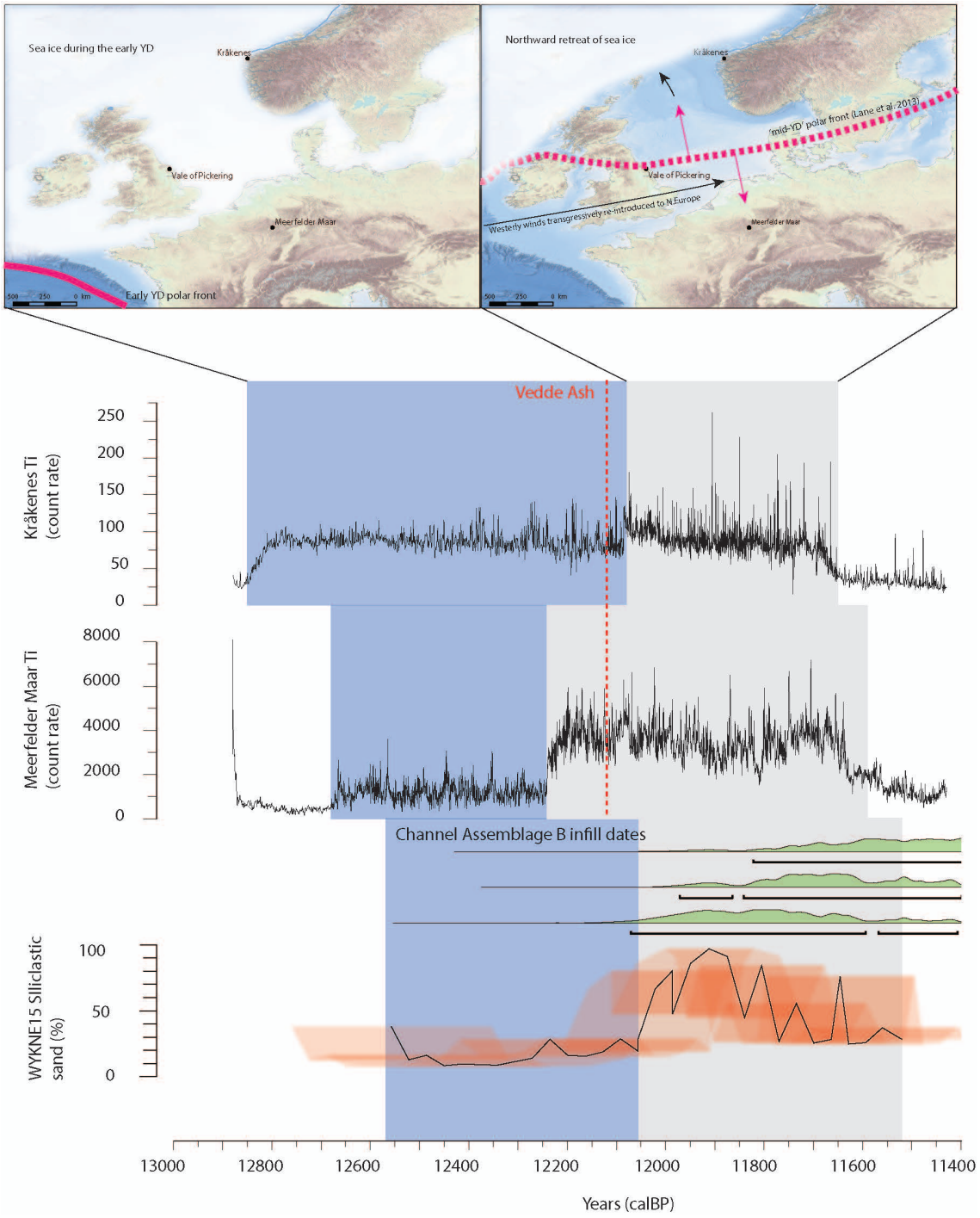

Figure 9.5. *Comparison of siliclastic particle size from the WYKNE15 record, palaeochannel infill dates of Channel Assemblage B channels at Wykeham Quarry (from Fraser et al., 2009). These data are compared to Ti records from Meerdelder Maar and Kråkenes which have been used by Bakke et al. (2009) and Lane et al. (2013) as evidence for a 'mid-YD transition' (see maps), transgressively bringing warmer and wetter conditions back to Northern Europe. The reactivation of river channels and consistently higher particle sizes and sedimentation rates deposits in the eVoP are thought to be related to this regional climatic shift, although more precisely constrained records are required to assess the timing of these changes.*

At the onset of the Holocene however, there was no direct glacial influence, meaning that the mechanisms behind these lags are not synonymous. The Pleistocene-Holocene boundary is characterised by an abrupt and near synchronous hemispheric climatic amelioration at 11.65 ± 0.1 ka BP (Walker *et al.,* 2009). The climatic amelioration into the Holocene was interrupted by a series of lower amplitude climatic oscillations over the first thousand years (e.g. Bjork *et al.,* 1997; Vincent and Cwynar, 2016). This interval can be split into two phases (phases 1-2), based

upon the amount and type of biomass cover, the elevation of the water table, and the characteristics of fluvial drainage and aggradation in the River Derwent floodplain. In phase 1 (*ca.* 11.65 and 11.4 cal ka BP), although hemispheric temperatures had ameliorated (Walker *et al.,* 2009), biomass cover remained low, and coarse-grained sediments continued to be deposited in the Derwent floodplain, In phase 2 (*ca.* 11.4 cal ka BP and 11 cal ka BP) palaeoenvironmental records at Wykeham show rapidly increasing biomass cover (rising pollen and macrofossil concentrations, and bulk organic content), increasing water table elevations, a resumption of carbonate precipitation in PF (Matthews *pers comm.*), and a decrease in siliclastic particle size in the Wykeham records, indicating a rapid increase in landscape stability at *ca.* 11.4 cal ka BP. The Wykeham records therefore show that the landscape took *ca.* 150-250 years to stabilise after the amelioration at the Pleistocene-Holocene boundary. This lag is thought to reflect an artefact of para- and/or peri-glacial processes operating across the landscape during the LLS (Ballantyne, 2002; Vandenberghe and Woo, 2002; Huijzer and Isarin, 1997), coupled with migrational vegetation lags (Birks and Birks, 2014), and the development of thick enough soils to sufficiently stabilise slopes and fluvial activity in lowland environs (Rose, 1995).

9.5. Human occupation in the eVoP

Archaeological sites around the margins of PF, demonstrate that humans with different technical and mobility strategies were present in the valley at intervals through the LGIT (Conneller, 2007; Coneller *et al.,* 2012). These sites can be subdivided into three periods of occupation based upon typological criteria (Conneller, 2007). These are: a) Final Palaeolithic sites at Seamer site K, which record occupation at some time between 13.8-13 cal ka BP (Schadla Hall, 1987; Conneller, 2007) b) Terminal Palaeolithic sites, including a horse butchery site on Flixton Island (Moore, 1954; Conneller, 2007), which has recently been re-dated (Bayliss *pers comm.*) c) Early Mesolithic occupation at Star Carr which has been extensively radiocarbon dated and tightly chronologically constrained (Clark, 1954; Mellars and Dark, 1998; Bayliss, *pers comm.*).

By using the chronological data associated with these archaeological remains, the timing of human occupation in the eVoP can be compared to the eVoP landscape model (Figure 9.6). The following sections analyse the three phases of human occupation with respect to the eVoP landscape model.

9.5.1. Final Palaeolithic occupation

Recolonization of the British Isles after the LGM by Creswellian industries, occurred prior to- and through the E-WI (Jacobi and Higham, 2011). No Creswellian remains are present in the eVoP, which is unsurprising, as these industries are extremely rare north of Derbyshire (Jacobi,

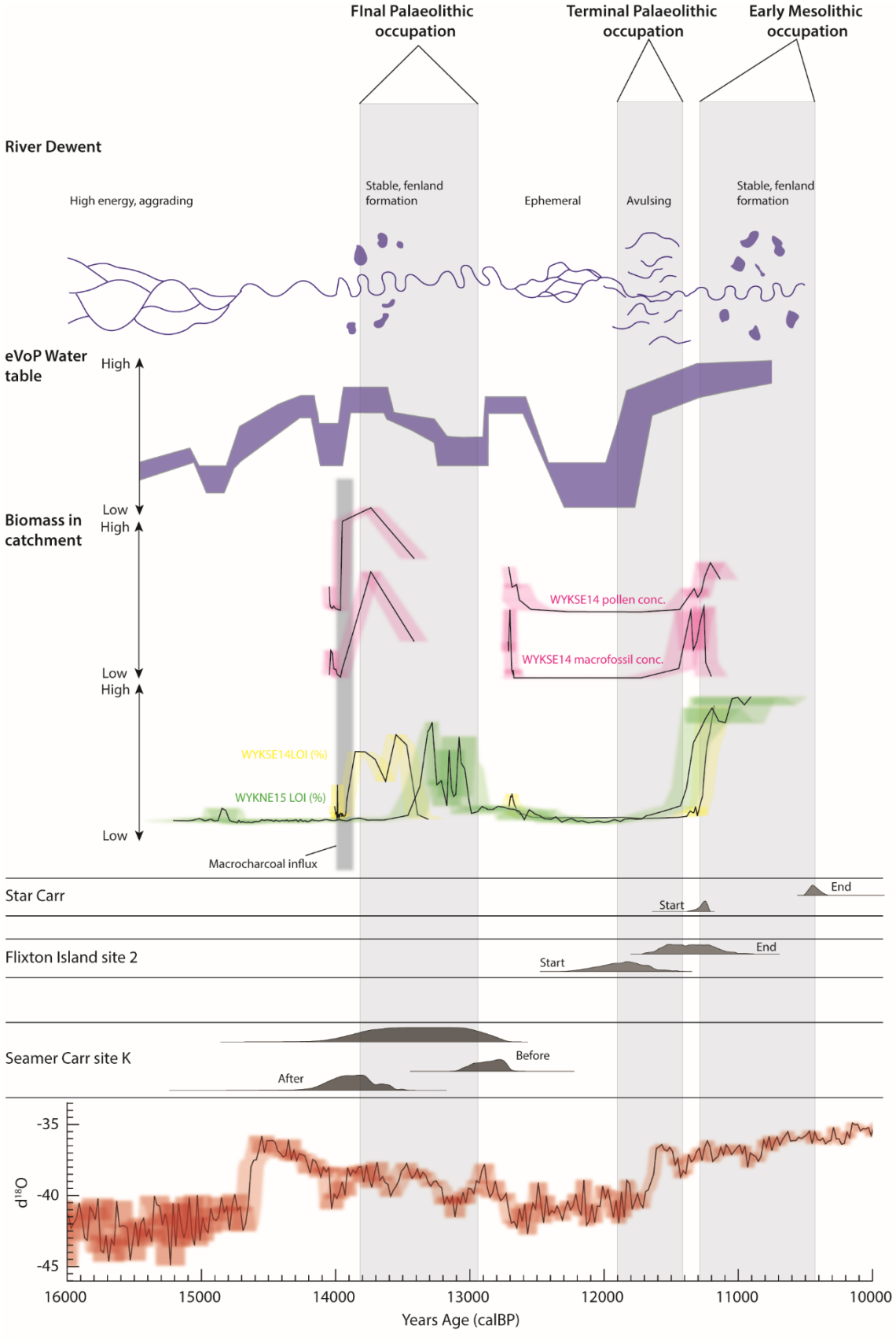

Figure 9.6. *Comparison of the timing of early human occupation in the eVoP to the palaeoenvironmental and landscape changes observed in the eVoP. The timing of Final Palaeolithic occupation is derived from the bracketing ages reported in Schadla-Hall (1987), whilst Flixton Island site 2 and Star Carr are from remodelled, and new ages on archaeological remains provided to the author by Alex Bayliss (POSTGLACIAL unpublished data). These data are from new research undertaken by Professor Nicky Milner and colleagues at the aforementioned sites. All data are calibrated IntCal 13 (Reimer et al. 2013).*

1991), likely as humans failed to migrate much further north of Creswell Crags prior to *ca.* 14 cal ka BP (Jacobi and Higham, 2011). The earliest chronologically constrained evidence of human occupation in the eVoP comes from Seamer Site K (Schadla-Hall, 1987) which is interpreted to be the first incursion of people into the area after the LGM (Conneller, 2007). These people are thought to have been highly mobile communities, travelling long distances in the search of food and materials (Conneller, 2007).

Two interpretations can be made from these regional trends. Firstly, the lack of Creswellian remains, attributed occupation during the E-WI (i.e. *ca.* 15-14 cal ka BP; Jacobi and Higham 2011) in the eVoP demonstrates that although temperatures were mild in this interval, the environmental conditions were not viable for occupation. The lack of Creswellian remains anywhere in the NE of England suggests that the unstable, and poorly vegetated landscape, in comparison to southern Britain, was not viable or favoured for human subsistence, possibly due to the delayed development of soils and vegetation cover required for sedentary mammalian presence. This is supported by the remains of cut-marked fauna (indicating human presence) preserved at Cresswell Crags, which show that during the E-WI, at the northernmost limit of E-WI human occupation, humans were hunting open ground and arctic adapted fauna such as *Lepus timidus* and *Equus ferus*, in a relatively barren landscape (Jacobi and Higham, 2011). Therefore, in the eVoP, which lies to the northeast of Creswell Crags, food resources may have been lower, and possibly insufficient to sustain the Creswellian populations. Furthermore, Creswellian sites in Britain are consistently south of the LGM ice limit, suggesting that the irregular, and unstable topography of the recently deglaciated outwash plains and proglacial lake sediments in the Vale of York and the VoP (Mitchell *et al.,* 2010), were an unfavourable and difficult landscape to traverse, particularly for highly mobile hunter gatherer populations. This demonstrates that although temperatures were warmest during this interval, the landscape differed sufficiently enough from southern Britain to prevent human migration into the area.

Whilst the age determination of the period of occupation is broad, it securely places the initiation of human presence in the eVoP into the M-L-WI, at a time when the landscape had become more accessible, and favourable for human presence. The landscape model constructed here invokes a rapid increase in landscape stability, higher water tables, and increasing biomass cover in the catchment between *ca.* 13.9-13.5 cal ka BP. Furthermore, the presence of dung beetles including *Aphodius* spp. in the WYKSE14 sequence indicates the presence of large herbivores in the catchment at this time (Jarosz, 2014), which would have provided a valuable material resource of human populations. The influx of *Federmessergruppen* hominins to similar landscapes during the mid to latter phases of the Allerød has recently been described by Tolksdorf *et al.* (2013) at Grabow in Northern Germany, suggesting that lowland low energy floodplains and wetlands were a favoured environment for these populations. These groups are thought to have vacated the British Isles during the LLS (Barton *et al.,* 2003).

9.5.2. Terminal Palaeolithic occupation

As with the Final Palaeolithic remains in the eVoP, the Terminal Palaeolithic site on Flixton Island represents the earliest occupation of NE England after the climatic amelioration at the Pleistocene-Holocene boundary (Conneller, 2007; Bayliss, *pers comm.*). This is unsurprising as lower sea-levels connected the eVoP to the continent, where pioneering populations would have migrated from, making the relatively higher ground of the eVoP an attractive locality for hunting forays, tracking herds of horse (Housely *et al.,* 1997; Conneller *et al.,* 2012). The Terminal Palaeolithic typologies in the eVoP demonstrate a pioneering, highly mobile population, differing from the Final Palaeolithic occupation in being well provisioned, suggesting a more flexible subsistence, being able to move without needing to restock with raw materials (Conneller, 2007).

The eVoP landscape model shows that the landscape in which these humans were present was markedly different to that of Final Palaeolithic, and the succeeding Early Mesolithic populations. The radiocarbon chronology constructed from the 'Flixton Island' deposits show that humans were occupying the eVoP either during the terminal period of the LLS, and/or phase 1 of the EH (*ca.* 11.65-11.4 cal ka BP), when the landscape was characterised by low biomass cover, lower water tables, and an active, laterally unstable river system crossing the River Derwent floodplain (infill of channel assemblage B coincides with 'Flixton Island' occupation; Figure 11.7). The open nature of the landscape is supported by the presence butchered horse remains which invoke an open landscape devoid of woodland cover (Coard and Chamberlain, 1999). Therefore, it is suggested that the more flexible mode of mobility of these human populations was due to the more unstable nature of the landscape in which they were hunting. Terminal Palaeolithic remains are located on a small topographic high, in the centre of the PF basin, suggesting that they were occupying an island whereby, transport to and from the locality would require a crossing of water.

Results presented here however suggest that during the Terminal Palaeolithic occupation of the eVoP, the water table (and therefore the lake level in PF) would have been lower (rising from *ca.* 22 to 24.5 m OD). Recent bathymetric surveys of PF, to the north of Flixton Island have identified areas of higher ground which provide the potential to have been dryland during the LLS and phase 1 of the EH (Palmer *et al.,* 2015). This has two implications. First, it demonstrates that when Terminal Palaeolithic populations were present in the eVoP, the morphology of PF was different, and the location of the 'Flixton Island' artefacts were probably deposited on a peninsula to deeper waterbodies rather than a true island. Second, as the morphology of PF changed in response to changing lake levels (Palmer *et al.,* 2015) it would suggest that other archaeological remains potentially exist in other areas of PF, which have subsequently been covered by EH lacustrine deposits as the water table rose.

This suggests that landscapes in which the 'Flixton Island' hominins were subsisting, differed substantially to that of the Early Mesolithic people at Star Carr. Furthermore, the regional hydrological work, invokes that the extent and morphology of the lake basin varied significantly through this interval, meaning further hominin remains may well be present in the eVoP, but have been hidden from the contemporary land surface by subsequent sedimentation.

9.5.3. Early Mesolithic occupation

The most famous period of prehistoric human occupation in the eVoP is the prolific flint assemblage (Clark, 1954; Mellars and Dark, 1998; Conneller and Schadla-Hall, 2003; Conneller *et al.,* 2009), and wealth of organic remains (Mellars and Dark, 1998; Conneller *et al.,* 2012; Innes *et al.,* 2013) associated with Early Mesolithic occupation at Star Carr, which has become a site of international archaeological importance (Innes *et al.,* 2013).

Early Mesolithic occupation in the eVoP differs from previous phases, with human populations spending considerable amounts of time at Star Carr and around PF, leaving abundant lithic and organic remains, as well as constructions, including platforms and dryland structures (Conneller *et al.,* 2012). This therefore points towards a sedentary lifestyle, in which the landscape was used in different ways to the pioneering, and highly mobile hunter-gatherer subsistence in the Final and Terminal Palaeolithic.

Recent remodelling of dates from Star Carr (Bayliss, *pers comm.;* Figure 11.7) show that occupation initiated at *ca.* 11.3-11.2 cal ka BP and ceased at 10.7-10.6 cal ka BP. This is in accord with phase 2 of the eVoP landscape model, characterised by birch woodland development, a high water table, and a stable, low energy fluvial regime, with wetland development in the Derwent floodplain. The timing of Early Mesolithic occupation at Star Carr therefore occurs after the 11.4 ka event, and soon after the development of a low energy, and stable landscape in the eVoP. The Mesolithic humans at Star Carr undoubtedly utilised the recently formed wetlands in the River Derwent floodplain for hunting and foraging (Innes *et al.,* 2013), whilst the River Derwent would also have provided a valuable resource for food and transport.

9.5.4. Synthesis

The Wykeham Quarry records allow the archaeological finds from the eVoP to be placed into a local landscape context. This suggests that the landscape of Northern Britain during the E-WI may not have been amenable to human occupation, principally due to the lag in landscape stabilisation. It also suggests that human occupation in these landscapes only becomes preferable after the ~GI-1d event during a brief period of stability lasting *ca.* 500 years. The terminal Upper Palaeolithic period occurred during a landscape which was characterised open conditions mass movements of clastic sediments and dramatically changing groundwater conditions. This appears

to be a very short-lived phase that finished with the stabilisation of the eVoP landscape, whereupon the transition into the Early Mesolithic occurred. Landscape stability and particularly paraglacial readjustment and responses to abrupt climatic changes (most likely reflecting changes in hydrology and driven by winter temperatures) are therefore suggested as being fundamental in understanding past human activity. However, these factors are not routinely reconstructed in palaeoenvironmental studies (Mellars and Dark, 1998). Rather, regional records of temperature and frequently summer temperatures are used to understand past populations from diverse areas (Blockley *et al.,* 2006). This suggests further studies local to archaeological sites and considering the whole range of driving factors are required to develop understanding further.

10. Conclusions

10.1. Key findings

This study has, through the application of multiproxy techniques, improved the understanding of: a) the landscape development of the eVoP through the Last Termination; b) the timing, amplitude, and phasing of palaeoclimatic shifts (palaeotemperature and palaeohydrology); and c) landscape response to climate change in NE England through the Last Termination. From this several key findings follow and these are:

1. The use of digital techniques in the mapping of landforms, supported by detailed sedimentological and stratigraphic work at Wykeham Quarry allows the following new model of landscape evolution in the eVoP:

a) Mapping of terrace levels determines that the elevation of Glacial Lake Pickering was initially controlled by the location of the NSIL and VOYL between *ca* 21-18 cal ka BP, before being controlled by the base level set by Glacial Lake Humber after ice recession in the Vale of York < *ca.* 18 cal ka BP.

b) The retreat of the NSIL in the eVoP initiated the formation of an ice-cored outwash plain, characterised by irregular topography viable for palaeochannel/palaeolake formation after ice recession. The minimum age for ice-free conditions in the eVoP is provided by the basal radiocarbon date from the WYKNE15 sequence (15.19-14.71 cal ka BP), which provides the first minimum constraining age for the evacuation of the NSIL from the valley.

c) The identification of palaeochannels in the eVoP, combined with detailed sedimentological analyses at Wykeham Quarry has enabled the construction of a model a fluvial activity in the River Derwent through the LGIT for the first time. This model demonstrates a repeated phase lag in fluvial system response to major climatic warming trends (i.e. Dimlington Stadial-WI, and LLS-EH). Similar lags are also identified in vegetation, and hydrological records from this study, suggesting a causal link between these phenomena.

2. A novel approach, combining sedimentological and stratigraphic analyses and depositional modelling of deposits at Wykeham Quarry in the eVoP has enabled the development of criteria (sedimentary characteristics, extent and thickness of deposits) for targeting the sites of greatest potential for high resolution palaeotemperature and palaeohydrological reconstructions from complex sedimentary sequences, whilst also identifying sites that may have further potential for preserving archaeological remains.

3. Two reliable age-modelled radiocarbon chronologies for two sites in the eVoP have been produced for the LGIT, a first for East Yorkshire.

4. A plant macrofossil summer and winter palaeotemperature reconstruction has been made for the UK, for the first time, and in combination with a coleopteran-based MCR the first Mutual MCR has been constructed for this period.

a) These data have been compared to chironomid (mean july) palaeotemperature reconstructions from Palaeolake Flixton, where the agreement between the records suggest that this is a robust comparison.
b) Climatic amelioration at the start of the WI in the VoP appears to pre-date amelioration in Greenland, although the peak of warming is coincident.
c) A short-lived early WI oscillation is recorded in the VoP prior to 14 ka cal BP.
d) The mutual MCR indicates that summer temperature is less significant than mean annual temperatures in driving environmental change during the entire LGIT, not only during YD as previously suggested.

5. Changes in water table elevation appear to be linked to threshold change across abrupt climate change boundaries. The precision of the eVoP age models allow this distinction to be made in the UK for the first time. These age models show that changes were occurring in phase with European sequences but not in phase with shifts identified in Greenland. Hydrology and winter temperature seem to have the greatest impact in driving changes in landscape stability through these thresholds.

6. Differences in the structure and amplitude of climatic signals in the British Isles are attributed to the relative proximity of sites to the North Atlantic. The records from the VoP show most similarities to those of continental Europe rather than those of the west coast of Ireland and Scotland, possibly reflecting the influence of continentality, with sites in the east of the landmass being subjected to higher amplitude changes in temperature, and potentially precipitation when fluctuations in AMOC strength occurred.

7. The reconstruction of the VoP landsystem through the LGIT enables insight into the rate of landscape stabilisation during deglaciation. After the onset of the climatic amelioration, at the start of the WI, it takes approximately 500 years for the landscape to stabilise, whereas the landscape appears to stabilise after 200 years from the amelioration at the start of the EH.

8. During the WI, the human recolonisation on a 'stable' landscape occurs in a relatively short time period in the middle of the interval, and after peak warmth had been reached. Human recolonisation at the start of the EH appears to be rapid due to stable landscapes being established within 200 years, but local factors may control their exact location.

10.2. Wider significance

This study demonstrates the importance of constructing quantitative, chronologically constrained, palaeoclimatic records across latitudinal and longitudinal gradients which allows the spatial variability in the response to abrupt climatic events in NW Europe to be reconstructed (Coope *et al.,* 1998; Brooks and Langdon, 2014).

This study has presented a body of evidence to suggest a consistent link between the timing landscape change (towards stable, low energy systems) and phases of human occupation of NE England. This indicates that climate change, and particularly summer temperature estimates, in isolation is insufficient to explain the patterns of human occupation in NE England. This suggests that further insights into the antecedent landscapes in which these populations were living, particularly during the WI, is vital to understand their mode of subsistence and landscape exploitation. This study provides a fresh perspective on the phasing and chronology of occupation and the relationship between hominin populations and the environment during the Upper Palaeolithic-Early Mesolithic. It also runs counter to more simplistic models of a temperature driven population dispersal (Blockley *et al.,* 2006) and may explain the pattern of modern human dispersal both into Britain (Jacobi and Higham, 2009) and indeed the dispersal out of glacial refugia in Europe, prior to the onset of warming in the LGIT (Gamble *et al.,* 2004; 2005).

This study is also provides data on the timing, and phasing of terrestrial landscape responses to high amplitude climate changes in lowland environments. As outlined in Chapter 1, the Last Termination represents a valuable time interval to further understanding on the potential landscape responses to future periods of climatic instability. If periods such as the Last Termination have a role to play as analogues of future climate change, then the understanding of landscape response to climate change is of major importance as it is the impact on the environment and landscapes, not just the amplitude of warming/cooling trends that needs to be understood, to enable societies to mitigate and plan for these changes. The data obtained in this thesis therefore provides a multiproxy dataset with which to better understand the terrestrial response in lowlands to phases of abrupt hydroclimatic change.

10.3. Future work

10.3.1. The VoP

Whilst the results presented here have improved understanding on the development of climatic and landscape regimes through the LGIT in NE England, landscape evolution through certain stages of the Last Termination require further investigation. This is most pertinent between *ca.* 13.5-13 cal ka BP where hiatuses in the Wykeham records preclude palaeoclimatic

reconstruction. Additionally, the records at Wykeham Quarry are largely infilled during the EH, limiting their potential for high-resolution palaeoclimatic reconstructions. Mapping of the eVoP has demonstrated that other lake archives exist with the potential for complete LGIT sequences to be preserved. Preliminary analysis of the palaeolake basin at Seamer (Chapter 5), demonstrates that these sites contain tripartite sedimentary infills, characteristic of deposition during the LGIT. Additionally, preliminary data demonstrates that these sites remained as open bodies of water much later into the Holocene than those at Wykeham Quarry (Appendices D-E). More detailed investigations into these deposits would: a) enable the hydroclimatic model for the LGIT in the eVoP to be tested, and provide potential to extend this record into the Holocene, b) test the potential of other sites in the eVoP for Mesolithic and late Upper Palaeolithic archaeological investigations, helping to further develop the model of early human occupation in the British Isles after ice recession.

In addition, the application of stable isotopic analysis from terrestrial and aquatic biomarkers have shown considerable potential for reconstructing high-resolution shifts in hydroclimatic regimes through the LGIT (Sasche *et al.,* 2012; Rach *et al.,* 2014; Muschitiello *et al.,* 2015b), and therefore their application to records from the VoP would provide a means to test the groundwater model constructed for the eVoP. Applying these techniques to sites such as Palaeolake Flixton, and potentially the Seamer basin therefore would also develop understanding on the mechanisms responsible for the model of groundwater variations reconstructed from Wykeham Quarry.

10.3.2. The British Isles and NW Europe

This study has demonstrated that the amplitude of abrupt climatic events was spatially heterogeneous across the British Isles. It has also demonstrated that via a combination of sedimentological, and biological techniques, carefully targeted sedimentary sequences from lowland palaeolake bodies and wetlands can be used to reconstruct hydroclimatic changes through the LGIT (Harrison and Digerfeldt, 1993; Magny and Ruffadi, 1995). Applying these methods to other deglaciated lowland areas (e.g. Evans *et al.,* 2005; Livingstone *et al.,* 2010; Chiverrell *et al.,* 2016) would develop understanding on the longitudinal effect of temperature and precipitation trends, providing a tool to understand the role of continentality across the European landmass through the LGIT (Coope *et al.,* 1998). Recording and analysing these changes is of critical importance to develop understanding of the phasing of hydroclimatic change, and landscape response to abrupt shifts in North Atlantic ocean circulation across different continental settings.

References

Aarnes, I., Kühl, N. and Birks, H.H., 2012. Quantitative climate reconstruction from late-glacial and early Holocene plant macrofossils in western Norway using the probability density function approach. *Review of Palaeobotany and Palynology*, *170*, pp.27-39.

Abatzoglou, J.T., Kolden, C.A., Balch, J.K. and Bradley, B.A., 2016. Controls on interannual variability in lightning-caused fire activity in the western US. *Environmental Research Letters*, *11*(4), p.045005.

Adamiec, G., Aitken, M., 1998. Dose-rate conversion factors: update. Ancient TL 16, 37-50. Bøtter-Jensen, L., Andersen, C.E., Duller, G.A.T., Murray, A.S., 2003. Developments in radiation, stimulation and observation facilities in luminescence measurements. *Radiat Meas 37*, 535-541.

Alley, R.B., 2007. Wally was right: predictive ability of the North Atlantic "conveyor belt" hypothesis for abrupt climate change. *Annu. Rev. Earth Planet. Sci.*, *35*, pp.241-272.

Ampel, L., Kylander, M.E., Steinthorsdottir, M. and Wohlfarth, B., 2015. Abrupt climate change and early lake development–the Lateglacial diatom flora at Hässeldala Port, southeastern Sweden. *Boreas*, *44*(1), pp.94-102.

Anadón, P., Utrilla, R. and Vázquez, A., 2000. Use of charophyte carbonates as proxy indicators of subtle hydrological and chemical changes in marl lakes: example from the Miocene Bicorb Basin, eastern Spain. *Sedimentary Geology*, *133*(3), pp.325-347.

Andrews, J.E., Coletta, P., Pentecost, A., Riding, R., Dennis, S., Dennis, P.F. and Spiro, B., 2004. Equilibrium and disequilibrium stable isotope effects in modern charophyte calcites: implications for palaeoenvironmental studies. *Palaeogeography, Palaeoclimatology, Palaeoecology*, *204*(1), pp.101-114.

Antoine, P., Munaut, A. V., Limondin-Lozouet, N., Ponel, P., Dupéron, J., and Dupéron, M. 2003. Response of the Selle River to climatic modifications during the Lateglacial and early Holocene (Somme Basin-Northern France).*Quaternary Science Reviews*, *22*(20), 2061-2076.

Apolinarska, K., Pełechaty, M. and Pukacz, A., 2011. $CaCO_3$ sedimentation by modern charophytes (Characeae): can calcified remains and carbonate $\delta^{13}C$ and $\delta^{18}O$ record the ecological state of lakes? – a review− Studia Limnol. *Telmat*, *5*, pp.23-41.

Arenas-Abad, C., Vázquez-Urbez, M., Pardo-Tirapu, G. and Sancho-Marcén, C., 2010. Fluvial and associated carbonate deposits. *Developments in Sedimentology*, *61*, pp.133-175.

Ashley, G.M., 1975. Rhythmic sedimentation in glacial lake Hitchcock, Massachusetts, Connecticut. In: Jopling, A.V., McDonald, B.C. (Eds.). Glaciofluvial and Glaciolacustrine Sedimentation. Society of Economic Palaeontologists and Mineralogists, Special Publication No. 23, pp. 304-320.

Astin, T.R., Scotchman, I.C., 1988. The diagenetic history of some spetarian concretions from the Kimmeridge Clay, England. Sedimentology 35, 349–368.

Atkinson, T. C., Briffa, K. R., and Coope, G. R. 1987. Seasonal temperatures in Britain during the past 22,000 years, reconstructed using beetle remains. *Nature*, *325*, 587-592.

Bakke, J., Lie, Ø., Heegaard, E., Dokken, T., Haug, G.H., Birks, H.H., Dulski, P. and Nilsen, T., 2009. Rapid oceanic and atmospheric changes during the Younger Dryas cold period. *Nature Geoscience*, *2*(3), pp.202-205.

Baldini, L.M., McDermott, F., Baldini, J.U., Arias, P., Cueto, M., Fairchild, I.J., Hoffmann, D.L., Mattey, D.P., Müller, W., Nita, D.C. and Ontañón, R., 2015. Regional temperature, atmospheric circulation, and sea-ice variability within the Younger Dryas Event constrained using a speleothem from northern Iberia. *Earth and Planetary Science Letters*, *419*, pp.101-110.

Ballantyne, C.K., 2002. Paraglacial geomorphology. *Quaternary Science Reviews*, *21*(18), pp.1935-2017.

Barber, K.E., Chambers, F.M., Maddy, D., Stoneman, R. and Brew, J.S., 1994. A sensitive high-resolution record of late Holocene climatic change from a raised bog in northern England. *The Holocene*, *4*(2), pp.198-205.

Bartley, D. D. 1962. The stratigraphy and pollen analysis of lake deposits near Tadcaster, Yorkshire. *New Phytologist*, *61*(3), 277-287.

Bartley, D. D., Chambers, C., and Hart-Jones, B. 1976. The vegetational history of parts of south and east Durham. *New Phytologist*, *77*(2), 437-468.

Barton, R.N.E., Jacobi, R.M., Stapert, D. and Street, M.J., 2003. The Late-glacial reoccupation of the British Isles and the Creswellian. *Journal of Quaternary Science*, *18*(7), pp.631-643.

Batchelor, C.R. 2009. Northern Extension and Southern Extensions, Wykeham Quarry: Geoarchaeological Deposit Models, Interim Report. Quaternary Scientific Unpublished Report

Bateman, M.D., 1998. The origin and age of coversand in north Lincolnshire, UK. *Permafrost and Periglacial Processes*, *9*(4), pp.313-325.

Bateman, M.D., Murton, J.B. and Crowe, W., 2000. Late Devensian and Holocene depositional environments associated with the coversand around Caistor, north Lincolnshire, UK. *Boreas*, *29*(1), pp.1-15.

Bateman, M. D., Buckland, P. C., Chase, B., Frederick, C. D., and Gaunt, G. D. 2008. The Late-Devensian proglacial Lake Humber: new evidence from littoral deposits at Ferrybridge, Yorkshire, England. *Boreas*, *37*(2), 195-210.

Bateman, M.D., Buckland, P.C., Whyte, M.A., Ashurst, R.A., Boulter, C. and Panagiotakopulu, E.V.A., 2011. Re-evaluation of the Last Glacial Maximum typesite at Dimlington, UK. *Boreas*, *40*(4), pp.573-584.

Bateman, M.D., Evans, D.J.A., Buckland, P.C., Connell, E.R., Friend, R.J., Hartmann, D., Moxon, H., Fairburn, W.A., Panagiotakopulu, E. and Ashurst, R.A., 2015. Last glacial dynamics of the Vale of York and North Sea lobes of the British and Irish Ice Sheet. *Proceedings of the Geologists' Association*,*126*(6), pp.712-730.

Bearcock, J.M., Smedley, P.L. and Milne, C.J., 2015. Baseline groundwater chemistry: the Corallian of the Vale of Pickering, Yorkshire.

Beckenbach, E., Müller, T., Seyfried, H. and Simon, T., 2014. Potential of a high-resolution DTM with large spatial coverage for visualization, identification and interpretation of young (Würmian) glacial geomorphology: a case study from Oberschwaben (southern Germany). *Quaternary Science Journal*, *63*, pp.107-129.

Becker, B. and Kromer, B., 1993. The continental tree-ring record—absolute chronology, 14 C calibration and climatic change at 11 ka. *Palaeogeography, Palaeoclimatology, Palaeoecology*, *103*(1), pp.67-71.

Beckett, S.C., 1981. Pollen diagrams from Holderness, north Humberside -.*Journal of Biogeography*, pp.177-198.

Bellamy, D. J., Bradshaw, M. E., Millington, G. R., and Simmons, L. G. 1966. Two Quaternary deposits in the lower Tees basin. *New Phytologist*,*65*(4), 429-442.

Bendle, J.M. and Glasser, N.F., 2012. Palaeoclimatic reconstruction from lateglacial (younger dryas chronozone) cirque glaciers in snowdonia, north wales. *Proceedings of the Geologists' Association*, *123*(1), pp.130-145.

Benn, D.I. and Evans, D.J.A., 2010. Glaciers and Glaciation. 802 pp. *Arnold, London*.

Bennett, K.D. and Willis, K.J., 2002. Pollen. In *Tracking environmental change using lake sediments* (pp. 5-32). Springer Netherlands.

Bennett, M.M. and Glasser, N.F. eds., 2009. *Glacial geology: ice sheets and landforms*. John Wiley and Sons.

Bennike, O., 1998. Fossil egg sacs of Diaptomus (Crustaceae: Copepoda) in Late Quaternary lake sediments. *Journal of Paleolimnology*, *19*(1), pp.77-79.

Bennike, O., Björck, S., Böcher, J. and Walker, I., 2000. The Quaternary arthropod fauna of Greenland: a review with new data. *Bulletin of the Geological Society of Denmark*, *47*, pp.111-134.

Benson, L., Burdett, J., Lund, S., Kashgarian, M. and Mensing, S., 1997. Nearly synchronous climate change in the Northern Hemisphere during the last glacial termination. *Nature*, *388*(6639), pp.263-265.

Berger, A. and Loutre, M.F., 1991. Insolation values for the climate of the last 10 million years. *Quaternary Science Reviews*, *10*(4), pp.297-317.

Berger, A. and Loutre, M.F., 2010. Modeling the 100-kyr glacial–interglacial cycles. *Global and Planetary Change*, *72*(4), pp.275-281.

Berggren, G., 1964. Atlas of Seeds. Part 2. Cyperaceae. Swedish Natural Science Research

Bicket, A., and Tizzard, L. 2015. A review of the submerged prehistory and palaeolandscapes of the British Isles. *Proceedings of the Geologists' Association*, *126*(6), 643-663.

Birks, H. H., 1980. Plant macrofossils in Quaternary lake sediments. Arch. Hydrobiol. 15: 1–60

Birks, H.H., 2000. Aquatic macrophyte vegetation development in Kråkenes Lake, western Norway, during the late-glacial and early-Holocene. *Journal of Paleolimnology*, *23*(1), pp.7-19.

Birks, H.H., 2002. Plant macrofossils. In *Tracking environmental change using lake sediments* (pp. 49-74). Springer Netherlands.

Birks, H. H., and Ammann, B. 2000. Two terrestrial records of rapid climatic change during the glacial–Holocene transition (14,000–9,000 calendar years BP) from Europe. *Proceedings of the National Academy of Sciences*, *97*(4), 1390-1394.

Birks, H.H. and Birks, H.J.B., 2014. To what extent did changes in July temperature influence Lateglacial vegetation patterns in NW Europe?. *Quaternary Science Reviews*, *106*, pp.262-277.

Birks, H.H. and Mathewes, R.W., 1978. Studies in the vegetational history of Scotland. *New Phytologist*, *80*(2), pp.455-484.

Birks, H.H. and van Dinter, M., 2010. Lateglacial and early Holocene vegetation and climate gradients in the Nordfjord–Ålesund area, western Norway. *Boreas*, *39*(4), pp.783-798.

Birks, H.H., Battarbee, R.W. and Birks, H.J.B., 2000. The development of the aquatic ecosystem at Kråkenes Lake, western Norway, during the late glacial and early Holocene-a synthesis. *Journal of Paleolimnology*, *23*(1), pp.91-114

Birks, H.J.B. and Birks, H.H., 2008. Biological responses to rapid climate change at the Younger Dryas—Holocene transition at Kråkenes, western Norway. *The Holocene*, *18*(1), pp.19-30.

Birks, H.J.B., 1985. Recent and possible future mathematical developments in quantitative palaeoecology. *Palaeogeography, Palaeoclimatology, Palaeoecology*, *50*(1), pp.107-147.

Bisat, W.S., 1939, January. Older and newer drift in East Yorkshire. In. *Proceedings of the Yorkshire Geological and Polytechnic Society* (Vol. 24, No. 3, pp. 137-151). Geological Society of London.

Björck S, and Wohlfarth B. 2001. ^{14}C chronostratigraphic techniques in paleolimnology. In: Last WM, Smol JP, eds. Tracking Environmental Change Using Lake Sediments. Volume 1: Basin

Analysis, Coring, and Chronological Techniques. Dordrecht, the Netherlands: Kluwer Academic Publishers. p 205–45

Björck, S., Rundgren, M., Ingolfsson, O., and Funder, S., 1997. The Preboreal oscillation around the Nordic seas: terrestrial and lacustrine responses. *Journal of Quaternary Science,* 12, 455–465

Björck, S., Walker, M.J., Cwynar, L.C., Johnsen, S., Knudsen, K.L., Lowe, J.J. and Wohlfarth, B., 1998. An event stratigraphy for the Last Termination in the North Atlantic region based on the Greenland ice-core record: a proposal by the INTIMATE group. *Journal of Quaternary Science*, *13*(4), pp.283-292.

Blackburn, K. B. 1952. The dating of a deposit containing an elk skeleton found at Neasham near Darlington, County Durham. *New Phytologist*, *51*(3), 364-377.

Blockley, S.P., Lowe, J.J., Walker, M.J., Asioli, A., Trincardi, F., Coope, G.R. and Donahue, R.E., 2004. Bayesian analysis of radiocarbon chronologies: examples from the European Late-glacial. *Journal of Quaternary Science*, *19*(2), pp.159-175.

Blockley, S.P.E., Pyne-O'Donnell, S.D.F., Lowe, J.J., Matthews, I.P., Stone, A., Pollard, A.M., Turney, C.S.M. and Molyneux, E.G., 2005. A new and less destructive laboratory procedure for the physical separation of distal glass tephra shards from sediments. *Quaternary Science Reviews*, *24*(16), pp.1952-1960.

Blockley, S.P.E., Blockley, S.M., Donahue, R.E., Lane, C.S., Lowe, J.J. and Pollard, A.M., 2006. The chronology of abrupt climate change and Late Upper Palaeolithic human adaptation in Europe. *Journal of Quaternary Science*, *21*(5), pp.575-584.

Blockley, S.P.E., Blaauw, M., Ramsey, C.B. and van der Plicht, J., 2007. Building and testing age models for radiocarbon dates in Lateglacial and Early Holocene sediments. *Quaternary Science Reviews*, *26*(15), pp.1915-1926.

Blockley, S.P.E., Lane, C.S., Hardiman, M., Rasmussen, S.O., Seierstad, I.K., Steffensen, J.P., Svensson, A., Lotter, A.F., Turney, C.S., Ramsey, C.B. and Intimate Members, 2012. Synchronisation of palaeoenvironmental records over the last 60,000 years, and an extended INTIMATE event stratigraphy to 48,000 b2k. *Quaternary Science Reviews*, *36*, pp.2-10.

Blunier, T. and Brook, E.J., 2001. Timing of millennial-scale climate change in Antarctica and Greenland during the last glacial period. *Science*, *291*(5501), pp.109-112.

Bodén, P., Fairbanks, R.G., Wright, J.D. and Burckle, L.H., 1997. High-resolution stable isotope records from southwest Sweden: The drainage of the Baltic Ice Lake and Younger Dryas Ice Margin Oscillations. *Paleoceanography*, *12*(1), pp.39-49.

Bohncke, S. and Wijmstra, L., 1988. Reconstruction of Late-Glacial lake-level fluctuations in The Netherlands based on palaeobotanical analyses, geochemical results and pollen-density data. *Boreas*, *17*(3), pp.403-425.

Bond et al. 1992. Evidence for massive discharges of icebergs into the North Atlantic Ocean during the last glacial period. *Nature,* 360, 245 - 249

Bondevik, S., Løvholt, F., Harbitz, C., Mangerud, J., Dawson, A., and Svendsen, J. I. 2005. The Storegga Slide tsunami—comparing field observations with numerical simulations. *Marine and Petroleum Geology*, *22*(1), 195-208.

Boreham, S. and West, R.G., 1993. Late Quaternary sediments with Chara encrustations in southern Fenland. *Geological Magazine*, *130*(04), pp.543-544.

Bos, J.A. and van Geel, B., 2016. Palaeoenvironmental reconstruction based on the Early Holocene Haelen sequence, near Roermond (southeastern Netherlands). *Netherlands Journal of Geosciences*, pp.1-16.

Bos, J.A., Bohncke, S.J. and Janssen, C.R., 2006. Lake-level fluctuations and small-scale vegetation patterns during the late glacial in The Netherlands. *Journal of Paleolimnology*, *35*(2), pp.211-238.

Bos, J.A.A., Verbruggen, F., Engels, S. and Crombé, P., 2013. The influence of environmental changes on local and regional vegetation patterns at Rieme (NW Belgium): implications for Final Palaeolithic habitation. *Vegetation history and archaeobotany*, *22*(1), pp.17-38.

Boston, C.M., Evans, D.J. and Cofaigh, C.Ó., 2010. Styles of till deposition at the margin of the Last Glacial Maximum North Sea lobe of the British–Irish Ice Sheet: an assessment based on geochemical properties of glacigenic deposits in eastern England. *Quaternary Science Reviews*,*29*(23), pp.3184-3211.

Boston, C.M., Lukas, S. and Carr, S.J., 2015. A Younger Dryas plateau icefield in the Monadhliath, Scotland, and implications for regional palaeoclimate. *Quaternary Science Reviews*, *108*, pp.139-162.

Bøtter-Jensen, L., Mejdahl, V., 1988. Assessment of beta dose-rate using a GM multicounter system. *International Journal of Radiation Applications and Instrumentation. 14*, 187-191

Boulton, G. and Hagdorn, M., 2006. Glaciology of the British Isles Ice Sheet during the last glacial cycle: form, flow, streams and lobes. *Quaternary Science Reviews*, *25*(23), pp.3359-3390.

Boulton, G.S., Smith, G.D., Jones, A.S. and Newsome, J., 1985. Glacial geology and glaciology of the last mid-latitude ice sheets. *Journal of the Geological Society*, *142*(3), pp.447-474.

Bowen, D.Q., 1973. The Pleistocene succession of the Irish Sea. *Proceedings of the Geologists' Association*, *84*(3), pp.249-IN2.

Bowen, D.Q., McCabe, A.M., Rose, J., Sutherland, D.G., 1986. Correlation of Quaternary Glaciations in England, Ireland, Scotland and Wales. In: Sibrava, V., Bowen, D.Q., Richmond, G.M. (Eds.), Quaternary Glaciations in the Northern Hemisphere, International Geological Correlation Programme Project 24. Quaternary Science Reviews 5, 199–340.

Bowen, D.Q., Phillips, F.M., McCabe, A.M., Knutz, P.C. and Sykes, G.A., 2002. New data for the last glacial maximum in Great Britain and Ireland. *Quaternary Science Reviews*, *21*(1), pp.89-101.

Bradley, S.L., Milne, G.A., Shennan, I. and Edwards, R., 2011. An improved glacial isostatic adjustment model for the British Isles. *Journal of Quaternary Science*, *26*(5), pp.541-552.

Brauer, A., Günter, C., Johnsen, S.J. and Negendank, J.F.W., 2000. Land-ice teleconnections of cold climatic periods during the last Glacial/Interglacial transition. *Climate Dynamics*, *16*(2-3), pp.229-239.

Brauer, A., Haug, G.H., Dulski, P., Sigman, D.M. and Negendank, J.F., 2008. An abrupt wind shift in western Europe at the onset of the Younger Dryas cold period. *Nature Geoscience*, *1*(8), pp.520-523.

Breckenridge, A., 2015. The Tintah-Campbell gap and implications for glacial Lake Agassiz drainage during the Younger Dryas cold interval. *Quaternary Science Reviews*, *117*, pp.124-134.

Bridge, J.S., 2003. *Rivers and floodplains: forms, processes, and sedimentary record*. John Wiley and Sons.

Bridgland, D. R., Westaway, R., Howard, A. J., Innes, J. B., Long, A. J., Mitchell, W. A., White, M.J. and White, T. S. 2010. The role of glacio-isostasy in the formation of post-glacial river terraces in relation to the MIS 2 ice limit: evidence from northern England. *Proceedings of the Geologists' Association*,*121*(2), 113-127.

Bridgland, D.R., Innes, J.B., Long, A.J. and Mitchell, W.A. 2011. *Late Quaternary Landscape Evolution of the Swale-Ure Washlands, North Yorkshire*. Oxford: Oxbow Books.

Brock, F., Higham, T., Ditchfield, P. and Bronk Ramsey, C., 2010. Current pretreatment methods for AMS radiocarbon dating at the Oxford Radiocarbon Accelerator Unit (ORAU). *Radiocarbon*, *52*(1), pp.103-12.

Brodzikowski, K. and Van Loon, A.J., 1991. Review of glacigenic sediments. *Development in Sedimentology*, *49*, p.688.

Broecker, W.S. and Denton, G.H., 1989. The role of ocean-atmosphere reorganizations in glacial cycles. *Geochimica et Cosmochimica Acta*, *53*(10), pp.2465-2501.

Broecker, W.S. and Kennett, J.P., 1989. Routing of meltwater from the Laurentide Ice Sheet during the Younger Dryas cold episode. *Nature*, *341*, p.28.

Broecker, W.S., 1998. Paleocean circulation during the last deglaciation: a bipolar seesaw?. *Paleoceanography*, *13*(2), pp.119-121.

Broecker, W.S., 2006. Abrupt climate change revisited. *Global and Planetary Change*, *54*(3), pp.211-215.

Broecker, W.S., Bond, G., Klas, M., Bonani, G. and Wolfli, W., 1990. A salt oscillator in the glacial Atlantic? 1. The concept. *Paleoceanography*, *5*(4), pp.469-477.

Broecker, W.S., Denton, G.H., Edwards, R.L., Cheng, H., Alley, R.B. and Putnam, A.E., 2010. Putting the Younger Dryas cold event into context. *Quaternary Science Reviews*, *29*(9), pp.1078-1081.

Bronk Ramsey, C. 2008. Deposition models for chronological records. *Quaternary Science Reviews, 27*(1-2), 42-60.

Bronk Ramsey, C. 2009a. Bayesian analysis of radiocarbon dates. *Radiocarbon, 51*(1), 337-360.

Bronk Ramsey, C. 2009b. Dealing with outliers and offsets in radiocarbon dating. *Radiocarbon, 51*(3), 1023-1045.\

Bronk Ramsey, C., and Lee, S., 2013. Recent and planned developments of the program OxCal. *Radiocarbon*, *55*(2–3), pp.720-730.

Bronk Ramsey, C., Albert, P.G., Blockley, S.P., Hardiman, M., Housley, R.A., Lane, C.S., Lee, S., Matthews, I.P., Smith, V.C. and Lowe, J.J., 2015. Improved age estimates for key Late Quaternary European tephra horizons in the RESET lattice. *Quaternary Science Reviews*, *118*, pp.18-32.

Brooks, S.J. and Birks, H.J.B., 2000a. Chironomid-inferred Late-glacial air temperatures at Whitrig Bog, Southeast Scotland. *Journal of Quaternary Science*, *15*(8), pp.759-764.

Brooks, S.J. and Birks, H.J.B., 2000b. Chironomid-inferred late-glacial and early-Holocene mean July air temperatures for Kråkenes Lake, western Norway. *Journal of Paleolimnology*, *23*(1), pp.77-89.

Brooks, S. J., and Langdon, P. G. 2014. Summer temperature gradients in northwest Europe during the Lateglacial to early Holocene transition (15–8 ka BP) inferred from chironomid assemblages. *Quaternary International*, *341*, 80-90.

Brooks, S.J., Matthews, I.P., Birks, H.H. and Birks, H.J.B., 2012. High resolution Lateglacial and early-Holocene summer air temperature records from Scotland inferred from chironomid assemblages. *Quaternary Science Reviews*, *41*, pp.67-82.

Brown, A.G., Keough, M.K. and Rice, R.J., 1994. Floodplain evolution in the East Midlands, United Kingdom: the Lateglacial and Flandrian alluvial record from the Soar and Nene valleys. *Philosophical Transactions of the Royal Society of London A: Mathematical, Physical and Engineering Sciences*, *348*(1687), pp.261-293.

Brown, T., Bradley, C., Grapes, T. and Boomer, I., 2013. Hydrological assessment of Star Carr and the Hertford catchment, Yorkshire, UK. *Journal of Wetland Archaeology*.

Buckland, P.I. and Buckland, P.C., 2006. Bugs Coleopteran Ecology Package (Versions: BugsCEP v7.63; Bugsdata v8.01; BugsMCR v2.02; BugStats v1.22).

Bull, W. B. 1991. Geomorphic responses to climatic change. *Oxford University Press,* Oxford.

Bullock, P., Fedoroff, N., Jongerius, A., Stoops, G., Tursina, T. 1985 *Handbook for soil thin section description,* Waine Research, Chicago.

Bunch, T.E., Hermes, R.E., Moore, A.M., Kennett, D.J., Weaver, J.C., Wittke, J.H., DeCarli, P.S., Bischoff, J.L., Hillman, G.C., Howard, G.A. and Kimbel, D.R., 2012. Very high-temperature impact melt products as evidence for cosmic airbursts and impacts 12,900 years ago. *Proceedings of the National Academy of Sciences*, *109*(28), pp.E1903-E1912.

Busfield, M.E., Lee, J.R., Riding, J.B., Zalasiewicz, J. and Lee, S.V., 2015. Pleistocene till provenance in east Yorkshire: reconstructing ice flow of the British North Sea Lobe. *Proceedings of the Geologists' Association*, *126*(1), pp.86-99.

Bush, M.B., 1993. An 11 400 year paleoecological history of a British chalk grassland. *Journal of Vegetation Science*, pp.47-66.

Busschers, F.S., Kasse, C., Van Balen, R.T., Vandenberghe, J., Cohen, K.M., Weerts, H.J.T., Wallinga, J., Johns, C., Cleveringa, P. and Bunnik, F.P.M., 2007. Late Pleistocene evolution of the Rhine-Meuse system in the southern North Sea basin: imprints of climate change, sea-level oscillation and glacio-isostacy. *Quaternary Science Reviews*, *26*(25), pp.3216-3248.

Candy, I., Farry, A., Darvill, C. M., Palmer, A., Blockley, S. P. E., Matthews, I. P., MacLeod, A., Deeprose, L., Farley, N., Kearney, R., Conneller, C., Taylor, B., and Milner, N., 2015. The evolution of Palaeolake Flixton and the environmental context of Star Carr: an oxygen and carbon isotopic record of environmental change for the early Holocene. *Proceedings of the Geologists' Association*, *126*(1), 60-71.

Candy, I., Abrook, A., Elliot, F., Lincoln, P., Matthews, I.P. and Palmer, A., 2016. Oxygen isotopic evidence for high-magnitude, abrupt climatic events during the Lateglacial Interstadial in north-west Europe: analysis of a lacustrine sequence from the site of Tirinie, Scottish Highlands. *Journal of Quaternary Science*, *31*(6), pp.607-621.

Cappers, R.T., René, T.J., Becker, R.M. and Jans, J.E., 2006. *Digital seed atlas of the Netherlands. Groningen Archaeological Studies, Volume 4*. Barkhuis Publishing and Groningen University Library, Groningen, 502pp. (in Dutch).

Carey, M.A. and Chadha, D., 1998. Modelling the hydraulic relationship between the River Derwent and the Corallian Limestone aquifer. *Quarterly Journal of Engineering Geology and Hydrogeology*, *31*(1), pp.63-72.

Carlson, A.E., Clark, P.U., Haley, B.A., Klinkhammer, G.P., Simmons, K., Brook, E.J. and Meissner, K.J., 2007. Geochemical proxies of North American freshwater routing during the Younger Dryas cold event. *Proceedings of the National Academy of Sciences*, *104*(16), pp.6556-6561.

Carr, S.J., Holmes, R.V.D., Van der Meer, J.J.M. and Rose, J., 2006. The Last Glacial Maximum in the North Sea Basin: micromorphological evidence of extensive glaciation. *Journal of Quaternary Science*, *21*(2), pp.131-153.

Catt, J.A., 1991a. Late Devensian glacial deposits and glaciations in eastern England and the adjoining offshore region. *Glacial deposits in Great Britain and Ireland. Balkema, Rotterdam*, pp.61-68.

Catt, J.A., 1991b. The Quaternary history and glacial deposits of East Yorkshire. *Glacial Deposits in Great Britain and Ireland. Balkema, Rotterdam*, pp.185-191.

Catt, J. A. 2007. The Pleistocene glaciations of eastern Yorkshire: a review. In *Proceedings of the Yorkshire Geological and Polytechnic Society*(Vol. 56, No. 3, pp. 177-207). Geological Society of London.

Catt, J.A. and Penny, L.F., 1966. The Pleistocene deposits of Holderness, East Yorkshire. *Proceedings of the Yorkshire Geological Society*, *35*(3), pp.375-420.

Cavalazzi, B., Agangi, A., Barbieri, R., Franchi, F. and Gasparotto, G., 2014. The formation of low-temperature sedimentary pyrite and its relationship with biologically-induced processes. *Geology of Ore Deposits*, *56*(5), pp.395-408.

Cerling, T.E. and Quade, J., 1993. Stable carbon and oxygen isotopes in soil carbonates. *Climate change in continental isotopic records*, pp.217-231.

Challis, K., 2006. Airborne laser altimetry in alluviated landscapes. *Archaeological Prospection*, *13*(2), pp.103-127.

Charman, D.J., Barber, K.E., Blaauw, M., Langdon, P.G., Mauquoy, D., Daley, T.J., Hughes, P.D. and Karofeld, E., 2009. Climate drivers for peatland palaeoclimate records. *Quaternary Science Reviews*, *28*(19), pp.1811-1819.

Cheng, H., Edwards, R.L., Broecker, W.S., Denton, G.H., Kong, X., Wang, Y., Zhang, R. and Wang, X., 2009. Ice age terminations. *Science*, *326*(5950), pp.248-252.

Chiverrell, R.C., 2001. A proxy record of late Holocene climate change from May Moss, northeast England. *Journal of Quaternary Science*, *16*(1), pp.9-29.

Chiverrell, R. C., and Thomas, G. S. 2010. Extent and timing of the Last Glacial Maximum (LGM) in Britain and Ireland: a review. *Journal of Quaternary Science*, *25*(4), 535-549.

Chiverrell, R.C., Burke, M.J. and Thomas, G.S., 2016. Morphological and sedimentary responses to ice mass interaction during the last deglaciation. *Journal of Quaternary Science*, *31*(3), pp.265-280.

Clark, C.D., Evans, D.J., Khatwa, A., Bradwell, T., Jordan, C.J., Marsh, S.H., Mitchell, W.A. and Bateman, M.D., 2004. Map and GIS database of glacial landforms and features related to the last British Ice Sheet. *Boreas*, *33*(4), pp.359-375.

Clark, C.D., Hughes, A.L., Greenwood, S.L., Jordan, C. and Sejrup, H.P., 2012. Pattern and timing of retreat of the last British-Irish Ice Sheet. *Quaternary Science Reviews*, *44*, pp.112-146.

Clark, G., 1954. *Excavations at Star Carr: an early mesolithic site at Seamer near Scarborough, Yorkshire*. CUP Archive.

Clark, P.U., Marshall, S.J., Clarke, G.K., Hostetler, S.W., Licciardi, J.M. and Teller, J.T., 2001. Freshwater forcing of abrupt climate change during the last glaciation. *Science*, *293*(5528), pp.283-287.

Clark, P.U., Pisias, N.G., Stocker, T.F. and Weaver, A.J., 2002. The role of the thermohaline circulation in abrupt climate change. *Nature*, *415*(6874), pp.863-869.

Clark, P.U., Shakun, J.D., Baker, P.A., Bartlein, P.J., Brewer, S., Brook, E., Carlson, A.E., Cheng, H., Kaufman, D.S., Liu, Z. and Marchitto, T.M., 2012. Global climate evolution during the last deglaciation. *Proceedings of the National Academy of Sciences*, *109*(19), pp.E1134-E1142.

Cloutman, E.W., 1988a. Palaeoenvironments in the Vale of Pickering. Part I: Stratigraphy and Palaeogeography of Seamer Carr, Star Carr and Flixton Carr. In *Proceedings of the Prehistoric Society* (Vol. 54, pp. 1-19). Cambridge University Press.

Cloutman, E.W., 1988b. Palaeoenvironments in the Vale of Pickering. Part 2: Environmental History at Seamer Carr. In *Proceedings of the Prehistoric Society* (Vol. 54, pp. 21-36). Cambridge University Press.

Cloutman, E.W. and Smith, A.G., 1988. Palaeoenvironments in the Vale of Pickering. Part 3: Environmental History at Star Carr. In *Proceedings of the Prehistoric Society* (Vol. 54, pp. 37-58). Cambridge University Press.

Cloutman, E.W., Mitchell, W.A., and Chambers, F.M., 2010. Wykeham Quarry Extension Phase 6a (WK09): Interim Fieldwork Report and Recommendations for Specialist Palaeoenvironmental Reconstructions.

Coard, R. and Chamberlain, A.T., 1999. The nature and timing of faunal change in the British Isles across the Pleistocene/Holocene transition. *The Holocene*, *9*(3), pp.372-376.

Cohen, A.S., 2003. *Paleolimnology: the history and evolution of lake systems*. Oxford University Press.

Coles, B. J. 1998. Doggerland: A Speculative Survey. In *Proceedings of the Prehistoric Society* (Vol. 64, pp. 45-81). Cambridge University Press.

Conneller, C., 2007. Inhabiting new landscapes: settlement and mobility in Britain after the last glacial maximum. *Oxford Journal of Archaeology*, *26*(3), pp.215-237.

Conneller, C. and Schadla-Hall, T., 2003. Beyond Star Carr: the Vale of Pickering in the 10th millennium BP. In *Proceedings-Prehistoric Society* (Vol. 69, pp. 85-106). The Prehistoric Society.

Conneller, C., Milner, N., Taylor, B. and Taylor, M., 2012. Substantial settlement in the European Early Mesolithic: new research at Star Carr. *Antiquity*, *86*(334), pp.1004-1020.

Conneller, C., Bayliss, A., Milner, N. and Taylor, B. 2016. The Resettlement of the British Landscape: Towards a chronology of Early Mesolithic lithic assemblage types, Internet Archaeology 42. http://dx.doi.org/10.11141/ia.42.12

Coope. G. R. 1977: The Windermere Interstadial of the Late Devensian. Phil. 7rata. *H.* Soc. *Lond.* B

Coope, G.R. and Brophy, J.A., 1972. Late Glacial environmental changes indicated by a coleopteran succession from North Wales. *Boreas*, *1*(2), pp.97-142.

Coope, G. R., and Lemdahl, G. 1995. Regional differences in the Lateglacial climate of northern Europe based on coleopteran analysis. *Journal of Quaternary Science*, *10*(4), 391-395.

Coope, G.R. and Lemdahl, G., 1996. Validations for the use of beetle remains as reliable indicators of Quaternary climates: a reply to the criticisms by Johan Andersen. *Journal of Biogeography*, pp.115-120.

Coope, G.R., Pennington, W., Mitchell, G.F., West, R.G., Morgan, A.V. and Peacock, J.D., 1977. Fossil coleopteran assemblages as sensitive indicators of climatic changes during the Devensian (Last) Cold Stage [and Discussion]. *Philosophical Transactions of the Royal Society of London B: Biological Sciences*, *280*(972), pp.313-340.

Coope, G. R., Lemdahl, G., Lowe, J. J., and Walkling, A. 1998. Temperature gradients in northern Europe during the last glacial–Holocene transition (14-9 ^{14}C kyr BP) interpreted from coleopteran assemblages. *Journal of Quaternary Science*, *13*(5), 419-433.

Coops, H., 2002. Ecology of charophytes: an introduction. *Aquatic Botany*. 72. 205–208.

Cummins, G. 2003. Impacts of hunter-gatherers on the vegetation history of the Eastern Vale of Pickering, Yorkshire. Unpublished PhD Thesis. University of Durham

Daley, T.J. and Barber, K.E., 2012. Multi-proxy Holocene palaeoclimate records from Walton Moss, northern England and Dosenmoor, northern Germany, assessed using three statistical approaches. *Quaternary International*, *268*, pp.111-127.

Dansgaard, W. 1964. Stable isotopes in precipitation. *Tellus*, *16* (4), 436-468.

Dansgaard, W., Johnsen, S.J., Clausen, H.B., Dahl-Jensen, D., Gundestrup, N.S., Hammer, C.U., Hvidberg, C.S., Steffensen, J.P., Sveinbjörnsdottir, A.E., Jouzel, J. and Bond, G., 1993. Evidence for general instability of past climate from a 250-kyr ice-core record. *Nature*, *364*(6434), pp.218-220.

Dark, P., Higham, T.F.G., Jacobi, R. and Lord, T.C., 2006. New radiocarbon accelerator dates on artefacts from the Early Mesolithic site of Star Carr, North Yorkshire. *Archaeometry*, *48*(1), pp.185-200.

Dark, P. 1998. Palaeoecological investigations. In Mellars, P. and Dark, P. (eds) Star Carr in Context. Chapters 9-15, 111-181. McDonald Institute Monographs, Oxbow Books, Oxford.

Darling, W. G. 2004. Hydrological factors in the interpretation of stable isotopic proxy data present and past: a European perspective. *Quaternary Science Reviews*, 23 (7), 743-770.

Davies, B.J., Roberts, D.H., Ó Cofaigh, C., Bridgland, D.R., Riding, J.B., Phillips, E.R. and Teasdale, D.A., 2009. Interlobate ice-sheet dynamics during the Last Glacial Maximum at Whitburn Bay, County Durham, England. *Boreas*, *38*(3), pp.555-578.

Davies, S.M., 2015. Cryptotephras: the revolution in correlation and precision dating. *Journal of Quaternary Science*, *30*(2), pp.114-130.

Day, P., 1996. Devensian Late-glacial and early Flandrian environmental history of the Vale of Pickering, Yorkshire, England. *Journal of Quaternary Science,* 11, 9-24.

Dean, W.E., 1974. Determination of carbonate and organic matter in calcareous sediments and sedimentary rocks by loss on ignition: comparison with other methods. *Journal of Sedimentary Research*, *44*(1).

Dearing, J., 1999. Magnetic susceptibility. *Environmental magnetism: A practical guide*, *6*, pp.35-62.

Dee, M. and Bronk Ramsey, C., 2000. Refinement of graphite target production at ORAU. *Nuclear Instruments and Methods in Physics Research Section B: Beam Interactions with Materials and Atoms*, *172*(1), pp.449-453.

Denton, G.H., Alley, R.B., Comer, G.C. and Broecker, W.S., 2005. The role of seasonality in abrupt climate change. *Quaternary Science Reviews*, *24*(10), pp.1159-1182.

Denton, G.H., Broecker, W.S. and Alley, R.B., 2006. The mystery interval 17.5 to 14.5 kyrs ago. *PAGES news*, *14*(20), pp.14-16.

Denton, G.H., Anderson, R.F., Toggweiler, J.R., Edwards, R.L., Schaefer, J.M. and Putnam, A.E., 2010. The last glacial termination. *Science*, *328*(5986), pp.1652-1656.

Dickson, B., Yashayaev, I., Meincke, J., Turrell, B., Dye, S. and Holfort, J., 2002. Rapid freshening of the deep North Atlantic Ocean over the past four decades. *Nature*, *416*(6883), pp.832-837.

Digerfeldt, G., 1988. Reconstruction and regional correlation of Holocene lake-level fluctuations in Lake Bysjön, South Sweden. *Boreas*, *17*(2), pp.165-182.

Drummond, C. N., Patterson, W. P., Walker, J. C. 1995. Climatic forcing of carbon-oxygen isotopic covariance in temperate-region marl lakes. *Geology*, *23*, 1031-1034.

Duller, G.A.T., Bøtter-Jensen, L., Murray, A.S., 2003. Combining infrared- and green-laser stimulation sources in single-grain luminescence measurements of feldspar and quartz. *Radiat Meas 37,* 543-550.

Edwards, C.A., 1978. *The Quaternary history and stratigraphy of north-east Yorkshire* (Unpublished PhD thesis, University of Hull).

Edwards, K J 1990 'Fire and the Scottish Mesolithic: evidence from microscopic charcoal', in Vermeersch, P M and Van Peer, P (eds), Contributions to the Mesolithic in Europe, Leuven, 71-9.

Edwards, K.J., Whittington, G. and Tipping, R., 2000. The incidence of microscopic charcoal in late glacial deposits. *Palaeogeography, Palaeoclimatology, Palaeoecology*, *164*(1), pp.247-262.

Ehlers, J. and Gibbard, P.L., 2004. *Quaternary glaciations-extent and chronology: part I: Europe* (Vol. 2). Elsevier.

Elias, S.A., 2001. Coleoptera and Trichoptera. In *Tracking environmental change using lake sediments* (pp. 67-80). Springer Netherland

Elias, S. A., and Matthews, I. P. 2013. A comparison of reconstructions based on aquatic and terrestrial beetle assemblages: Late glacial–Early Holocene temperature reconstructions for the British Isles. *Quaternary International*, *341*, 69-79.

Engels, S., Brauer, A., Buddelmeijer, N., Martín-Puertas, C., Rach, O., Sachse, D. and Van Geel, B., 2016. Subdecadal-scale vegetation responses to a previously unknown late-Allerød climate fluctuation and Younger Dryas cooling at Lake Meerfelder Maar (Germany). *Journal of Quaternary Science*, *31*(7), pp.741-752.

Evans, D.J. and Twigg, D.R., 2002. The active temperate glacial landsystem: a model based on Breiðamerkurjökull and Fjallsjökull, Iceland. *Quaternary science reviews*, *21*(20), pp.2143-2177.

Evans, D.J., and Thomson, S. A. 2010. Glacial sediments and landforms of Holderness, eastern England: a glacial depositional model for the North Sea Lobe of the British–Irish Ice Sheet. *Earth-Science Reviews*, *101*(3), 147-189.

Evans, D.J., Owen, L.A. and Roberts, D., 1995. Stratigraphy and sedimentology of Devensian (Dimlington Stadial) glacial deposits, east Yorkshire, England. *Journal of Quaternary Science*, *10*(3), pp.241-265.

Evans, D.J., Thomson, S. and Clark, C.D., 2001. The glacial history of east Yorkshire. *The quaternary of east Yorkshire and north Lincolnshire, field guide. Quaternary Research Association, London*, pp.1-12.

Evans, D.J., Bateman, M.D., Roberts, D.H., Medialdea, A., Hayes, L., Duller, G.A., Fabel, D. and Clark, C.D., 2016. Glacial Lake Pickering: stratigraphy and chronology of a proglacial lake dammed by the North Sea Lobe of the British–Irish Ice Sheet. *Journal of Quaternary Science*.

Fairburn, W.A., 2009. Landforms and the geological evolution of the Vale of York during the Late Devensian. *Proceedings of the Yorkshire Geological Society*, *57*(3-4), pp.145-154.

Fairburn, W.A., 2011. The Pocklington alluvial fans of Yorkshire and their relationship with Late Devensian shorelines of proglacial Lake Humber.*Quaternary Newsletter*, *124*, pp.7-18.

Fairburn, W.A. and Bateman, M.D., 2016. A new multi-stage recession model for Proglacial Lake Humber during the retreat of the last British–Irish Ice Sheet. *Boreas*, *45*(1), pp.133-151.

Farrington, A. and Mitchell, G.F., 1951. The end-moraine north of Flamborough Head. *Proceedings of the Geologists' Association*, *62*(2), pp.100-106.

Fay, H., 2002. Formation of kettle holes following a glacial outburst flood (jökulhlaup), Skeidarársandur, southern Iceland. *The Extremes of the Extremes: Extraordinary Floods, Int. Assoc. Hydrol. Sci. Publ*, *271*, pp.205-210.

Ferguson, R. 1987: Hydraulic and sedimentary controls of channel pattern. In Richards, K., editor, River channels: environment and process, Institute of British Geographers Special Publication 18, Oxford: Blackwell, 129–58.

Firestone, R.B., West, A., Kennett, J.P., Becker, L., Bunch, T.E., Revay, Z.S., Schultz, P.H., Belgya, T., Kennett, D.J., Erlandson, J.M. and Dickenson, O.J., 2007. Evidence for an extraterrestrial impact 12,900 years ago that contributed to the megafaunal extinctions and the Younger Dryas cooling. *Proceedings of the National Academy of Sciences*, *104*(41), pp.16016-16021.

Foster, S.W., 1985. The late glacial and post glacial history of the Vale of Pickering and northern Yorkshire Wolds. *Unpublished PhD thesis*, University of Hull.

Franks, A.C., 1987. A re-evaluation of Late Quaternary events in the eastern half of the Vale of Pickering. *Unpublished PhD thesis.*

Fraser, M., Cloutman, E., Mitchell, W. & Chambers, F. 2009. Recording Phases 2 to 5, Interim Report, Wykeham Quarry, Eastern Extension, Vale of Pickering, North Yorkshire. Northern Archaeological Associates Unpublished Report

Freytet, P. and Verrecchia, E.P., 2002. Lacustrine and palustrine carbonate petrography: an overview. *Journal of Paleolimnology*, *27*(2), pp.221-237.

Galbraith, R.F., Roberts, R.G., Laslett, G.M., Yoshida, H., Olley, J.M., 1999. Optical dating of single and multiple grains of quartz from Jinmium rock shelter, northern Australia: Part I, experimental design and statistical models. *Archaeometry 41*, 339-364.

Gale, S. J. and Hoare, P. G. 1991 *Quaternary sediments: petrographic methods for the study of unlithified rocks*, Belhaven, London.

Gamble, C., Davies, W., Pettitt, P., Hazelwood, L., Richards, M., 2005. The Archaeological and Genetic Foundations of the European Population during the Lateglacial: Implications for "Agricultural Thinking." Cambridge Archaeological Journal 15, 193–223.

Gamble, C., Davies, W., Pettitt, P., Richards, M., 2004. Climate change and evolving human diversity in Europe during the last glacial. Philos. Trans. R. Soc. Lond. B Biol. Sci. 359, 243–53; discussion 253–4.

Gao, C., Boreham, S., Preece, R.C., Gibbard, P.L. and Briant, R.M., 2007. Fluvial response to rapid climate change during the Devensian (Weichselian) Lateglacial in the River Great Ouse, southern England, UK. *Sedimentary Geology*, *202*(1), pp.193-210.

Garnett, E.R., Andrews, J.E., Preece, R.C. and Dennis, P.F., 2004. Climatic change recorded by stable isotopes and trace elements in a British Holocene tufa. *Journal of Quaternary Science*, *19*(3), pp.251-262.

Gaunt, G.D., 1976. The Devensian maximum ice limit in the Vale of York. In *Proceedings of the Yorkshire Geological and Polytechnic Society* (Vol. 40, No. 4, pp. 631-637). Geological Society of London.

Gaunt, G.D., 1981. Quaternary history of the southern part of the Vale of York. *The Quaternary in Britain*, pp.82-97.

Gaunt, G.D., Jarvis, R.A. and Matthews, B. 1971. The late Weichselian sequence in the Vale of York. *Proceedings of the Yorkshire Geological Society*, 38, 281–284.

Gearey, B. R. 2008. Lateglacial vegetation change in East Yorkshire: a radiocarbon dated pollen sequence from Routh Quarry, Beverley.*Proceedings of the Yorkshire Geological Society*, *57*(2), 113-122.

Gibbard, P.L. and Clark, C.D., 2011. Pleistocene glaciation limits in Great Britain. *Quaternary Glaciation Extent and Chronology: A Closer Look. Elsevier, Amsterdam*, pp.75-94.

Gibbard, P.L. and Lewin, J., 2002. Climate and related controls on interglacial fluvial sedimentation in lowland Britain. *Sedimentary Geology*, *151*(3), pp.187-210.

Giles, J. R. A. 1992. Late Devensian and early Flandrian environments at Dishforth Bog, North Yorkshire. In *Proceedings of the Yorkshire Geological and Polytechnic Society* (Vol. 49, No. 1, pp. 1-9). Geological Society of London

Greenwood, S.L., Clark, C.D. and Hughes, A.L., 2007. Formalising an inversion methodology for reconstructing ice-sheet retreat patterns from meltwater channels: application to the British Ice Sheet. *Journal of Quaternary Science*, *22*(6), pp.637-645.

Grimm, S. B., and Weber, M. J. 2008. The chronological framework of the Hamburgian in the light of old and new ^{14}C dates. *Quartär*, *55*, 17-40.

Guilderson, T.P., Reimer, P.J. and Brown, T.A., 2005. The boon and bane of radiocarbon dating. *Science*, *307*(5708), pp.362-364.

Hammarlund, D., Björck, S., Buchardt, B., Israelson, C. and Thomsen C.T., 2003. Rapid hydrological changes during the Holocene revealed by stable isotope records of lacustrine carbonates from Lake Igelsjön, southern Sweden. Quaternary Science Reviews 22, 353–370.

Hammen, T. and Geel, B., 2008. Charcoal in soils of the Allerød-Younger Dryas transition were the result of natural fires and not necessarily the effect of an extra-terrestrial impact. *Geologie and Mijnbouw*, *87*(4), pp.359-361.

Hannon, G.E. and Gaillard, M.J., 1997. The plant-macrofossil record of past lake-level changes. *Journal of Paleolimnology*, *18*(1), pp.15-28.

Hardt, J., Hebenstreit, R., Lüthgens, C. and Böse, M., 2015. High-resolution mapping of ice-marginal landforms in the Barnim region, northeast Germany. *Geomorphology*, *250*, pp.41-52.

Harrison, S.P. and Digerfeldt, G., 1993. European lakes as palaeohydrological and palaeoclimatic indicators. *Quaternary Science Reviews*, *12*(4), pp.233-248.

Haynes, C.V., 2008. Younger Dryas "black mats" and the Rancholabrean termination in North America. *Proceedings of the National Academy of Sciences*, *105*(18), pp.6520-6525.

Hays, J.D., Imbrie, J. and Shackleton, N.J., 1976, December. Variations in the Earth's orbit: pacemaker of the ice ages. *Science, 194*(4270)

Hegerl, G.C. and Bindoff, N.L., 2005. Warming the world's oceans. *Science*, *309*(5732), pp.254-255.

Hegerl, G.C., F. W. Zwiers, P. Braconnot, N.P. Gillett, Y. Luo, J.A. Marengo Orsini, N. Nicholls, J.E. Penner and P.A. Stott, 2007: Understanding and Attributing Climate Change. In: Climate Change 2007: The Physical Science Basis. Contribution of Working Group I to the Fourth Assessment Report of the Intergovernmental Panel on Climate Change [Solomon, S., D. Qin, M. Manning, Z. Chen, M. Marquis, K.B. Averyt, M. Tignor and H.L. Miller (eds.)]. Cambridge University Press, Cambridge, United Kingdom and New York, NY, USA.

Heiri, O., Lotter, A.F. and Lemcke, G., 2001. Loss on ignition as a method for estimating organic and carbonate content in sediments: reproducibility and comparability of results. *Journal of paleolimnology*, *25*(1), pp.101-110.

Heiri, O., Cremer, H., Engels, S., Hoek, W.Z., Peeters, W. and Lotter, A.F., 2007. Lateglacial summer temperatures in the Northwest European lowlands: a chironomid record from Hijkermeer, the Netherlands. *Quaternary Science Reviews*, *26*(19), pp.2420-2437.

Hemming, S.R., 2004. Heinrich events: Massive late Pleistocene detritus layers of the North Atlantic and their global climate imprint. *Reviews of Geophysics*, *42*(1).

Hijmans, R.J., Cameron, S.E., Parra, J.L., Jones, P.G. and Jarvis, A., 2005. Very high resolution interpolated climate surfaces for global land areas. *International journal of climatology*, *25*(15), pp.1965-1978.

Hoek, W.Z., 1997. Late-glacial and early Holocene climatic events and chronology of vegetation development in the Netherlands. *Vegetation History and Archaeobotany*, *6*(4), pp.197-213.

Hoek, W.Z., 2008. The last glacial-interglacial transition. *Episodes*, *31*(2), pp.226-229.

Hoek, W.Z. and Bohncke, S.J.P., 2002. Climatic and environmental events over the Last Termination, as recorded in The Netherlands: a review. *Netherlands Journal of Geosciences/Geologie en Mijnbouw*, *81*(1).

Hoek, W.Z., Bohncke, S.J., Ganssen, G.M. and Meijer, T.M., 1999. Lateglacial environmental changes recorded in calcareous gyttja deposits at Gulickshof, southern Netherlands. *Boreas*, *28*(3), pp.416-432.

Hogg, A., Southon, J., Turney, C., Palmer, J., Ramsey, C.B., Fenwick, P., Boswijk, G., Friedrich, M., Helle, G., Hughen, K. and Jones, R., 2016. Punctuated Shutdown of Atlantic Meridional Overturning Circulation during Greenland Stadial 1. *Scientific reports*, *6*.

Holden N. 2004. LIDAR. The Environment Agency. http://www.environment-agency.gov.uk/science/monitoring/131047/?lang=_e

Holliday, V.T., Surovell, T., Meltzer, D.J., Grayson, D.K. and Boslough, M., 2014. The Younger Dryas impact hypothesis: a cosmic catastrophe. *Journal of Quaternary Science*, *29*(6), pp.515-530.

Holmes, J.A., Atkinson, T., Darbyshire, D.F., Horne, D.J., Joordens, J., Roberts, M.B., Sinka, K.J. and Whittaker, J.E., 2010. Middle Pleistocene climate and hydrological environment at the Boxgrove hominin site (West Sussex, UK) from ostracod records. *Quaternary Science Reviews*, *29*(13), pp.1515-1527.

Horton, T.W., Defliese, W.F., Tripati, A.K. and Oze, C., 2016. Evaporation induced 18 O and 13 C enrichment in lake systems: A global perspective on hydrologic balance effects. *Quaternary Science Reviews*, *131*, pp.365-379.

Housley, R.A., Gamble, C.S., Street, M. and Pettitt, P., 1997. Radiocarbon evidence for the Lateglacial Human Recolonisation of Northern Europe. In *Proceedings of the Prehistoric Society* (Vol. 63, pp. 25-54). Cambridge University Press.

Hsü, K. 1979. Non-annual cycles of varve-like sedimentation in Walensee, Switzerland, Hudson, J.D., 1978. Concretions, isotopes, and the diagenetic history of the Oxford Clay (Jurassic) of central England. Sedimentology 25, 339–370

Hubbard, B. and Glasser, N.F., 2005. *Field techniques in glaciology and glacial geomorphology*. John Wiley & Sons.

Huisink, M. 1997. Late-glacial sedimentological and morphological changes in a lowland river in response to climatic change: the Maas, southern Netherlands. *Journal of Quaternary Science*, *12*(3), 209-223.

Huijzer, A.S. and Isarin, R.F.B., 1997. The reconstruction of past climates using multi-proxy evidence: an example of the Weichselian Pleniglacial in northwest and central Europe. *Quaternary Science Reviews*, *16*(6), pp.513-533.

Huijzer, A.S., Vandenberghe, J., 1998. Climatic reconstruction of the Weichselian Pleniglacial in northwestern and central Europe. Journal of Quaternary Science 13, 391–417.

Hunt, C.O., Hall, A.R. and Gilbertson, D.D. 1984. The palaeobotany of the Late-Devensian sequence at Skipsea Withow Mere. In: Gilbertson, D.D. (ed.), Late Quaternary Environments and Man in Holderness, BAR Series 134, 81-108.

Imbrie, J. and Imbrie, J.Z., 1980. Modeling the climatic response to orbital variations. *Science*, *207*(4434), pp.943-953.

Innes, J. B. 2002. Introduction to the Late Devensian. In Quaternary of Northern England. Huddart, D. and Glasser, N. F. London: Geological Conservation Review Series 25. Joint Nature Conservation Committee. 211-220.

Innes, J. B., Rutherford, M. M., O'Brien, C. E., Bridgland, D. R., Mitchell, W. A., and Long, A. J. 2009. Late Devensian environments in the Vale of Mowbray, North Yorkshire, UK: evidence from palynology. *Proceedings of the Geologists' Association*, *120*(4), 199-208.

Innes, J.B., Blackford, J.J. and Simmons, I.G., 2011. Mesolithic environments at Star Carr, the eastern Vale of Pickering and environs: local and regional contexts. *Journal of Wetland Archaeology*.

Intermap Technologies (2007): NEXTMap British Digital Terrain Model Dataset Produced by Intermap. NERC Earth Observation Data Centre, *date of citation*. http://catalogue.ceda.ac.uk/uuid/8f6e1598372c058f07b0aeac2442366d

Irwin, H., Curtis, C., Coleman, M., 1977. Isotopic evidence for source of diagenetic carbonates formed during burial of organic-rich sediments. Nature 269, 209–213.

Isarin, R.F. and Bohncke, S.J., 1999. Mean July temperatures during the Younger Dryas in northwestern and central Europe as inferred from climate indicator plant species. *Quaternary Research*, *51*(2), pp.158-173.

Isarin, R.F., Renssen, H. and Vandenberghe, J., 1998. The impact of the North Atlantic Ocean on the Younger Dryas climate in northwestern and central Europe. *Journal of Quaternary Science*, *13*(5), pp.447-453.

Isarin, R.F., Renssen, H. and Vandenberghe, J., 1998. The impact of the North Atlantic Ocean on the Younger Dryas climate in northwestern and central Europe. *Journal of Quaternary Science*, *13*(5), pp.447-453.

Iversen, J., 1954. The late-glacial flora of Denmark and its relation to climate and soil. *Danmarks geologiske undersøgelse*, *2*(80), pp.87-119.

Jacobi, R., 1991. The Creswellian, Creswell and Cheddar. In: Barton, N., Roberts, A.J., Roe, D.A. (Eds.), The Late Glacial in north-west Europe: human adaptation and environmental change at the end of the Pleistocene. London, Council for British Archaeology, pp. 128–140.

Jacobi, R. M., and Higham, T. F. G. 2009. The early Lateglacial re-colonization of Britain: new radiocarbon evidence from Gough's Cave, southwest England. *Quaternary Science Reviews*, *28*(19), 1895-1913.

Jacobi, R. M., and Higham, T. F. G. 2011. Jacobi, R. and Higham, T., 2010. The Later Upper Palaeolithic recolonisation of Britain: new results from AMS radiocarbon dating. *The Ancient Human Occupation of Britain, Developments in Quaternary Science*, *14*, pp.223-247.

Jarosz, S. C., 2014. A Lateglacial environmental and temperature record from Wykeham, Yorkshire, interpreted from subfossil beetles (Coleoptera). *RHUL unpublished MSc thesis*

Jelgersma, S. 1979. Sea-level changes in the North Sea basin. In *The Quaternary History of the North Sea* (Vol. 2, pp. 233-248). Acta Universitatis Upsaliensis Symposia Universitatis Upsaliensis Annum Quingentesimum Celebrantis.

Johnsen, S.J., Clausen, H.B., Dansgaard, W., Fuhrert, K., Gundestrup, N., Hammer, C.U., Iversen, P., Jouzel, I. and Stauffer, B., 1992. Irregular glacial interstadials•, recorded in a new Greenland. *Nature*, *359*, p.24.

Jones, A.F., Brewer, P.A., Johnstone, E. and Macklin, M.G., 2007. High-resolution interpretative geomorphological mapping of river valley environments using airborne LiDAR data. *Earth Surface Processes and Landforms*, *32*(10), pp.1574-1592.

Jones, A.P., Tucker, M.E., and Hart, J.K., Eds. 1999. The description and analysis of Quaternary stratigraphic field sections. Technical Guide No. 7, Quaternary Research Association, London, 1999, 293pp.

Jones, R. L. 1977. Late Devensian deposits from Kildale, north-east Yorkshire. In *Proceedings of the Yorkshire Geological and Polytechnic Society* (Vol. 41, No. 2, pp. 185-188). Geological Society of London.

Jones, R.T., Marshall, J.D., Crowley, S.F., Bedford, A., Richardson, N., Bloemendal, J. and Oldfield, F., 2002. A high resolution, multiproxy Late-glacial record of climate change and intrasystem responses in northwest England. *Journal of Quaternary Science*, *17*(4), pp.329-340.

Jones, R.T., Marshall, J.D., Fisher, E., Hatton, J., Patrick, C., Anderson, K., Lang, B., Bedford, A. and Oldfield, F., 2011. Controls on lake level in the early to mid Holocene, Hawes Water, Lancashire, UK. *The Holocene*, *21*(7), pp.1061-1072.

Josephs, A. (2010). Wykeham Quarry Proposed Extension: Cultural Heritage Assessment. *Unpublished report.*

Jouzel, J., Stievenard, M., Johnsen, S.J., Landais, A., Masson-Delmotte, V., Sveinbjornsdottir, A., Vimeux, F., Von Grafenstein, U. and White, J.W., 2007. The GRIP deuterium-excess record. *Quaternary Science Reviews*, *26*(1), pp.1-17.

Kageyama, M., Valdes, P.J., Ramstein, G., Hewitt, C. and Wyputta, U., 1999. Northern Hemisphere Storm Tracks in Present Day and Last Glacial Maximum Climate Simulations: A Comparison of the European PMIP Models*. *Journal of Climate*, *12*(3), pp.742-760.

Kantorowicz, J.D., 1990, May. Lateral and vertical variations in pedogenesis and other early diagenetic phenomena, Middle Jurassic Ravenscar Group, Yorkshire. In *Proceedings of the Yorkshire Geological and Polytechnic Society* (Vol. 48, No. 1, pp. 61-74). Geological Society of London.

Kasse, C., Vandenberghe, J., and Bohncke, S. 1995. Climatic change and fluvial dynamics of the Maas during the late Weichselian and early Holocene. *Paläoklimaforschung*, *14*, 123-150.

Kasse, C., Vandenberghe, J., Van Huissteden, J., Bohncke, S.J.P. and Bos, J.A.A., 2003. Sensitivity of Weichselian fluvial systems to climate change (Nochten mine, eastern Germany). *Quaternary Science Reviews*, *22*(20), pp.2141-2156.

Kasse, C., Hoek, W. Z., Bohncke, S. J. P., Konert, M., Weijers, J. W. H., Cassee, M. L., and Van der Zee, R. M. 2005. Late Glacial fluvial response of the Niers-Rhine (western Germany) to climate and vegetation change. *Journal of Quaternary Science*, *20*(4), 377-394.

Keen, D.H., Jones, R.L. and Robinson, J.E., 1984, February. A Late Devensian and early Flandrian fauna and flora from Kildale, North-east Yorkshire. In *Proceedings of the Yorkshire Geological and Polytechnic Society* (Vol. 44, No. 4, pp. 385-397). Geological Society of London.

Keen, D. H., Jones, R. L., Evans, R. A., and Robinson, J. E. 1988. Faunal and floral assemblages from Bingley Bog, West Yorkshire, and their significance for Late Devensian and early Flandrian environmental changes. In *Proceedings of the Yorkshire Geological and Polytechnic Society* (Vol. 47, No. 2, pp. 125-138). Geological Society of London.

Kendall, P.F., 1902. A system of glacier-lakes in the Cleveland Hills. *Quarterly Journal of the Geological Society*, *58*(1-4), pp.471-571.

Kendall, P.F. and Wroot, H.E., 1924. *Geology of Yorkshire: an illustration of the evolution of Northern England* (Vol. 2).

Kleiven, H.K.F., Kissel, C., Laj, C., Ninnemann, U.S., Richter, T.O. and Cortijo, E., 2008. Reduced North Atlantic deep water coeval with the glacial Lake Agassiz freshwater outburst. *Science*, *319*(5859), pp.60-64.

Köhler, P., Knorr, G. and Bard, E., 2014. Permafrost thawing as a possible source of abrupt carbon release at the onset of the Bølling/Allerød. *Nature communications*, *5*.

Kozarski, S. 1983. River channel changes in the middle reach of the Warta Valley, Great Poland Lowland. *Quaternary studies in Poland*, *4*, 159-169.

Kühl, N., Gebhardt, C., Litt, T. and Hense, A., 2002. Probability density functions as botanical-climatological transfer functions for climate reconstruction. *Quaternary Research*, *58*(3), pp.381-392.

Lambeck, K., Rouby, H., Purcell, A., Sun, Y. and Sambridge, M., 2014. Sea level and global ice volumes from the Last Glacial Maximum to the Holocene. *Proceedings of the National Academy of Sciences*, *111*(43), pp.15296-15303.

Lamoureux, S.F., Gilbert, R. and Lewis, T., 2002. Lacustrine sedimentary environments in High Arctic proglacial Bear Lake, Devon Island, Nunavut, Canada. *Arctic, Antarctic, and Alpine Research*, pp.130-141.

Lane, C.S., Brauer, A., Blockley, S.P. and Dulski, P., 2013. Volcanic ash reveals time-transgressive abrupt climate change during the Younger Dryas. *Geology*, *41*(12), pp.1251-1254.

Lang, B., Brooks, S. J., Bedford, A., Jones, R. T., Birks, H. J. B., and Marshall, J. D. 2010. Regional consistency in Lateglacial chironomid-inferred temperatures from five sites in north-west England. *Quaternary Science Reviews*, *29*(13), 1528-1538.

Langford, H.E., Boreham, S., Briant, R.M., Coope, G.R., Horne, D.J., Schreve, D.C., Whittaker, J.E. and Whitehouse, N.J., 2014. Middle to Late Pleistocene palaeoecological reconstructions and palaeotemperature estimates for cold/cool stage deposits at Whittlesey, eastern England. *Quaternary International*, *341*, pp.6-26.

Laurie, T. 2003. Researching the Prehistory of Wensleydale, Swaledale and Teesdale. *The Archaeology of Yorkshire* ed. Manby, T.G., Moorhouse, S., and Ottaway, P. Yorkshire Archaeological Society Occasional Paper No. 3.

Lehman, S. J., and L. D. Keigwin 1992, Sudden changes in North Atlantic circulation during the last deglaciation, Nature, 356, 757–762.

Lekens, W.A.H., Sejrup, H.P., Haflidason, H., Petersen, G.Ø., Hjelstuen, B. and Knorr, G., 2005. Laminated sediments preceding Heinrich event 1 in the Northern North Sea and Southern Norwegian Sea: origin, processes and regional linkage. *Marine Geology*, *216*(1), pp.27-50.

Leng, M.J., Jones, M.D., Frogley, M.R., Eastwood, W.J., Kendrick, C.P. and Roberts, C.N., 2010. Detrital carbonate influences on bulk oxygen and carbon isotope composition of lacustrine sediments from the Mediterranean. *Global and Planetary Change*, *71*(3), pp.175-182.

Leng, M. J., and Marshall, J. D. 2004. Palaeoclimate interpretation of stable isotope data from lake sediment archives. *Quaternary Science Reviews*, 23 (7), 811-831.

Lewis, H.C., 1894. *Papers and notes on the glacial of Great Britain and Ireland*. Longmans, Green, and Company.

Lewis, S.G. and Maddy, D., 1999. Description and analysis of Quaternary fluvial sediments: a case study from the Upper River Thames, UK. *The description and analysis of Quaternary stratigraphic field sections. Quaternary Research Association, London*, pp.111-135.

Li, H.C. and Ku, T.L., 1997. $\delta^{13}C$– $\delta^{18}C$ covariance as a paleohydrological indicator for closed-basin lakes. *Palaeogeography, Palaeoclimatology, Palaeoecology*, *133*(1), pp.69-80.

Lian L. B. and Huntley D. J. 2001. Luminescence dating. In Tracking Environmental Change Using Lake Sediments, Vol. 1 ed. W. M. L. a. J. P. Smol, pp. 261-282. Kluwer Academic Publishers.

Lipps, S., and Caspers, G. 1990. Spätglazial und Holozän auf der Stolzenauer Terrasse im Mittelwesertal. *Eiszeitalter und Gegenwart*, *40*, 111-119.

Lisiecki, L.E. and Raymo, M.E., 2005. A Pliocene-Pleistocene stack of 57 globally distributed benthic $\delta^{18}O$ records. *Paleoceanography*, *20*(1).

Litt, T., Brauer, A., Goslar, T., Merkt, J., Bałaga, K., Müller, H., Ralska-Jasiewiczowa, M., Stebich, M. and Negendank, J.F., 2001. Correlation and synchronisation of Lateglacial continental sequences in northern central Europe based on annually laminated lacustrine sediments. *Quaternary Science Reviews*, *20*(11), pp.1233-1249.

Livingstone, S.J., Evans, D.J., Cofaigh, C.Ó. and Hopkins, J., 2010. The Brampton kame belt and Pennine escarpment meltwater channel system (Cumbria, UK): morphology, sedimentology and formation. *Proceedings of the Geologists' Association*, *121*(4), pp.423-443.

Livingstone, S.J., Evans, D.J., Cofaigh, C.Ó., Davies, B.J., Merritt, J.W., Huddart, D., Mitchell, W.A., Roberts, D.H. and Yorke, L., 2012. Glaciodynamics of the central sector of the last British–Irish Ice Sheet in Northern England. *Earth-Science Reviews*, *111*(1), pp.25-55.

Livingstone, S.J., Roberts, D.H., Davies, B.J., Evans, D.J., Ó Cofaigh, C. and Gheorghiu, D.M., 2015. Late Devensian deglaciation of the Tyne Gap Palaeo-Ice Stream, northern England. *Journal of Quaternary Science*, *30*(8), pp.790-804.

Livingstone, S.J., Piotrowski, J.A., Bateman, M.D., Ely, J.C. and Clark, C.D., 2015b. Discriminating between subglacial and proglacial lake sediments: an example from the Dänischer Wohld Peninsula, northern Germany. *Quaternary Science Reviews*, *112*, pp.86-108.

Lohne, Ø.S., Bondevik, S., Mangerud, J. and Svendsen, J.I., 2007. Sea-level fluctuations imply that the Younger Dryas ice-sheet expansion in western Norway commenced during the Allerød. *Quaternary Science Reviews*, *26*(17), pp.2128-2151.

Lohne, Ø.S., Mangerud, J.A.N. and Birks, H.H., 2013. Precise ^{14}C ages of the Vedde and Saksunarvatn ashes and the Younger Dryas boundaries from western Norway and their comparison with the Greenland Ice Core (GICC05) chronology. *Journal of Quaternary Science*, *28*(5), pp.490-500.

Lohne, Ø.S., Mangerud, J.A.N. and Birks, H.H., 2014. IntCal13 calibrated ages of the Vedde and Saksunarvatn ashes and the Younger Dryas boundaries from Kråkenes, western Norway. *Journal of Quaternary Science*, *29*(5), pp.506-507.

Lotter, A.F. and Anderson, N.J., 2012. Limnological responses to environmental changes at inter-annual to decadal time-scales. In *Tracking environmental change using lake sediments* (pp. 557-578). Springer Netherlands.

Lowe, J.J. and Turney, C.S., 1997. Vedde Ash layer discovered in a small lake basin on the Scottish mainland. *Journal of the Geological Society*, *154*(4), pp.605-612.

Lowe, J.J. and Walker, M.J.C., 1986. Lateglacial and early Flandrian environmental history of the Isle of Mull, Inner Hebrides, Scotland. *Transactions of the Royal Society of Edinburgh: Earth Sciences*, *77*(01), pp.1-20.

Lowe, J.J. and Walker, M.J.C., 2000. Radiocarbon dating the last glacial-interglacial transition (Ca. 14-9 ^{14}C ka BP) in terrestrial and marine records: the need for new quality assurance protocols. *Radiocarbon*, *42*(1), pp.53-68.

Lowe, J.J. and Walker, M.J., 2014. *Reconstructing quaternary environments*. Routledge.

Lowe, J.J., Ammann, B., Birks, H.H., Björck, S., Coope, G.R., Cwynar, L., De Beaulieu, J.L., Mott, R.J., Peteet, D.M. and Walker, M.J.C., 1994. Climatic changes in areas adjacent to the North Atlantic during the last glacial-interglacial transition (14-9 ka BP): A contribution to IGCP-253. *Journal of Quaternary Science*, *9*(2), pp.185-198.

Lowe, J.J., Coope, G.R., Sheldrick, C., Harkness, D.D. and Walker, M.J.C., 1995. Direct comparison of UK temperatures and Greenland snow accumulation rates, 15000—12000 yr ago. *Journal of Quaternary Science*, *10*(2), pp.175-180.

Lowe, J.J., Hoek, W.Z. and group1, I.N.T.I.M.A.T.E., 2001. Inter-regional correlation of palaeoclimatic records for the Last Glacial–Interglacial Transition: a protocol for improved precision recommended by the INTIMATE project group. *Quaternary Science Reviews*, *20*(11), pp.1175-1187.

Lowe, J.J., Rasmussen, S.O., Björck, S., Hoek, W.Z., Steffensen, J.P., Walker, M.J. and Yu, Z.C., 2008. Synchronisation of palaeoenvironmental events in the North Atlantic region during the Last Termination: a revised protocol recommended by the INTIMATE group. *Quaternary Science Reviews*, *27*(1), pp.6-17.

Macklin, M. G. 1997. Fluvial geomorphology of North-east England. In *Fluvial Geomorphology of Great Britain* (pp. 201-238). Springer Netherlands.

MacLeod, A., Palmer, A., Lowe, J., Rose, J., Bryant, C. and Merritt, J., 2011. Timing of glacier response to Younger Dryas climatic cooling in Scotland. *Global and Planetary Change*, *79*(3), pp.264-274.

Madgett, P.A. and Catt, J.A., 1978, March. Petrography, stratigraphy and weathering of Late Pleistocene tills in East Yorkshire, Lincolnshire and north Norfolk. In *Proceedings of the Yorkshire Geological and Polytechnic Society*(Vol. 42, No. 1, pp. 55-108). Geological Society of London.

Magny, M., Vannière, B., De Beaulieu, J.L., Bégeot, C., Heiri, O., Millet, L., Peyron, O. and Walter-Simonnet, A.V., 2007. Early-Holocene climatic oscillations recorded by lake-level fluctuations in west-central Europe and in central Italy. *Quaternary Science Reviews*, *26*(15), pp.1951-1964.

Magny, M., 2012. Palaeoclimatology and archaeology in the wetlands, in F. Menotti and A. O'Sullivan (ed.) The Oxford handbook of wetland archaeology: 585–97. Oxford: Oxford University Press.

Magny, M., 2013. Climatic and environmental changes reflected by lake-level fluctuations at Gerzensee from 14,850 to 13,050 yrBP. *Palaeogeography, Palaeoclimatology, Palaeoecology*, *391*, pp.33-39.

Magny, M. and Ruffadi, P., 1995. Younger Dryas and early Holocene lake-level fluctuations in the Jura mountains, France. *Boreas*, *24*(2), pp.155-172.

Magny, M., Aalbersberg, G., Bégeot, C., Benoit-Ruffaldi, P., Bossuet, G., Disnar, J.R., Heiri, O., Laggoun-Défarge, F., Mazier, F., Millet, L. and Peyron, O., 2006. Environmental and climatic changes in the Jura mountains (eastern France) during the Lateglacial–Holocene transition: a multi-proxy record from Lake Lautrey. *Quaternary Science Reviews*, *25*(5), pp.414-445.

Maher, L.J., 1981. Statistics for microfossil concentration measurements employing samples spiked with marker grains. *Review of Palaeobotany and Palynology*, *32*(2), pp.153-191.

Makaske, B., 2001. Anastomosing rivers: a review of their classification, origin and sedimentary products. *Earth-Science Reviews*, *53*(3), pp.149-196.

Mangerud, J., Andersen, S.T., Berglund, B.E. and Donner, J.J., 1974. Quaternary stratigraphy of Norden, a proposal for terminology and classification. *Boreas*, *3*(3), pp.109-126.

Mangili, C., Plessen, B., Wolff, C. and Brauer, A., 2010. Climatic implications of annual to decadal resolution stable isotope data from calcite varves of the Piànico interglacial lake record, Southern Alps. *Global and Planetary Change*, *71*(3), pp.168-174.

Markgraf, V., 1991. Younger Dryas in southern South America? *Boreas*, *20*(1), pp.63-69.

Marshall, J. D., Jones, R. T., Crowley, S. F., Oldfield, F., Nash, S., and Bedford, A. 2002. A high resolution late-glacial isotopic record from Hawes Water, northwest England: Climatic oscillations: Calibration and comparison of palaeotemperature proxies. *Palaeogeography, Palaeoclimatology, Palaeoecology*, *185*(1), 25-40.

Marshall, J. D., Lang, B., Crowley, S. F., Weedon, G. P., van Calsteren, P., Fisher, E. H., Holme, R., Holmes, J.A., Jones, R.T., Bedford, A. and Brooks, S. J. (2007). Terrestrial impact of abrupt changes in the North Atlantic thermohaline circulation: Early Holocene, UK. *Geology*,*35*(7), 639-642.

Masson-Delmotte, V., Jouzel, J., Landais, A., Stievenard, M., Johnsen, S.J., White, J.W.C., Werner, M., Sveinbjornsdottir, A. and Fuhrer, K., 2005. GRIP deuterium excess reveals rapid and orbital-scale changes in Greenland moisture origin. *Science*, *309*(5731), pp.118-121.

Matthews, I.P., Birks, H.H., Bourne, A.J., Brooks, S.J., Lowe, J.J., MacLeod, A. and Pyne-O'Donnell, S.D.F., 2011. New age estimates and climatostratigraphic correlations for the Borrobol and Penifiler Tephras: evidence from Abernethy Forest, Scotland. *Journal of Quaternary Science*, *26*(3), pp.247-252.

Mauquoy D, van Geel B. 2007. Mire and peat macros. In Encyclopedia of Quaternary Science, Vol. 3, Elias SA (ed.). Elsevier: Amsterdam; 2315–2336.

Mayle, F. E., Bell, M., Birks, H. H., Brooks, S. J., Coope, G. R., Lowe, J. J., Sheldrick, C., Shijie, L., Turney, C.S.M., and Walker, M. J. C. 1999. Climate variations in Britain during the Last Glacial–Holocene transition (15.0–11.5 cal ka BP): comparison with the GRIP ice-core record. *Journal of the Geological Society*, *156*(2), 411-423.

McCabe, A.M., Clark, P.U., Clark, J. and Dunlop, P., 2007. Radiocarbon constraints on readvances of the British–Irish Ice Sheet in the northern Irish Sea Basin during the last deglaciation. *Quaternary Science Reviews*, *26*(9), pp.1204-1211.

McConnaughey, T., 1991. Calcification in Chara corallina: CO_2 hydroxylation generates protons for bicarbonate assimilation. *Limnology and Oceanography*, *36*(4), pp.619-628.

McManus, J.F., Francois, R., Gherardi, J.M., Keigwin, L.D. and Brown-Leger, S., 2004. Collapse and rapid resumption of Atlantic meridional circulation linked to deglacial climate changes. *Nature*, *428*(6985), pp.834-837.

Mellars, P. and Dark, P. eds., 1998. *Star Carr in context: new archaeological and palaeoecolgical investigations at the early Mesolithic site of Star Carr, North Yorkshire*. McDonald Inst of Archeological.

Melmore, S., 1935. *The glacial geology of Holderness and the Vale of York*. S. Melmore.

Menuge, N.J., 2001. *A Guide to the Wetland Heritage of the Vale of Pickering*. PLACE Research Centre.

Merritt, R., 2006. *Atlas of the water beetles (Coleoptera) and water bugs (Hemiptera) of Derbyshire, Nottinghamshire and South Yorkshire, 1993-2005*. Sorby Natural History Society.

Metcalfe, S.E., Ellis, S., Horton, B.P., Innes, J.B., McArthur, J., Mitlehner, A., Parkes, A., Pethick, J.S., Rees, J., Ridgway, J. and Rutherford, M.M., 2000. The Holocene evolution of the Humber Estuary: reconstructing change in a dynamic environment. *Geological Society, London, Special Publications*,*166*(1), pp.97-118.

Miall, A.D., 1977. Lithofacies types and vertical profile models in braided river deposits: a summary.

Miall, A.D., 1985. Architectural-element analysis: a new method of facies analysis applied to fluvial deposits.

Miall, A.D., 1996. The geology of fluvial deposits. *Sedimentary facies, basin analysis, and petroleum geology*.

Milankovitch, M.M., 1941. *Canon of insolation and the ice-age problem* (in German) Publication

132 Mathematical and Natural Sciences, 33. Royal Serbian Sciences, Belgrade (English translation, Israel Program for Scientific Translation, Jerusalem (1969)).

Minchin, P.R., 1987. An evaluation of the relative robustness of techniques for ecological ordination. In *Theory and models in vegetation science* (pp. 89-107). Springer Netherlands.

Mitchell, W.A. 1991. Western Pennines. Field Guide. *Quaternary Research Association*, London.

Mitchell, W.A., 1996. Significance of snowblow in the generation of Loch Lomond Stadial (Younger Dryas) glaciers in the western Pennines, northern England. *Journal of Quaternary Science*, *11*(3), pp.233-248.

Mitchell, W.A., 2007, Reconstructions of the Late Devensian (Dimlington Stadial) British-Irish Ice Sheet: the role of the upper Tees drumlin field, north Pennines, England. In *Proceedings of the Yorkshire Geological and Polytechnic Society* (Vol. 56, No. 4, pp. 221-234). Geological Society of London.

Mitchell, W.A., Bridgland, D.R. and Innes, J.B., 2010. Late Quaternary evolution of the Tees–Swale interfluve east of the Pennines: the role of glaciation in the development of river systems in northern England. *Proceedings of the Geologists' Association*, *121*(4), pp.410-422.

Mix, A.C., Bard, E. and Schneider, R., 2001. Environmental processes of the ice age: land, oceans, glaciers (EPILOG). *Quaternary Science Reviews*, *20*(4), pp.627-657.

Moore, J.W., 1954. Excavations at Flixton, site 2. *JGD Clark Excavations at Star Carr*, pp.192-4.

Moore, P.D., 1989. The ecology of peat-forming processes: a review. *International Journal of Coal Geology*, *12*(1-4), pp.89-103.

Mortensen, M. F., Birks, H. H., Christensen, C., Holm, J., Noe-Nygaard, N., Odgaard, B. V., Olsen, J. and Rasmussen, K. L. 2011. Lateglacial vegetation development in Denmark–new evidence based on macrofossils and pollen from Slotseng, a small-scale site in southern Jutland. *Quaternary Science Reviews*, *30*(19), 2534-2550.

Mortensen, M.F., Henriksen, P.S. and Bennike, O., 2014. Living on the good soil: relationships between soils, vegetation and human settlement during the late Allerød period in Denmark. *Vegetation history and archaeobotany*, *23*(3), pp.195-205.

Murphy, D.H. and Wilkinson, B.H., 1980. Carbonate deposition and facies distribution in a central Michigan marl lake. *Sedimentology*, *27*(2), pp.123-135.

Murray, A.S., Wintle, A.G., 2000. Luminescence dating of quartz using an improved single-aliquot regenerative-dose protocol. *Radiat Meas, 32*, 57-73.

Murton, D.K., Pawley, S.M. and Murton, J.B., 2009. Sedimentology and luminescence ages of Glacial Lake Humber deposits in the central Vale of York. *Proceedings of the Geologists Association*, *120*(4), pp.209-222.

Murton, J.B., Bateman, M.D., Dallimore, S.R., Teller, J.T. and Yang, Z., 2010. Identification of Younger Dryas outburst flood path from Lake Agassiz to the Arctic Ocean. *Nature*, *464*(7289), pp.740-743.

Muschitiello, F. and Wohlfarth, B., 2015. Time-transgressive environmental shifts across Northern Europe at the onset of the Younger Dryas. *Quaternary Science Reviews*, *109*, pp.49-56.

Muschitiello, F., Pausata, F.S., Watson, J.E., Smittenberg, R.H., Salih, A.A., Brooks, S.J., Whitehouse, N.J., Karlatou-Charalampopoulou, A. and Wohlfarth, B., 2015. Fennoscandian freshwater control on Greenland hydroclimate shifts at the onset of the Younger Dryas. *Nature communications*, *6*.

Nanson, G.C. and Croke, J.C., 1992. A genetic classification of floodplains. *Geomorphology*, *4*(6), pp.459-486.

Neugebauer, I., Brauer, A., Dräger, N., Dulski, P., Wulf, S., Plessen, B., Mingram, J., Herzschuh, U. and Brande, A., 2012. A Younger Dryas varve chronology from the Rehwiese palaeolake record in NE-Germany. *Quaternary Science Reviews*, *36*, pp.91-102.

Nilsson, A.N., 1995. The larval stages of *Agabus approximatus* Fall. and *A. congener* (Thunberg) (Col. Dytiscidae). *Aquatic Insects: International Journal of Freshwater Entomology*, vol. 5, iss. 1.

Økland, K.A. and Økland, J., 2000. Freshwater bryozoans (Bryozoa) of Norway: distribution and ecology of Cristatella mucedo and Paludicella articulata. *Hydrobiologia*, *421*(1), pp.1-24.

Oswald, W.W., Anderson, P.M., Brown, T.A., Brubaker, L.B., Hu, F.S., Lozhkin, A.V., Tinner, W. and Kaltenrieder, P., 2005. Effects of sample mass and macrofossil type on radiocarbon dating of arctic and boreal lake sediments. *The Holocene*, *15*(5), pp.758-767.

Palmer, A.P., Rose, J., Lowe, J.J. and Walker, M.J.C., 2008a. Annually laminated Late Pleistocene sediments from Llangorse Lake, South Wales, UK: a chronology for the pattern of ice wastage. *Proceedings of the Geologists' Association*, *119*(3), pp.245-258.

Palmer, A. P., Lee, J.A., Kemp, R.A., Carr, S.J. 2008b. *Revised laboratory procedures for the preparation of thin sections from unconsolidated material*. Unpublished Internal Report, Royal Holloway, University of London.

Palmer, A.P., Rose, J., Lowe, J.J. and MacLeod, A., 2010. Annually resolved events of Younger Dryas glaciation in Lochaber (Glen Roy and Glen Spean), Western Scottish Highlands. *Journal of Quaternary Science*, *25*(4), pp.581-596.

Palmer, A.P., Matthews, I.P., Candy, I., Blockley, S.P.E., MacLeod, A., Darvill, C.M., Milner, N., Conneller, C. and Taylor, B., 2015. The evolution of Palaeolake Flixton and the environmental context of Star Carr, NE. Yorkshire: stratigraphy and sedimentology of the Last Glacial-Interglacial Transition (LGIT) lacustrine sequences. *Proceedings of the Geologists' Association*, *126*(1), pp.50-59.

Paus, A., 1995. The Late Weichselian and early Holocene history of tree birch in south Norway and the Bølling Betula time-lag in northwest Europe. *Review of Palaeobotany and Palynology*, *85*(3), pp.243-262.

Pawley, S.M., Bailey, R.M., Rose, J., Moorlock, B.S., Hamblin, R.J., Booth, S.J. and Lee, J.R., 2008. Age limits on Middle Pleistocene glacial sediments from OSL dating, north Norfolk, UK. *Quaternary Science Reviews*, *27*(13), pp.1363-1377.

Pawłowski, D., Borówka, R.K., Kowalewski, G.A., Luoto, T.P., Milecka, K., Nevalainen, L., Okupny, D., Tomkowiak, J. and Zieliński, T., 2016. Late Weichselian and Holocene record of the paleoenvironmental changes in a small river valley in Central Poland. *Quaternary Science Reviews*, *135*, pp.24-40.

Pennington, W. 1973. Absolute pollen frequencies in the sediments of lakes of different morphometry. In *Symposium of the British Ecological Society*.

Pennington, W. 1975. A chronostratigraphic comparison of Late-Weichselian and Late-Devensian subdivisions, illustrated by two radiocarbon-dated profiles from western Britain. *Boreas*, *4*(3), 157-171.

Pennington, W., 1986. Lags in adjustment of vegetation to climate caused by the pace of soil development. Evidence from Britain. *Vegetatio*, *67*(2), pp.105-118.

Pennington, W., and Bonny, A. P. 1970. Absolute pollen diagram from the British late-glacial. *Nature* 226, 871 – 873

Penny, L.F., and Rawson, P.F., 1969. Field meeting in East Yorkshire and North Lincolnshire. *Proceedings of the Geologists' Association*, 80, 193–218.

Pentecost, A., Andrews, J.E., Dennis, P.F., Marca-Bell, A. and Dennis, S., 2006. Charophyte growth in small temperate water bodies: extreme isotopic disequilibrium and implications for the palaeoecology of shallow marl lakes. *Palaeogeography, Palaeoclimatology, Palaeoecology*, *240*(3), pp.389-404.

Phillips, E.R. and Auton, C.A., 2000. Micromorphological evidence for polyphase deformation of glaciolacustrine sediments from Strathspey, Scotland. *Geological Society, London, Special Publications*, *176*(1), pp.279-292.

Pickering, K., Stow, D., Watson, M. and Hiscott, R., 1986. Deep-water facies, processes and models: a review and classification scheme for modern and ancient sediments. *Earth-Science Reviews*, *23*(2), pp.75-174.

Pieńkowski, P., 2008. Distribution of small, water-filled depressions as a component of the analysis of ice-sheet retreat dynamics in young glacial areas. *Landform Analysis*, *6*, pp.41-46.

Pigott, C. D., and Pigott, M. E. 1963. Late-glacial and Post-glacial deposits at Malham, Yorkshire. *New Phytologist*, *62*(3), 317-334.

Pinter, N., Scott, A.C., Daulton, T.L., Podoll, A., Koeberl, C., Anderson, R.S. and Ishman, S.E., 2011. The Younger Dryas impact hypothesis: A requiem. *Earth-Science Reviews*, *106*(3), pp.247-264.

Powell, J.H., Ford, J.R. and Riding, J.B., 2016. Diamicton from the Vale of Pickering and Tabular Hills, north-east Yorkshire: evidence for a Middle Pleistocene (MIS 8) glaciation? *Proceedings of the Geologists' Association*, *127*(5), pp.575-594.

Prescott, J.R., Hutton, J.T., 1988. Cosmic ray and gamma ray dosimetry for TL and ESR. *International Journal of Radiation Applications and Instrumentation. 14*, 223-227.

Price, G.D., 1998, May. Isotopic variation in fossils and matrix of the Cretaceous Red Chalk at Speeton and South Ferriby, Yorkshire, England. In *Proceedings of the Yorkshire Geological and Polytechnic Society* (Vol. 52, No. 1, pp. 107-112). Geological Society of London.

Price, G.D., Ruffell, A.H., Jones, C.E., Kalin, R.M. and Mutterlose, J., 2000. Isotopic evidence for temperature variation during the early Cretaceous (late Ryazanian–mid-Hauterivian). *Journal of the Geological Society*, *157*(2), pp.335-343.

Proctor, C. J., and Smart, P. L. 1989. *A new survey of Kent's Cavern, Devon*. University of Bristol Spelaeological Society.

Pyne-O'Donnell, S.D., 2007. Three new distal tephras in sediments spanning the Last Glacial–Interglacial Transition in Scotland. *Journal of Quaternary Science*, *22*(6), pp.559-570.

Rach, O., Brauer, A., Wilkes, H. and Sachse, D., 2014. Delayed hydrological response to Greenland cooling at the onset of the Younger Dryas in western Europe. *Nature Geoscience*, *7*(2), pp.109-112.

Rahmstorf, S., 1996. On the freshwater forcing and transport of the Atlantic thermohaline circulation. *Climate Dynamics*, *12*(12), pp.799-811.

Rahmstorf, S., Feulner, G., Mann, M.E., Robinson, A., Rutherford, S. and Schaffernicht, E.J., 2015. Exceptional twentieth-century slowdown in Atlantic Ocean overturning circulation. *Nature climate change*, *5*(5), pp.475-480.

Raistrick, A., 1926, January. The Glaciation of Wensleydale, Swaledale, and adjoining parts of the Pennines. In *Proceedings of the Yorkshire Geological and Polytechnic Society* (Vol. 20, No. 3, pp. 366-410). Geological Society of London.

Ralska-Jasiewiczowa, M., Goslar, T., Różański, K., Wacnik, A., Czernik, J. and Chróst, L., 2003. Very fast environmental changes at the Pleistocene/Holocene boundary, recorded in laminated sediments of Lake Gościąż, Poland. *Palaeogeography, Palaeoclimatology, Palaeoecology*, *193*(2), pp.225-247.

Rasmussen, S.O., Andersen, K.K., Svensson, A.M., Steffensen, J.P., Vinther, B.M., Clausen, H.B., Siggaard-Andersen, M.L., Johnsen, S.J., Larsen, L.B., Dahl-Jensen, D. and Bigler, M., 2006. A new Greenland ice core chronology for the last glacial termination. *Journal of Geophysical Research: Atmospheres*, *111*(D6).

Rasmussen, S.O., Vinther, B.M., Clausen, H.B. and Andersen, K.K., 2007. Early Holocene climate oscillations recorded in three Greenland ice cores. *Quaternary Science Reviews*, *26*(15), pp.1907-1914.

Rasmussen, S.O., Bigler, M., Blockley, S.P., Blunier, T., Buchardt, S.L., Clausen, H.B., Cvijanovic, I., Dahl-Jensen, D., Johnsen, S.J., Fischer, H. and Gkinis, V., 2014. A stratigraphic framework for abrupt climatic changes during the Last Glacial period based on three synchronized Greenland ice-core records: refining and extending the INTIMATE event stratigraphy. *Quaternary Science Reviews*, *106*, pp.14-28.

Rayburn, J.A., Cronin, T.M., Franzi, D.A., Knuepfer, P.L. and Willard, D.A., 2011. Timing and duration of North American glacial lake discharges and the Younger Dryas climate reversal. *Quaternary Research*, *75*(3), pp.541-551.

Reimer, P.J., Baillie, M.G., Bard, E., Bayliss, A., Beck, J.W., Blackwell, P.G., Bronk, R.C., Buck, C.E., Burr, G.S., Edwards, R.L. and Friedrich, M., 2009. IntCal09 and Marine09 radiocarbon age calibration curves, 0-50,000 years cal BP. *Radiocarbon*, *51*(4), pp.1111-1150.

Reimer, P.J., Bard, E., Bayliss, A., Beck, J.W., Blackwell, P.G., Bronk Ramsey, C., Buck, C.E., Cheng, H., Edwards, R.L., Friedrich, M. and Grootes, P.M., 2013. IntCal13 and Marine13 radiocarbon age calibration curves 0-50,000 years cal BP.

Renssen, H. and Isarin, R.F., 2001. The two major warming phases of the last deglaciation at~ 14.7 and~ 11.5 ka cal BP in Europe: climate reconstructions and AGCM experiments. *Global and Planetary Change*, *30*(1), pp.117-153.

Renssen, H. and Vandenberghe, J., 2003. Investigation of the relationship between permafrost distribution in NW Europe and extensive winter sea-ice cover in the North Atlantic Ocean during the cold phases of the Last Glaciation. *Quaternary Science Reviews*, *22*(2), pp.209-223.

Renssen, H., Mairesse, A., Goosse, H., Mathiot, P., Heiri, O., Roche, D.M., Nisancioglu, K.H. and Valdes, P.J., 2015. Multiple causes of the Younger Dryas cold period. *Nature Geoscience*.

Rhein, M., S.R. Rintoul, S. Aoki, E. Campos, D. Chambers, R.A. Feely, S. Gulev, G.C. Johnson, S.A. Josey, A. Kostianoy, C. Mauritzen, D. Roemmich, L.D. Talley and F. Wang, 2013: Observations: Ocean. In: Climate Change 2013: The Physical Science Basis. Contribution of Working Group I to the Fifth Assessment Report of the Intergovernmental Panel on Climate Change [Stocker, T.F., D. Qin, G.-K. Plattner, M. Tignor, S.K. Allen, J. Boschung, A. Nauels, Y. Xia, V. Bex and P.M. Midgley (eds.)]. Cambridge University Press, Cambridge, United Kingdom and New York, NY, USA.

Roberts, R.G., Lian, O.B., 2015. Dating techniques: Illuminating the past. *Nature*, *520*(7548), pp.438-439.

Roberts, R.G., Galbraith, R.F., Olley, J.M., Yoshida, H., Laslett, G.M., 1999. Optical dating of single and multiple grains of quartz from Jinmium rock shelter, northern Australia: Part II, results and implications. *Archaeometry 41*, 365-395.

Rodwell, J.S., ed., 1995. British plant communities Volume 4: Aquatic communities, swamps and tall-herb Fens. Cambridge, Cambridge University Press

Rose, J. 1985. The Dimlington Stadial/Dimlington Chronozone: a proposal for naming the main glacial episode of the Late Devensian in Britain. *Boreas*,*14*(3), pp.225-230.

Rose, J., 1995. Lateglacial and early Holocene river activity in lowland Britain. *European river activity and climatic change during the Lateglacial and early Holocene*, *14*, pp.51-74.

Rose, J., 2010. The Quaternary of the British Isles: factors forcing environmental change. *Journal of Quaternary Science*, *25*(4), pp.399-418.

Rose, J., Boardman, J., 1983. River activity in relation to short-term climatic deterioration. *Quaternary Studies in Poland*, 4, 189–198.

Rose, J., Turner, C., Coope, G.R. and Bryan, M.D., 1980. Channel changes in a lowland river catchment over the last 13,000 years. *Timescales in Geomorphology. Wiley, Chichester*, pp.159-175.

Rose, J., Lee, J.A., Candy, I. and Lewis, S.G., 1999. Early and Middle Pleistocene river systems in eastern England: evidence from Leet Hill, southern Norfolk, England. *Journal of Quaternary Science*, *14*(4), pp.347-360.

Rosen, J.L., Brook, E.J., Severinghaus, J.P., Blunier, T., Mitchell, L.E., Lee, J.E., Edwards, J.S. and Gkinis, V., 2014. An ice core record of near-synchronous global climate changes at the Bolling transition. *Nature Geoscience*, *7*(6), pp.459-463.

Rowe, P. 2006. *Nosterfield 2005: Intervention 11: The Flasks– Flint Report*. Report for Field Archaeological Specialists.

Rozanski, K., Araguás-Araguás, L., Gonfiantini, R. 1992. Relation between long-term trends of oxygen-18 isotope composition of precipitation and climate. *Science*, 258, 981-985.

Rozanski, K., Araguás-Araguás, L., Gonfiantini, R. 1993. Isotopic Patterns in Modern Global Precipitation. In: Swart, P. K., Lohmann, K. C., McKenizie, J. Savin, S. (Eds) *Climate Change in Continental Isotopic Systems,* American Geophysical Union, Washington, D. C.

Ruddiman, W.F. and McIntyre, A., 1981. The North Atlantic Ocean during the last deglaciation. *Palaeogeography, Palaeoclimatology, Palaeoecology*, *35*, pp.145-214.

Sachse, D., Billault, I., Bowen, G.J., Chikaraishi, Y., Dawson, T.E., Feakins, S.J., Freeman, K.H., Magill, C.R., McInerney, F.A., Van Der Meer, M.T. and Polissar, P., 2012. Molecular paleohydrology: interpreting the hydrogen-isotopic composition of lipid biomarkers from photosynthesizing organisms.

Sarmaja-Korjonen, K., 2003. Chydoid ephippia as indicators of environmental change biostratigraphical evidence from two lakes in southern Finland. *The Holocene*, *13*(5), pp.691-700.

Sarmaja-Korjonen, K., Seppänen, A. and Bennike, O., 2006. Pediastrum algae from the classic late glacial Bølling Sø site, Denmark: response of aquatic biota to climate change. *Review of Palaeobotany and Palynology*, *138*(2), pp.95-107.

Schadla-Hall, T. 1987. Recent investigations of the early Mesolithic landscape in the Vale of Pickering. In: *Mesolithic Northwest Europe: Recent Trends* (eds M. Zvelebil and H. Blankholm), pp. 46–54. Department of Archaeology, University of Sheffield.

Schillereff, D.N., Chiverrell, R.C., Macdonald, N. and Hooke, J.M., 2014. Flood stratigraphies in lake sediments: A review. *Earth-Science Reviews*, *135*, pp.17-37.

Schnurrenberger, D., Russell, J. and Kelts, K., 2003. Classification of lacustrine sediments based on sedimentary components. *Journal of Paleolimnology*, *29*(2), pp.141-154.

Schumm, S.A., 1985. Patterns of alluvial rivers. *Annual Review of Earth and Planetary Sciences*, *13*, p.5.

Sejrup, H.P., Hjelstuen, B.O., Nygård, A., Haflidason, H. and Mardal, I., 2015. Late Devensian ice-marginal features in the central North Sea–processes and chronology. *Boreas*, *44*(1), pp.1-13.

Severinghaus, J.P. and Brook, E.J., 1999. Abrupt climate change at the end of the last glacial period inferred from trapped air in polar ice. *Science*, *286*(5441), pp.930-934.

Severinghaus, J.P., 2009. Climate change: Southern see-saw seen. *Nature*, *457*(7233), pp.1093-1094.

Severinghaus, J.P., Sowers, T., Brook, E.J., Alley, R.B. and Bender, M.L., 1998. Timing of abrupt climate change at the end of the Younger Dryas interval from thermally fractionated gases in polar ice. *Nature*, *391*(6663), pp.141-146.

Shackleton, N.J. and Opdyke, N.D., 1973. Oxygen isotope and palaeomagnetic stratigraphy of equatorial Pacific core V28-238: Oxygen isotope temperatures and ice volumes on a 10 5 year and 10 6 year scale. *Quaternary research*, *3*(1), pp.39-55.

Sheldrick, C.D., 1997. *Plant macrofossil records from UK lake sediments spanning the last glacial-interglacial transition, ca. 14-9 C Ka BP. Unpublished PhD thesis,* University of London.

Sheldrick, C.D., Lowe, J.J. and Reynier, M.J., 1997. Palaeolithic Barbed Point from Gransmoor, East Yorkshire, England. In *Proceedings of the Prehistoric Society* (Vol. 63, pp. 359-370). Cambridge University Press.

Shotton, F.W. 1986. Glaciations in the United Kingdom. Quaternary Science Reviews 5, 293-297.

Sissons, J. B. 1974. The Quaternary in Scotland: a review. *Scottish Journal of Geology*, *10*(4), 311-337.

Sissons, J.B., 1979. The later lakes and associated fluvial terraces of Glen Roy, Glen Spean and vicinity. *Transactions of the Institute of British Geographers*, pp.12-29.

Skinner, L.C., Fallon, S., Waelbroeck, C., Michel, E. and Barker, S., 2010. Ventilation of the deep Southern Ocean and deglacial CO2 rise. *Science*, *328*(5982), pp.1147-1151.

Smith, A.G., 1984. Newferry and the Boreal-Atlantic transition. *New Phytologist*, *98*(1), pp.35-55.

Smith, A.J.E. and Smith, R., 2004. *The moss flora of Britain and Ireland*. Cambridge University Press.

Solomon, S., D. Qin, M. Manning, R.B. Alley, T. Berntsen, N.L. Bindoff, Z. Chen, A. Chidthaisong, J.M. Gregory, G.C. Hegerl, M. Heimann, B. Hewitson, B.J. Hoskins, F. Joos, J. Jouzel, V. Kattsov, U. Lohmann, T. Matsuno, M. Molina, N. Nicholls, J. Overpeck, G. Raga, V. Ramaswamy, J. Ren, M. Rusticucci, R. Somerville, T.F. Stocker, P. Whetton, R.A. Wood and D. Wratt, 2007: Technical Summary. In: Climate Change 2007: The Physical Science Basis. Contribution of Working Group I to the Fourth Assessment Report of the Intergovernmental Panel on Climate Change [Solomon, S., D. Qin, M. Manning, Z. Chen, M. Marquis, K.B. Averyt, M. Tignor and H.L. Miller (eds.)]. Cambridge University Press, Cambridge, United Kingdom and New York, NY, USA.

Stanford, J.D., Rohling, E.J., Hunter, S.E., Roberts, A.P., Rasmussen, S.O., Bard, E., McManus, J. and Fairbanks, R.G., 2006. Timing of meltwater pulse 1a and climate responses to meltwater injections. *Paleoceanography*, *21*(4).

Steffensen, J.P., Andersen, K.K., Bigler, M., Clausen, H.B., Dahl-Jensen, D., Fischer, H., Goto-Azuma, K., Hansson, M., Johnsen, S.J., Jouzel, J. and Masson-Delmotte, V., 2008. High-resolution Greenland ice core data show abrupt climate change happens in few years. *Science*, *321*(5889), pp.680-684.

Stocker, T.F., D. Qin, G.-K. Plattner, L.V. Alexander, S.K. Allen, N.L. Bindoff, F.-M. Bréon, J.A. Church, U. Cubasch, S. Emori, P. Forster, P. Friedlingstein, N. Gillett, J.M. Gregory, D.L. Hartmann, E. Jansen, B. Kirtman, R. Knutti, K. Krishna Kumar, P. Lemke, J. Marotzke, V. Masson-Delmotte, G.A. Meehl, I.I. Mokhov, S. Piao, V. Ramaswamy, D. Randall, M. Rhein, M. Rojas, C. Sabine, D. Shindell, L.D. Talley, D.G. Vaughan and S.-P. Xie, 2013: Technical Summary. In: Climate Change 2013: The Physical Science Basis. Contribution of Working Group I to the Fifth Assessment Report of the Intergovernmental Panel on Climate Change [Stocker, T.F., D. Qin, G.-K. Plattner, M. Tignor, S.K. Allen, J. Boschung, A. Nauels, Y. Xia, V. Bex and P.M. Midgley (eds.)]. Cambridge University Press, Cambridge, United Kingdom and New York, NY, USA.

Stott, L., Timmermann, A. and Thunell, R., 2007. Southern hemisphere and deep-sea warming led deglacial atmospheric CO2 rise and tropical warming. *Science*, *318*(5849), pp.435-438.

Straw, A., 1961. Drifts, meltwater channels and ice-margins in the Lincolnshire Wolds. *Transactions and Papers (Institute of British Geographers)*, (29), pp.115-128.

Straw, A., 1979. The Devensian glaciation. In: Straw, A., Clayton, K.M. (Eds.), The geomorphology of the British Isles: eastern and central England. Methuen, London, pp. 21– 45.

Straw, A., and Clayton, K.M. (Eds.). 1979. The geomorphology of the British Isles: eastern and central England. Methuen, London, pp. 21– 45.

Stuiver M, and Reimer PJ. 1993. Extended ^{14}C data base and revised CALIB 3.0 ^{14}C age calibration program. *Radiocarbon*, 35(1):215–30.

Suggate, R.P., West, R.G., 1959. On the extent of the last glaciation in eastern England. Proceedings of the Royal Society B, 150, 263– 283.

Surovell, T.A., Holliday, V.T., Gingerich, J.A., Ketron, C., Haynes, C.V., Hilman, I., Wagner, D.P., Johnson, E. and Claeys, P., 2009. An independent evaluation of the Younger Dryas extraterrestrial impact hypothesis. *Proceedings of the National Academy of Sciences*, *106*(43), pp.18155-18158.

Talbot, M.R., 1990. A review of the palaeohydrological interpretation of carbon and oxygen isotopic ratios in primary lacustrine carbonates. *Chemical Geology: Isotope Geoscience Section*, *80*(4), pp.261-279.

Taylor, B.J., 1971. *British regional geology: northern England* (No. 7). HM Stationery Office.

Taylor, B., 2011. Early Mesolithic activity in the wetlands of the Lake flixton basin. *Journal of Wetland Archaeology*.

Tebbens, L. A., Veldkamp, A., Westerhoff, W., and Kroonenberg, S. B. 1999. Fluvial incision and channel downcutting as a response to Late-glacial and Early Holocene climate change: the lower reach of the River Meuse (Maas), the Netherlands. *Journal of Quaternary Science*, *14*(1), 59-75.

Teller, J.T., Leverington, D.W. and Mann, J.D., 2002. Freshwater outbursts to the oceans from glacial Lake Agassiz and their role in climate change during the last deglaciation. *Quaternary Science Reviews*, *21*(8), pp.879-887.

Thiagarajan, N., Subhas, A.V., Southon, J.R., Eiler, J.M. and Adkins, J.F., 2014. Abrupt pre-Bolling-Allerod warming and circulation changes in the deep ocean. *Nature*, *511*(7507), pp.75-78.

Thomas, G.S.P., 1999. Northern England. In: Bowen, D.Q. (Ed.), A revised correlation of quaternary deposits in the British Isles, Geological Society Special Report, vol. 23, pp. 91–98.

Thomas, G.S.P. and Connell, R.J., 1985. Iceberg drop, dump, and grounding structures from Pleistocene glacio-lacustrine sediments, Scotland. *Journal of Sedimentary Research*, *55*(2).

Thórsson, Æ.T., Salmela, E. and Anamthawat-Jónsson, K., 2001. Morphological, cytogenetic, and molecular evidence for introgressive hybridization in birch. *Journal of Heredity*, *92*(5), pp.404-408.

Thrasher, I.M., Mauz, B., Chiverrell, R.C., Lang, A. and Thomas, G.S.P., 2009. Testing an approach to OSL dating of Late Devensian glaciofluvial sediments of the British Isles. *Journal of Quaternary Science*, *24*(7), pp.785-801.

Tipping, R., 1995. Holocene evolution of a lowland Scottish landscape: Kirkpatrick Fleming. Part I, peat-and pollen-stratigraphic evidence for raised moss development and climatic change. *The Holocene*, *5*(1), pp.69-81.

Tolksdorf, J.F., Turner, F., Kaiser, K., Eckmeier, E., Stahlschmidt, M., Housley, R.A., Breest, K. and Veil, S., 2013. Multiproxy analyses of stratigraphy and palaeoenvironment of the late Palaeolithic Grabow floodplain site, northern Germany. *Geoarchaeology*, *28*(1), pp.50-65.

Toucanne, S., Soulet, G., Freslon, N., Jacinto, R.S., Dennielou, B., Zaragosi, S., Eynaud, F., Bourillet, J.F. and Bayon, G., 2015. Millennial-scale fluctuations of the European Ice Sheet at the end of the last glacial, and their potential impact on global climate. *Quaternary Science Reviews*,*123*, pp.113-133.

Treese, K.L. and Wilkinson, B.H., 1982. Peat-marl deposition in a Holocene paludal-lacustrine basin—Sucker Lake, Michigan. *Sedimentology*, *29*(3), pp.375-390.

Turner, F., Tolksdorf, J. F., Viehberg, F., Schwalb, A., Kaiser, K., Bittmann, F., von Bramann, U., Pott, R., Staesche, U., Breest, K. and Veil, S. 2013. Lateglacial/early Holocene fluvial reactions of the Jeetzel river (Elbe valley, northern Germany) to abrupt climatic and environmental changes. *Quaternary Science Reviews*, *60*, 91-109.

Turner, J. and Kershaw, A.P. 1973. A Late- and Post-glacial pollen diagram from Cranberry Bog, near Beamish, County Durham. *New Phytologist*, 72, 915–928.

Turner, J.N., Holmes, N., Davis, S.R., Leng, M.J., Langdon, C. and Scaife, R.G., 2015. A multiproxy (micro-XRF, pollen, chironomid and stable isotope) lake sediment record for the Lateglacial to Holocene transition from Thomastown Bog, Ireland. *Journal of Quaternary Science*, *30*(6), pp.514-528

Turney, C.S., 1998. Extraction of rhyolitic component of Vedde microtephra from minerogenic lake sediments. *Journal of Paleolimnology*, *19*(2), pp.199-206.

Turney, C.S., Harkness, D.D. and Lowe, J.J., 1997. Rapid Communication: The use of microtephra horizons to correlate Late-glacial lake sediment successions in Scotland. *Journal of Quaternary Science*, *12*(6), pp.525-531.

Turney, C.S., Coope, G.R., Harkness, D.D., Lowe, J.J. and Walker, M.J., 2000. Implications for the dating of Wisconsinan (Weichselian) Late-Glacial events of systematic radiocarbon age differences between terrestrial plant macrofossils from a site in SW Ireland. *Quaternary Research*, *53*(1), pp.114-121.

Tweddle, J.C., 2000. *A high resolution palynological study of the Holocene vegetational development of central Holderness, eastern Yorkshire, with particular emphasis on the detection of prehistoric human activity* (Doctoral dissertation, University of Sheffield).

Tweddle, J.C., 2001. Regional vegetational history. In: Bateman, M.D., Buckland, P.C., Frederick, C.D., Whitehouse, N.J. (Eds.), The Quaternary of East Yorkshire and North Lincolnshire Field Guide. Quaternary Research Association, London, pp. 35–46.

Tye, G.J., Sherriff, J., Candy, I., Coxon, P., Palmer, A., McClymont, E.L. and Schreve, D.C., 2016. The $\delta^{18}O$ stratigraphy of the Hoxnian lacustrine sequence at Marks Tey, Essex, UK: implications for the climatic structure of MIS 11 in Britain. *Journal of Quaternary Science*, *31*(2), pp.75-92.

Valentin, H., 1957. Glaziamorphologische Untersuchungen in Ostengland. Abhandlungen Geographischen Institute Freien Universitat Berlin, 4, 1– 84.

Väliranta, M., Weckström, J., Siitonen, S., Seppä, H., Alkio, J., Juutinen, S. and Tuittila, E.S., 2011. Holocene aquatic ecosystem change in the boreal vegetation zone of northern Finland. *Journal of Paleolimnology*, *45*(3), pp.339-352.

Väliranta, M., Salonen, J.S., Heikkilä, M., Amon, L., Helmens, K., Klimaschewski, A., Kuhry, P., Kultti, S., Poska, A., Shala, S. and Veski, S., 2015. Plant macrofossil evidence for an early onset of the Holocene summer thermal maximum in northernmost Europe. *Nature communications*, *6*.

van Asch, N., Lutz, A. F., Duijkers, M. C., Heiri, O., Brooks, S. J., and Hoek, W. Z. 2012. Rapid climate change during the Weichselian Lateglacial in Ireland: Chironomid-inferred summer temperatures from Fiddaun, Co. Galway. *Palaeogeography, Palaeoclimatology, Palaeoecology*, *315*, 1-11.

van Asch, N., Heiri, O., Bohncke, S. J., and Hoek, W. Z. 2013. Climatic and environmental changes during the Weichselian Lateglacial Interstadial in the Weerterbos region, the Netherlands. *Boreas*, *42*(1), 123-139.

van Dinter, M. and Birks, H.H., 1996. Distinguishing fossil Betula nana and B. pubescens using their wingless fruits: implications for the late-glacial vegetational history of western Norway. *Vegetation History and Archaeobotany*, *5*(3), pp.229-240.

Van Geel, B., Bohncke, S.J.P. and Dee, H., 1980. A palaeoecological study of an upper Late Glacial and Holocene sequence from "De Borchert", The Netherlands. *Review of Palaeobotany and Palynology*, *31*, pp.367-448.

Van Geel, B., De Lange, L., and Wiegers, J. 1984. Reconstruction and interpretation of the local vegetation succession of a Lateglacial deposit from Usselo (The Netherlands), based on the analysis of micro- and macrofossils. *Acta Botanica Neerlandica*, *33*(4), 535-546.

Van Geel, B., Coope, G. R., and Van Der Hammen, T. 1989. Palaeoecology and stratigraphy of the Lateglacial type section at Usselo (The Netherlands).*Review of Palaeobotany and Palynology*, *60*(1), 25-129.

van Raden, U.J., Colombaroli, D., Gilli, A., Schwander, J., Bernasconi, S.M., van Leeuwen, J., Leuenberger, M. and Eicher, U., 2013. High-resolution late-glacial chronology for the Gerzensee lake record (Switzerland): $\delta^{18}O$ correlation between a Gerzensee-stack and NGRIP. *Palaeogeography, Palaeoclimatology, Palaeoecology*, *391*, pp.13-24.

Vandenberghe, J., 2002 The relation between climate and river processes, landforms and deposits during the Quaternary. *Quaternary International* 91, 17-23.

Vandenberghe, J. 2003. Climate forcing of fluvial system development: an evolution of ideas. *Quaternary Science Reviews*, *22*(20), 2053-2060.

Vandenberghe, J., and Woo, M. K. 2002. Modern and ancient periglacial river types. *Progress in Physical Geography*, *26*(4), 479-506.

Vandenberghe, J., Kasse, C., Bohncke, S., and Kozarski, S. 1994. Climate-related river activity at the Weichselian-Holocene transition: a comparative study of the Warta and Maas rivers. *Terra Nova*, *6*(5), 476-485.

Vandenberghe, J., Lowe, J.J, Coope, R., Litt, T., and Züller, L. 2004. Climatic and environmental variability in the mid-latitude Europe sector during the last interglacial-glacial cycle. In *Past Climate Variability through Europe and Africa* (pp. 393-416). Springer Netherlands.

Veblen, T.T., Baker, W.L., Montenegro, G. and Swetnam, T.W. eds., 2006. *Fire and climatic change in temperate ecosystems of the western Americas* (Vol. 160). Springer Science and Business Media.

Vellinga, M. and Wood, R.A., 2002. Global climatic impacts of a collapse of the Atlantic thermohaline circulation. *Climatic change*, *54*(3), pp.251-267.

Vellinga, M. and Wood, R.A., 2008. Impacts of thermohaline circulation shutdown in the twenty-first century. *Climatic Change*, *91*(1-2), pp.43-63.

Vincent, J.H. and Cwynar, L.C., 2016. A temperature reversal within the rapid Younger Dryas-Holocene warming in the North Atlantic?. *Quaternary Science Reviews*, *153*, pp.199-207.

von Grafenstein, U., Erlenkeuser, H., Brauer, A., Jouzel, J. and Johnsen, S.J., 1999. A mid-European decadal isotope-climate record from 15,500 to 5000 years BP. *Science*, *284*(5420), pp.1654-1657.

von Grafenstein, U., Belmecheri, S., Eicher, U., van Raden, U.J., Erlenkeuser, H., Andersen, N. and Ammann, B., 2013. The oxygen and carbon isotopic signatures of biogenic carbonates in

Gerzensee, Switzerland, during the rapid warming around 14,685 years BP and the following interstadial. *Palaeogeography, Palaeoclimatology, Palaeoecology*, *391*, pp.25-32.

Wade, P.M., 1990. The colonisation of disturbed freshwater habitats by Characeae. *Folia Geobotanica et Phytotaxonomica*, *25*(3), pp.275-278.

Walker, D. and Godwin, H., 1954. Lake stratigraphy, pollen analysis and vegetational history. *Excavations at Star Carr*, pp.25-69.

Walker, M.J.C., 1995. Climatic changes in Europe during the last glacial/interglacial transition. *Quaternary International*, *28*, pp.63-76.

Walker, M.J.C., 2001. Rapid climate change during the last glacial–interglacial transition; implications for stratigraphic subdivision, correlation and dating. *Global and Planetary Change*, *30*(1), pp.59-72.

Walker, M. J. C. 2004. A Lateglacial pollen record from Hallsenna Moor, near Seascale, Cumbria, NW England, with evidence for arid conditions during the Loch Lomond (Younger Dryas) Stadial and early Holocene. In *Proceedings of the Yorkshire Geological and Polytechnic Society* (Vol. 55, No. 1, pp. 33-42). Geological Society of London.

Walker, M. J. C., and Harkness, D. D. 1990. Radiocarbon dating the Devensian Lateglacial in Britain: new evidence from Llanilid, South Wales. *Journal of Quaternary Science*, *5*(2), 135-144.

Walker, M.J.C., Coope, G.R. and Lowe, J.J., 1993. The Devensian (Weichselian) Lateglacial palaeoenvironmental record from Gransmoor, East Yorkshire, England: A contribution to the 'North Atlantic seaboard programme'of IGCP-253,'Termination of the Pleistocene'. *Quaternary Science Reviews*, *12*(8), pp.659-680.

Walker, M. J. C., Bohncke, S. J. P., Coope, G. R., O'Connell, M., Usinger, H., and Verbruggen, C. 1994. The Devensian/Weichselian Late-glacial in northwest Europe (Ireland, Britain, north Belgium, The Netherlands, northwest Germany). *Journal of Quaternary Science*, *9*(2), 109-118.

Walker, M.J.C., Björck, S., Lowe, J.J., Cwynar, L.C., Johnsen, S., Knudsen, K.L. and Wohlfarth, B., 1999. Isotopic 'events' in the GRIP ice core: a stratotype for the Late Pleistocene. *Quaternary Science Reviews*, *18*(10), pp.1143-1150.

Walker, M.J.C., Bryant, C., Coope, G.R., Harkness, D.D., Lowe, J.J. and Scott, E.M., 2001. Towards a radiocarbon chronology of the Late-Glacial: sample selection strategies. *Radiocarbon*, *43*(2B), pp.1007-1019.

Walker, M.J.C., Coope, G.R., Sheldrick, C., Turney, C.S.M., Lowe, J.J., Blockley, S.P.E. and Harkness, D.D., 2003. Devensian Lateglacial environmental changes in Britain: a multi-proxy environmental record from Llanilid, South Wales, UK. *Quaternary Science Reviews*, *22*(5), pp.475-520.

Walker, M.J.C., Johnsen, S., Rasmussen, S.O., Popp, T., Steffensen, J.P., Gibbard, P., Hoek, W., Lowe, J., Andrews, J., Björck, S. and Cwynar, L.C., 2009. Formal definition and dating of the GSSP (Global Stratotype Section and Point) for the base of the Holocene using the Greenland NGRIP ice core, and selected auxiliary records. *Journal of Quaternary Science*, *24*(1), pp.3-17.

Walker, M.J.C., Lowe, J.J., Blockley, S.P., Bryant, C., Coombes, P., Davies, S., Hardiman, M., Turney, C.S. and Watson, J., 2012. Lateglacial and early Holocene palaeoenvironmental 'events' in Sluggan Bog, Northern Ireland: comparisons with the Greenland NGRIP GICC05 event stratigraphy. *Quaternary Science Reviews*, *36*, pp.124-13.

Wallinga, J., Murray, A., Duller, G., 2000. Underestimation of equivalent dose in single-aliquot optical dating of feldspars caused by preheating. *Radiat Meas 32*, 691-695.

Ward, S. L., Neill, S. P., Scourse, J. D., Bradley, S. L., & Uehara, K. (2016). Sensitivity of palaeotidal models of the northwest European shelf seas to glacial isostatic adjustment since the Last Glacial Maximum. *Quaternary Science Reviews*, *151*, 198-211.

Watson, E.V., 1981. *British Mosses and Liverworts: An Introductory Work*. Cambridge University Press.

Watson, J.E., Brooks, S.J., Whitehouse, N.J., Reimer, P.J., Birks, H.J.B. and Turney, C., 2010. Chironomid-inferred late-glacial summer air temperatures from Lough Nadourcan, Co. Donegal, Ireland. *Journal of Quaternary Science*, *25*(8), pp.1200-1210.

Watts, W.A., 1977. The Late Devensian vegetation of Ireland. Philosophical Transactions of the Royal Society of London, B280, 273–93

Weninger, B., Schulting, R., Bradtmöller, M., Clare, L., Collard, M., Edinborough, K., Hilpert, J., Jöris, O., Niekus, M., Rohling, E.J. and Wagner, B., 2008. The catastrophic final flooding of Doggerland by the Storegga Slide tsunami. *Documenta Praehistorica*, *35*(15), pp.1-24.

Wheeler, B.D., Shaw, S. and Tanner, K., 2009. A wetland framework for impact assessment at statutory sites in England and Wales. *Environment Agency RandD Technical Report*.

Wheeler, D., 2013. Regional weather and climates of the British Isles–Part 4: North East England and Yorkshire. *Weather*, *68*(7), pp.184-190.

Wheeler, J.A., Cortés, A.J., Sedlacek, J., Karrenberg, S., Kleunen, M., Wipf, S., Hoch, G., Bossdorf, O. and Rixen, C., 2016. The snow and the willows: earlier spring snowmelt reduces performance in the low-lying alpine shrub Salix herbacea. *Journal of Ecology*.

White, T.S., Bridgland, D.R., Westaway, R. and Straw, A., 2016. Evidence for late Middle Pleistocene glaciation of the British margin of the southern North Sea. *Journal of Quaternary Science*.

Whittington, G., Edwards, K. J., Zanchetta, G., Keen, D. H., Bunting, M. J., Fallick, A. E., & Bryant, C. L. 2015. Lateglacial and early Holocene climates of the Atlantic margins of Europe: Stable isotope, mollusc and pollen records from Orkney, Scotland. *Quaternary Science Reviews*, *122*, 112-130.

Wiik, E., Bennion, H., Sayer, C.D., Davidson, T.A., Clarke, S.J., McGowan, S., Prentice, S., Simpson, G. and Stone, L., 2015. The coming and going of a marl lake: multi-indicator palaeolimnology reveals abrupt ecological change and alternative views of reference conditions. *Frontiers in Ecology and Evolution*, *3*, p.82.

Wilkin, R.T. and Barnes, H.L., 1997. Formation processes of framboidal pyrite. *Geochimica et Cosmochimica Acta*, *61*(2), pp.323-339.

Williams, N.E., 1988. The use of caddisflies (Trichoptera) in palaeoecology. *Palaeogeography, Palaeoclimatology, Palaeoecology*, *62*(1-4), pp.493-500.

Wilson, D.J., Crocket, K.C., Flierdt, T., Robinson, L.F. and Adkins, J.F., 2014. Dynamic intermediate ocean circulation in the North Atlantic during Heinrich Stadial 1: A radiocarbon and neodymium isotope perspective. *Paleoceanography*, *29*(11), pp.1072-1093.

Wing, S.L., 1984. Relation of paleovegetation to geometry and cyclicity of some fluvial carbonaceous deposits. *Journal of Sedimentary Research*, *54*(1).

Wohlfarth, B., 1996. The chronology of the last termination: a review of radiocarbon-dated, high-resolution terrestrial stratigraphies. *Quaternary Science Reviews*, *15*(4), pp.267-284.

Wohlfarth, B., Blaauw, M., Davies, S.M., Andersson, M., Wastegard, S., Hormes, A. and Possnert, G., 2006. Constraining the age of Lateglacial and early Holocene pollen zones and tephra horizons in southern Sweden with Bayesian probability methods. *Journal of Quaternary Science*, *21*(4), pp.321-334.

Wohlfarth, B., Blaauw, M., Davies, S.M., Andersson, M., Wastegard, S., Hormes, A. and Possnert, G., 2006. Constraining the age of Lateglacial and early Holocene pollen zones and tephra horizons in southern Sweden with Bayesian probability methods. *Journal of Quaternary Science*, *21*(4), pp.321-334.

Wohlfarth, B., Skog, G., Possnert, G. and Holmquist, B., 1998. Pitfalls in the AMS radiocarbon-dating of terrestrial macrofossils. *Journal of Quaternary Science*, *13*(2), pp.137-145.

Woolacott, D. 1905. The superficial deposits and pre-glacial valleys of the Northumberland and Durham coalfield. *Quarterly Journal of the Geological Society*, *61*(1-4), 64-96.

Wunsch, C., 2006. Abrupt climate change: An alternative view. *Quaternary Research*, *65*(2), pp.191-203.

Yorke, L., Rumsby, B.T. and Chiverrell, R.C., 2012. Depositional history of the Tyne valley associated with retreat and stagnation of Late Devensian Ice Streams. *Proceedings of the Geologists' Association*, *123*(4), pp.608-625.

Yu, Z. and Eicher, U., 1998. Abrupt climate oscillations during the last deglaciation in central North America. *Science*, *282*(5397), pp.2235-2238.

Zhao, Y., Sayer, C.D., Birks, H.H., Hughes, M. and Peglar, S.M., 2006. Spatial representation of aquatic vegetation by macrofossils and pollen in a small and shallow lake. *Journal of Paleolimnology*, *35*(2), pp.335-350.

Appendices

The attached data CD includes the appendices for this thesis. These are as follows:

A. GIS comparisons to borehole data at Wykeham Quarry (Chapter 4).

B. Location and sediment descriptions from the records obtained from Wykeham Quarry (Chapters 4 and 5).

C. Stratigraphic logs from the RHULS-1-3 sequences (Chapter 5).

D. Summary figures for work undertaken on the Seamer basin (Chapter 5).

E. Sediment descriptions and bulk sediment data from the Seamer Basin (Chapter 5).

F. Output of the inverse distance weighted model runs on sedimentary sequences at Wykeham Quarry (Chapter 5).

G. Raw data obtained from the WYKNE15 sequence (bulk sedimentology, plant macrofossils, stable isotopes, age model; Chapter 6).

H. NMDS output from the plant macrofossil assemblage data in the WYKNE15 sequence (Chapter 6).

I. Raw data obtained from the WYSE14 sequence (bulk sedimentology, pollen, plant macrofossils, age model; Chapter 6).

J. Coleopteran assemblage from the WYKSE14 sequence (Chapter 6).

K. NMDS output from the plant macrofossil assemblage data in the WYKSE14 sequence (Chapter 6).

Appendices Data CD

If missing, please contact:
Paul Lincoln
Department of Geography
Royal Holloway, University of London
Egham
Surrey
TW20 OEX
Paul.Lincoln.2010@live.rhul.ac.uk